

THESIS

SEQUENCE STRATIGRAPHIC FRAMEWORK FOR TOP SEAL DEVELOPMENT:
EXAMPLES FROM THE SKULL CREEK AND GRANEROS SHALES,
DENVER BASIN.

Submitted by

Kimberly K. Edwards

Earth Resources Department

In partial fulfillment of the requirements

For the Degree of Masters of Science

Colorado State University

Fort Collins, CO

Fall 1999

QE
471.15
S5
E47
1999
THESIS

COLORADO STATE UNIVERSITY

November 10, 1999

WE HEREBY RECOMMEND THAT THE THESIS PREPARED UNDER OUR SUPERVISION BY KIMBERLY K. EDWARDS ENTITLED SEQUENCE STRATIGRAPHIC FRAMEWORK FOR TOP SEAL DEVELOPMENT: EXAMPLES FROM THE SKULL CREEK AND GRANEROS SHALES, DENVER BASIN BE ACCEPTED AS FULLFILLING IN PART REQUIREMENTS FOR THE DEGREE OF MASTERS OF SCIENCE.

Committee on Graduate Work

William R. Alcorn

Dean Hall

Sally J. Sutton

Advisor

Frank G. Ehridge

Co-Advisor

Judith L. Hall

Department Head/Director

ABSTRACT OF THESIS

SEQUENCE STRATIGRAPHIC FRAMEWORK FOR TOP SEAL DEVELOPMENT: EXAMPLES FROM THE SKULL CREEK AND GRANEROS SHALES, DENVER BASIN.

In general, the distal open marine shelf setting, typified by the Graneros Shale produces a rock with a greater and more uniform seal capacity relative to the rocks of a proximal open marine shelf setting, such as those of the Skull Creek Shale. A distal setting, which usually corresponds to the time of maximum transgression, may produce better seals because there is less coarse clastic sediment input, which allows slow deposition of clays from suspension to be the dominant depositional process. In this study, the higher capacity seal rocks occur in the upper parts of the TST, either within the condensed section or below it. The Skull Creek locations show seal occurrence to be stratigraphically higher on depositional topographic highs, and lower in areas that were topographically low at the time of deposition. Top seal capacity was quantified with mercury injection capillary pressure (MICP) analysis. Other physical characteristics of these marine shales were studied but only porosity, permeability, total clay, and hydrogen index consistently demonstrated a significant correlation with seal capacity in both units. Shales that are well laminated with a high percentage of total clay and/or total organic carbon with a type I-II (marine) kerogen may or may not qualify as the best seal. Top seal capacity may be more a function of rock fabric rather than mineralogy. For example, two samples may have exactly the same amount of quartz, as shown by XRD analysis, but thin section examination reveals that the majority of quartz in one sample is present as grains and in the other sample as cement. Samples with cement usually provide a better seal because they decrease the pore throat diameter, thus increasing the amount of hydrocarbons that can be trapped. Seal quality in both the Skull Creek and Graneros Shales is quite variable throughout each of the facies within the TST deposits.

Kimberly K. Edwards
Earth Resources Department
Colorado State University
Fort Collins, CO 80523
Fall 1999

TABLE OF CONTENTS

ABSTRACT	ii
LIST OF FIGURES	vii
LIST OF TABLES	x
LIST OF APPENDICES	xi
ACKNOWLEDGEMENTS	xii
Chapter 1. INTRODUCTION	1
1.1 Purpose and scope of study	1
1.2 Background	2
1.3 Location	4
1.4 Regional Geology	5
Denver Basin	5
Tectonic History	8
Sequence Stratigraphy	9
Chapter 2. SAMPLING PROCEDURES	18
2.1 Outcrop sampling procedures	18
2.2 Core sampling procedures	20
2.3 Outcrop Gamma ray procedures	20
Chapter 3. METHODOLOGY	21
3.1 Capillary Pressure	21
3.2 Thin Section Petrography	24
3.3 X-Ray Diffraction	25
Whole Rock Analysis	25
Clay Mineral Analysis	26
3.4 Scanning Electron Microscopy	27
3.5 Organic Geochemistry	27
Chapter 4. SOLDIER CANYON DAM (SKULL CREEK) OUTCROP RESULTS	30
4.1 Facies Description	30
4.2 Lithology Description	41
Thin-Section petrography	44
Scanning Electron Microscopy	48
Whole Rock Mineralogy	49
Clay Mineralogy	49
4.3 Petrophysical Description	52
4.4 Summary	61

Chapter 5. BELLEVUE (SKULL CREEK) OUTCROP RESULTS	63
5.1 Facies Description	63
5.2 Lithology Description	69
Thin Section Petrography	76
Scanning Electron Microscopy	80
Whole Rock Mineralogy	81
Clay Mineralogy	81
5.3 Petrophysical Description	84
5.4 Summary	90
Chapter 6. TURKEY CREEK (SKULL CREEK) OUTCROP RESULTS	92
6.1 Facies Description	92
6.2 Lithology Description	96
Thin Section Petrography	102
Whole Rock Mineralogy	107
6.3 Petrophysical Description	107
6.4 Summary	113
Chapter 7. MEADOW SPRINGS (SKULL CREEK) CORE RESULTS	115
7.1 Facies Description	115
7.2 Lithology Description	130
Thin Section Petrography	136
Scanning Electron Microscopy	138
Whole Rock Mineralogy	140
Clay Mineralogy	140
7.3 Petrophysical Description	141
7.4 Summary	149
Chapter 8. ROONEY RANCH OUTCROP (GRANEROS) RESULTS	152
8.1 Facies Description	152
8.2 Lithology Description	158
Thin Section Petrography	168
Whole Rock Mineralogy	169
8.3 Petrophysical Description	171
8.4 Summary	177
CHAPTER 9. YOUNGS CORE (GRANEROS) RESULTS	179
9.1 Facies Description	179
9.2 Lithology Description	184
Thin Section Petrography	186
Whole Rock Mineralogy	191
9.3 Petrophysical Description	191
9.4 Summary	192

CHAPTER 10. DISCUSSION	195
10.1 Skull Creek Summary	195
10.2 Graneros Shale Summary	198
10.2 Correlations	201
10.3 Seal Classification	214
CHAPTER 11. CONCLUSIONS	219
11.1 Future Work Statement	221

LIST OF FIGURES

Figure 1.1	Generalized stratigraphic column for Denver Basin	6
Figure 1.2	Location map of outcrop and core in study area.....	7
Figure 1.3	North-south stratigraphic cross section of the Dakota Group	12
Figure 1.4	Dakota Group descriptions/interpretations and Skull Creek legend.....	14
Figure 2.1	Photo of sampling protocol.....	19
Figure 4.1	Stratigraphic column for Soldier Canyon Dam (Skull Creek)	31
Figure 4.2	Facies K in outcrop at Soldier Canyon Dam	32
Figure 4.3	Facies A in outcrop at Soldier Canyon Dam	35
Figure 4.4	Facies B in outcrop at Soldier Canyon Dam	37
Figure 4.5	Facies C in outcrop at Soldier Canyon Dam	39
Figure 4.6	Stratigraphic height vs. MICP, permeability, porosity and density.....	43
Figure 4.7	Stratigraphic height vs. total clay, quartz, feldspar, and carbonate	45
Figure 4.8	Stratigraphic height vs. TOC, HI, HI/OI	46
Figure 4.9a	Drainage curve for facies K at Soldier Canyon Dam	54
Figure 4.9b	Drainage curve for facies A at Soldier Canyon Dam	55
Figure 4.9c	Drainage curve for facies B at Soldier Canyon Dam	57
Figure 4.9d	Drainage curve for facies C at Soldier Canyon Dam	58
Figure 4.9e	Drainage curve for horizontal samples of facies A at Soldier Canyon.....	59
Figure 4.10	Soldier Canyon Histograms of Injection Pressures for each facies.....	62
Figure 5.1	Stratigraphic column for Bellevue outcrop (Skull Creek Shale)	64
Figure 5.2	Facies K in outcrop at Bellevue.....	65
Figure 5.3	Facies A in outcrop at Bellevue.....	67
Figure 5.4	Facies B in outcrop at Bellevue.....	70
Figure 5.5	Facies C in outcrop at Bellevue.....	72
Figure 5.6	Stratigraphic height vs. MICP, permeability, porosity and density.....	75
Figure 5.7	Stratigraphic height vs. total clay, quartz, feldspar, and carbonate	77
Figure 5.8	Stratigraphic height vs. TOC, HI, HI/OI	78
Figure 5.9a	Drainage curve for facies K at Bellevue.....	86
Figure 5.9b	Drainage curve for facies A at Bellevue.....	87
Figure 5.9c	Drainage curve for facies B at Bellevue.....	88
Figure 5.9d	Drainage curve for facies C at Bellevue.....	89
Figure 5.10	Bellevue Histograms of Injection Pressures for each facies.....	91
Figure 6.1	Stratigraphic column for Turkey Creek outcrop (Skull Creek Shale)	93
Figure 6.2	Facies A in outcrop at Turkey Creek.....	94
Figure 6.3	Facies B in outcrop at Turkey Creek.....	97
Figure 6.4	Facies C in outcrop at Turkey Creek.....	99
Figure 6.5	Stratigraphic height vs. MICP, permeability, porosity and density.....	103
Figure 6.6	Stratigraphic height vs. total clay, quartz, feldspar, and carbonate	104
Figure 6.7	Stratigraphic height vs. TOC, HI, HI/OI	105
Figure 6.8a	Drainage curve for facies A at Turkey Creek.....	110
Figure 6.8b	Drainage curve for facies B at Turkey Creek.....	111
Figure 6.8c	Drainage curve for facies C at Turkey Creek.....	112
Figure 6.9	Turkey Creek Histograms of Injection Pressures for each facies.....	114

Figure 7.1	Stratigraphic column for Meadow Springs Core (Skull Creek Shale) ...	116
Figure 7.2	Meadow Springs Core photos from 7935-7944 ft (facies A)	117
Figure 7.3	Meadow Springs Core photos from 7924-7934 ft (facies B)	119
Figure 7.4	Meadow Springs Core photos from 7912-7923 ft (facies C)	122
Figure 7.5	Meadow Springs Core photos from 7901-7911 ft (facies C)	123
Figure 7.6	Meadow Springs Core photos from 7888-7900 ft (facies D)	125
Figure 7.7	Meadow Springs Core photos from 7878-7886 ft (facies D)	127
Figure 7.8	Meadow Springs Core photos from 7864-7876 ft (facies E, paleosol, and Mowry Shale)	128
Figure 7.9	Stratigraphic height vs. MICP, permeability, porosity and density	133
Figure 7.10	Stratigraphic height vs. total clay, quartz, feldspar, and carbonate	134
Figure 7.11	Stratigraphic height vs. TOC, HI, HI/OI	135
Figure 7.12a	Drainage curve for facies A at Meadow Springs	144
Figure 7.12b	Drainage curve for facies B at Meadow Springs	145
Figure 7.12c	Drainage curve for facies C at Meadow Springs	146
Figure 7.12d	Drainage curve for facies D at Meadow Springs	147
Figure 7.12e	Drainage curve for facies E, paleosol, and Mowry Shale at Meadow Springs	148
Figure 7.13	Meadow Springs Histograms of Injection Pressures for each facies	151
Figure 8.1	Stratigraphic column for Rooney Ranch Outcrop (Graneros Shale)	153
Figure 8.2	Facies X in outcrop at Rooney Ranch	154
Figure 8.3	Lower Facies Y in outcrop at Rooney Ranch	156
Figure 8.4	Facies Z in outcrop at Rooney Ranch	159
Figure 8.5	Upper Facies Y in outcrop at Rooney Ranch	161
Figure 8.6	Stratigraphic height vs. MICP, permeability, porosity and density	165
Figure 8.7	Stratigraphic height vs. total clay, quartz, feldspar, and carbonate	166
Figure 8.8	Stratigraphic height vs. TOC, HI, HI/OI	167
Figure 8.9a	Drainage curve for facies X at Rooney Ranch	173
Figure 8.9b	Drainage curve for lower facies Y at Rooney Ranch	174
Figure 8.9c	Drainage curve for facies Z at Rooney Ranch	175
Figure 8.9d	Drainage curve for upper facies Y at Rooney Ranch	176
Figure 8.10	Rooney Ranch Histograms of Injection Pressures for each facies	178
Figure 9.1	Stratigraphic column for Youngs #34 Core	180
Figure 9.2	Youngs #34 core photos from 5762-5780 ft	181
Figure 9.3	Youngs #34 core photos from 5780-5798 ft	182
Figure 9.4	Youngs #34 core photos from 5800-5709 ft	183
Figure 9.5	Organic Matter Type for Youngs #34 Core	185
Figure 9.6	Stratigraphic height vs. MICP, permeability, porosity and density	187
Figure 9.7	Stratigraphic height vs. total clay, quartz, feldspar, and carbonate	188
Figure 9.8	Stratigraphic height vs. TOC, HI, HI/OI	189
Figure 9.9	Drainage Curve for Youngs #34 Core	193
Figure 9.10	Youngs Core Histograms of Injection Pressures for each facies	194
Figure 10.1	Stratigraphic cross-section of the Skull Creek Shale	196
Figure 10.2	Skull Creek Histograms for the Injection Pressures at each location	199
Figure 10.3	Stratigraphic cross-section of the Graneros Shale	200
Figure 10.4	Graneros Histogram for the Injection pressures as each location	202

Figure 10.5	Skull Creek Shale MICP vs. porosity and permeability	203
Figure 10.6	Skull Creek Shale MICP vs. total clay, quartz, carbonate	204
Figure 10.7	Skull Creek Shale MICP vs. TOC and HI	206
Figure 10.8	Skull Creek Shale MICP vs. HI/OI and density	207
Figure 10.9	Graneros Shale MICP vs. porosity and permeability	208
Figure 10.10	Graneros Shale MICP vs. total clay, quartz, and carbonate	209
Figure 10.11	Graneros Shale MICP vs. TOC and HI.....	210
Figure 10.12	Graneros Shale MICP vs. HI/OI and density.....	211
Figure 10.13	Thin-section photos of the condensed section.....	213

LIST OF TABLES

Table 1.1	GPS Coordinates for Outcrop Locations	5
Table 4.1	Statistics of Main features for Soldier Canyon Dam Outcrop.....	42
Table 4.2	Thin Section Petrography for Soldier Canyon Dam Outcrop.....	47
Table 4.3	Whole Rock Mineralogy for Soldier Canyon Dam Outcrop.....	50
Table 4.4	Clay Mineralogy for Soldier Canyon Dam Outcrop.....	51
Table 4.5	Injection Pressures at 10% Mercury Saturation for Soldier Canyon.....	53
Table 5.1	Statistics of Main features for Bellevue Outcrop	74
Table 5.2	Thin Section Petrography for Bellevue Outcrop	79
Table 5.3	Whole Rock Mineralogy for Bellevue Outcrop.....	82
Table 5.4	Clay Mineralogy for Bellevue Outcrop	83
Table 5.5	Injection Pressures at 10% Mercury Saturation for Bellevue.....	85
Table 6.1	Statistics of Main features for Turkey Creek Outcrop.....	101
Table 6.2	Thin Section Petrography for Turkey Creek Outcrop	106
Table 6.3	Whole Rock Mineralogy for Turkey Creek Outcrop.....	108
Table 6.4	Injection Pressures at 10% Mercury Saturation for Turkey Creek.....	109
Table 7.1	Statistics of Main features for Meadow Springs Core.....	131
Table 7.2	Thin Section Petrography for Meadow Springs Core.....	137
Table 7.3	Whole Rock Mineralogy for Meadow Springs Core.....	141
Table 7.4	Clay Mineralogy for Meadow Springs Core	142
Table 7.5	Injection Pressures at 10% Mercury Saturation for Meadow Springs.....	143
Table 8.1	Statistics of Main features for Rooney Ranch Outcrop.....	163
Table 8.2	Thin Section Petrography for Rooney Ranch Outcrop.....	169
Table 8.3	Whole Rock Mineralogy for Rooney Ranch Outcrop.....	170
Table 8.4	Injection Pressures at 10% Mercury Saturation for Rooney Ranch	172
Table 9.1	Statistics of Main features for Youngs Core.....	186
Table 9.2	Thin Section Petrography for Youngs Core	190
Table 9.3	Whole Rock Mineralogy for Youngs Core.....	191
Table 9.4	Injection Pressures at 10% Mercury Saturation for Youngs Core.....	192
Table 10.1	Skull Creek and Graneros Shales in Sneider's Seal Classification	215

LIST OF APPENDICES

Appendix A	Soldier Canyon Dam Thin Section Petrography.....	226
Appendix B	Soldier Canyon Dam SEM Images.....	239
Appendix C	Soldier Canyon Dam MICP graphs.....	248
Appendix D	Bellevue Thin Section Petrography.....	297
Appendix E	Bellevue SEM Images.....	306
Appendix F	Bellevue MICP graphs.....	317
Appendix G	Turkey Creek Thin Section Petrography.....	339
Appendix H	Turkey Creek MICP graphs.....	348
Appendix I	Meadow Springs Thin Section Petrography.....	361
Appendix J	Meadow Springs SEM Images.....	372
Appendix K	Meadow Springs MICP graphs.....	383
Appendix L	Rooney Ranch Thin Section Petrography.....	393
Appendix M	Rooney Ranch MICP graphs.....	408
Appendix N	Youngs Core Thin Section Petrography.....	434
Appendix O	Youngs Core MICP graphs.....	445
Appendix P	Organic Geochemistry for all locations.....	457

ACKNOWLEDGEMENTS

There are many acknowledgements to make as this project involved many different people. First of all, I would like to thank Dr. Sally Sutton for taking me as a graduate student and Dr. Frank Ethridge for also advising this project. Dr. W.R. Almon and Dr. W.C. Dawson provided the backbone for this research not only with funding from Texaco but with their limitless knowledge on seal capacity and petroleum geology in general. I learned more from these people than they probably realize. I also must acknowledge the generous financial support I received from Texaco EPTD, American Association of Petroleum Geologists, and the Department of Earth Resources at Colorado State University.

I would also like to thank Dr. R.J. Weimer and Jim Jones who generously lent their core and expertise of the Denver Basin. I would also like to thank Keith Etchells who was a wonderful field assistant to collect shale with for the summer.

There are many other people within Texaco and HARC that greatly contributed to this project. W.T. Lawrence kept a large number of samples and myself organized, in addition to the photography and being a tremendous help in the field. Dr. D.K. McCarty provided an immense amount of work and dedication in instructing the XRD techniques and analyses used. Dr. Victor Drits also contributed his vast knowledge of clay mineral analysis. Dr. B.J. Katz instructed how organic geochemistry is used to characterize the organic content in shales. J. Jones always provided help with both XRD analysis and SEM work. A. Blackwell prepared samples for X-ray analysis. G. Vardillos cut thin sections of selected shale samples.

I must thank all my family and friends as I would not have made it through without them. They too were a support more than they probably realized, and I think they realized it was a lot. I have had the opportunity to experience some incredible people and some of them are excellent geologists in their own right and will always have an endless amount of respect from me. And Geo Prizms are really good cars.

Chapter 1. INTRODUCTION

"Possibly many may think that the deposition and consolidation of fine-grained mud must be a very simple matter, and the results of little interest. However, when carefully studied experimentally it is soon found to be so complex a question, and the results dependent on so many variable conditions, that one might feel inclined to abandon the inquiry, were it not that so much of the history of our rocks appears to be written in this language."

Henry Clifton Sorby, 1908

1.1 Purpose and scope of study

It is the goal of this study to predict seal occurrence within a sequence stratigraphic framework using the Cretaceous Skull Creek and Graneros Shale in the Denver Basin. To do this we must answer several questions:

1. What type of rock makes the "best" seal?
2. What are the physical properties of this rock?
3. What type of depositional environment produced this rock?
4. How does this rock fit into the overall sequence or parasequence?
5. How does the integrity and/or position of the seal change across the basin?

Ideally, a seal is an impermeable caprock or barrier that traps oil/gas. For a seal to trap hydrocarbons, it must be laterally continuous, thick, and ductile. Fracturing and faulting can disrupt a seal by offsetting beds, thus allowing a pathway for hydrocarbons to migrate. Seal failure can also occur if a unit is discontinuous or too thin to cover the reservoir in question (Allen and Allen, 1990).

The integrity of a top seal is primarily controlled by capillary pressure, barring larger scale heterogeneities like faults or joints. Capillary pressure is the pressure needed to displace a wetting phase in the capillary with a non-wetting phase (Jennings, 1987).

The seal's capillary pressure can be used to calculate the hydrocarbon column height that it can hold (Allen and Allen, 1990). Capillary pressure is a function of pore throat size, shape, and organization (Vavra et al., 1992). Generally, a small or odd-shaped pore throat that is not connected to another pore would increase the potential of the seal because it would be more difficult for hydrocarbons to migrate. A seal is only as good as the largest pore throat in the system (Yang and Aplin, 1998). Dewhurst and Aplin (1998) have done experimental studies on mudstones that show the finer muds to have a less stable pore packing arrangement than the silt-rich samples. The pores of the fine-grained muds are more likely to collapse and compress with increasing strain. The coarser grained samples have a stronger framework to support the arrangement of the pores, and are less likely to collapse. Therefore, the porosity and permeability of mudstones are somewhat controlled by lithology, but compaction and diagenesis must also be factored in (Dewhurst and Aplin, 1998).

In this study, the following physical characteristics were examined to determine their affect if any, on seal character: size and organization of pore networks, lithology (or mineralogy), grain size, sorting, bedding features, laminations, organic matter type and content, and overall texture, cementation, and compaction. These characteristics were analyzed along with the prospective seal's depositional environment and sequence stratigraphic position. Lastly, these characteristics were put into a conceptual sequence stratigraphic framework to permit general conclusions about seal occurrence.

1.2 Background

Schutter (1998) states that the different shales within stratigraphic sequences have predictable enough characteristics to provide modeling tools for economic assessment. TST (Transgressive Systems Tract) shales are associated with a relative increase in sea

level and are often thin, reworked or discontinuous, but can produce thick shale wedges if deposited under high sedimentation rates. Condensed section shales are distinctive areas in late stages of TST or early HST (Highstand Systems Tract) where sediment has been starved but abundant organic matter, chemical precipitates, and fossil debris, such as phosphatic material, remain. These units are often continuous and may provide hydrocarbon source rocks or seals. Although these units are continuous, there is lateral variation that may produce two facies of the condensed section. The lower facies is a fissile black shale that has a low amount of total organic carbon with type III (terrestrial) organic matter, which may have been undiluted by sedimentation. This marks the condensed section relative to sea level rise. The upper facies is brownish-black blocky shale that marks the maximum highstand, and has a type I-II (marine) organic matter, along with a greater rate of sedimentation. Schutter (1998) states that in proximal locations only the black shale facies may be present, but both facies (black and brown) are usually found in more distal locations. Shales in HST are usually heterogeneous and have increasing amounts of sand, along with storm deposits of alternating shale and sandstone or limestone. These discontinuous deposits are not of economic value.

Bohacs (1998) provides a framework for studying the sequence stratigraphy of mudrocks. He classifies the Skull Creek and Mowry Shales in Powder River Basin, WY in a marine, constructional shelf margin setting. This setting generally thins toward the basin and the clay mineralogy is controlled by river and wind input and ocean circulation. The organic matter content increases in the mid-sequence downlap surface or condensed section. These shales may contain 1-20% TOC, with decreasing algal matter (type I-II kerogen) towards the shoreline. The Skull Creek Shale is a distal to proximal open

marine shelf environment that grades from a TST into a HST. The Mowry Shale ranges from a lower shoreface/subtidal to distal open-marine shelf environment of a LST (Lowstand Systems Tract).

In addition to understanding the nature of mudrocks, there is a need to classify the rocks that make top seals. Sneider et al. (1997) has developed a classification system for seals. A type "A" seal is predominantly clay with limited grain support and has little pore space. A type "B" seal has some grain support and intergranular detrital clays, with minor pore space. A type "C" seal shows grain support with more infrequent amounts of intergranular clays with increased amounts of pore space. A type "D" seal is grain supported with abundant pore space. Sneider et al. (1997) has found that there is good to excellent agreement between the actual field rocks that have trapped hydrocarbons and the calculated hydrocarbon column heights from the mercury injection pressure curves for vertical plugs. He has calculated an empirical adjustment factor (EAF) to compare core samples to cuttings. This study has avoided using an EAF by preparing simulated cuttings for all the samples, including the cores.

1.4 Location

This study includes both outcrop and subsurface samples of the Skull Creek and Graneros Shales in the Denver basin. Both units are Cretaceous, with the Skull Creek being lower Cretaceous, approximately Albian in age. The younger Graneros falls into the lowest portion of the Upper Cretaceous. A generalized stratigraphic column for the Denver basin shows the ages of the Skull Creek and Graneros Shale relative to the surrounding units (Fig. 1.1). The approximate locations of the outcrop and core in this study area are shown on the Denver basin (Fig. 1.2). The Soldier Canyon Dam outcrop

of the Skull Creek Shale is located in Larimer County west of Fort Collins. Adjacent to Soldier Canyon Dam is the most northern dam on the east side of Horsetooth Reservoir. The Bellevue outcrop of the Skull Creek Shale, also in Larimer County, is 5.5 miles north of Soldier Canyon to the east of the Bellevue Dome. The Meadow Springs Core of the Skull Creek Shale is in Larimer County, approximately 20 miles northeast of the Bellevue outcrop. The Turkey Creek outcrop of the Skull Creek shale is approximately 65 miles south of Soldier Canyon and located on US 285, 5 miles south of I-70, southwest of Denver. The Rooney Ranch outcrop of the Graneros is located just south of Golden, CO on the east side of Dinosaur Ridge. Youngs #34 Core of the Graneros is located in Morgan County, 20 miles east of Loveland and 9 miles south of Fort Morgan. The township and range coordinates are given on the stratigraphic columns for each location in the following chapters. The GPS coordinates for the outcrops are in the following table and do not include core coordinates.

Table 1.1 GPS Coordinates for Outcrop Locations

Bellevue Outcrop- Skull Creek Shale	N 40° 39.338	W 105° 10.722
Soldier Canyon Dam- Skull Creek Shale	N 39° 35.541	W 105° 09.807
Turkey Creek- Skull Creek Shale	N 39° 38.063	W 105° 10.14
Rooney Ranch- Graneros Shale	N 39° 40.650	W 105° 11.485

1.3 Regional Geology

Denver Basin

The Denver basin encircles northeast Colorado, southeast Wyoming and southwest Nebraska. It is an asymmetrical syncline formed on thick continental crust with the axis on the folded and faulted western flank that parallels the Front Range (Weimer, 1996). This foreland basin encompasses 70,000 mi² (Higley, 1989).

		<i>WEST FLANK</i>	<i>EAST FLANK</i>
UPPER CRETACEOUS	LARAMIE FORMATION		LARAMIE FORMATION
	FOX HILLS SANDSTONE		FOX HILLS SANDSTONE
	PIERRE SHALE	TERRY SANDSTONE	SUSSEX SANDSTONE
		HYGIENE SANDSTONE	SHANNON MEMBER
		SHARON SPRINGS MEMBER	SHARON SPRINGS MEMBER
	NIORARA FM.	SMOKY HILL	SMOKY HILL
		FORT HAYS LIMESTONE	FORT HAYS LIMESTONE
	CODELL SANDSTONE		CODELL SANDSTONE
	CARLILE SHALE		CARLILE SHALE
	GREENHORN LIMESTONE		GREENHORN LIMESTONE
	GRANEROS SHALE		GRANEROS SHALE
			D SANDSTONE
			HUNTSMAN SHALE
LOWER CRETACEOUS	DAKOTA GROUP	MOWRY SHALE	MUDDY (J) SANDSTONE
		HORSETOOTH MEMBER	
		FORT COLLINS MEMBER	
		SKULL CREEK SHALE	
		PLAINVIEW FORMATION	SKULL CREEK SHALE
		LYTLE FORMATION	INYAN KARA GROUP

Figure 1.1 Generalized stratigraphic column of the Denver Basin for the Cretaceous units. Modified from Higley (1999).

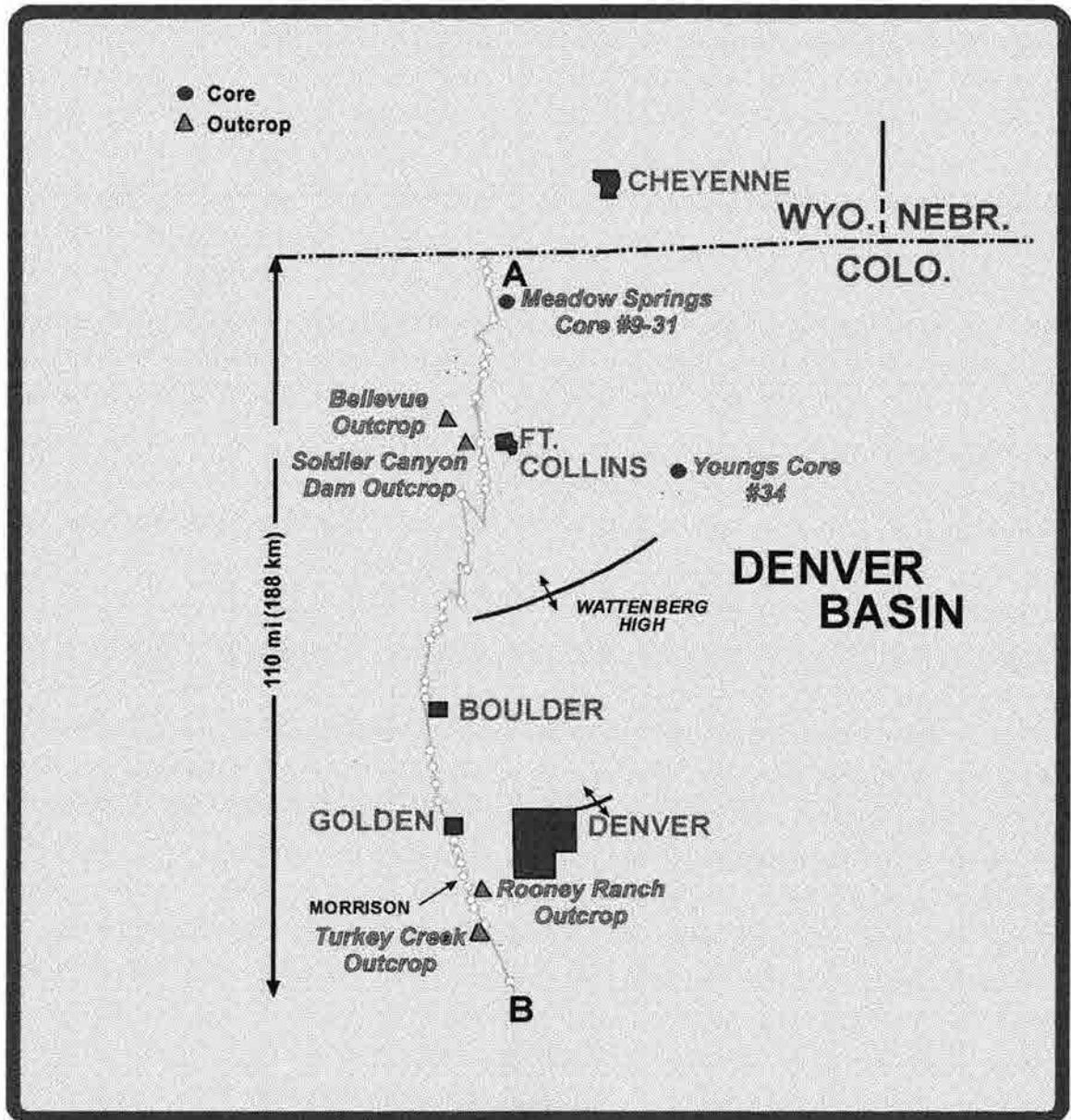


Figure 1.2 Location Map showing approximate locations of the outcrop and core in the Denver Basin. Modified from Weimer (1996).

The basement is composed of Precambrian igneous and metamorphic rocks that are 1.6 Ga in age. Of the 13,000 ft (4000 m) of stratigraphic section exposed in the Denver basin, 9500 ft (2200 m) are Cretaceous and Lower Tertiary with 80% being marine sediments of the Upper Cretaceous. The lower 3500 ft (1080 m) of the section consists of Late Paleozoic and Mesozoic rocks (Weimer, 1996).

The Western Interior Cretaceous Seaway was an elongate, asymmetrical basin that periodically filled with a shallow epicontinental sea. It extended from the Arctic to the Gulf of Mexico, and occupied a 500 to 1000 mi wide basin that was bounded to the west by a fold and thrust belt and to the east by the Canadian Shield (Weimer, 1994; Pietraszek-Mattner, 1995).

Tectonic History

The general history of the movement within the Rocky Mountain Foreland can be separated into three phases, as done by Dolson and Weimer (1992):

1. During the Jurassic a passive margin setting existed with the hingeline lying in Utah and western Wyoming. This was disturbed by uplift that created the Ancestral Rocky Mountains and other Pennsylvanian basins, such as the Paradox (Utah) and Eagle Basins (Colorado).
2. During the mid-Jurassic to late Cretaceous periods, a Sevier orogenic phase developed which is related to creation of the Cretaceous inland seaway. This phase is further known for the high sediment influx from the west.
3. During the Tertiary, this foreland basin was further separated into smaller basins and ranges due to subduction that resulted in hydrocarbon generation.

Sequence Stratigraphy

Some fundamentals of sequence stratigraphy will be reviewed before interpreting the Dakota Group and Graneros sequence stratigraphy. Sequence stratigraphy is the “study of rock relationships within a chronostratigraphic framework of repetitive, genetically related strata bounded by surfaces of erosion or no deposition and their correlative conformities” (p. 110, Van Wagoner et al., 1988). Galloway (1989) uses condensed sections and their correlative transgressive surfaces of erosion to separate the genetically related strata into sequences. This paper will use the sequence stratigraphic fundamentals defined by Van Wagoner et al. (1988). A “sequence” is the basic unit and is bounded above and below by unconformities and their correlative conformities (Mitchum, 1977; Van Wagoner et al., 1988). These sequences are thought to be responses from the interaction of eustatic sea level, subsidence, and sedimentation (Reading, 1996). Unconformities separate younger and older strata with surfaces that show non-deposition or subaerial/submarine erosion (Weimer, 1996; Van Wagoner et al., 1988). A sequence can be further divided into systems tracts, which are defined as linked depositional environments (Reading, 1996), and by their stacking patterns of parasequences (Van Wagoner, 1985). Marine flooding surfaces (MFS) and their correlative conformities bound parasequences. These MFS separate younger strata from older, by obvious increases in water depth that may show minor submarine erosion. They may be correlated to coastal plain environments that have local erosion from fluvial processes or minor subaerial exposure (Van Wagoner et al., 1988).

Progradation occurs when the rate of deposition is greater than the rate of creation of accommodation space. Retrogradation or “backstepping” occurs when the rate of

deposition is less than the rate of creation of accommodation space. Aggradation refers to the rate of deposition equaling the rate at which accommodation space is created (Van Wagoner et al., 1988). A lowstand systems tract (LST) is deposited in a basin ramp margin when relative SL fall produces a lowstand wedge, eventually stabilizes, then slowly rises causing a basinward shift in facies (Van Wagoner et al., 1988; Reading, 1996). A rapidly rising relative SL forms a transgressive systems tract (TST) on the continental shelf (Van Wagoner et al., 1988). The transgressive surface of erosion (TSE), or the initial flooding of the shoreline that fills the incised valleys (IVF), is succeeded by a retrogradational parasequence (Reading, 1996). The TSE is bounded by a MFS, which is usually indicated in a condensed section (CS). A CS is thought to be a product of maximum “sediment starvation” that is preserved in the rock record by small amounts of clay-rich sediment that represents long periods of time (Loutit et al., 1988). The MFS is also known as a downlap surface onto which “the toes of prograding clinoforms in the overlying highstand systems downlap” (Van Wagoner et al., 1988). It marks the transition of TST (retrogradational parasequences) to HST (aggradational parasequences). A highstand systems tract (HST) forms when a decrease in relative SL rise occurs and the stacked parasequences are aggradational until the accommodation space decreases due to a lowering of relative SL, causing a progradational parasequence (Van Wagoner et al., 1988).

Weimer (1996) has developed facies models to interpret the sequences and unconformities of the Cretaceous Dakota Group. The transition from the marine Skull Creek Shale to the overlying Muddy sandstone to the Benton Shale is a classic example of a transgressive-regressive-transgressive cycle (Weimer, 1996). There are three

sequences within the Dakota Group that are bounded on both sides by unconformities, as seen in the N-S stratigraphic cross-section from Turkey Creek to Fort Collins (Fig. 1.3) modified from MacKenzie (1971); Weimer (1994). Sequence 1 includes the non-marine deposits of the Lytle Formation. Sequence 2 incorporates the Plainview Formation and Skull Creek and the Fort Collins member of the Muddy (J) Sandstone where present. Sequence 3 is only partially represented in this diagram (Fig. 1.4) and includes the Muddy (J) Sandstone, Mowry or Huntsman Shale, and Benton Group that includes the overlying Graneros. In the Fort Collins area, sequence 3 would include the Horsetooth member of the Muddy Sandstone; and in the Denver area the Muddy (J) Sandstone would include the Kassler SS, Van Bibber Shale, and the first sandstone member. It should also be noted from Figure 1.3, that the Skull Creek is much thicker in the Fort Collins area, with a correspondingly thinner Muddy Sandstone. Further south, by Denver, the Skull Creek is thinner with a thicker Muddy Sandstone.

The non-marine Lytle Formation grades from a chert-pebble conglomerate at the bottom to interbedded fine-medium grained sandstones and multicolored shales or mudstones at the top (Weimer, 1996). This has been interpreted as a transition from a braided stream to a floodplain/fluvial environment. The lack of carbonaceous material indicates a highly oxidizing environment, common to fluvial environments (Graham and Ethridge, 1995; Weimer, 1996).

The lowstand surface of erosion (LSE) or unconformity between the Lytle and the overlying Plainview is composed of yellowish-brown claystones that show signs of oxidation (Weimer, 1996; MacKenzie, 1971). The Plainview Formation is a burrowed sandstone with carbonaceous debris interpreted as a coastal plain environment and known

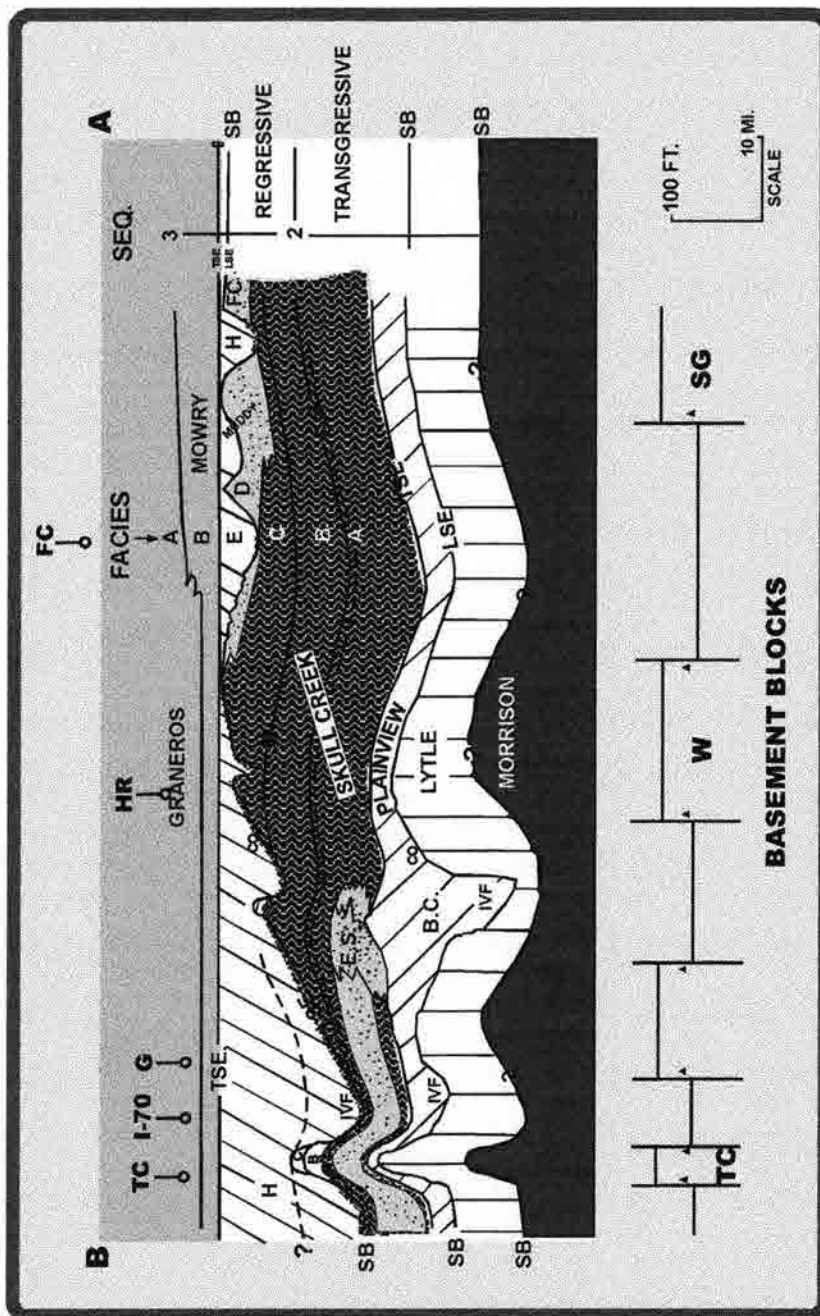


Figure 1.3 North-south stratigraphic cross section of the Lower Cretaceous Dakota Group. Modified from MacKenzie, 1971; Weimer, 1994. Legend is as follows: for formations---Muddy Formation: Fort Collins Member (FC), and Horsetooth member (H); Skull Creek facies members: C, B, A, regional marker bed (M); Eldorado Springs sandstone (ES), Bear Canyon sandstone (BC). Basement fault blocks: Turkey Creek (TC), Wattenburg (W), and Skin Gulch (SG); geographic locations---Fort Collins (FC), Hygiene Road (HR), Golden (G) and Turkey Creek (TC); sequence stratigraphy---sequence boundary (SB), incised valley fill (IVF), lowstand surface of erosion (LSE), transgressive surface of erosion (TSE), condensed section (CS). Location of A-B cross section is located on the Location Map in Figure 1.2.

as facies E in Weimer's lithology descriptions/interpretations for the regressive facies. Figure 1.4 shows Weimer's facies descriptions/interpretations modified, in addition to the legend for all the Skull Creek and Graneros stratigraphic columns presented in this paper. The contact between the Plainview Formation and overlying Skull Creek Shale is a transgressive surface of erosion (TSE) represented by a thin transgressive lag of conglomeratic sandstones (Graham and Ethridge, 1995; Weimer, 1996). The Skull Creek Shale is a carbonaceous silty shale to alternating shale/sandstone that represents open marine shelf to lower shoreface environments. Weimer (1996) estimates a 200-ft average water depth for the Skull Creek by decompacting a sedimentary column. A parasequence boundary or a marine flooding surface separates the transgressive systems tract deposits (TST) that include facies K and A from the highstand systems tract deposits (HST) that include facies B and C. Some of the Skull Creek samples do not have enough total organic carbon (1%) to permit accurate assessment of organic matter with the Van Krevelen diagrams.

There are four facies (K, A, B, and C) that characterize the Skull Creek Shale. Facies K is a grayish-black carbonaceous shelf mudstone to shale located stratigraphically under the condensed section. This clay rich rock may have been deposited in an offshore environment during the transgression of the Skull Creek seaway.

The condensed section or facies A is a grayish-black, well laminated silty shale. It is usually characterized by two bentonite layers, Inoceramid fragments, and visible silt laminations in hand sample. This facies has been interpreted by Weimer (1996) as an offshore or deeper neritic environment that was deposited in anaerobic conditions.

**LEGEND FOR SKULL CREEK DESCRIPTIONS
FACIES DESCRIPTIONS**

FORMATION	FACIES	LITHOLOGY	DEPOSITIONAL ENV.
Muddy (J) Horsetooth member	E	Gray FG to MG x-stratified ss, shale; coaly	Incised Valley Fill, Coastal Plain
Fort Collins member	D	Gray burrowed or x-stratified ss and shale	Shoreline, Upper Delta Front
Skull Creek	C	Gray alt ss and shale Extensive bioturbation	Lower Delta Front
	B	Gray-black shale, siltstone, graded/ hummocky bedding	Prodelta
	A	Gray-black shale w/ silt lam., Inoceramus, Condensed Section	Offshore
	K	Black shale, claystone Planar bedding	Further Offshore
Regressive Deposits			
Transgressive Deposits			

*Modified from Weimer (1996)

Sedimentary Structures

 Cross bedding	 Climbing ripples
 Planar bedding	 Hummocky x-strata
 Lenticular bedding	 Swaley x-strata
 Flaser bedding	 Bioturbation
 Slump structure	 Gutter Cast
 Wave ripples	 Cone-in-cone structure
	 Ironstone

Fossils

 Horizontal or "white-walled" burrows
 Vertical burrows
 U-shaped or Diplocriterion burrows
 Root Structures
 Plant fragments
 Bivalves
 Inoceramus shells
 Carbonized woody debris

Sequence Stratigraphy

LSE	Lowstand Surface of Erosion
TSE	Transgressive Surface of Erosion
CS	Condensed Section
IVF	Incised Valley Fill
MFS	Maximum Flooding Surface

Contacts

 Sharp
 Unconformity
 Gradational

Figure 1.4 Facies Descriptions for the Skull Creek Shale modified from Weimer (1996) and Legend for the Skull Creek and Graneros stratigraphic columns

Facies B is a tannish-brown silty shale to siltstone that can lie above and below facies A, if not eroded. This facies marks the beginning of the HST deposits and shows a dramatic increase in the amount of quartz relative to the TST deposits. The bedding ranges from graded laminations to hummocky or swaley cross-stratification. Gutter casts or storm deposits are found in this facies, in addition to horizontal (or “white-walled”) and vertical burrows. Weimer (1996) has interpreted this facies as a prodeltaic environment.

Facies B grades into facies C when the level of bioturbation completely destroys all previous bedding features. Facies C is the coarsest with the highest silt content and corresponding lowest clay content. Kaolinite is present in the upper part of facies C. This facies is cut by a diastem, or minor surface of erosion with the overlying Fort Collins Member of the Muddy sandstone. Weimer (1996) has interpreted facies C as a lower delta front environment.

Overlying the Skull Creek Shale is facies D, a fine to medium grained burrowed sandstone that represents an upper delta front environment. In the Fort Collins area, this facies is known as the Fort Collins member of the Muddy Sandstone (MacKenzie, 1971; Weimer, 1996). However, this facies has been eroded in some areas and replaced by incised valley fill deposits, or facies E, characteristic of the Horsetooth member of the Muddy Sandstone (Graham and Ethridge, 1995). Between these two members of the Muddy is a major sequence boundary, or LSE. At the Turkey Creek outcrop, the LSE directly separates the Skull Creek from the overlying Muddy sandstone. At the top of the Muddy lies another TSE which is inferred from the thin conglomeratic sandstone lag deposit to mark a switch from regressive to transgressive deposits (Weimer, 1996). A

rapid rise in sea level formed the lower silty shales and siltstones that grade into the organic rich black shales of the Mowry Shale. From the ammonite impressions found water depth is estimated have been 100-150 ft for the Mowry seaway (Cobban et al., 1994; Weimer, 1996).

On the western flank of the Denver Basin, the Graneros Shale directly overlies the Mowry Shale. However, the Huntsman shale is equivalent to the Mowry shale on the eastern side (Fig. 1.1). Stratigraphically above the Huntsman is the Muddy 'D' Sandstone, with the Graneros Shale above the D Sandstone.

The Graneros Shale represents another transgressive-regressive-transgressive cycle and has three distinguishable facies delineated by Pietraszek-Mattner (1995). The stratigraphic column shows an overall fining upward - coarsening upward sequence. The lowest facies is termed facies X and composed of interbedded hematitic silty shales and Fe-rich siltstones or ironstones. This facies has the highest silt content and is well laminated with flaggy to platy parting. This shale has a type III (terrestrial) organic matter and appears to be relatively organic-poor and has lower gamma ray readings when compared to the other facies.

Facies Y is a well-laminated, carbonaceous shale with numerous thick bentonites. This facies clearly displays a type II (marine) to type III (terrestrial) organic matter. Splintery lenses of iron oxides are prominent throughout this facies.

Facies Z is approximately the stratigraphic middle of the Graneros Shale. It is a blackish-gray to olive-gray shale with considerable carbonaceous debris in hand sample. It displays fissile to platy parting and comes off in sheets when extracted from outcrop. An algal kerogen (marine organic matter) is evident in this facies. This facies has the

highest radioactivity in the section and is known as the “hot zone”. This facies is most likely to hold or be a condensed section and represents the maximum transgression for the Graneros seaway. This is followed by the coarsening upward sequence of the regressive deposits.

Chapter 2. SAMPLING PROCEDURES

2.1 Outcrop sampling procedures

Outcrop samples were collected with detailed descriptions delineating sequence and parasequence boundaries. Digital photography documented the lithology in the field. Rock descriptions included: rockname, color, texture, mineralogy, organic content, laminations, bedding, degree and type of bioturbation, additional sedimentary structures, and fossils present. Other factors such as the extent of weathering and outcrop conditions, for example groundwater seepage along joint planes, were noted.

Samples were taken in three dimensions: perpendicular to bedding, parallel to bedding and perpendicular to outcrop surface (Fig. 2.1). The goal was to gather moderately unweathered samples along the transect perpendicular to bedding. Samples perpendicular to bedding were taken every 1 vertical feet until the sand content increase was significant enough to extend sampling to every 2-ft. A 1-ft deep trench was dug perpendicular to bedding to obtain acceptable moderately unweathered material. Sampling extended one foot into the outcrop because these shales are jointed and weathered so extensively, it was unrealistic to easily obtain “unweathered” material. It was more realistic to gather the “moderately unweathered” material that is in the first several feet into the outcrop than it was to dig another 6-10 feet to reach the unweathered material. The trench was dug into the weathered shale with a pick ax, chisel or shovel. “Moderately unweathered” material was judged in the field and laboratory by the color

and texture. Care was taken to collect shale with a “darker” color and to avoid weathering products, such as iron oxides, jarosite, etc. Samples were taken every ten feet along the horizontal transect in the condensed section at Soldier Canyon Dam. Flags were used as transect reference points.

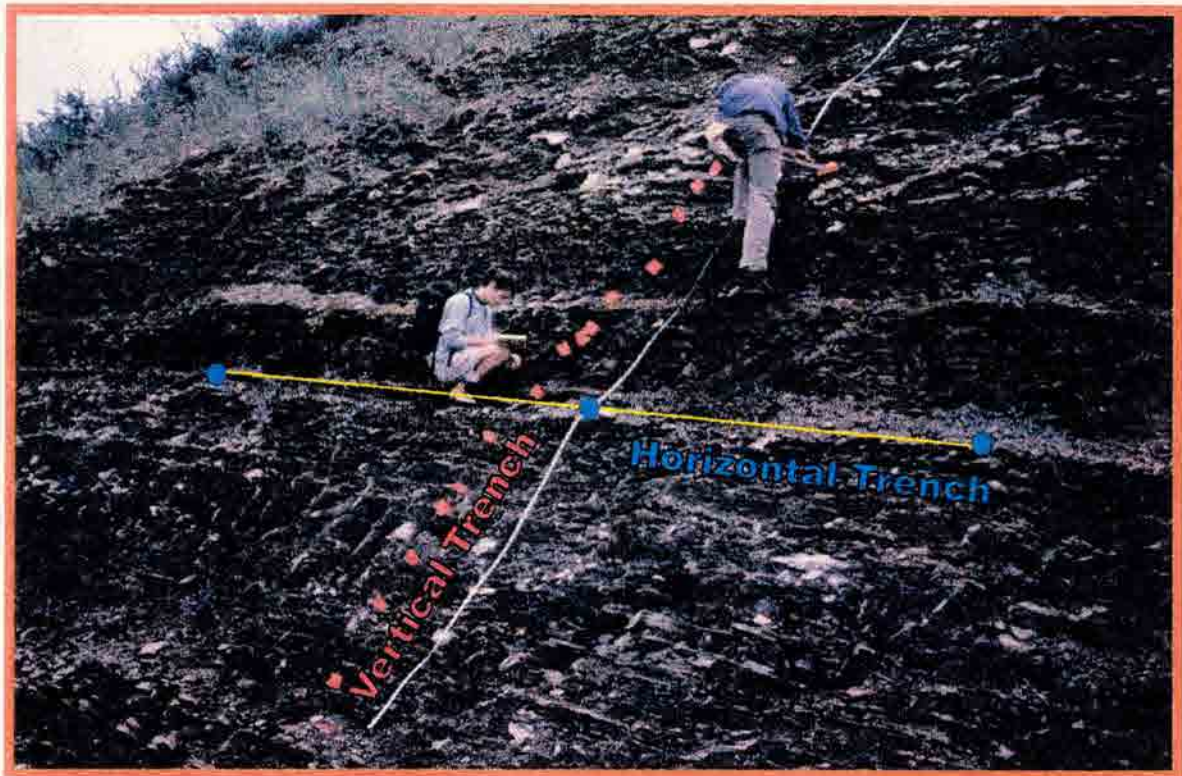


Figure 2.1 Sampling procedure along the vertical and horizontal trenches.

2.2 *Core sampling procedures*

Detailed core descriptions were drawn noting sharp erosional surfaces that might represent unconformities and maximum flooding surfaces. Rock descriptions again included: rockname, color, texture, mineralogy, organic content, laminations, bedding, level and type of bioturbation, sedimentary structures, and/or fossils present. Digital photographs were taken to document the core.

Samples were taken along a one dimensional transect, perpendicular to bedding. They were collected from the back of the core or from thin shale laminations to prevent unnecessary damage to the core.

2.3 *Outcrop Gamma ray procedures*

Gamma ray readings of the outcrops were obtained to compare with core wireline logs. The outcrop gamma ray device delineates sharp changes in lithology (i.e. shale to sand), and may also be used to detect “hot” shales that have a noticeable increase in radioactivity (Slatt et al., 1995).

The Scintex EDA GRS-500 differential gamma-ray spectrometer/ scintillometer was used for the outcrop gamma ray measurements. The machine was calibrated by taking a reading from a reference rock periodically and adjusting the measurements relative to that rock. To obtain the measurement, five readings were taken at each sampling interval; the first and last reading were discarded and the remaining three were averaged (Slatt et al., 1995). These gamma ray measurements were then plotted against the stratigraphic height, producing a curve similar to the gamma ray wireline log.

Chapter 3. METHODOLOGY

3.1 Capillary Pressure

Mercury injection capillary pressure (MICP) measurements were used to determine the seal capacity of samples. Any rock can be a seal if the minimum displacement pressure of the potential seal is greater than the buoyant pressure generated by the accumulation of the hydrocarbon column (Sneider, 1987). The controlling factors for the displacement pressure of a seal rock, and its capacity to contain hydrocarbons are the diameter of the largest, interconnected continuous pore throats, the hydrocarbon/water contact angle, and the interfacial tension of the hydrocarbon/water system. The buoyant counterforce attempting to break the seal is a function of the relative densities of the hydrocarbon and formation water.

Data collection for capillary pressure began with injecting mercury into an evacuated, cleaned rock sample. Mercury injection pressure was increased in a step-wise manner and the percentage of the rock volume saturated by mercury at each step was recorded, after allowing sufficient time for equilibrium to be established. The pressure was then plotted against the mercury saturation, resulting in the injection curve. Initial pressure increases caused mercury to fill all the surface irregularities, such as nicks, gouges, small fractures or vugs on the sample surface. "Closure" is the term used for the point when mercury first entered the actual sample pore system as opposed to just surrounding the sample. Mercury injection capillary pressure data must be corrected for

closure before the data is applied to field studies. After closure has been picked, the pressure at which mercury first entered the pore system is termed “entry” (P_e). The percentage of pore volume saturated by mercury at the maximum pressure is termed the “maximum saturation” (S_{max}). The value of the maximum saturation is dependent on the pressure applied and the duration of the experiment (Wardlaw and Taylor, 1976).

Data from the mercury injection curve can be used to approximate the distribution of pore volume accessible by pore throats of a given size by using the equation:

$$r_d = \frac{2 \delta \cos \Theta}{P_d}$$

where δ is the interfacial tension of the air/mercury system, Θ is the air/mercury/solid contact angle, P_d is the capillary displacement pressure in dynes/cm² (1 psi = 68,948 dynes/cm²) and r_d is either the radius of a cylindrical capillary tube or the distance (in cm) between two parallel, infinite plates. These two geometries model tubular and slot-like or sheet-like pore throats respectively (Wardlaw, 1976). Using $\delta = 485$ dynes/cm, $\Theta = 140$ degrees, and converting to pressure in psi and r_d in microns, the equation becomes:

$$r_d = \frac{107.6}{P_d}$$

To evaluate the capacity of a seal for a particular hydrocarbon/water system, the laboratory measurements from the air/mercury system must be converted to an approximation of the hydrocarbon/water system. In the absence of specific data, a good approximation of oil/water systems can be made by the equation:

$$P_{Cw/o} = 0.1 P_{Co/Hg} \text{ (approximately)}$$

An approximation for gas/water systems is given by:

$$P_{Cw/g} = 0.5 P_{Co/Hg}$$

Detailed estimates for water/oil and water/gas capillary pressures need to be adjusted for the hydrocarbon composition, temperature, and pressure of each individual reservoir. Once converted to the appropriate system, the capillary pressure data from the suspected seal rock can be used to determine the maximum hydrocarbon column that can be retained in a reservoir before the seal begins to leak (Watts, 1987). The maximum hydrocarbon column that a seal can retain is given by:

$$h_{\max} = \frac{P_{ds} - P_{dr}}{0.433 (\rho_w - \rho_{hc})}$$

where h_{\max} is the height in feet of the hydrocarbon column that will induce membrane seal failure, ρ_w and ρ_{hc} are the respective densities of the water and hydrocarbon phases under reservoir conditions, and P_{ds} and P_{dr} are the brine/hydrocarbon displacement pressures (in psia) of the seal and the reservoir rocks, respectively.

The MICP data are in the appendices, with three graphs for each sample. The first graph of mercury saturation (%) vs. mercury injection pressure (psia) represents the P_e (entry pressure) needed to intrude the pore network after closure has been picked. The shape of this curve can give important information, for example a broad flat plateau suggests a high P_e , with an even distribution of PTD (pore throat diameters). Conversely, a curve with a steeper slope usually caused by a lower P_e , suggests the PTD are unevenly distributed. The other two graphs represent the sorting and median distribution of the PTD. The lower right graph plots PTD (microns) against Cumulative Pore Volume (percent). The Y-axis is a probability scale that gives the percentage of pore volume

occupied by a specific population. A line has been drawn through the populations to help the reader quickly determine how many PTD populations are present in each sample. A well-sorted PTD is represented in this graph by a steep line. The upper right graph shows the size of the median PTD, and a narrower curve suggests a well-sorted PTD.

3.2 *Thin Section Petrography*

Preparation of thin sections was done at Texaco EPTD, Houston, TX. Because of the incoherent nature of shale, thin sections were prepared by using kerosene instead of water to finish the slides. Thin sections were cut perpendicular to bedding to show the laminations and/or bedding, if present. Samples were impregnated with blue epoxy so porosity could be easily analyzed under plane polarized light using a petrographic microscope.

Representative thin section photomicrographs were taken to show the dominant features of each facies. Detailed descriptions were supplemented with point count analysis for representative thin sections of each facies. Visual estimates were used to assess the mineralogy for the remainder of thin sections. Grain size analysis of thirty points was used to determine the average grain size for each sample. The Wentworth size classification was used and the size class boundaries are as follows: clay 0.00006-0.0039 mm, very fine silt 0.0039-0.0078 mm, fine silt 0.0078-0.0156 mm; medium silt 0.0156-0.031 mm; coarse silt 0.031-0.0625 mm; very fine sand 0.0625-0.125 mm; fine sand 0.125-0.25 mm; and medium sand 0.25-0.50 mm

Thin section petrography was used to examine how the mineralogy, organic matter, and pore network, if visible, were organized in the sample. Each thin section was classified with a rockname based on visible mineralogy. The size, shape, roundness, and

sorting of hard grains (quartz, feldspars, pyrite etc.) were noted. The matrix was classified as either: homogeneous, bioturbated, or mottled; weak, moderate, or well-laminated; wispy or discontinuous laminations; and/or wavy bedding. The distribution of organic matter was of primary interest; however, it was also examined for fluorescence, which suggests an oil-prone kerogen. Two types of primary porosity were noted: intercrystalline or matrix porosity, and intergranular porosity located between hard grains.

The authigenic mineral growth was placed into three categories: replacement of original detrital grains or “psuedomorphs”, cement, or new crystal growth (Potter et al., 1980). Authigenic carbonates such as dolomite, calcite, and siderite were distinguished by having a much larger grain size than the surrounding clay matrix with an occasional euhedral shape. Sericite is a common replacement feature of feldspars. Both clay minerals and carbonates were found as prevalent cements.

3.3 X-Ray Diffraction

Whole rock and clay mineralogy was characterized by X-ray diffraction (XRD). Diffraction data was collected in a Siemens D5000 diffractometer using Cu K α radiation transmitted through a 2 mm beam slit. The diffractometer is equipped with a 40 position sample holder, theta-theta goniometer, and a Kevex Peltier cooled silicon solid state detector. The accelerating voltage of the system was 50-kV with a 40-mA current.

Whole Rock Analysis

Random powder diffraction mounts for the whole rock were first prepared by hand grinding the sample in a mortar and pestle. Care was taken not to bias the sample with respect to the harder and softer minerals by grinding it thoroughly. The powder was

then passed through a 425-micron sieve and retained for grinding in a McCrone grinding mill. To avoid contamination, a “pre-grind” run for 20 seconds in the McCrone grinder was made by using 1 or 2 cc of sample and 6 cc of acetone. The sample to be analyzed was then ground using 2-cc sample and 6-cc acetone for 45 seconds. The ground sample was then poured into an aluminum boat and evaporated on a warming tray. To finish preparation, samples were lightly ground in a mortar and packed into a 25-mm diameter front loading sample holder accommodating about 600 mg of samples. Step diffraction scans were made from 2 to 52 °2θ with a step increment of 0.02 °2θ and counting rate of 2 seconds per step.

Whole rock mineral identification was based on the correlation of experimental d -values with the diagnostic hkl reflections from the International Centre for Diffraction Data (1993), (ICDD) reference file and/or other published works. The semi-quantitative interpretation used the method of Schultz (1964) and Reynolds (1989).

Clay Mineral Analysis

Whole rock samples were hand ground dry in a porcelain mortar and passed through a 425 μm sieve. The <2.0 μm equivalent spherical diameter size fractions were separated from the <425 μm powder by centrifugation after disaggregation with an ultrasonic probe in deionized water with several drops of 1N Na-hexametaphosphate as a dispersion agent. Approximately 1 gram of sample was dispersed in 200 ml of deionized water. The <2.0 μm suspension was decanted after the first centrifuge run, and then a second centrifuge separation was made on each sample to minimize incorporation of non-clay minerals in the <2.0 μm size fraction.

Oriented sample preparations were made by vacuum filtration of the clay suspension onto 0.8 μm silver metal membrane filters. The silver metal membrane and clay aggregates were laminated to 25-mm diameter metal disks. Glycol solvated treatments were made by placing these preparations in a heated chamber at 60 °C under a glycol-wet paper lab towel for one to three hours.

Diffraction scans for each sample were collected in treated and untreated states with the same diffractometer configuration as for the whole rock scans. Step diffraction scans were made from 2 to 32 °2 θ with a 0.02 °2 θ step increment and counting rate of 2 s per step.

The semi-quantitative interpretation used the method of Moore and Reynolds (1997). Mineral intensity factors in the semi-quantitative analysis, and illite-smectite expandability determinations were based on calculated diffraction scans from NEWMOD[®] (Reynolds, 1985).

3.4 Scanning Electron Microscopy

Scanning Electron Microscopy (SEM) work was done in conjunction with XRD analysis. The XRD gave information on what minerals were present and SEM provided a three dimensional view of texture or how the mineral grains were arranged with respect to pore networks, if visible. SEM images were collected at Texaco EPTD on the Phillips E-3 environmental scanning electron microscope.

3.5 Organic Geochemistry

Total organic carbon (TOC) sample preparation began with grinding the rock into a homogeneous powder. 200-mg of sample was weighed out in a ceramic crucible and treated with hydrochloric acid to remove any carbonate material. Sample was then

washed to remove remaining acid. The carbon-sulfur content was analyzed with the Leco CS-344, an infrared detector, by applying a ballistic heat of 900 °C in a oxygen atmosphere.

Rock-Eval pyrolysis was then performed on samples with a TOC greater than 1%. A 100-mg sample is placed in an inert atmosphere up to 550 °C. This is done to simulate burial conditions, not to burn the sample. The Rock-Eval measurements were made in three increments. The first measurement or S₁ peak measured the free hydrocarbons. These hydrocarbons become volatile at a temperature below 300 °C (Espitalie et al., 1977). The second peak, S₂, measured the maximum hydrocarbon unit or the maximum temperature reached. This peak is produced by the cracking of kerogens up to 550 °C (Espitalie et al., 1977). S₂ can also referred to as the hydrogen index as it measured the hydrogen to carbon ratio in the organic matter. The third curve, S₃, measured the carbon dioxide given off by the sample. This is also referred to as the oxygen index because it measures the oxygen to carbon ratio in the organic matter. The Rock-Eval pyrolysis tests were run relative to the Woodford shale standard.

Various types of kerogen can be characterized with modified Van Krevelen diagrams and may be used to describe the environment in which the sediment was deposited. These diagrams are called modified because they use the hydrogen and oxygen indexes instead of the atomic H/C and atomic O/C ratios originally used by Espitalie et al. (1977). The reliability of these modified diagrams becomes questionable when there is significant variations in the matrix mineralogy and organic enrichment (Katz, 1983).

A type I kerogen has a high hydrogen index with a lower oxygen index. Type I kerogen has high petroleum potential as it produces large amounts of oil and gas during catagenesis. This production of hydrocarbon compounds occurs during Rock-Eval pyrolysis between 400 to 500 °C. Rocks with a type I signature would be an excellent source due to their algal organic matter (Espitalie et al., 1977). Type III kerogen has a high oxygen index with a lower hydrogen index. This type of kerogen is gas prone and has low petroleum potential. The origin of this material is upper plant detritus and humic terrestrial matter. Type II kerogen has an intermediate position of being both oil and gas prone, but is still considered a good source rock. This kerogen is typically found in marine environments. The petroleum potential of a rock is calculated by adding the S1 and S2 peaks, so it would include the hydrocarbons currently in the rock and the hydrocarbons that would continue to produce should the rock become more mature (Espitalie et al., 1977).

Thin section photomicrographs, SEM images, and MICP graphs are displayed separately for all six locations in Appendix A-O. Appendix P contains the organic geochemistry results for all six locations.

Chapter 4. SOLDIER CANYON DAM (SKULL CREEK SHALE) OUTCROP RESULTS

4.1 Facies Description

At Soldier Canyon Dam, a 154-ft section of Skull Creek Shale was measured and gamma ray logged (Fig. 4.1). The underlying contact with the Plainview Formation is sharp and lies below the road along Soldier Canyon Dam. The overlying contact with the Fort Collins member of the Muddy Sandstone appears gradational. A sharp color change from the tannish-brown Skull Creek to the whitish-orange Fort Collins member was used in the field to define the boundary between these two units. All of the facies designated for the Skull Creek Shale (K, A, B, and C) are present at this outcrop. Overall, the gamma ray log has a higher response in the TST deposits.

Facies K composes the lowest 59-ft of the outcrop. The lowest 14-ft directly overlie the Plainview Formation and comprise an alternating series of tannish-brown siltstones and shales, with graded bedding and no signs of bioturbation (Fig. 4.2a). The lower portions of this section may represent the reworking of the underlying TSE. Overlying this is 36 ft of olive-gray to dk-grayish black mudstone with a blocky to splintery texture (Fig. 4.2b). The upper 9-ft of facies K is a well-laminated grayish black shale with gypsum along joint surfaces. Overall, this facies has two bentonites and a relatively high outcrop gamma ray despite heavy weathering. The organic matter type for this facies is type III (terrestrial) (Fig. 4.2c).

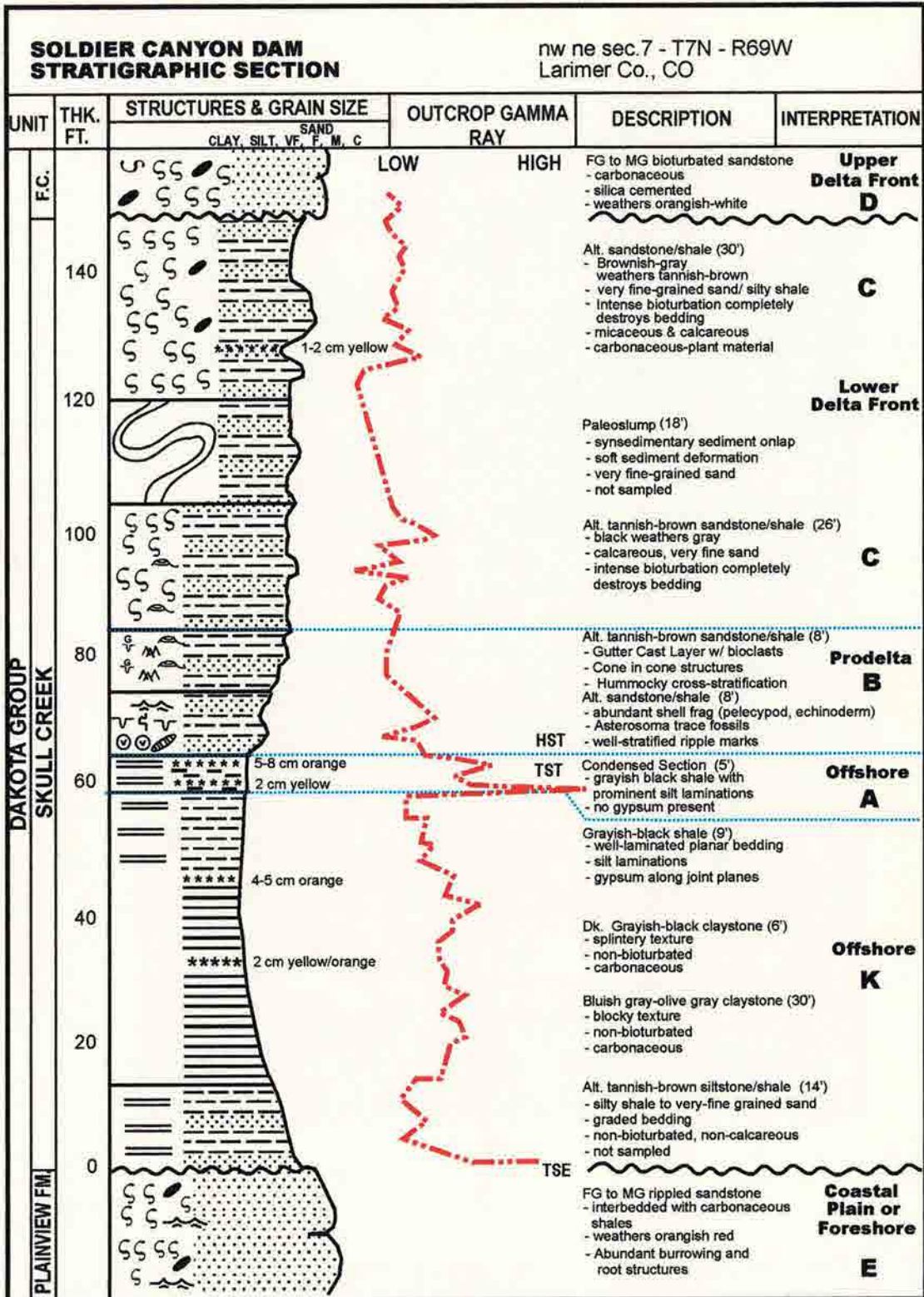
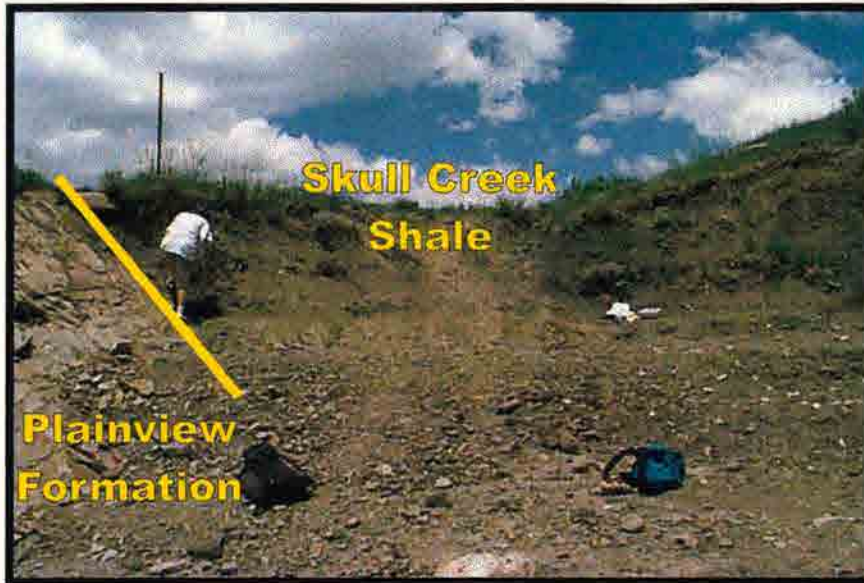


Figure 4.1 Stratigraphic column for Soldier Canyon Outcrop, including detailed descriptions, interpretations, and logged outcrop gamma ray.

A.



B.



Figure 4.2 A) Sharp contact between the Skull Creek Shale and Plainview Fm.; B) overall view of the heavily weathered mudstone; C) Van Krevelen diagram shows type III (terrestrial) organic matter for facies K. Flags mark samples taken in 1-ft increments.

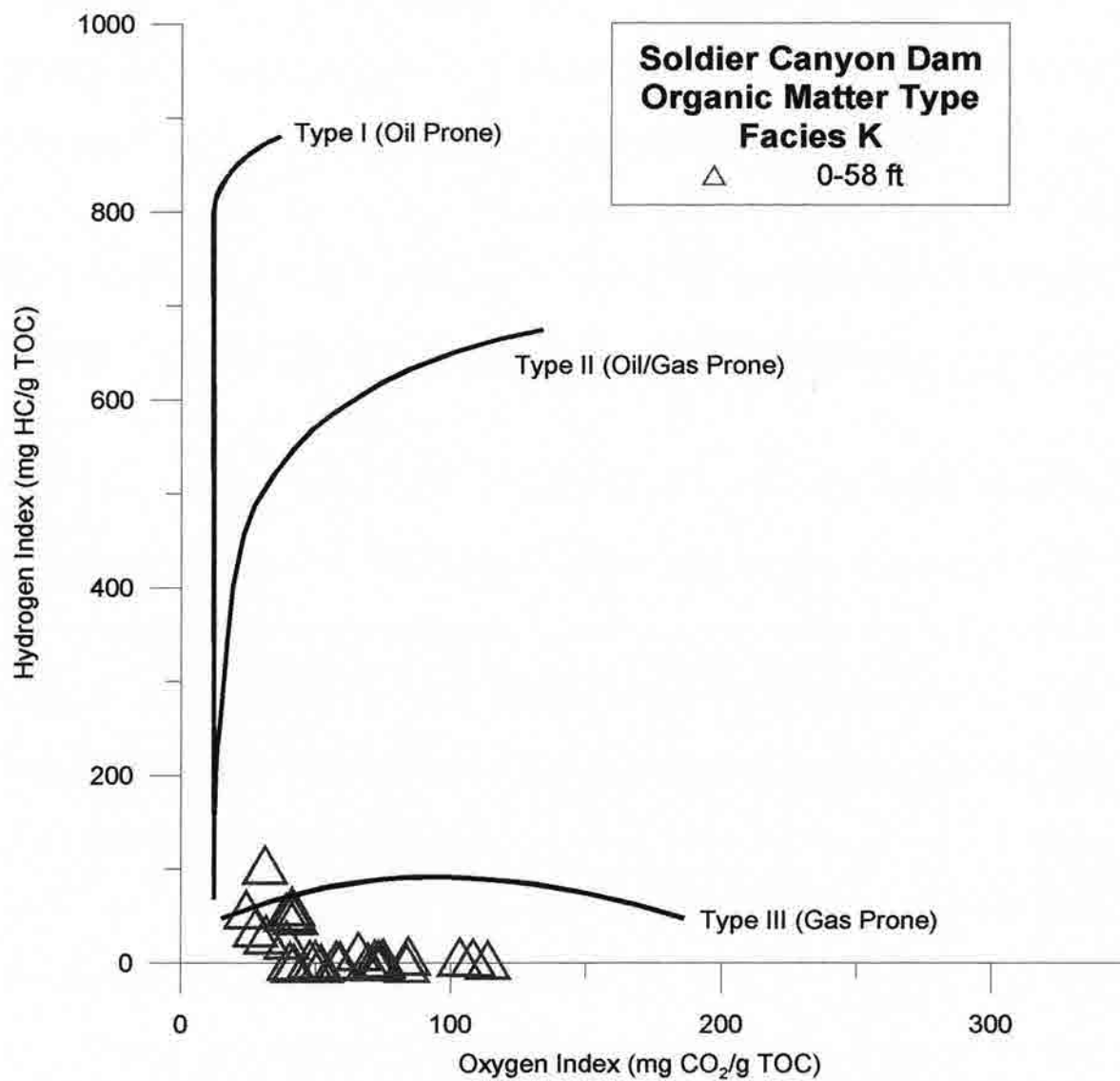


Figure 4.2 C.

The condensed section (CS) of facies A is 5 ft thick and includes two bentonites (Fig. 4.3). It is possible to delineate this facies in outcrop because of the well-developed fissility, in addition, to the relatively high outcrop gamma ray response (Fig. 4.1). Graham and Ethridge (1995) reported the prominent 5-8 cm thick yellowish-orange bentonite in the CS at Soldier Canyon is hypothesized to be the equivalent of the basal bentonite in the Skull Creek of the Northern Black Hills that was dated at 104.4 ± 0.5 Ma using argon/argon analyses (Cobban et al., 1994). The grayish-black shale of the CS contains prominent silt laminations, Inoceramid fragments and carbonaceous debris. No gypsum was found along joint planes.

Overlying the CS, is 16 ft of facies B that is a tannish-brown alternating sandstone/ shale (Fig. 4.4a). The bottom 8 ft of this well-stratified facies contains ripple marks, abundant pelecypod and echnioderm shell fragments, and *Astersoma* trace fossils (Graham and Ethridge, 1995). The upper 8-ft of facies B displays hummocky cross-stratification, cone in cone structures (Fig. 4.4b), and scoured surfaces that have been filled in with silt and bioclastic debris. This later feature has been interpreted to be a gutter cast from a storm deposit (Graham and Ethridge, 1995). The organic matter type for this facies is type III or terrestrial (Fig. 4.4c).

Facies C is represented by the overlying 74 ft of alternating sandstones and shale (Fig. 4.5). The bottom 26-ft includes a calcareous, tannish-brown interbedded sandstone/shale that has been bioturbated to the degree that has destroyed any previous bedding or sedimentary structures. Overlying this is an 18-ft paleoslump feature that was

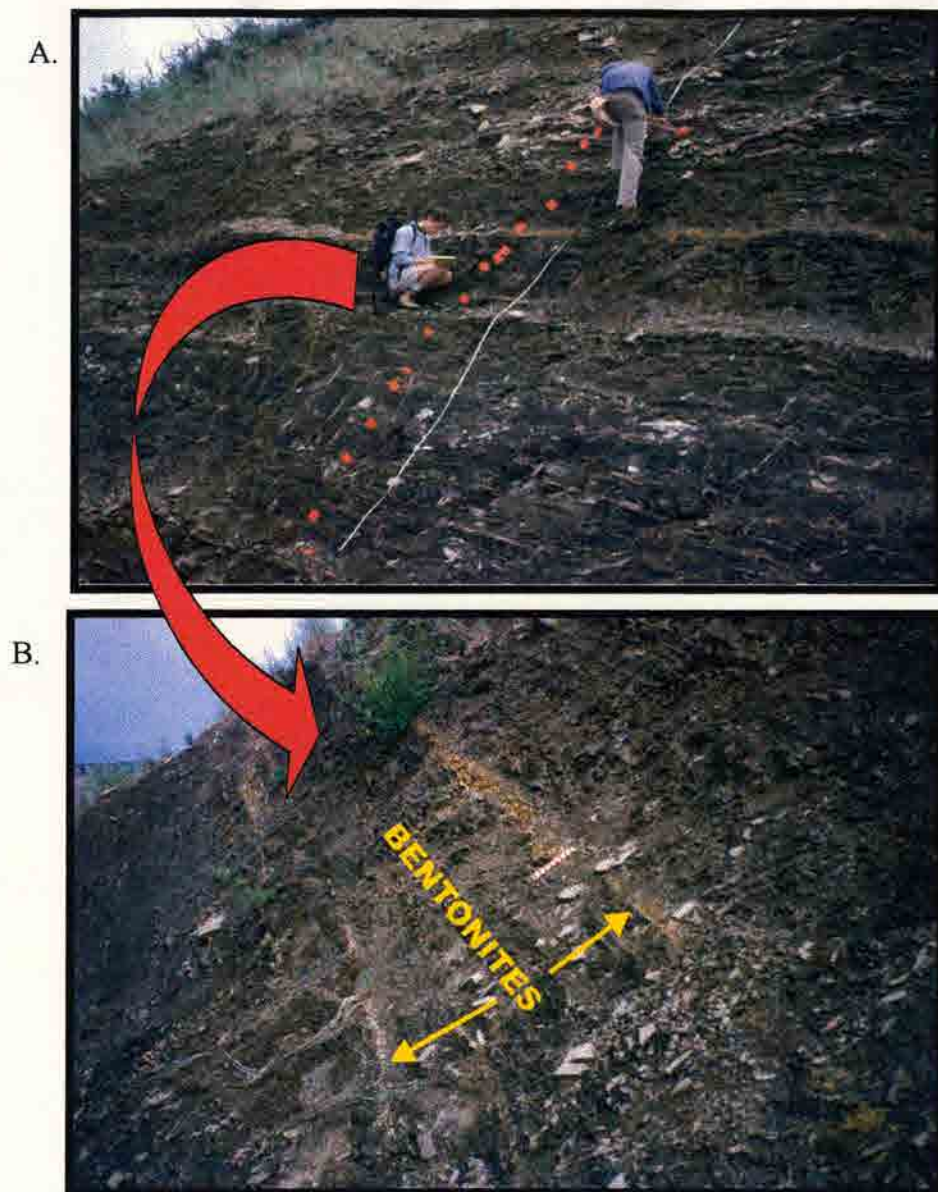


Figure 4.3 A) Overall view of grayish-black fissile shale; B) close-up view of two bentonites in the CS; C) Van Krevelen diagram shows organic matter for facies A. 1-ft ruler for scale. Samples were taken in 1-ft increments.

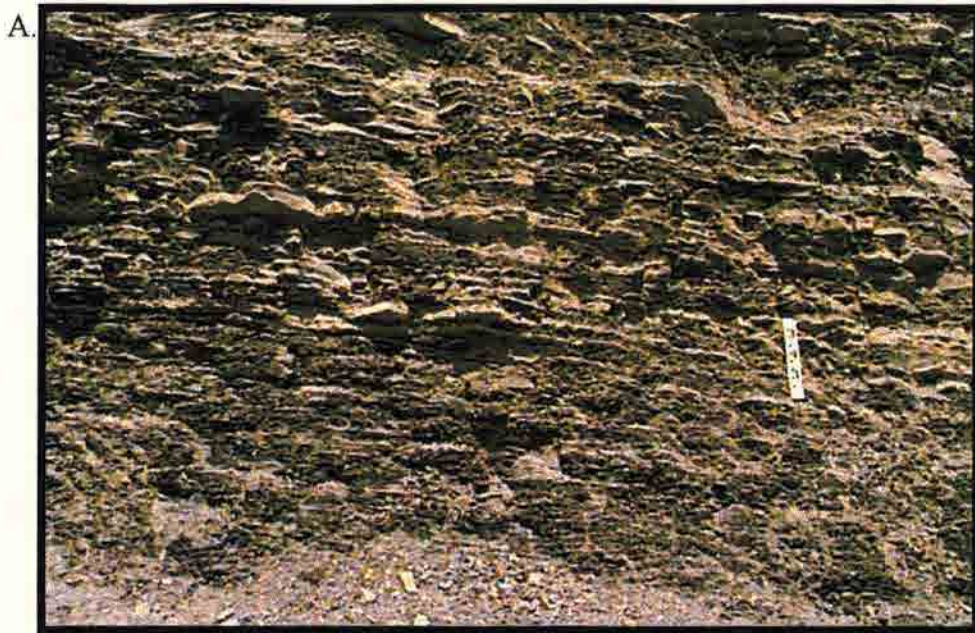


Figure 4.4 A) Overall view of hummocky cross-stratification bedding; B) close-up view of cone-in cone structures; C) Van Krevelen diagram shows type II-III organic matter for facies B. 1-ft ruler for scale, left side of ruler is centimeters and right side is inches..

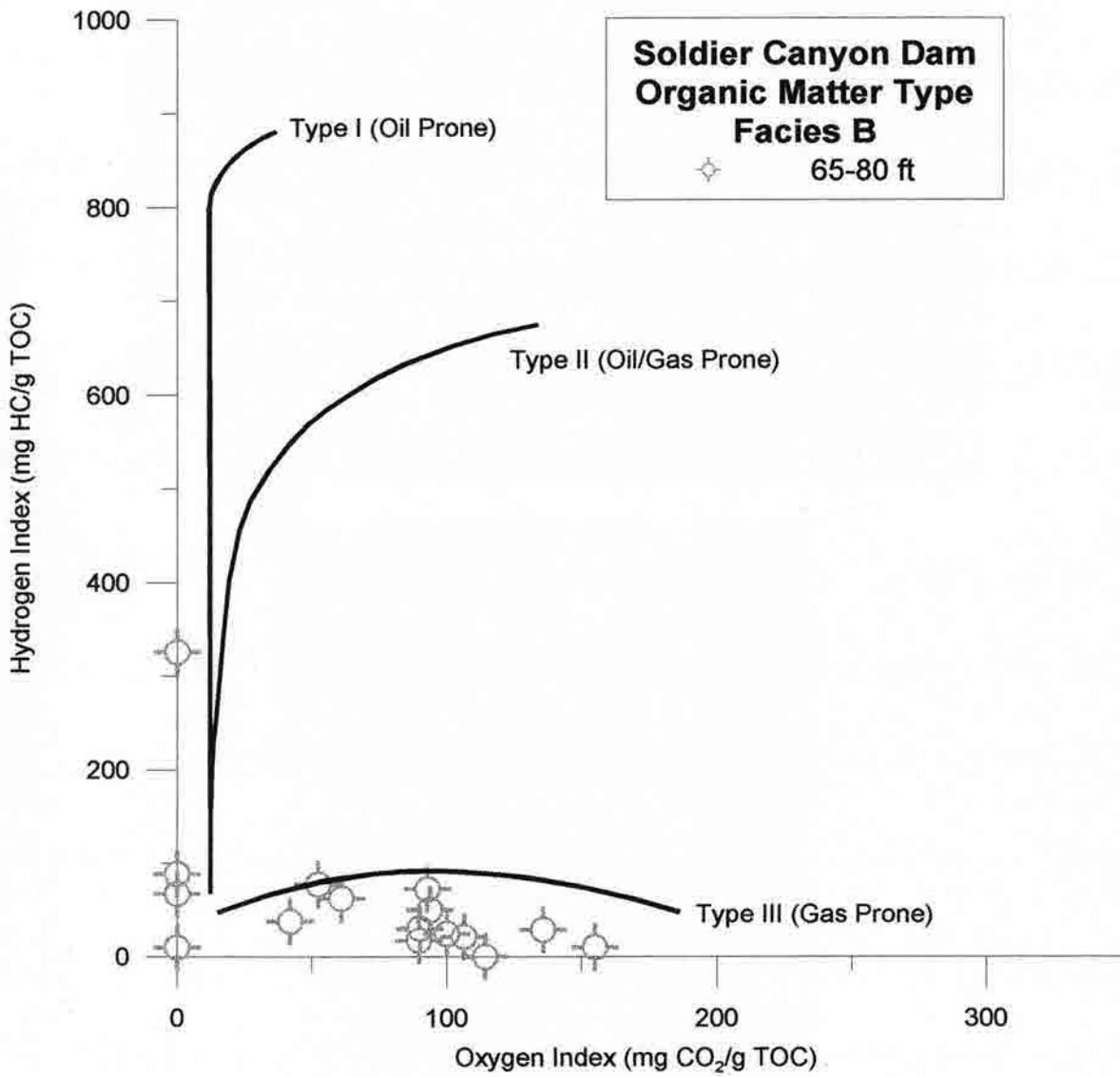


Figure 4.4 C.

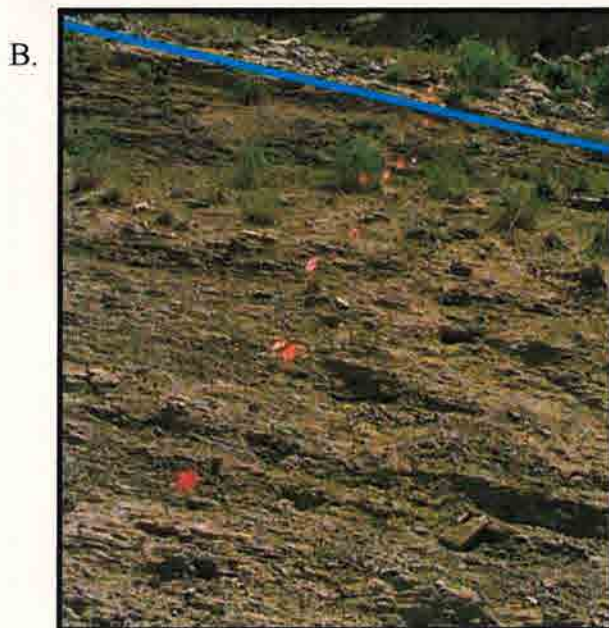
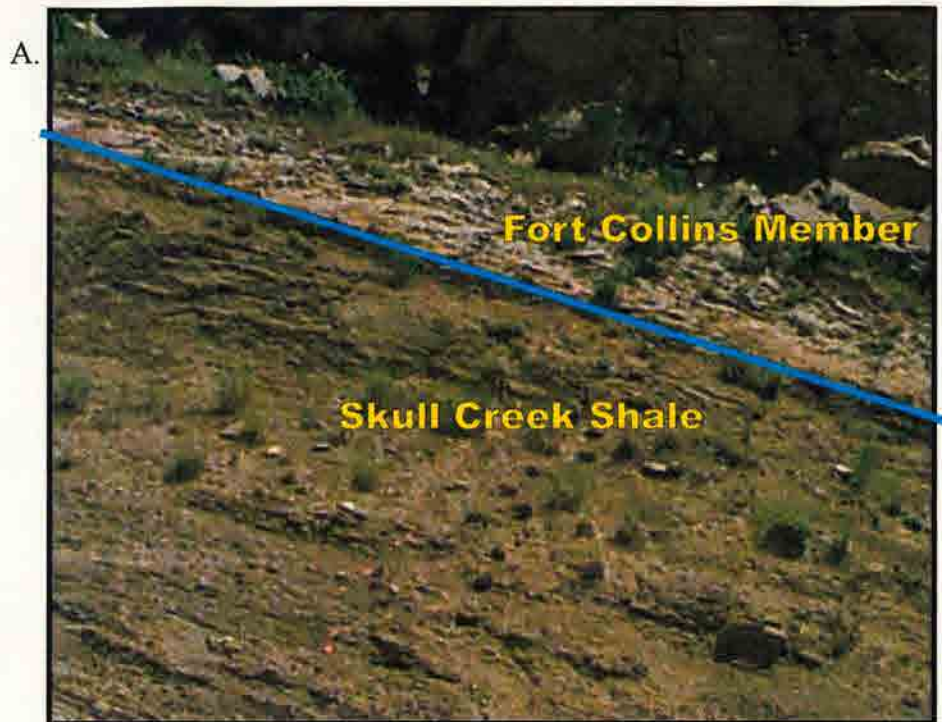


Figure 4.5 A) Contact between the Skull Creek Shale and the Fort Collins member; B) interbedded sandstone and shale lithology; C) Van Krevelen diagram shows a Type III organic matter for facies C. Flags mark the samples that were taken in two foot increments.

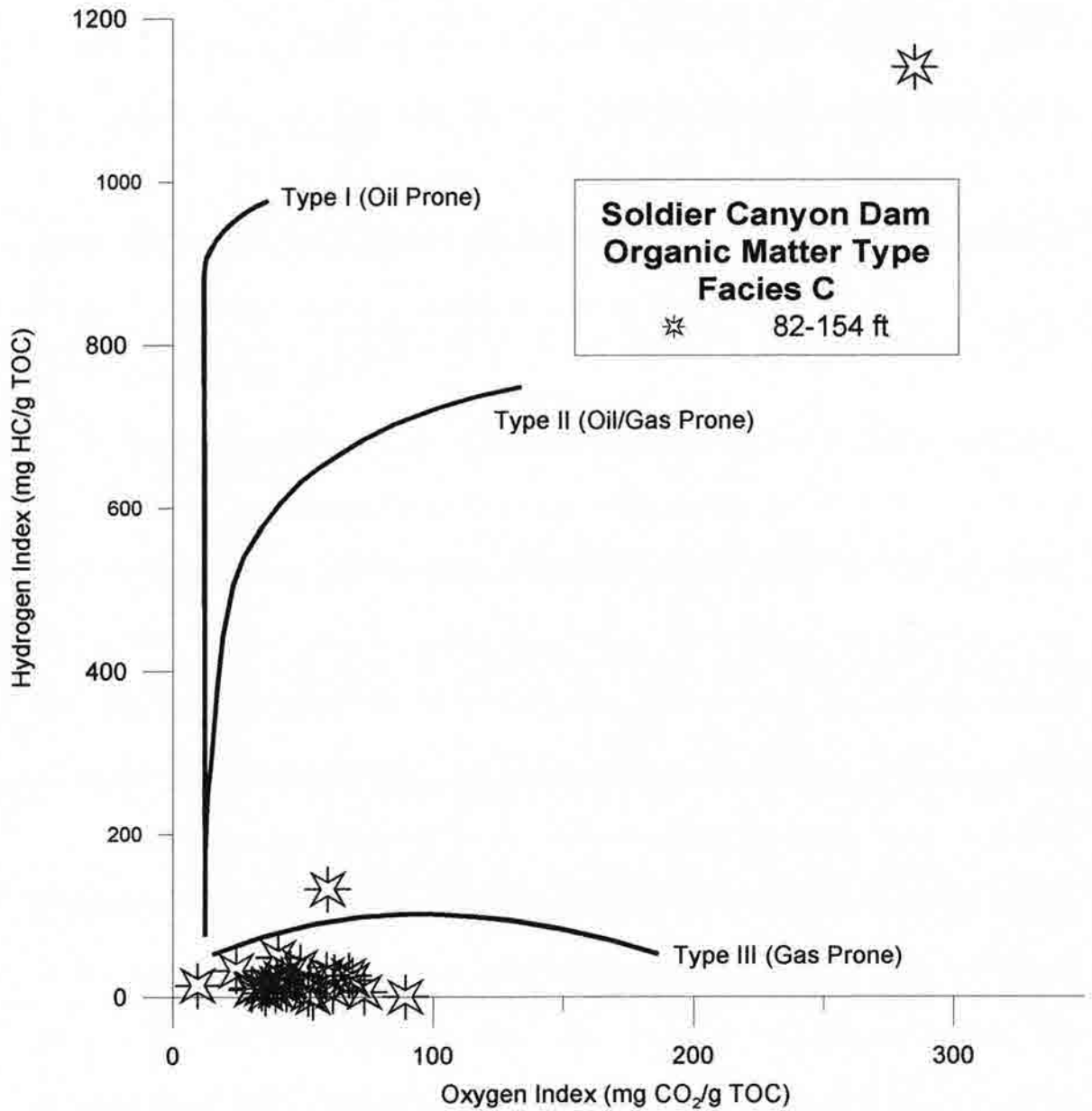


Figure 4.5 C.

not sampled. This “paleoslump” has tight folds that indicate soft sediment deformation prior to lithification. Onlapping lenticular sandstones sharply define the upper contact of this “paleoslump” (Graham and Ethridge, 1995). Graham and Ethridge (1995) determined that the axis of this slump is parallel to the N-S trend of the presumed Skull Creek paleoshoreline in this area. Another 30 ft of facies C overlies the paleoslump. Facies C displays type III (terrestrial) organic matter (Fig. 4.5c).

4.2 Lithology Description

Table 4.1 gives the average value and standard deviation of the Skull Creek facies data at Soldier Canyon Dam. There is a clear difference between the TST (facies K and A) and HST (facies B and C) deposits. Thermal maturity (T_{max}) data is not reliable unless TOC is greater than 1% (Barry Katz, 1983). Since TOC is below 1% in all the HST deposits and in most of the TST deposits, T_{max} thermal maturity data will be disregarded for this outcrop.

The horizontal samples of facies A or the condensed section have the highest percentage of total organic carbon and carbonate with the lowest permeability and the vertical samples of facies A have the highest percentage of total clay (54%). The vertical samples may have more variability and higher percentages of total clay because they include two bentonites. Facies K has the second highest percentage of total clay (47%) and the second lowest permeability.

The HST deposits have lower amounts of TOC and total clay with increased amounts of quartz and carbonate relative to the TST deposits. Overall, the HST deposits

Table 4.1 Soldier Canyon Statistics for Data

Facies		Total Organic Carbon (%)	Hydrogen Index (mg HC/g TOC)	Hydrogen Index/Oxygen Index (mg HC/mg CO ₂)	Total Clay (wt%)	Quartz (wt%)	Feldspar (wt%)	Carbonate (wt%)	Porosity (%)	Permeability (md)	Density (g/cc)
	# of Analyses	28	28	28	0	0	10	10	9	9	9
K	Average	0.73	20	1	47	42	5	5	14.3	0.0040	2.64
	Std Dev	0.39	27	1	7	5	1	5	2.0	0.003	0.04
Vert. A	# of Analyses	6	6	2	6	6	6	6	6	6	6
	Average	1.20	104	1	54	32	5	8	15.9	0.0080	2.66
	Std Dev	0.61	113	1	20	17	1	4	3.8	2.12	0.04
Hor. A	# of Analyses	6	5	5	6	6	6	6	6	6	6
	Average	2.39	138	5	43	40	4	11	16.2	0.0049	2.64
	Std Deviation	1.3	62.9	0.9	15.0	13.4	1	2.2	3.8	0.003	0.04
	# of Analyses	16	16	13	5	5	5	5	5	5	5
B	Average	0.81	38	0	24	54	6	16	12.6	0.066	2.68
	Std Dev	0.58	28	0	6	6	1	4	1.2	0.04	0.04
	# of Analyses	29	29	29	13	13	13	13	13	13	13
C	Average	0.35	23	1	22	63	4	11	13.0	0.23	2.68
	Std Dev	0.10	26	1	3	7	1	6	1.9	0.229	0.04

of facies B and C have lower porosity and higher permeability and density than the TST deposits.

The data has been plotted against stratigraphic height to permit comparison to seal capacity. The best seals are located in the upper parts of the TST deposits, in particular facies K and facies A (Fig. 4.6a). Porosity values are generally higher in the TST deposits than in the HST deposits (Fig. 4.6b). The lowest permeability values are in the upper parts of facies K followed by facies A, and increase in the HST deposits (Fig. 4.6c). Density values do not vary much, although the HST samples have a somewhat greater density than the TST samples (Fig. 4.6d).

The TST deposits have higher total clay content than the HST deposits, the spike in facies A is caused by a clay rich bentonite (Fig. 4.7a). Quartz shows an inverse relationship to clay, and is higher in the HST deposits (Fig. 4.7b). The amount of

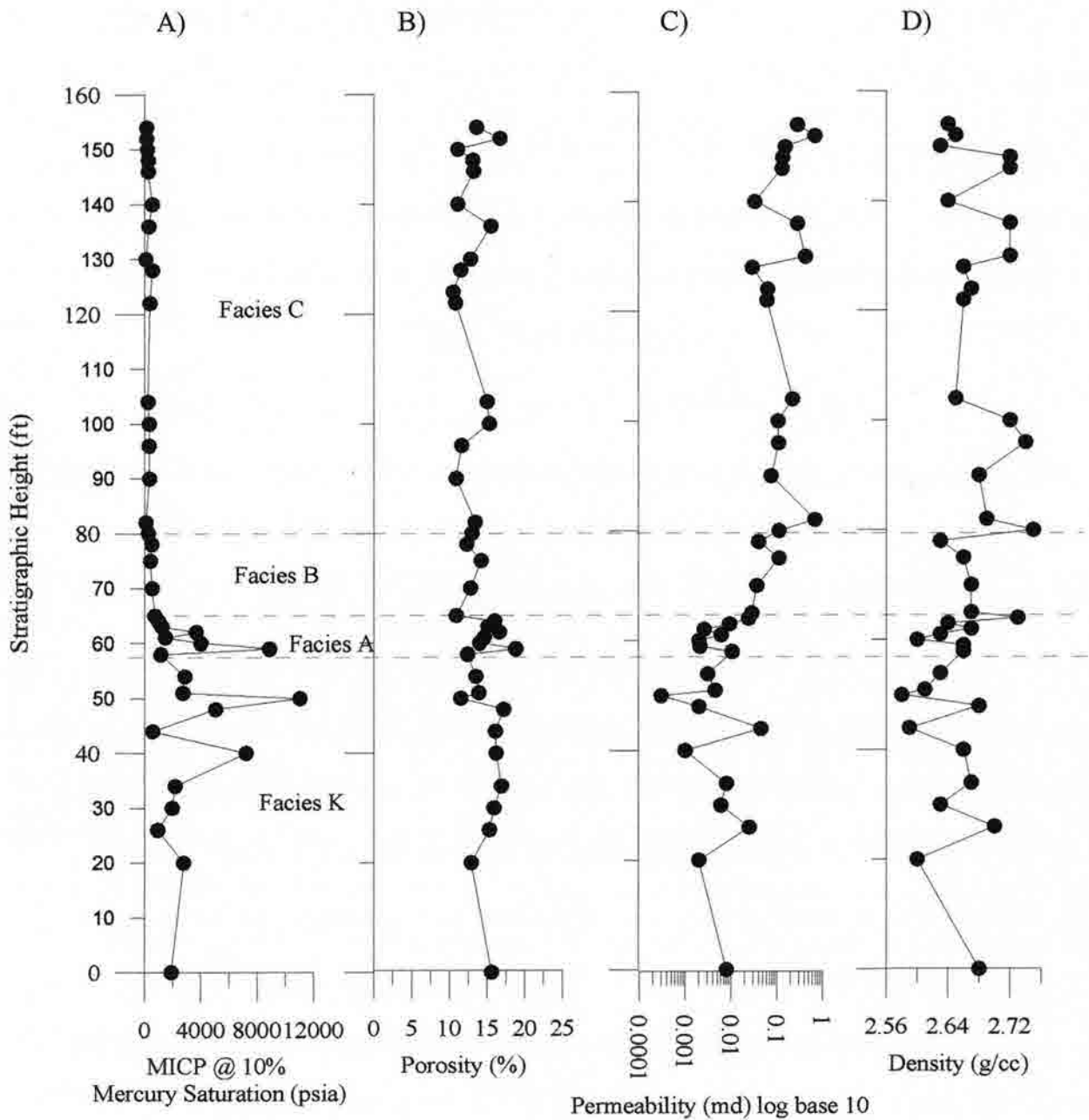


Figure 4.6 Stratigraphic height versus MICP (A), porosity (B), permeability (C), and density (D) at Soldier Canyon Dam for the Skull Creek.

feldspar varies but seems to be slightly higher in the TST deposits (4.7c). Carbonate is clearly higher in the HST deposits but have peaks in the TST deposits that correspond to relatively high seal capacity (Fig. 4.7d).

The greatest amount of TOC is found in the upper parts of the facies K and in facies A (Fig. 4.8a). Hydrogen index values are low for facies K but peak in facies A (Fig. 4.8b). The ratio of HI/OI shows a corresponding peak to the HI (Fig. 4.8b) in facies K and A. A detailed summary of the organic geochemistry is found in Appendix P.

Thin-Section petrography

Table 4.2 summarizes the petrographic observations for each thin section. This table includes a few representative point counts for each of the facies, along with visual estimates for the other thin sections. Grain size analysis reveals an overall coarsening upward trend. Appendix A includes representative thin section photomicrographs for each of the facies, along with detailed petrographic descriptions.

The basal layers of facies K consist of dark grayish brown carbonaceous mudstones with approximately 50-60% clay, 2% organic matter and no pyrite or carbonate. The detrital grains of quartz, feldspar and sedimentary rock fragments are silt-size, subrounded, spherical, and moderately well sorted. These mudstones are not laminated but appear to be slightly “mottled”. The upper part of facies K contains more silt and well-developed laminations. No fossils or porosity is detected in this facies.

The condensed section (facies A) is a well compacted, carbonaceous silty shale with approximately 65-80% clay, 15-25% quartz, 1-3% organic matter, 0-8% authigenic carbonate with minor amounts of pyrite. The detrital grains of quartz, feldspar and mica are silt to fine-grained sand size, well rounded, elongate-spherical, and well sorted. This

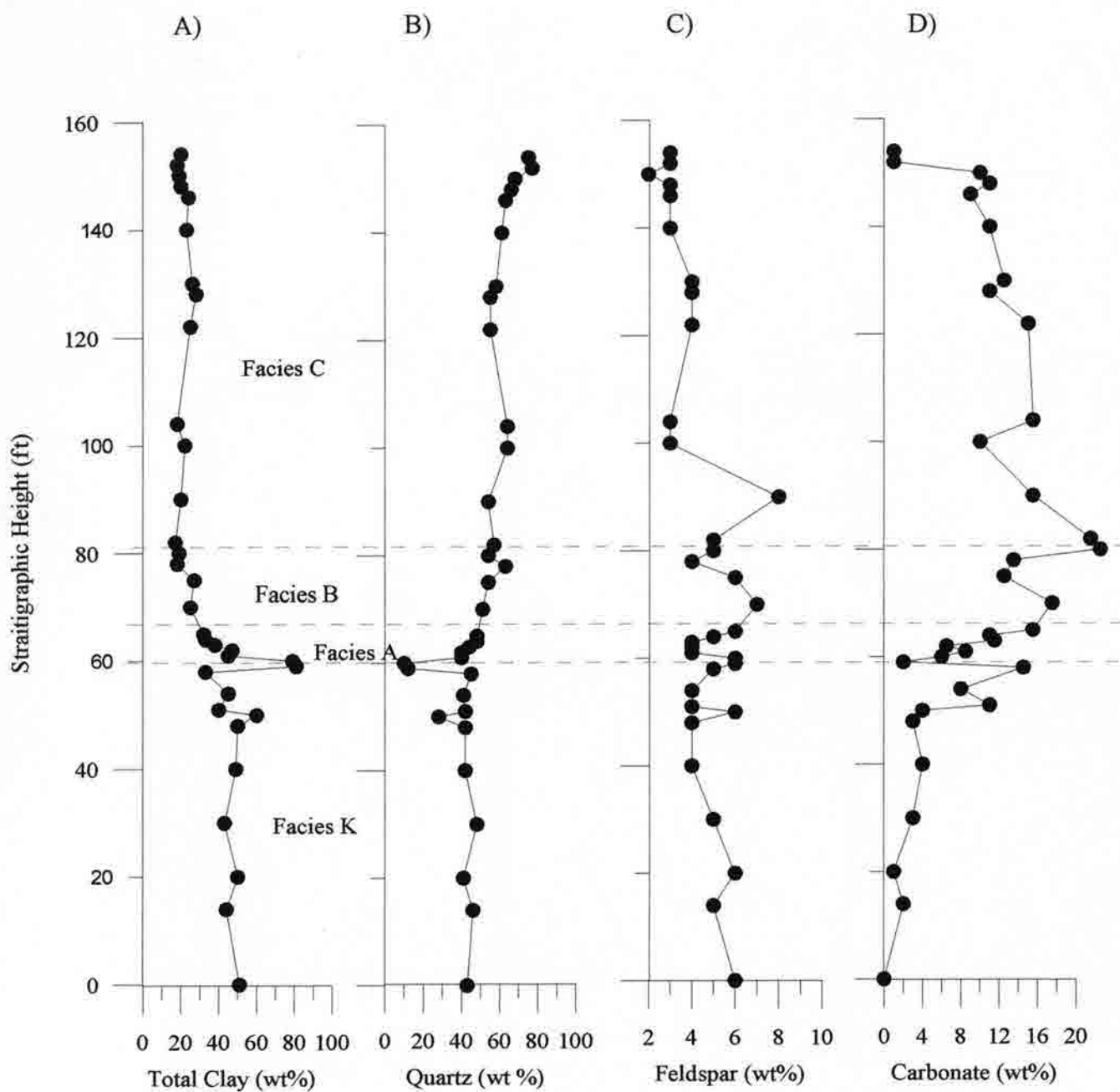


Figure 4.7 Stratigraphic height versus total clay (A), quartz (B), feldspar (C), and carbonate (D) at Soldier Canyon Dam for the Skull Creek.

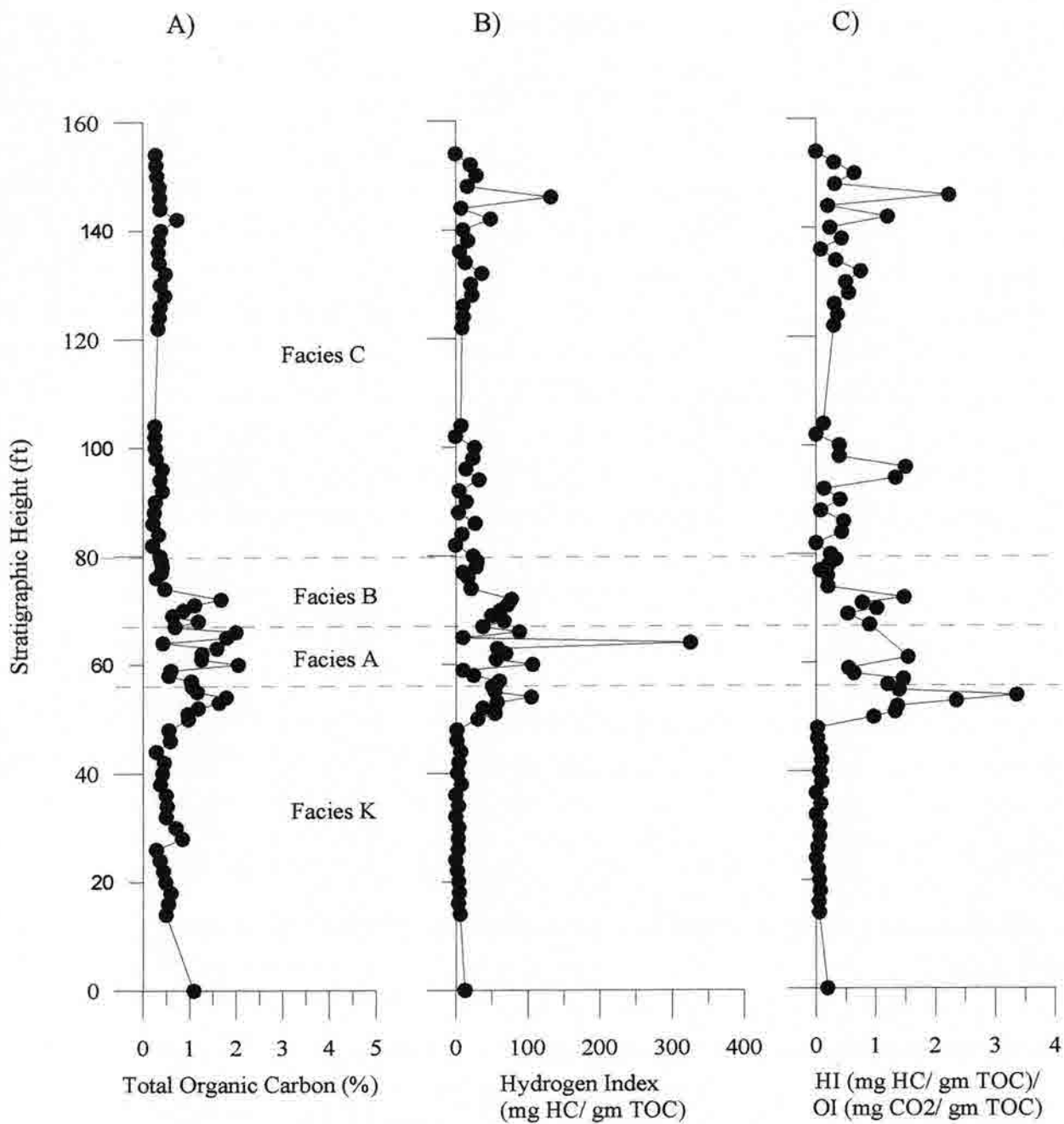


Figure 4.8 Stratigraphic height versus total organic carbon (A), hydrogen index (B), and hydrogen index / oxygen index (C) at Soldier Canyon Dam for the Skull Creek.

Table 4.2 Soldier Canyon Dam Thin Section Petrography

Facies	FT	Rock name	Avg. Grain Size (μ)	COMPOSITION						Laminations	Bioturbation	Pressure Solution	Fossils	Porosity
				QTZ	CLAY	ORG	CARB	PYR	OTHER					
C	154	sandstone	108	77	19	1	2	1	glauc	N	Y	Y	Y	3%
C	140	siltstone	(vf sand)	68	22	2	7	1	glauc	N	Y	Y	Y	3%
C	102	siltstone	(vf sand)	68	22	2	7	1	glauc	Y	Y	Y	Y	2%
C	100	siltstone	(vf sand)	58	24	2	15	1	glauc	Y	Y	Y	Y	2%
B	80	siltstone	83	55	30	2	12	1	glauc	Y	Y	Y	Y	N
B	65	silty shale	24	52	35	2	10	1	mica	Y	N	Y	Y	N
A	63	silty shale	(silt)	23	65	3	8	1	mica	Y	N	Y	N	N
A	62	silty shale	31	24	66	3	6	1	mica	Y	N	Y	Y	N
A	59	bentonite	68	15	84	1	0	0		N	N	Y	Y	N
K	54	silty shale	18	46	49	2	3	0	mica	Y	N	Y	N	N
K	48	mudstone	49	36	62	2	0	0	mica	N	N	N	N	N
K	42	mudstone	26	36	62	2	0	0	mica	N	N	N	N	N

*NOTE: Point count percentages are in bold, other percentages are estimates.

**NOTE: 1/256 <silt <1/16 mm, 1/16 <VF sand <1/8 mm, 1/8 <F sand <1/4 mm, 1/4 <M sand <1/2 mm

LEGEND:

QTZ= Quartz

ORG= Organic Matter

CARB= Carbonate (calcite, dolomite, siderite)

feld= Feldspar

phos= Phosphate

mic= Mica

hem= Hematite

glauc= Glauconite

pyr= Pyrite

facies has well-developed laminations of silt, clay, and organic matter. There are no signs of bioturbation disrupting the laminations. Inoceramid fragments are commonly found in this facies. No matrix porosity is evident.

Facies B is a well-compacted, carbonaceous silty shale to argillaceous siltstone with approximately 53-54% quartz, 32-33% clay, 2% organic matter, 11% authigenic carbonate and minor amounts of pyrite and glauconite. These authigenic carbonates include dolomite, calcite, and siderite. The detrital grains of quartz, feldspar, and mica are silt to very-fine sand size, rounded, spherical, and well sorted. This silty shale to siltstone shows well-developed laminations that are occasionally disrupted by minor

burrowing, thus giving a “mottled” appearance. Abundant pelecypod and echinoderm debris is present in the gutter cast layer at 65 ft. No matrix porosity is visible in this facies.

Facies C represents a well-compacted, argillaceous sandstone with approximately 60-75% quartz, 20-25% clay, 1-2% organic matter, 2-15% authigenic carbonate with minor amounts of pyrite and glauconite. The detrital grains of quartz, feldspar and mica are silt to fine sand size, rounded, spherical, and well sorted. Intense bioturbation has completely destroyed any relic bedding features or sedimentary structures. Up to 3% intergranular porosity is visible in this facies.

Scanning Electron Microscopy

The purpose of SEM is to determine the organization of the pore throat system and the overall microtexture of the shale. SEM is done in conjunction with XRD to determine the mineralogy of the fabric seen in SEM. Appendix B provides representative photomicrographs for each facies, along with detailed descriptions.

The TST deposits (facies K and A) are a well sorted, subangular, framework supported silty shale. The framework particle size ranges from 10 to 30 μm and is homogeneously distributed throughout the sample. The framework mineralogy primarily consists of detrital quartz grains with secondary amounts of feldspars and carbonate. Most of the clay occurs as grain coatings and interstitial fines. Illite/smectite is coating the hard grains and appears to be blocking the pore network. Small booklets of kaolinite are present. There is no significant micropore or macropore intergranular system. Most of the pores noticed are caused by grain plucking that can be an artifact of sample preparation.

The HST deposits (facies B and C) are a moderately sorted, subrounded, framework supported siltstone to sandstone. The framework particle size ranges from 10 to 50 μm and comprises the bulk of this sample. The framework mineralogy consists of detrital quartz grains with secondary amounts of carbonate and feldspars. Most of the clays occur as grain coatings or pore filling interstitial fines. Kaolinite books are common throughout these facies. A moderately developed intergranular micropore and macropore system is evident.

Whole Rock Mineralogy

The XRD analysis of the whole rock mineralogy is shown in Table 4.3. Vertical sampling of facies A has the highest percentage of total clay with almost no pyrite. Horizontal sampling shows less total clay with minor amounts of pyrite. The carbonates in facies A are mainly dolomite with smaller amounts of calcite and siderite. Facies K has the second highest total clay, with more gypsum and jarosite and less carbonate than facies A.

Feldspar includes both potassium feldspar and plagioclase and is 5% or less throughout the TST and HST deposits. There is a dramatic shift in the mineralogy between the TST and HST deposits. The majority of facies B and C is quartz with considerably more dolomite than the TST deposits.

Clay Mineralogy

The XRD analysis of the clay mineralogy is shown in Table 4.4. Facies K averages 61% total I/S, with the bottom 30-ft having a R1 ordering and the upper 29 ft having an R0 ordering. This is complimented by an average of 28% illite, 10% kaolinite and 1% chlorite. In general, illite and I/S show an inverse relationship. This R1

Table 4.3 Whole Rock Mineralogy from XRD (wt%): Soldier Canyon Dam Outcrop

Facies	Sample #	FT	TCL	QTZ	KSP	PLAG	CAL	DOL	PYR	SID	CLINO	PHIL	GYP	JARO
C	SC-058	154	19	75	2	1	ND	1	TR	1	ND	ND	ND	ND
	SC-057	152	17	77	2	1	1	ND	TR	1	ND	ND	ND	ND
	SC-056	150	18	68	2	ND	1	8	TR	1	ND	ND	1	ND
	SC-055	148	20	64	2	1	1	10	TR	1	ND	ND	ND	ND
	SC-054	146	23	62	2	1	2	7	TR	2	ND	ND	ND	ND
	SC-051	140	23	62	2	1	1	10	ND	1	ND	ND	ND	ND
	SC-046	130	25	57	2	2	1	11	TR	1	ND	0.5	ND	ND
	SC-045	128	28	55	2	2	1	10	TR	1	ND	ND	ND	ND
	SC-042a	122	25	54	2	2	1	14	TR	1	ND	ND	ND	ND
	SC-042	104	17	63	2	1	1	14	TR	1	ND	TR	ND	ND
	SC-040	100	22	63	2	1	1	8	TR	1	1	ND	ND	ND
	SC-035	90	20	55	2	6	1	14	TR	1	ND	TR	ND	ND
SC-031	82	17	56	2	3	1	20	TR	ND	ND	TR	ND	ND	
Average		21	62	2	2	1	11	0	1	1	1	1	1	0
B	SC-030	80	19	53	2	3	8	14	TR	ND	ND	TR	ND	ND
	SC-028	78	18	63	2	2	1	12	TR	1	ND	TR	ND	ND
	SC-025	75	26	53	2	4	ND	11	TR	2	1	TR	ND	ND
	SC-020	70	25	50	3	4	2	15	TR	ND	ND	TR	ND	ND
	SC-015	65	31	47	3	3	3	11	TR	ND	ND	TR	1	ND
	Average		24	53	2	3	4	13	0	2	1	0	1	0
A	SC-014	64	33	48	2	3	ND	11	TR	2	ND	ND	ND	ND
	SC-013	63	38	44	2	2	ND	8	TR	2	ND	TR	1	2
	SC-012	62	47	40	2	2	ND	6	TR	2	ND	TR	ND	ND
	SC-011	61	45	40	2	2	2	6	TR	2	ND	TR	ND	ND
	SC-010	60	78	10	3	3	3	3	ND	ND	ND	ND	ND	ND
	SC-009	59	80	12	3	3	ND	2	ND	ND	ND	ND	ND	ND
	Average		54	32	2	3	3	6	0	2	0	0	1	2
K	SC-008	58	33	45	2	3	1	12	TR	2	1	TR	ND	ND
	SC-004	54	45	41	2	2	ND	8	ND	2	ND	ND	ND	ND
	SC-001	51	41	42	2	2	ND	9	ND	2	ND	ND	2	ND
	BSC-019	50	60	28	3	3	ND	0	ND	2	ND	ND	ND	4
	BSC-018	48	49	42	2	2	ND	0	ND	2	ND	ND	ND	3
	BSC-014	40	50	42	2	2	ND	0	ND	ND	ND	ND	ND	4
	BSC-009	30	42	48	3	2	ND	0	ND	2	ND	ND	ND	3
	BSC-004	20	50	41	3	3	ND	1	ND	2	ND	ND	ND	ND
	BSC-001	14	45	46	3	2	1	1	ND	2	ND	ND	ND	ND
	BSC-000	0	51	43	4	2	ND	ND	ND	TR	ND	ND	ND	ND
Average		47	42	3	2	1	3	0	2	1	0	2	4	
HORIZONTAL SAMPLING OF THE CONDENSED SECTION														
A	West 40'		46	39	2	0	3	5	4	2	ND	ND	ND	ND
	West 30'		47	36	2	2	3	5	4	2	ND	ND	ND	ND
	West 20'		37	44	2	2	3	7	4	2	ND	ND	ND	ND
	West 10'		37	44	2	2	3	7	4	2	ND	ND	ND	ND
	East 10'		43	38	2	2	3	7	4	2	ND	ND	ND	ND
	East 20'		45	39	2	2	0	6	4	2	ND	ND	ND	ND
	East 30'		43	40	2	2	3	5	4	2	ND	ND	ND	ND
	Average		43	40	2	2	3	6	4	2	0	0	0	0

LEGEND:

TCL= Total Clay and Mica

QTZ= Quartz

KSP= K-Feldspar

PLAG= Plagioclase

Mg-CAL= Mg-rich calcite

CAL= Calcite

DOL= Dolomite

PYR= Pyrite

SID= Siderite

GYP= Gypsum

CLINO= Clinoptilolite

PHIL= Philipsite

ANHY= Anhydrite

JARO= Jarosite

TR= Trace

ND= Not Detected

Table 4.4 Soldier Canyon Dam Clay Mineralogy

Facies	Sample #	Height (ft)	R1 I/S	R0 I/S	Total amt. I/S	Illite	Kaol	Chlorite	Verm
C	SC-058	154	ND	32	32	40	18	TR	10
	SC-057	152	ND	40	40	32	18	TR	10
	SC-056	150	ND	50	50	30	10	TR	10
	SC-055	148	ND	55	55	31	7	TR	7
	SC-054	146	ND	66	66	21	8	TR	5
	SC-051	140	ND	36	36	24	23	12	5
	SC-046	130	ND	79	79	7	8	2	4
	SC-045	128	ND	70	70	19	7	TR	4
	SC-042a	122	ND	49	49	24	19	5	3
	SC-042	104	ND	70	70	21	6	TR	3
	SC-040	100	ND	76	76	12	6	3	3
	SC-035	90	ND	69	69	15	9	4	3
	SC-031	82	ND	62	62	21	12	TR	5
	Average					58	23	12	5
B	SC-030	80	ND	77	77	16	7	TR	5
	SC-028	78	ND	65	65	25	9	TR	TR
	SC-025	75	ND	63	63	30	6	TR	1
	SC-020	70	ND	71	71	24	4	TR	TR
	SC-015	65	ND	74	74	21	4	1	TR
	Average					70	23	6	1
A	SC-014	64	ND	74	74	25	2	ND	TR
	SC-013	63	ND	67	67	30	3	ND	ND
	SC-012	62	ND	70	70	28	2	ND	ND
	SC-011	61	ND	65	65	35	TR	ND	ND
	SC-010	60	ND	86	86	ND	14	ND	ND
	SC-009	59	ND	100	100	ND	TR	ND	ND
	Average					77	30	5	0
K	SC-008	58	ND	78	78	22	1	TR	ND
	SC-004	54	ND	57	57	42	1	TR	ND
	SC-001	51	ND	66	66	32	2	TR	ND
	BSC-019	50	ND	48	48	42	9	1	ND
	BSC-018	48	ND	50	50	40	9	1	ND
	BSC-014	40	ND	65	65	20	14	1	ND
	BSC-009	30	65	ND	65	19	15	1	ND
	BSC-004	20	55	ND	55	30	14	1	ND
	BSC-001	14	67	ND	67	15	17	1	ND
	BSC-000	0	59	ND	59	20	20	1	ND
	Average					61	28	10	1

LEGEND:

R1 I/S= Ordered Illite/Smectite (Reichweite=1)

R0 I/S= Randomly Ordered Illite/Smectite (Reichweite=0)

Kaol= Kaolinite (1:1 Clay)

Serp= Serpentine (1:1 Clay)

Verm= Vermiculite (2:1 Clay)

I/S is the only example of an ordered I/S at the Soldier Canyon Dam outcrop. The condensed section or facies A has the greatest concentration of I/S (avg. 77%) with R0 ordering. 30% illite and 5% kaolinite compliment this clay mineralogy. Facies B averages 70% R0 I/S, 23% illite, and 6% kaolinite, with minor amounts of vermiculite and chlorite. The clays in facies C average 58% R0 I/S, 23% illite, 12% kaolinite, 6% vermiculite, and 5% chlorite. Overall, the amount of kaolinite is higher in facies K and C. Vermiculite and chlorite are also most concentrated in facies C.

4.3 *Petrophysical Description*

The MICP (mercury-injection capillary pressure) data is important because it provides key information on the organization of the pore network. The injection pressures and HCH (hydrocarbon column height, ft) are displayed in Table 4.5. The highest injection pressure at 10% mercury saturation is 11,040 psia and holds a corresponding HCH of 3,095 ft. This sample is located in facies K at 50 ft. This rock is the best seal at Soldier Canyon Dam, because it requires the highest psia to intrude the pore network. The next high injection pressure is 8,870 psia for a sample located in the CS at 59 ft. The next high injection pressures are 7,210 psia and 5,050 psia for samples located in facies K at 40 and 48 ft, respectively.

There is a dramatic difference in the shape of the drainage curves for the TST (facies K and A) and the HST (facies B and C). The drainage curves for facies K show significant variability, but the best seals have a broadly sloping upper curve with entry pressures around 2,000 psia (Fig. 4.9a). The best seals in facies A also have a gently sloping upper curve with entry pressures between 1,000-3,000 psia (Fig. 4.9b). Facies B has very low entry pressures (100-400 psia) with a steeply sloping upper curve

Table 4.5 Soldier Canyon Injection Pressures (psia) at 10% Mercury Saturation

Facies	Sample#	FT	PSIA@10% SAT.	HCH (ft)
C	SC-058	154	173	40
C	SC-057	152	173	40
C	SC-056	150	223	50
C	SC-055	148	280	70
C	SC-054	146	281	70
C	SC-051	140	556	145
C	SC-049	136	316	80
C	SC-046	130	106	20
C	SC-045	128	575	150
C	SC-042a	122	389	100
C	SC-042	104	261	65
C	SC-040	100	347	85
C	SC-038	96	333	85
C	SC-035	90	360	90
C	SC-031	82	112	20
B	SC-030	80	280	70
B	SC-028	78	519	135
B	SC-025	75	425	110
B	SC-020	70	553	145
B	SC-015	65	730	195
A	SC-014	64	1010	275
A	SC-013	63	1240	340
A	SC-012	62	3680	1030
A	SC-011	61	1490	410
A	SC-010	60	4010	1120
A	SC-009	59	8870	2490
K	SC-008	58	1170	320
K	SC-004	54	2870	795
K	SC-001	51	2730	760
K	BSC-019	50	11040	3095
K	BSC-018	48	5050	1410
K	BSC-016	44	585	155
K	BSC-014	40	7210	2020
K	BSC-011	34	2180	605
K	BSC-009	30	1970	545
K	BSC-007	26	946	255
K	BSC-004	20	2780	775
K	BSC-000	0	1910	525
A	SCCS1	West 40	5402	1510
A	SCCS2	West 30	1830	505
A	SCCS3	West 20	2530	700
A	SCCS4	West 10	3020	840
A	SCCS5	East 10	1750	480
A	SCCS6	East 20	1210	330
A	SCCS7	East 30	1860	515

Soldier Canyon Drainage Curve (Facies K)

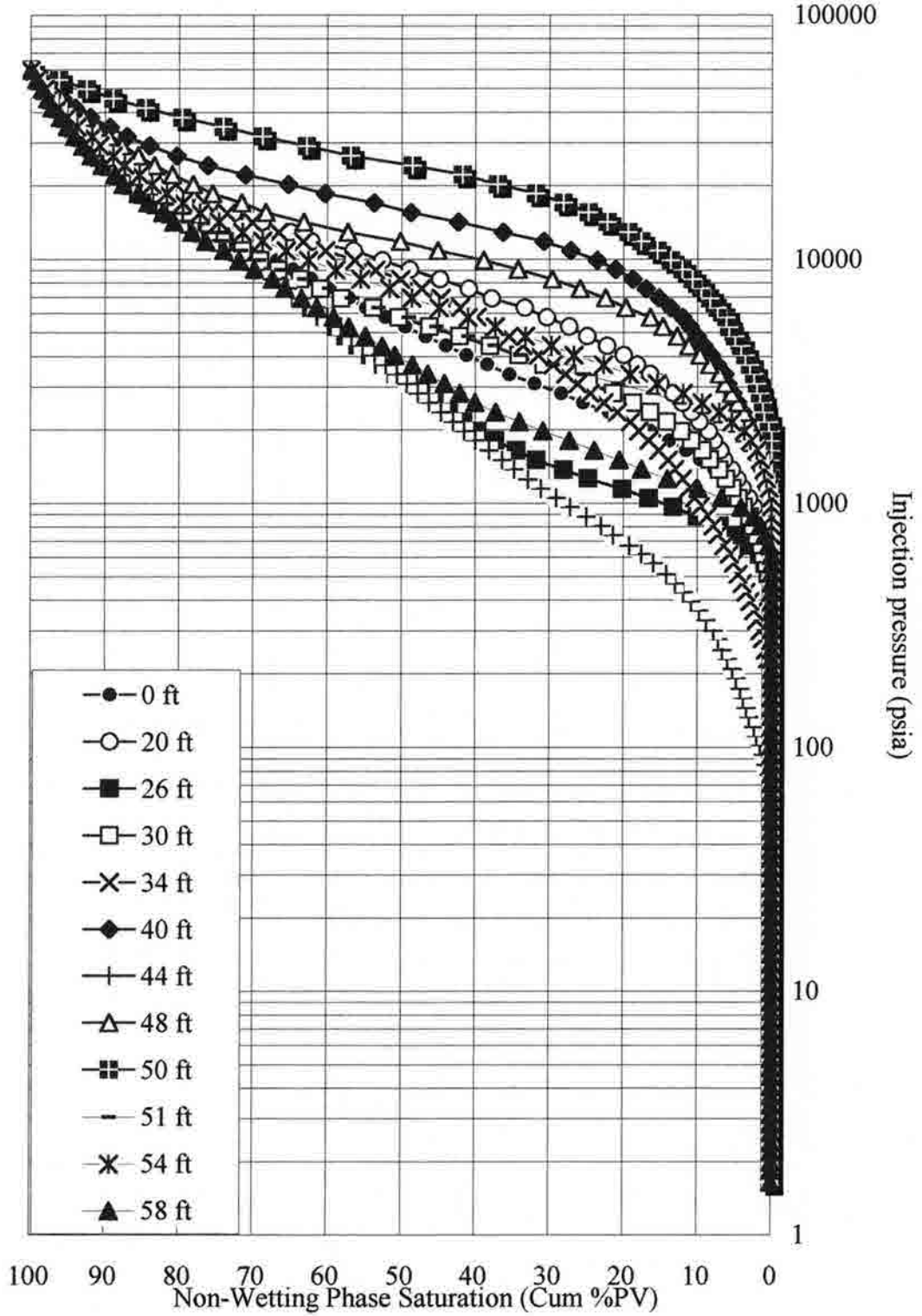


Figure 4.9a Drainage Curve for facies K at Solider Canyon Dam for the Skull Creek.

Soldier Canyon Drainage Curve (Facies A)

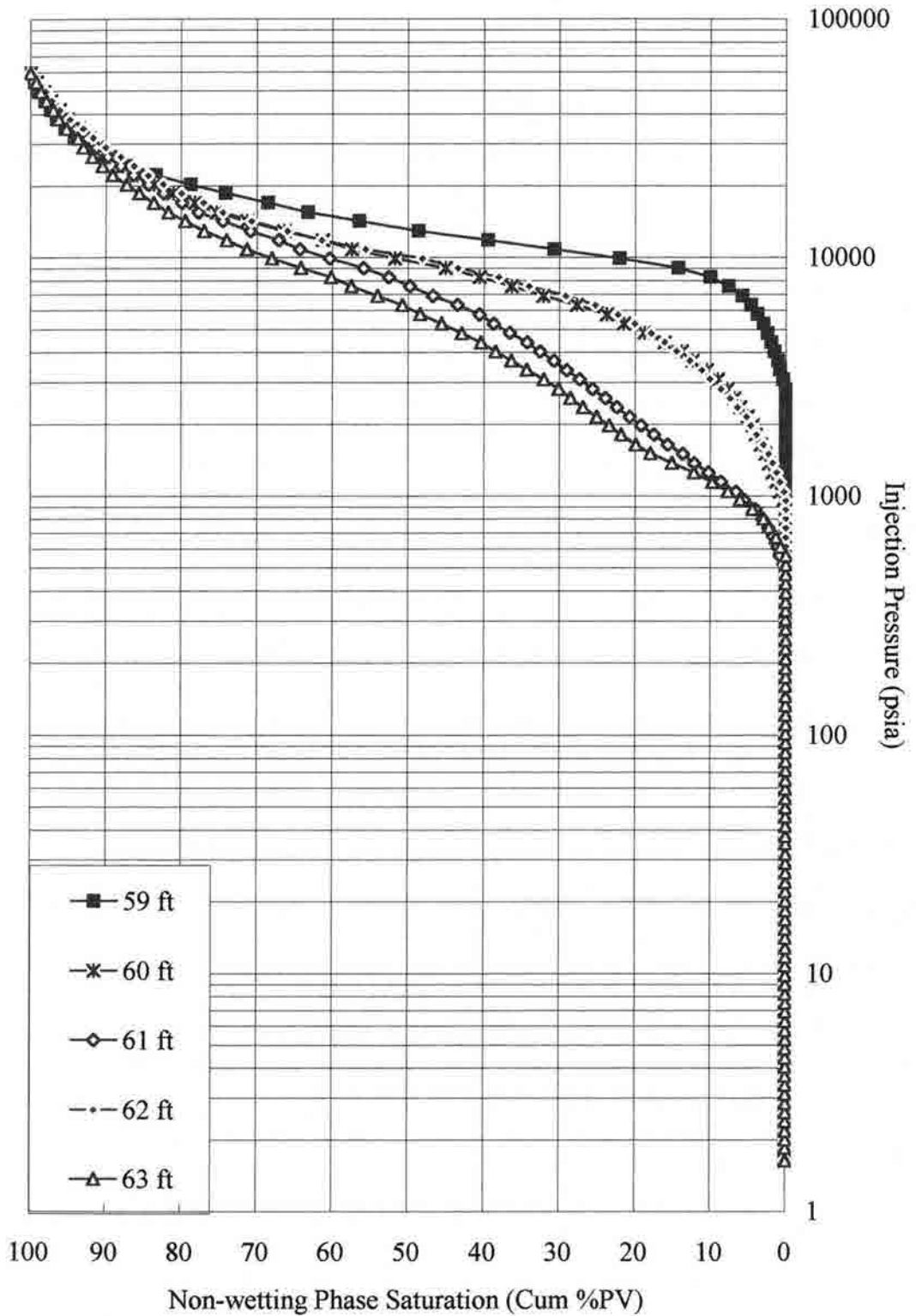


Figure 4.9b Drainage Curve for facies A at Solider Canyon Dam for the Skull Creek.

(Fig. 4.9c). Facies C has even lower entry pressures ranging from 30 to 200 psia with a very steep curve (Fig. 4.9d). The drainage curves for the horizontal sampling of facies A show significant variability within the CS, in terms of the range of psia values (5402-1211 psia) needed to intrude the pore network (Fig. 4.9e).

Appendix C shows the individual MICP graphs for the Soldier Canyon Dam samples. The first 7 pages of Appendix C are the horizontal samples of the CS, which again show variability within facies A. Overall, the median PTD ranges from one to two populations of 0.025 to 0.04 microns in size and is moderately to very well sorted. This variation in PTD can be explained by the different layers of silt, clays, and bentonites within the CS each having different entry pressures. For example, sample SCCS6 has a strong bentonite component that has significantly lowered the entry pressure needed to intrude that pore system. Bentonites would typically show one population that is very poorly sorted (broad curve) due to the clay shrinking and swelling, as seen in Appendix C. Sample SCCS2 shows two populations, one being a well-sorted silt that composes 25% of the PV (pore volume), which lowers the entry pressure. Samples SCCS1, SCCS3 and SCCS4 all show very well sorted clay (0.01 micron) PTD (pore throat diameter) populations that notably increase the entry pressure. SCCS1 has another small (30% PV) population of clay-size (<0.01 micron) PTD that makes it the best seal in the horizontal sampling of the CS, in that it requires the highest psia to intrude the pore network.

In general, facies K has more than one population of PTD with the median PTD ranging 0.015 to 0.2 microns. The PTD sorting is variable and ranges from poor to very good. This wide variety in median PTD has several different possible explanations. This sharp change in PTD may be due to a change in source area that introduces recycled and

Soldier Canyon Drainage Curve (Facies B)

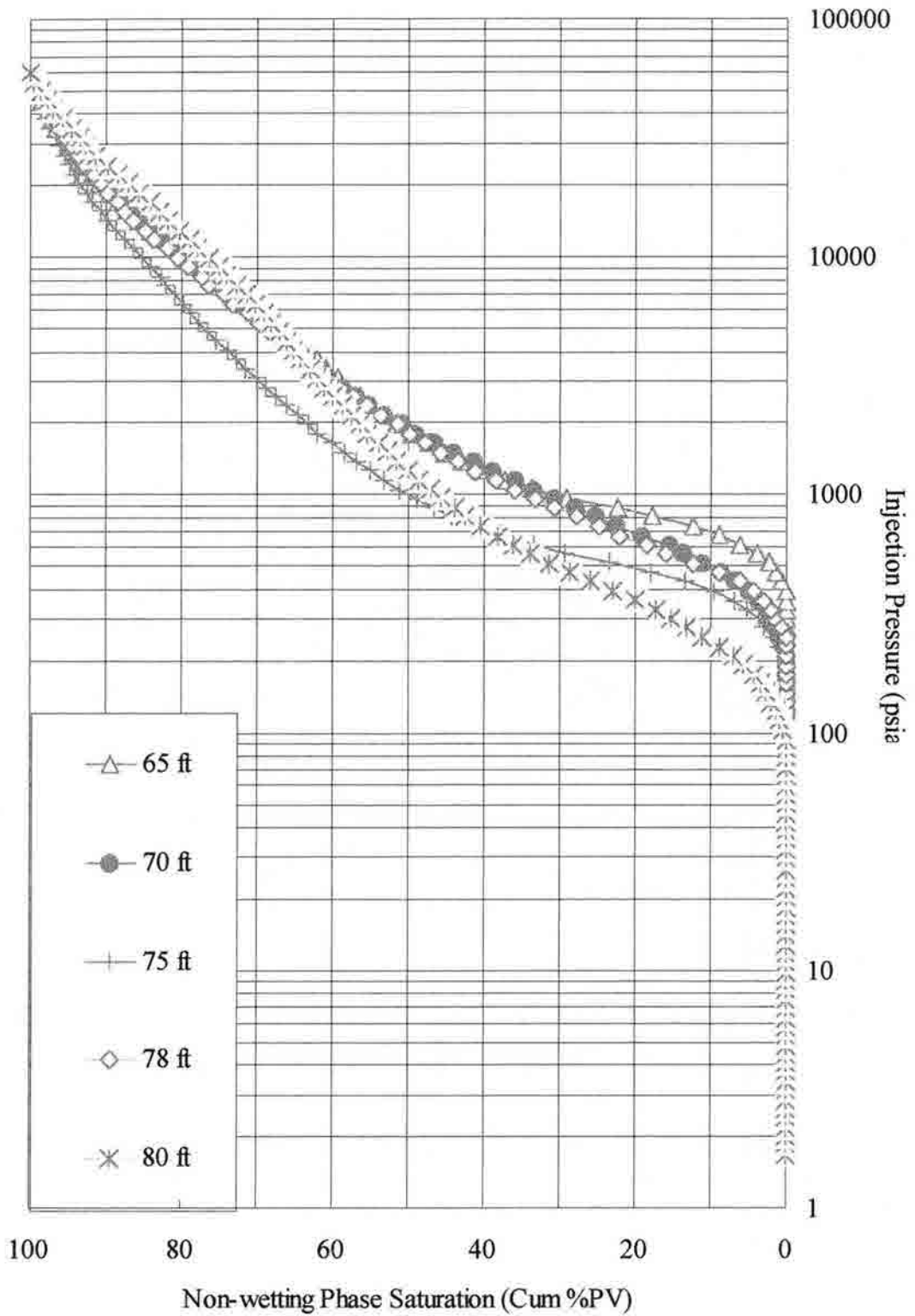


Figure 4.9c Drainage Curve for facies B at Solider Canyon Dam for the Skull Creek.

Soldier Canyon Drainage Curve (facies C)

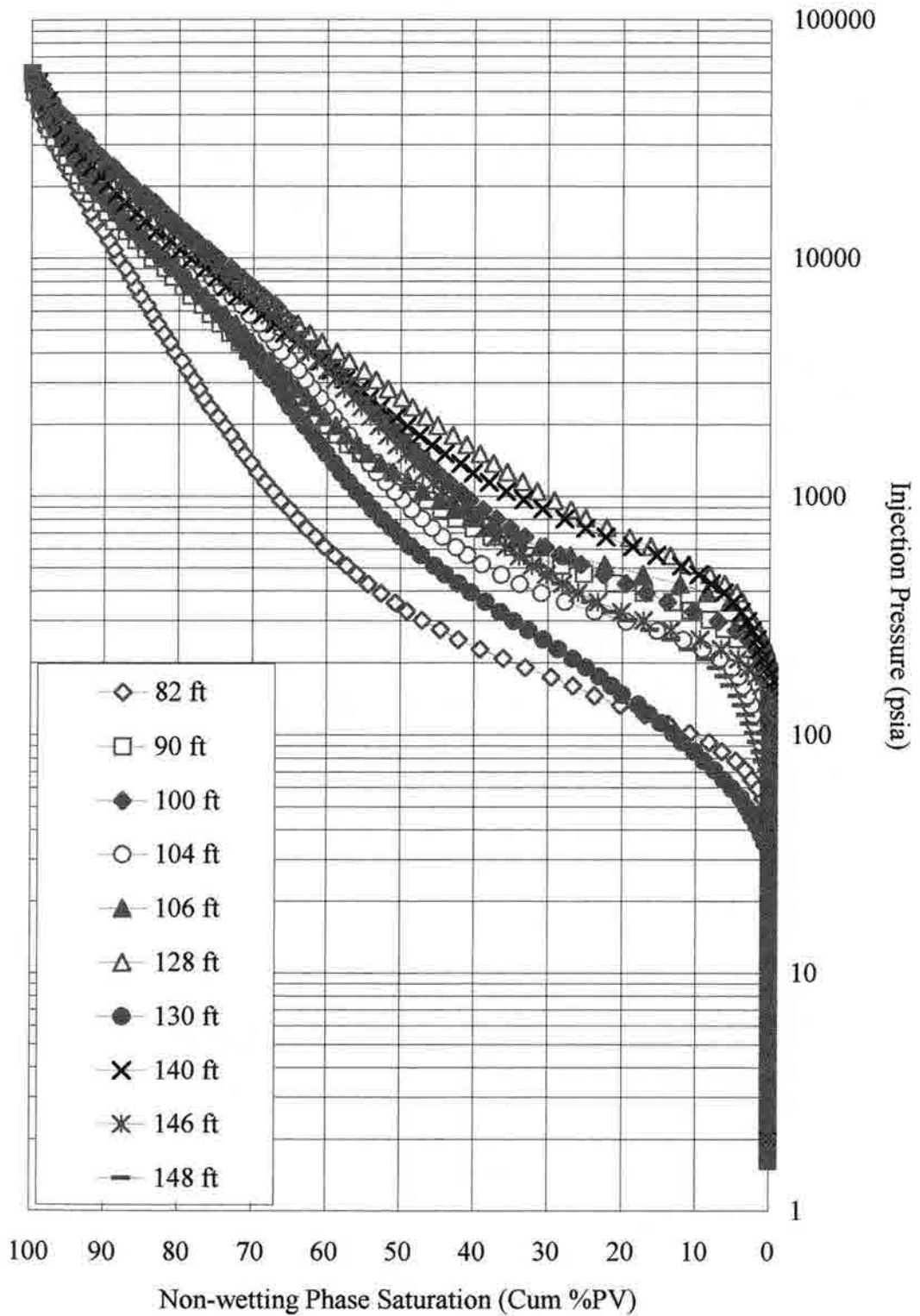


Figure 4.9d Drainage Curve for facies C at Solider Canyon Dam for the Skull Creek.

Soldier Canyon (Facies A) Horizontal Sampling Drainage Curve

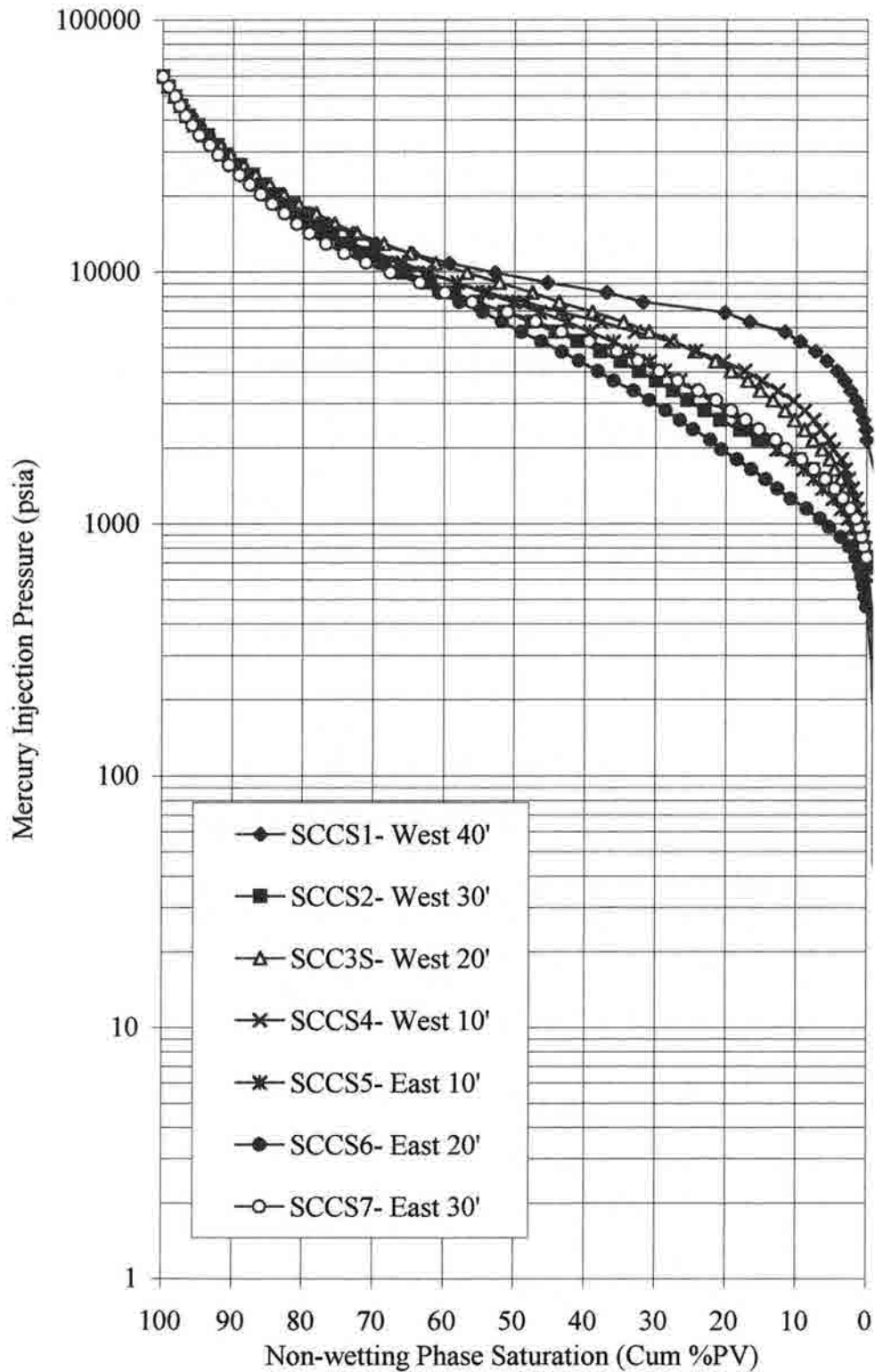


Figure 4.9e Drainage Curve for horizontal samples of facies A at Solider Canyon Dam.

unrecycled material that has a variety of pore throat diameters. The PTD sorting drastically improves at 40 and 48 ft as the best seal is reached at 50 ft with one well-sorted population with the median PTD of 0.008 microns.

The next layers with good sealing capacity are in the CS. These samples display a well-sorted, median PTD of 0.02 microns and usually have a second population of silt size spaces that compose 10% of the pore volume. At 59 ft, one well-sorted PTD population with a 0.02-micron median PTD stands out as the second best seal at Soldier Canyon Dam. Quality seals are also located at 60 and 62 ft with one population of moderately well sorted, median PTD of 0.02 microns. Samples at 61, 63 and 64 ft may have bentonite components that could increase the median PTD thus resulting in poor sorting from the shrinking and swelling.

The PTD drastically changes at 65 ft (onset of HST deposits) to 3 populations incorporating 30% of the PV into one well-sorted population with the median PTD of 0.25 microns, another 60% of the PV has the median PTD of 0.06 micron, and the remaining 10% includes a poorly sorted median PTD of 0.015 micron. The median, moderately-well sorted PTD increases at 80 ft to 0.5-0.6 microns, which comprises 30% of the PV. These samples have 2 other populations with poor to moderate sorting. It is interesting to note that the shape, size and sorting of PTD does not change at 100 ft when facies C begins. This further suggests a gradational contact between the two facies. A significant change occurs at 150 ft when 20% of the PV has a well-sorted, median PTD of 1.0 microns, 50% has poorly sorted 0.2 micron median PTD, and the remaining 30% has a poorly sorted 0.02 micron median PTD. This PTD change in the last 4 ft of the

section is probably related to modern day weathering between the top of the Skull Creek and the bottom of the Fort Collins member of the Muddy Sandstone.

4.4 Summary

The best seal delineated by MICP is located in the upper parts of the TST deposits, in particular facies K, which is below the CS. However, the CS does contain rocks with potential seal properties. The following is a list of characteristics displayed by the rock with the highest sealing properties:

1. Located at 50 ft, which is stratigraphically below the CS.
2. 1% total organic carbon content (not the highest).
3. Type III (terrestrial) organic matter.
4. No continuous laminations or fossils in hand sample.
5. Density value of 2.58 g/cc.
6. 11% porosity with 0.0003-md permeability.
7. No notable bioturbation, fossils or matrix porosity in thin section.
8. Point count data with 62% clay, 36% quartz, 2% organic matter, and no visible pyrite or carbonate.
9. XRD data with 60% clay, 28% quartz, 6% feldspars, 2% siderite and no calcite, dolomite or pyrite detected.
10. Clay mineralogy consists of 48% R0 illite/smectite, 42% illite, 9% kaolinite, with trace amounts of chlorite.
11. 11,000 psia at 10% mercury saturation.
12. One well-sorted PTD population with a median PTD of 0.008-micron.

Figure 4.10 shows the histograms for the injection pressures at 10% mercury saturation for each facies grouped into columns of 2000 psia. Facies K has one sample in the 12,000 column and one in the 8,000 column. Facies A has one sample in the 10,000 column and one in the 6,000 column. Facies B and C have all their samples in the 2,000 column.

Soldier Canyon (Skull Creek) Distribution of Injection Pressures at 10% sat.

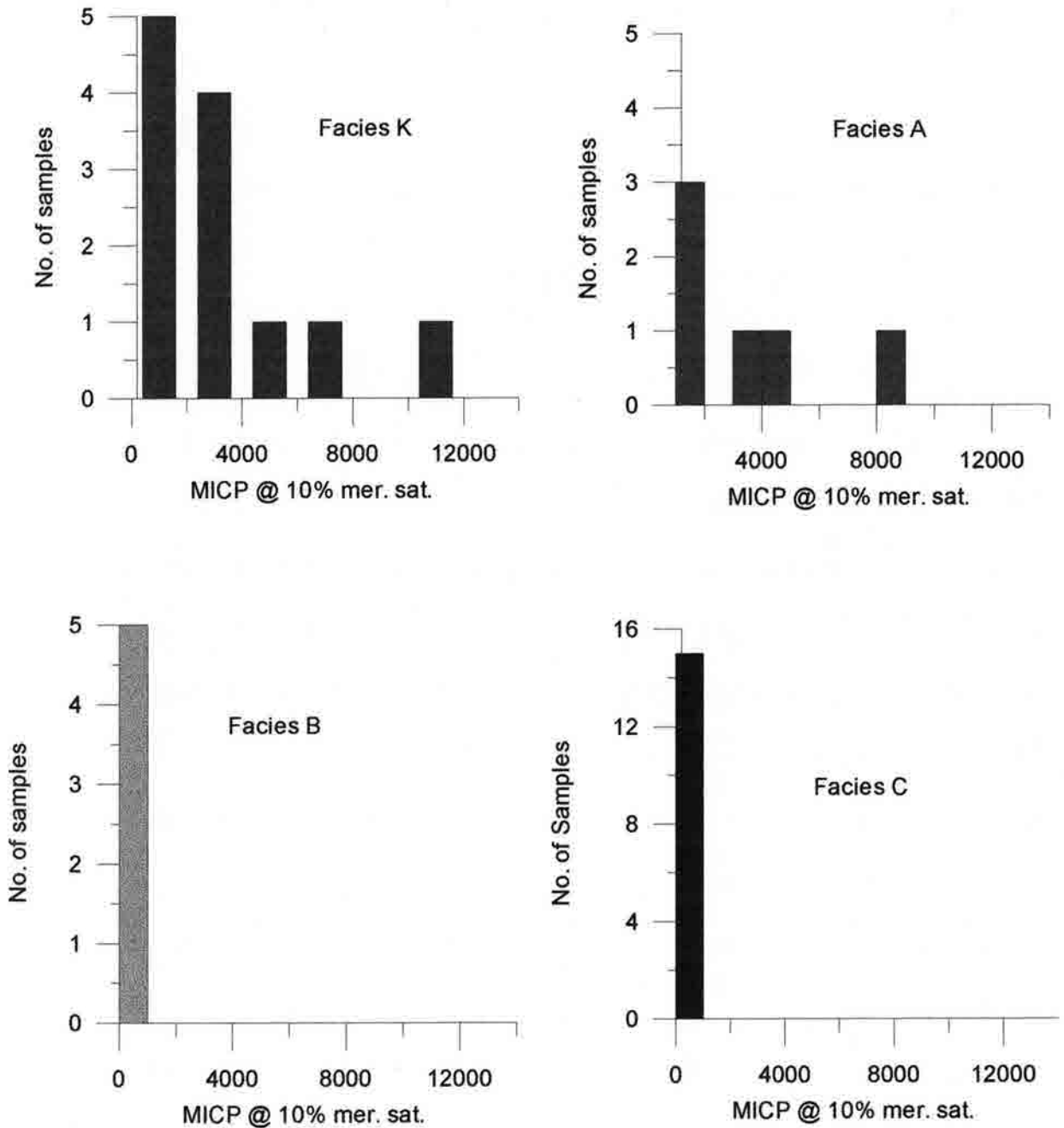


Figure 4.10 Soldier Canyon Dam Histograms for the MICP @ 10% Mercury Saturation (psia).

Chapter 5. BELLEVUE (SKULL CREEK SHALE) OUTCROP RESULTS

5.1 Facies Description

At the Bellevue outcrop, a 130-ft section of the Skull Creek was measured and gamma ray logged (Fig. 5.1). No distinct contacts were evident with the underlying Plainview Formation or the overlying Muddy 'J' Sandstone (Dolson, 1985). This outcrop has been heavily weathered, making the individual facies more difficult to distinguish in outcrop. All the facies designated for the Skull Creek in this study (K, A, B, and C) are present. The outcrop gamma ray does not show much difference between the TST and HST deposits but seems to respond strongly to the bentonites as seen in Figure 5.1.

The lowest 49-ft of the exposed outcrop belongs to Facies K (Fig. 5.2a). In hand sample, this dark grayish-black shale weathers light brownish-gray and has flaggy to platy parting. Splintery gypsum has been deposited along jointing planes, where it joins other weathering products such as Fe-oxides and yellowish clays (possibly jarosite) (Fig. 5.2b). At Bellevue facies K has six bentonites, which is significantly more than Soldier Canyon. As at Soldier Canyon, the Bellevue facies K has type III (terrestrial) kerogen but is stratigraphically thicker at Bellevue (Fig. 5.2c).

Facies A could not be distinguished in outcrop because it is covered (Fig. 5.3). Since a condensed section represents the maximum transgression in a marine environment, (Van Wagoner et al., 1988) type II organic matter could be used to

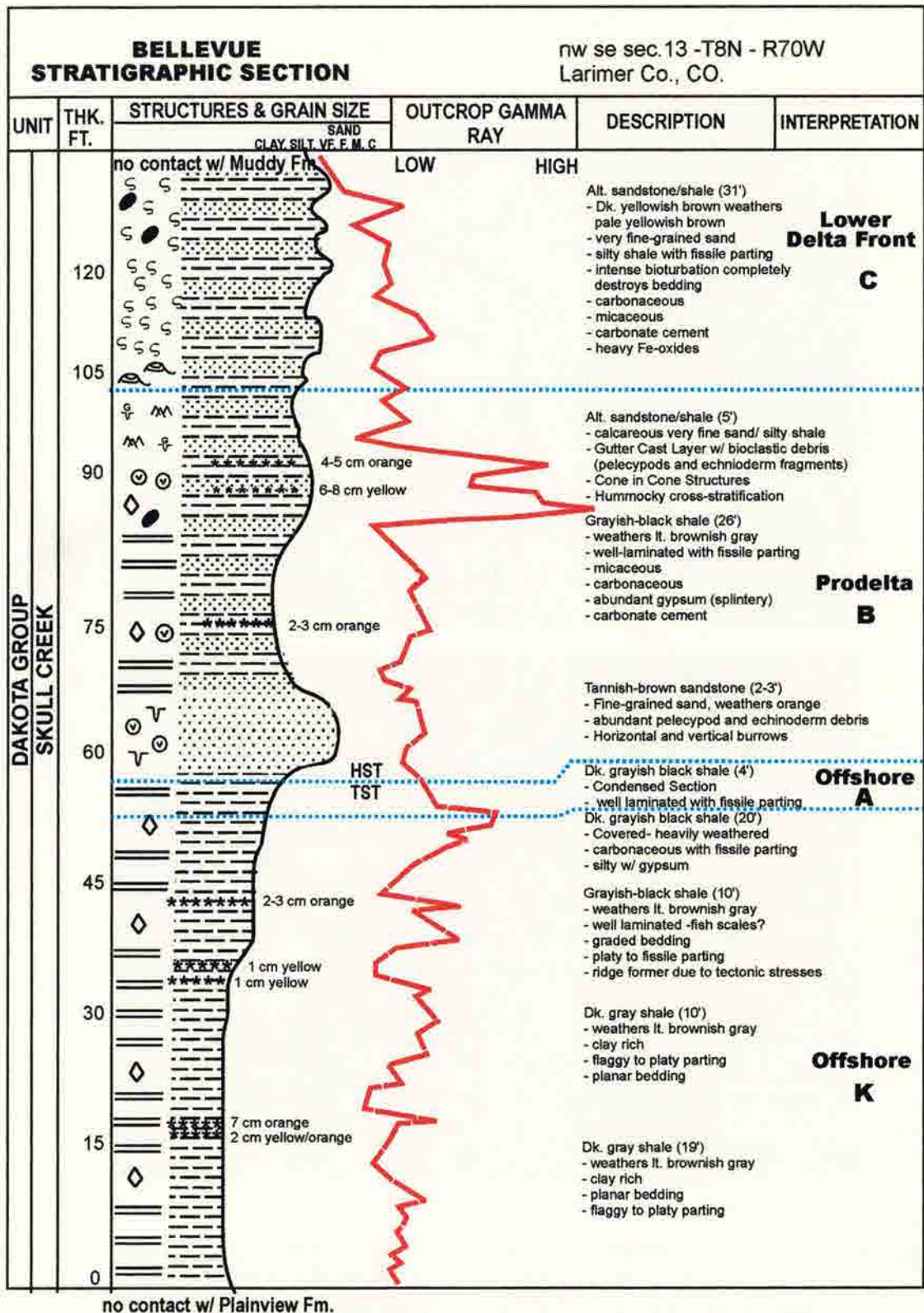


Figure 5.1 Stratigraphic column for Bellevue Outcrop, including detailed descriptions, interpretations, and logged outcrop gamma ray.

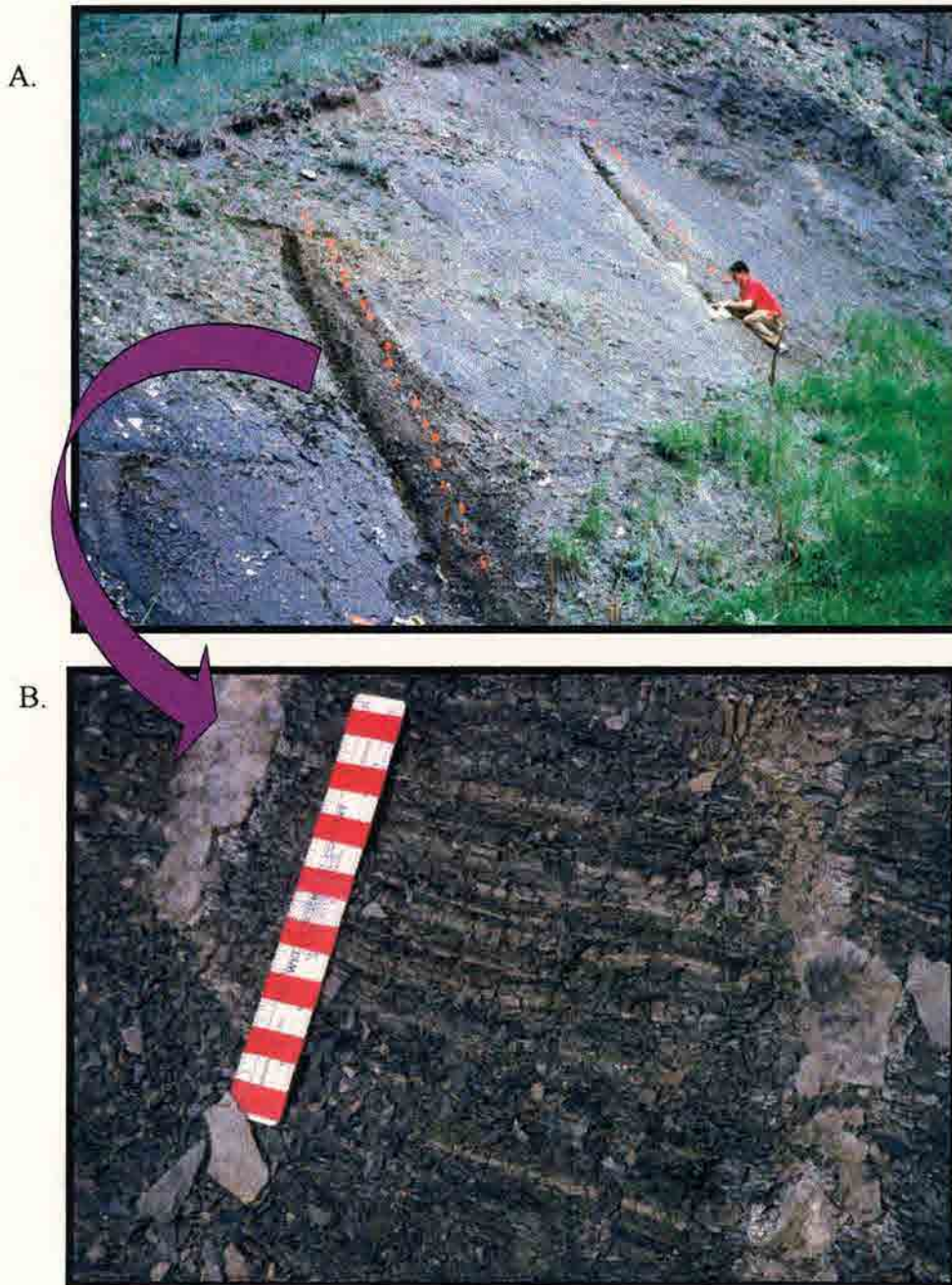


Figure 5.2 A) Overall view of moderately weathered shale with platy parting; B) close-up view of gypsum along the jointing planes of fissile shale. C) Van Krevelen diagram showing type III (terrestrial) organic matter. 1-ft ruler for scale, each increment marks a centimeter, Flags mark sampling every foot.

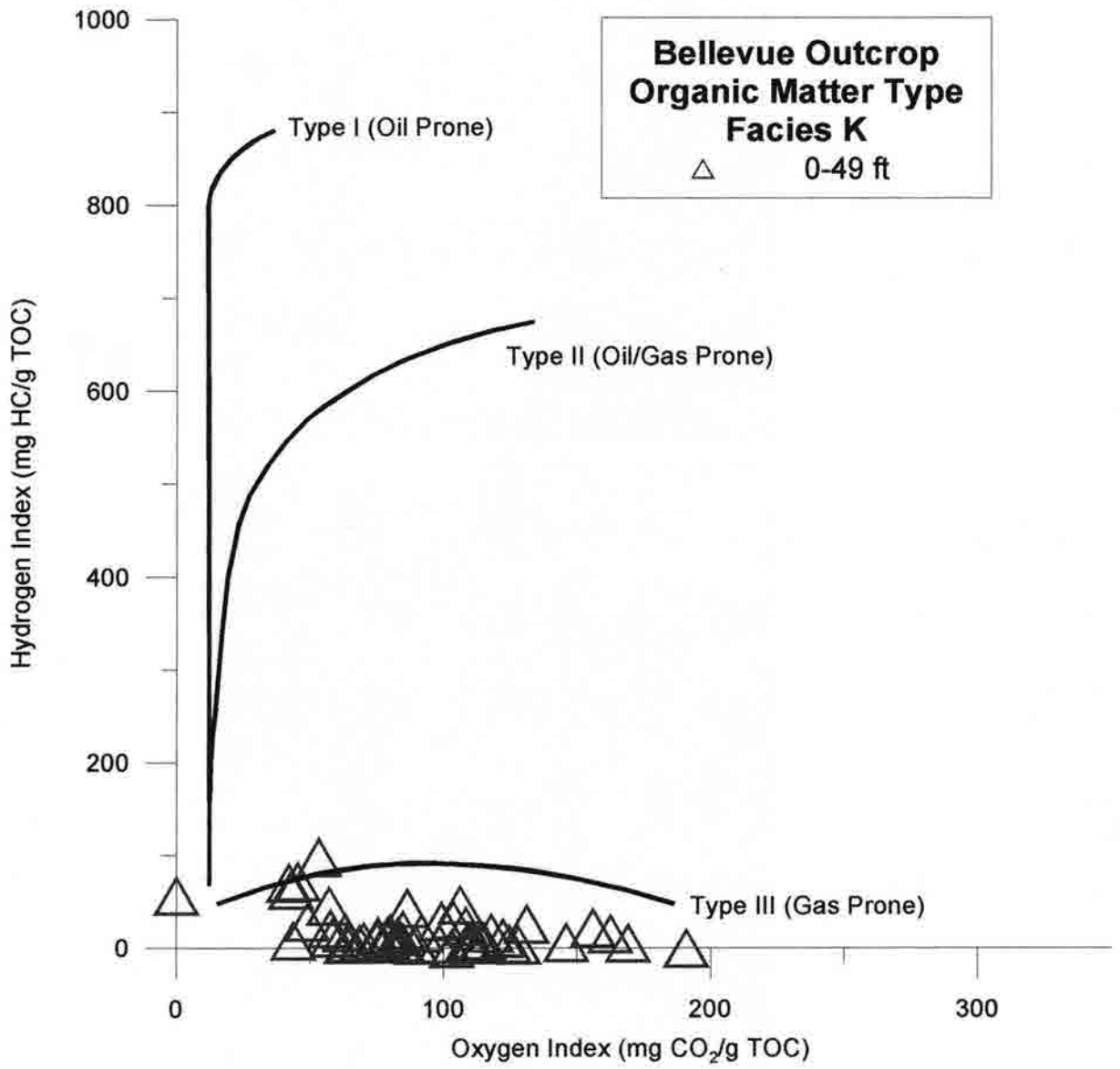


Figure 5.2 C.

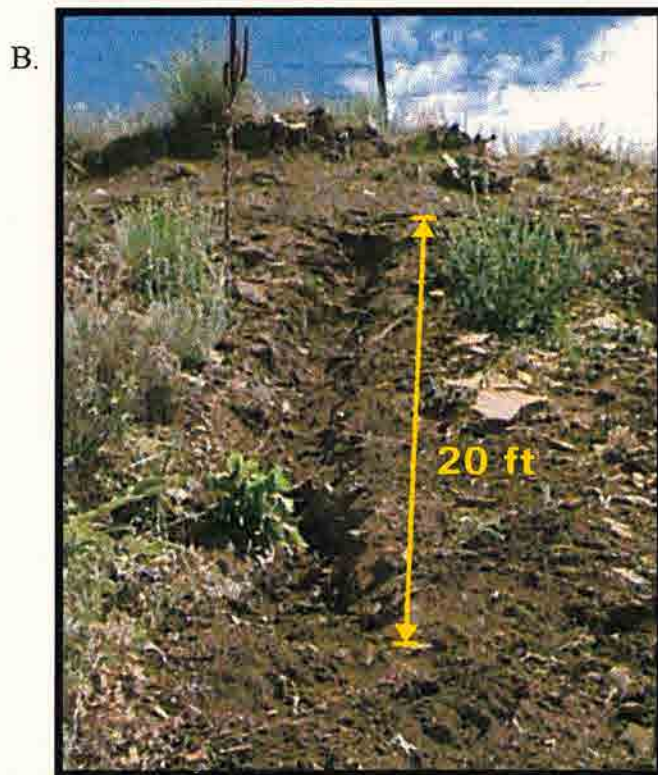
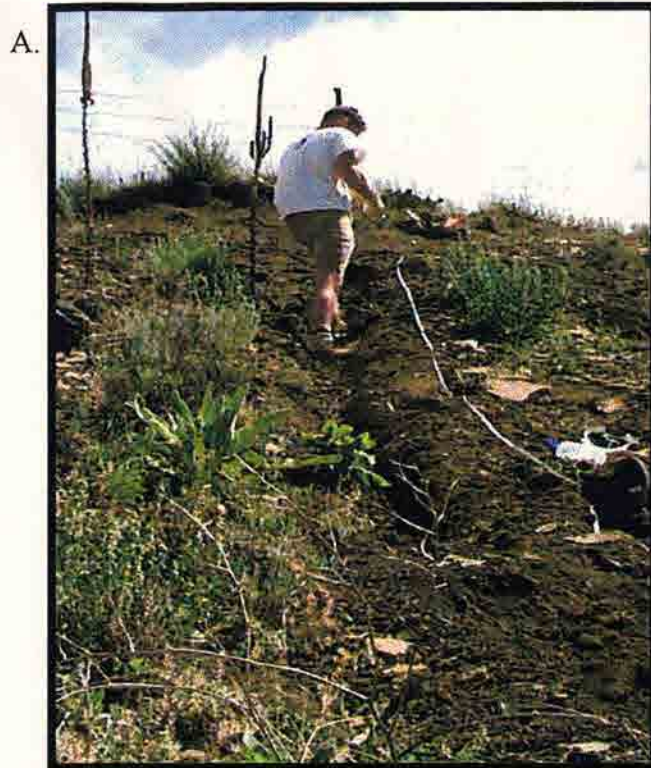


Figure 5.3 A) Overall view of heavily weathered, well-laminated shale; B) closer view of the collapsible nature of shale with sheetlike parting; C) Van Krevelen diagram of organic matter for facies A. Trench is 20 stratigraphic feet as seen in both pictures.

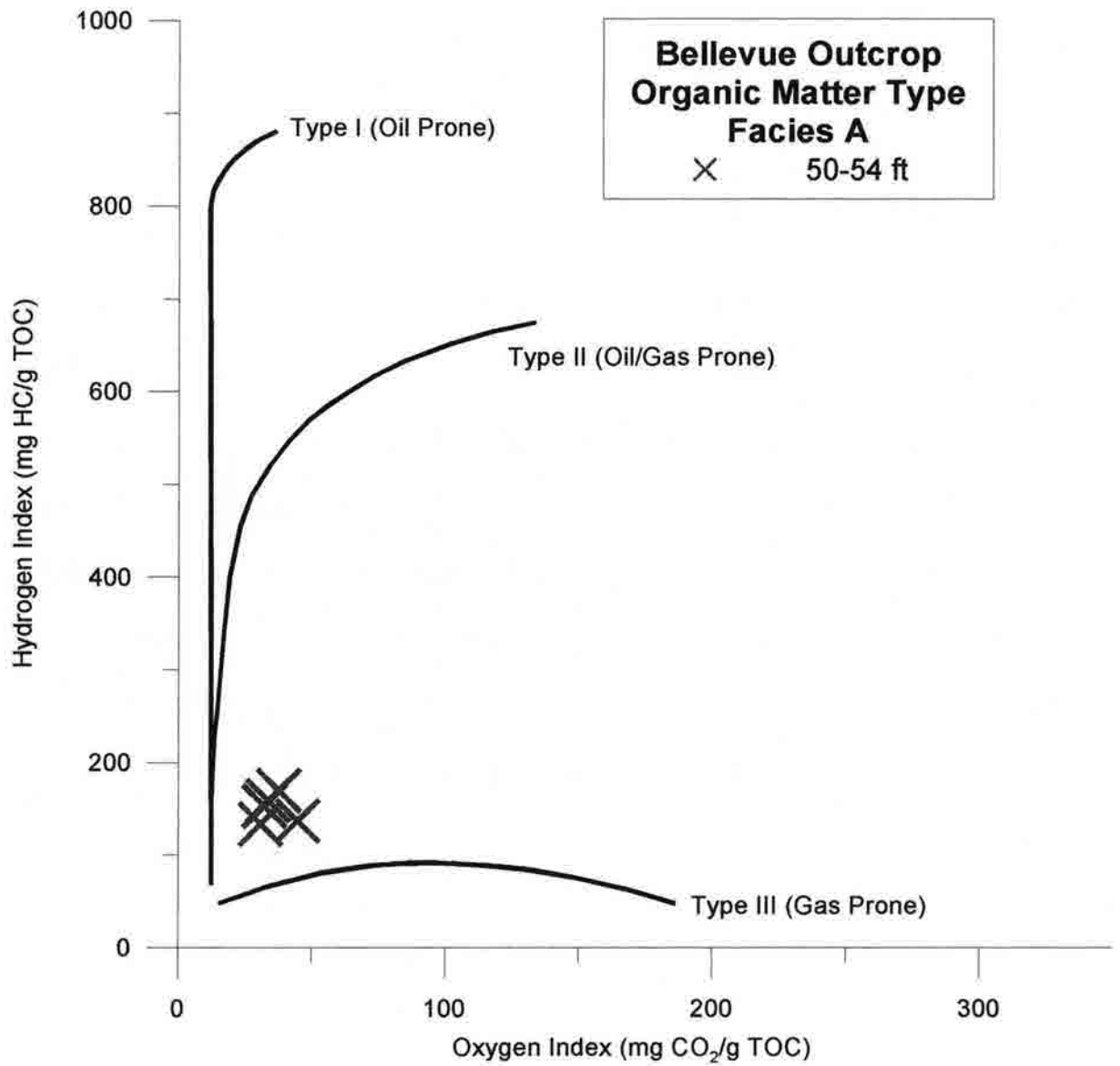


Figure 5.3 C.

classify this condensed section. However, it is not possible to determine whether the organic matter is type I, II, or III on the Van Krevelen diagram. The boundaries for this condensed section lie under the fossiliferous sandstone layer that marks the beginning of the HST deposits, which correlates with the position of the CS at Soldier Canyon Dam. This well-laminated shale is very fissile and easily collapses in outcrop. Silt laminations are not as prominent as in the CS at Soldier Canyon.

The onset of highstand deposits is clearly shown in the grayish-black alternating sandstone/shale layers of facies B. Hummocky bedding is beautifully displayed as seen in Figure 5.4a. Surfaces scoured into the shale are filled with sand and interpreted to be “gutter-casts” layers that were generated by storms (Fig. 5.4b). Cone-in-cone structures are found near the gutter cast layers, and are interpreted to be a pressure solution phenomenon. This unit has type III (terrestrial) organic matter (Fig. 5.4c). Facies B is stratigraphically thicker than at Soldier Canyon.

Facies C is stratigraphically thinner than at Soldier Canyon (Fig. 5.5). Facies C has alternating layers of dark-yellowish brown sandstone and shale that have undergone intense bioturbation, and are characterized by type III (terrestrial) kerogen.

5.2 Lithology Description

Table 5.1 summarizes the data for each of the facies at Bellevue. Facies A averages the highest percent of total organic carbon and total clay with the lowest permeability. The TST deposits (facies K and A) have lower permeability and higher porosity than the HST deposits. However, the mineralogy of facies B is not that different from facies A and K. Facies K averages 48% total clay while facies B has slightly less total clay with 46%. Facies B has the second highest total organic carbon, and averages

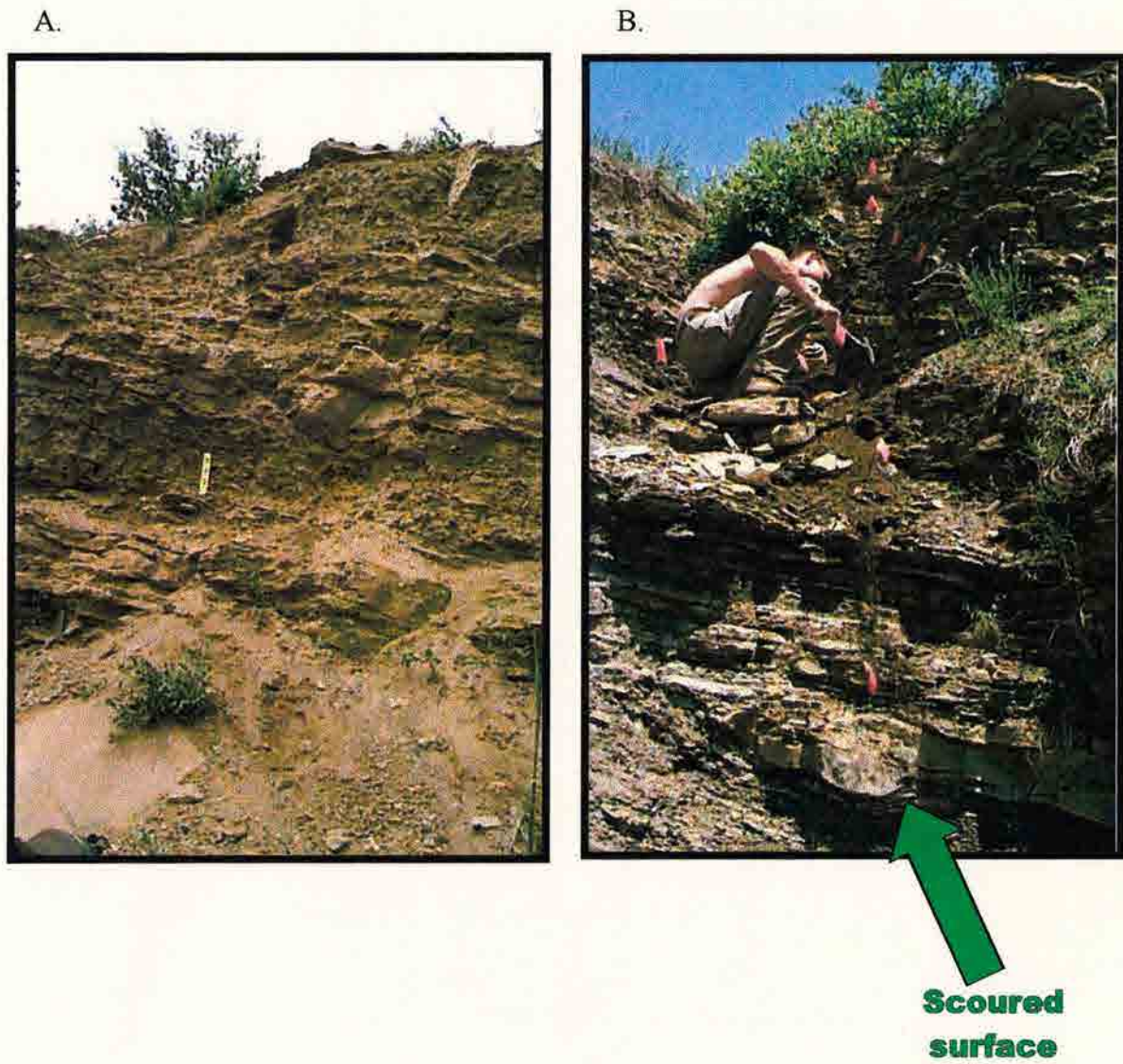


Figure 5.4 A) Overall view of hummocky bedding in alternating shale and sandstone; B) "gutter-cast" layer shows a scoured surface in shale filled in by sandstone; C) Van Krevelen diagram type II-III organic matter for facies B. 1-ft ruler for scale, flags mark sampling every 2 feet.

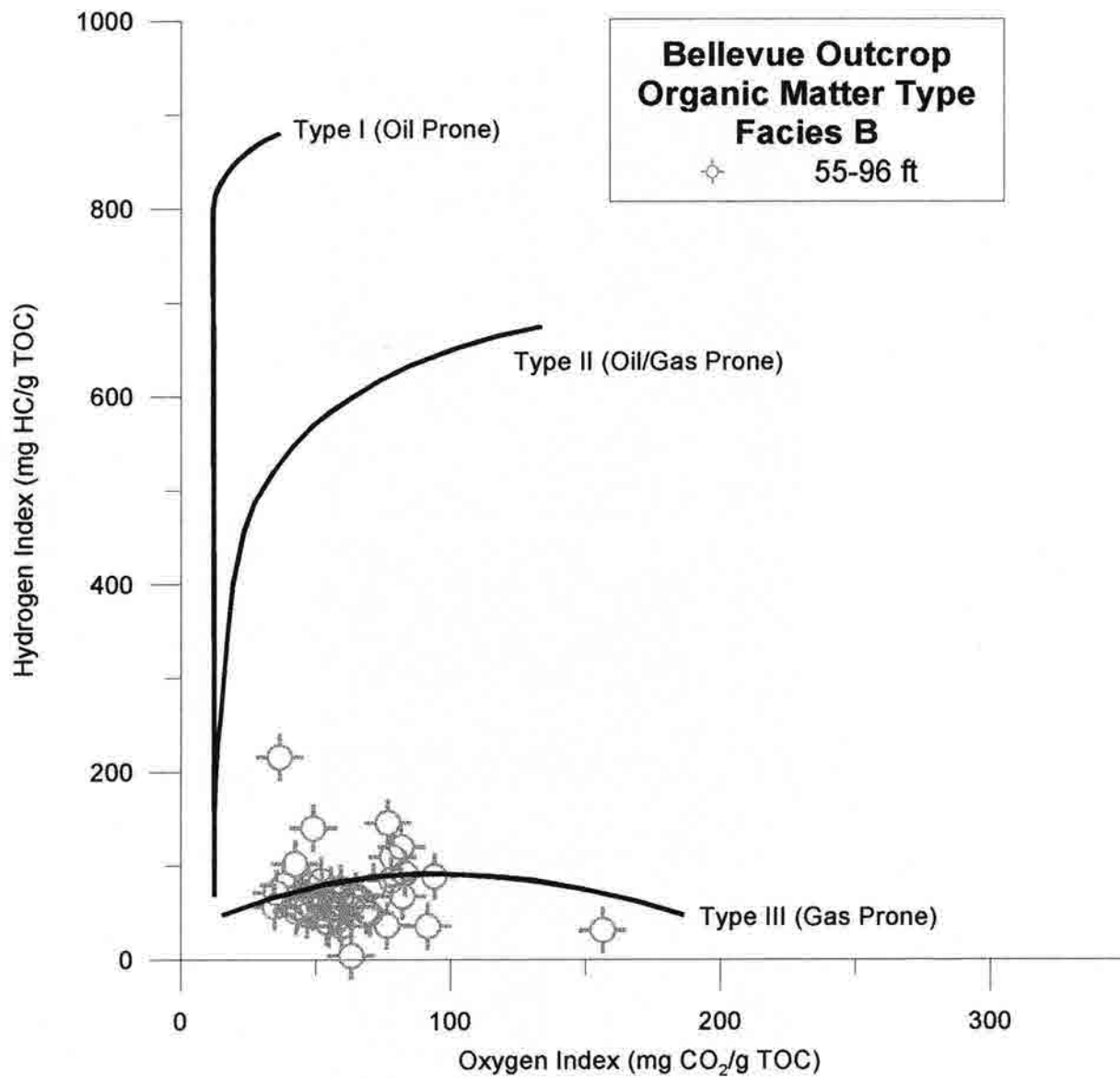
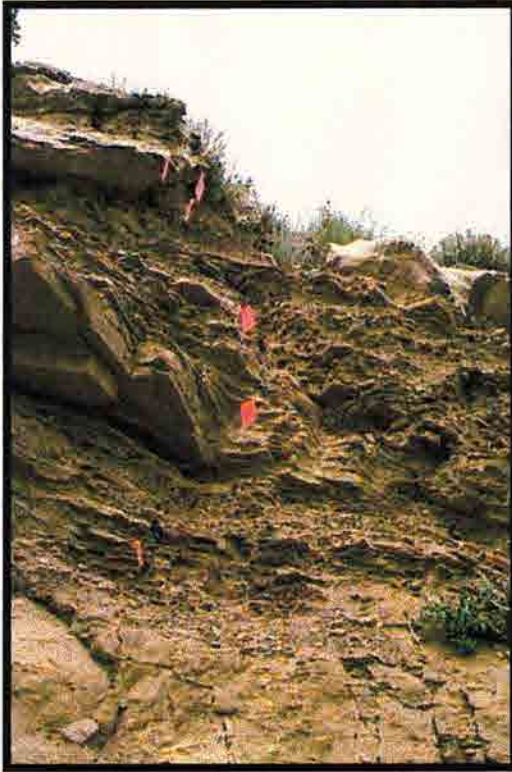


Figure 5.4 C.

A.



B.



Figure 5.5 A) Overall view of bioturbated, alternating shale and sandstone; B) close-up view of well-developed bedding of alternating shale and sandstone; C) Van Krevelen diagram type III (terrestrial) organic matter for facies C. 1-ft ruler for scale, flags mark 2-ft sampling increments.

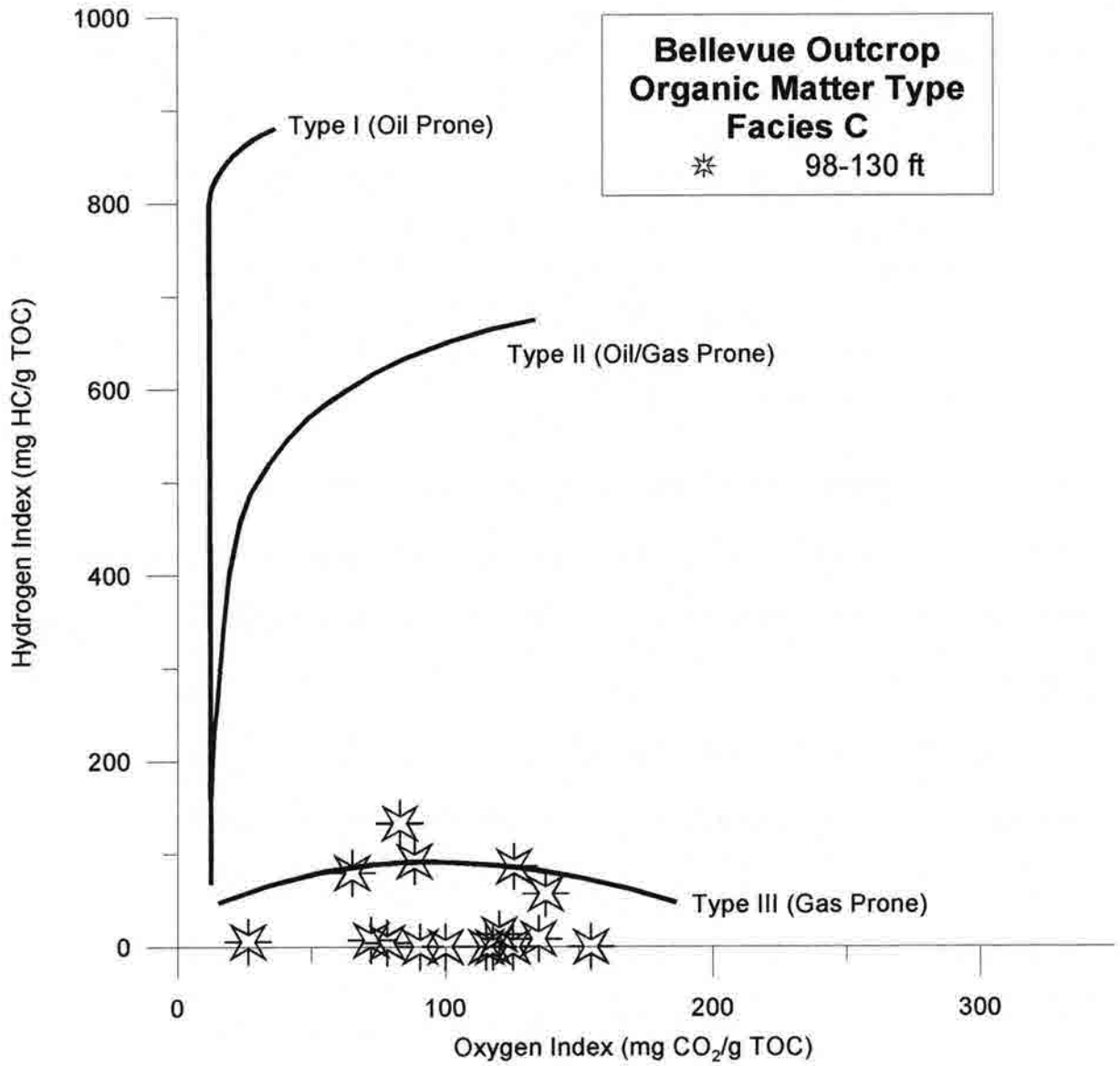


Figure 5.5 C.

Table 5.1 Statistics of Bellevue Outcrop Data

Facies		Total Organic Carbon (%)	Hydrogen Index (mg HC/g TOC)	Hydrogen Index/Oxygen Index (mg HC/mg CO ₂)	Total Clay (wt %)	Quartz (wt %)	Feldspar (wt %)	Carbonate (wt %)	Porosity (%)	Permeability (md)	Density (g/cc)
	# of Analyses	50	50	48	11	11	11	11	10	10	10
K	Average	0.84	19	10	48	46	6	0	15.4	0.014	2.63
	Std Dev	0.37	21	9	15	13	2	0	2.2	0.022	0.05
	# of Analyses	5	5	5	1	1	1	1	1	1	1
A	Average	2.90	150	0	53	42	5	0	18.1	0.0040	2.58
	Std Dev	0.41	15	0							
	# of Analyses	41	41	41	9	9	9	9	8	8	8
B	Average	1.28	71	1	46	43	5	6	13.2	0.027	2.66
	Std Dev	0.66	37	2	16	11	2	6	4.7	0.03	0.05
	# of Analyses	17	17	10	2	2	2	2	7	7	3
C	Average	0.54	29	6	19	58	6	19	11.2	0.038	2.73
	Std Dev	0.55	43	6	3	6	1	2	3.5	0.036	0.01

6% more carbonate than the TST deposits. On average the lowest permeability is found in facies A, K, and B respectively. Facies C has dramatically more quartz and carbonate than facies K, A, or B. The rocks of facies C are also considerably more permeable and dense.

This data has been plotted against stratigraphic height to permit comparison to seal capacity, as measured by MICP (Fig. 5.6). The best seals are located in facies K (Fig. 5.6a) at 4 ft, 9 ft and 40 ft. Porosity is variable throughout both the TST and HST deposits (Fig. 5.6b). The lowest permeability values are in facies K and correspond with the highest seal capacity (Fig. 5.6c). Overall, the TST deposits are less dense than the HST deposits (Fig. 5.6d).

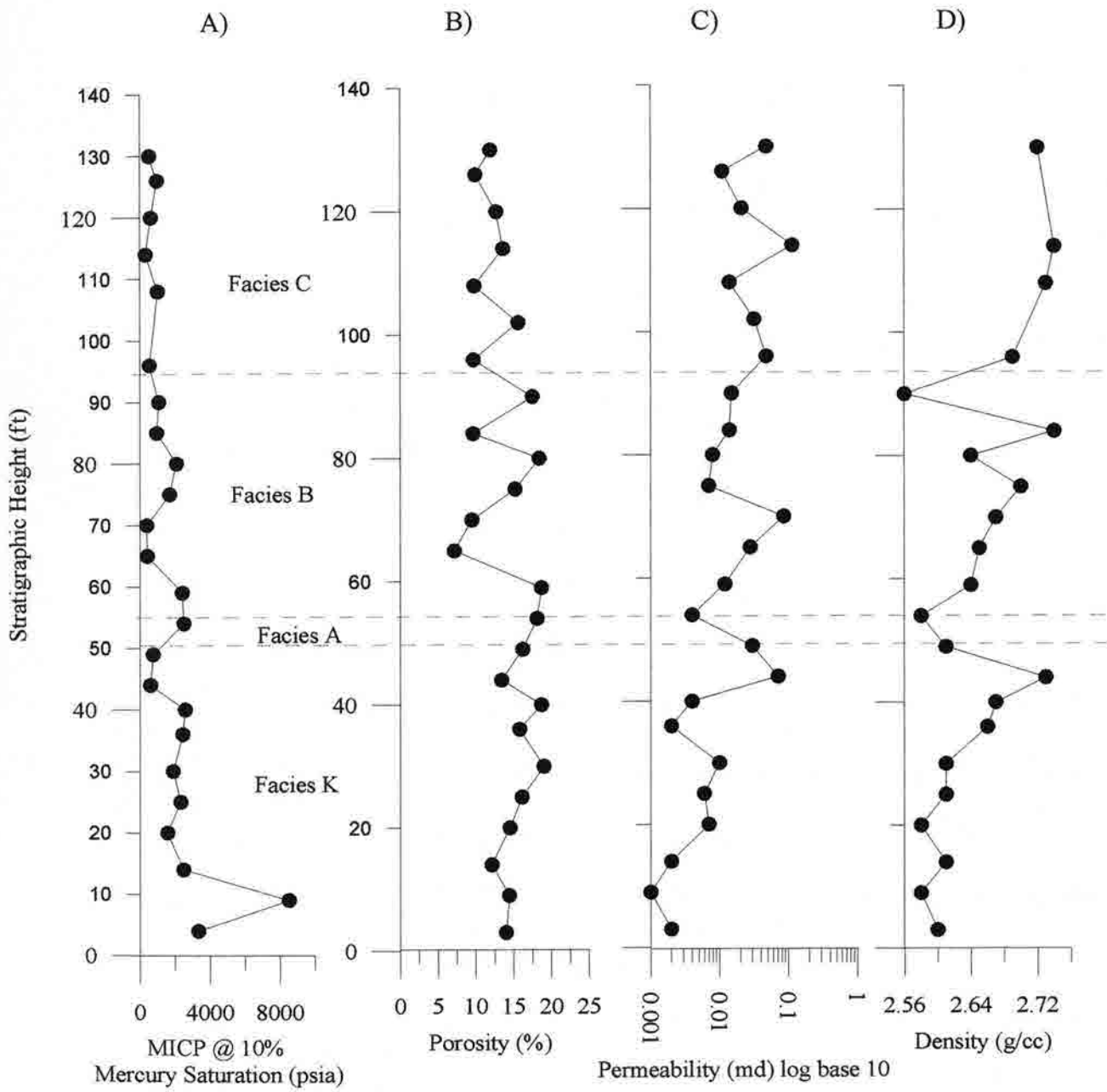


Figure 5.6 Stratigraphic height versus MICP (A), porosity (B), permeability (C), and density (D) at the Bellevue Outcrop for the Skull Creek.

The amount of total clay does not vary significantly between the TST and HST deposits, the spike in facies K is caused by a clay rich bentonite (Fig. 5.7a). Quartz shows an inverse relationship to clay (Fig. 5.7b). The amount of feldspar varies and shows a sharp decrease in the bentonite at 42 ft (5.7c). Carbonate is clearly higher in the HST deposits (Fig. 5.7d).

The greatest amount of TOC is found in facies A, (Fig. 5.8a) and also corresponds to high hydrogen index values (Fig. 5.8b). The HST deposits also show some spikes in high TOC and HI values. The ratio of HI/OI shows a corresponding peak to the HI (Fig. 5.8b) in facies K and A. Detailed organic geochemistry for the Bellevue outcrop is presented in Appendix P.

Thin Section Petrography

The thin section petrography data are displayed in Table 5.2 and Appendix D includes the thin section photomicrographs. The lowest exposed section of facies K is a carbonaceous mudstone. Point count analysis shows one sample to have 71% clay, 21% quartz, and minor amounts of organic matter, authigenic carbonate, pyrite and mica. Hematite staining is common throughout these thin sections, in addition to authigenic framboidal pyrite and altered siderite. The hard grains (quartz, feldspar) are well sorted, silt size, and spherical. No laminations are present, except for small wispy laminations of organic matter. Facies K becomes more laminated from 20-50 ft and is classified as a silty shale with a dramatic increase in quartz grains. No matrix porosity is evident throughout this facies.

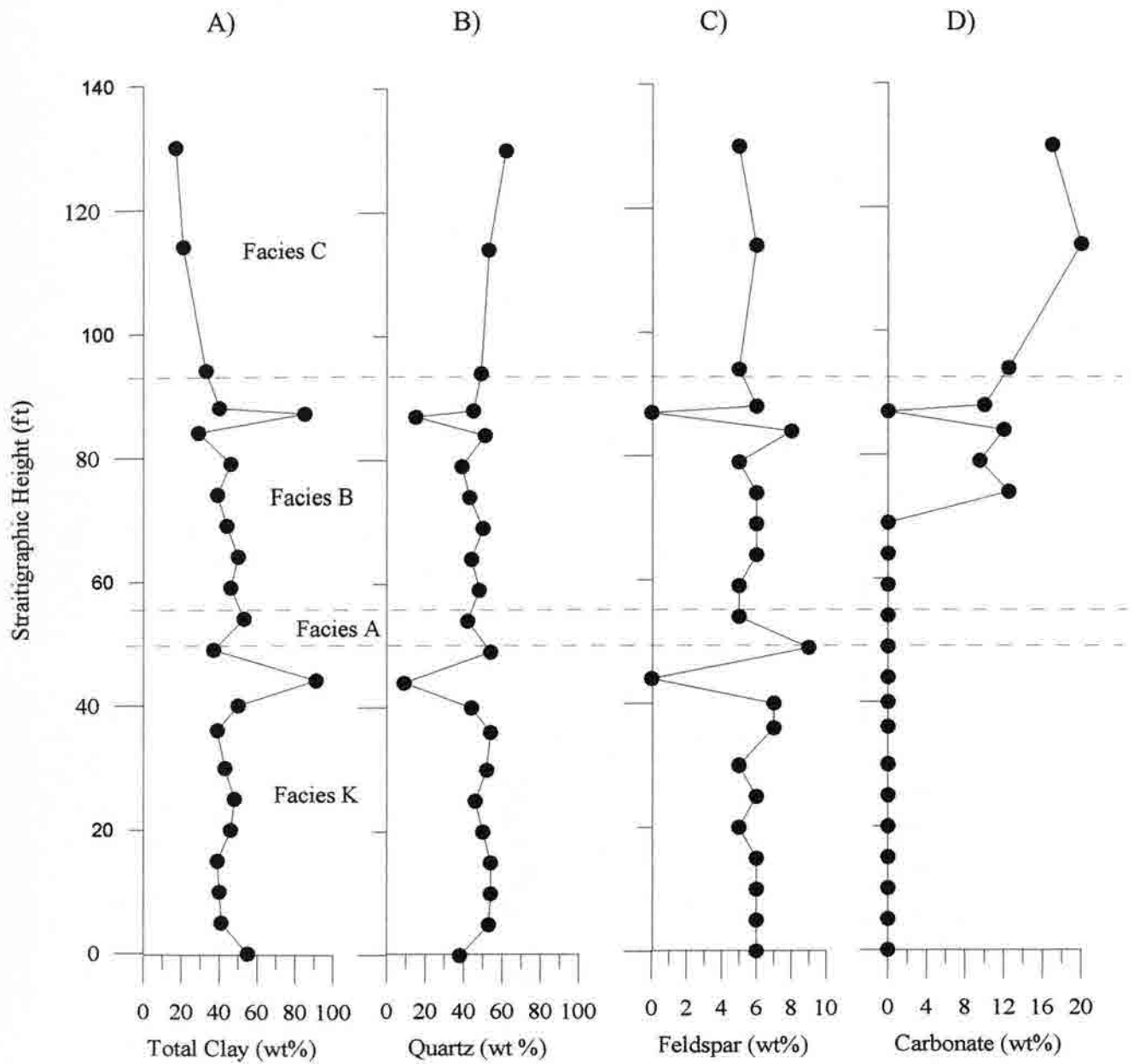


Figure 5.7 Stratigraphic height versus total clay (A), quartz (B), feldspar (C), and carbonate (D) at the Bellevue Outcrop for the Skull Creek.

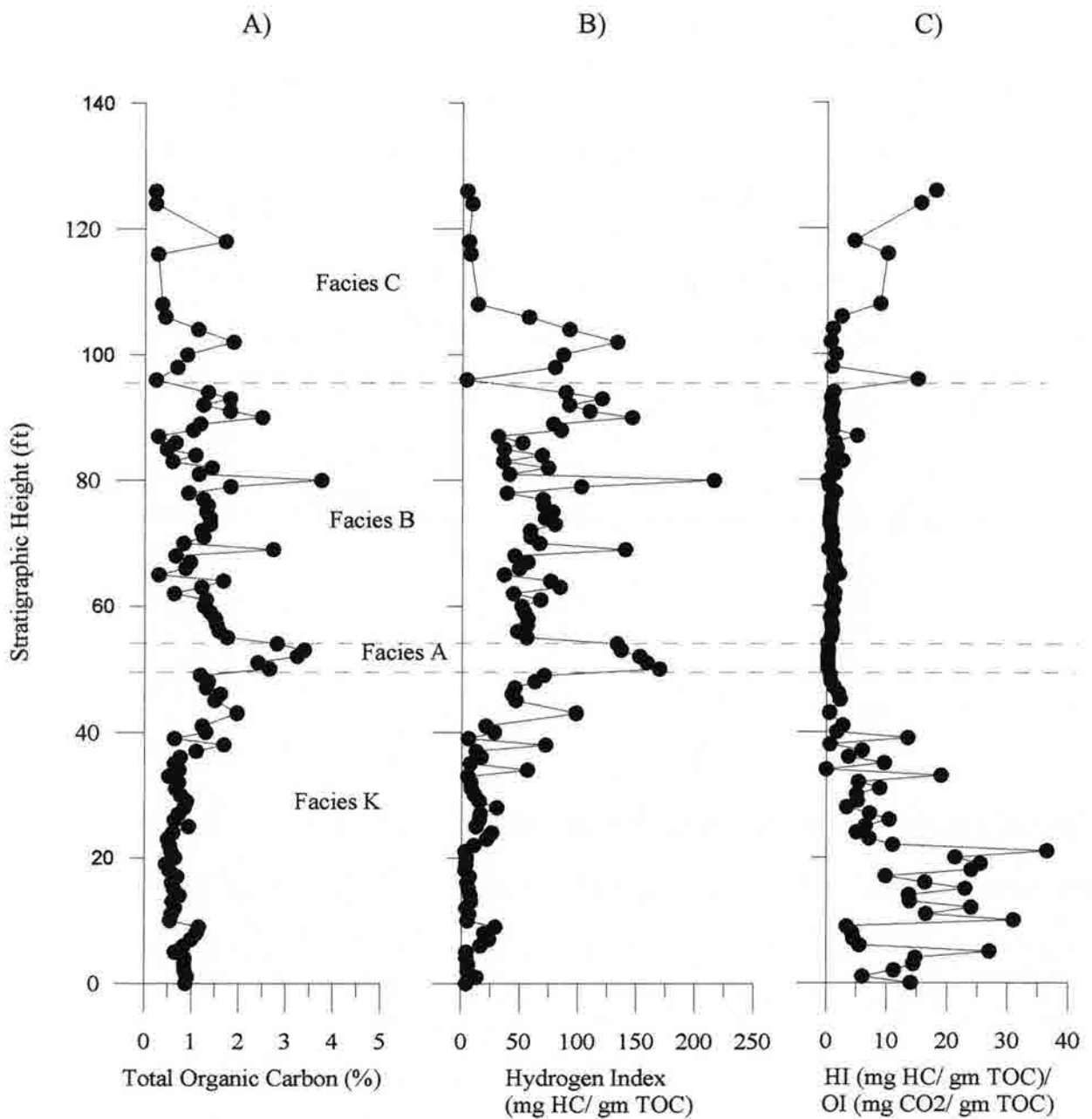


Figure 5.8 Stratigraphic height versus TOC (A), Hydrogen Index (B), Hydrogen Index / Oxygen Index (C) at the Bellevue outcrop for the Skull Creek Shale.

Table 5.2 Bellevue Thin Section Petrography

Facies	FT	Rockname	Avg. Grain Size (μ)	COMPOSITION						Laminations	Bioturbation	Pressure Solution	Fossils	Porosity
				QTZ	CLAY	ORG	CARB	PYR	OTHER					
C	108	siltstone	35	56	33	1	8	2	mica	Y	Y	Y	N	5%
B	94	siltstone	32	55	36	1	6	2	mica	N	Y	Y	N	N
B	87	bentonite	30	14	80	0	5	1	mica	N	N	N	N	N
B	69	siltstone	34	42	50	3	4	1	mica, feld	Y	N	Y	Y	N
A	59	silty shale	41	34	61	3	2	0	mica, feld	Y	N	Y	N	N
K	44	silty shale	27	37	60	3	0	0	mica, feld	Y	N	Y	N	N
K	30	silty shale	31	40	54	2	3	1	mica, feld	Y	N	Y	N	N
K	20	silty shale	39	50	43	2	3	2	mica	Y	N	N	N	N
K	5	mudstone	36	21	71	3	3	2	mica	N	N	N	N	N
K	3	mudstone	40	22	72	3	3	0	mica	N	N	N	N	N

*NOTE: Point count percentages are in bold, other percentages are estimates.

**NOTE: 1/256 < silt < 1/16 mm, 1/16 < VF sand < 1/8 mm, 1/8 < F sand < 1/4 mm, 1/4 < M sand < 1/2 mm

LEGEND:

QTZ= Quartz

ORG= Organic Matter

CARB= Carbonate (calcite, dolomite, siderite)

feld= Feldspar

phos= Phosphate

mic= Mica

hem= Hematite

Facies A is a strongly compacted, carbonaceous, silty shale. The one sample examined contains 61% clay, 34% quartz, 3% organic matter, 2% authigenic carbonate (specifically siderite) with secondary amounts of mica and no pyrite. The hard grains (quartz and feldspar) are well sorted, subrounded, spherical, and the size of silt to very fine sand. Wispy laminations of organic matter are present. Microscopic scoured surfaces in the clay matrix have been infilled with silt. No bioturbation or matrix porosity is detected.

Facies B is strongly compacted, carbonate-cemented, carbonaceous, interbedded siltstone and shale. The mineralogy of this rock is 42% quartz, 50% clay, 3% organic matter, 4% authigenic siderite with some phosphatic debris. The quartz grains are well

sorted, subrounded, spherical, and silt-size. Wispy laminations of organic matter are present, in addition to larger laminations of silt and clay. Some burrowing has occurred in this overall well-laminated shale. No matrix porosity is evident.

A strongly compacted, carbonate-cemented, carbonaceous, interbedded siltstones and shales are also common to facies C. Point count analysis for one sample shows 56% quartz, 33% clay, 1% organic matter, 8% authigenic carbonate, and 2% pyrite. Bioturbation has destroyed most of the clay laminations. Wispy laminations of organic matter are present. The quartz grains are well sorted, subrounded, spherical, and silt to fine sand size. Up to 5% intergranular porosity is visible in this facies.

Scanning Electron Microscopy

Appendix E provides representative photomicrographs for each facies, along with detailed descriptions of the images. The TST deposits (facies K and A) are moderately sorted, angular to subrounded, framework supported silty shales. The framework particle size ranges from 30 to 50 μ and is homogeneously distributed throughout the sample. The framework mineralogy primarily consists of detrital quartz grains with secondary amounts of feldspars and carbonates. Most of the clay occurs as grain coating and interstitial fines. Clays can be seen “bending” around the hard grains. Small booklets of kaolinite and discrete illite flakes are present. There is no significant micropore or macropore intergranular system. Most of the pores noticed are caused by grain plucking that can be an artifact of sample preparation.

The HST deposits (facies B and C) are well-sorted, subrounded, framework supported siltstones to sandstones. The bulk of these samples are composed of framework particles with the size ranging from 10 to 30 μ . The framework mineralogy

consists of detrital quartz grains with secondary amounts of carbonate, pyrite, and feldspars. Most of the clays occur as grain coating or pore filling interstitial fines. Again, kaolinite books and discrete illite are commonly identified in these facies. A moderately developed intergranular micropore and macropore system is visible.

Whole Rock Mineralogy

Table 5.3 displays the quantitative whole rock mineralogy for the Bellevue outcrop. Facies K has high amounts of total clay averaging 46% and ranging from 34-91%, the higher end member being a bentonite. The quartz content has an inverse relationship and averages 44%. The amounts of potassium feldspar and plagioclase remain relatively constant at 4-6% throughout the entire outcrop. Facies K contains little carbonate and anhydrite. The carbonate includes magnesium-rich calcite (~4%) with smaller amounts of dolomite, and siderite. The condensed section has slightly higher amounts of total clay, averaging 48% with minor amounts of feldspars, high Mg-calcite, dolomite, and siderite.

As seen in the Soldier Canyon outcrop, the amount of total clay is less in the HST deposits. However, the amount of quartz remains relatively constant. This difference in facies B is increased carbonate, including 7% dolomite, 4% high Mg-calcite, 2% calcite, and 2% siderite. Unlike the TST deposits, pyrite is present, averaging 5%. Facies C averages 55% quartz, 18% total clay, 17% dolomite with minor amounts of pyrite, plagioclase, potassium feldspar, and calcite.

Clay Mineralogy

The XRD analysis of the clay mineralogy is displayed in Table 5.4. Facies K contains R0 I/S (illite/smectite) with the total amount of I/S (avg. 67%) ranging from 40

Table 5.3 Whole Rock Mineralogy (wt%): Bellevue Outcrop

Facies	Sample#	FT	TCL	QTZ	KSP	PLAG	CAL	Mg-CAL	DOL	PYR	SID	ANHY
C	JY088	130	16	59	2	2	2	ND	15	4	TR	ND
	JY080	114	20	51	2	3	1	ND	18	4	1	ND
	Average		18	55	2	3	2	0	17	4	1	0
B	JY070	94	31	44	2	3	ND	3	10	5	2	ND
	JY064	88	39	44	3	2	ND	3	9	ND	TR	ND
	JY063	87	69	12	ND	ND	ND	8	3	8	TR	ND
	JY060	84	28	49	4	3	ND	ND	11	4	1	ND
	JY055	79	20	73	1	1	1	ND	3	ND	1	ND
	JY050	74	35	40	2	3	2	3	9	4	2	TR
	JY045	69	37	41	2	3	ND	ND	10	5	2	TR
	JYC020	64	47	42	3	3	ND	ND	3	ND	2	TR
	Average		38	43	2	3	2	4	7	5	2	0
A	JYC015	59	44	46	2	3	ND	3	ND	ND	2	TR
	JYC010	54	50	39	2	3	ND	3	1	ND	2	TR
	Average		47	43	2	3	0	3	1	0	2	0
K	JYC005	49	34	50	3	5	ND	3	ND	3	2	TR
	JYC000	44	91	9	ND	ND	ND	ND	ND	ND	TR	TR
	JY040	40	44	40	2	3	ND	8	2	ND	TR	1
	JY036	36	36	51	3	3	ND	3	1	ND	2	1
	JY030	30	40	49	2	3	ND	3	1	ND	1	1
	JY025	25	44	43	3	3	ND	3	1	ND	2	1
	JY020	20	43	46	2	2	ND	3	1	ND	2	1
	JY015	15	37	52	3	3	ND	3	1	ND	TR	1
	JY010	10	38	50	3	3	ND	3	ND	ND	2	1
	JY005	5	39	50	3	3	ND	3	1	ND	TR	1
	JY000	0	55	39	4	2	ND	ND	ND	ND	ND	ND
	Average		46	44	3	3	0	4	1	3	2	1
	LEGEND:			CAL= Calcite Mg-CAL= Mg-rich calcite DOL= Dolomite				SID= Siderite ANHY= Anhydrite PYR= Pyrite			ND= Not Detected TR= Trace	
TCL= Total Clay and Mica			QTZ= Quartz				KSP= K-Feldspar			PLAG= Plagioclase		

to 100%. The 100% end member of I/S is a bentonite. Table 5.4 shows concentration and expandability of both R0 and R1 I/S for each sample. The ratio of the 25% expandable I/S to the 65% expandable is 2:1. Illite averages 29% with minor amounts of kaolinite (4%) and serpentine. The condensed section is very similar to facies K, with the addition of 5% R1 I/S with the expandability of 50%. The total amount of I/S averages 76%, with 21% illite and 3% kaolinite. No smectite or serpentine is detected in this facies.

Table 5.4 Bellevue Clay Mineralogy

Facies	Sample #	Ht (ft)	R1 I/S		R0 I/S				Total amt. I/S	Illite	Kaol	Smec.	Serp
			Exp.	Con.	Exp.	Con.	Exp.	Con.					
C	JY088	130	50	13	35	40	25	7	60	19	17	4	0
	JY080	114	50	21	35	40		0	61	9	28	2	0
	Average								61	14	23	3	0
B	JY070	94		0	25	47	65	24	71	28	1	0	0
	JY064	88		0	25	60	65	27	87	12	1	0	0
	JY063	87	50	5	35	85		0	90	0	6	4	0
	JY060	84		0	25	49	65	25	74	25	2	0	0
	JY055	79		0	25	63	65	19	82	17	0.8	0	0.2
	JY050	74	50	2	25	50	65	23	75	24	1	0	0
	JY045	69	50	2	25	51	65	23	76	20	4	0	0
	JYC020	64	50	2	25	52	65	25	79	17	4	0	0
Average								79	18	3	1	0	
A	JYC015	59	50	3	25	52	65	26	81	17	2	0	0
	JYC010	54	50	6	25	54	65	10	70	25	5	0	0
	Average								76	21	3	0	0
K	JYC005	49		0	25	62	65	16	78	20	1.5	0	0.5
	JYC000	44		0	50	99		0	99	0	1	0	0
	JY040	40		0	25	26	65	14	40	55	4	0	0
	JY036	36		0	25	42	65	21	63	29	7	0	0
	JY030	30		0	25	36	65	18	54	42	4	0	0
	JY025	25		0	25	41	65	20	61	34	6	0	0
	JY020	20		0	25	47	65	23	70	30	1	0	0
	JY015	15		0	25	41	65	20	61	32	7	0	0
	JY010	10		0	25	47	65	23	70	24	6	0	0
	JY005	5		0	25	42	65	21	63	30	7	0	0
	JY000	0		0	25	56	65	18	74	22	3.8	0	0.2
Average								67	29	4	0	0	

LEGEND:

R1 I/S= Ordered Illite/Smectite (Reichweite=1); (2:1 mixed-layer clay)

R0 I/S= Randomly Ordered Illite/Smectite (Reichweite=0); (2:1 mixed-layer clay)

Kaol= Kaolinite (1:1 Clay)

Smec= Smectite (2:1 Clay)

Serp= Serpentine (1:1 Clay)

Facies B averages 79% I/S, mostly with R0 ordering and 25% expandability, and smaller amounts of R0 I/S with 65% expandability and R1 I/S with 50% expandability. Again, the ratio of the 25% expandable I/S to the 65% expandable is 2:1. Illite averages 18%, and has an inverse relationship to the amount of I/S. These clays are further complimented by an average of 3% kaolinite and 1% smectite. There is significantly more R1 I/S in facies C, where the average rises to 17% with 50% expandability. The

total amount of I/S in facies C averages 61%, with most of the remaining R0 I/S having the expandability of 35%. Kaolinite is very significant in facies C, averaging 23%, with 14% illite and 3% smectite.

5.3 *Petrophysical Description*

The MICP injection pressures and corresponding hydrocarbon column heights are presented in Table 5.5. Facies K includes the three samples with the highest injection pressures (psia). At 9 ft, the injection pressure at 10% mercury saturation is 8,520 psia that can hold a HCH of 2,390 ft. This is considerably less than the highest injection pressure at Soldier Canyon. The next highest injection pressures drop significantly to 3,320 psia (925 ft HCH) and 2,570 psia (715 ft HCH), which correspond to 4 ft and 40 ft respectively also located in facies K. This is closely followed by a sample in facies A which holds a HCH of 690 ft at 2,500 psia.

Again, there is considerable variability in facies K as shown by the drainage curves with entry pressure ranging from 400 to 2,000 psia (Fig. 5.9a). The lowest psia value at 44 ft corresponds to a thick bentonite. The drainage curve for facies A (Fig. 5.9b) shows a broad sloping upper curve with an entry pressure around 1,000 psia.

The drainage curves for facies B (Fig. 5.9c) show entry pressures ranging from 300 to 1,000 psia. The entry pressures for facies C (Fig. 5.9d), range from 200 to 700 psia. The MICP data (Fig. 5.9) for HST deposits are indicating an interconnected pore network, which is allowing a non-wetting fluid to move through it at low pressures.

MICP data for the distribution of pore throat diameters are shown in Appendix F. In general, the PTD for the TST deposits are not as well sorted as Soldier Canyon. The

Table 5.5 Bellevue Injection Pressures (psia) at 10% Mercury Saturation

Facies	Sample#	FT	PSIA@10% SAT.	HCH (ft)
C	JY-088	130	512	135
C	JY086	126	959	260
C	JY083	120	607	160
C	JY-080	114	308	75
C	JY077	108	1000	270
B	JY-071	96	536	140
B	JY-066	90	1060	290
B	JY-061	85	947	255
B	JY-056	80	2080	575
B	JY-051	75	1683	465
B	JY-046	70	379	95
B	JYC-021	65	407	105
B	JYC-015	59	2400	665
A	JYC-010	54	2500	690
K	JYC-005	49	736	195
K	JY-044	44	583	155
K	JY-040	40	2570	715
K	JY-036	36	2430	675
K	JY-030	30	1880	520
K	JY-025	25	2310	640
K	JY-020	20	1560	430
K	JY-014	14	2470	685
K	JY-009	9	8520	2390
K	JY-004	4	3320	925

9-ft shale in facies K has 60% of its pore volume with a median PTD of 0.01 micron with the remaining 40% having a median, 0.02-micron PTD. The median PTD diameter shifts to 0.02-0.04 microns in the remaining samples for facies K. Lesser cumulative pore volumes of one to two other poorly sorted populations of either 0.1 micron PTD or 0.015 microns PTD supplement this population. The CS sample at 54 ft shows two poorly sorted populations, with 70% of the PV having a median PTD of 0.015 microns with the remaining 30% having a median PTD of 0.07 microns.

The HST deposits have 40-50% of their pore volume composed of a moderately sorted median PTD ranging from 0.03-0.3 microns. A second population of very poorly sorted PTD supplements this, with the median PTD ranging from 0.008-0.01 microns.

Bellevue Drainage Curve (Facies K)

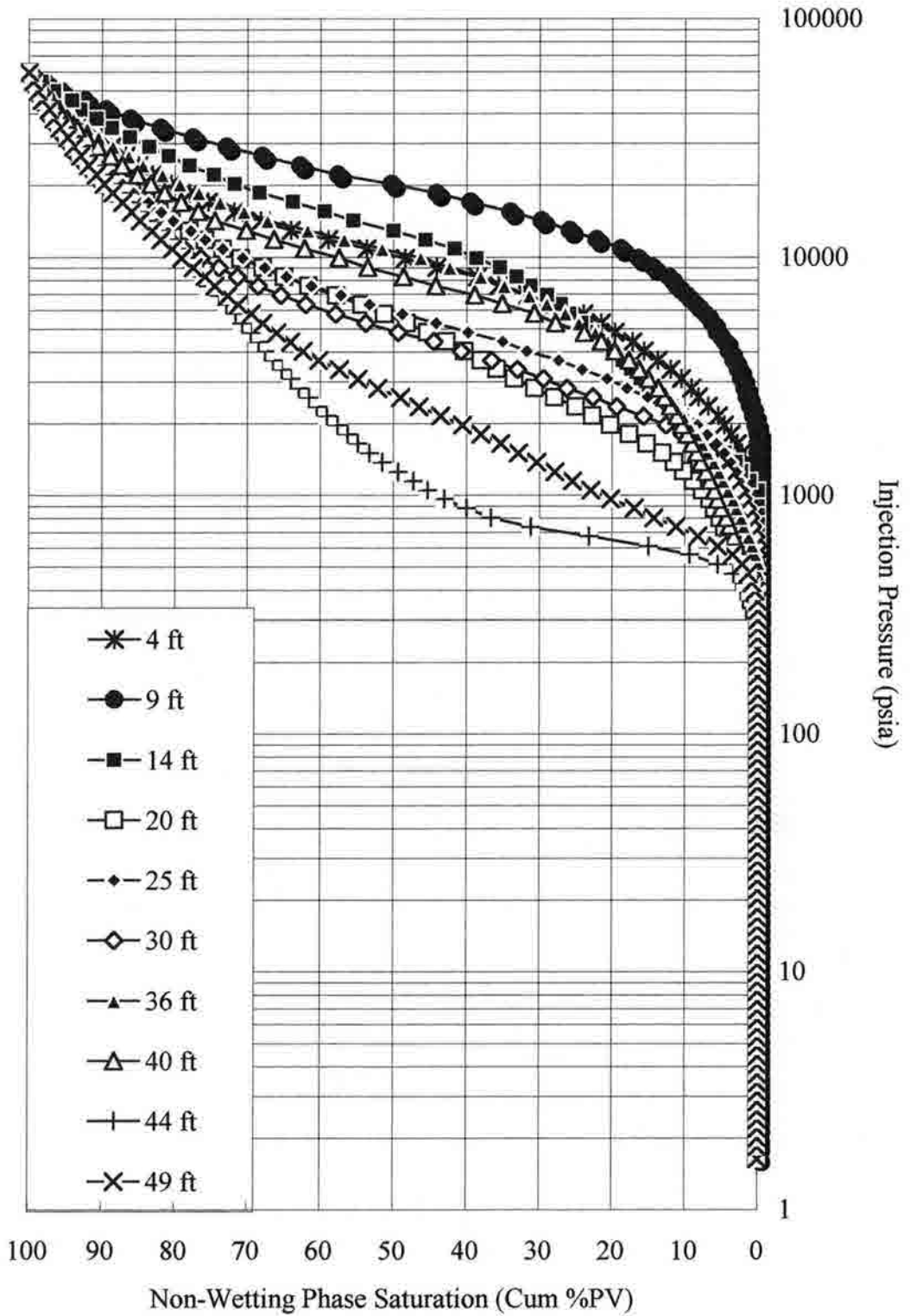


Figure 5.9a Drainage Curve for facies K at Bellevue Outcrop.

Bellevue Drainage Curve (Facies A)

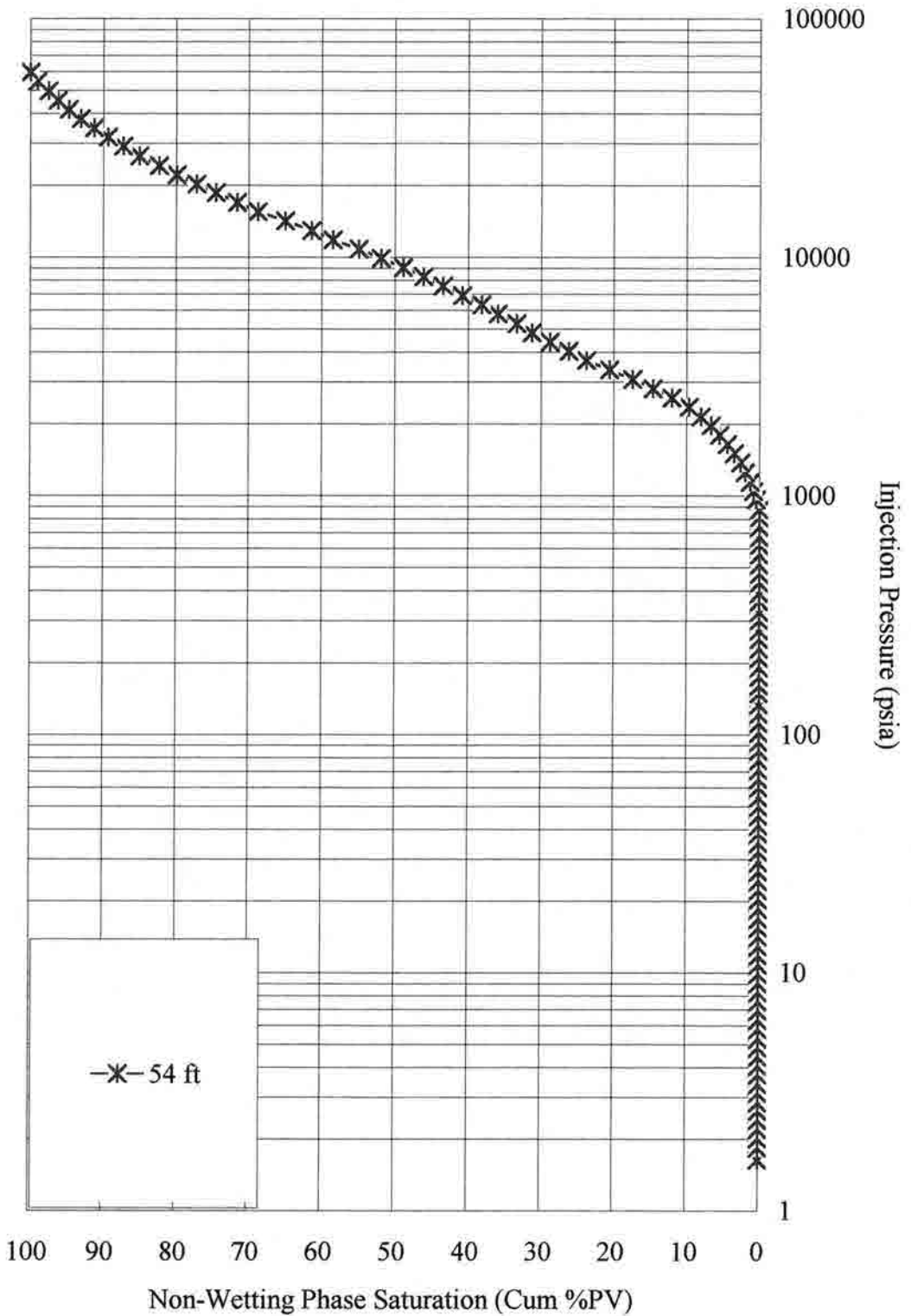


Figure 5.9b Drainage Curve for Facies A at Bellevue Outcrop.

Bellevue Drainage Curve (Facies B)

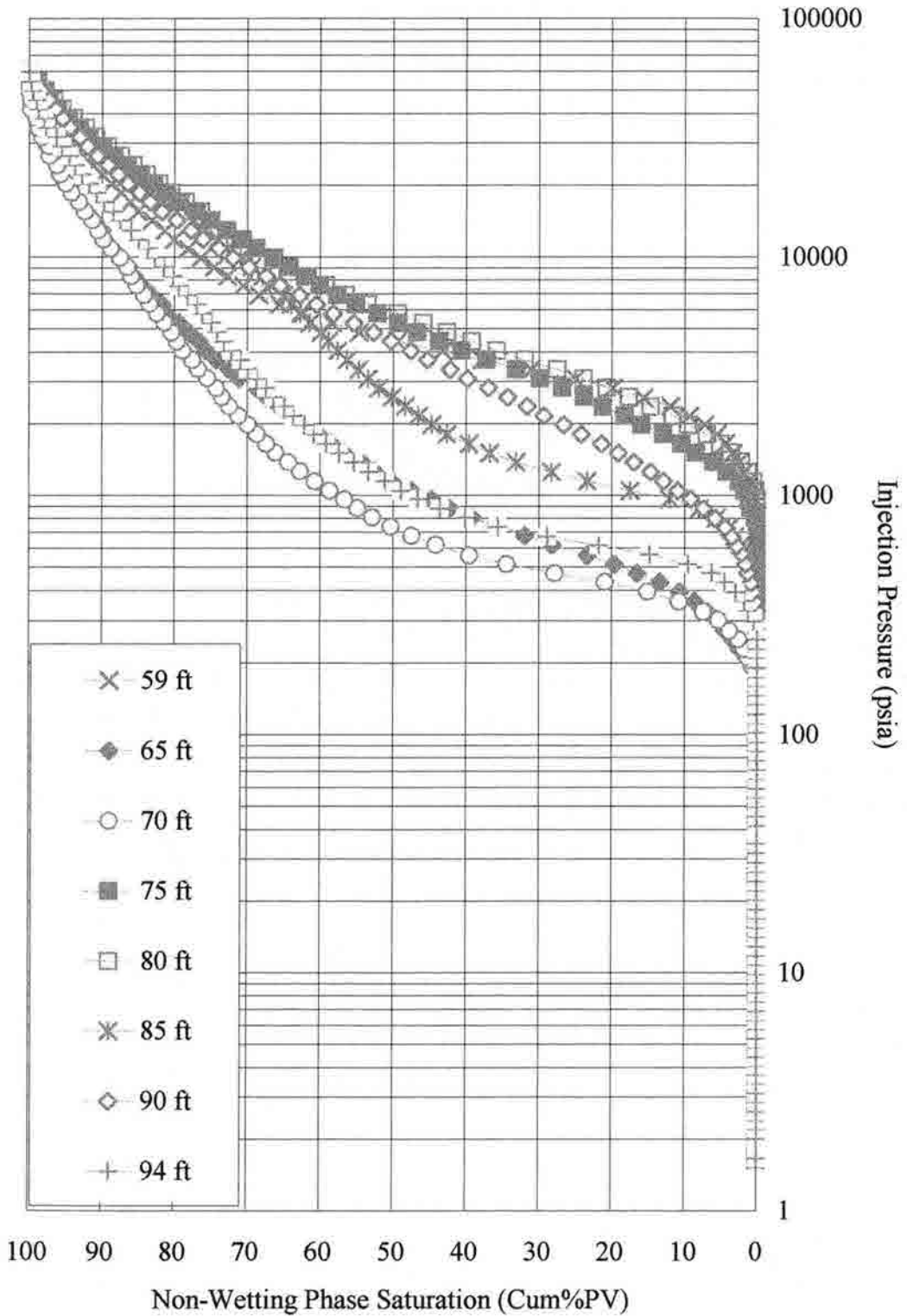


Figure 5.9c Drainage Curve for Facies B at Bellevue Outcrop.

Bellevue Drainage Curve (Facies C)

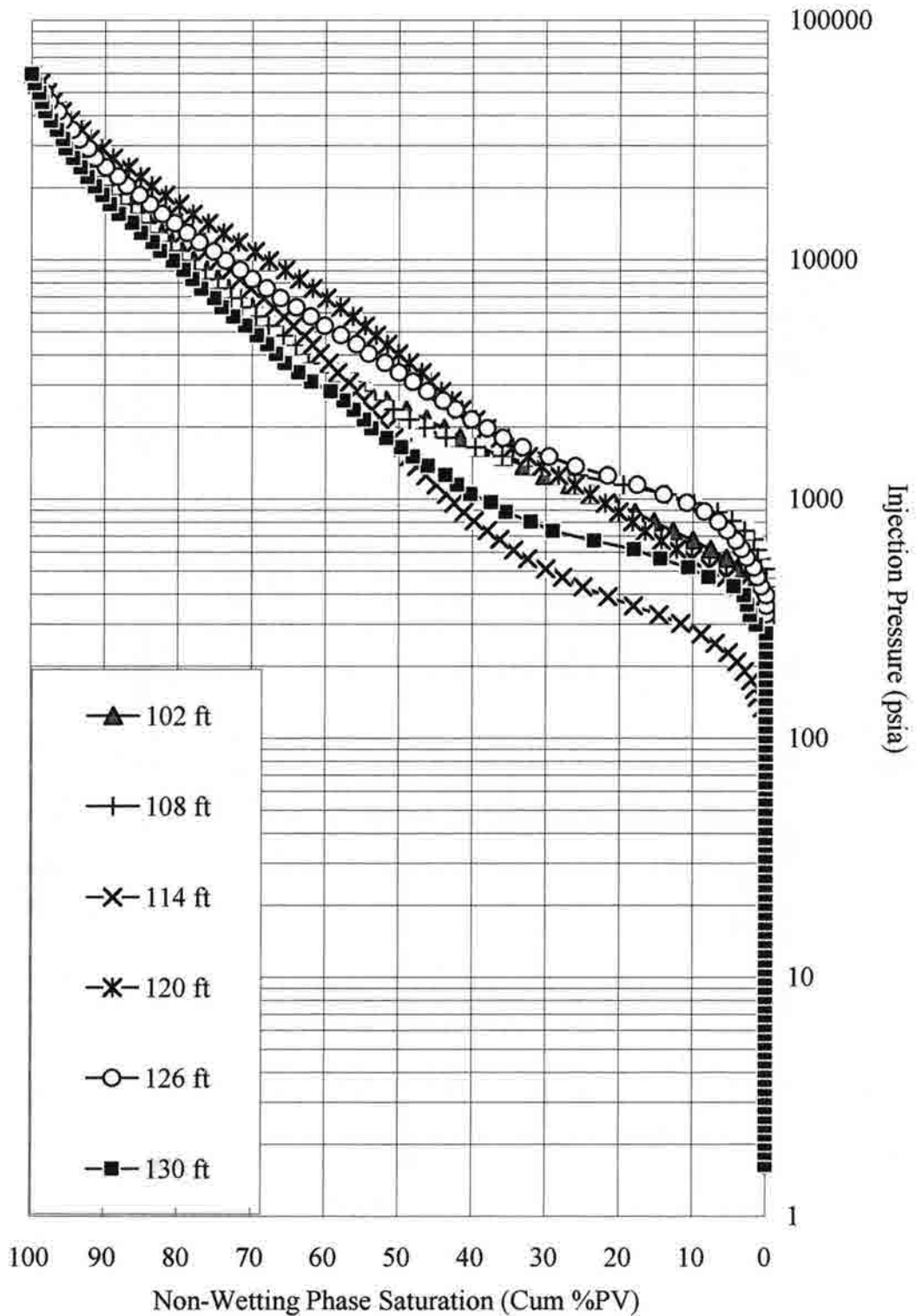


Figure 5.9d Drainage Curve for Facies C at Bellevue Outcrop.

This trend continues into facies C, as the median PTD gradually increases in size with some variability. This larger median PTD in the HST deposits is enough of a difference from the TST deposits to allow non-wetting fluids to permeate these rocks.

5.4 *Summary*

The best seal delineated by MICP is located in the upper parts of the TST deposits, in particular facies K, which is below the CS. However, the CS does contain rocks with significant seal properties. The following is a list of characteristics displayed by the rock with the highest sealing properties:

1. Located at 9 ft, which is stratigraphically below the CS.
2. 1.16% total organic carbon content.
3. Type III (terrestrial) organic matter.
4. No continuous laminations or fossils in hand sample.
5. Density value of 2.58 g/cc.
6. 14.4% porosity with 0.001-md permeability.
7. No notable bioturbation, fossils or matrix porosity in thin section.
8. Point count data with 71% clay, 21% quartz, 3% organic matter, 3% carbonate, and 2% pyrite.
9. XRD data with 50% clay, 38% quartz, 6% feldspars, 3% mg-calcite, and 2% siderite.
10. Clay mineralogy consists of 70% R0 illite/smectite (with 47% having 25% expandability and 23% has 63% expandability), 24% illite, and 6% kaolinite.
11. 8,517 psia at 10% mercury saturation with a HCH of 2,285 ft.
12. Two populations with 60% of the PV having a well-sorted median PTD of 0.01 microns and 40% with a moderately sorted median PTD of 0.025 microns.

Figure 5.10 shows the histograms for the injection pressures at 10% mercury saturation for each facies grouped into columns of 2000 psia. Facies K has one sample in the 10,000 column and five in the 4,000 column. Facies A has one sample in the 4,000 column. Facies B has two samples in the 4,000 column and six samples in the 2,000 column. Facies C has five samples in the 2,000 psia column.

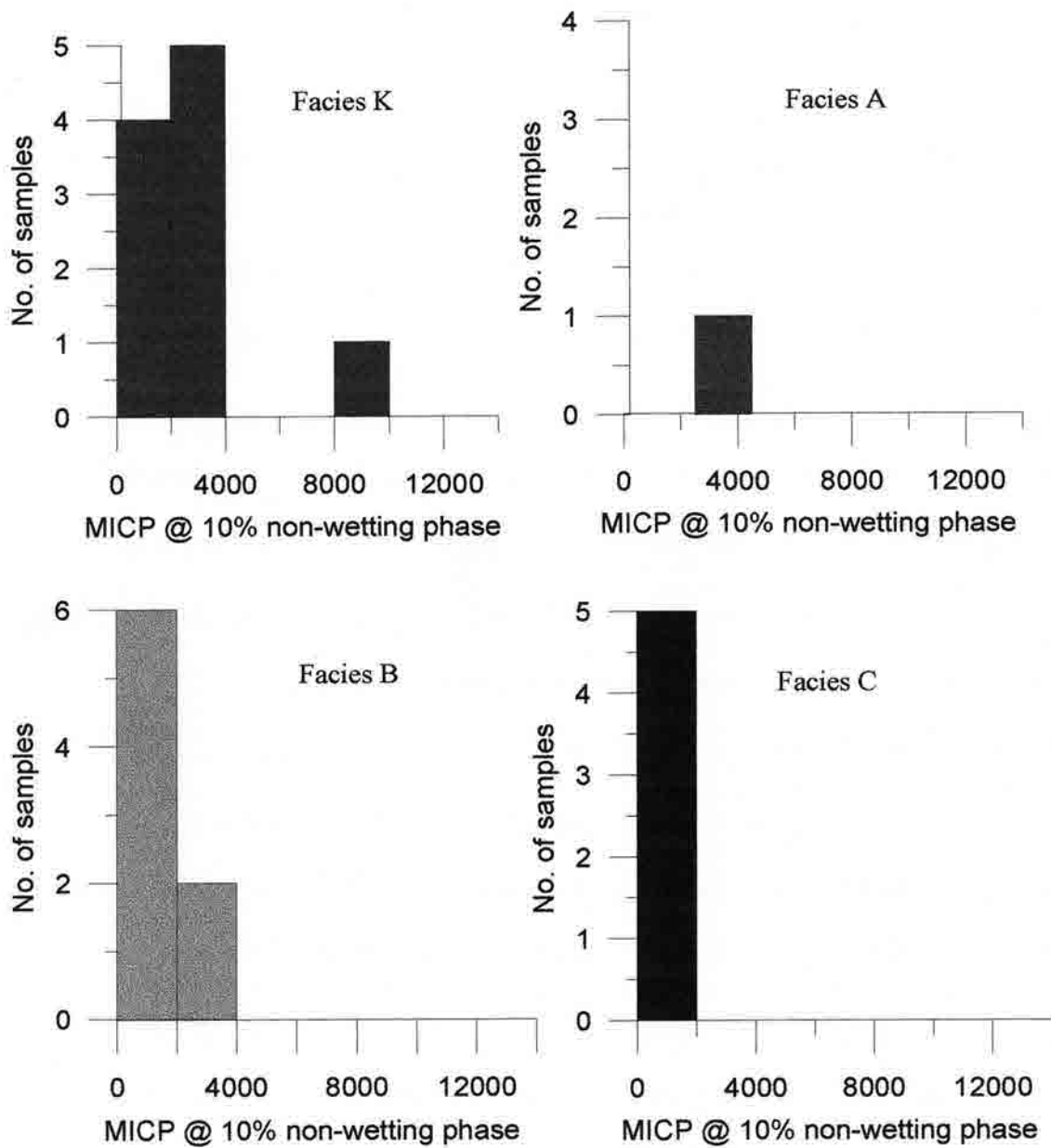


Figure 5.10 Bellevue Histograms of MICP at 10% Mercury Saturation for each facies.

CHAPTER 6. TURKEY CREEK (SKULL CREEK SHALE) OUTCROP RESULTS

6.1 *Facies Description*

At the Turkey Creek outcrop, 94 ft of the Skull Creek Shale was measured and gamma ray logged (Fig. 6.1). This location has a sharp underlying contact with the Plainview Formation and a sharp overlying contact with the Muddy 'J' Sandstone. The Skull Creek is much siltier at this outcrop in the southern part of the Denver compared to the northern outcrops around Fort Collins. All the Skull Creek facies (A, B, and C) are present with the exception of the mudstone/shale of facies K. Overall, the gamma ray response is consistent throughout facies A, B, and C but increases towards the top of the outcrop due to radioactivity found in the overlying Muddy Sandstone.

Facies A is the only representative of the TST deposits at this location. The CS or facies A is slightly thicker (8') than at the other two outcrops (4-5') (Fig. 6.2a). It is distinguishable in outcrop by being a clay-rich, organic-rich, grayish-black fissile shale that incorporates two 1 in. yellow bentonites (Fig. 6.2b). It has well-developed laminations of silt. This facies clearly displays a type I-II (marine) organic matter (Fig. 6.2c). This "marine" signature in the CS is more explicit at Turkey Creek than at either Soldier Canyon or Bellevue. At Turkey Creek, the HST deposits (facies B and C) occur both stratigraphically above and below the condensed section.

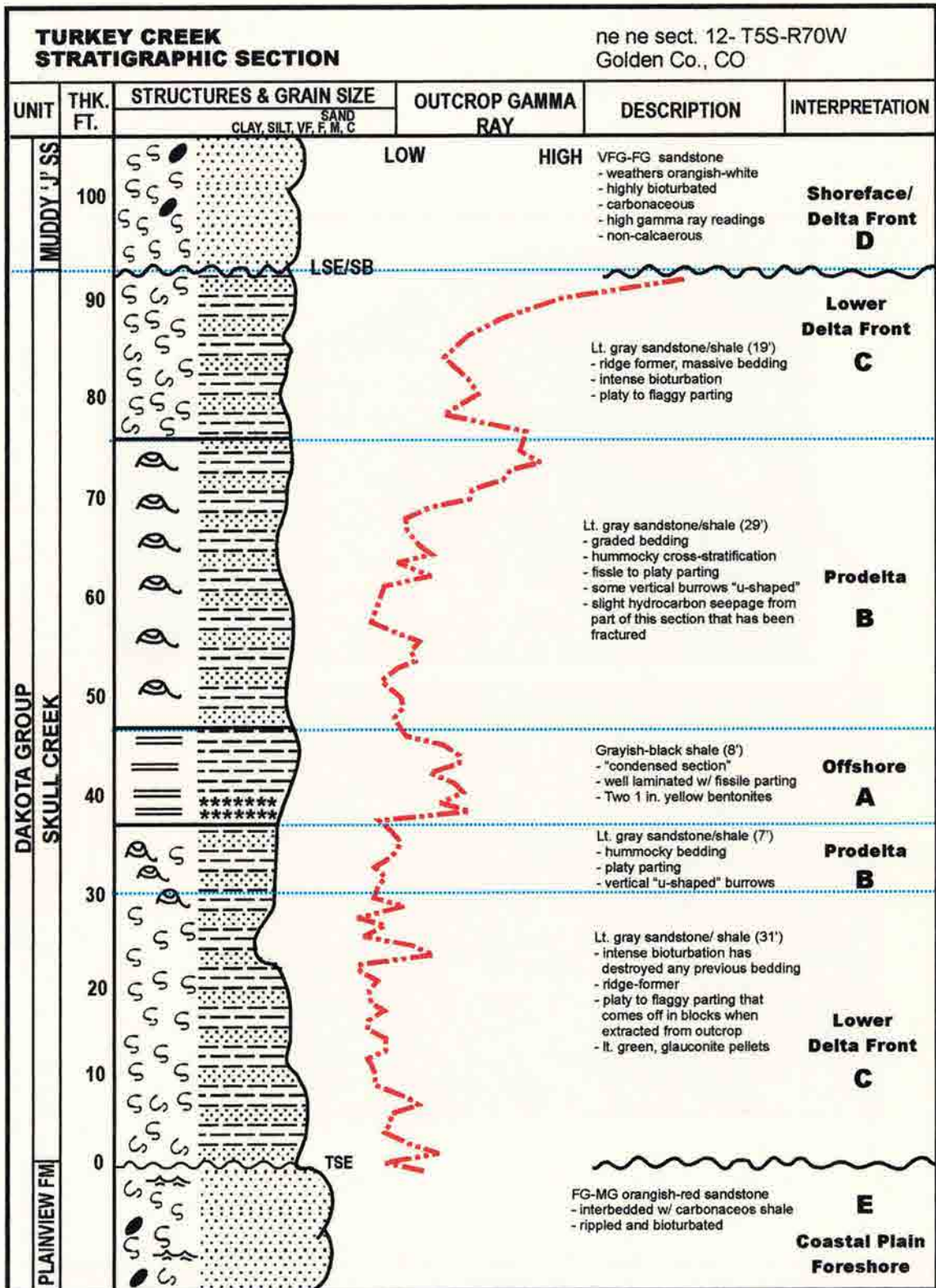


Figure 6.1 Stratigraphic column for Turkey Creek Outcrop, including detailed descriptions, interpretations, and logged outcrop gamma ray.

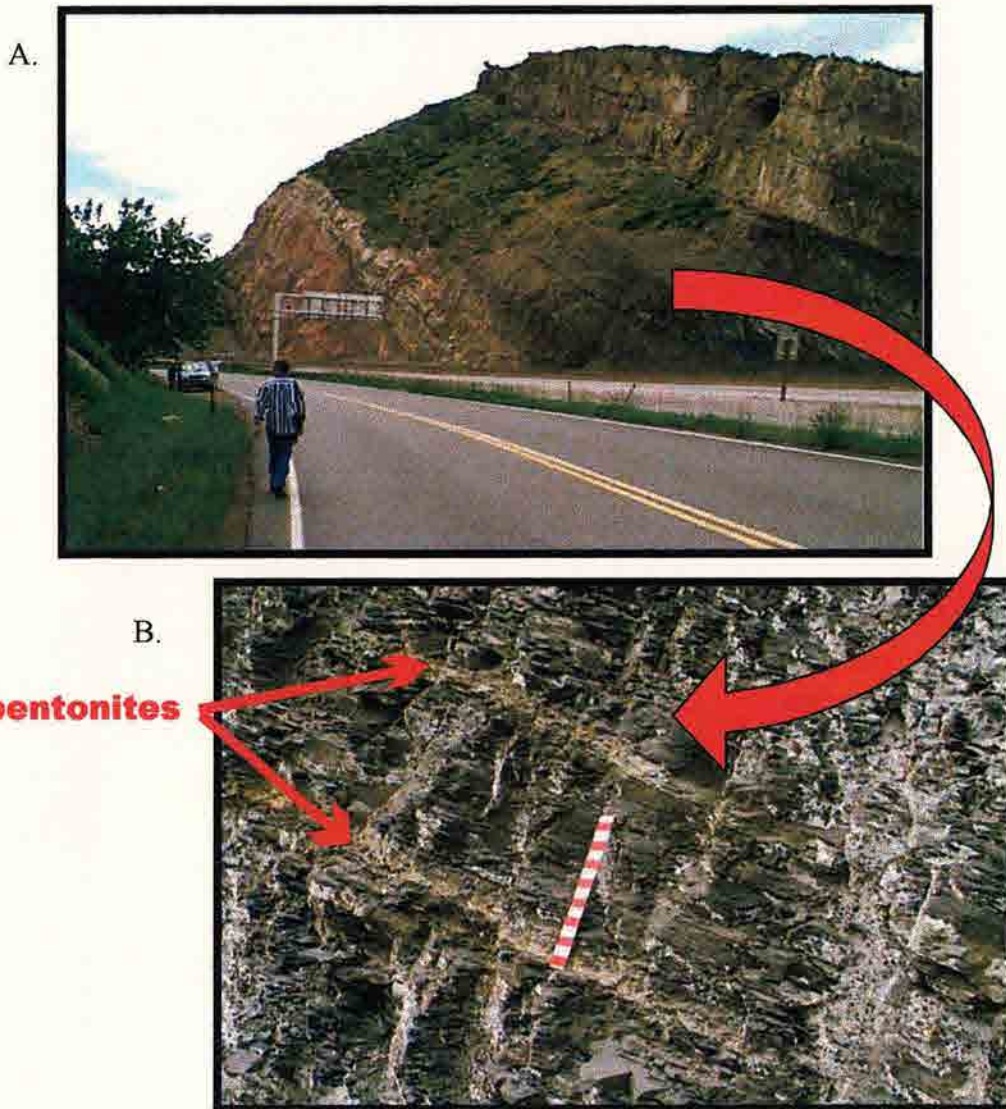


Figure 6.2 A) middle section of Turkey Creek is the fissile shale in the condensed section; B) closer view of facies A with two small bentonites approx. 1-ft apart; C) Van Krevelen diagram of type I-II (marine) organic matter for facies A. Overall exposure of Skull Creek is 85 ft thick.

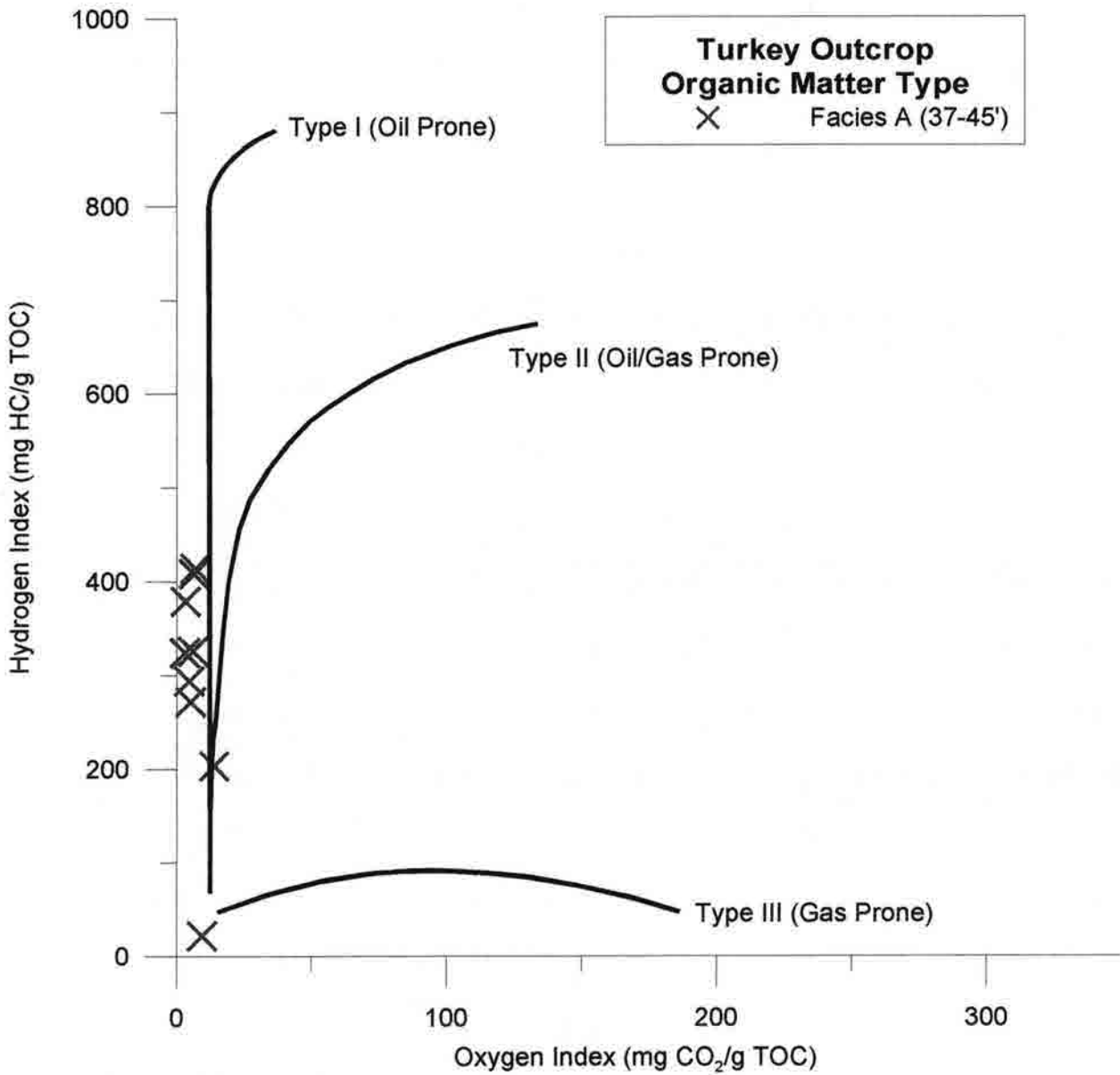


Figure 6.2 C.

Facies B is a light gray interbedded shale and sandstone that ranges from graded bedding to hummocky cross-stratification (Fig. 6.3a,b). This shale has platy parting and comes off in blocks when extracted from the outcrop. The organic matter is type II (marine) which is different than the type III (terrestrial) kerogen that is found in facies B at the other two outcrops, but is similar to the type II kerogen found in the core for facies B (Fig. 6.3c).

Facies C is also a light gray shale/sandstone that is distinguishable from facies B by the intense bioturbation that has destroyed any previous bedding features (Fig. 6.4a). In outcrop, this facies is massively bedded. In hand sample, light green glauconite pellets are visible, in addition to the “white-walled” burrows (Fig. 6.4b). The organic matter for this facies is type III (terrestrial) (Fig. 6.4c).

6.2 Lithology Description

Table 6.1 displays the averages and standard deviations for the Turkey Creek data. TOC values are greater for facies A at Turkey Creek than found at Soldier Canyon and Bellevue, as it ranges from <1 to 4%, with the average value of 3%. Overall, the Turkey Creek location has higher hydrogen indexes with the average value of 294 mg HC/g TOC, than the other two outcrops. This shale is dominated by quartz that ranges from 50-70% (avg. 39%) with lesser amounts of total clay (avg. 36%) and carbonate (avg. 12%) with the lowest permeability values. The density values are lower (avg. 2.58 g/cc) than in the other facies at Turkey Creek.

A significant decrease in the amount of ductile material is noted in the HST deposits, which is compensated by an increase in carbonate. There is considerably less carbonate in facies B and C below the CS than above it. Facies B ranges from 53% quartz

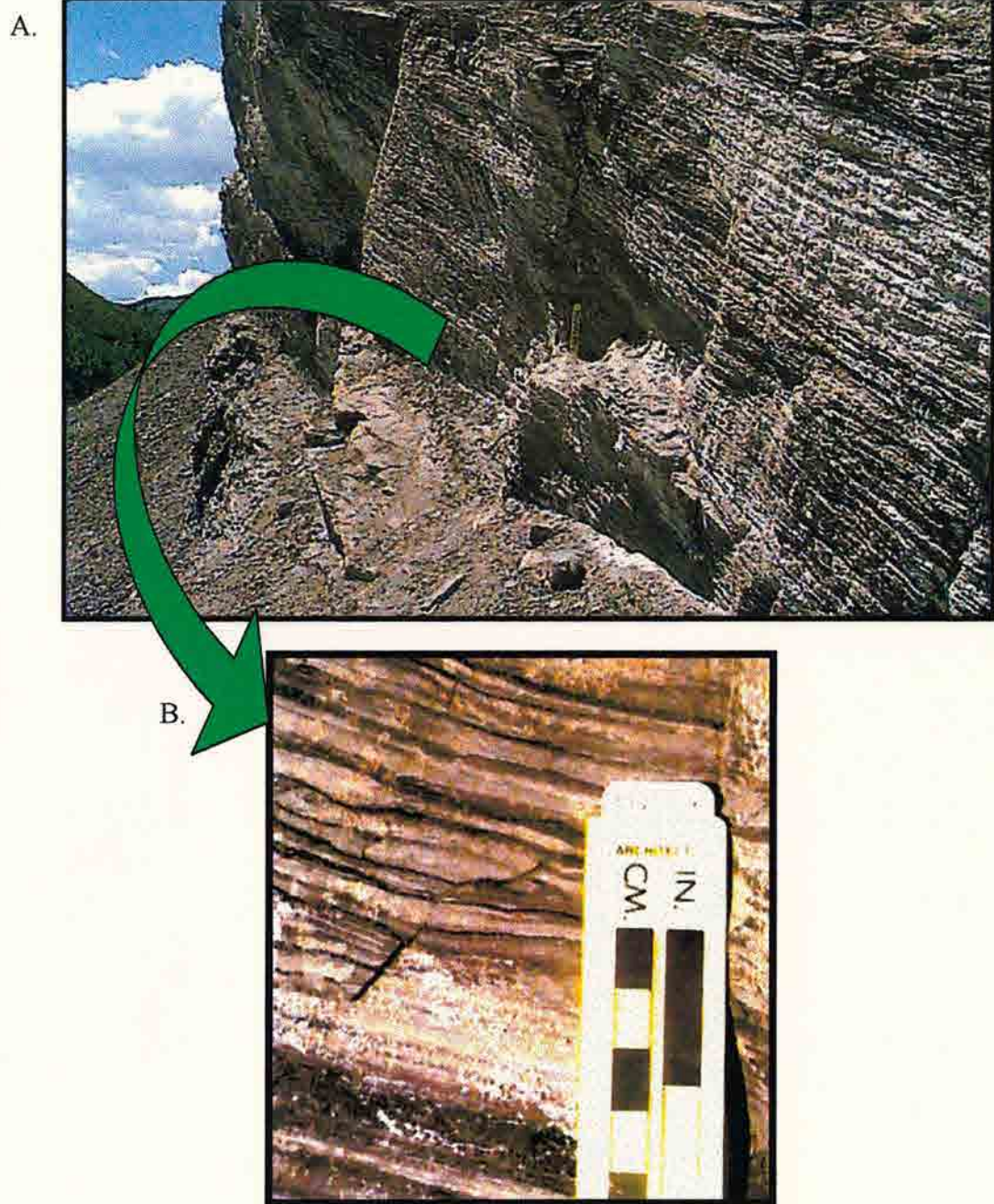


Figure 6.3 A) Overall view of hummocky bedding in alternating silty shale and siltstone; B) closer view of small scale graded bedding; C) Van Krevelen diagram of type I-II (marine) organic matter for facies B. 1-ft ruler for scale.

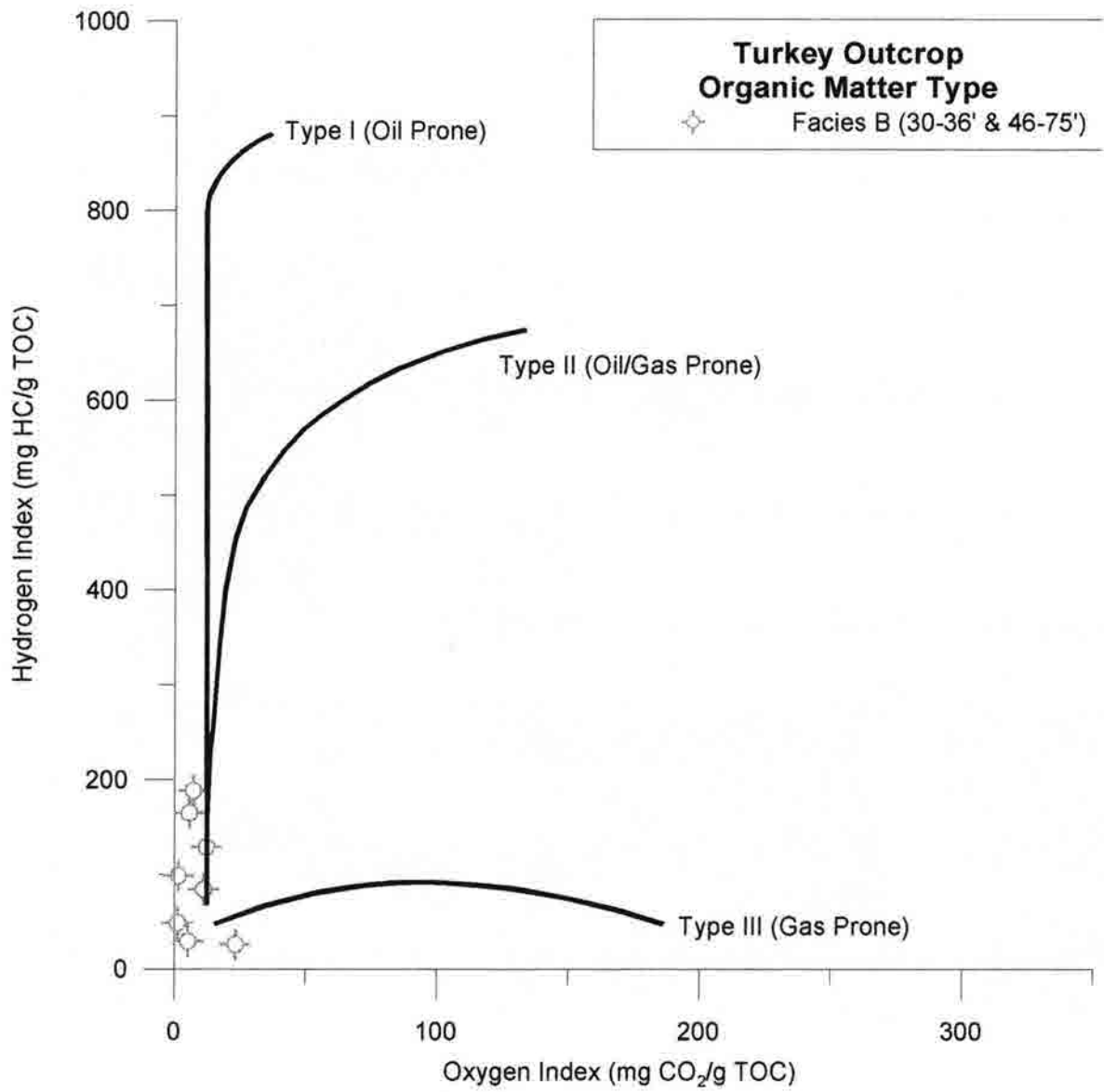


Figure 6.3 C.

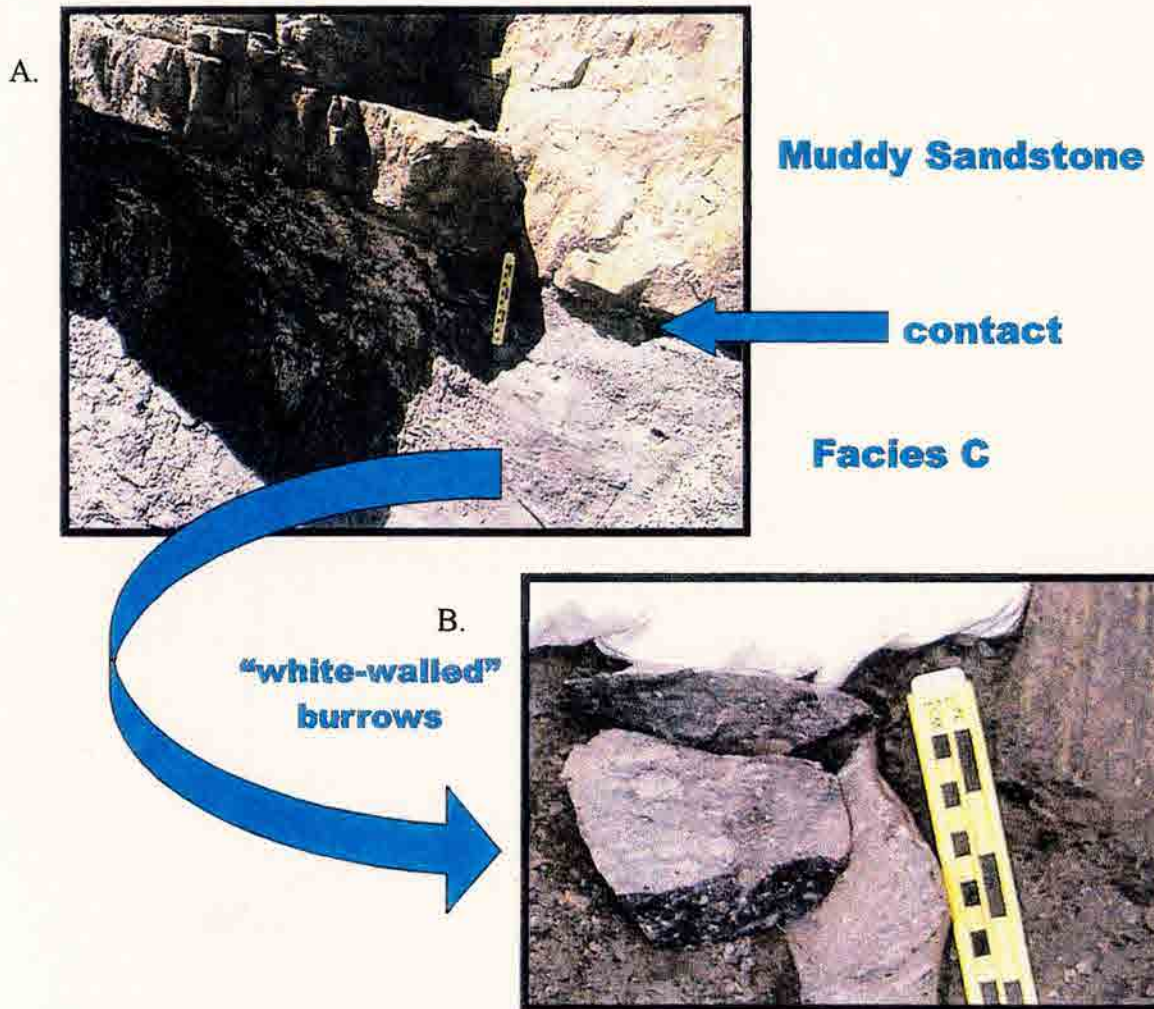


Figure 6.4 A) Sharp contact of facies C with the overlying Muddy sandstone; B) closer view of heavily burrowed siltstone; C) Van Krevelen diagram of type III (terrestrial) organic matter for facies C. 1-ft ruler for scale, centimeters to the left and inches to the right..

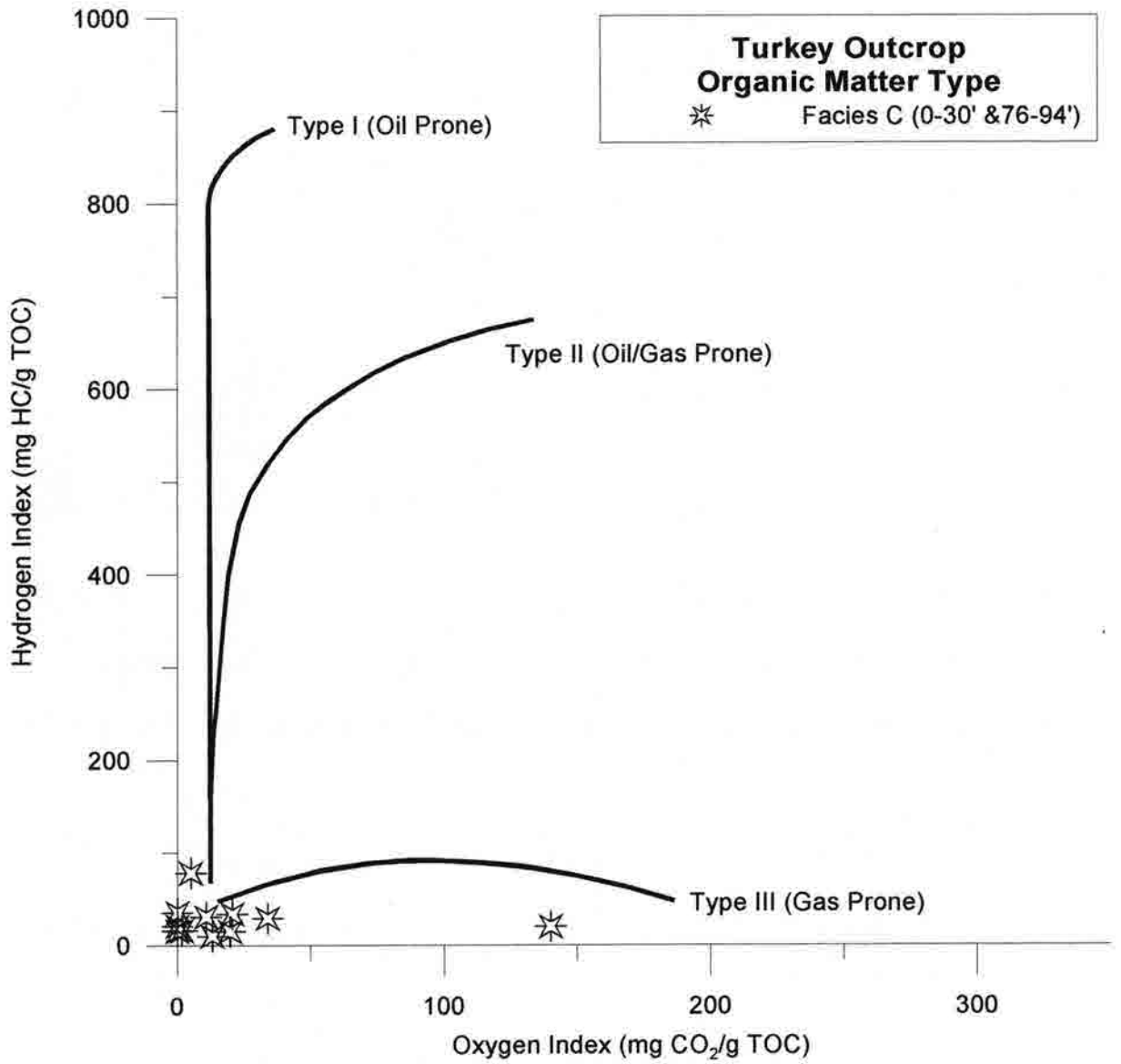


Figure 6.4 C.

Table 6.1 Statistics for Turkey Creek Outcrop data.

Facies		Total Organic Carbon (%)	Hydrogen Index (mg HC/g TOC)	Hydrogen Index/Oxygen Index (mg HC/mg CO ₂)	Total Clay (wt %)	Quartz (wt %)	Feldspar (wt %)	Carbonate (wt %)	Porosity (%)	Permeability (md)	Density (g/cc)
	# of Analyses	4	4	2	4	4	4	4	2	2	2
C	Average	0.81	20	5	25	63	0	9	12.6	1.13	2.70
	Std Dev	0.16	10	7	7	9	1	13	3.5	1.59	0.13
	# of Analyses	5	5	5	5	5	5	5	3	3	3
B	Average	1.11	106	33	23	53	1	17	7.4	0.002	2.70
	Std Dev	0.59	70	21	4	4	1	6	1.0	0.00	0.08
	# of Analyses	9	9	9	9	9	9	9	2	2	2
A	Average	3.00	294	60	36	39	2	12	9.5	4E-04	2.58
	Std Dev	1.23	122	37	9	5	0	5	0.2	2E-04	0.02
	# of Analyses	3	3	3	3	3	3	3	2	2	2
B	Average	1.31	80	6	23	58	3	13	7.7	6E-04	2.60
	Std Dev	0.50	51	5	9	5	1	9	1.1	4E-04	0.03
	# of Analyses	7	7	6	7	7	7	7	3	3	3
C	Average	0.75	32	4	26	66	2	2	11.2	0.020	2.61
	Std Dev	0.41	22	6	6	7	1	1	2.2	0.015	0.03

above the CS, to 58% below the CS with total clay averaging 23%. Carbonate averages 17% above, and 13% (avg.) below the CS. Porosity values range from 6-8% with 0.0003-0.004 md permeability. Density values average slightly heavier above the CS (2.7 g/cc) than below (2.6 g/cc).

Facies C averages the highest amount of quartz with the lowest amounts of total clay and total organic carbon. In turn, these rocks have the highest permeability. Overall, facies A is the most organic, clay rich rock with the lowest permeability. However, facies B also contains relatively high amounts of total organic carbon with high HI values and low permeabilities. Facies B has the highest percentage of carbonate.

This data has been plotted against stratigraphic height to permit comparison to seal capacity, as measured by MICP (Fig. 6.5). The best seals are located in facies A (Fig. 6.5a) and directly above and below the CS in facies B. Porosity is variable

throughout both the TST and HST deposits (Fig. 6.5b). The lowest permeability values are in the CS and correspond with the highest seal capacity (Fig. 6.5c). In the TST deposits, the samples with the highest sealing capacity also have the lowest density (Fig. 6.5d).

The highest amount of total clay is found in facies A (CS) K (Fig. 6.6a). Quartz shows an inverse relationship to clay (Fig. 6.6b). The amount of feldspar is variable but decreases towards the top (6.6c). Carbonate is clearly more concentrated towards the top of the outcrop (Fig. 6.6d). The greatest amount of TOC is found in facies A, (Fig. 6.7a) and also corresponds to high hydrogen index values (Fig. 6.7b). The ratio of HI/OI also shows a corresponding trend seen in the TOC and HI graphs (Fig. 6.7b). Appendix P contains a complete description of the organic geochemistry.

Thin Section Petrography

Table 6.2 is a composite of the main features observed with thin section petrography. Thin section photomicrographs for representative samples of the facies at Turkey Creek are in Appendix G. Facies A is a strongly compacted, carbonaceous silty shale. It has a well-sorted matrix that contains clay minerals and silt size detrital grains (quartz, feldspar, and mica). The hard grains are angular, spherical-elongate and silt size. Point count analysis of one sample shows 49% quartz, 40% clay, 3% organic matter, 4% authigenic carbonate, and 4% pyrite. Very large authigenic framboidal pyrite nodules are noted. This shale has well-developed laminations that are absent of bioturbation or porosity. Under high power, the quartz grains exhibit sutured boundaries between grains. Facies B is a strongly compacted, argillaceous, carbonate-cemented sandstone/shale. The matrix is composed of clay minerals and silt size detrital grains (quartz, feldspar, and

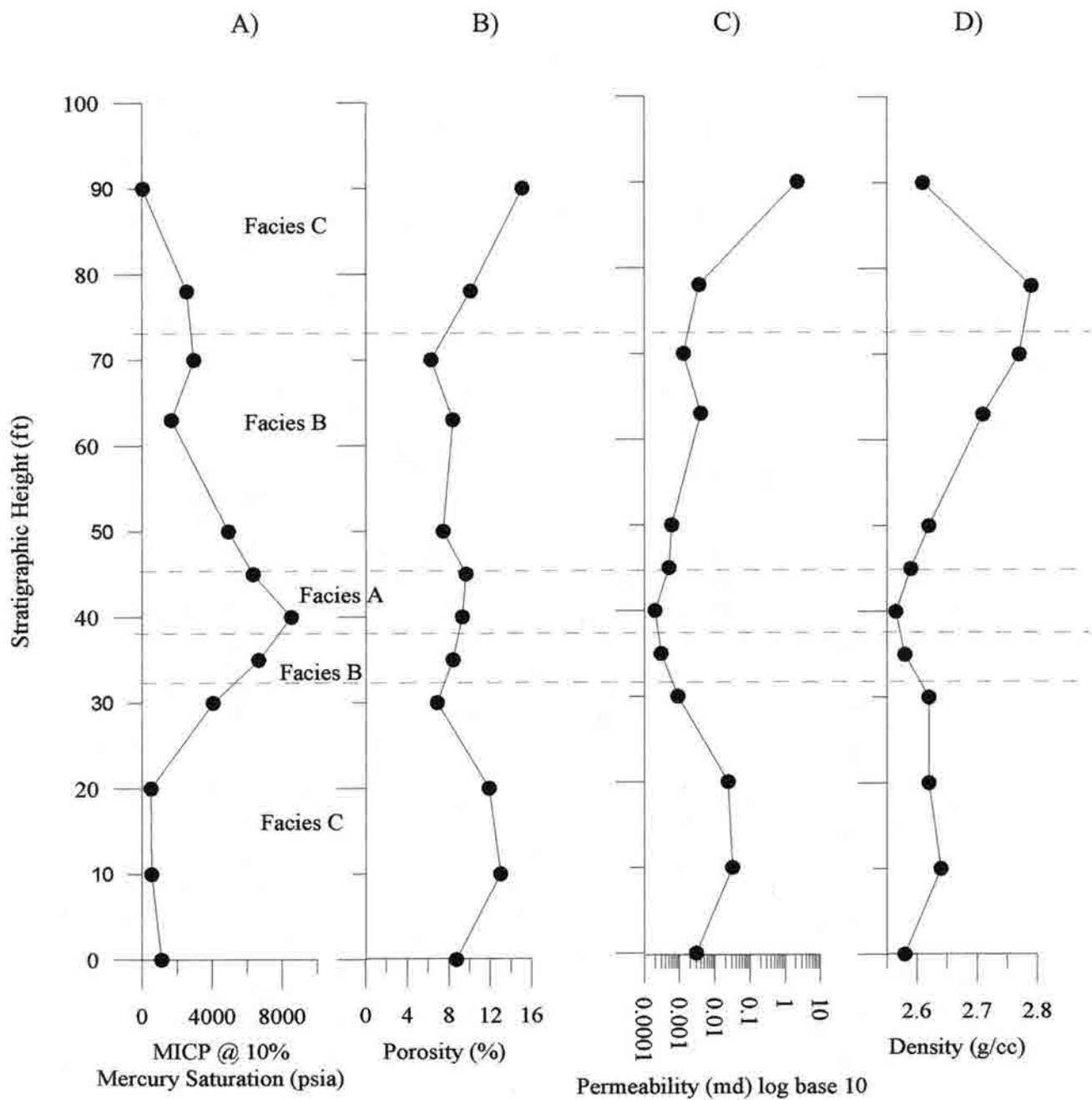


Figure 6.5 Stratigraphic height versus MICP (A), porosity (B), permeability (C), and density (D) at the Turkey Creek Outcrop for the Skull Creek.

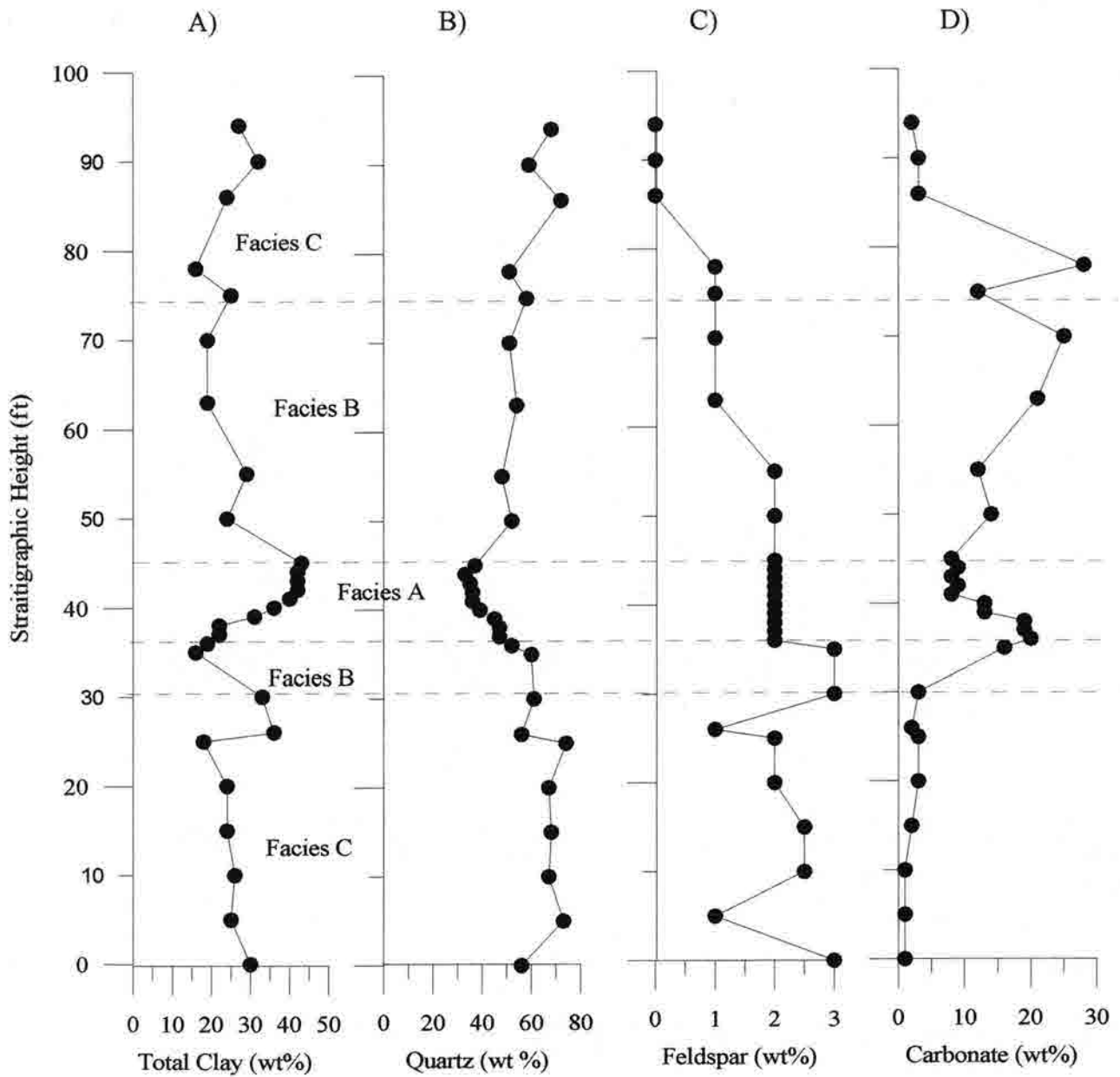


Figure 6.6 Stratigraphic height versus total clay (A), quartz (B), feldspar (C), and carbonate (D) at the Turkey Creek Outcrop for the Skull Creek.

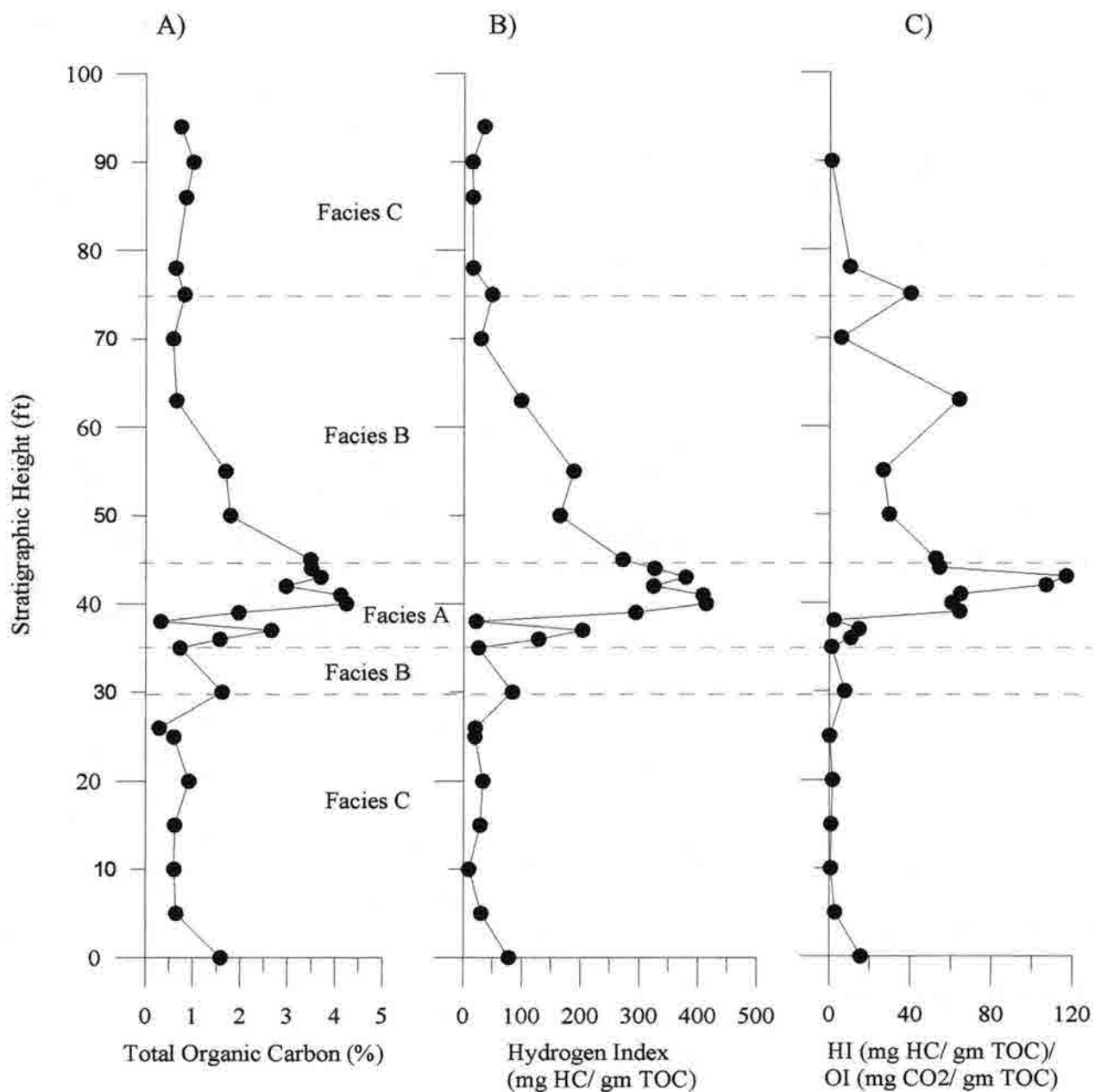


Figure 6.7 Stratigraphic height versus TOC (A), hydrogen index (B), hydrogen index / oxygen index (C) at the Turkey Creek Outcrop for the Skull Creek.

Table 6.2 Turkey Creek Thin Section Petrography

Facies	FT	Rockname	Avg. Grain Size (μ)	COMPOSITION						Laminations	Bioturbation	Pressure Solution	Fossils	Porosity
				QTZ	CLAY	ORG	CARB	PYR	OTHER					
C	90	siltstone	45	68	25	2	2	3	mica, feld	N	Y	Y	N	5
C	80	siltstone	44	60	27	2	8	3	mica, feld	N	Y	Y	N	5
C	70	siltstone	64	68	20	1	8	3	mica, feld	N	Y	Y	N	2
B	63	siltstone	44	70	18	2	8	2	mica, feld	Y	Y	Y	N	5
B	50	siltstone	44	66	23	2	6	3	mica, feld	Y	Y	Y	N	2
A	45	silty shale	22	49	40	3	3	5	mica, feld	Y	Y	Y	N	2
A	40	silty shale	32	49	40	3	4	4	glauc, mica	Y	N	Y	N	N
B	35	siltstone	85	71	20	3	4	2	glauc, mica	N	Y	Y	N	2
C	30	siltstone	47	72	23	2	3	0	mica, feld	N	Y	Y	N	5
C	20	siltstone	58	65	29	2	2	2	mica, feld	N	Y	Y	N	5
C	10	siltstone	54	65	30	1	2	2	mica, feld	Y	Y	Y	N	10
C	6	siltstone	38	60	34	2	1	3	mica, feld	Y	Y	Y	N	15-20

*NOTE: Point count percentages are in bold, other percentages are estimates.

**NOTE: 1/256 < silt < 1/16 mm, 1/16 < VF sand < 1/8 mm, 1/8 < F sand < 1/4 mm, 1/4 < M sand < 1/2 mm

LEGEND:

QTZ= Quartz

ORG= Organic Matter

CARB= Carbonate (calcite, dolomite, siderite)

feld= Feldspar

phos= Phosphate

mic= Mica

hem= Hematite

mica). The hard grains are well sorted, subangular, spherical-elongate, and silt size with scarce fine-grained sand. It is composed of 70% quartz, 18% clay, 2% organic matter, 8% carbonate, and 2% pyrite. Patchy carbonate cement surrounds the hard grains and gives them appearance of “floating”. Well-developed laminations of clays and organics are present along with distinct graded bedding and minor burrowing. Grain boundaries are sometimes hard to distinguish between quartz and feldspar grains. Intergranular porosity is 2-5%.

Facies C is a strongly compacted, argillaceous, carbonate-cemented alternating siltstone and shale. The matrix is again composed of clay minerals and silt size detrital

grains (quartz, feldspar, and mica). The hard grains are moderately-well sorted, subangular, spherical-elongate, and silt size with an occasional fine-grained sand size particle. It is composed of ~65% quartz, ~27% clay, ~2% organic matter, ~5% authigenic carbonate, and 2-3% pyrite. Faint laminations of organic matter are visible in addition to silt-filled burrows. Intergranular porosity is very noticeable and ranges from 2-20%.

Whole Rock Mineralogy

The quantitative XRD analysis of the whole rock mineralogy is shown in Table 6.3. The condensed section has the most total clay, averaging 36%. This is complimented with minor amounts of siderite, dolomite, high Mg-calcite, potassium feldspar, and gypsum. Pyrite is significantly more concentrated (avg. 10%) in the CS than in the other facies here and at the other two Skull Creek outcrops.

The transition into the overlying and underlying facies B provides a decrease in the amount of total clay to an average of 23%, with 55% quartz. Dolomite is the highest in facies and averages 12% with 5% pyrite, potassium feldspar, siderite, and gypsum. Facies C is predominantly quartz (avg. 65%) with 25% total clay and minor amounts of potassium feldspar, high Mg-calcite, dolomite, pyrite, plagioclase, siderite and gypsum.

6.3 Petrophysical Description

Table 6.4 provides the injection pressures at 10% mercury saturation and the corresponding hydrocarbon column heights (HCH). The highest injection pressure found at 40 ft in facies A, is 8,530 psia and can hold a HCH of 2390 ft. This is followed by 6,650 psia at 35 ft, which is located in facies B below the CS and can hold a HCH of 1870 ft. The psia at 10% mercury saturation for facies A ranges from 6,500-8,500 psia.

Table 6.3 Whole Rock Mineralogy (wt%): Turkey Creek Outcrop

Facies	Sample#	FT	TCL	QTZ	KSP	PLAG	MG-CAL	DOL	PYR	SID	GYP
C	TC085	94	27	68	ND	ND	ND	1	3	1	ND
	TC083	90	32	59	ND	ND	ND	2	5	1	1
	TC081	86	24	72	ND	ND	2	1	ND	ND	1
	TC078	80	16	51	1	ND	1	26	3	1	1
	Average		25	63	1	0	2	8	4	1	1
B	TC075	75	25	58	1	ND	1	10	3	1	1
	TC070	70	19	51	1	ND	2	22	3	1	1
	TC063	63	19	54	1	ND	ND	20	4	1	1
	TC055	55	29	48	2	ND	1	10	7	1	2
	TC050	50	24	52	2	ND	2	11	7	1	1
	Average		23	53	1	0	2	15	5	1	1
A	TC045	45	43	37	2	ND	2	4	10	2	ND
	TC044	44	42	33	2	ND	3	3	12	3	2
	TC043	43	42	35	2	ND	3	3	12	2	1
	TC042	42	42	36	2	ND	3	2	10	4	1
	TC041	41	40	36	2	ND	3	2	13	3	1
	TC040	40	36	39	2	ND	3	4	9	6	1
	TC039	39	31	45	2	ND	2	5	7	6	2
	TC038	38	22	47	2	ND	2	6	9	11	1
	TC037	37	22	47	2	ND	2	6	9	11	1
	Average		36	39	2	0	3	4	10	5	1
B	TC036	36	19	52	2	ND	2	13	6	5	1
	TC035	35	16	60	3	ND	2	10	4	4	1
	TC030	30	33	61	3	ND	2	1	ND	ND	ND
	Average		23	58	3	0	2	8	5	5	1
C	TC026	26	36	56	1	ND	1	1	4	ND	1
	TC025	25	18	74	2	ND	ND	1	3	2	ND
	TC020	20	24	67	2	ND	ND	1	3	2	1
	TC015	15	24	68	2	TR	ND	1	3	1	1
	TC010	10	26	67	2	TR	ND	ND	3	1	1
	TC005	5	25	73	TR	TR	ND	1	ND	TR	1
	TC000	0	30	56	2	1	ND	ND	10	1	ND
	Average		26	66	2	TR	1	1	4	1	1

LEGEND:
 QTZ= Quartz
 TCL= Total Clay and Mica
 KSP= K-Feldspar
 PLAG= Plagioclase
 MG-CAL= Mg-rich Calcite
 DOL= Dolomite
 PYR= Pyrite
 SID= Siderite
 GYP= Gypsum
 ND= Not Detected
 TR= Trace

The psia values for facies B range from 1,600-6,600 psia, with the lowest psia values corresponding to rocks above the CS. There is a clear separation in the psia values for facies C. The highest injection pressures at 10% mercury saturation is 2500 psia.

Table 6.4 Turkey Creek Injection Pressures at 10% Mercury Saturation

Facies	Sample#	FT	PSIA@10% SAT.	HCH (ft)
C	TC-083	90	35	1
C	TC-078	78	2550	710
B	TC-070	70	2950	820
B	TC-063	63	1670	460
B	TC-050	50	4930	1330
A	TC-045	45	6340	1780
A	TC-040	40	8530	2390
B	TC-035	35	6650	1870
B	TC-030	30	4050	1130
C	TC-020	20	510	135
C	TC-010	10	550	145
C	TC-000	0	1120	305

The drainage curves for facies A show two gently sloping upper curves with entry pressures around 2,000 psia (Fig. 6.8a). The drainage curves for facies B also show gently sloping upper curves with slightly lower entry pressure ranging from 1,000 to 2,000 psia (Fig. 6.8b). The drainage curves for facies C have a steeper sloping upper curve with entry pressures ranging from 10-1000 psia (Fig. 6.8c).

The MICP data in Appendix H show the smallest median PTD to be 0.0075 microns and located at 40 ft in facies A. This well sorted population composes 70% of Figure 6.8a the PV and is supplemented by a small population (30% PV) of 0.045 microns median PTD. Facies B has two populations of median PTD ranging from 0.007-0.01 microns, with moderate to very well sorted. Facies C has two to three populations with the median PTD ranging from 0.008-20 microns, with poor to moderate sorting.

Turkey Creek Drainage Curve (Facies A)

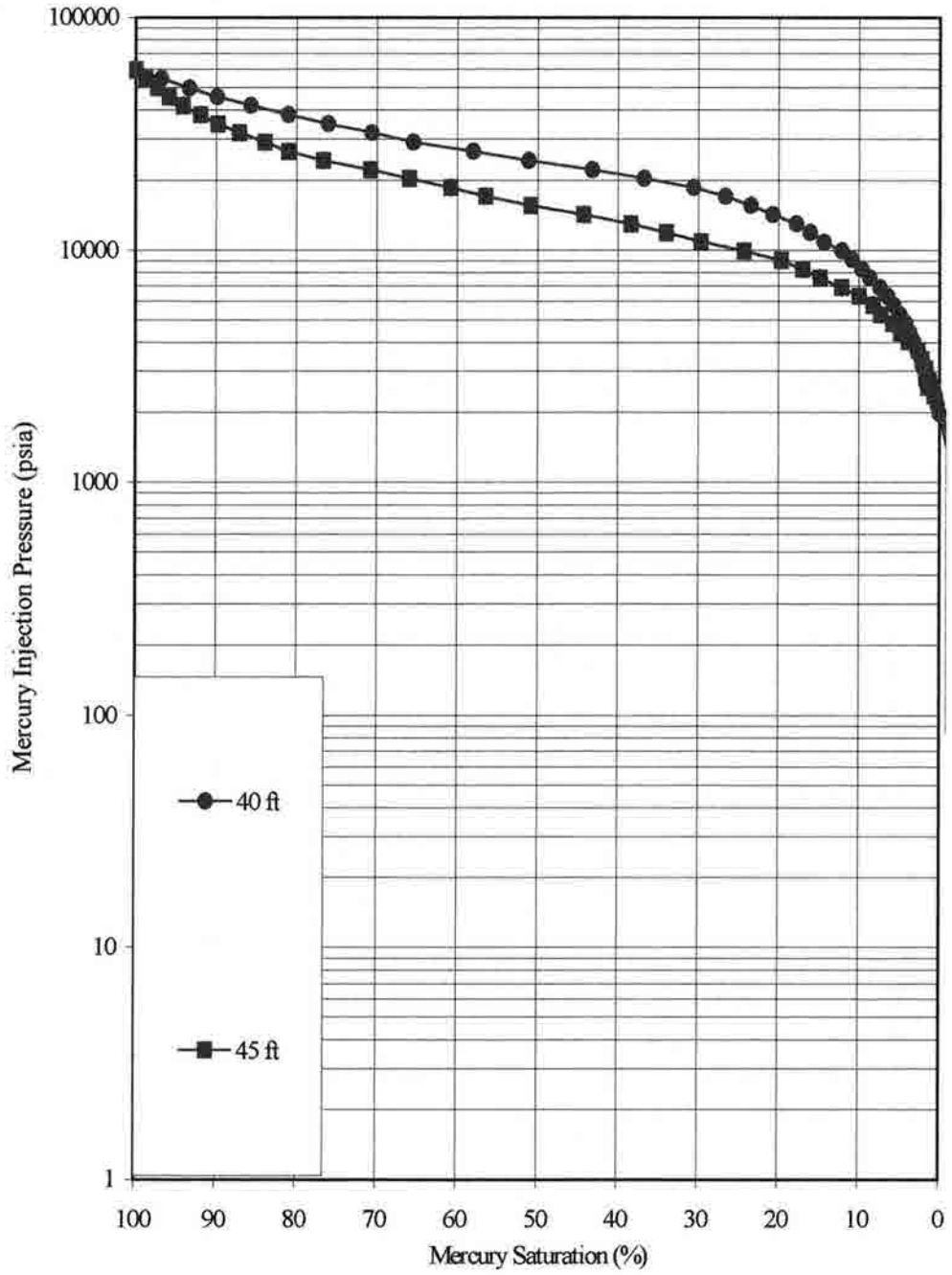


Figure 6.8a Drainage Curve for facies A at Turkey Creek.

Turkey Creek Drainage Curve (Facies B)

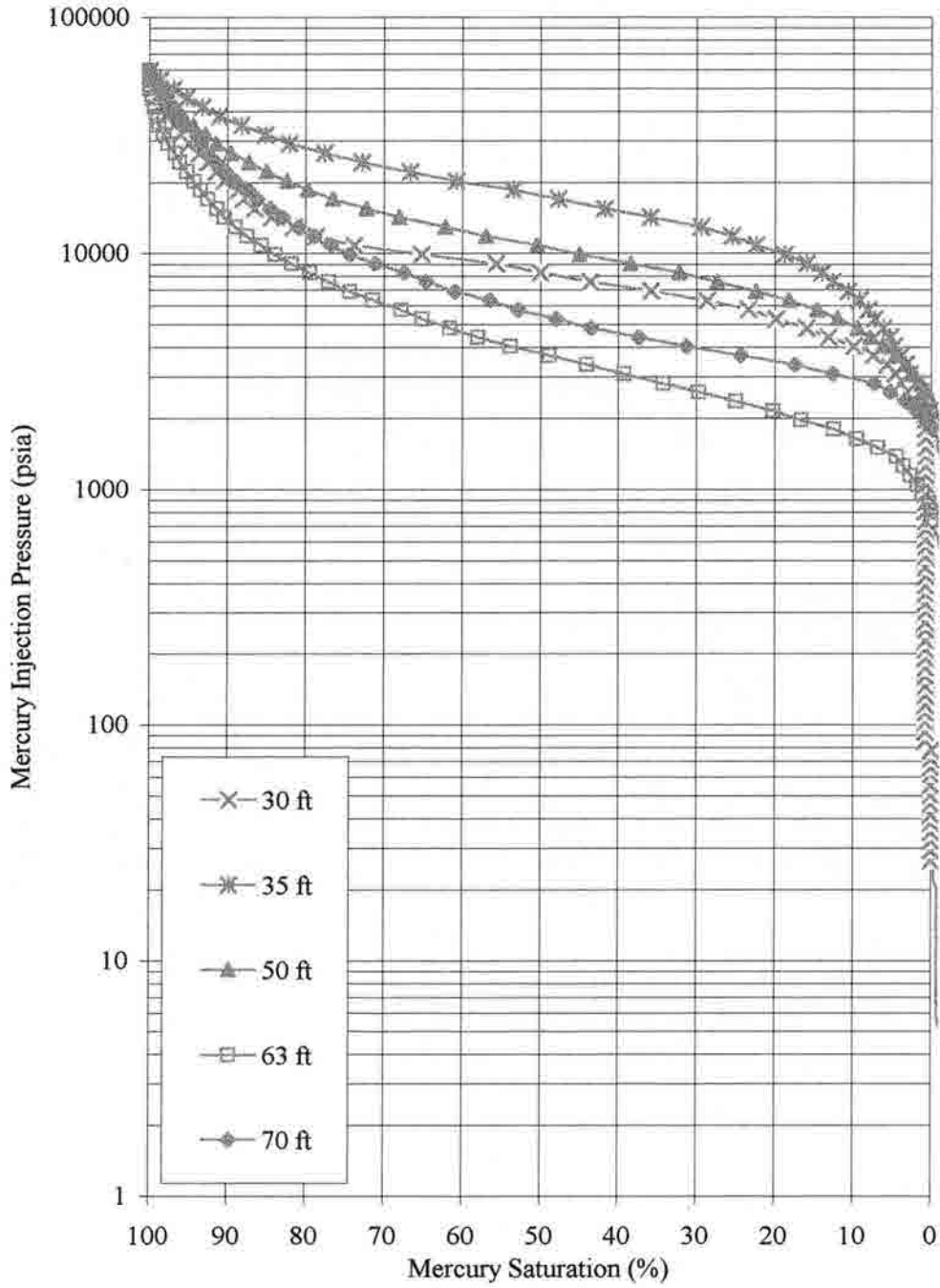


Figure 6.8b Drainage Curve for Facies B at Turkey Creek.

Turkey Creek Drainage Curve (Facies C)

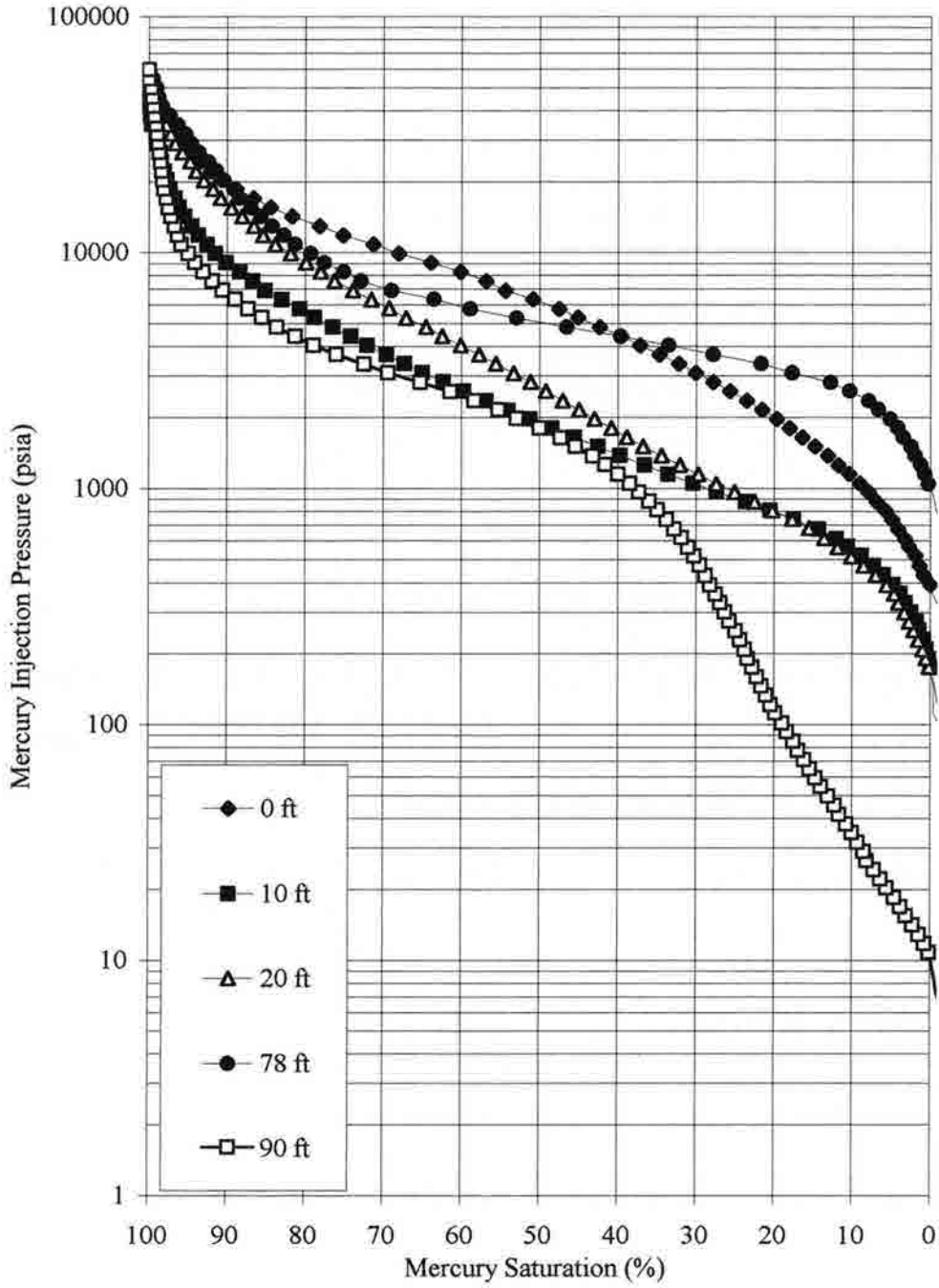


Figure 6.8c Drainage Curve for Facies C at Turkey Creek.

6.4 Summary

The best seal delineated by MICP is located in the condensed section or facies A.

The following is the characteristics of the rock with the highest sealing properties:

1. Located at 40 ft in the CS.
2. 4.24% total organic carbon content (the highest).
3. Type I (marine) organic matter.
4. Well-developed laminations and Inoceramus fossils in hand sample.
5. Density value of 2.58 g/cc.
6. 9.31% porosity with 0.0002-md permeability.
7. No notable bioturbation or matrix porosity in thin section.
8. Point count data with 40% clay, 49% hard grains, 3% organic matter, 4% carbonate, and 4% pyrite.
9. XRD data with 36% clay, 39% quartz, 9% pyrite, 6% siderite, 4% dolomite, 3% mg-calcite, 2% feldspars, and 1% gypsum.
10. 8,525 psia at 10% mercury saturation with a HCH of 2390 ft.
11. Two PTD populations with a very well sorted median PTD of 0.008-microns that composes 70% of the PV, along with another moderately sorted median PTD of 0.02-microns.

Figure 6.9 shows histograms for the injection pressures of each facies. Facies A has one sample in the 10,000 column, and one sample in the 8,000 column. Facies B has one sample in the 8,000 column and two samples in the 6,000 column. Facies C has one sample in the 4,000 column with four samples in the 2,000 column.

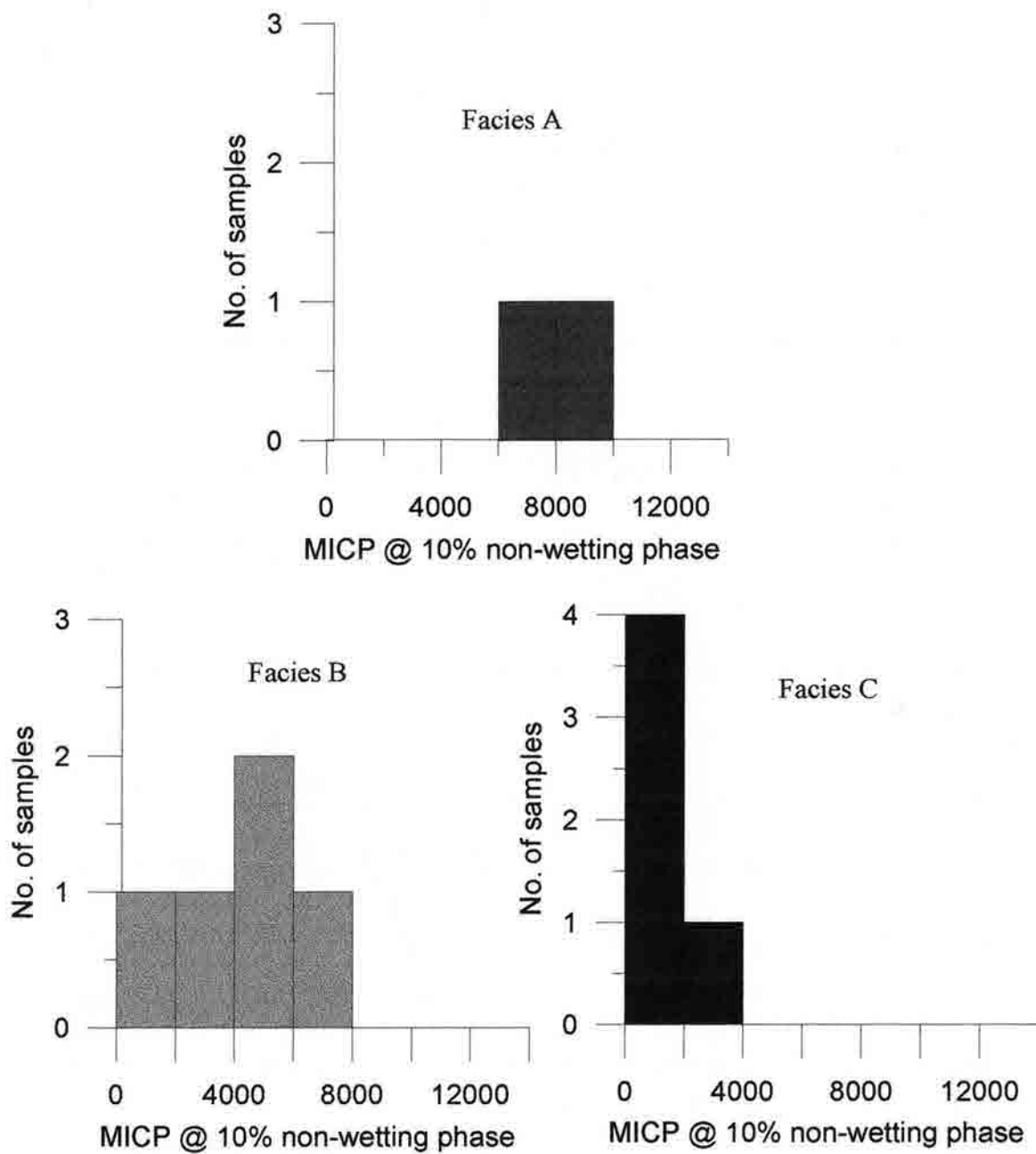


Figure 6.9 Turkey Creek Histogram of MICP at 10% Mercury Saturation for each facies.

Chapter 7. MEADOW SPRINGS (SKULL CREEK SHALE) CORE RESULTS

7.1 Facies Description

The Meadow Springs core is an 80-ft thick interval from 7864-7944 ft that includes the Skull Creek Shale, Muddy “J” Sandstone, and Mowry Shale. The Skull Creek is the bottom 39 ft of this core. Within this interval, there is no underlying contact with the Plainview Formation or any other facies that might underlie the condensed section. The Skull Creek facies present are A, B, and C, with facies K being absent. A diastem or minor surface of erosion separates the Skull Creek from the overlying Muddy sandstone.

The lowest 5.5-ft of the core belongs to facies A or the CS and is the only record of the TST deposits for the Skull Creek in this core. It is a well-laminated, fissile, dark-grayish black shale (Fig. 7.2a). Prominent silt laminations can be seen in hand sample, in addition to intact and broken *Inoceramus*. Some of the silt lenses appear to be small-scale density flows, where silt has been deposited on a slope of clay (Weimer, 1991). A layer of bentonite is located towards the bottom of the core. This facies has type I-II (marine) organic matter (Fig. 7.2b).

The next 20.5-ft of grayish black silty shale overlying the CS, belong to facies B (Fig. 7.3). This silty shale grades into a siltstone, in which fissility is not apparent. This facies includes both graded bedding and hummocky cross-stratification. Diplocriterion or “u-shaped” vertical burrows and “white-walled” or horizontal burrows

A.

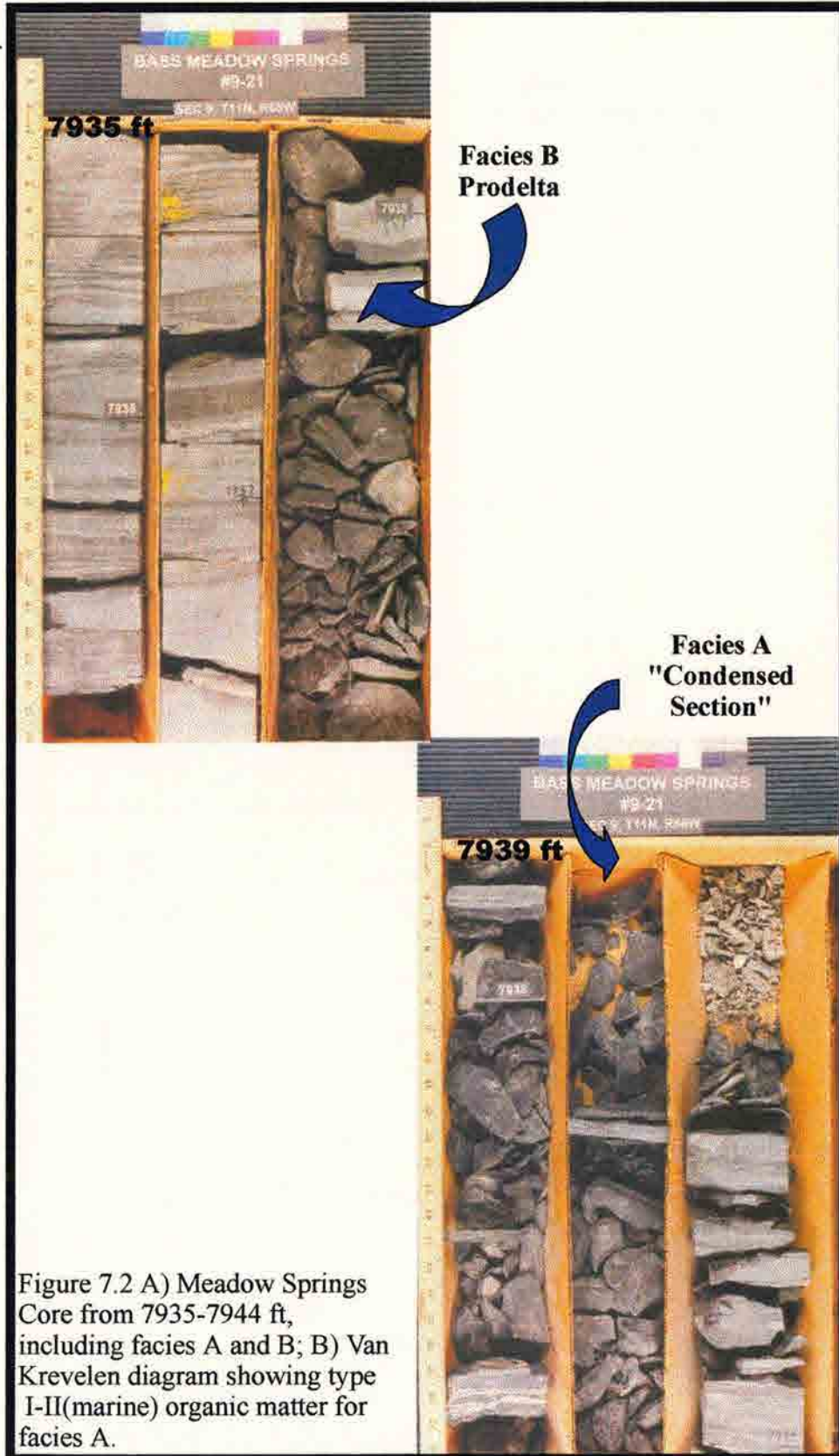


Figure 7.2 A) Meadow Springs Core from 7935-7944 ft, including facies A and B; B) Van Krevelen diagram showing type I-II(marine) organic matter for facies A.

Bottom of Core

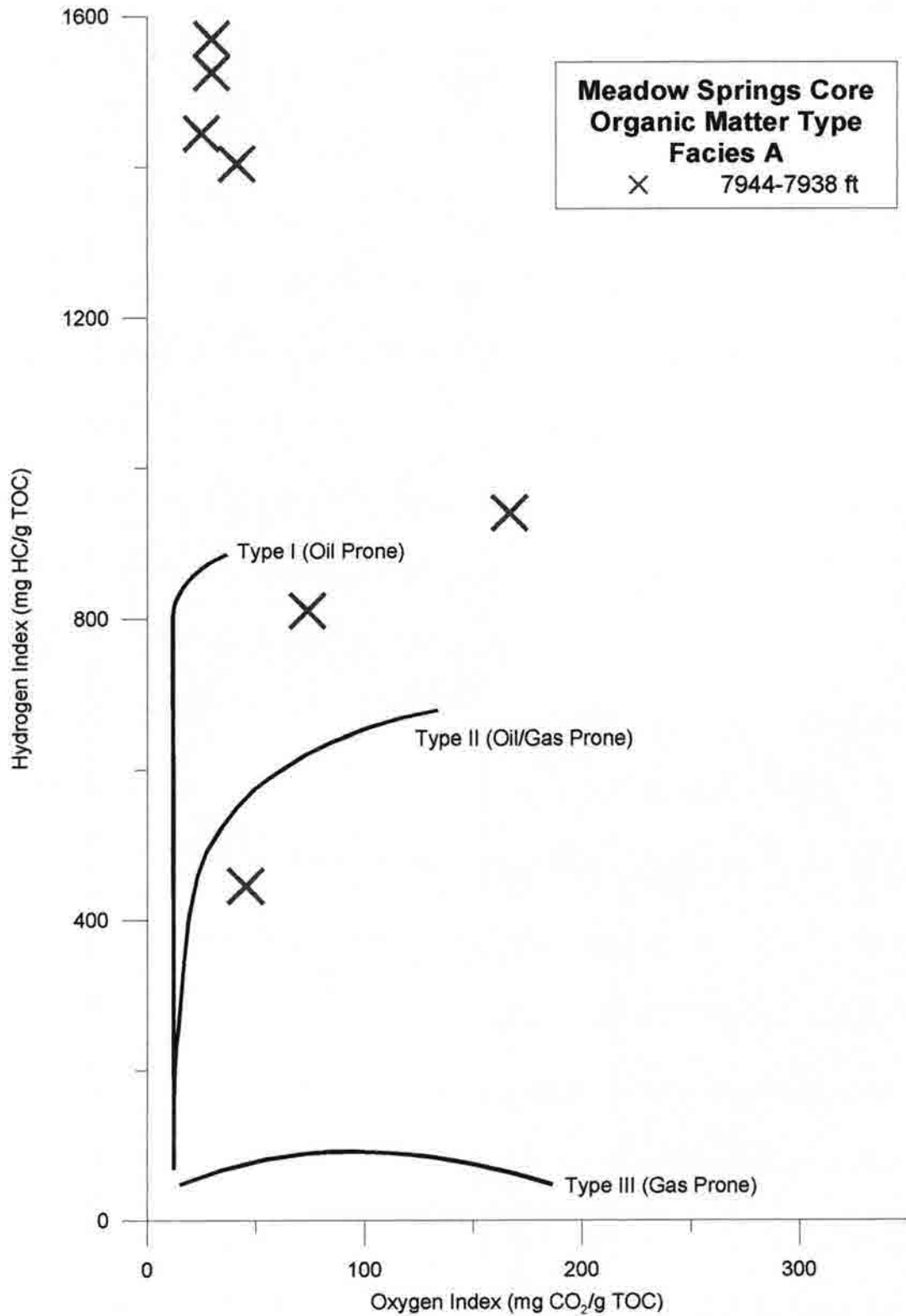


Figure 7.2 B.

A.

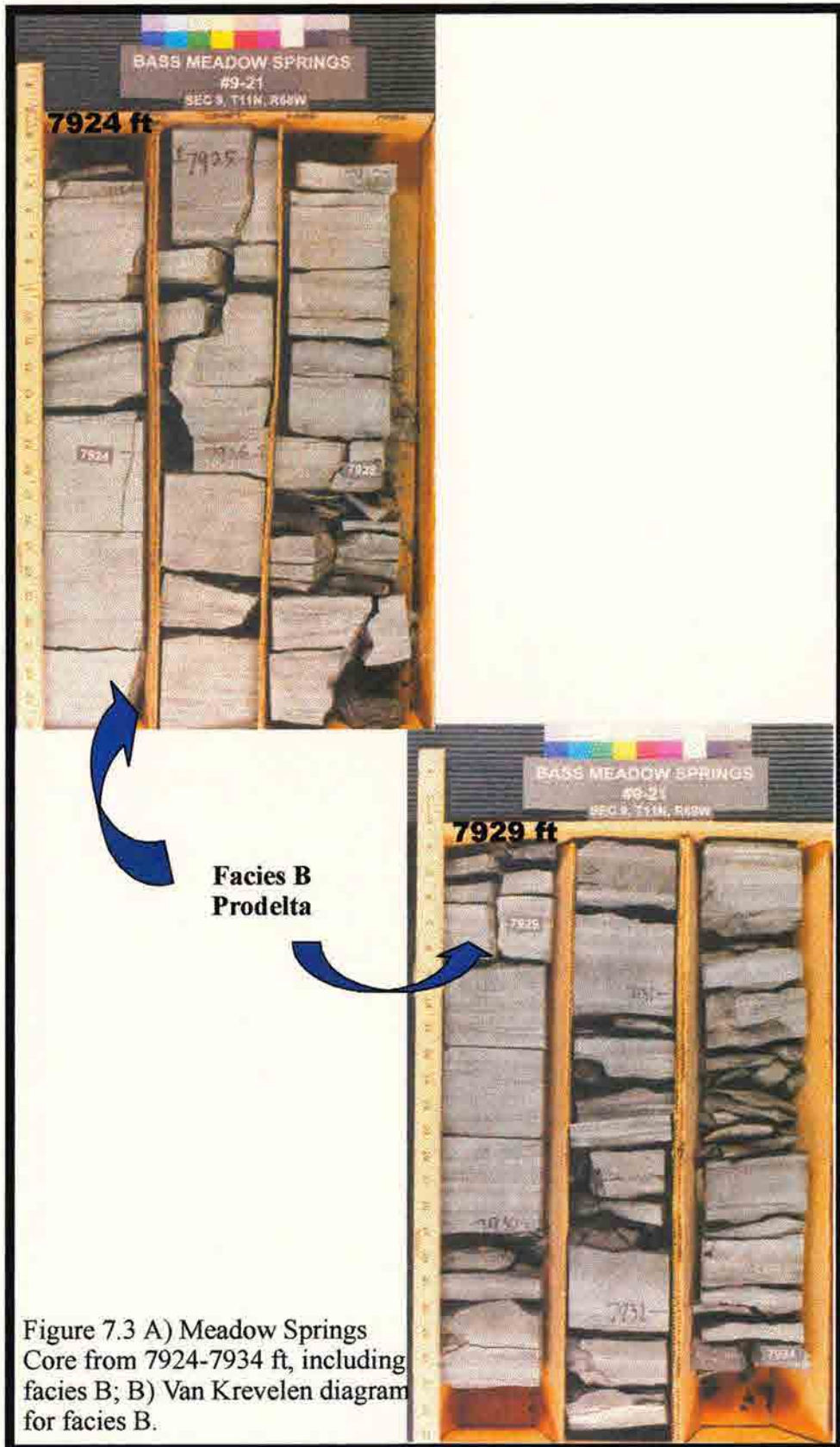


Figure 7.3 A) Meadow Springs Core from 7924-7934 ft, including facies B; B) Van Krevelen diagram for facies B.

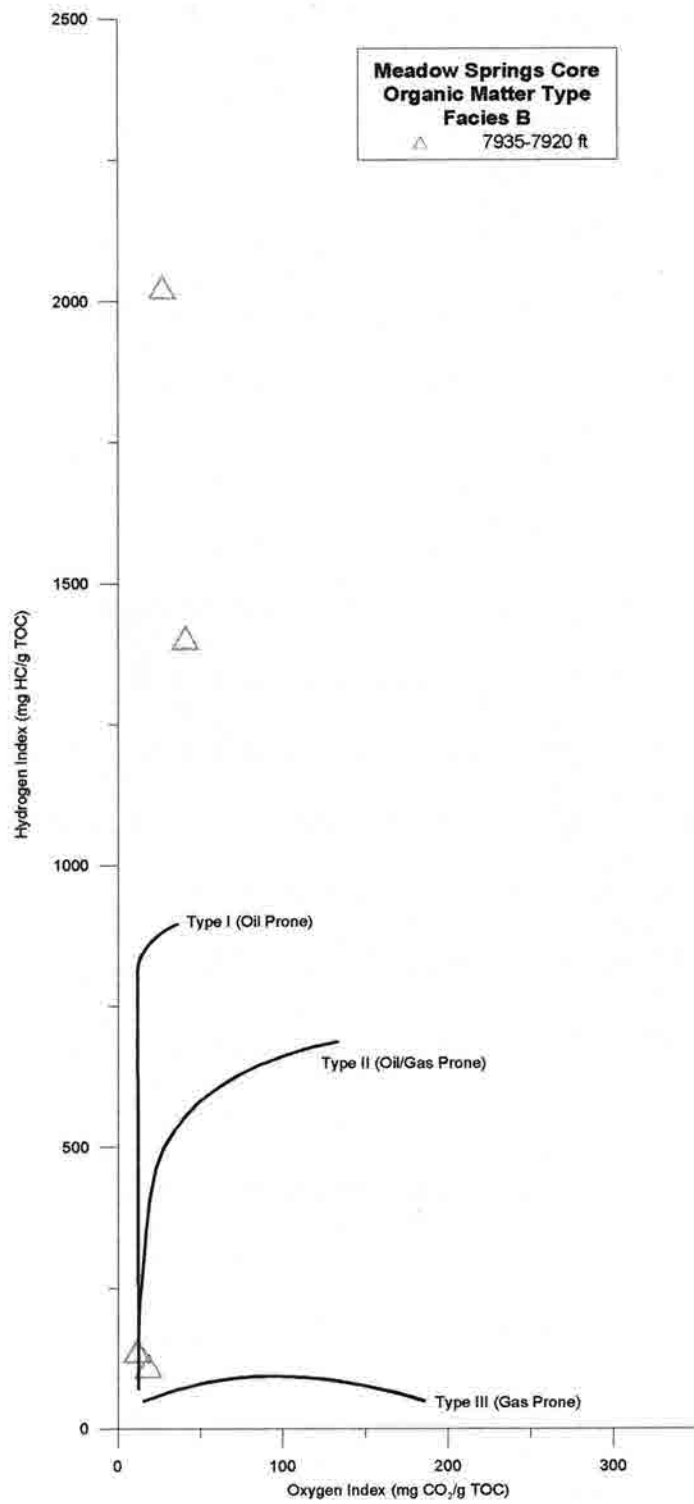


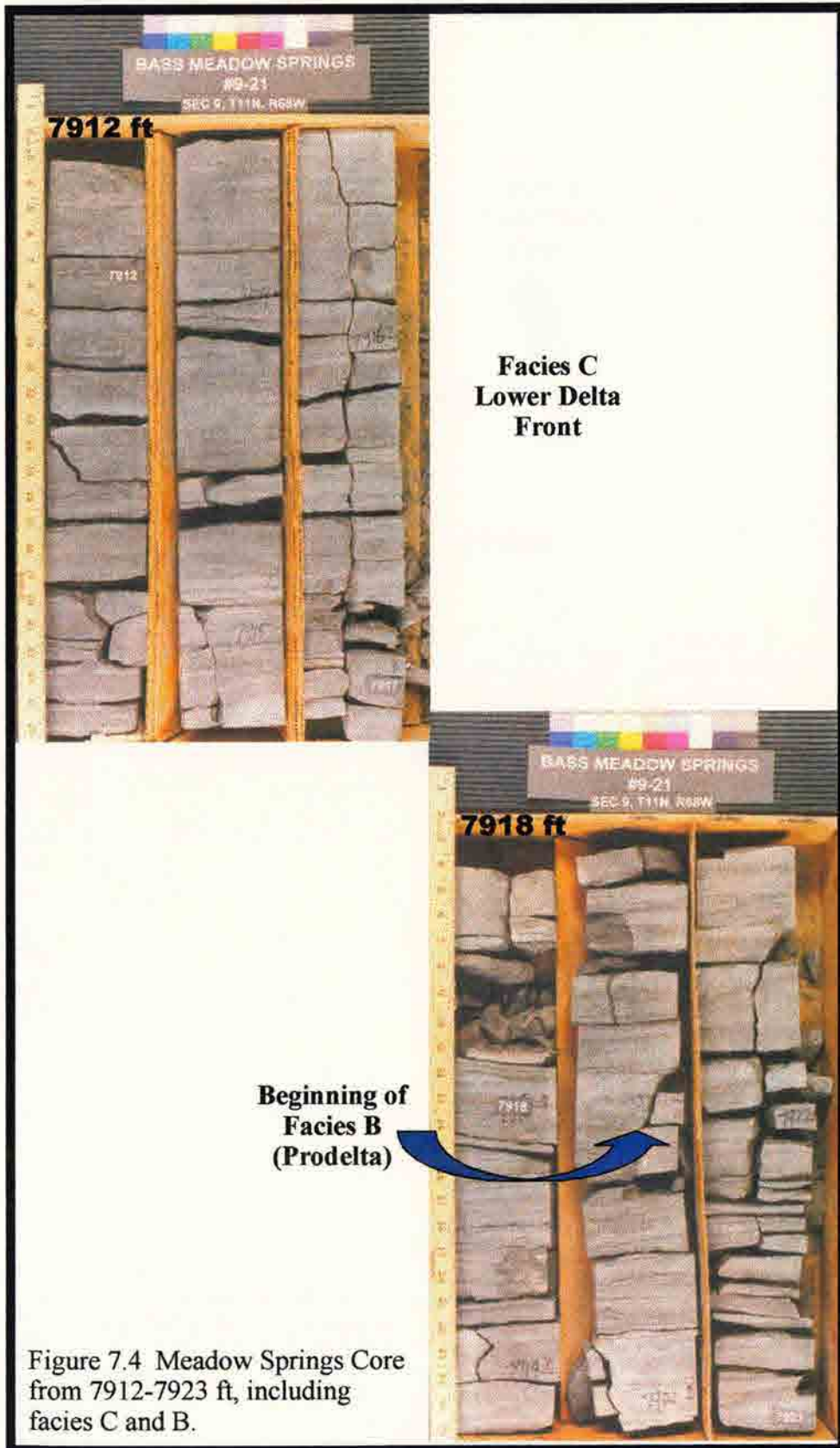
Figure 7.3 B.

are present, in addition to *Inoceramus* debris. Siderite cemented mudclasts can be found throughout facies, along with multiple generations of burrowing. Some structures may be evidence of dewatering.

Overlying facies B, is 16 ft of grayish-black, alternating fine-grained sandstone/silty shale that is represented by facies C (Fig. 7.4a and 7.5a). Intense bioturbation has completely destroyed any relic bedding in this facies. The bioturbation again shows multiple generations of burrowing. The data points are too close to the origin to determine the organic matter, as shown in Figure 7.5b. A coaly deposit is found at a diastem, which is at the top of this facies and represents the end of the Skull Creek. The wireline gamma ray shows no fluctuations throughout the Skull Creek facies A, B, or C.

The next 17.5-ft of whitish-tan sandstone that overlies the diastem, belongs to facies D and the onset of the Muddy sandstone unit (Fig. 7.6a and 7.7a). The wireline gamma ray shows a sharp decrease at this diastem. The diagenetic silica cement has made this a “tight” sandstone. It is fractured and oil stained. Climbing ripples, clay drapes, and carbonized woody debris is found throughout this fluvial facies (Weimer, 1991). It is not possible to determine the type of organic matter because the data are too close to the origin (Fig. 7.6b).

A 3.5-ft paleosol sharply overlies facies D (Fig. 7.8a) (Weimer, 1991). It consists of a very fine grained, light gray clay matrix. Carbonized woody debris, siderite, and pyrite are present. The data points are too close to the origin to determine the organic matter type (Fig. 7.8b).



A.

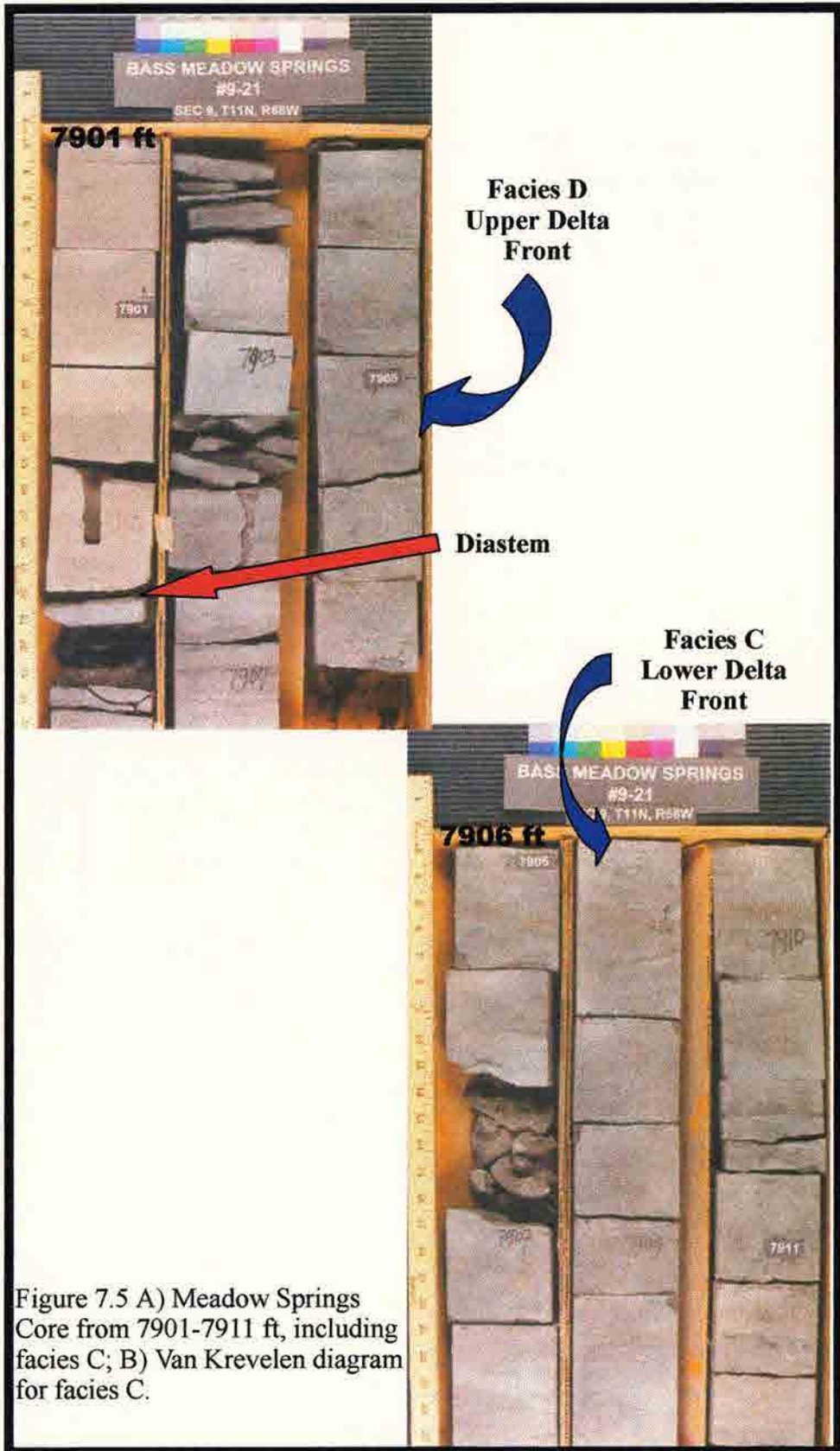


Figure 7.5 A) Meadow Springs Core from 7901-7911 ft, including facies C; B) Van Krevelen diagram for facies C.

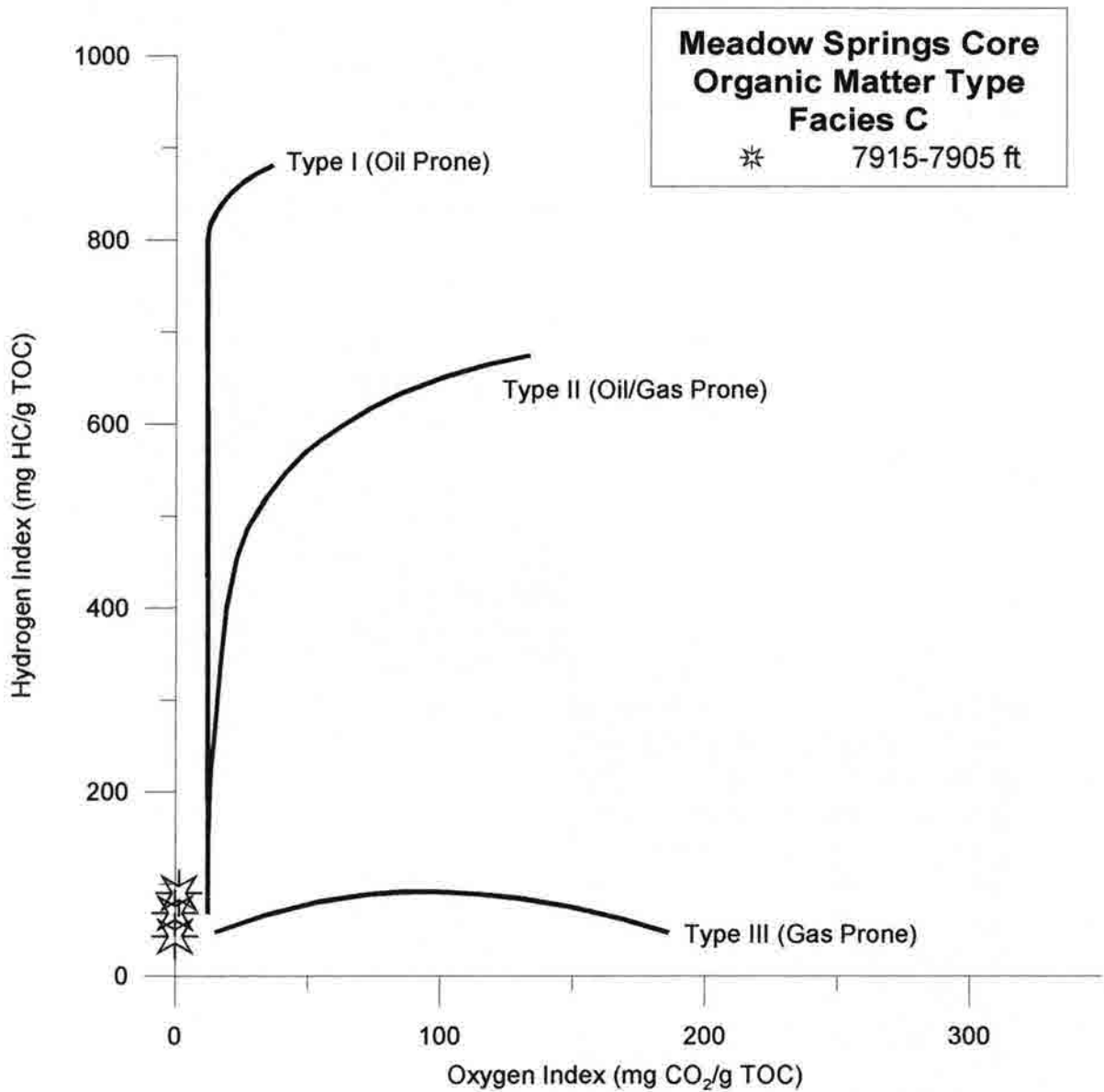


Figure 7.5 B.

A.

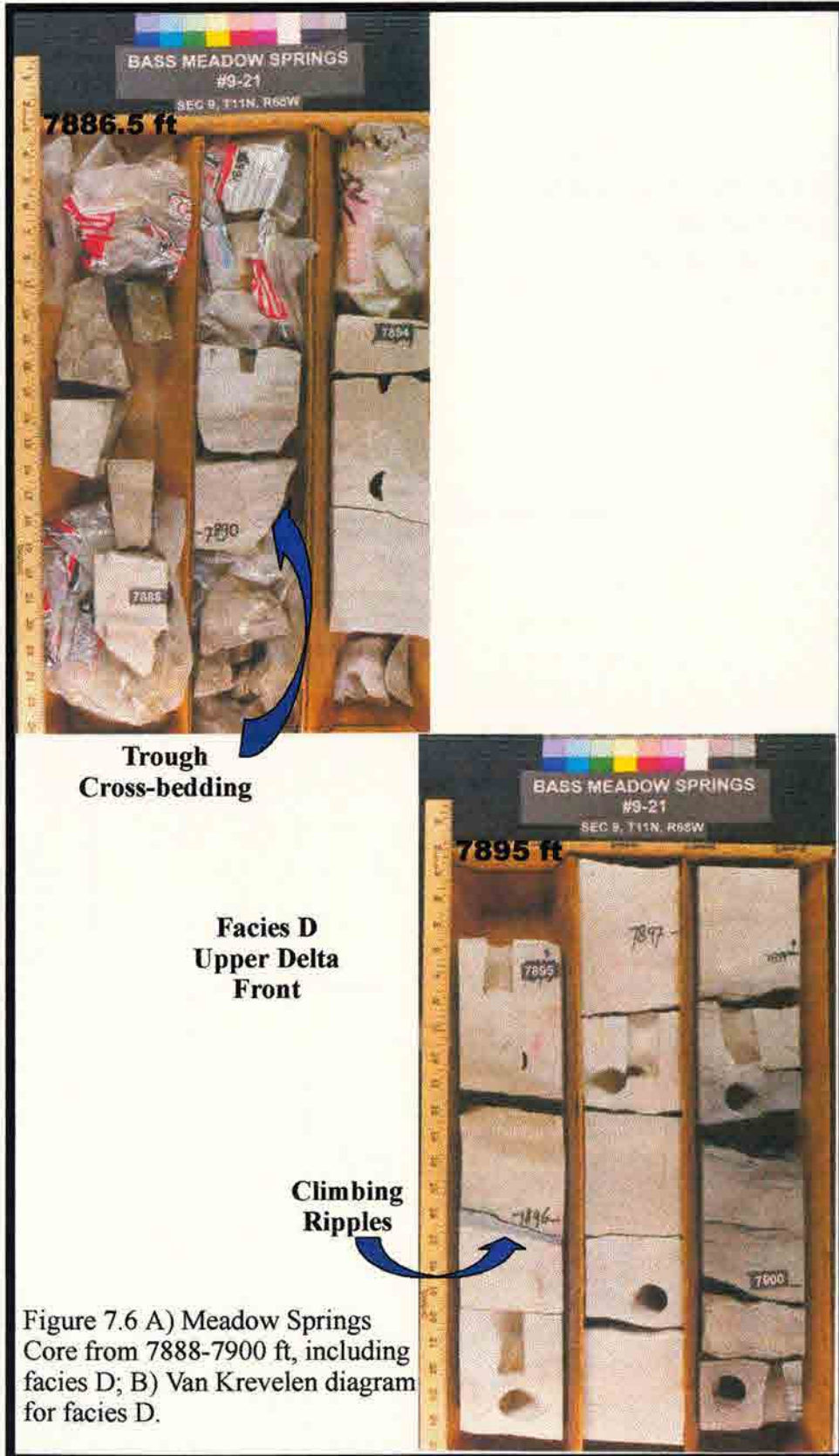


Figure 7.6 A) Meadow Springs Core from 7888-7900 ft, including facies D; B) Van Krevelen diagram for facies D.

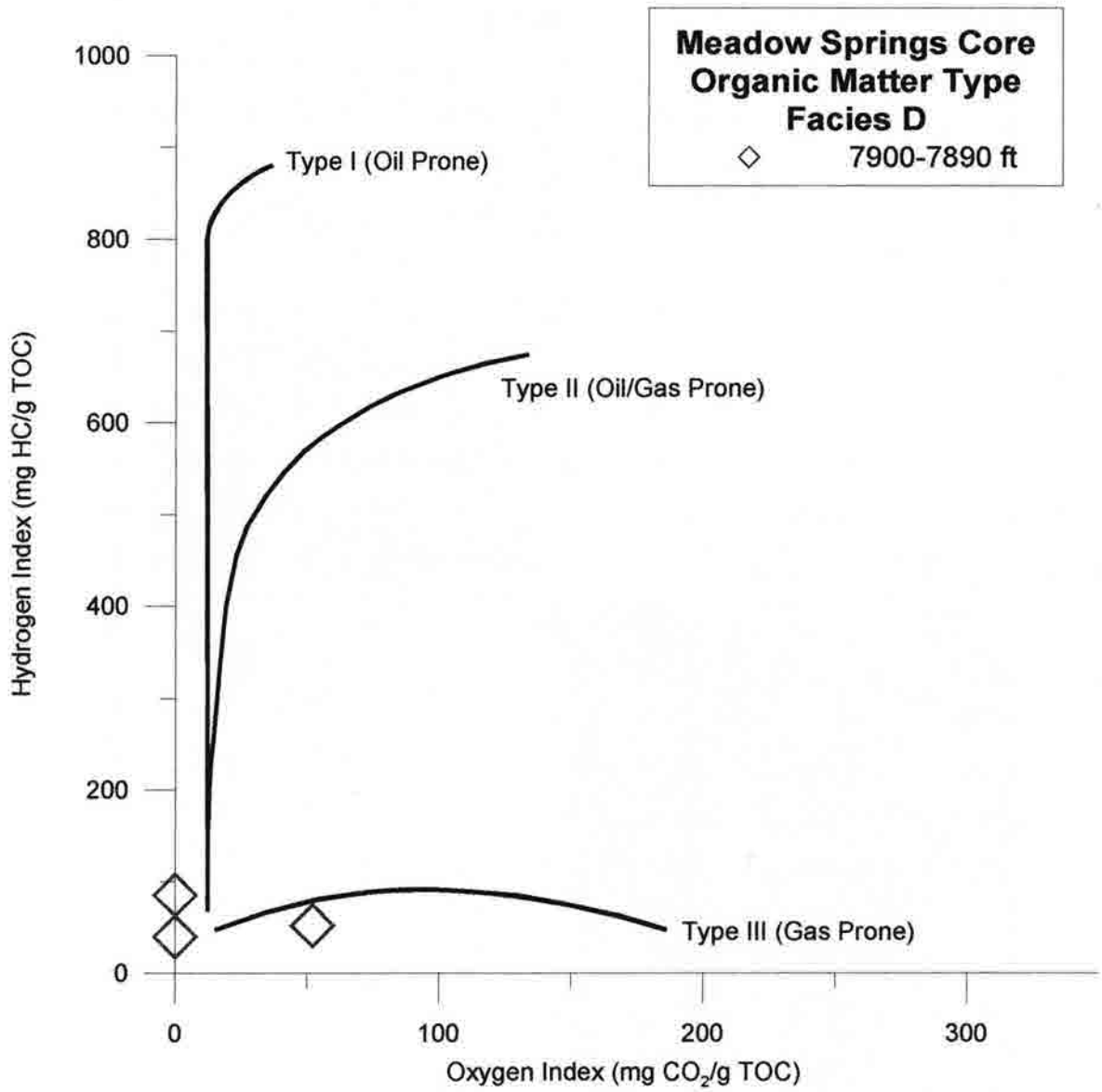


Figure 7.6 B.

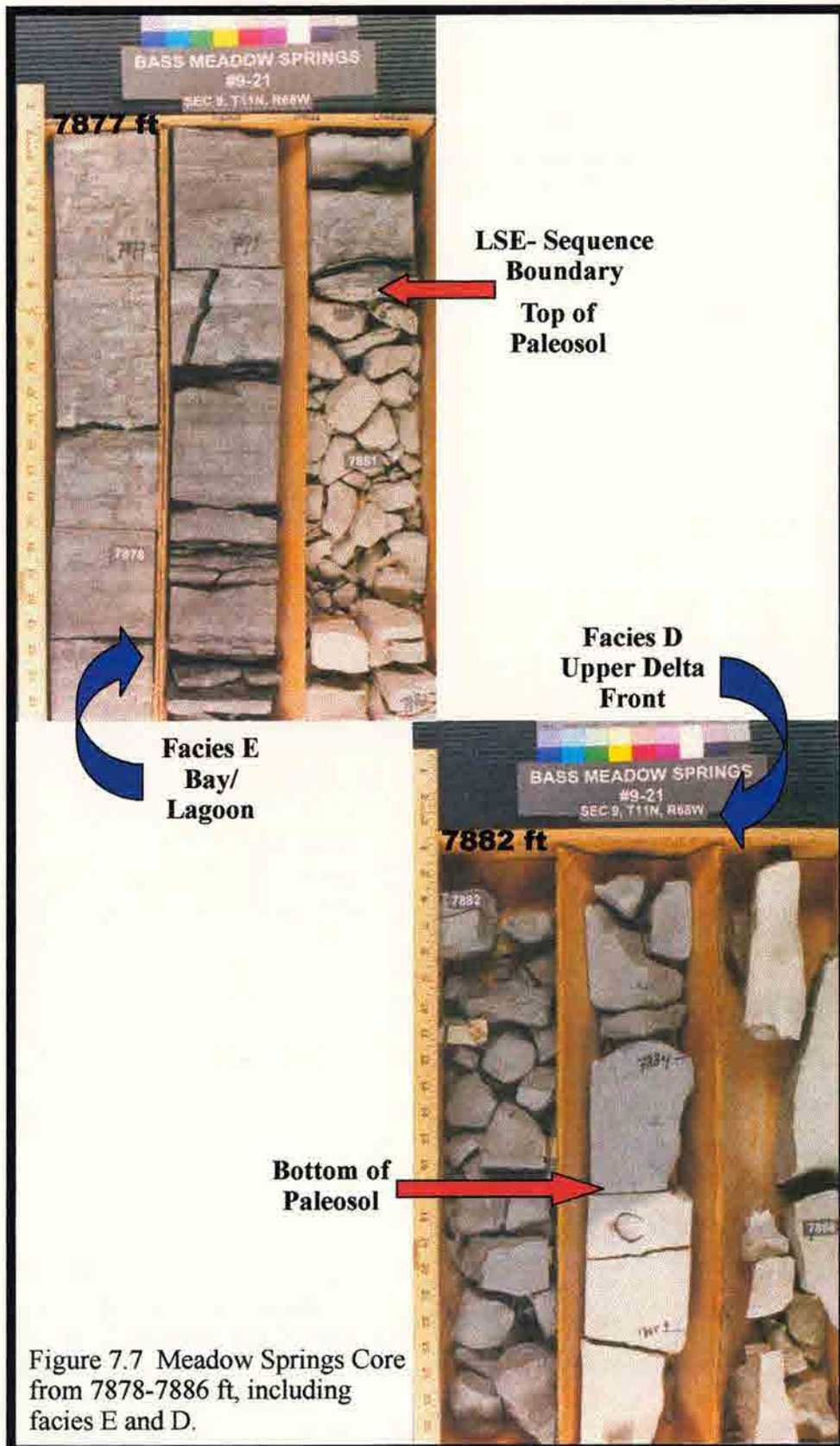


Figure 7.7 Meadow Springs Core from 7878-7886 ft, including facies E and D.

A.

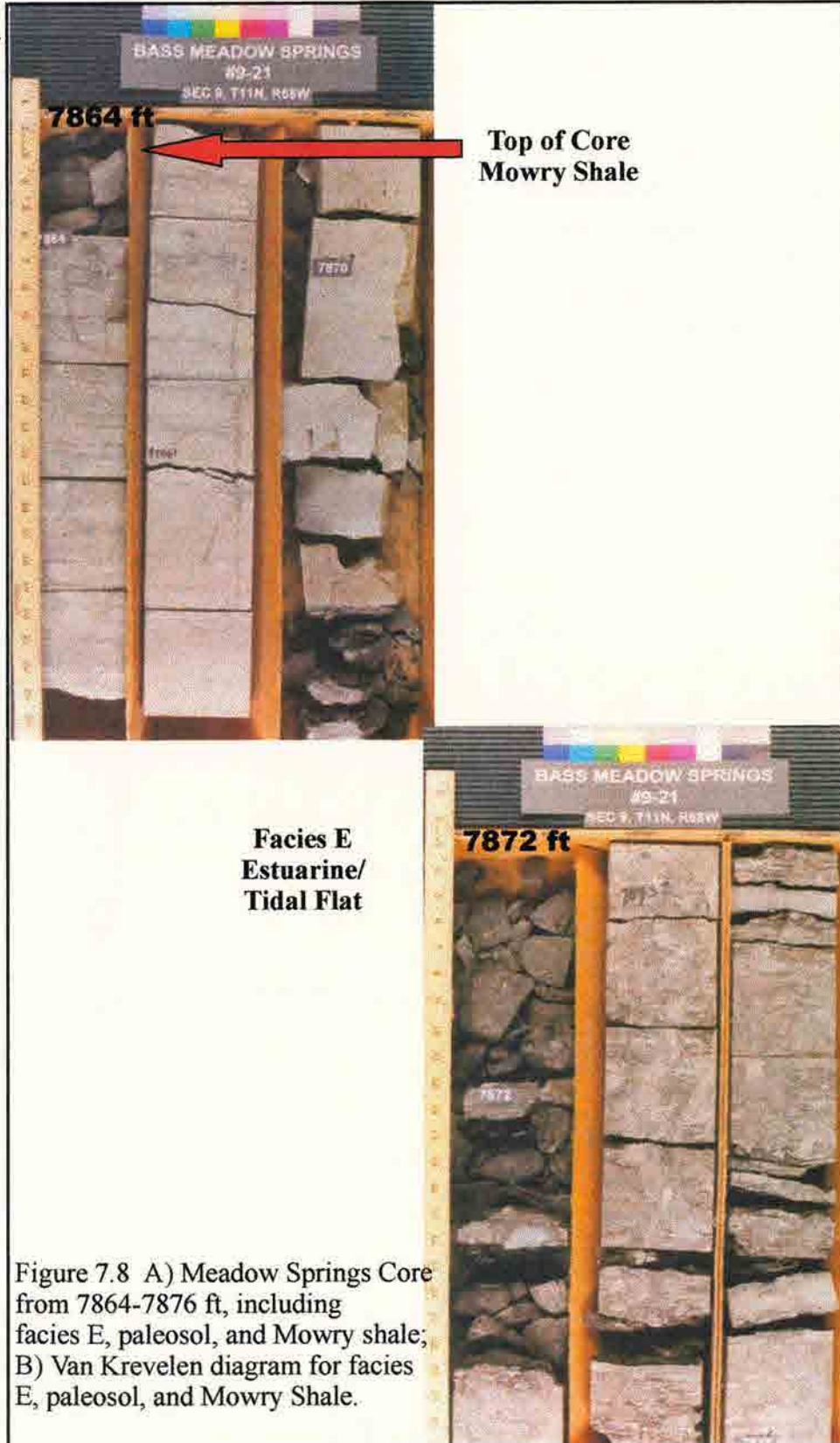


Figure 7.8 A) Meadow Springs Core from 7864-7876 ft, including facies E, paleosol, and Mowry shale; B) Van Krevelen diagram for facies E, paleosol, and Mowry Shale.

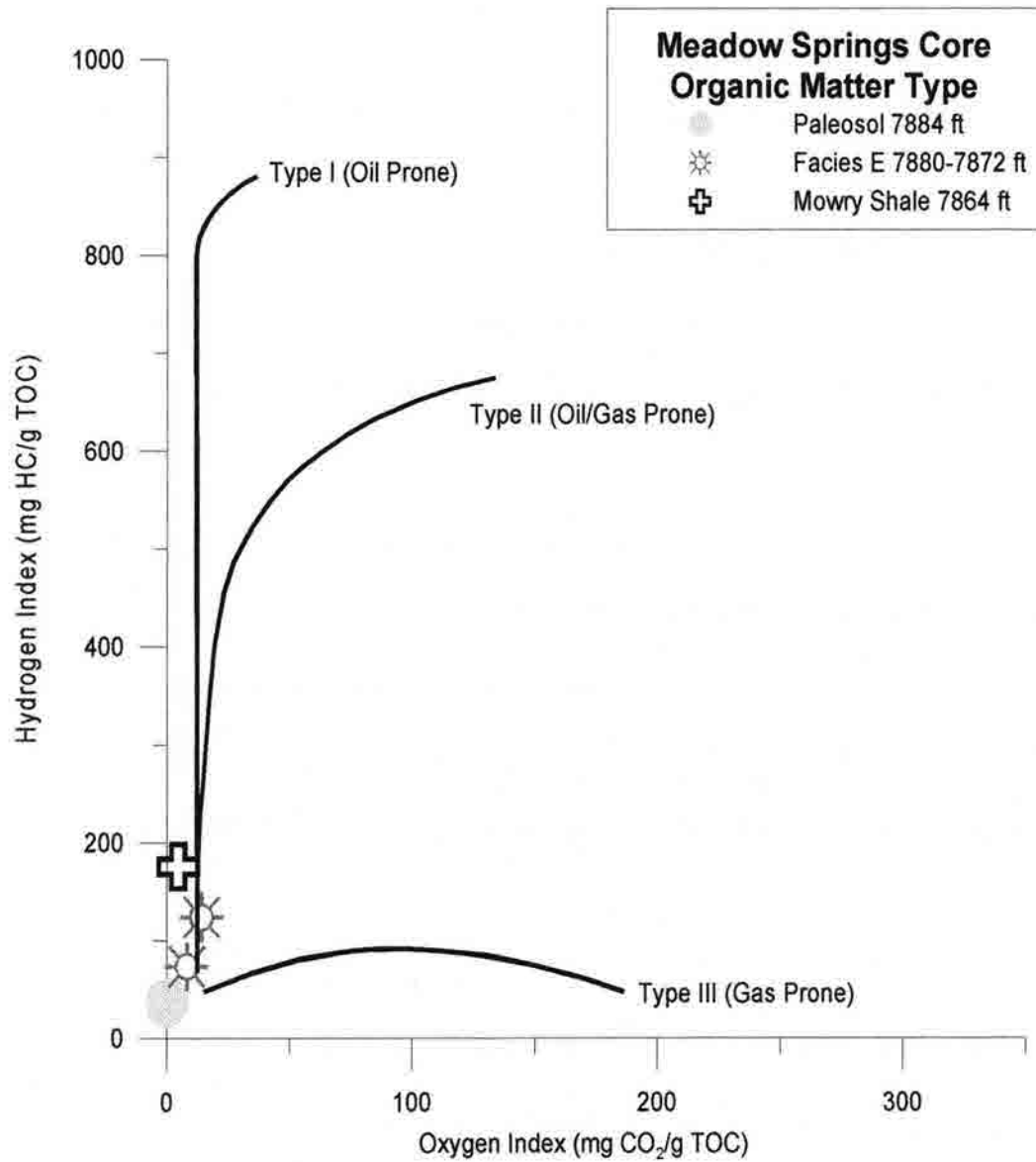


Figure 7.8 B.

At the top of the paleosol, "piping" or vertical burrowing is present, in addition to root traces. Paleosols represent a time of subaerial exposure or a maximum lowstand surface of erosion and represent a time of subaerial exposure.

Above the paleosol, is 10 ft of grayish-black silty shale to siltstone of facies E (Fig. 7.8). This facies has been heavily burrowed and contains white walled burrows and 6-8 in. long Diplocraterion or u-shaped burrows and may be representing a bay/lagoon environment (Weimer, 1991). Facies E is also represented by the overlying 6 ft of light gray, very-fine to fine grained sandstone. This sandstone contains carbonized woody debris and numerous clay drapes. The top of facies E represents the end of the HST deposits.

Directly overlying the HST deposits, is a TSE that is shown by the 1-ft medium grayish black, organic rich shale (Fig. 7.8a). This clay rich shale is well laminated and breaks apart in conchoidal sheets, which are also known as "poker-chip" shale. This 1-ft unit is the extent of the Mowry Shale for this core. This rock has more of a type II (marine) organic matter than the underlying facies E. The wireline gamma ray begins to increase in this unit.

7.2 Lithology Description

Table 7.1 shows the averages and standard deviations for the Meadow Springs Core data. Facies A or the CS has the lowest amount of TOC with the highest hydrogen index in the Skull Creek facies. The CS also has the highest percentage of total clay with both facies A and B having considerable amounts of carbonate (10-12%). Facies B has the highest amounts of total organic carbon. Quartz becomes the major component of the shale in facies C.

Table 7.1 Statistics for the Meadow Springs Core data.

Facies		Total Organic Carbon (%)	Hydrogen Index (mg HC/g TOC)	Hydrogen Index/Oxygen Index (mg HC/mg CO ₂)	Total Clay (wt%)	Quartz (wt%)	Feldspar (wt%)	Carbonate (wt%)	Porosity (%)	Permeability (md)	Density (g/cc)
	# of Analyses	1	1	1	1	1	1	1	1	1	1
Mowry	7864	1.78	176	39	51	41	5	2	3.4	0.00003	2.62
	# of Analyses	2	2	2	2	2	2	2	1	1	1
E	Average	1.96	99	9	37	59	4	0	5.7	0.00028	2.60
	Std Dev										
	# of Analyses	1	1	1	1	1	1	1	1	1	1
Paleosol	7884	0.11	36		59	39	0	2	0.9	3E-06	2.57
	# of Analyses	3	3	1	3	3	3	3	2	2	2
D	Average	0.36	59	1	10	90	0	0	13	0.0175	2.62
	Std Dev	0.3	24		4	4	0	0			
	# of Analyses	3	3	1	3	3	3	3	1	1	1
C	Average	0.59	67	64	29	61	6	3	4.9	0.0008	2.68
	Std Dev	0.14	24		1	8	1	4			
	# of Analyses	4	4	4	4	4	4	4	2	2	2
B	Average	1.23	479	20	33	42	6	12	3.9	0.00011	2.69
	Std Dev	0.53	698	21	7	10	0.5	2			
	# of Analyses	6	7	7	7	7	7	7	2	2	2
A	Average	0.35	1234	35	39	40	5	10	3.9	5.5E-05	2.64
	Std Dev	0.16	532	27	6	7	1	2			

The next three facies (D, E and the paleosol) represent the water shallowing events that lead to the maximum sealevel lowstand or sequence boundary (LSE). Facies D is mainly composed of quartz and very low amounts of total organic carbon with high porosity and permeability. Most of the overlying paleosol is composed of clay with almost no total organic carbon. This paleosol has very low porosity and permeability. Facies E overlies the paleosol and is composed mainly of quartz, but with considerably higher amounts of TOC and no carbonate. Clay is the main constituent of the Mowry

Shale at the top of the core. This corresponds with a relatively high hydrogen index. This shale has very low porosity and permeability values.

These main features have been plotted against stratigraphic height to determine where changes occur relative to seal capacity. The best seal is located in the condensed section or facies A for the Skull Creek, but the paleosol and the Mowry Shale also make excellent seals (Fig. 7.9a). Porosity values are highest in the HST deposits of facies D and lowest in the paleosol (Fig. 7.9b). The lowest permeability values are in facies A, the paleosol and the Mowry Shale (Fig. 7.9c). Density values do not vary much but the samples with the highest sealing capacity seem to have the lowest density (Fig. 7.9d).

The highest amounts of total clay are in facies A, the paleosol and the Mowry Shale (Fig. 7.10a). Quartz shows an inverse relationship to total clay, and is higher in the HST deposits (Fig. 7.10b). Feldspar is not present in the fluvial deposits of facies D, but remains relatively constant throughout the other facies (7.10c). Carbonate is clearly present in the Skull Creek Shale, especially in facies B, than sharply drops off at the beginning of facies D (Fig. 7.10d).

The greatest amount of TOC is found in facies B of the Skull Creek and in facies E (Fig. 7.11a). Hydrogen index values are highest in facies A, with a spike at 7938 ft, which corresponds to high seal capacity (Fig. 7.11b). The ratio of HI/OI shows a corresponding peak to the HI (Fig. 7.11c) in facies A, with another spike at 7915 ft. Appendix P has a detailed summary of the organic geochemistry for this core.

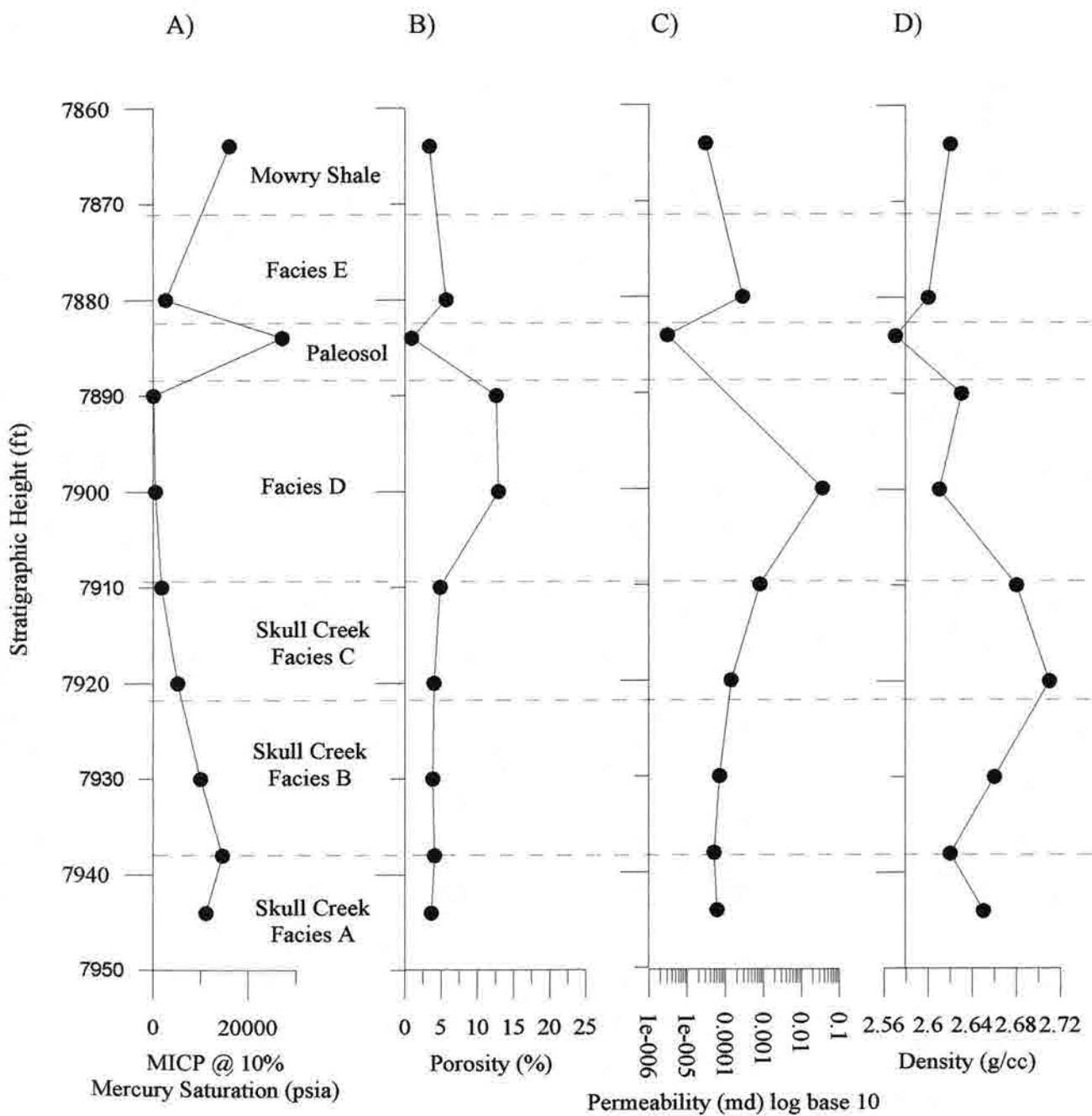


Figure 7.9 Stratigraphic Height vs. MICP (A), porosity (B), permeability (C), and density (D) for Meadow Springs core.

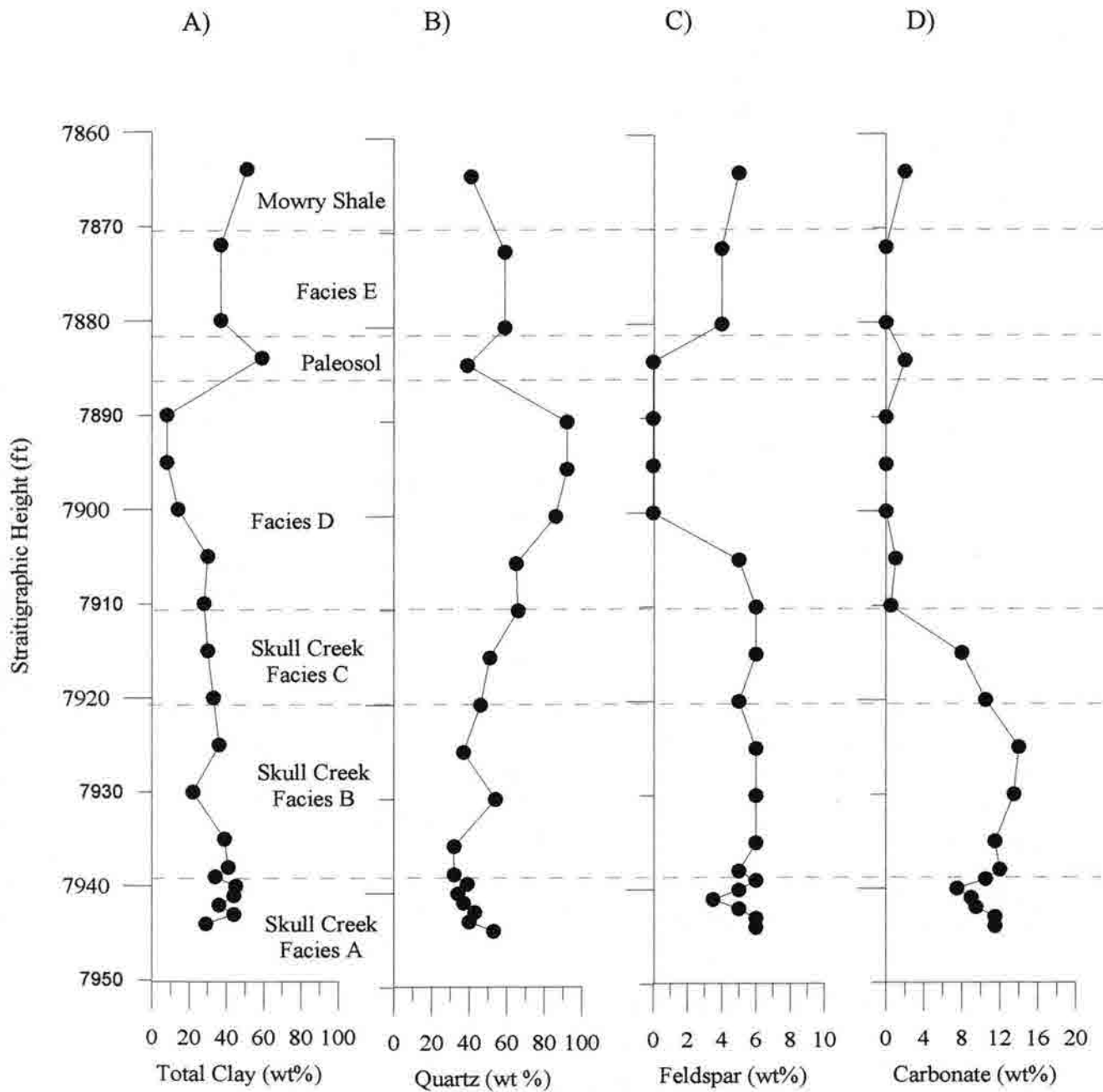


Figure 7.10 Stratigraphic height vs. total clay (A), quartz (B), feldspar (C), and carbonate (D) for Meadow Springs core.

Thin Section Petrography

The thin section petrography data is displayed in Table 7.2, more detailed information is found in Appendix I. Facies A is a well compacted, carbonaceous silty shale with approximately 40% quartz, 38% clay, 5% organic matter, 10-15% carbonate, 2-7% pyrite with minor amounts of feldspar, mica and phosphate. Dolomite, calcite, and siderite are the carbonates present as major cements. The quartz grains are well sorted, subrounded, spherical to elongate, and the size of fine silt to very fine sand. This rock is finely laminated with distinct silt laminations that have a strong preferred grain orientation. Some of the discontinuous laminations of organic matter fluoresce under ultraviolet light, which is a characteristic property of hydrocarbons. Intact and broken Inoceramus are present without any burrowing. No matrix porosity is evident.

Facies B is a well compacted, carbonaceous silty shale to siltstone that ranges from 36-55% quartz, 27-29% clay, 8-25% carbonate, 3-5% organic matter, 3-5% pyrite, and 3-5% mica. The cementation of this facies is provided by dolomite, calcite, and siderite. The quartz grains are well sorted, subrounded, spherical to elongate, and the size of silt to very fine sand. This rock has alternating lamination of clays and silt, with some discontinuous lamination of organic matter. Burrowing has disturbed some of these laminations. Inoceramus debris is found throughout this facies. Some microfracturing has occurred, and may be an artifact of sample preparation. No matrix porosity is detected.

Facies C is a well-compacted, carbonaceous siltstone to sandstone that ranges from 45-66% quartz, ~30% clay, ~2% organic matter, 2-15% carbonate with minor amounts of mica, pyrite, and glauconite. The quartz grains are moderately sorted,

Table 7.2 Meadow Springs Core Thin Section Petrography

Facies	FT	Rockname	Avg. Grain Size (μ)	COMPOSITION						Laminations	Bioturbation	Pressure Solution	Fossils	Porosity
				QTZ	CLAY	ORG	CARB	PYR	OTHER					
E	7880	siltstone	83	60	37	3	0	0	mica, feld	Y	Y	N	N	5
Paleo	7884	paleosol	80	39	60	1	0	0		N	N	N	N	N
D	7895	sandstone	101	87	9	2	0	2	mica, feld	N	N	Y	N	15-20
C	7905	sandstone	82	65	30	2	0	Y	3% mica, glauc	N	Y	Y	N	5
C	7910	siltstone	77	66	30	2	2	Y	mica, glauc.	N	Y	Y	N	N
C	7915	siltstone	58	45	27	3	15	5	5% mica	N	Y	Y	N	N
B	7920	siltstone	52	37	27	3	25	3	5% mica	Y	Y	Y	N	N
B	7925	siltstone	40	36	29	4	25	3	3% mica, sid	Y	Y	Y	Y	N
B	7930	silty shale	31	55	27	5	8	5	siderite	Y	Y	Y	N	N
A	7938	silty shale	26	42	37	4	10	7	mica,	Y	N	Y	Y	N
A	7939	silty shale	18	42	38	5	10	5	mica, phosp.	Y	N	Y	Y	N
A	7944	silty shale	31	40	38	5	15	2	feld, mica	Y	N	Y	Y	N

*NOTE: Point count percentages are in bold, other percentages are estimates.

**NOTE: 1/256 < silt < 1/16 mm, 1/16 < VF sand < 1/8 mm, 1/8 < F sand < 1/4 mm, 1/4 < M sand < 1/2 mm

LEGEND:

QTZ= Quartz

ORG= Organic Matter

CARB= Carbonate (calcite, dolomite, siderite)

feld= Feldspar

phos= Phosphate

mic= Mica

hem= Hematite

subrounded, spherical to elongate, and the size of silt to fine sand. Dolomite, calcite, and siderite are the carbonates that form the major cement. No laminations are noted in this facies as the intense bioturbation has probably destroyed any bedding features. Minor intergranular porosity up to 5% is visible.

Facies D is a fine-grained sandstone with approximately 85% quartz, 10% clay, 2% organic matter, 3% pyrite and minor amounts of mica and feldspars. The quartz grains are moderately sorted, subrounded, spherical to elongate and the size of silt to medium sand. No laminations or fossils are present, with the exception of some lenticular laminations of organic matter. However, burrowing may have destroyed some

of the previous bedding features. Up to 15-20% intergranular porosity with minor intercrystalline porosity is detected.

The paleosol has a 60% clay matrix with 39% of the quartz grains being very fine sand sized. Minor amounts (1%) of organic matter occur as wispy laminations. Overall, the clay matrix is not laminated or bioturbated but does show evidence of root traces, with Fe-staining along with some phosphate material. No porosity is evident.

Facies E is a carbonaceous siltstone with approximately 60% quartz, 37% clay, 3% carbonate with minor amounts of mica and feldspars. Quartz grains are well sorted, subrounded, spherical to elongate, and the size of silt to fine sand. This siltstone has alternating laminations of silt and clay with wispy laminations of organic matter. Some of these laminations have been disturbed by burrowing or soft sediment deformation. Up to 5% intergranular porosity is visible.

Scanning Electron Microscopy

Appendix J contains SEM photomicrographs along with detailed descriptions for each facies. Facies A is a moderately sorted, angular to subrounded, framework supported silty shale. The framework particle size ranges from 10 to 50 μm . The framework mineralogy consists of detrital quartz with significant amounts of authigenic framboidal pyrite and minor amounts of carbonate and/or feldspars. This facies also contains shell fragments. The clays in this rock occur primarily as grain coatings and pore fillings. Discrete illite can be distinguished by its "flake-like" appearance. This facies exhibits a poorly developed intergranular macropore system and a poorly developed micropore system. Molds of plucked grains (pyrite and quartz) are found throughout this sample.

Facies B is a moderately to well sorted, subangular to subrounded, framework supported silty shale. The framework particle size ranges from 10 to 50 μm . The framework mineralogy consists of detrital quartz with significant amounts of authigenic framboidal pyrite, and minor amounts of carbonate and/or feldspars. The clays in this rock occur primarily as grain coatings and pore fillings. Individual clays, such as discrete illite and small "books" of kaolinite can be distinguished. This facies exhibits a poorly developed intergranular macropore system and a poorly developed micropore system. Molds of plucked grains are found throughout this sample.

Facies C is a moderately to well sorted, subangular to subrounded, framework supported silty shale. The framework particle size ranges from 20 to 50 μm . The framework mineralogy consists of detrital quartz with minor amounts of feldspars. The clays in this rock occur primarily as grain coatings and pore fillings. Individual booklets of kaolinite are prominent throughout this sample. This facies exhibits a poor to moderately developed intergranular macropore system and a poorly developed micropore system.

Facies E is a moderately sorted, subangular to subrounded, framework supported silty shale. The framework particle size ranges from 10 to 50 μm . The framework mineralogy consists of detrital quartz with minor amounts of feldspars. The clays in this rock occur primarily as grain coatings and pore fillings. Individual clays, such as discrete illite and small "books" of kaolinite can be distinguished. This facies exhibits a moderately developed intergranular macropore system and a moderately developed micropore system.

Whole Rock Mineralogy

The whole rock mineralogy for the entire core is provided in Table 7.3. Facies A averages the highest amounts of total clay (39%) and pyrite (9%) for the Skull Creek facies with 9% pyrite, 8% dolomite, and minor amounts of plagioclase, potassium feldspar, calcite, and siderite. Facies B has the highest amount of dolomite and less clay and more quartz than the condensed section. A dramatic increase in the amount of quartz is seen in facies C with the average of 61% quartz, with minor amounts of dolomite, pyrite, plagioclase, potassium feldspar, and siderite.

Facies D consists almost entirely of quartz (90%). The paleosol averages 59% total clay, 39% quartz, and 2% siderite. Facies E averages 59% quartz and 37% total clay, while the Mowry Shale averages 51% total clay and 42% quartz. The amount of dolomite and calcite is much less in the Muddy Sandstone and Mowry Shale than in the Skull Creek. For the entire core, total clay is highest in the paleosol, followed by the Mowry Shale and facies A of the Skull Creek, respectively.

Clay Mineralogy

The clay mineralogy for the entire Meadow Springs core is displayed in Table 7.4. Facies A has the average value of 71% for the total amount of illite/smectite (I/S), all of which has R0 ordering. It is complimented by 26% illite, 2% chlorite, and 1% kaolinite. Facies B is very similar with the average of 69% R0 I/S, 26% illite, 4% kaolinite, and 1% chlorite. Facies C averages 67% R0 I/S, 19% kaolinite, 11% illite, and 3% chlorite. This facies has significantly more kaolinite than either facies A or B. Facies D provides a dramatic change from the clay mineralogy found in the Skull Creek.

Table 7.3 Whole Rock Mineralogy (wt%): Bass Meadow Springs Core

Facies	Sample#	Depth (FT)	TCL	QTZ	KSP	PLAG	CAL	DOL	PYR	SID	ANH
Mowry	MS066	7864	51	42	2	3	ND	ND	0	2	ND
E	MS062	7872	37	59	2	2	ND	ND	TR	ND	ND
	MS058	7880	37	59	2	2	ND	ND	TR	ND	ND
	Average		37	59	2	2	0	0	0	0	0
Paleo	MS055	7884	59	39	ND	ND	ND	ND	ND	2	ND
D	MS052	7890	8	92	ND	ND	ND	ND	ND	ND	TR
	MS049	7895	8	92	ND	ND	ND	ND	ND	ND	TR
	MS044	7900	14	86	ND	ND	ND	ND	ND	ND	ND
	Average		10	90	0	0	0	0	0	0	0
C	MS039	7905	30	65	2	3	ND	TR	TR	TR	ND
	MS034	7910	28	66	2	4	ND	TR	TR	ND	ND
	MS029	7915	30	51	2	4	ND	6	5	2	ND
	Average		29	61	2	4	0	6	5	2	0
B	MS024	7920	33	47	2	3	ND	10	5	TR	ND
	MS019	7925	36	38	2	4	1	11	6	2	ND
	MS014	7930	22	54	2	4	TR	12	5	1	ND
	MS009	7935	39	32	2	4	TR	9	12	2	ND
	Average		33	43	2	4	1	11	7	2	0
A	MS006	7938	41	33	2	3	2	8	9	2	ND
	MS005	7939	34	40	2	4	TR	8	10	2	ND
	MS004	7940	45	34	2	3	TR	5	9	2	ND
	MS003	7941	44	37	TR	3	TR	8	8	TR	ND
	MS002	7942	36	43	2	3	2	7	7	TR	ND
	MS001	7943	44	39	2	4	2	9	TR	TR	ND
	MS000	7944	29	54	2	4	ND	11	TR	TR	ND
	Average		39	40	2	3	2	8	9	2	0

LEGEND: QTZ= Quartz SID= Siderite GYP= Gypsum
TCL= Total Clay and Mica PYR= Pyrite TR= Trace ND= Not Detected
DOL= Dolomite JAR= Jarosite PLAG= Plagioclase MG-CAL= Mg-rich Calcite
ANHY= Anhydrite KSP= K-Feldspar

It averages 75% kaolinite, 12% serpentine, and 10% I/S with R1 ordering. The paleosol clay minerals are 100% kaolinite. Facies E averages 76% R0 I/S, 20% kaolinite, 2% illite, and 2% chlorite. The clays in the Mowry Shale are more akin to what is found in the Skull Creek with 70% R0 I/S, 25% illite, 4% kaolinite, and 2% chlorite.

7.3 Petrophysical Description

The Meadow Springs core injection pressures (psia) at 10% mercury saturation and the corresponding hydrocarbon column heights (HCH) are displayed in Table 7.5. They are sorted in descending order of injection pressures. The highest pressure is the

Table 7.4 Meadow Springs Clay Mineralogy

Facies	Sample #	Depth (ft)	R1 I/S		R0 I/S		Total amt. I/S	Illite	Kaol	Chlorite	Serp.	Laumontite
			Exp.	Con.	Exp.	Con.						
Mowry	MS066	7864		0	10	60	70	25	4	2	0	0
					40	10						
E	MS062	7872		0	48	73	73	3	20	4	0	0
	MS058	7880		0	40	60	79	1	20	0	0	0
					10	19						
	Average							76	2	20	2	0
Paleo	MS055	7884		0		0	0	0	100	0	0	0
D	MS052	7890	50	10		0	10	5	85	0	0	0
	MS049	7895	50	10		0	10	5	85	0	0	0
	MS044	7900	55	10		0	10	1	55	0	35	0
	Average							10	4	75	0	12
C	MS039	7905		0	34	62	62	3	30	5	0	0
	MS034	7910		0	47	69	69	2	25	4	0	0
	MS029	7915		0	31	70	70	27	2	1	0	0
	Average							67	11	19	3	0
B	MS024	7920		0	28	67	67	27	4	2	0	0
	MS019	7925		0	20	69	69	26	4	1	0	0
	MS014	7930		0	28	44	44	45	9	2	0	0
	MS009	7935		0	17	94	94	5	1	1	0	0
	Average							69	26	4	1	0
A	MS006	7938		0	25	70	70	29	1	1	0	0
	MS005	7939		0	27	70	70	27	1	2	0	TR
	MS004	7940		0	38	70	70	29	1	1	0	TR
	MS003	7941		0	35	78	78	21	1	1	0	0
	MS002	7942		0	36	70	70	27	1	2	0	TR
	MS001	7943		0	22	67	67	27	2	4	0	TR
	MS000	7944		0	31	71	71	23	2	4	0	0
	Average							71	26	1	2	0

LEGEND:

R1 I/S= Ordered Illite/Smectite (Reichweite=1); (2:1 mixed-layer clay)

R0 I/S= Randomly Ordered Illite/Smectite (Reichweite=0); (2:1 mixed-layer clay)

Kaol= Kaolinite (1:1 Clay)

Serp= Serpentine (1:1 Clay)

paleosol at 27,120 psia, with a corresponding HCH of 7630 ft. This is by far the highest sealing capacity of all the rocks that have been examined in this study. This is followed by the Mowry Shale which holds a 4,305 ft HCH at an injection pressure of 16,030 psia. The third highest injection pressure is found in facies A of the Skull Creek at 14,600 psia which holds a HCH of 4100 ft.

Table 7.5 Meadow Spring Core Injection Pressures (psia) at 10% Mercury Saturation

Facies	Sample#	FT	PSIA@10% SAT.	HCH (ft)
Mowry	MS066	7864	16030	4310
E	MS058	7880	2616	725
Paleo	MS055	7884	27120	7630
D	MS052	7890	67	10
D	MS044	7900	509	135
C	MS034	7910	1790	495
B	MS024	7920	5220	1460
B	MS014	7930	10000	2810
A	MS006	7938	14600	4100
A	MS000	7944	11150	3130

The overall shapes of the drainage curves are displayed in Figures 7.12a, b, c, d, and e. Facies A shows two broadly sloping upper curves with entry pressures between 3,000 and 4,000 psia (Fig 7.12a). Facies B has two similar shaped drainage curves with slightly lower entry pressures (Fig 7.12b). Facies C has a much steeper sloping upper curve with a much lower entry pressure around 600 psia (7.12c). Facies D provides an even steeper sloping upper curve with extremely low entry pressures (7.12d). The paleosol and the Mowry Shale (Fig. 7.12e) show broadly sloping upper curves with entry pressures around 6-7,000 psia. Facies E has a steeper slope with a lower entry pressure.

Appendix K shows the individual MICP graphs for each sample of the Meadow Springs core. Facies A generally shows one population with a well sorted median PTD that ranges from 0.007-0.01 microns. Facies B shows one population of a moderately well sorted median PTD that ranges from 0.01-0.0175 microns. Facies C displays two populations with a moderately well sorted median PTD of 0.0175 microns that composes 80% of the sample with the remaining 20% PV having a very sorted median PTD of 0.15 microns.

Meadow Springs Drainage Curve (facies A)

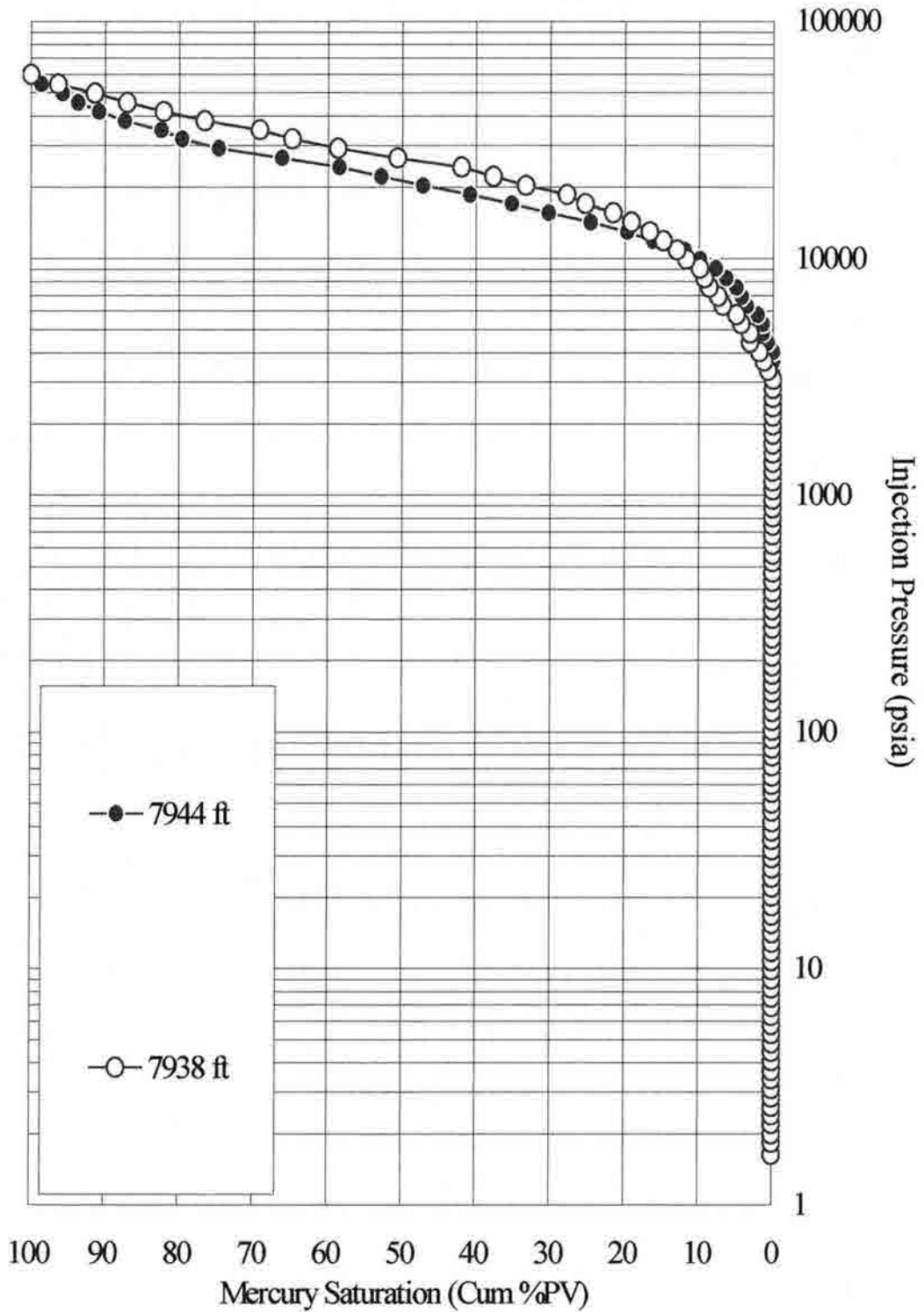


Figure 7.12a Drainage Curve of Facies A for Meadow Springs Core.

Meadow Springs Drainage Curve (facies B)

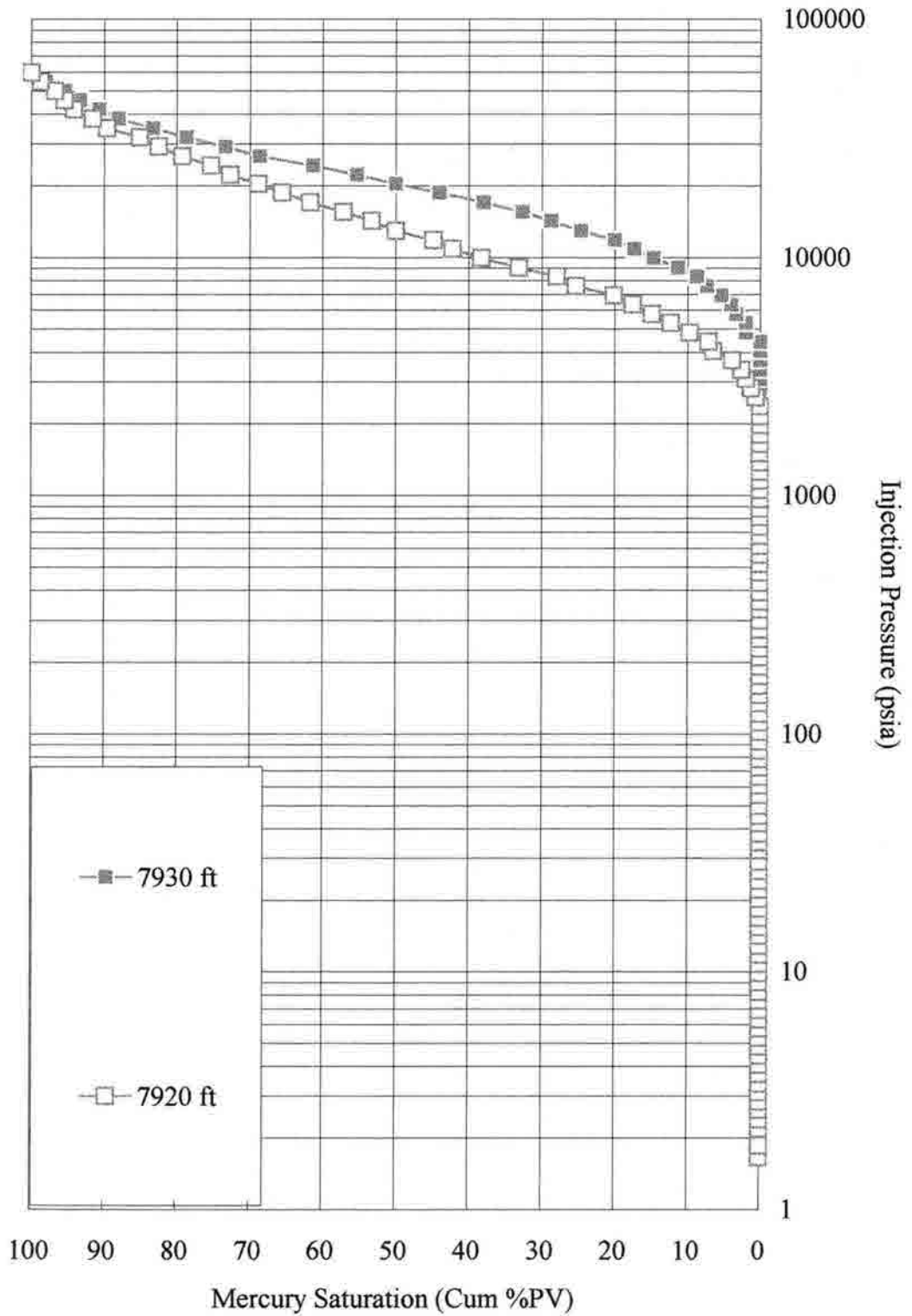


Figure 7.12b Drainage Curve of facies B for Meadow Springs Core.

Meadow Springs Drainage Curve (facies C)

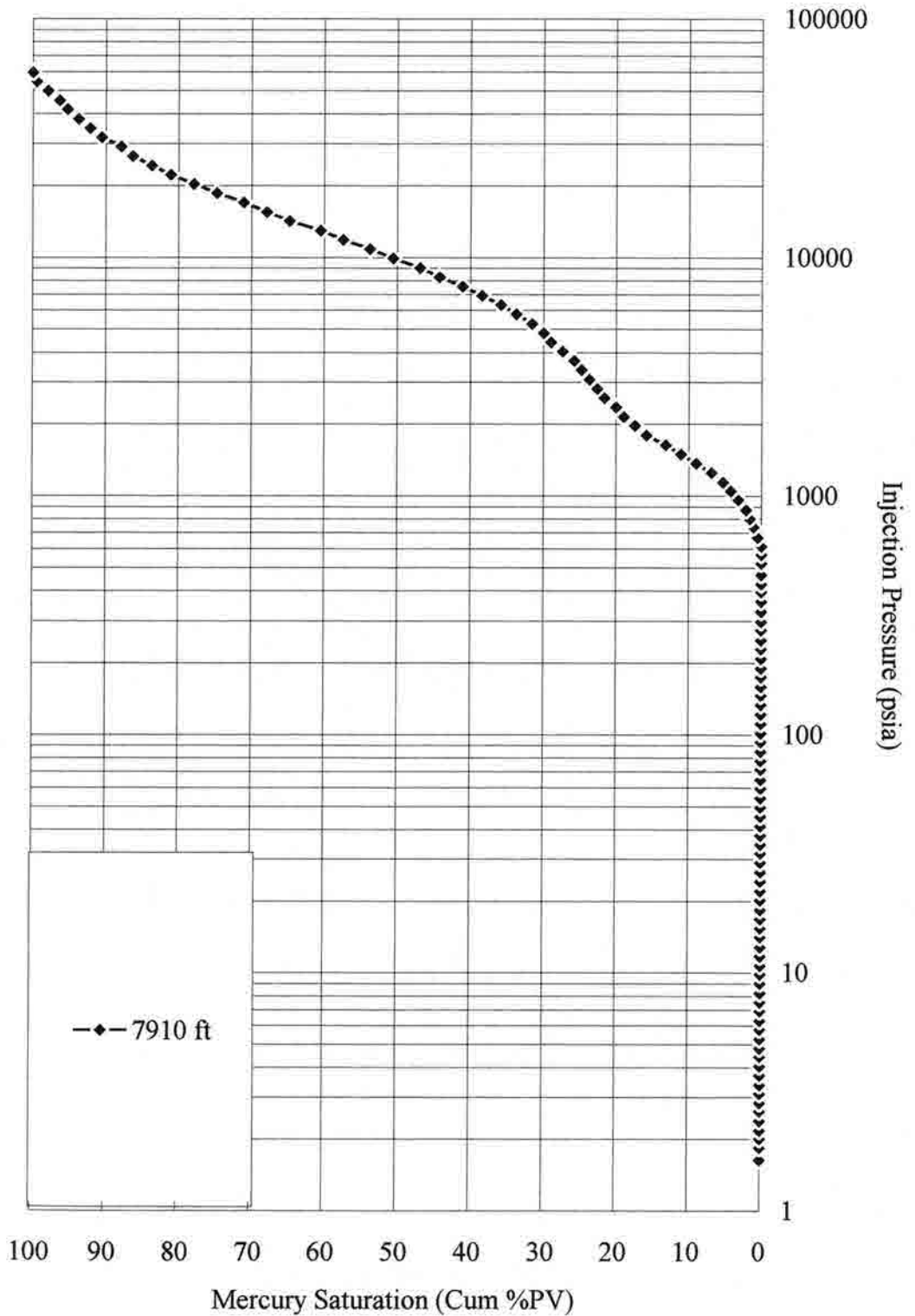


Figure 7.12c Drainage curve of Facies C for Meadow Springs Core.

Meadow Springs Drainage Curve (facies D)

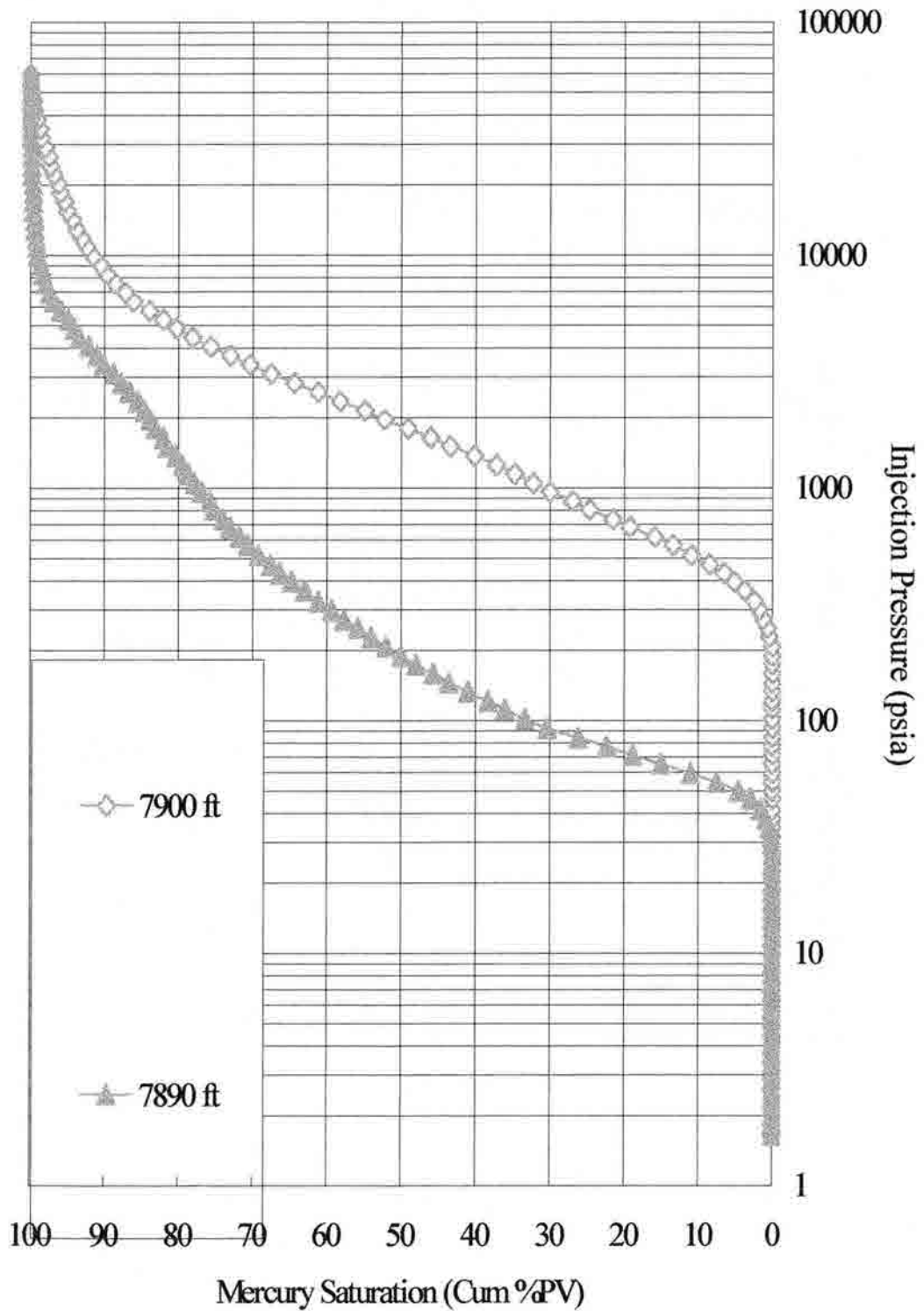


Figure 7.12d Drainage Curve of Facies D for Meadow Springs Core.

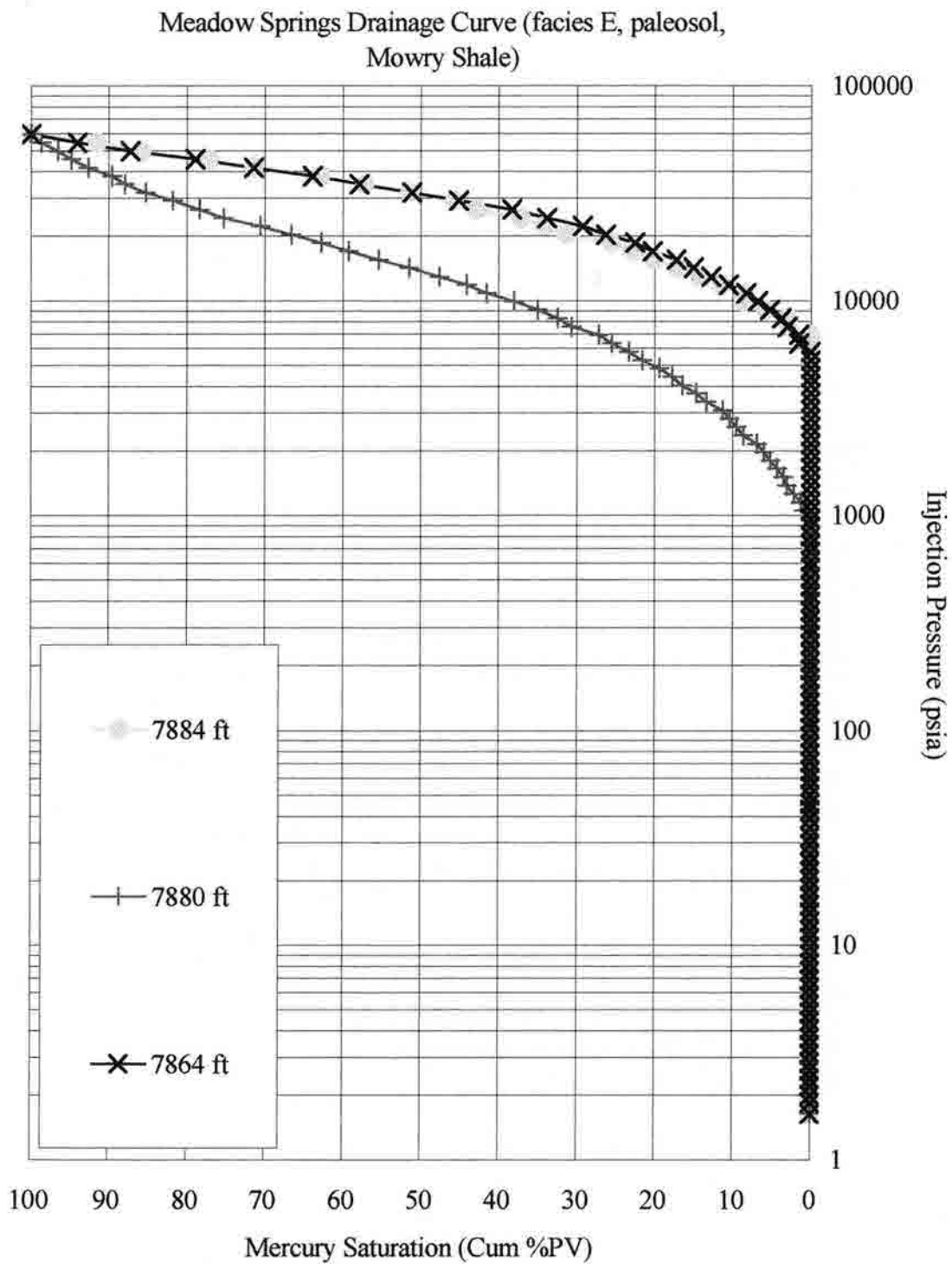


Figure 7.12e Drainage Curve for facies E, paleosol, Mowry Shale for Meadow Springs.

The Muddy Sandstone shows a much larger pore throat diameter in facies D with 80% of the sample having a medium sorted PTD of 0.1 microns and 20% with a well sorted median PTD of 0.3 microns. Conversely, the paleosol has one population of a very well sorted median PTD of 0.005 microns. This data is almost identical to that of the Mowry Shale, which has one population of a well-sorted median PTD of 0.005 microns.

7.4 Summary

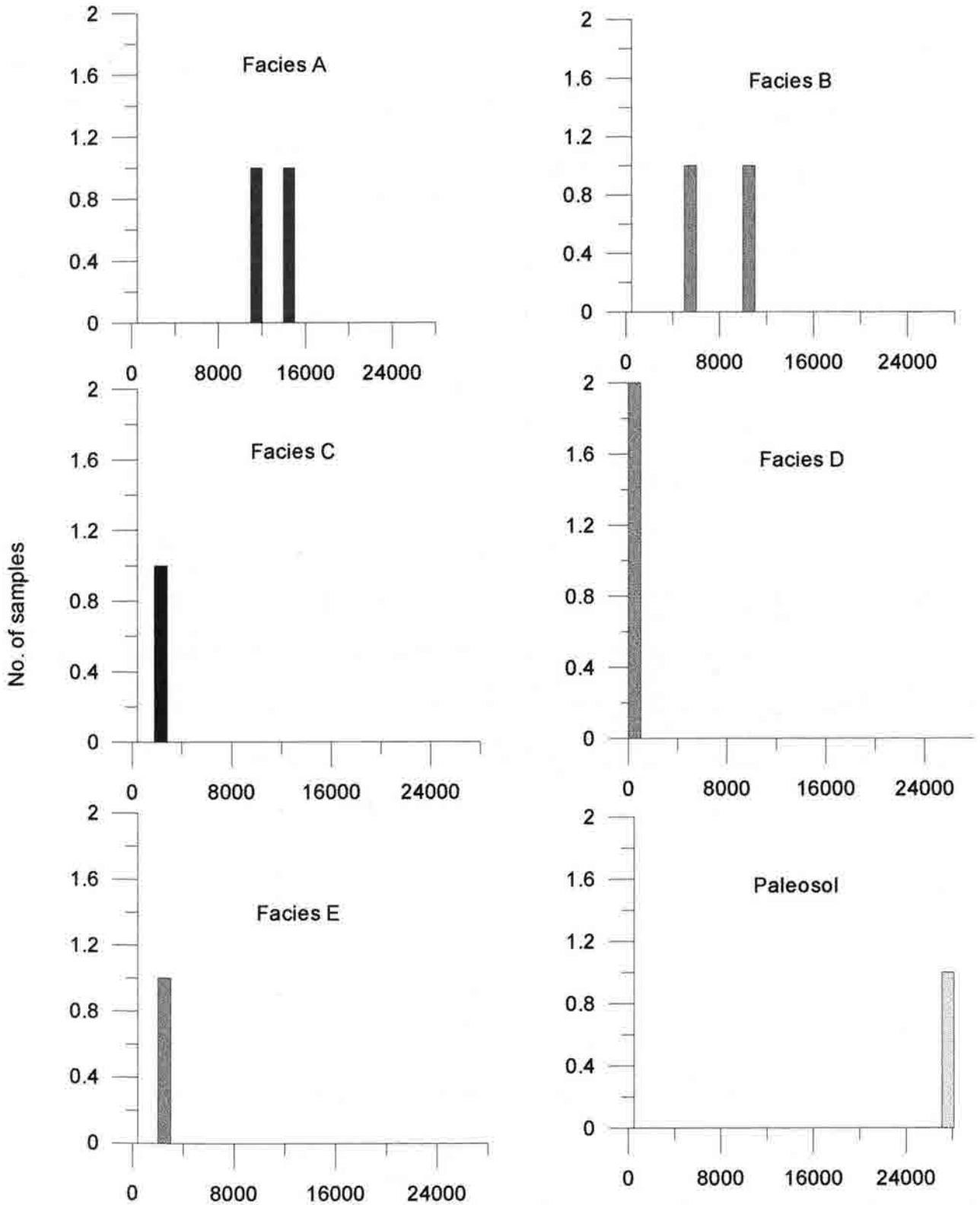
The best seal delineated by MICP for the Skull Creek in the Meadow Springs Core is located in facies A or the CS, although stronger sealing capacities are found in the paleosol and the Mowry Shale. The following is a list of characteristics displayed by the rock with the highest sealing properties:

1. Located at 7938 ft in the condensed section.
2. 0.46% total organic carbon content (not the highest).
3. Type I-II (marine) organic matter.
4. Well developed lamination and *Inoceramus* fossils in hand sample.
5. Density value of 2.62 g/cc.
6. 4.07% porosity with 0.00005-md permeability.
7. No notable bioturbation or matrix porosity in thin section.
8. Point count data with 37% clay, 42% quartz, 25% carbonate, 4% organic matter, 3% pyrite, 3% mica and siderite.
9. XRD data with 41% clay, 33% quartz, 9% pyrite, 8% dolomite, 5% feldspars, 2% siderite and 2% calcite.
10. Clay mineralogy consists of 70% R0 illite/smectite with 25% expandability, 29% illite, 1% kaolinite, and 1% chlorite.
11. 14,601 psia at 10% mercury saturation with a HCH of 4,100 ft.
12. One well-sorted PTD population with a median PTD of 0.007-micron.

Figure 7.13 shows the histograms for each of the facies, in which the injection pressures at 10% mercury saturation for each facies are grouped into columns of 2000 psia. Facies A has one sample in the 16,000 column and one in the 12,000 column. Facies B has one sample in the 12,000 column and one sample in the 6,000 column.

Facies C has one sample in the 4,000 column. Facies D has two samples in the 2,000 column. Facies E has one sample in the 4,000 column. The Mowry Shale has one sample in the 18,000 column and the paleosol is in the 28,000 column.

Meadow Springs Core (Skull Creek)
 Distribution of Injection Pressures at 10% sat.



MICP @ 10% non-wetting phase

Figure 7.13 Histograms of MICP for Meadow Springs Core.

Chapter 8. ROONEY RANCH OUTCROP (GRANEROS SHALE) RESULTS

8.1 Facies Description

The Rooney Ranch outcrop exposes 124 ft of the Graneros Shale, which was measured and gamma ray logged (Fig. 8.1). The underlying contact with the Mowry Shale is gradational, and a two-foot thick ironstone layer was used as the boundary between these two shales. The overlying contact with the Greenhorn Formation is covered and not apparent at the Rooney Ranch location (Pietraszek-Mattner, 1995).

Facies X has been designated to represent the lowest 30-ft of the 124-ft exposure of the Graneros Shale. Prominent interbedded ironstone layers easily separate this facies from the others (Fig. 8.2a,b). This carbonaceous shale has a gray blackish-brown color and is very well laminated. It displays fissile parting and gives relatively low gamma ray readings. This shale has type III (terrestrial) organic matter, and appears to be relatively organic-poor compared to the other facies (Fig. 8.2c).

Facies Y is a well-laminated, carbonaceous shale that is characterized by the numerous thick bentonites present. This facies appears twice in this outcrop at Rooney Ranch. The first occurrence is stratigraphically above facies X, and will be referred to as the lower Y facies. The second occurrence is at the stratigraphic top of this exposure above facies Z, and will be referred to as the Upper Y facies. The lower Y facies (Fig. 8.3a,b) is 20-ft thick and has a grayish-black color with fissile to platy parting that

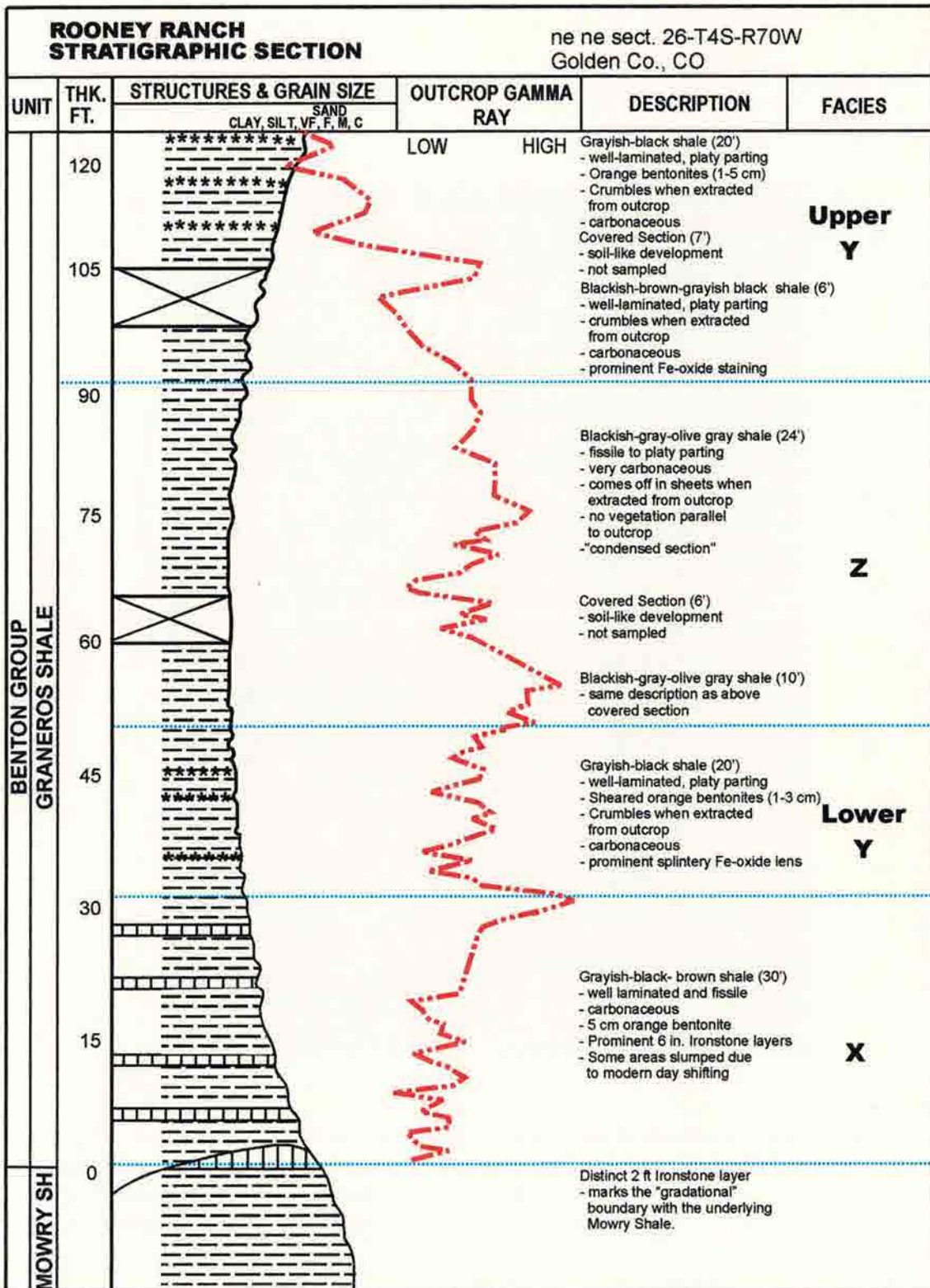


Figure 8.1 Stratigraphic column for Rooney Ranch Outcrop, including detailed descriptions, interpretations, and logged outcrop gamma ray.

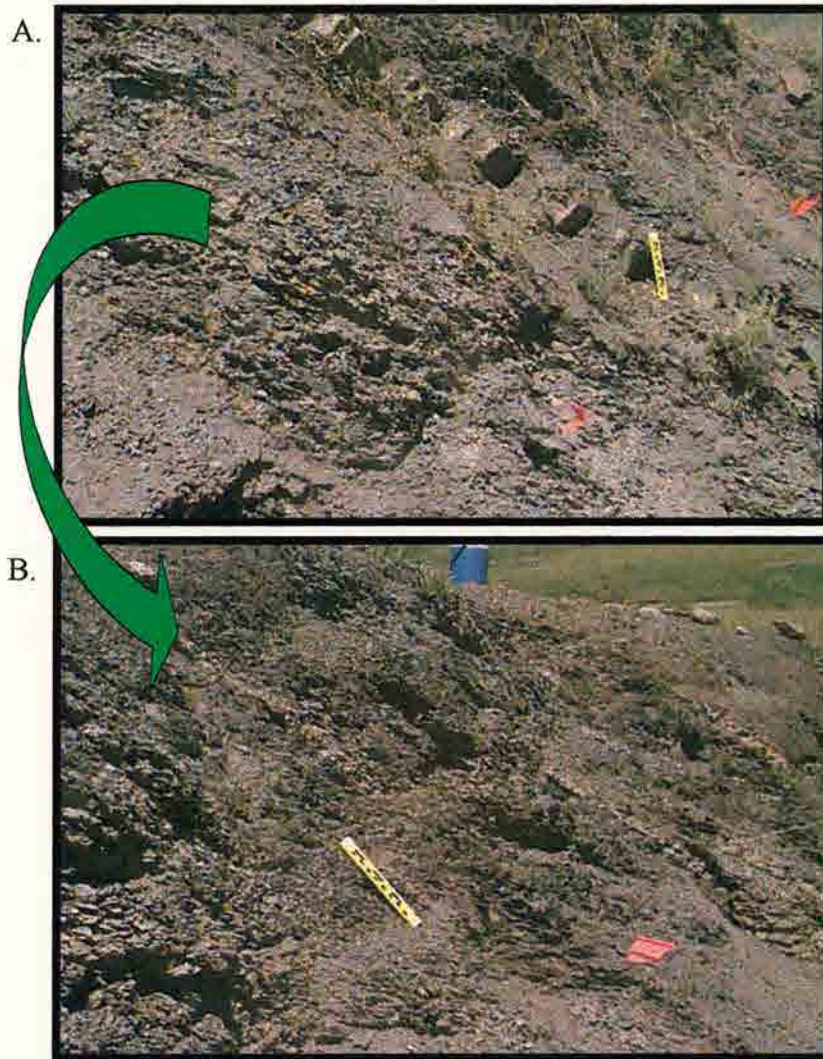


Figure 8.2 A) Overall view of gray blackish-brown shale interbedded with thick ironstones; B) fissile parting of this shale; C) Van Krevelen diagram shows type III (terrestrial) organic matter for facies X. Samples were taken in 1-ft increments, 1-ft ruler for scale.

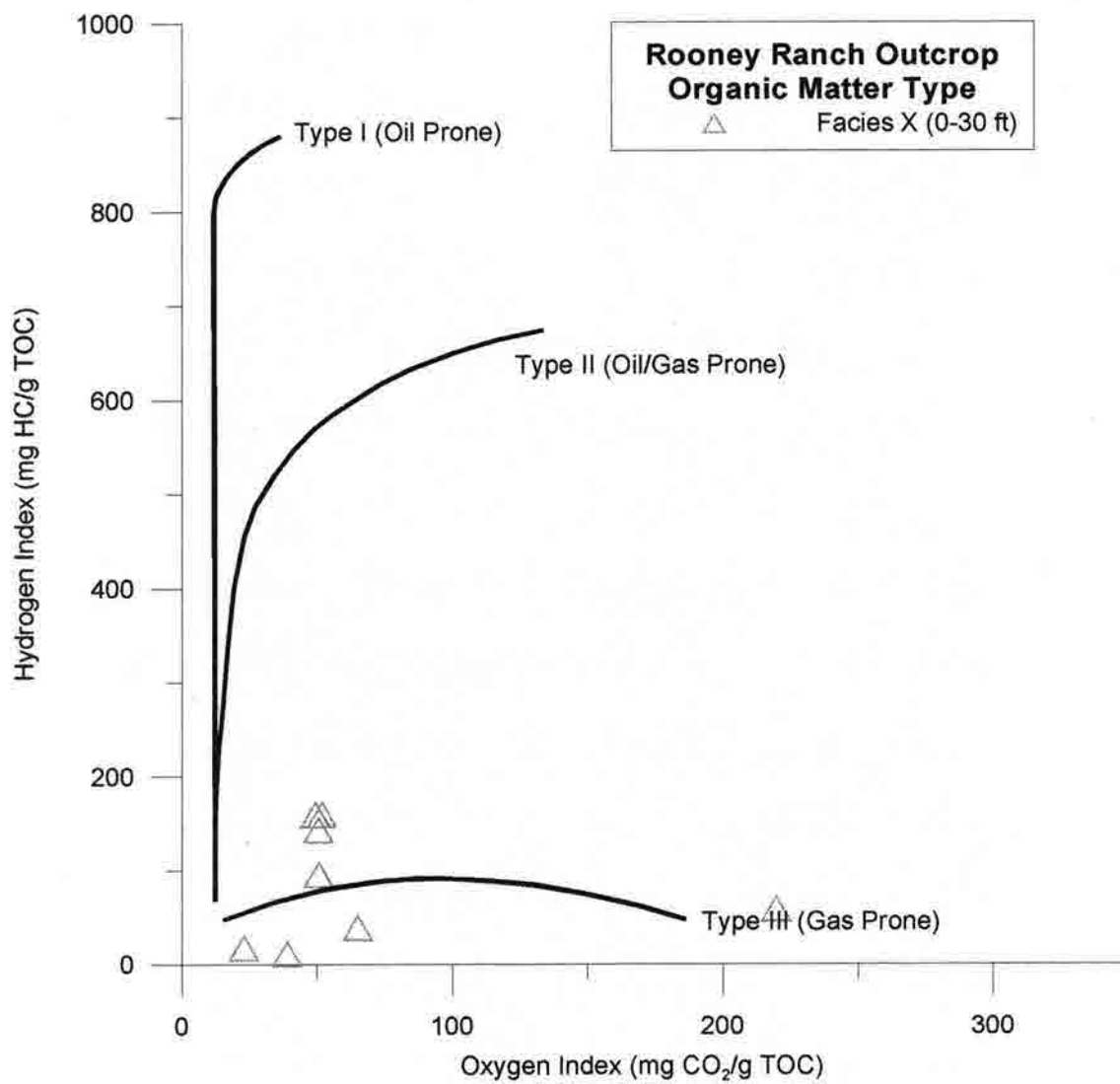


Figure 8.2 C.

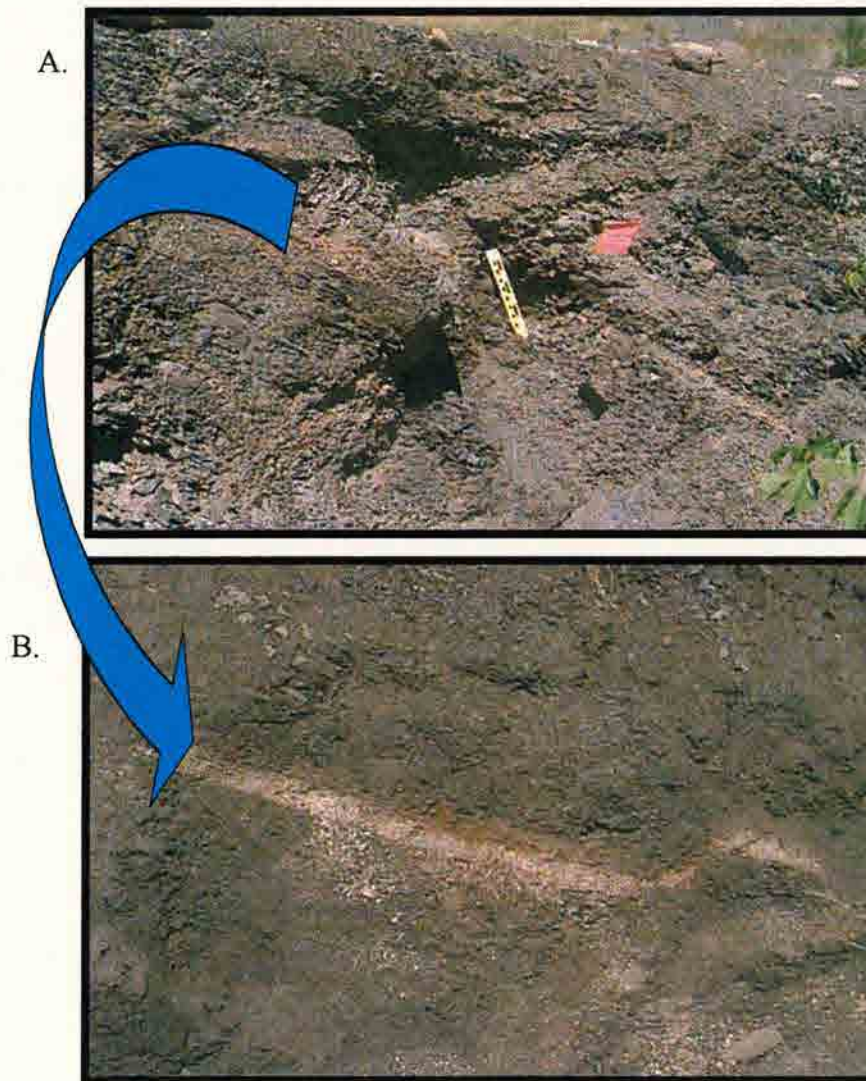


Figure 8.3 A) Overall view of grayish-black fissile shale with a prominent bentonite layer; B) a well preserved 6 in. bentonite; C) Van Krevelen diagram shows a distinct type II (marine) organic matter for the lower Y facies. Samples were taken in 1-ft increments, 1-ft ruler for scale.

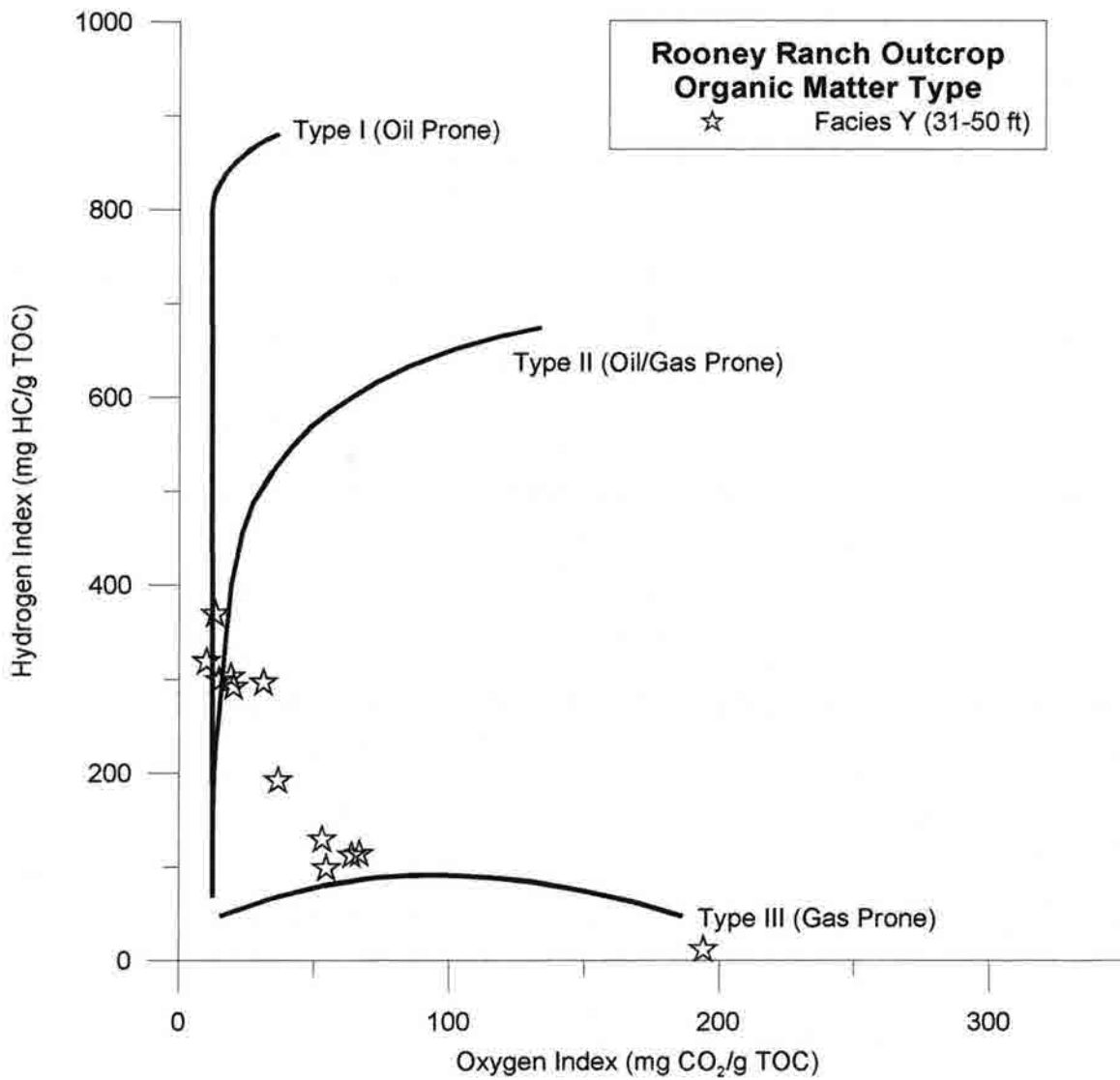


Figure 8.3 C.

crumbles when extracted from the outcrop. This facies appears to be organic rich and displays a variable organic matter type (Fig. 8.3). Splintery lenses of iron oxides are prominent throughout this facies.

Facies Z is 40 ft thick and is approximately in the stratigraphic middle of this section. It is a blackish-gray to olive-gray shale with considerable carbonaceous debris. It displays fissile to platy parting and comes off in sheets when extracted from outcrop (Fig. 8.4a,b). These organic rich shales display a type II (marine) organic matter (Fig. 8.4c). This facies was distinguished by Pietrasnek-Mattner (1995) as having the highest radioactivity measured with the outcrop gamma ray scintillator. In this study, facies Z gives two significant gamma ray peaks and has relatively high readings. However, a significant peak in gamma ray is also shown between the X and lower Y facies, and it must be noted that the lower Y facies also has relatively high gamma ray readings (Fig. 8.1). However, field observations such as the absence of vegetation growing parallel to facies Z, further suggest that it may have the highest radioactivity or be the “hot zone” (Pietrasnek-Mattner, 1995).

The upper Y facies is 33 ft thick and is a well-laminated, grayish-black to blackish-brown carbonaceous shale (Fig. 8.5a). It displays platy parting and crumbles when extracted from outcrop. Three thick (1-5 cm), orange bentonites are present, which are characteristic of this facies (Fig. 8.5b). This shale has both type II (marine) and type III (terrestrial) organic matter (Fig. 8.5c).

8.2 Lithology Description

Table 8.1 provides the averages and standard deviations for the Graneros Shale data at the Rooney Ranch outcrop. Facies X has the lowest TOC with the highest

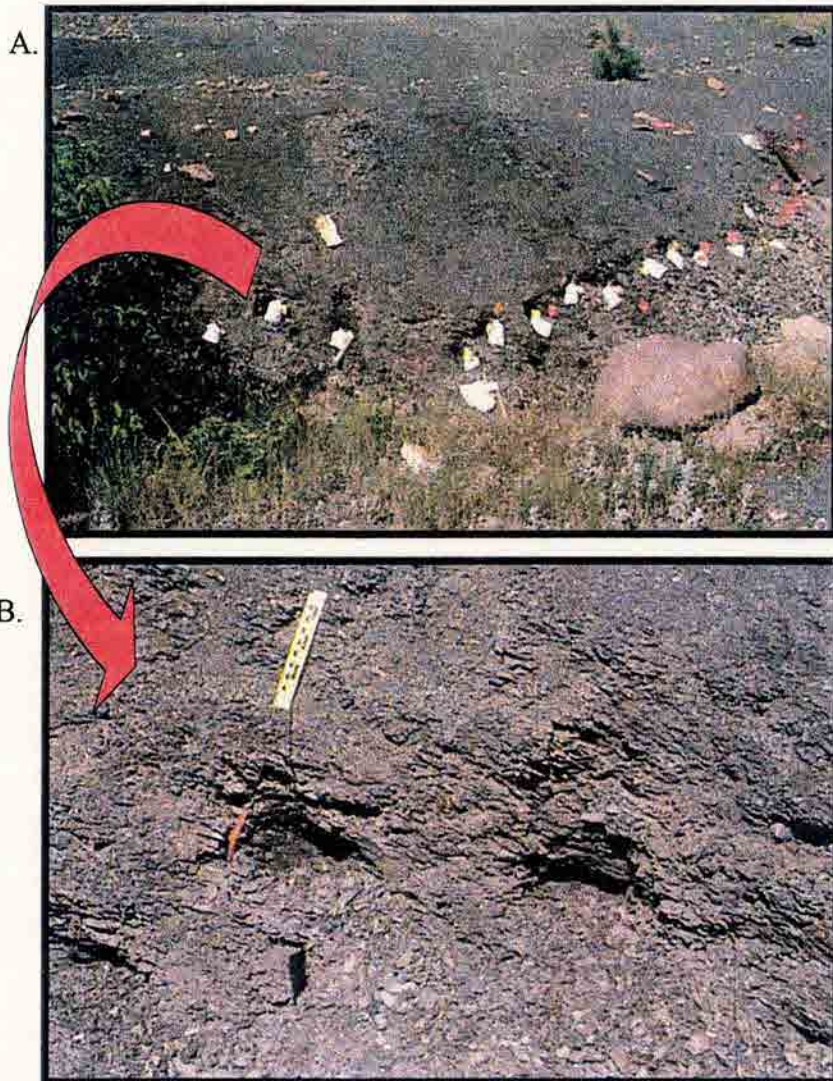


Figure 8.4 A) Overall view of grayish-black fissile shale with no vegetation parallel to outcrop; B) closer view of sheetlike parting of this shale; C) Van Krevelen diagram shows a type II (marine) organic matter for facies Z. Samples were taken in 1-ft increments, 1-ft ruler for scale.

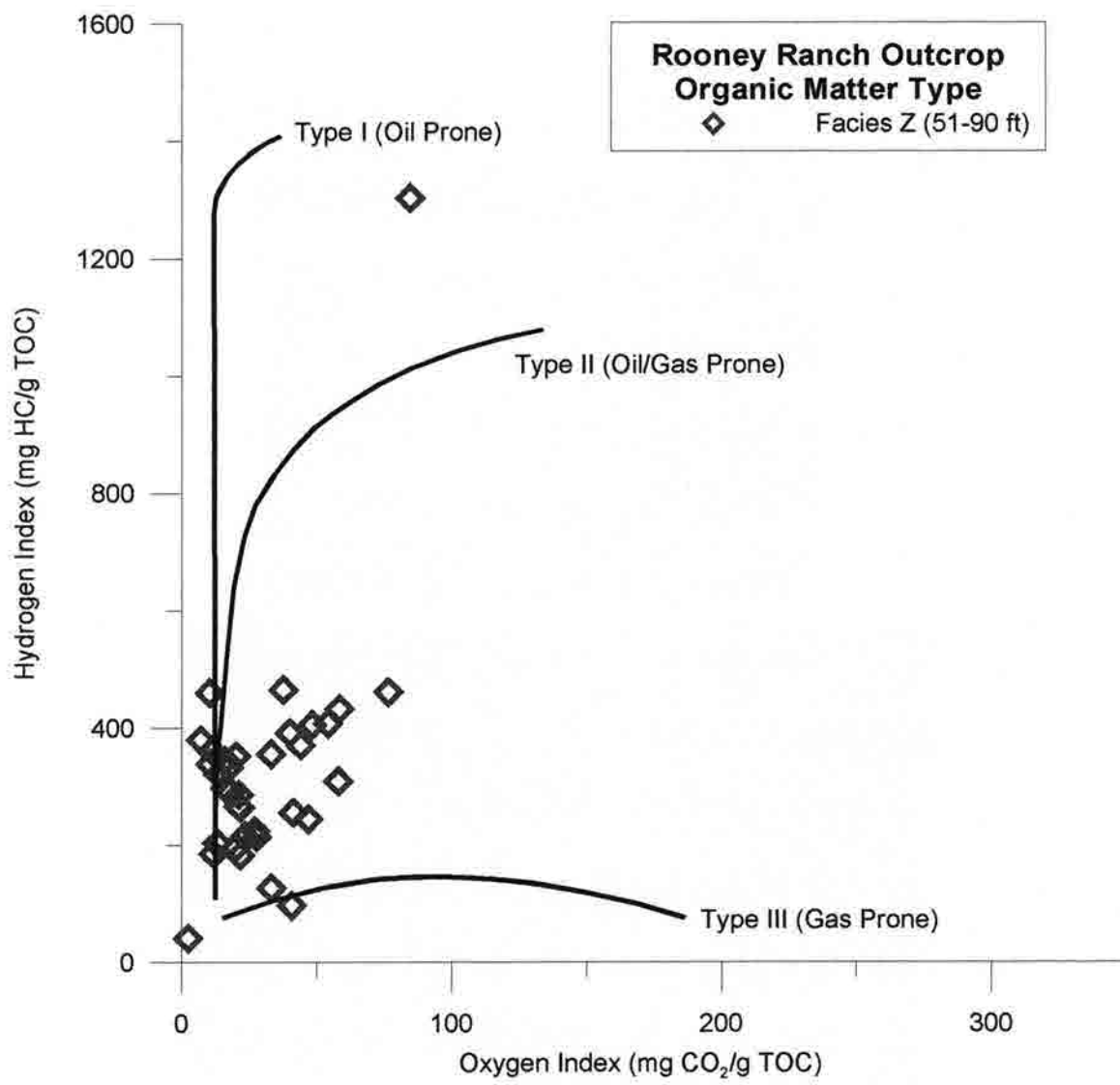


Figure 8.4 C.

A.



B.



Figure 8.5 A) Overall view of grayish-black fissile shale with Fe-staining; B) 4-5 cm thick bentonite interbedded with a well-laminated shale; C) Van Krevelen diagram shows type III (terrestrial) organic matter for upper facies Y. 1-ft ruler for scale, each red tick on bottom ruler equals one centimeter.

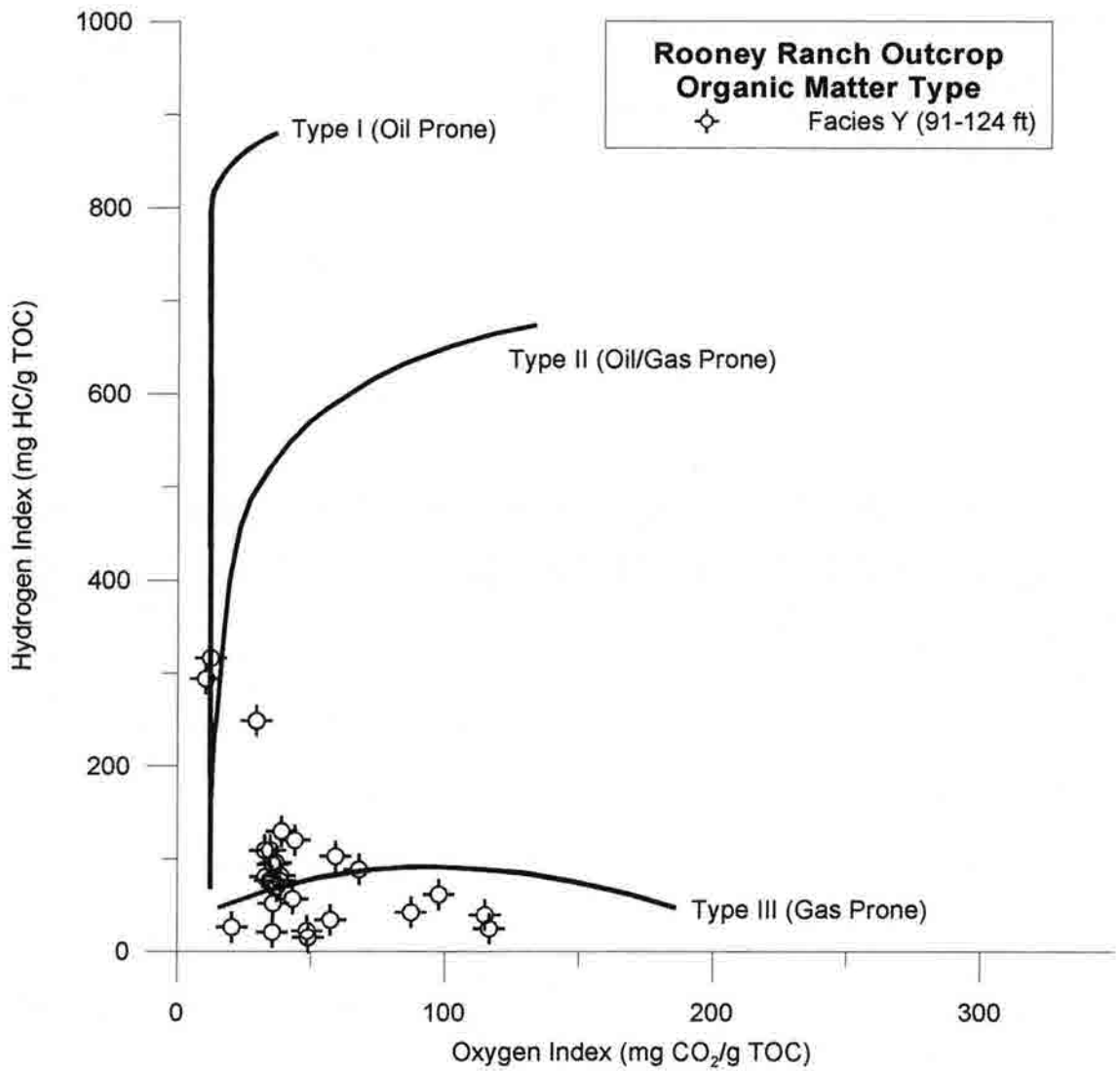


Figure 8.5 C.

Table 8.1 Statistics for the Rooney Ranch (Graneros Shale) data

Facies		Total Organic Carbon (%)	Hydrogen Index (mg HC/g TOC)	Hydrogen Index/Oxygen Index (mg HC/mg CO ₂)	Total Clay (wt%)	Quartz (wt%)	Feldspar (wt%)	Carbonate (wt%)	Porosity (%)	Permeability (md)	Density (g/cc)
	# of Analyses	28	28	28	9	9	9	9	8	8	4
Upper	Average	2.73	92	4	51	38	3	6	16.4	0.032	2.54
Y	Std Dev	0.96	76	7	12	9	1	1	2.8	0.062	0.05
	# of Analyses	35	35	35	7	7	7	7	8	8	4
Z	Average	4.21	325	15	43	38	3	10	12.6	0.00069	2.50
	Std Dev	1.15	199	11	6	5	0	5	3.8	0.00069	0.06
	# of Analyses	12	12	12	4	4	4	4	3.0	3	1
Lower	Average	3.17	211	11	50	33	2	6	14.2	0.0057	2.57
Y	Std Dev	1.16	115	11	7	7	1	2	2.7	0.0082	
	# of Analyses	8	8	8	5	5	5	5	4	4	1
X	Average	1.51	86	2	45	33	2	17	15.9	0.0022	2.63
	Std Dev	0.58	62	1	15	13	1	26	2.9	0.0020	

of quartz and carbonate with the second lowest average permeability values. The density of this shale averages 2.63 g/cc and is slightly greater than that of the other facies by 0.06 to 0.13 g/cc.

Both of the Y facies have approximately 3% TOC with ~35% quartz, ~50% total clay, and ~6% carbonate. However, the lower Y facies has a significantly higher hydrogen index by about 120 mg HC/g TOC. The lower Y facies also averages low permeability of 0.0057 md, with 14.17% porosity. The upper Y facies has a higher permeability of 0.0323 md with an average porosity of 16.44%.

Facies Z has the highest average TOC at 4.21% and the highest average hydrogen index at 325 mg HC/g TOC. The organic geochemistry data clearly distinguishes it from the other facies. However, the average percentage of ductile grains is lower than in both Y facies. This may be due to the numerous bentonite layers in facies Y increasing the

average percentage of ductile grains. Overall, facies Z averages 38% quartz, 43% total clay, and 10% carbonate. Facies Z averages the lowest permeability (0.0007 md) and 12.6% porosity with a density of 2.5 g/cc. This is the “lightest” rock of the section.

These data were plotted against stratigraphic height to compare these characteristics to seal capacity as determined by MICP. The best seals are located in facies Z or the CS and at 15 ft in facies X (Fig. 8.6a). Porosity is variable throughout the section, but generally lower for the samples with high seal capacity (8.6b). The lowest permeability values also correspond with high seal capacity as seen in facies Z and X (Fig. 8.6c). The CS or facies Z contain samples with the lowest density (Fig. 8.6d).

The amount of total clay does not vary significantly throughout any of the facies (Fig. 8.7a). Quartz again shows an inverse relationship to clay, and is low in the carbonate rich rock of facies X (Fig. 8.7b). The amount of feldspar varies but seems to be slightly higher in the TST deposits (8.7c). Carbonate remains constant throughout all the facies except for the sharp peak in facies X which corresponds to a considerable amount of siderite that is shown in the whole rock mineralogy (Fig. 8.7d).

TOC corresponds with the overall fining upward/ coarsening upward sequence. It peaks in the CS or facies Z that is also the finest grained rock of the section (Fig. 8.8a). Hydrogen index values mimic this same trend and reach their highest point in facies Z (Fig. 8.8b). The ratio of HI/OI reaches its height (Fig. 8.8b) in facies Z. A detailed summary of the organic geochemistry is presented in Appendix P.

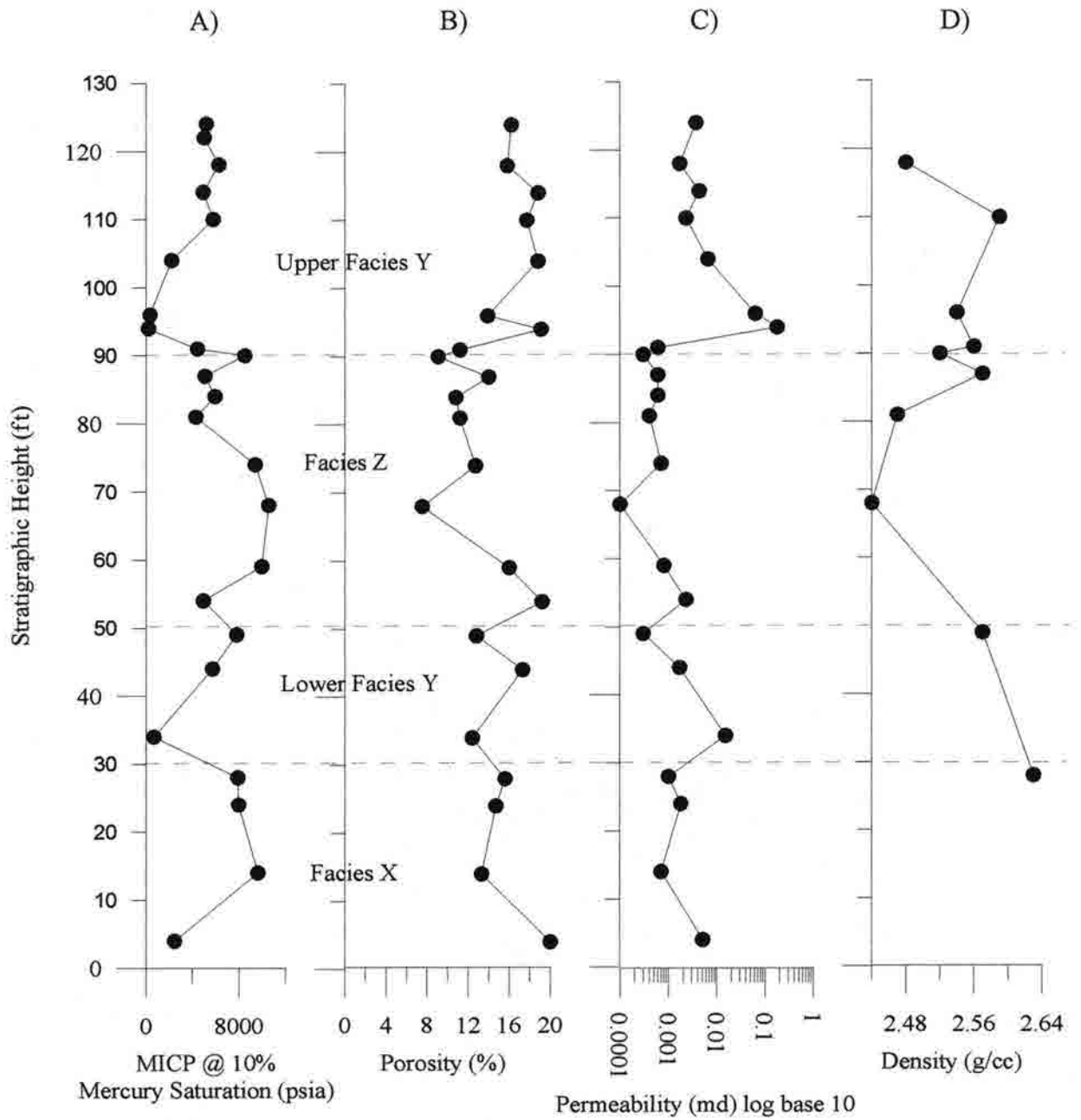


Figure 8.6 Stratigraphic height vs. MICP (A), porosity (B), permeability (C) and density (D) for Rooney Ranch.

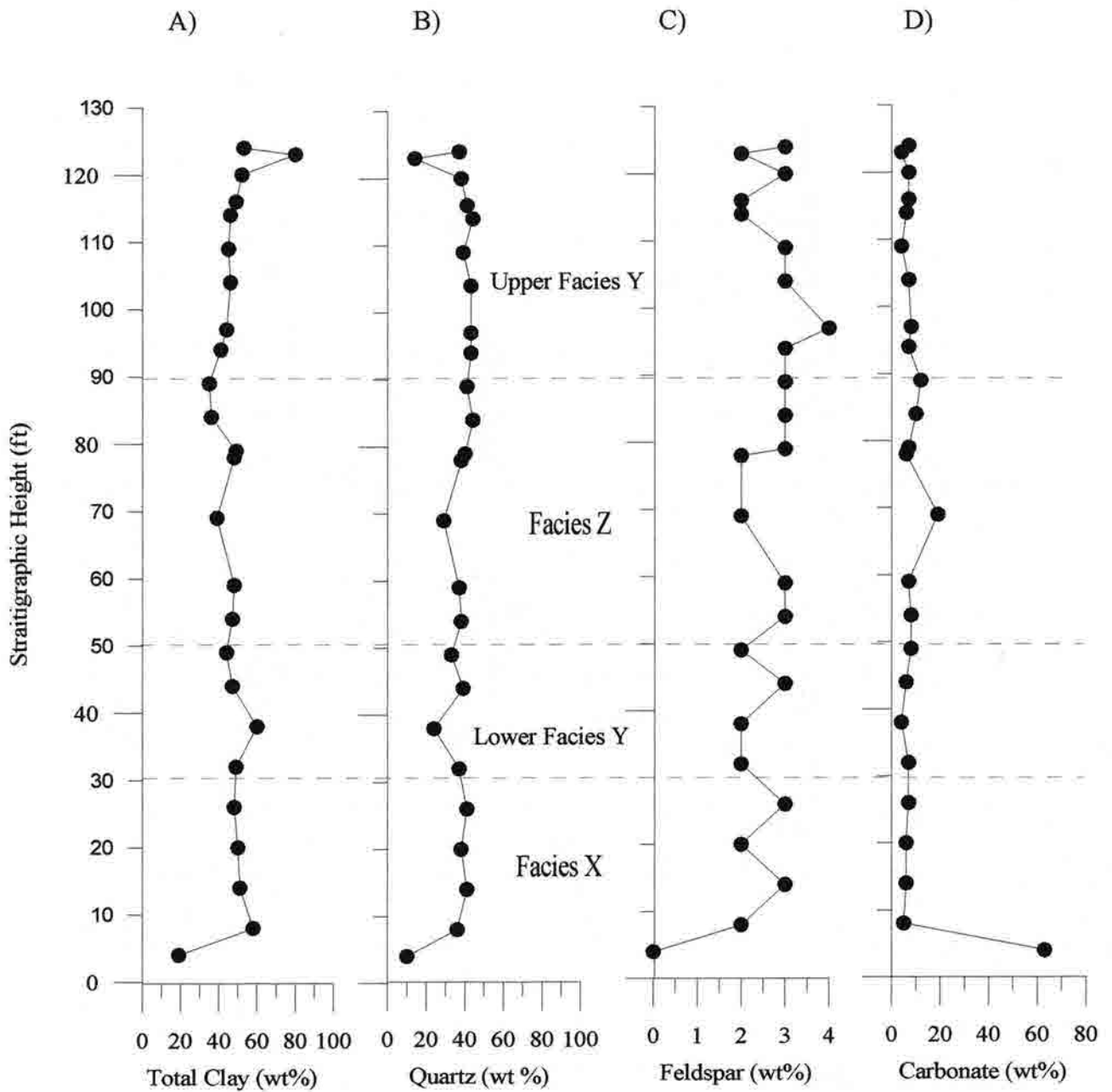


Figure 8.7 Stratigraphic height vs. total clay (A), quartz (B), feldspar (C), and carbonate (D) for Rooney Ranch.

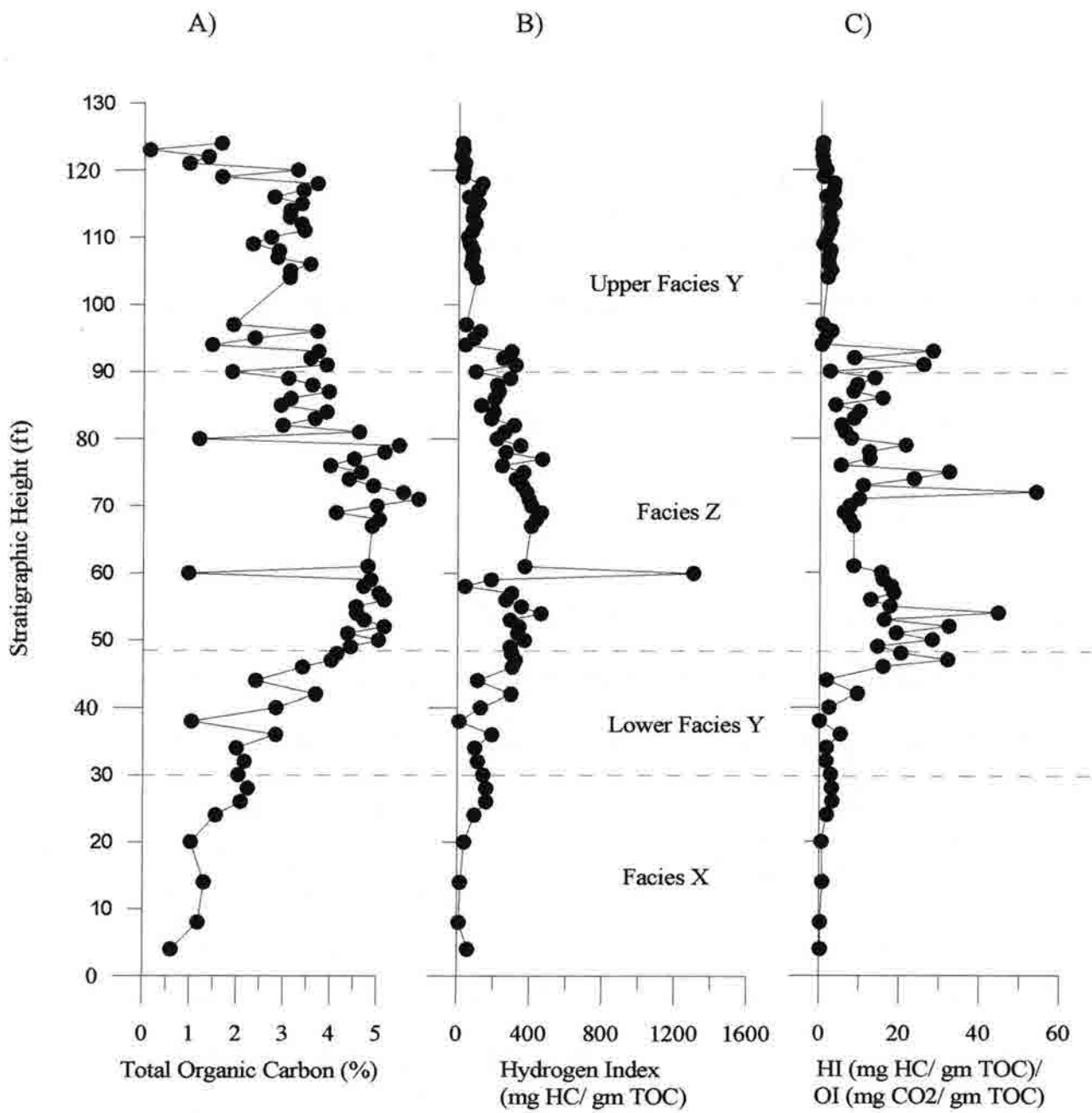


Figure 8.8 Stratigraphic height vs. TOC (A), hydrogen index (B), and hydrogen index/oxygen index (C) for Rooney Ranch.

Thin Section Petrography

The thin section observations are consolidated into Table 8.2 and Appendix L, which includes the representative thin section photomicrographs for this outcrop. Facies X ranges from a Fe-rich argillaceous siltstone to a silty shale. The siderite-cemented siltstone has well-sorted, subrounded, spherical, silt size detrital grains. Large nodules of pyrite and hematite are common along with altered siderite and phosphatic debris. The silty shale is compacted with well-sorted, silt size detrital grains (quartz, feldspar and mica). The mineralogy estimated for one sample is 50% quartz, 43% clay, 3% carbonate, 3% pyrite, 1% organic matter, with minor amounts of hematite and phosphate. No matrix porosity is visible.

The lower Y facies is a silty shale that is sometimes interbedded with argillaceous siltstones. The estimated mineralogy averages 43% quartz, 50% clay, 3% pyrite, 2% carbonate, 2% organic matter, with minor amounts of mica and phosphate. The detrital grains are well sorted, spherical to elongate, and silt size. Phosphatic debris is scattered throughout this facies. Wispy laminations of organic matter are also present. No porosity is detected.

Facies Z is a silty shale with one sample showing approximately 41% quartz, 52% clay, 3% organic matter, 2% carbonate, and 2% pyrite with minor amounts of mica and phosphate. The detrital grains are well sorted, subangular, spherical-elongate, and silt size. Some of the quartz grains are elongated parallel to the laminations. Organic matter forms discontinuous laminations. Nodules of authigenic framboidal pyrite and phosphate are scattered throughout. No porosity is evident in this facies.

Table 8.2 Rooney Ranch Thin Section Petrography

Facies	FT	Rockname	Grain Size	COMPOSITION						Laminations	Bioturbation	Pressure Solution	Fossils	Porosity
				QTZ	CLAY	ORG	CARB	PYR	OTHER					
Y	116	silty shale	silt-VFG			2	3			Y	N	Y	Y	N
Y	114	silty shale	silt-VFG	40	55	1	3	1	phos,mic	Y	N	Y	Y	N
Y	104	silty shale	silt-VFG							Y	N	Y	Y	N
Y	94	silty shale	silt-VFG	39	52	3	5	1	phos,mic	Y	N	Y	Y	N
Z	84	silty shale	coarse silt	39	52	3	5	1	phos,mic	Y	N	Y	Y	N
Z	74	silty shale	coarse silt	40	52	4	2	2	phos,mic	Y	N	Y	Y	N
Z	59	silty shale	coarse silt	41	52	3	2	2	phos,mic	Y	N	Y	Y	N
Z	54	silty shale	coarse silt	42	50	3	2	3	phos,mic	Y	N	Y	Y	N
Y	44	silty shale	coarse silt	43	50	2	2	3	phos,mic	Y	N	Y	Y	N
Y	34	silty shale	coarse silt	43	50	2	2	3	phos,mic	Y	N	Y	Y	N
X	24	silty shale	coarse silt							Y	N	Y	Y	N
X	14	silty shale	silt-VFG	50	43	1	3	3	hem, phos	Y	N	Y	Y	N

**NOTE: 1/256 <silt <1/16 mm, 1/16 <VF sand <1/8 mm, 1/8 <F sand<1/4 mm, 1/4 <M sand <1/2 mm

LEGEND:

QTZ= Quartz

ORG= Organic Matter

CARB= Carbonate (calcite, dolomite, siderite)

feld= Feldspar

phos= Phosphate

mic= Mica

hem= Hematite

The upper Y facies is also a silty shale but with detrital grains that range from silt to very fine sand size and are well sorted. The estimated mineralogy is approximately 40% quartz, 55% clay, 3% carbonate, 1% organic matter, 1% pyrite and minor amounts of mica and phosphate. Wispy laminations of organic matter and clays enhance the fissile appearance. Accessory constituents include phosphate and hematite nodules, authigenic framboidal pyrite, and siderite has replaced some feldspar. No porosity is evident in this facies.

Whole Rock Mineralogy

Table 8.3 shows the XRD analysis of the whole rock mineralogy for the Rooney Ranch outcrop. The whole rock mineralogy does not vary within the Graneros Shale as

Table 8.3 Whole Rock Mineralogy (wt%): Rooney Ranch Outcrop (Graneros)

Facies	Sample #	FT	TCL	QTZ	KSP	PLAG	Mg-CAL	DOL	PYR	SID	ANHY
Upper Y	GR000	124	53	36	3	ND	4	1	ND	2	1
	GR001	123	80	14	2	ND	TR	2	ND	2	ND
	GR004	120	52	37	3	ND	4	1	ND	2	1
	GR008	116	49	41	2	ND	4	1	ND	2	1
	GR010	114	46	45	2	ND	3	1	ND	2	1
	GR015	109	45	39	3	ND	3	1	8	ND	1
	GR020	104	46	43	3	ND	4	1	ND	2	1
	GR021	97	44	43	4	ND	5	1	ND	2	1
	GR024	94	41	44	3	ND	4	1	4	2	1
	Average		51	38	3	0	4	1	6	2	1
Z	GR029	89	35	42	3	ND	4	6	7	2	1
	GR034	84	35	43	3	ND	4	3	8	3	1
	GR039	79	49	40	3	ND	4	1	ND	2	1
	GR044	74	48	38	2	ND	3	1	5	2	1
	GR049	69	39	28	2	ND	4	11	9	4	3
	GR059	59	48	37	3	ND	4	1	4	2	1
	GR064	54	47	38	3	ND	5	1	3	2	1
	Average		43	38	3	0	4	3	6	2	1
Lower Y	GR069	49	44	34	2	ND	4	1	12	3	ND
	GR073	44	47	39	3	ND	3	1	4	2	1
	GR076	38	60	25	2	ND	3	1	9	TR	ND
	GR079	32	49	38	2	ND	4	1	3	2	1
		Average		50	34	2	0	4	1	7	2
X	GR082	26	48	41	3	ND	4	1	ND	2	1
	GR085	20	50	39	2	ND	3	1	3	2	ND
	GR088	14	51	40	3	ND	3	1	ND	2	ND
	GR091	8	58	35	0	2	3	0	ND	2	ND
	GR093	4	19	10	0	ND	0	0	8	63	ND
		Average		45	33	2	2	3	1	6	14

LEGEND: QTZ= Quartz SID= Siderite GYP= Gypsum
TCL= Total Clay and Mica PYR= Pyrite TR= Trace ND= Not Detected
DOL= Dolomite JAR= Jarosite PLAG= Plagioclase Mg-CAL= Mg-rich calcite
ANHY= Anhydrite KSP= K-Feldspar

much as it did within the Skull Creek Shale. This entire section of the Graneros Shale is matrix supported or dominated by clay and contains relatively high amounts of pyrite (avg. 6-7%). Facies X averages 45% total clay, 33% quartz, and 6% pyrite with minor feldspars, high Mg-calcite, and dolomite. A large amount of siderite is concentrated in the ironstone sample (4 ft). The lower and upper Y facies have the highest percentage of

total clay with 6-7% pyrite. Facies Z has less total clay and slightly more carbonate than the Y facies.

8.3 *Petrophysical Description*

Table 8.4 shows the injection pressures at 10% mercury saturation and the corresponding hydrocarbon column heights (HCH) they can hold. The highest injection pressure is located in facies Z at 68 ft with 10,570 psia, which can hold a 2970 ft HCH. Following this at 59 ft is a sample with 9,980 psia, which can hold 2,800 ft of HCH. Next is a sample in facies X at 14 ft that requires 9,410 psia, which can hold 2,710 ft of HCH.

All of the drainage curves for the Graneros Shale at Rooney Ranch show a similar shape with some outliers. Overall, they have a broadly dipping upper curve with a relatively high entry pressure. Facies X shows four samples that have entry pressures ranging from 1,000 to 3,000 psia. The lowest entry pressure correlates to the Ironstone sample, instead of shale (Fig. 8.9a). The lower Y facies has two broadly sloping curves with approximately 2,000 psia of entry pressure (Fig. 8.9b). The remaining sample has a steeply sloping curve with a 200 psia entry pressure. The samples of facies Z show remarkable uniformity with entry pressures around 2,000-4,000 psia (Fig. 8.9c). The upper Y facies samples have three outliers with steeply dipping curves and entry pressures around 100-1,000 psia. Overall, the better seals in this facies have entry pressures around 1,000-2,000 psia (Fig. 8.9d).

The MICP data for the distribution of pore throat diameters is in Appendix M. Facies X has two to three populations of median PTD ranging from 0.008-0.02 microns and moderately to very well sorted, with the 0.02 micron PTD being the dominant one.

Table 8.4 Rooney Ranch Injection Pressures (psia) at 10% Mercury Saturation

Facies	Sample#	FT	PSIA@10%SAT	HCH (ft)
Y	GR000	124	5200	1460
Y	GR002	122	5030	1410
Y	GR006	118	6290	1760
Y	GR010	114	4930	1380
Y	GR014	110	5790	1620
Y	GR020	104	2200	610
Y	GR022	96	334	85
Y	GR024	94	197	45
Y	GR027	91	4440	1240
Z	GR028	90	8520	2390
Z	GR031	87	5080	1420
Z	GR034	84	5950	1665
Z	GR037	81	4300	1200
Z	GR044	74	9410	2640
Z	GR050	68	10570	2970
Z	GR059	59	9980	2800
Z	GR064	54	4940	1380
Y	GR069	49	7820	2190
Y	GR073	44	5730	1610
Y	GR078	34	659	175
X	GR081	28	7910	2220
X	GR083	24	7990	2240
X	GR088	14	9640	2710
X	GR093	4	2450	680

The lower Y facies also has two to three populations of median PTD ranging from 0.006-0.15 microns and poorly to very well sorted, with the 0.02 micron PTD being predominant. Facies Z generally has two populations of median PTD ranging from 0.006-0.03 microns and poorly to very well sorted, respectively, with the 0.01 micron PTD dominating the pore volume. The upper Y facies has two to three populations of median PTD ranging from 0.008-0.1 and poorly to very well sorted, with the 0.025 micron PTD being the dominant one.

Rooney Ranch Drainage Curve (Facies X)

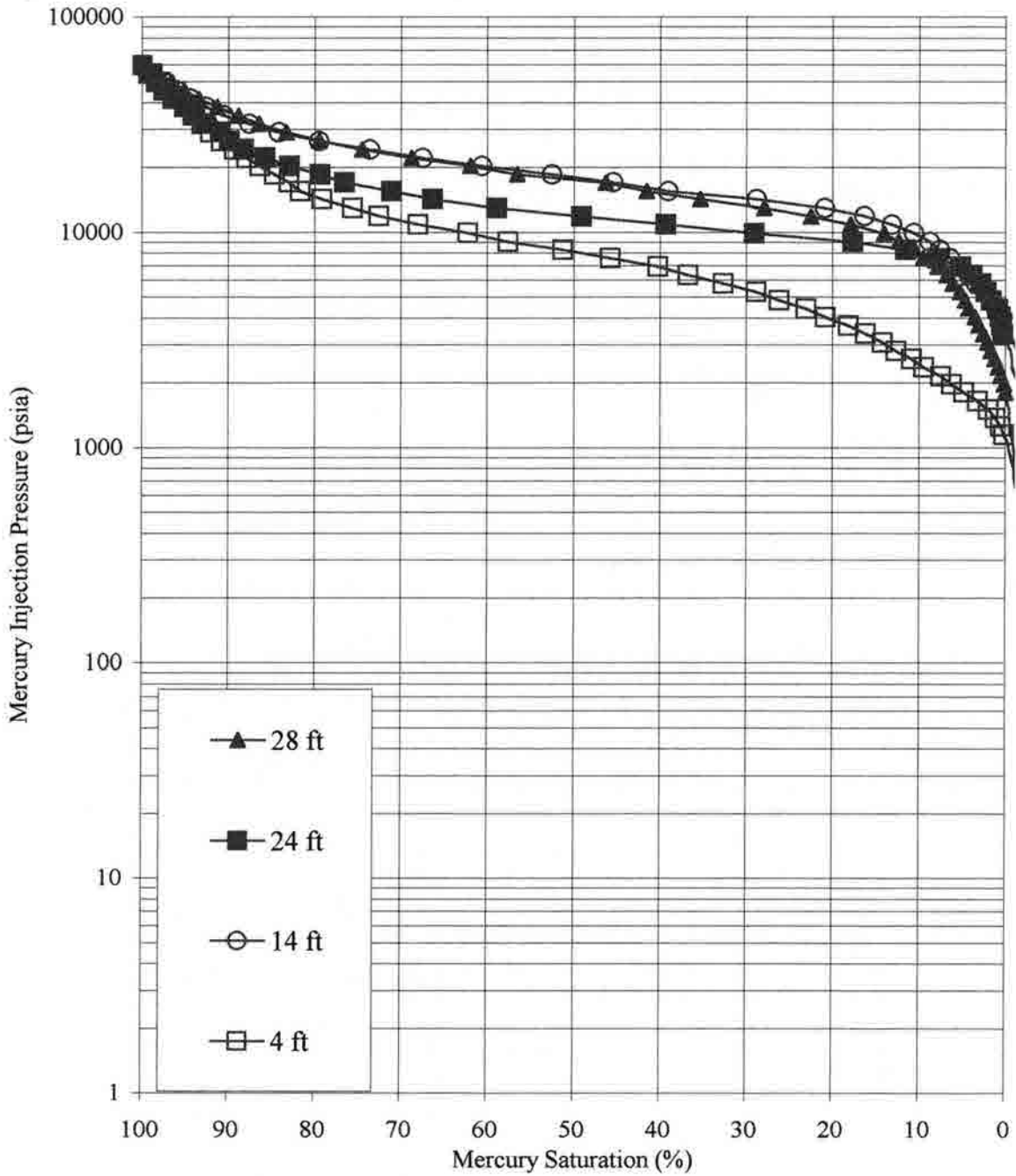


Figure 8.9a Drainage Curve for Facies X at Rooney Ranch.

Rooney Ranch Drainage Curve (Lower facies Y)

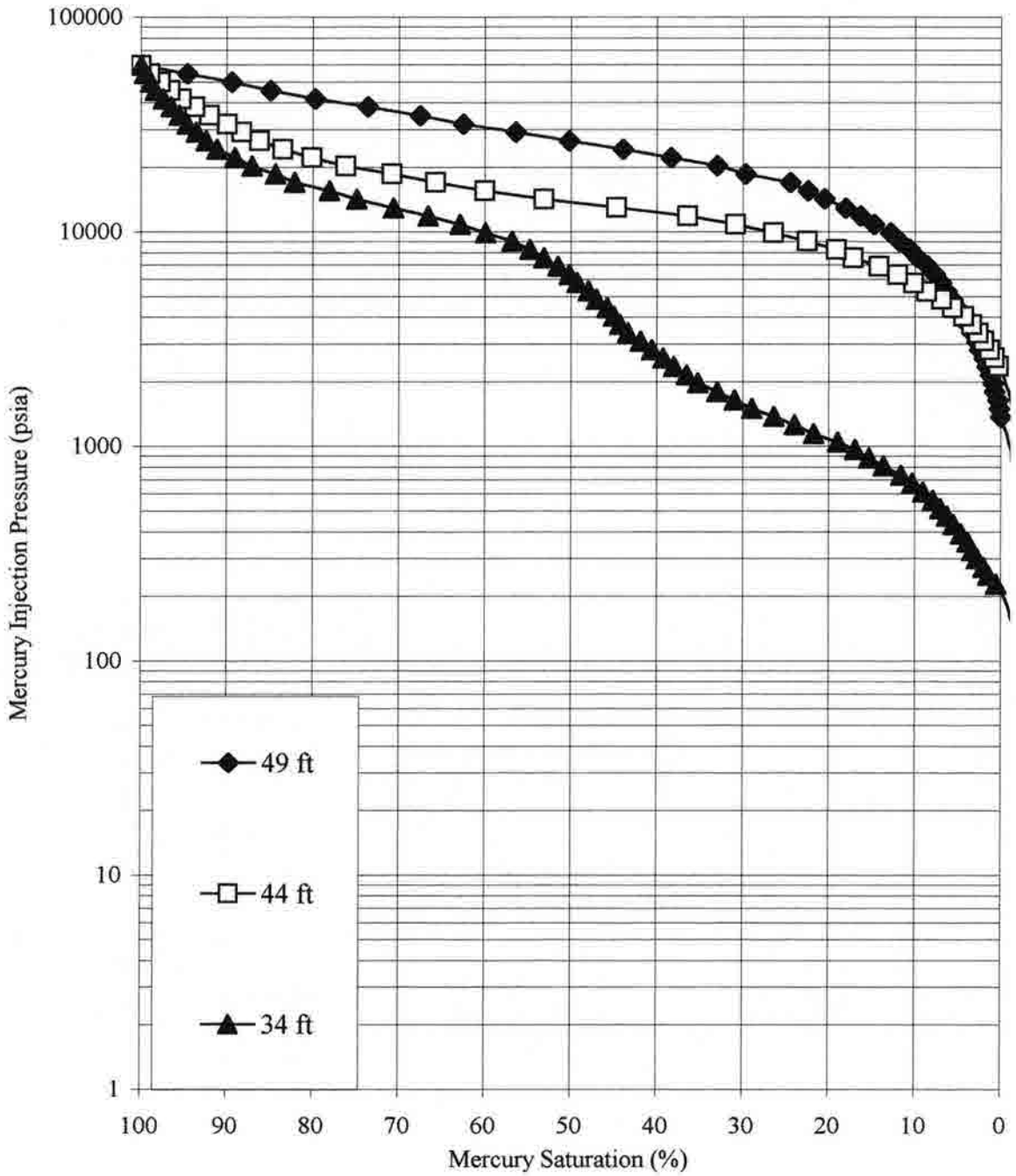


Figure 8.9b Drainage Curve for the lower Y facies at Rooney Ranch.

Rooney Ranch Drainage Curve (Facies Z)

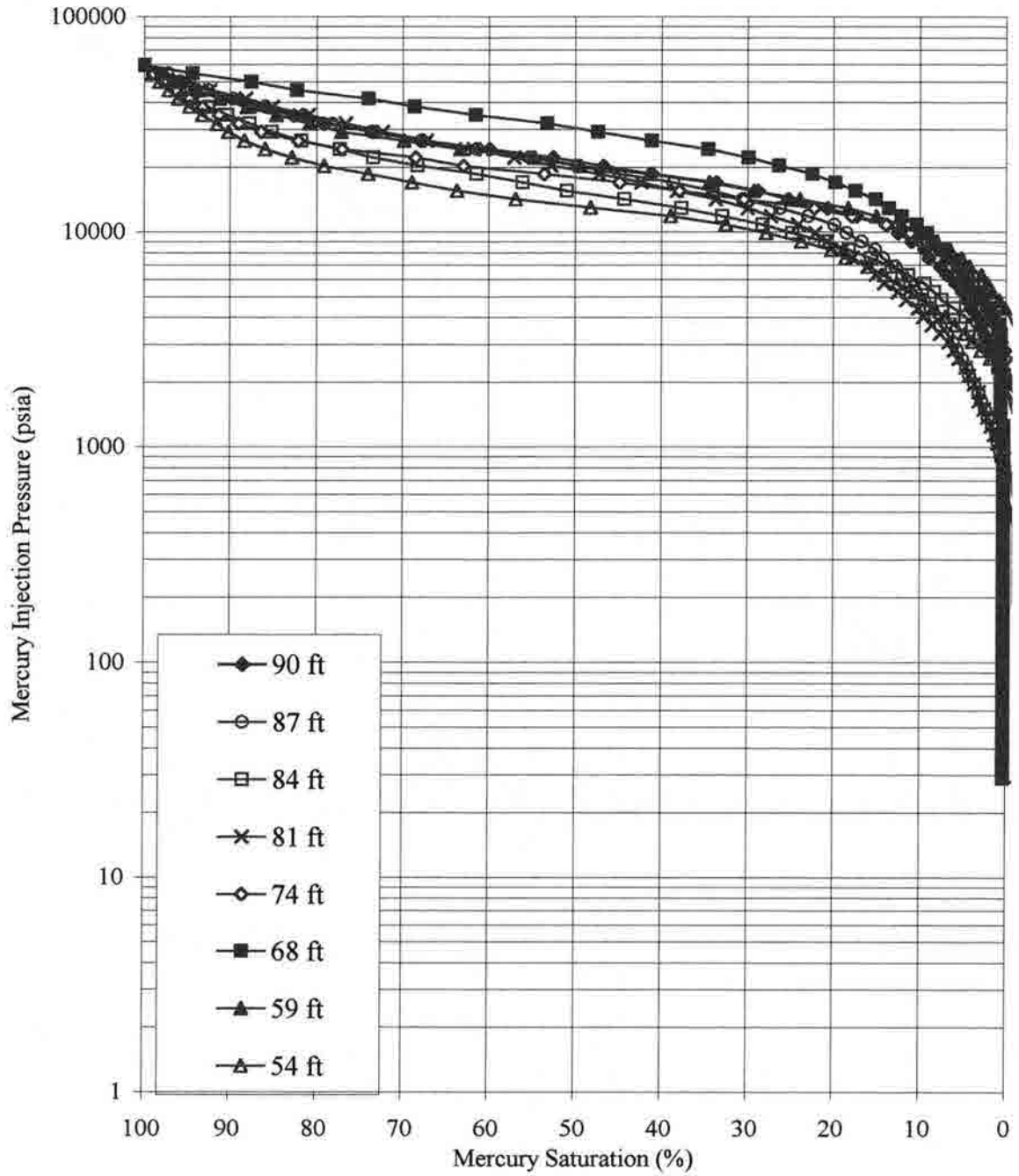


Figure 8.9c Drainage Curve for Facies Z (CS) at Rooney Ranch.

Rooney Ranch Drainage Curve (Upper facies Y)

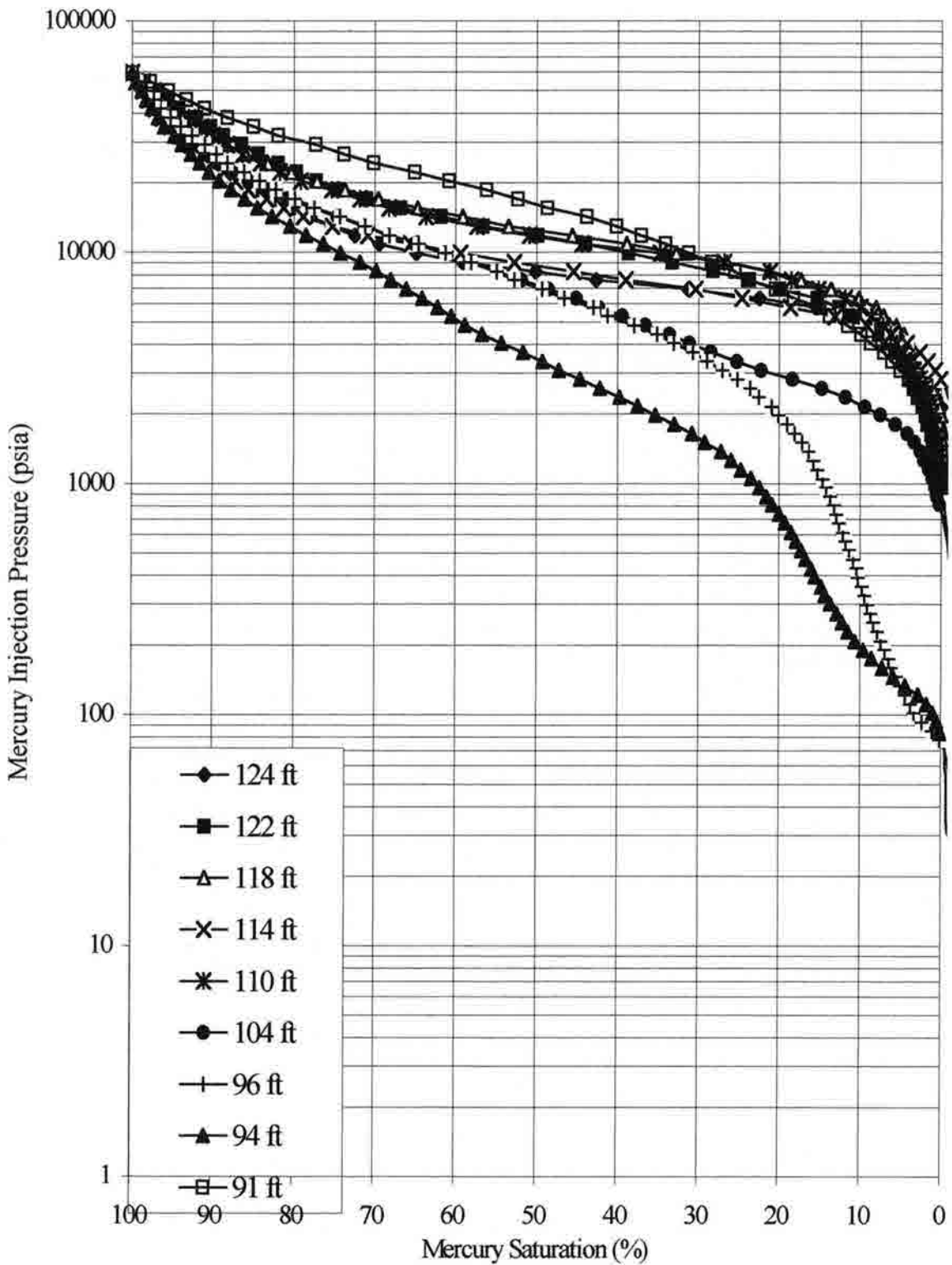


Figure 8.9d Drainage curve for the upper Y facies at Rooney Ranch.

8.4 Summary

The best seal delineated by MICP for the Graneros shale is located in facies Z or the condensed section, although potential seals are also located in facies X. The following is a list of characteristics displayed by the rock with the highest sealing properties:

1. Located at 68 ft in the "hot zone".
2. 5.04% total organic carbon content (the highest).
3. Type I-II (marine) organic matter.
4. Well developed lamination in hand sample.
5. Density value of 2.44 g/cc.
6. 4.07% porosity with 0.00005-md permeability.
7. No notable bioturbation or matrix porosity in thin section.
8. XRD data with 39% clay, 28% quartz, 9% pyrite, 11% dolomite, 4% mg-calcite, 4% siderite, 3% anhydrite, and 2% feldspars.
9. 10,566 psia at 10% mercury saturation with a HCH of 2965 ft.
10. Two PTD populations with a very well sorted, median PTD of 0.0055-micron composing 70% of the PV and the remaining 30% has a moderately sorted, median PTD of 0.015 microns.

Figure 8.10 shows the histograms for the injection pressures at 10% mercury saturation for each facies grouped into columns of 2000. Facies X has one sample in the 10,000 column and two in the 8,000 column. Facies Y has one sample in the 8,000 column and six in the 6,000 column. Facies Z has one sample in the 12,000 column and three in the 10,000 column.

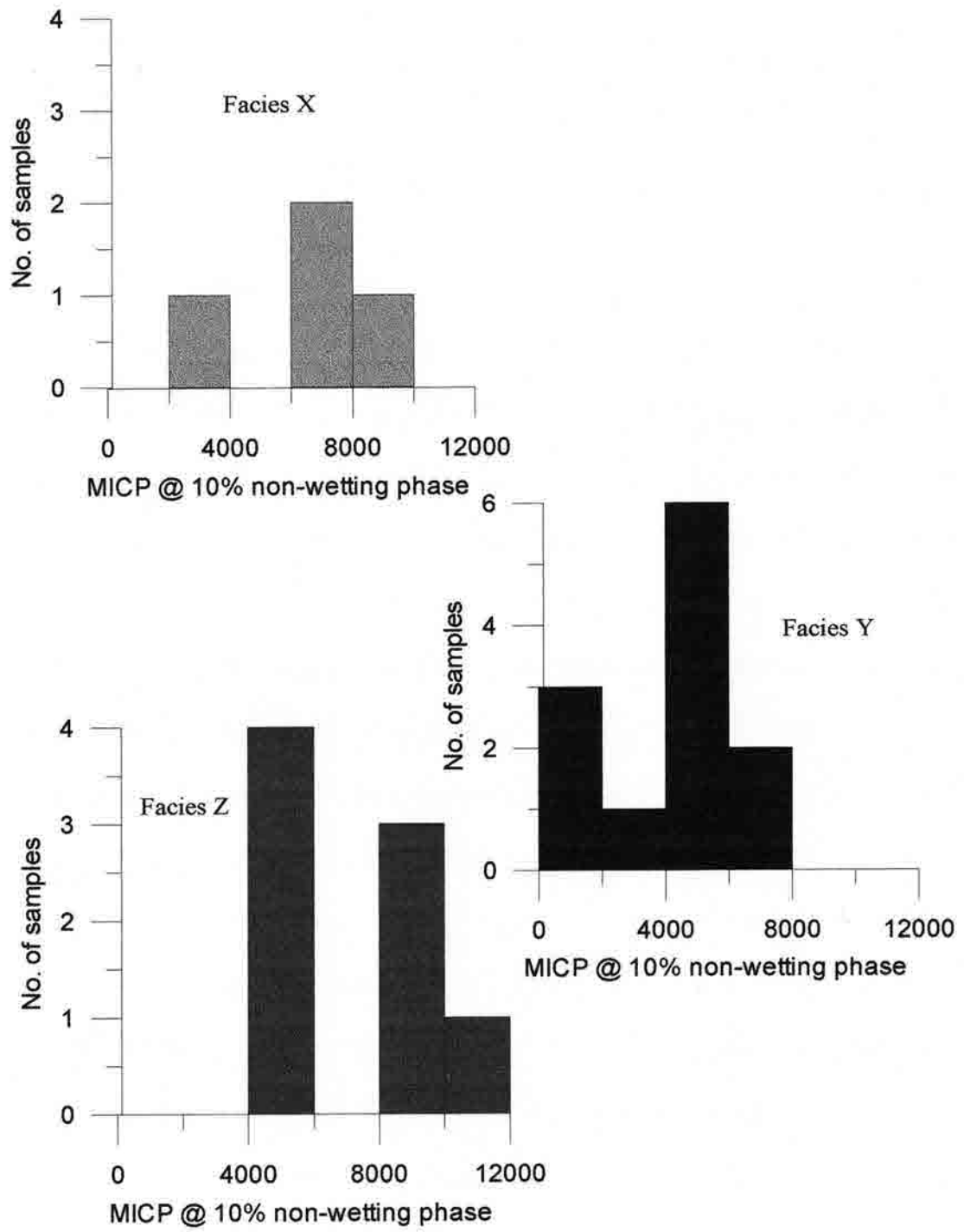


Figure 8.10 Histogram of MICP at 10% Mercury Saturation for Rooney Ranch.

CHAPTER 9. YOUNGS CORE (GRANEROS SHALE) RESULTS

9.1 Facies Description

The Graneros Shale is exposed in 45 ft of the 46 ft Youngs #34 core. The bottom foot of this core (5805 ft) is the Muddy D Sandstone and forms a sharp contact with the overlying Graneros Shale. No overlying contact is found at the top of this core and it is assumed that the Graneros Shale continues stratigraphically upward. Distinguishing facies within the Graneros section of the Youngs core was difficult based on the uniformity of the shale in hand sample. The overall mineralogy and drainage curves also show little variation among these samples. Since most of Youngs core is in the radioactive or "hot zone", all of the Graneros samples are termed facies Z here. There are no bentonites in this core to group samples with facies Y, and there are no Ironstone layers to group it with facies X. By examining the wireline gamma ray log the "hot zone" can be distinguished from 5780-5800 ft (Fig. 9.1). There is a transitional interval from the Muddy D Sandstone to the Graneros at 5804 ft. It is burrowed silty shale with siderite-cemented mudclasts and pyrite nodules. Overall, the samples are a grayish-black shale with no notable silt in hand sample. Well-developed laminations give this shale a fissile to crumbly appearance.

The bottom of the core begins with the Muddy 'D' Sand and is overlain by a burrowed silty shale deposit (Fig. 9.2). This gradually becomes more organic rich in facies Z (Fig. 9.3). Facies Z is seen all the way to the top of the core (Fig. 9.4).

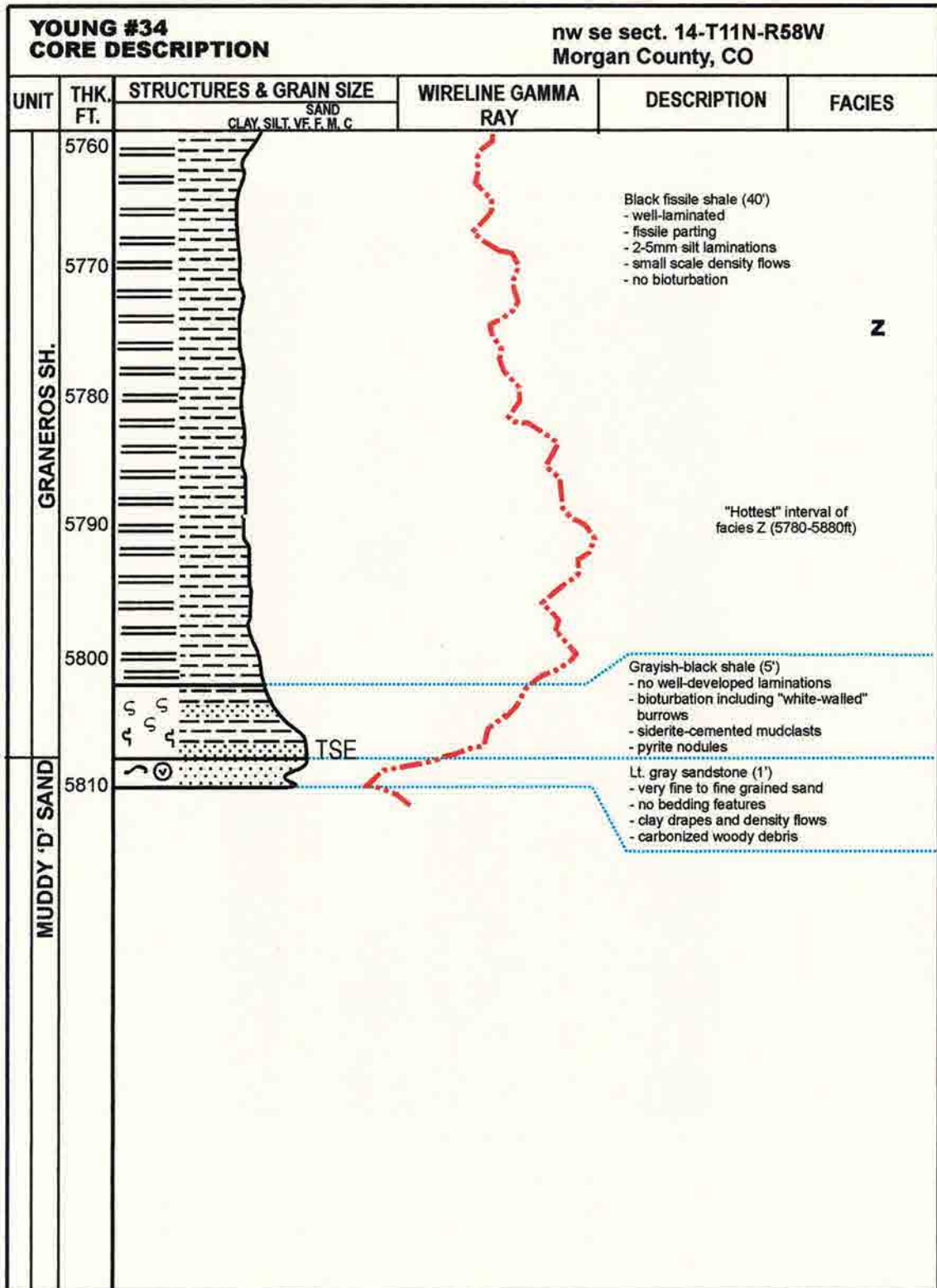
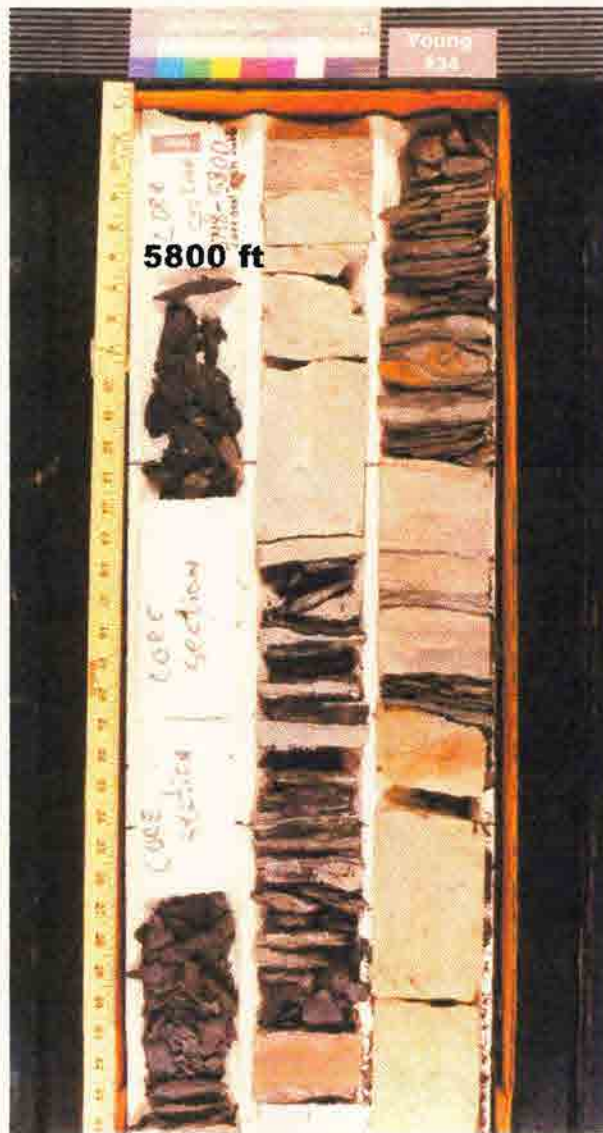


Figure 9.1 Stratigraphic column for Youngs #34 Core, including detailed descriptions interpretations, and wireline gamma ray log.



**Bottom of Core
5809 ft**

Figure 9.2 Youngs Core photos from 5800-5809, including Facies Z and the Muddy 'D' sandstone at the bottom of the core.

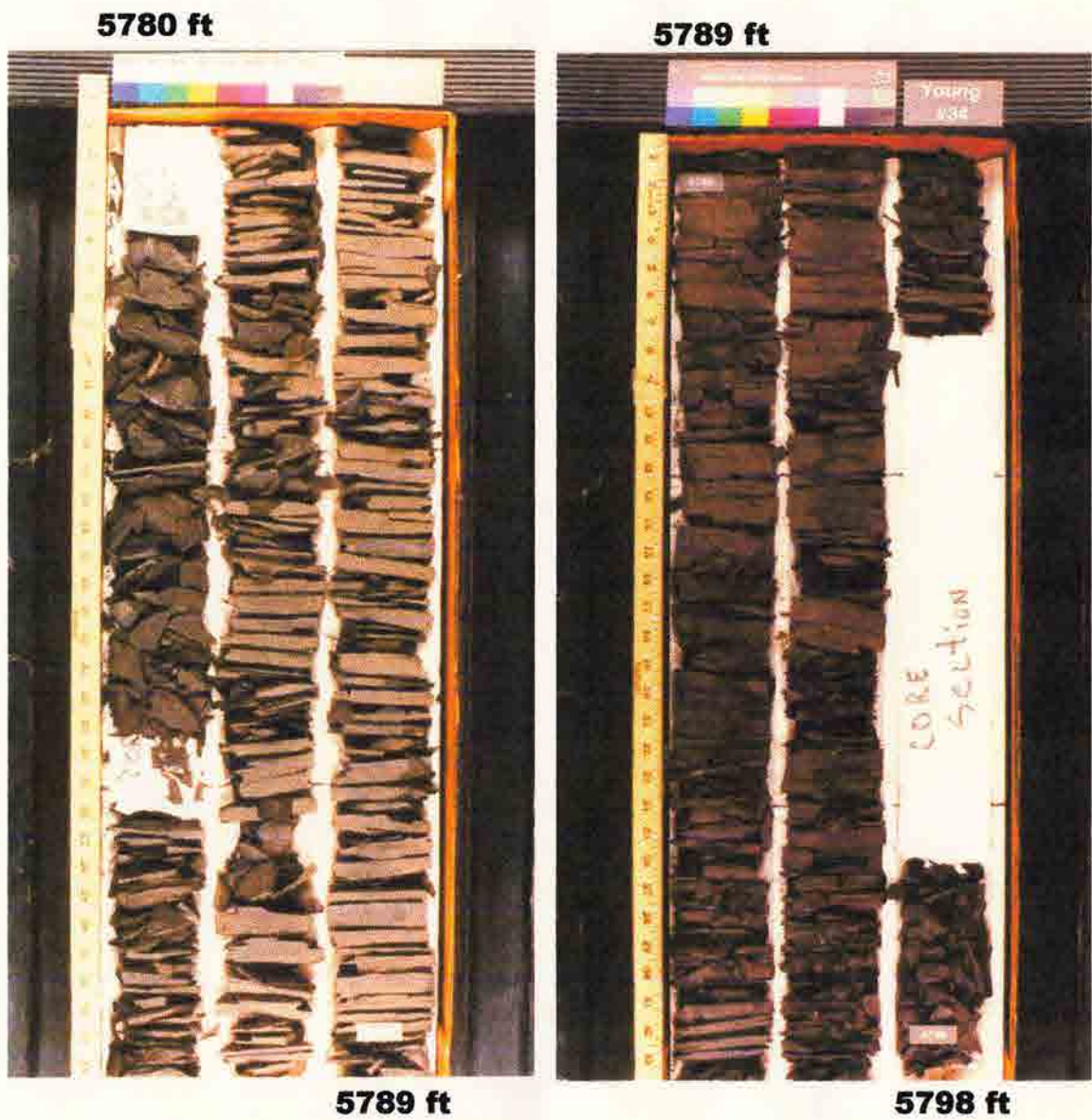


Figure 9.3 Youngs Core photos from 5780-5798, including Facies Z.



Figure 9.4 Youngs Core photos starting from the top of the core at 5762-5780, including Facies Z.

Figure 9.5 shows a clear type I (marine) organic matter. The samples with the lowest HI correspond to the Muddy 'D' sand.

9.2 *Lithology Description*

Table 9.1 displays the statistics for the Youngs Core data. Overall, the TOC values range from 1.56-5.36% with the average of 4.15%. Since the weathering of organic matter in outcrop is a concern when examining TOC, it is interesting that the average outcrop values are not much lower than the core values. The Youngs Core rocks have an average HI value of 411 mg HC/g TOC, which corresponds with a type I (marine) kerogen. It should be noted that the burrowed silty shale at 5804 ft has a low HI value although it has a significant amount of TOC. Another unusual sample is located at 5800 ft and has 1.56% TOC with an unusually high HI (925 mg HC/g TOC), relative to the other Graneros samples. The Graneros samples average 29% quartz, 49% total clay, and 6% carbonate. The porosity values average 4.18% with 0.000047 md of permeability and 2.52 g/cc of density. The sample at 5800 ft has an unusually high amount of total clay at 61%, with 34% quartz, and 5% carbonate. This sample also has the lowest porosity (1.71%) and permeability 0.00001-md values. This sample also has the highest density at 2.72 g/cc.

The D Sandstone is clearly separated from the Graneros Shale with 1.48% TOC with a low HI (28 mg HC/ mg TOC). It is composed of 83% quartz, 10% total clay, with 4% cement and 6.57% porosity with 0.0637 md of permeability.

The data in Table 9.1 were plotted against stratigraphic height to compare them to sealing capacity, as determined by MICP. The best seal is located in facies Z or the CS at 5804 ft (Fig. 9.6a).

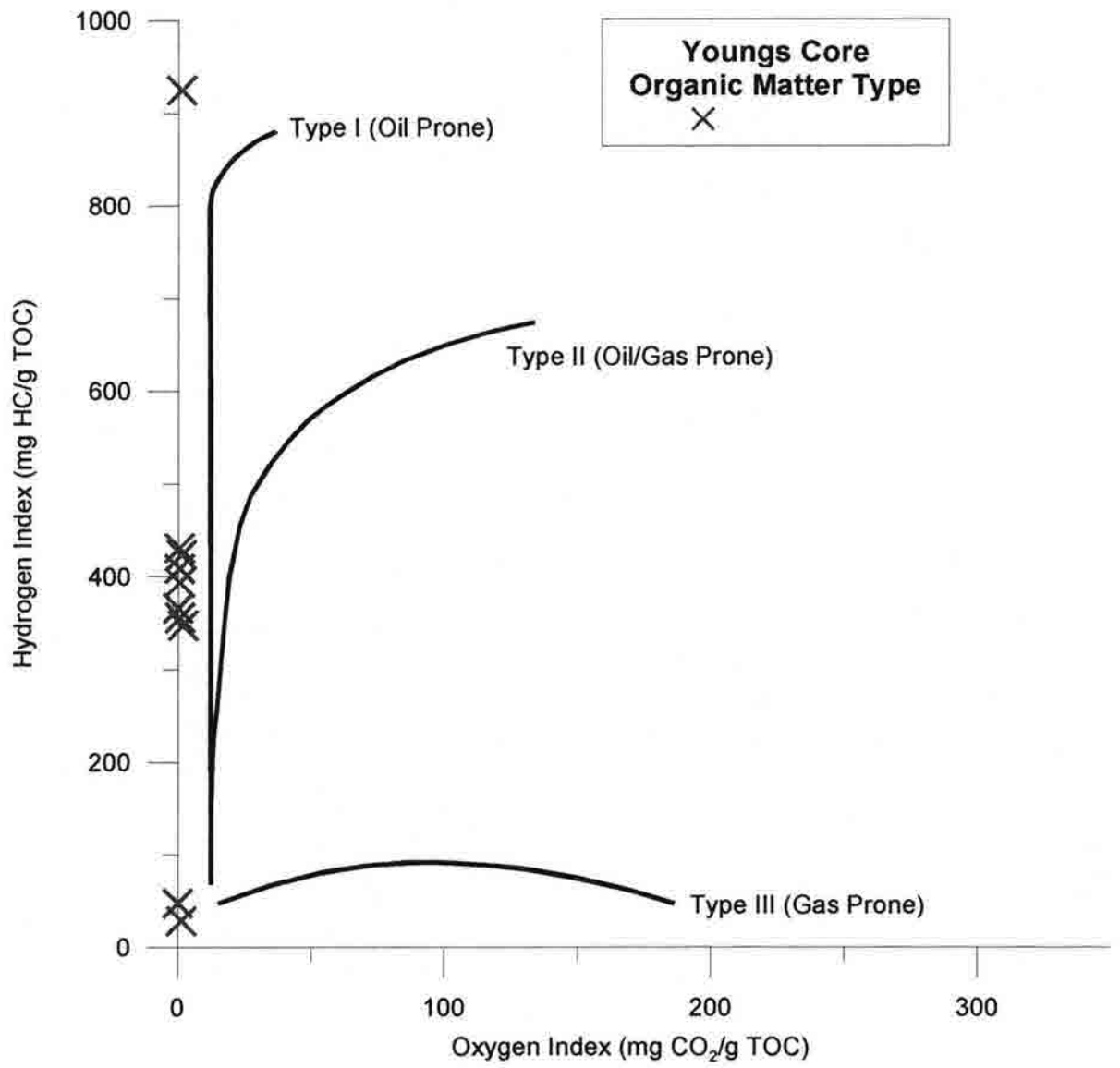


Figure 9.5

Table 9.1 Statistics for the Youngs Core (Graneros Shale) data

Youngs Core		Total Organic Carbon (%)	Hydrogen Index (mg HC/g TOC)	Hydrogen Index/Oxygen Index (mg HC/mg CO ₂)	Total Clay (wt%)	Quartz (wt%)	Feldspar (wt%)	Carbonate (wt%)	Porosity (%)	Permeability (md)	Density (g/cc)
	# of Analyses	9	9	9	9	9	9	9	9	9	9
Z	Average	4.15	411	1894	49	29	4	6	4.18	4.7E-05	2.52
	Std Dev	1.24	225	3600	5	3	1	1	1.14	2.2E-05	0.08
	# of Analyses	1	1	1	1	1	1	1	1	1	1
D sand		1.48	28	21	10	83	3	4	6.57	0.0637	2.69

Porosity is variable throughout, but shows a sharp decrease at 5804 ft (Fig. 9.6b). The lowest permeability value also corresponds with the highest value for seal capacity (Fig. 9.6c). This sample at 5804 ft also has the greatest density (Fig. 9.6d).

The amount of total clay does not vary much, but shows a slight increase at 5804 ft (Fig. 9.7a). Quartz shows an inverse relationship to clay (Fig. 9.7b). The amount of feldspar does not vary significantly (Fig. 9.7c). Carbonate shows a slight decrease at 5780 ft (Fig. 9.7d).

TOC reaches its peak towards the middle of the core in facies Z or the CS (Fig. 9.8a). The hydrogen index values peaks at 5800 ft (Fig. 9.8b). However, ratio of HI/OI does not correspond to this peak at 5800 ft, but peaks further upsection in facies Z (Fig. 9.8c).

Thin Section Petrography

Table 9.2 shows the thin section petrographic observations and Appendix N displays the representative thin section photomicrographs for the Youngs Core. Overall, the thin section petrography shows these samples to be a well compacted, carbonaceous

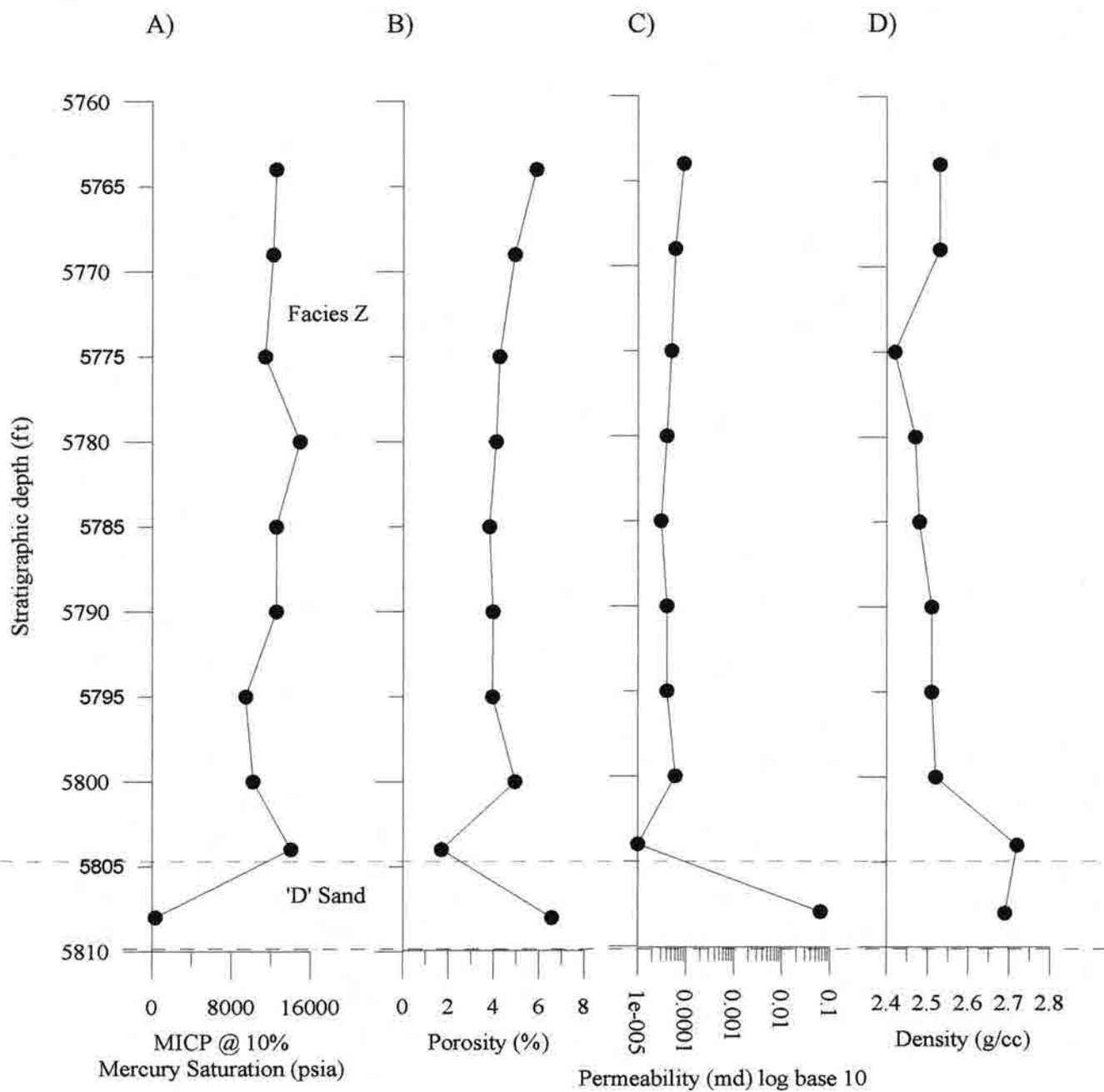


Figure 9.6 Stratigraphic height vs. MICP (A), porosity (B), permeability (C), and density (D) for the Youngs Core.

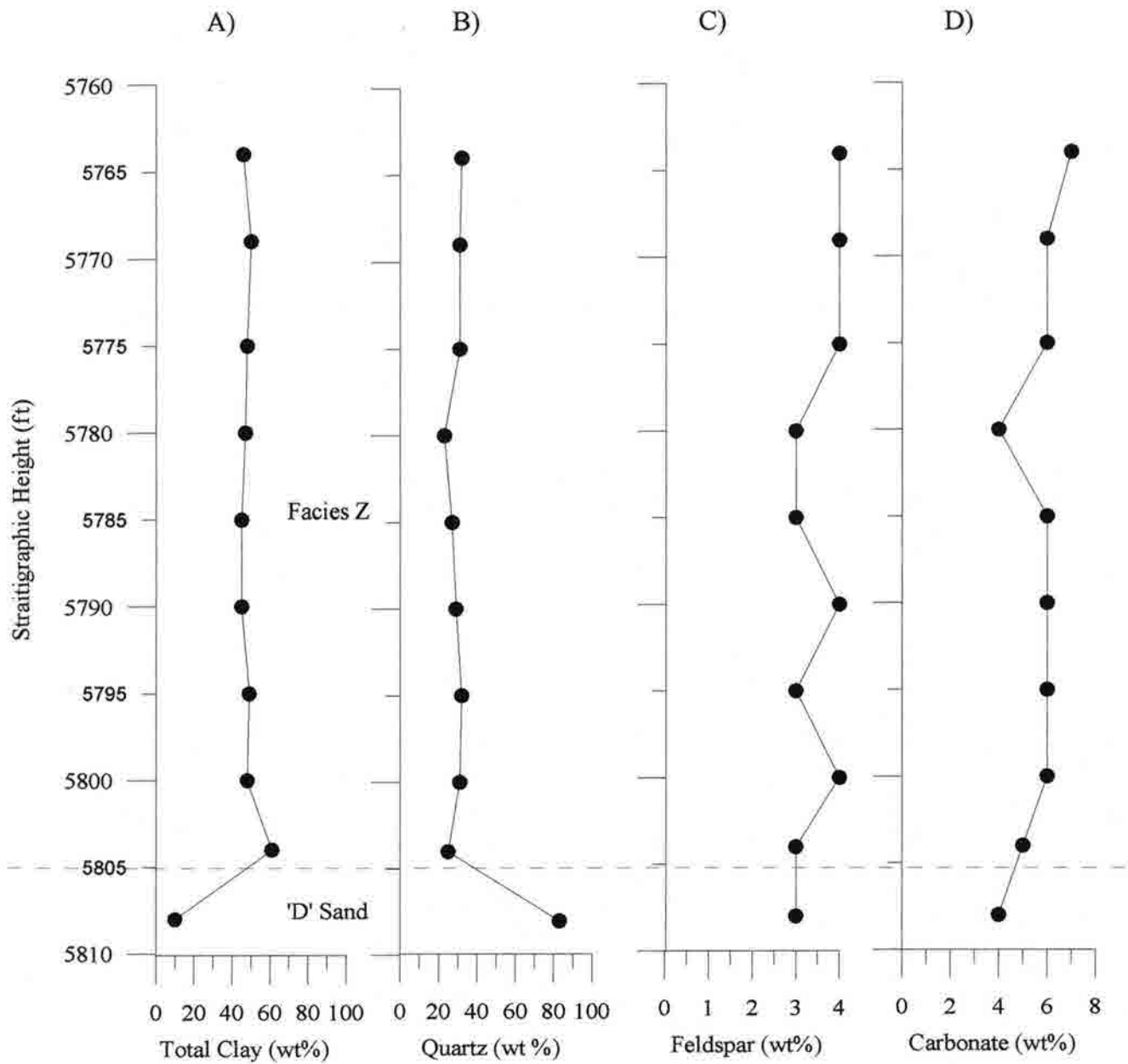


Figure 9.7 Stratigraphic height vs. total clay (A), quartz (B), feldspar (C), and carbonate (D) for the Youngs Core.

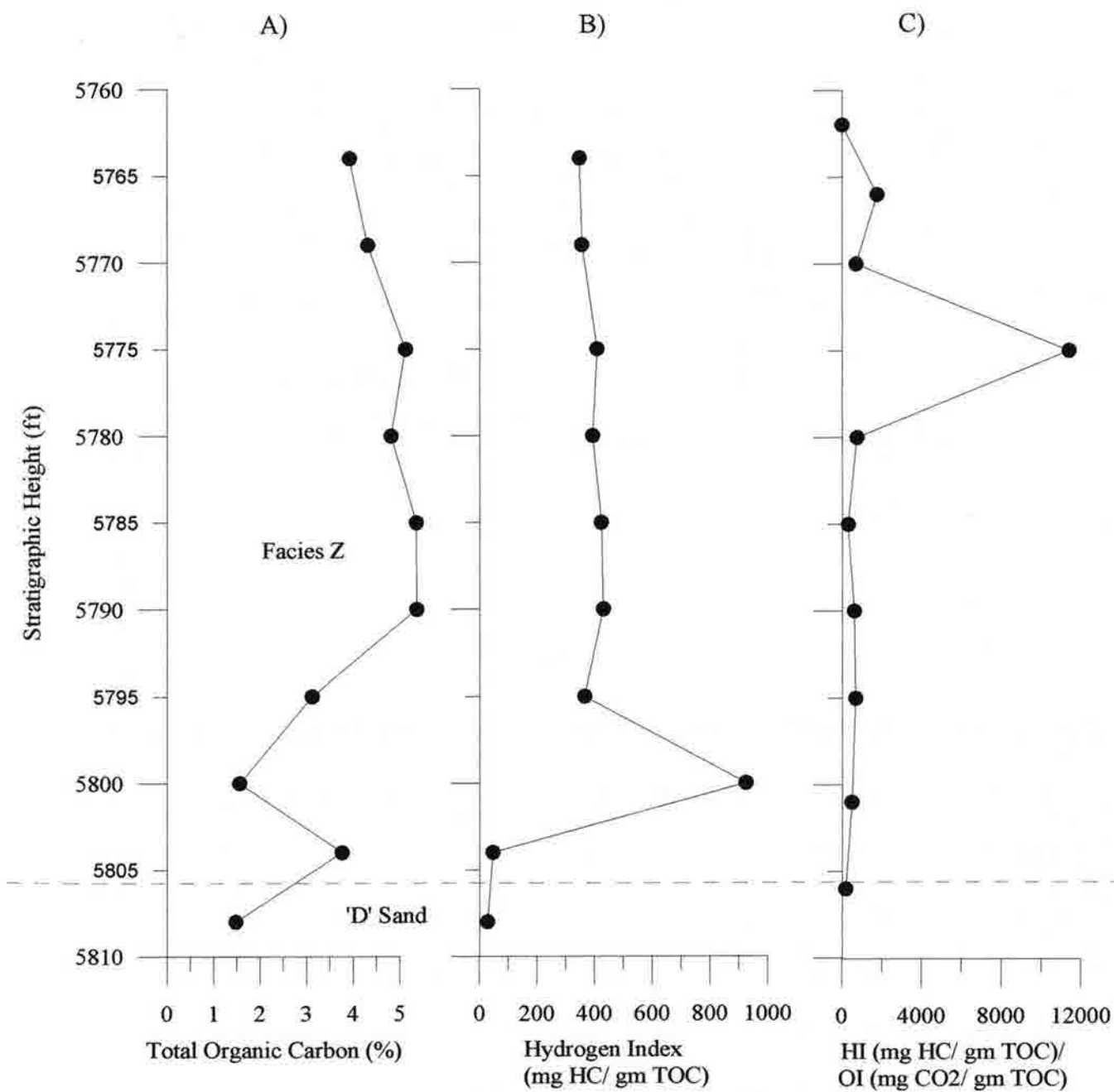


Figure 9.8 Stratigraphic height vs. TOC (A), hydrogen index (B), and hydrogen index / oxygen index (C) for Youngs Core.

Table 9.2 Youngs Core Thin Section Petrography

Facies	FT	Rockname	Grain Size	COMPOSITION						Laminations	Bioturbation	Pressure Solution	Fossils	Porosity
				QTZ	CLAY	ORG	CARB	PYR	OTHER					
Z	5764	mudstone	silt	41	52	2	1	4	phos	Y	Y	Y	Y	N
	5769	mudstone	silt	39	53	3	1	4	phos	Y	Y	Y	Y	N
	5780	mudstone	silt	34	54	4	1	7	phos	Y	N	Y	Y	N
	5790	mudstone	silt	35	54	4	1	6	phos	Y	N	Y	Y	N
	5800	mudstone	silt	28	63	3	1	5	phos	Y	N	Y	Y	N
	5804	mudstone	silt	27	63	3	2	5	phos	N	N	Y	Y	N
D sand	5808	sandstone	F-M sand	90	7	2	1	0	mica	N	N	Y	Y	N

**NOTE: 1/256 < silt < 1/16 mm, 1/16 < VF sand < 1/8 mm, 1/8 < F sand < 1/4 mm, 1/4 < M sand < 1/2 mm

QTZ= Quartz

ORG= Organic Matter

CARB= Carbonate (calcite, dolomite, siderite)

feld= Feldspar

phos= Phosphate

mic= Mica

hem= Hematite

silty shale. The detrital grains (quartz, feldspars, and mica) are well sorted, subangular, spherical-elongate, and silt size. These grains have a strong preferred orientation that enhances the well-laminated appearance. Wispy laminations of organic matter are also present. Authigenic framboidal pyrite and phosphatic nodules are minor constituents to the predominant clay matrix and detrital grains. The mineralogy for facies Z of the Youngs Core averages 57% clay, 34% quartz, 5% pyrite, 3% organic matter, and 1% authigenic carbonate (dolomite, calcite, and siderite). Some burrowing is present in the thin section towards the top of the core, but overall these shales remain unbioturbated. No intergranular or intercrystalline porosity is visible.

Whole Rock Mineralogy

The XRD analysis of the whole rock mineralogy is displayed in Table 9.3. Overall, the samples have a nearly uniform mineralogy that averages 49% total clay, 29% quartz, 13% pyrite, 4% plagioclase, 3% high Mg-calcite, 2% siderite, 1% dolomite, and 1% anhydrite. Again, the sample at 5804 ft is predominantly clay with 61% total clay, 25% quartz, 6% pyrite, 4% high Mg-calcite, 3% plagioclase with minor amounts of dolomite.

Table 9.3 Whole Rock Mineralogy (wt%): Youngs Core (Graneros Shale)

Facies	Sample #	DEPTH (FT)	TCL	QTZ	PLAG	Mg-CAL	DOL	PYR	SID	ANHY
Z	Y044	5764	46	32	4	3	1	11	3	TR
	Y039	5769	50	30	4	3	1	10	2	TR
	Y033	5775	48	31	4	3	1	11	2	TR
	Y028	5780	47	23	3	3	1	23	ND	TR
	Y023	5785	45	27	3	3	1	18	2	1
	Y018	5790	45	29	4	3	1	15	2	1
	Y013	5795	49	32	3	3	1	10	2	TR
	Y008	5800	48	31	4	3	1	11	2	TR
	Y004	5804	61	25	3	4	1	6	ND	TR
	Average			49	29	4	3	1	13	2
D-sand	Y000	5808	10	83	3	1	1	ND	2	TR

LEGEND:

TCL= Total Clay and Mica
 QTZ= Quartz
 PLAG= Plagioclase
 Mg-CAL= High Mg-Calcite
 DOL= Dolomite
 PYR= Pyrite
 SID= Siderite
 ANHY= Anhydrite

9.3 Petrophysical Description

Table 9.4 shows the injection pressures at 10% mercury saturation and the corresponding hydrocarbon column heights (HCH) they can hold. The highest injection pressure is located at 5780 ft with 14,940 psia, which can hold 4,200 ft HCH. Following this at 5804 ft is the burrowed sample with 14,050 psia, which can hold 3,920 ft of HCH.

Table 9.4 Young's Core Injection Pressures (psia) at 10% Mercury Saturation

Facies	Sample#	FT	PSIA@10%SAT.	HCH (ft)
Z	YO-044	5764	12540	3520
Z	YO-039	5769	12240	3440
Z	YO-033	5775	11420	3210
Z	YO-028	5780	14940	4200
Z	YO-023	5785	12540	3520
Z	YO-018	5790	12550	3530
Z	YO-013	5795	9450	2620
Z	YO-008	5800	10205	2860
Z	YO-004	5804	14047	3915
D-sand	YO-000	5808	349	90

This is followed by a sample 5,790 ft that requires 12,550 psia, which can hold 3,530 ft of HCH. The drainage curves for these samples show remarkable similarity (Fig. 9.9). They all have a gently sloping curve, with the exception of the D-sandstone sample at 5808 ft. Their entry pressures range from 3,000-10,000 psia.

Appendix O shows the MICP data for each of these samples. Overall, they have one population of a well-sorted median PTD ranging from 0.0045-0.015 microns. The burrowed sample at 5,804 ft has one very well sorted median PTD population of 0.0045 microns. This is somewhat unusual that a burrowed sample would have such a small PTD. This sample does not have an unusual amount of cement, but does have a high amount of total clay.

9.4 Summary

The best seal delineated by MICP for the Graneros is located in facies Z or the CS. The following is a list of characteristics displayed by the rock with the highest sealing properties:

1. Located at 5780 ft in the "hot zone".
2. 4.81% total organic carbon content (not the highest).
3. Type I-II (marine) organic matter.

Youngs #34 Core Drainage Curve (Facies Z and 'D' sandstone)

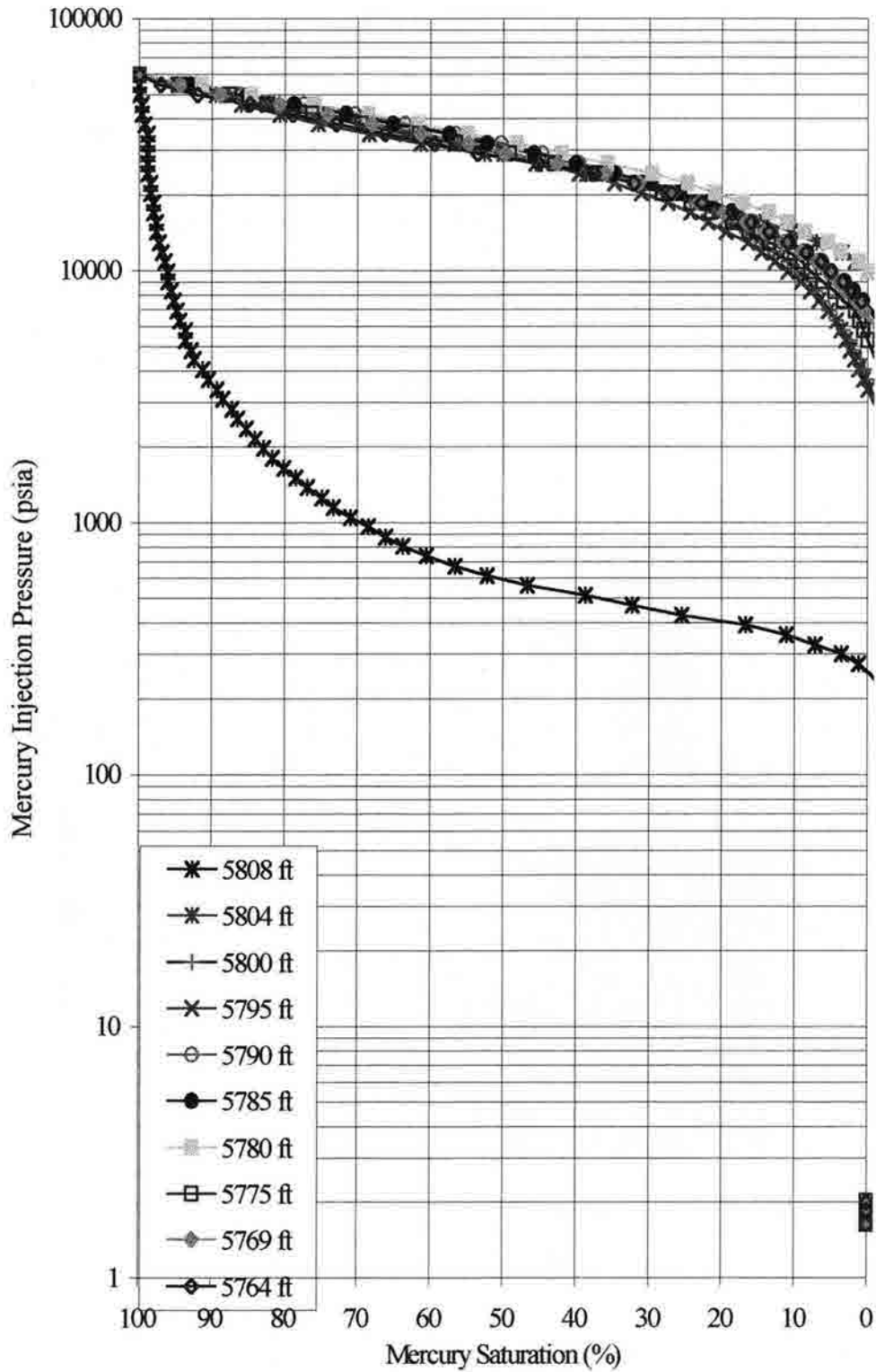


Figure 9.9 Drainage Curve for Youngs core (Graneros Shale).

4. Well developed lamination in hand sample.
5. Density value of 2.47 g/cc.
6. 4.12% porosity with 0.00004-md permeability.
7. No notable bioturbation or matrix porosity in thin section.
8. XRD data with 47% clay, 23% quartz, 23% pyrite, 1% dolomite, 3% mg-calcite, and 3% feldspars.
9. 14,942 psia at 10% mercury saturation with a HCH of 4195 ft.
10. One population with a well sorted, median PTD of 0.0045 microns.

Figure 9.10 shows a histogram for the injection pressures at 10% mercury saturation grouped into columns of 2000 psia. Facies Z has two samples in the 16,000 column and four in the 14,000 column.

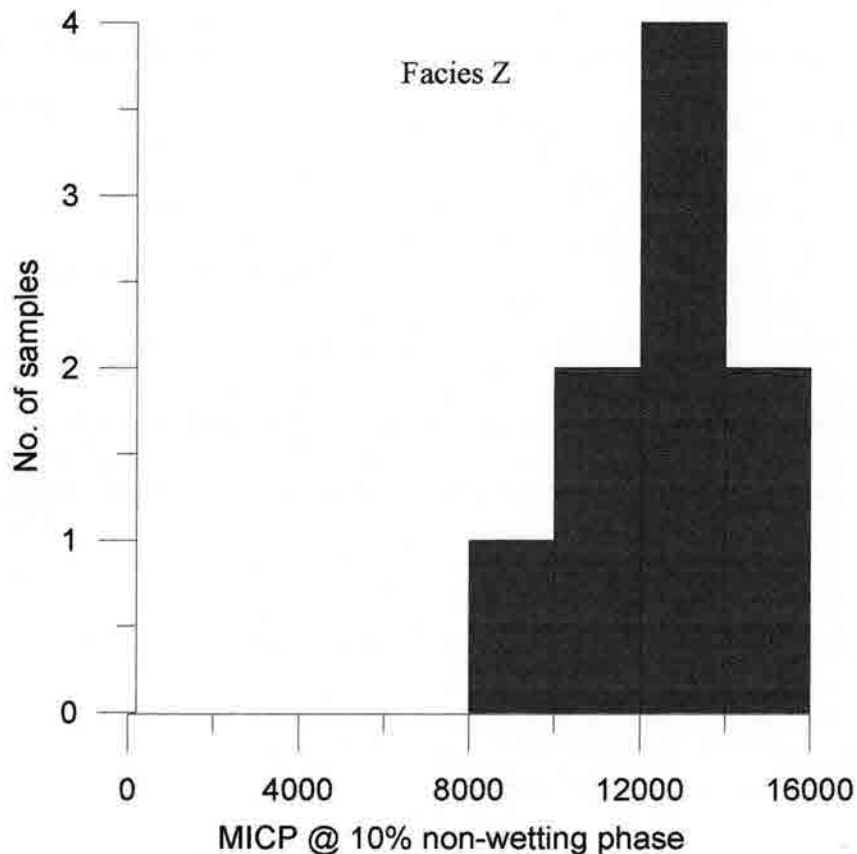


Figure 9.10 Histogram of MICP for Youngs Core (Graneros Shale).

CHAPTER 10. DISCUSSION

The Skull Creek and Graneros are two examples of marine Cretaceous shales. There is considerable variability between and within these shales. The Graneros is a fissile, organic-rich, phosphatic black shale that was deposited in a distal, open marine shelf environment (Bohacs, 1998). Conversely, the Skull Creek Shale is a well-laminated, fossiliferous silty shale that is organic poor relative to the Graneros. It was also deposited in an open marine shelf environment, but probably with a greater sediment input that may be caused by a more proximal location to a shoreline.

10.1 *Skull Creek Summary*

A stratigraphic cross-section of the Skull Creek Shale for the locations in this study is shown in Figure 10.1. In general, the shales with the greatest sealing capacity are located in the upper parts of the transgressive units, in places below the condensed section.

Facies K is only present at the Soldier Canyon and Bellevue outcrops and consists of a mudstone with relatively high amounts of total clay and low TOC, with type III (terrestrial) organic matter. The best seal is located at 50 ft in the upper part of facies K at Soldier Canyon. At Bellevue, the best seal is found lower in facies K at 9 ft. Bellevue samples have the lowest sealing capacity of all Skull Creek locations, probably due to the poorly sorted PTDs. This study agrees with Schutter (1998) in that the TST deposits are variable in mineralogy and generally have terrestrial organic matter. However, Schutter

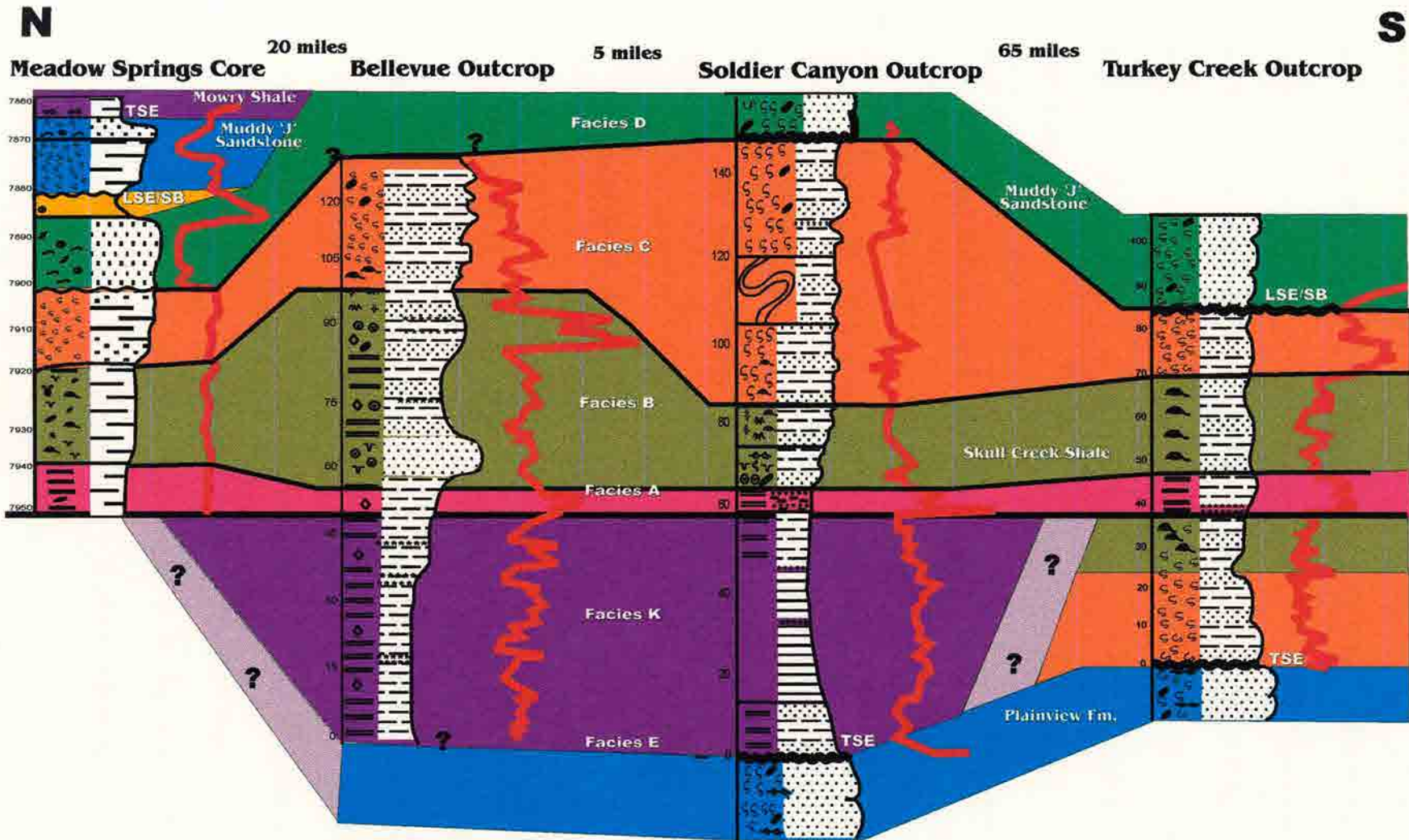


Figure 10.1 Stratigraphic cross-section of the Skull Creek Shale locations. Red lines are gamma ray curves. Vertical scale is approximate, horizontal representation is not to scale.

(1998) assumes this variability prevents TST deposits from providing adequate seal capacity. Data generated in this study suggests that some TST deposits are adequate seals. The Meadow Springs core, which is northeast of both Soldier Canyon Dam and Bellevue, does not include facies K because the core terminates in facies A. The best seal in the core for the Skull Creek Shale is located in facies A, which contains type I (marine) organic matter and has relatively low amounts of total clay and TOC. These core samples generally have higher injection pressures than the outcrop samples, due to their unweathered nature. At the Turkey Creek location, which is 65 miles south of Fort Collins, the best seal is also positioned in facies A. These TST deposits do not include facies K, but only the condensed section that is characterized by a type I (marine) organic matter and relatively low amounts of total clay and high amounts of TOC. The data in this study agrees with previous research by Schutter (1998) in that the condensed section shales contain volcanic ash layers and are well laminated, continuous units that provide a barrier for hydrocarbon migration.

The greatest seal capacity changes position from facies A at Meadow Springs and Turkey Creek to facies K at Bellevue and Soldier Canyon. Although, we can not determine if facies K would be a better seal at Meadow Springs, because the core is missing that facies. Possible explanations for this variability may relate to topography or position relative to shoreline during deposition. Turkey Creek and Meadow Springs may have been a topographically high or removed from an area of terrestrial sediment input, thus preventing dilution of type I (marine) organic matter. The presence of facies K and a type III (terrestrial) organic matter with relatively high amounts of total clay at Soldier

Canyon and Bellevue suggest that it was a relatively topographic low area or a deltaic depocenter during deposition.

The sealing capacity for each location can be seen in the histograms of injection pressures at 10% mercury saturation in Figure 10.2. These histograms group the samples into columns of 2,000 psia to visualize where the data is clustering. The Meadow Springs Core clearly shows the highest injection pressures, followed by Soldier Canyon Dam, Turkey Creek, and Bellevue respectively.

10.2 Graneros Shale Summary

A stratigraphic cross section of the two locations for the Graneros Shale is shown in Figure 10.3. There is no obvious marker bed on which to hang this section, so the “hot zone” or facies Z at the Rooney Ranch outcrop is correlated with the Youngs core because of the similarity of the gamma ray logs. The core directly overlies the Muddy D Sandstone member and is missing the underlying Mowry Shale. The core displays a thinner section of the Graneros Shale than found in outcrop. Facies X and Y that are present at Rooney Ranch are missing in the core. The highest seal capacity at both locations is in the condensed section of facies Z. In outcrop, the second highest sealing capacity is in the ironstone-bearing facies X below the condensed section. These shales are tightly cemented with siderite and hematite and provide good seals.

The Graneros Shale in the Youngs core has higher sealing capacity than the Rooney Ranch outcrop. However, the amount of TOC and total clay is similar in the outcrop and core, thus indicating that these materials have not been weathered out of the outcrop. Rooney Ranch is located near the axis of the Denver Basin which was an area of hydrocarbon generation (Pietrasnek-Matner, 1995). It might be possible the Graneros

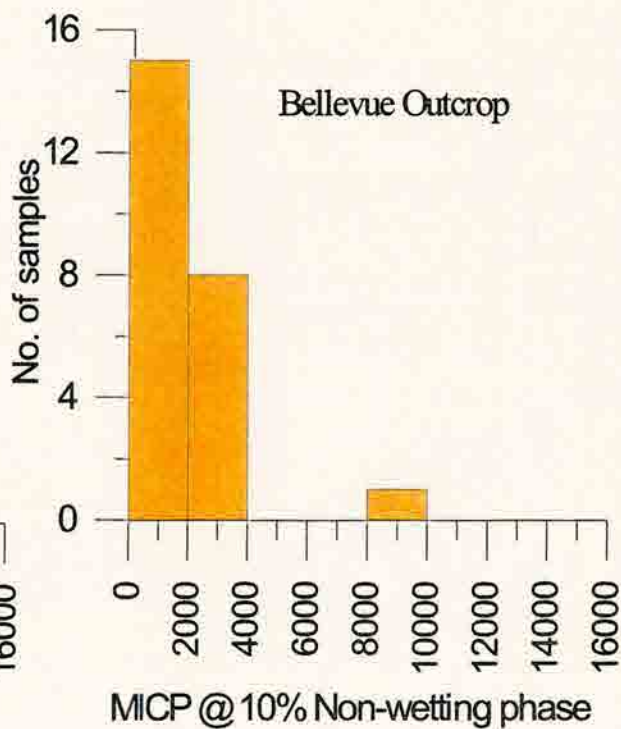
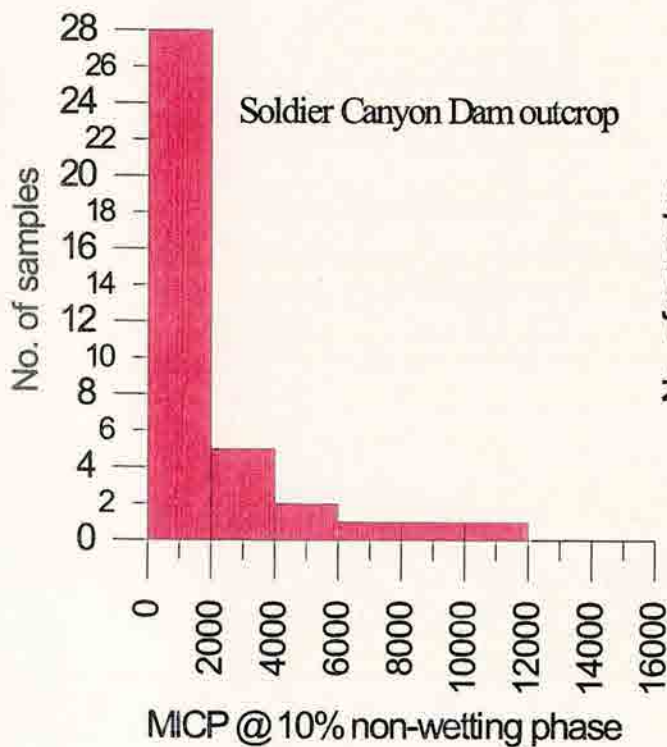
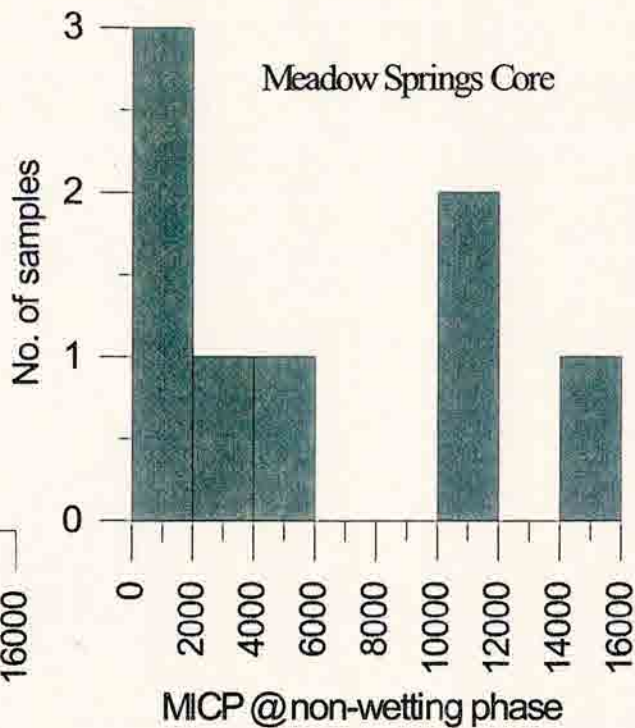
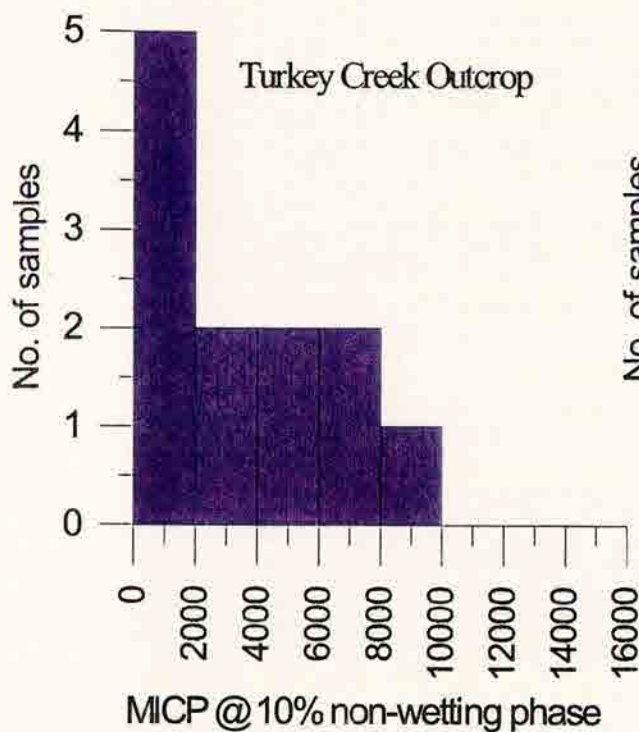


Figure 10.2 Skull Creek Histogram for the MICP at 10% mercury saturation at each location.

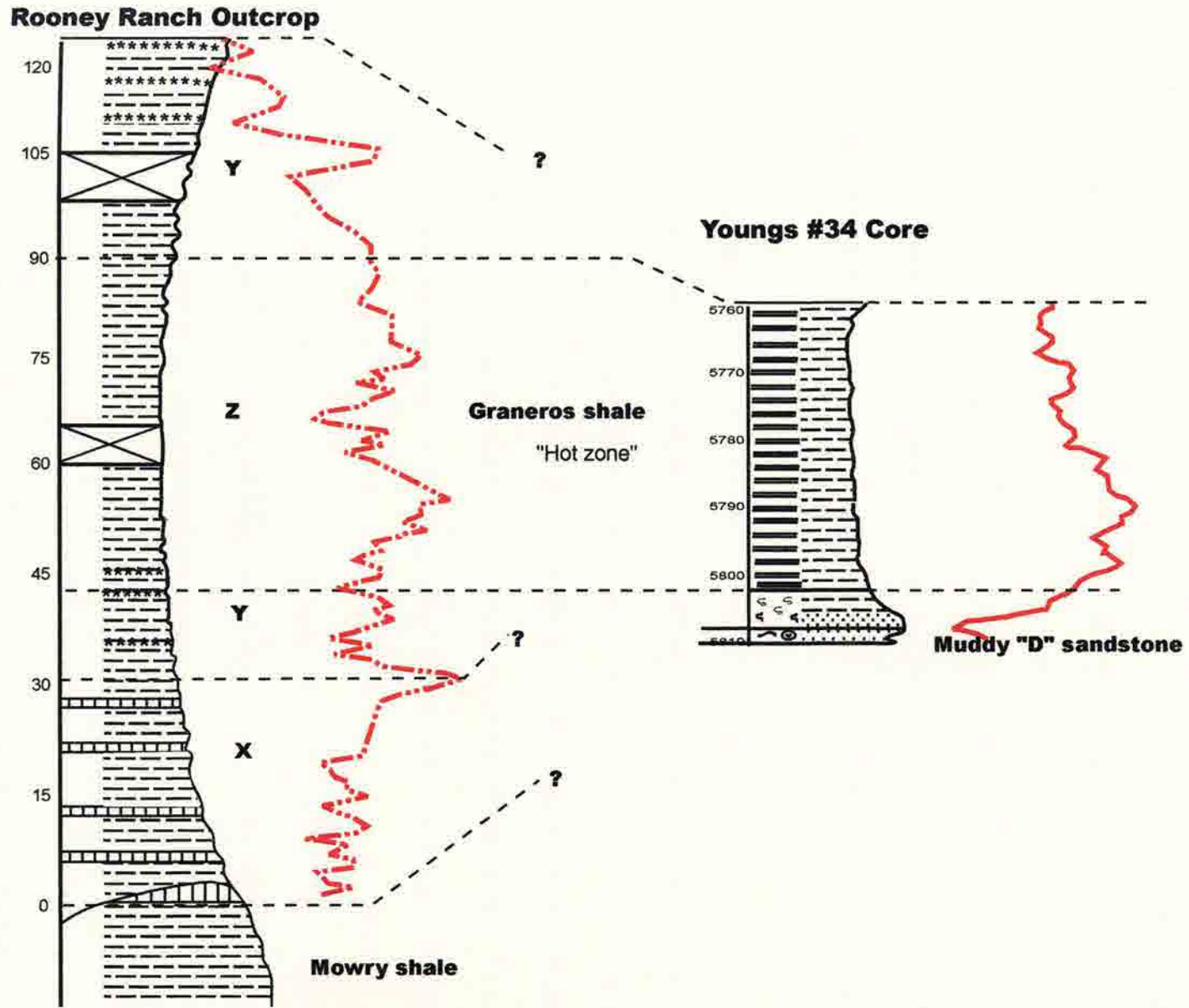


Figure 10.3 Stratigraphic cross-section of the Graneros locations. Red lines are gamma ray curves. Vertical scale is approximate, horizontal representation is not to scale.

Shale at Rooney Ranch has decreased seal capacity due to microfractures created by hydrocarbon generation.

Seal capacity is shown in the histograms (Fig. 10.4) with the samples grouped into columns of 2,000 psia. The greatest sealing capacity is shown in Youngs Core with two samples in the 16,000 bin and four samples in the 14,000 bin. The Youngs core also has the highest amount of total clay (49%) and TOC (4.15%). However, the Rooney Ranch outcrop is not far behind with 43% total clay and 4.21% TOC for facies Z. The injection pressures for the Graneros Shale are generally higher than those found in Skull Creek.

10.3 Correlation

Several of the physical characteristics of the Skull Creek and Graneros Shales, that may relate to seal capacity (MICP), have been plotted for both the Skull Creek and Graneros Shales. Correlation values are displayed in the upper right corner of each graph (Fig. 10.5-10.12). Correlation at the 0.05 level is signified by an (*), and at the 0.01 level by a (**) for a two-tailed test. For the Skull Creek Shale, porosity and log permeability both show the strongest relatively high negative correlation, with $R = -0.349^{**}$ for porosity (Fig. 10.5a), and $R = -0.835^{**}$ for permeability (Fig. 10.5b). These negative correlations reiterate the obvious conclusion that fine-grained rocks with small, non-connected pore networks generally make the best seals.

Total clay shows a significant positive correlation to Skull Creek MICP ($R = 0.313^{**}$; Fig. 10.6a). Quartz shows a negative correlation ($R = -0.383^{**}$; Fig. 10.6b). However, carbonate (Fig. 10.6c) does not have significant correlation with MICP. The ductility and small pore sizes of clays may account for the relatively high positive

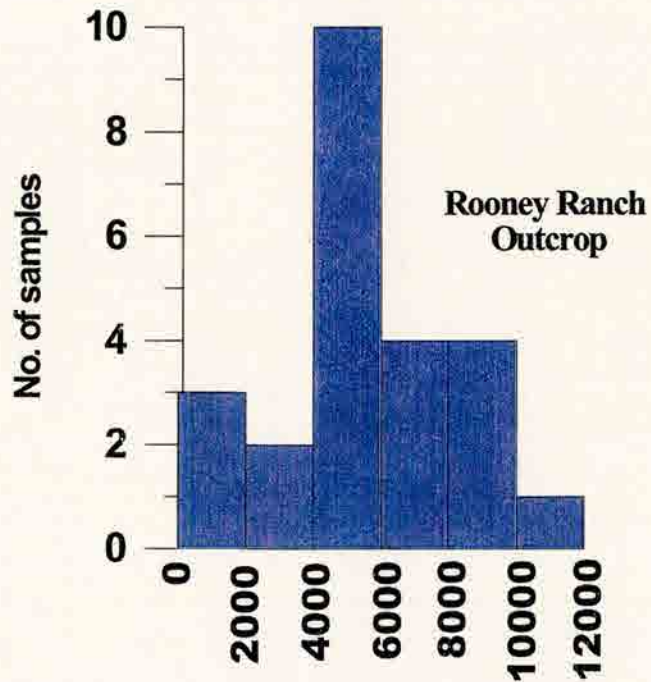
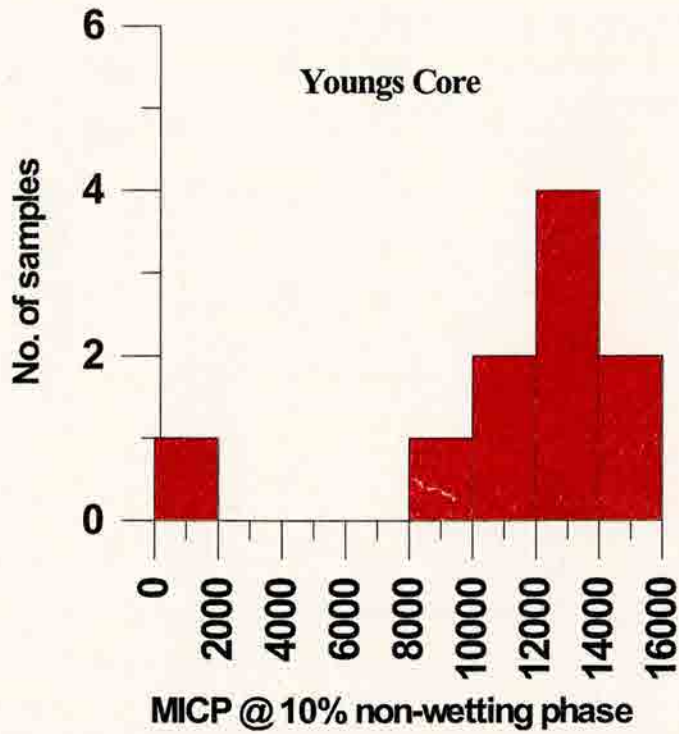


Figure 10.4 Graneros Shale Histogram of MICP at 10% mercury saturation for each location

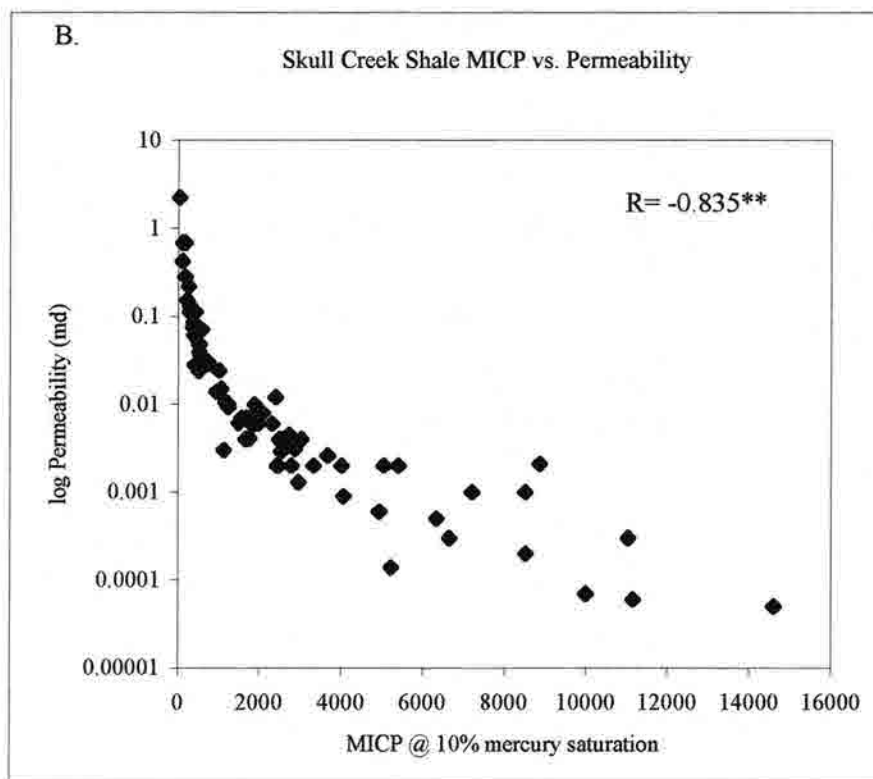
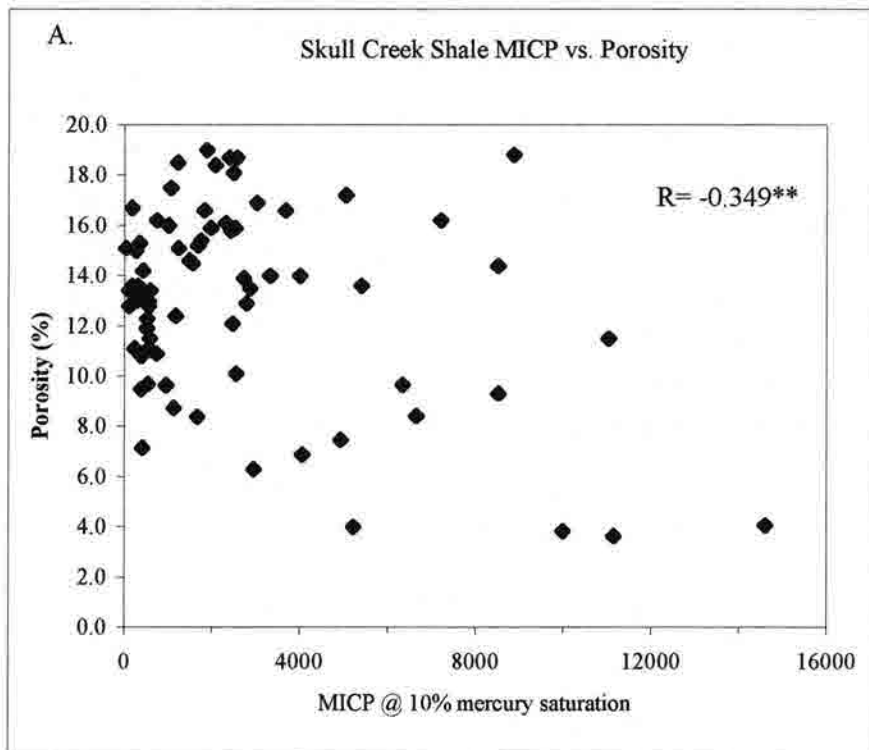


Figure 10.5 Skull Creek MICP vs. Porosity (A) and Permeability (B).

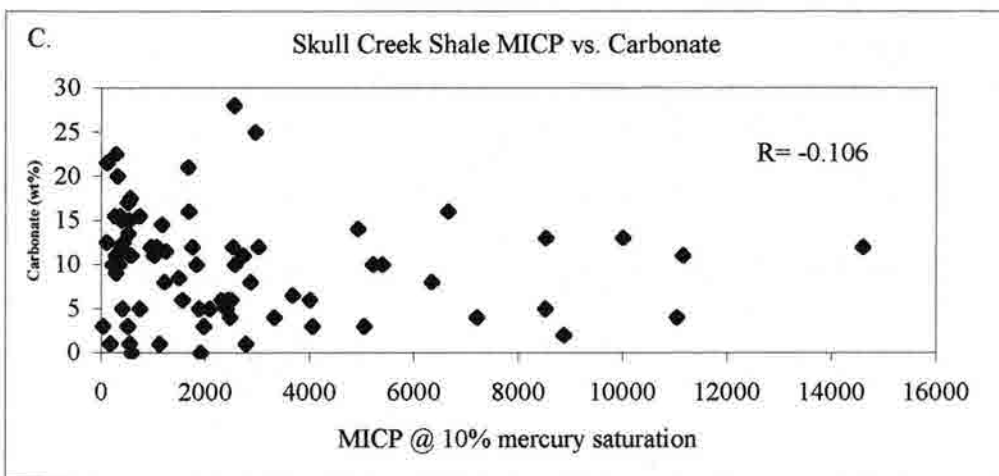
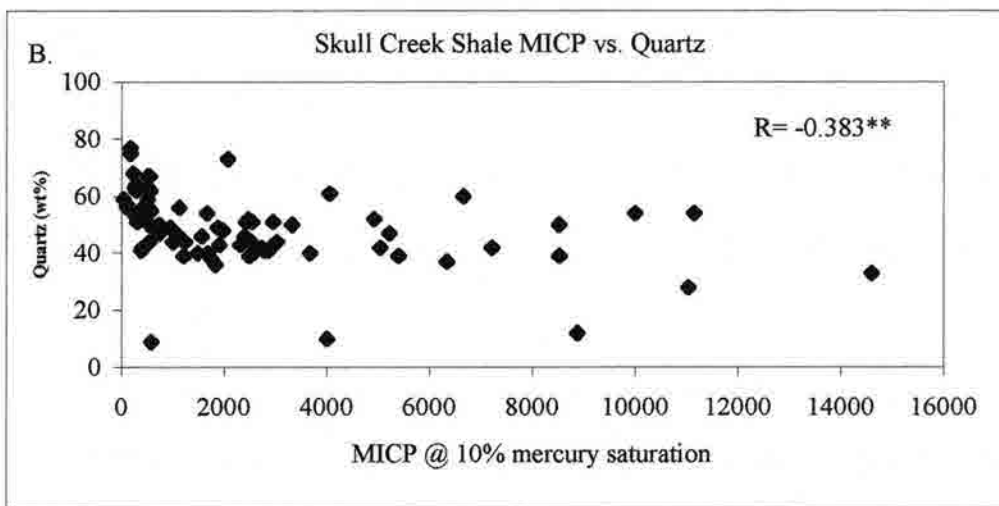
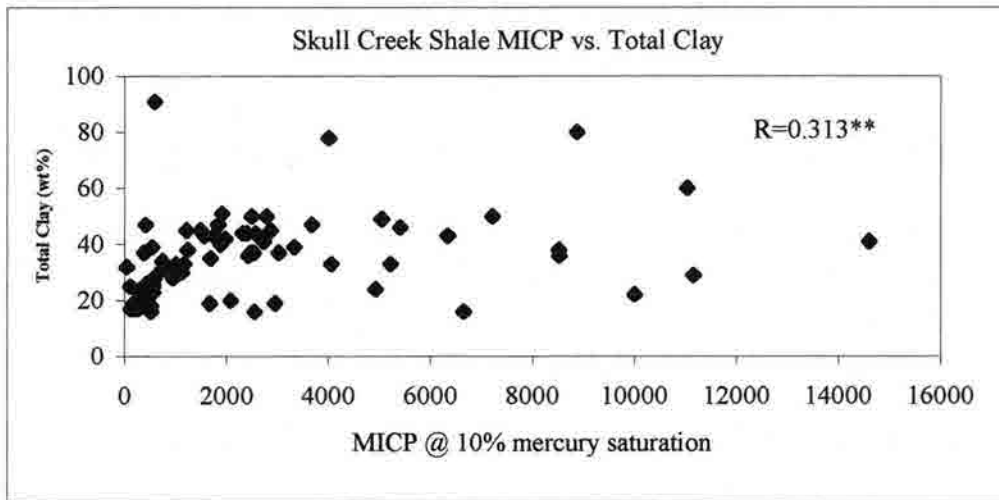


Figure 10.6 Skull Creek MICP vs. total clay (A), quartz (B), and carbonate (C).

correlation with MICP. The negative correlation between quartz and MICP can be explained, if the quartz occurs primarily as grains.

The percentage of total organic carbon does not have a significant correlation with MICP (Fig. 10.7a). However, hydrogen index has a significant positive correlation ($R=0.598^{**}$; Fig. 10.7b). This suggests that higher MICP values in the Skull Creek samples are associated with a more algal type of organic matter, that is indicated by a higher hydrogen index, but not necessarily with the total amount of organic matter. The ratio of hydrogen index to oxygen index does not show a significant correlation (Fig. 10.8a). Density shows a significant negative relationship to MICP ($R=-0.333^{**}$; Fig. 10.8b). A negative relationship suggests that density values are lower at higher MICP, which may be indicating that less dense minerals or greater porosity or both are present in samples with higher MICP.

The Graneros Shale also shows porosity and log permeability to have the strongest correlations ($R=-0.777^{**}$; Fig. 10.9a and $R=-0.905^{**}$; Fig. 10.9b). Total clay again shows a positive correlation with $R=0.497^{**}$ (Fig. 10.10a). Neither quartz nor carbonate have a significant correlation with MICP (Fig. 10.10b and Fig. 10.10c). The percentage of total organic carbon does show a significant correlation in the Graneros Shale (Fig. 10.11a) with $R=0.467^{**}$, in addition to the hydrogen index showing a significant positive correlation (Fig. 10.11b). The ratio of hydrogen index to oxygen index and density do not have a significant correlation with MICP (Fig. 10.12a and (Fig. 10.12b). Both the Skull Creek and the Graneros show significant correlation between MICP (psia) and porosity, log permeability, total clay, and hydrogen index. The consistency of correlations of these four variables with MICP suggests that they may be

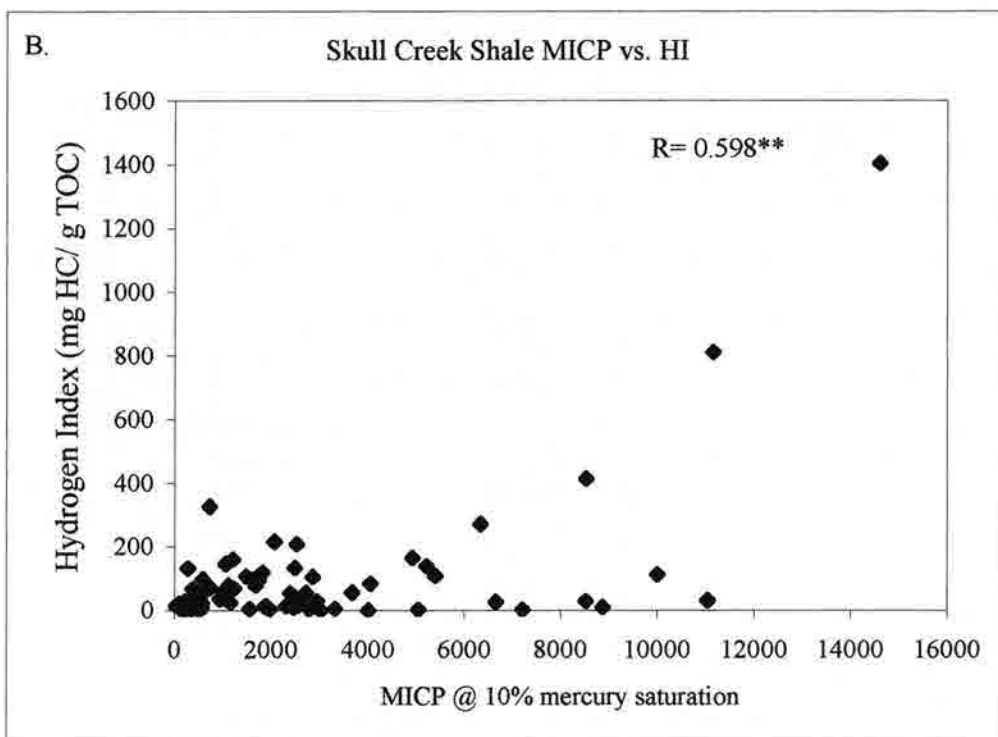
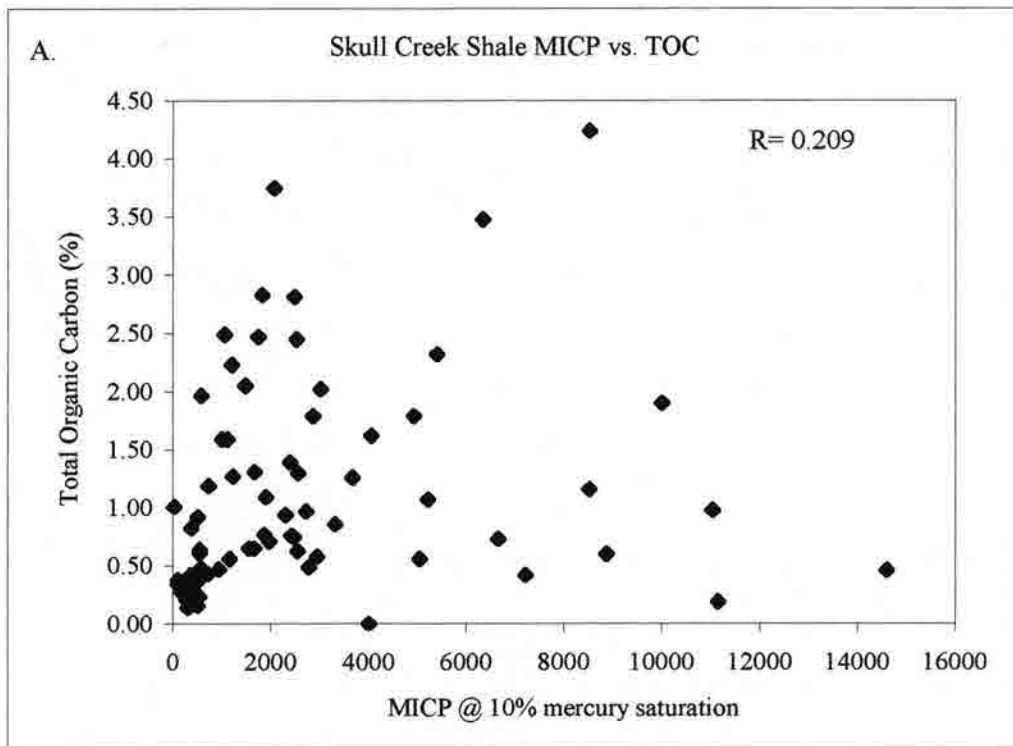


Figure 10.7 Skull Creek MICP vs. total organic carbon (A) and hydrogen index (B).

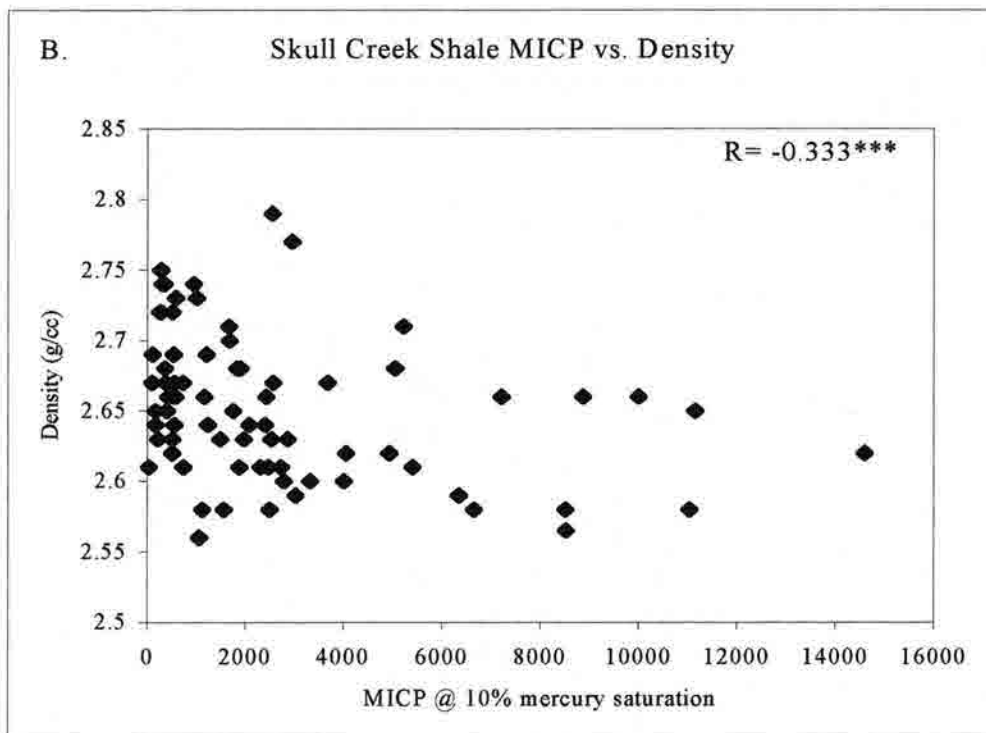
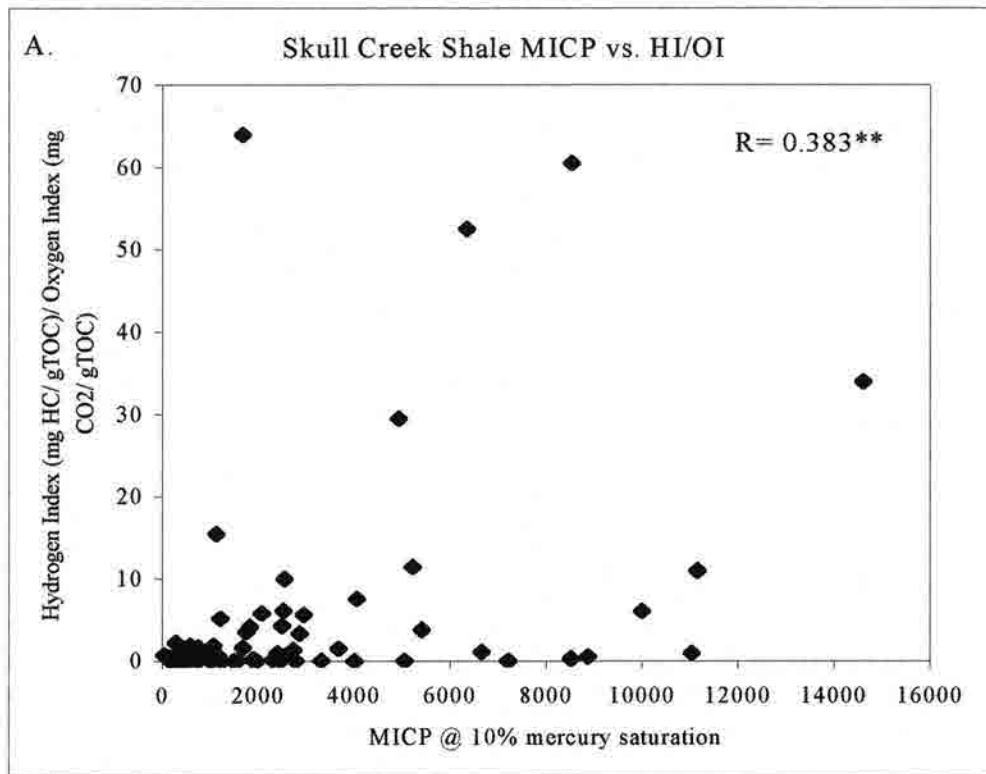


Figure 10.8 Skull Creek MICP vs. hydrogen index/ oxygen index (A) and density (B).

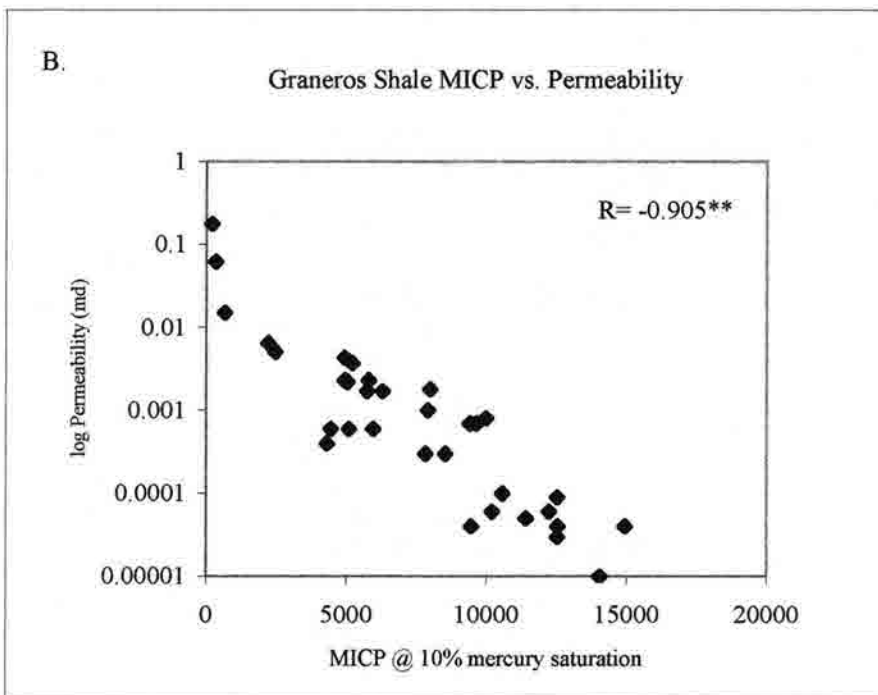
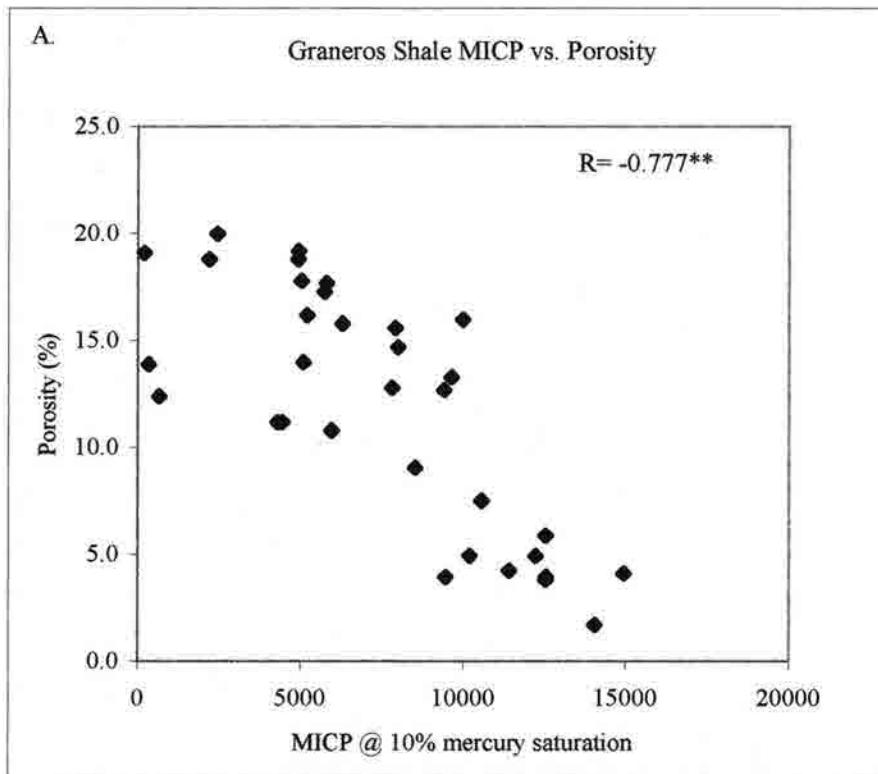


Figure 10.9 Graneros Shale MICP vs. porosity (A) and log permeability (B).

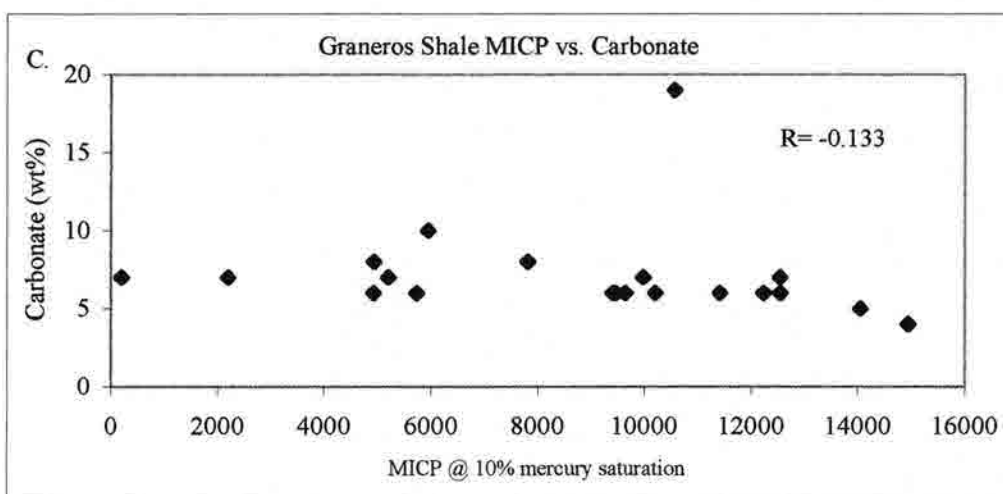
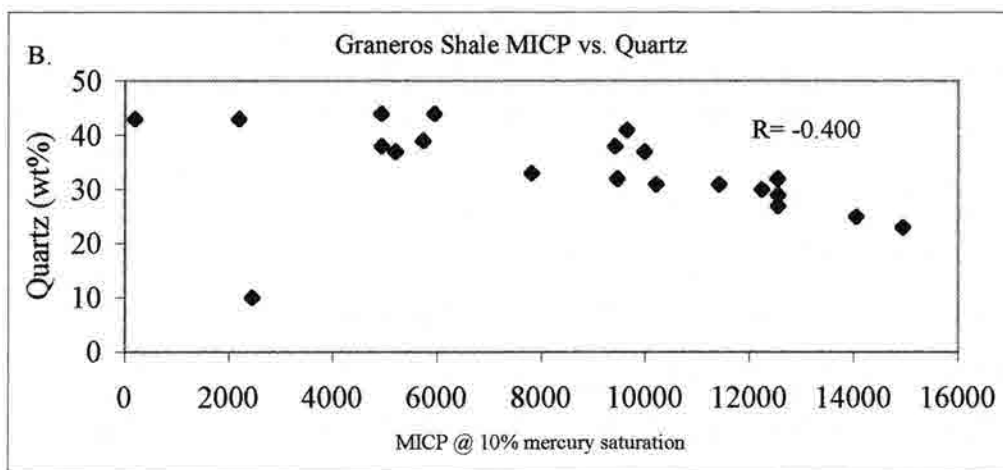
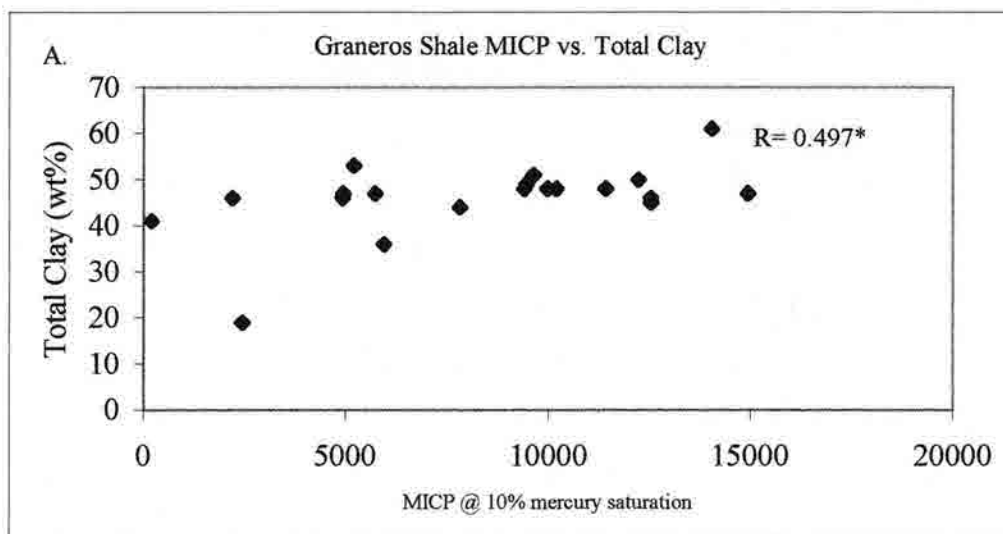


Figure 10.10 Graneros Shale MICP vs. total clay (A), quartz (B), and carbonate (C).

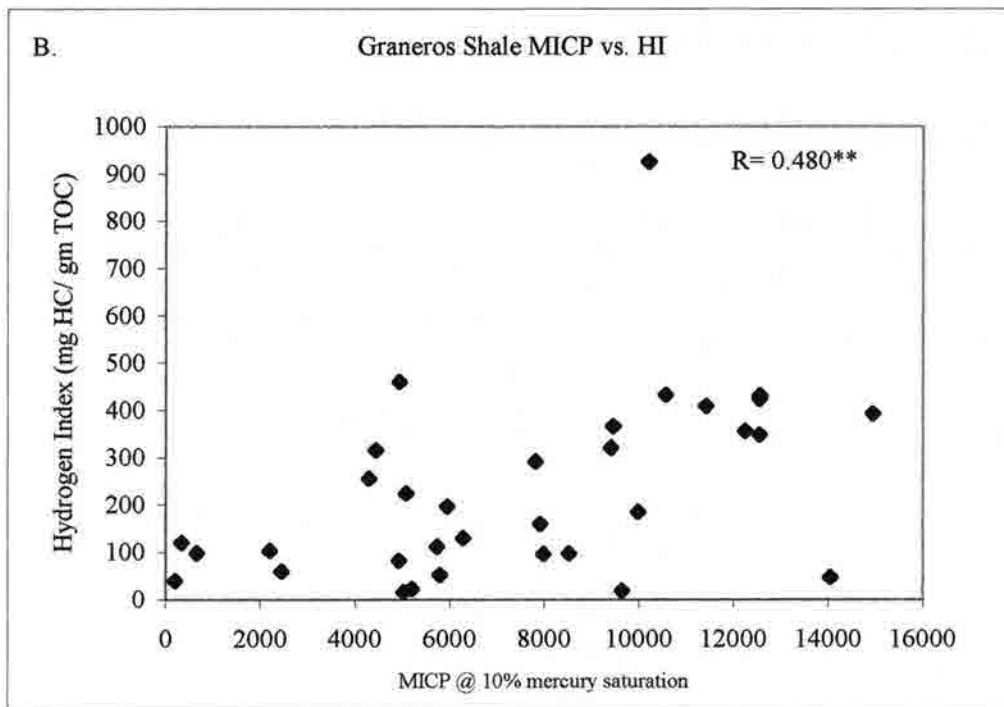
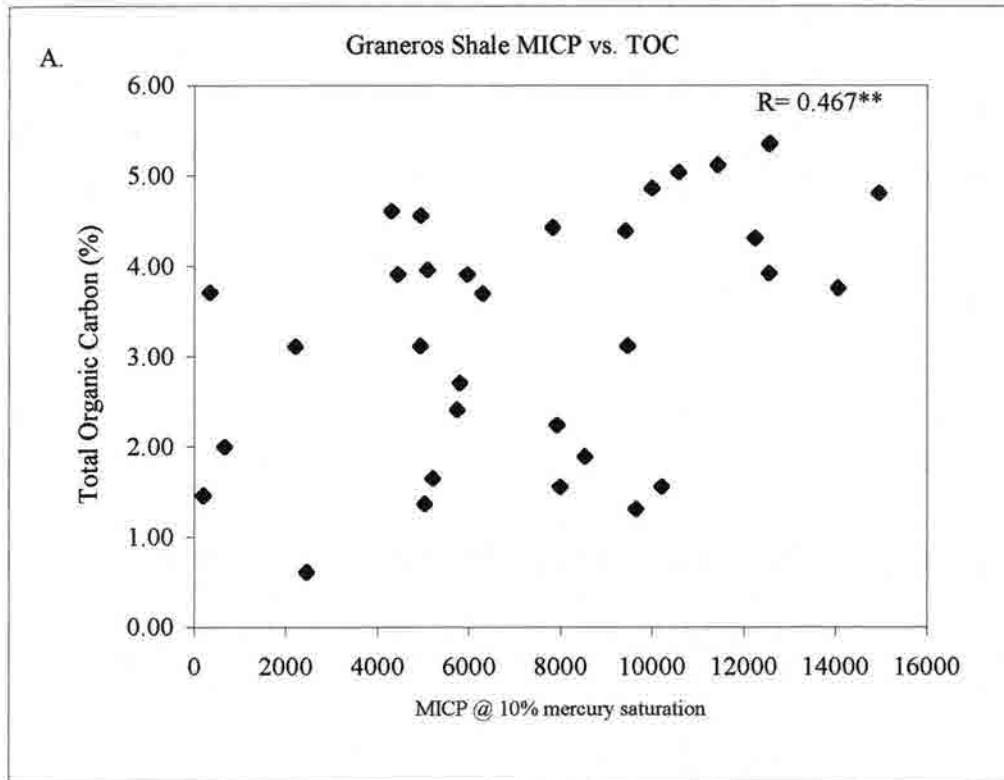


Figure 10.11 Graneros Shale MICP vs. total organic carbon (A) and hydrogen index (B).

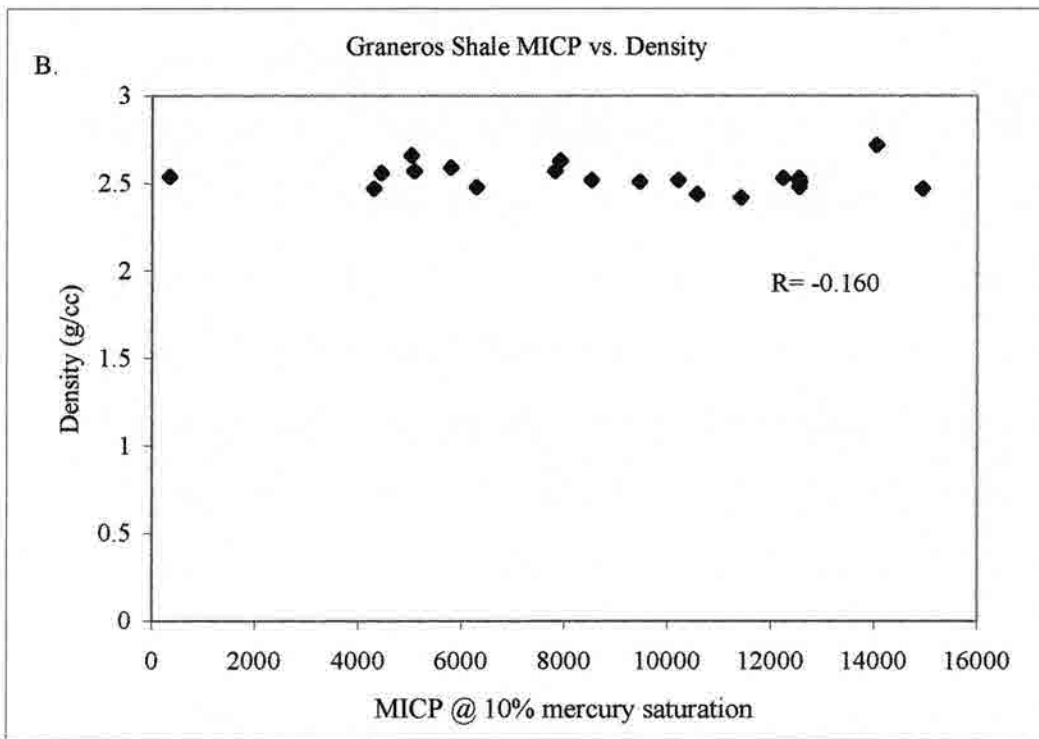
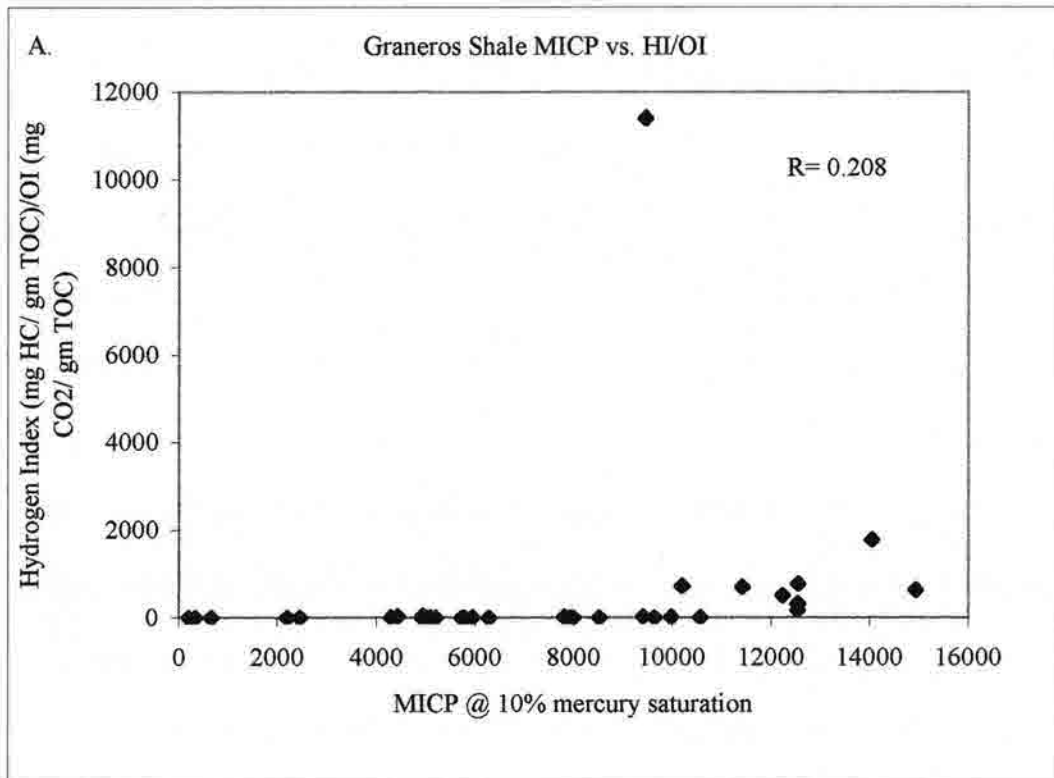


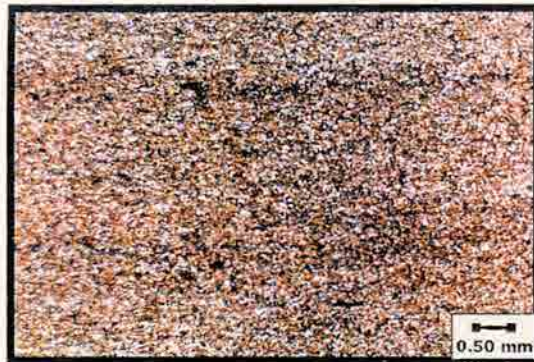
Figure 10.12 Graneros Shale MICP vs. hydrogen index/ oxygen index (A) and density (B).

reliable indicators of seal capacity. Other variables are not consistently correlated with MICP and are thus not considered reliable indicators of seal capacity.

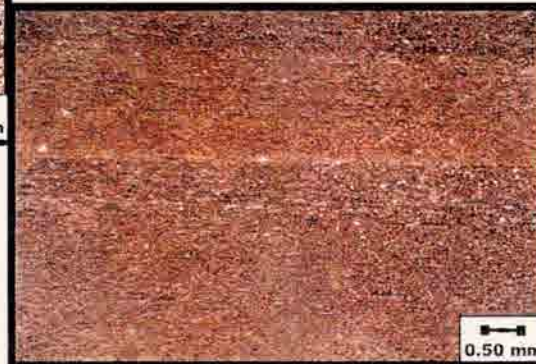
In an attempt to avoid the variability among the various facies of each shale, the condensed sections from each outcrop have been compared. This eliminates the problem of comparing a siltstone of facies B in the Skull Creek to the organic rich fissile shale in facies Z of the Graneros. In figure 10.13, an outcrop sample of the condensed section at Soldier Canyon Dam is compared to an outcrop sample of the CS at Rooney Ranch and to a core sample of the CS in the Youngs Core. The Soldier Canyon CS clearly has larger quartz grains than the other two condensed sections. These quartz grains seem to be providing a framework that may hindered compaction and supported pores from collapsing under increasing strain, thus explaining why this sample has a much lower psia value at 10% mercury saturation.

XRD analyses of the whole rock mineralogy show 32% quartz for the Soldier Canyon sample and 38% quartz at Rooney Ranch. This similar quartz content is surprising since the thin section of Soldier Canyon, appears to have considerable more quartz than Rooney Ranch. So the real difference becomes not the amount of quartz, but whether or not it is in grain form. This is a very important observation since the Rooney Ranch sample can hold approximately 3900 psia more than the Skull Creek sample, probably because the quartz is in the form of cement that is further narrowing the pore throat diameter.

There is also a difference in psia within the Graneros Shale. The Youngs Core holds 4700 psia more than the Rooney Ranch outcrop. The condensed section in Youngs Core CS averages 6% more total clay and 9% less quartz than Rooney Ranch. This



Soldier Canyon: Condensed Sections
54% total clay, 32% quartz
1.2% TOC
3400 psia @ 10% mer. sat.



Rooney Ranch:
43% total clay, 38% quartz
4% TOC
7300 psia @ 10% mer. sat.

Youngs Core:
49% total clay, 29% quartz
4.2% TOC
12,000 psia @ 10% mer. sat.

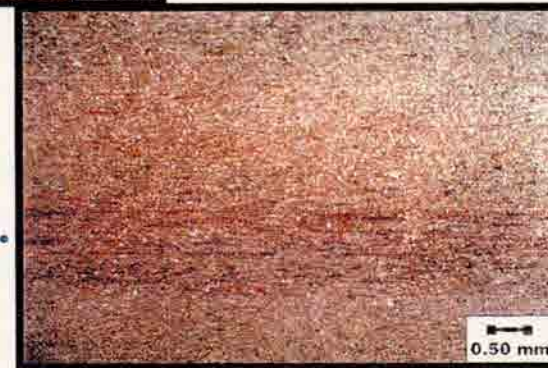


Figure 10.13 Thin section Photos of Condensed Sections at Soldier Canyon, Rooney Ranch, and Youngs Core.

change in percent mineralogy does not seem to be enough to explain the difference in psia, and there does not seem to be a change in the amount of visible grains. The difference may be caused by weathering of the outcrop sample.

10.4 Seal Classification

Sneider's (1997) seal classification system based on calculated hydrocarbon column heights (HCH) was used to classify all the MICP samples in this study (Table 10.1). This classification table provides a broad perspective on how seal capacity changes within the two shales and how the two shales relate to each other.

The process of grouping these samples into separate classes of seals shows that some generalizations can be made. However, there is still considerable variability within these shales that makes it difficult to predict where the highest seal capacity will be. Generally, the core samples have the highest seal capacity, which is not surprising. The outcrop samples in the upper parts of the TST deposits (facies K and A in the Skull Creek and facies Z and X in the Graneros) are also in the same A* seal category as the core samples.

Facies X in the Graneros Shale is not near the top of the TST deposits or facies Z. This rock has siderite cement, which has probably narrowed the pore throat diameter and increased its seal capacity. The good seals found in facies X may or may not be a function of sequence stratigraphic position, but are definitely related to rock fabric, which includes the amount and distribution of cement.

Table 10.1 Sneider's Seal Classification for the Skull Creek and Graneros Shales

<i>Facies</i>	<i>Location</i>	<i>FT</i>	<i>PSIA @ 10%SAT.</i>	<i>Sneider's HCH</i>	<i>Sneider's classification</i>
Paleo	Meadow	7884	27119	19743	
Mowry	Meadow	7872	16032	11671	
Z	Youngs	5780	14942	10878	
A	Meadow	7938	14601	10630	
Z	Youngs	5804	14047	10226	
Z	Youngs	5790	12552	9138	
Z	Youngs	5785	12542	9131	
Z	Youngs	5764	12540	9129	
Z	Youngs	5769	12235	8907	
Z	Youngs	5775	11419	8313	
A	Meadow	7944	11153	8119	
K	Soldier	50	11037	8035	
Z	Rooney	68	10566	7692	
Z	Youngs	5800	10205	7429	A*
B	Meadow	7930	10001	7281	
Z	Rooney	59	9983	7268	
X	Rooney	14	9643	7020	
Z	Youngs	5795	9459	6886	
Z	Rooney	74	9412	6852	
A	Soldier	59	8872	6459	
A	Turkey	40	8525	6206	
Z	Rooney	90	8523	6205	
K	Bellevue	9	8517	6200	
X	Rooney	24	7989	5816	
X	Rooney	28	7913	5761	
Y	Rooney	49	7815	5689	
K	Soldier	40	7210	5249	
B	Turkey	35	6654	4844	
A	Turkey	45	6339	4615	
Y	Rooney	118	6285	4575	
Z	Rooney	84	5948	4330	
Y	Rooney	110	5791	4216	
Y	Rooney	44	5732	4173	
A	Soldier	West 40	5402	3933	
B	Meadow	7920	5218	3799	
Y	Rooney	124	5200	3786	
Z	Rooney	87	5080	3698	
K	Soldier	48	5046	3673	A
Y	Rooney	122	5026	3659	
Z	Rooney	54	4936	3593	
B	Turkey	50	4928	3588	
Y	Rooney	114	4926	3586	
Y	Rooney	91	4436	3229	
Z	Rooney	81	4295	3127	
B	Turkey	30	4054	2951	
A	Soldier	60	4009	2919	
A	Soldier	62	3675	2675	

<i>Facies</i>	<i>Location</i>	<i>FT</i>	<i>PSIA @ 10%SAT.</i>	<i>Sneider's HCH</i>	<i>Sneider's classification</i>
K	Bellevue	4	3324	2420	
A	Soldier	West 10	3024	2201	
B	Turkey	70	2954	2151	
K	Soldier	54	2866	2086	
K	Soldier	20	2784	2027	
K	Soldier	51	2729	1987	
E	Meadow	7880	2616	1904	
K	Bellevue	40	2568	1870	
C	Turkey	78	2551	1857	
A	Soldier	West 20	2532	1843	
A	Bellevue	54	2495	1816	
K	Bellevue	14	2472	1800	
X	Rooney	4	2450	1784	
K	Bellevue	36	2428	1768	
B	Bellevue	59	2401	1748	
K	Bellevue	25	2311	1682	A
Y	Rooney	104	2201	1602	
K	Soldier	34	2180	1587	
B	Bellevue	80	2078	1513	
K	Soldier	30	1973	1436	
K	Soldier	0	1907	1388	
K	Bellevue	30	1876	1366	
A	Soldier	East 30	1860	1354	
A	Soldier	West 30	1830	1332	
C	Meadow	7910	1794	1306	
A	Soldier	East 10	1750	1274	
B	Bellevue	75	1683	1225	
B	Turkey	63	1668	1214	
K	Bellevue	20	1560	1136	
A	Soldier	61	1487	1083	
A	Soldier	63	1236	900	
A	Soldier	East 20	1211	882	
K	Soldier	58	1166	849	
C	Turkey	0	1122	817	
B	Bellevue	90	1063	774	
A	Soldier	64	1008	734	B
C	Bellevue	108	1003	730	
C	Bellevue	126	959	698	
B	Bellevue	85	947	689	
K	Soldier	26	946	689	
K	Bellevue	49	736	536	
B	Soldier	65	730	531	
Y	Rooney	34	659	480	
C	Bellevue	120	607	442	
K	Soldier	44	585	426	
K	Bellevue	44	583	424	
C	Soldier	128	575	419	C
C	Soldier	140	556	405	
B	Soldier	70	553	403	
C	Turkey	10	550	400	

<i>Facies</i>	<i>Location</i>	<i>FT</i>	<i>PSIA @ 10%SAT.</i>	<i>Sneider's HCH</i>	<i>Sneider's classification</i>
B	Bellevue	96	536	390	
B	Soldier	78	519	378	
C	Bellevue	130	512	373	
C	Turkey	20	510	371	
D	Meadow	7900	509	371	
B	Soldier	75	425	309	
B	Bellevue	65	407	296	
C	Soldier	122	389	283	
B	Bellevue	70	379	276	
C	Soldier	90	360	262	
Z	Youngs	5808	349	254	
C	Soldier	100	347	253	
Y	Rooney	96	334	243	C
C	Soldier	96	333	242	
C	Soldier	136	316	230	
C	Bellevue	114	308	224	
C	Soldier	146	281	205	
C	Soldier	148	280	204	
B	Soldier	80	280	204	
C	Soldier	104	261	190	
C	Soldier	150	223	162	
Y	Rooney	94	197	143	
C	Soldier	154	173	126	
C	Soldier	152	173	126	
C	Soldier	82	112	82	D
C	Soldier	130	106	77	
D	Meadow	7890	67	49	Waste Zone
C	Turkey	90	35	25	Zone
KEY: A* seal > 5000 ft HCH A seal 1000-5000 ft HCH B seal 500-1000 ft HCH C seal 100-500 ft HCH D seal 50-100 ft HCH E seal < 50 ft HCH F = Waste Zone- no seal capacity					

Some of the Skull Creek condensed section samples are classified as A* seals which can hold over 5,000 ft of hydrocarbons and some are classified as B seals, which holds 500-1000 ft of hydrocarbons. This again indicates that these shales are variable. It is possible to say that the condensed section generally holds the best seal, but some isolated sample of the condensed section may not be a good seal, and another sample below the condensed section may be a better seal.

So when looking for the best seals in a section, do not just look for the highest total clay or total organic carbon indicators, but look at the rock fabric and amount and distribution of cement. The arrangement of the silt grains provides a framework for the pores to remain open or not, as previously stated by Dewhurst and Aplin (1998), and cement may further narrow the pore network to provide an obstacle to hydrocarbon migration.

CHAPTER 11. CONCLUSIONS

The following is a summary of the results of this study for the questions asked at the beginning of chapter 1:

1. What type of rock makes the “best” seal?
 - The best seal is most consistently a very fine-grained shale or mudstone that has a very small pore throat diameter. Diagenesis can further decrease the size of the pore throat diameter through the precipitation of cements.
 - Black fissile shale, typical of a condensed section, does not always have the highest amounts of TOC and is not always the best seal in the section.
2. What are the physical properties of the best seal rock?
 - The samples with the highest seal capacity are significantly correlated with low values of porosity and permeability, and high values for hydrogen index and total clay.
 - Previous research suggests that rocks with a high percentage of total clay, or total organic carbon with a type I-II (algal) kerogen typify the best seal. This study has not shown that to be a consistent correlation.
 - Sometimes the best seal rock is well laminated like the condensed section shales, but not always as seen in mudstones of facies K in the Skull Creek.
 - Rock fabric, including grain orientation, packing, and cementation, may be an important factor in controlling seal capacity. Shale with quartz cement

usually has higher seal capacity than mudstone with quartz grains, other factors being equal. Additional research is needed to verify this tentative conclusion

3. What type of depositional environment produces the best seal rock?
 - In general, a distal open marine shelf setting, typified by the Graneros Shale, produces a rock with a greater and more uniform seal capacity relative to the rocks of a more proximal open marine shelf setting of the Skull Creek Shale.
 - A distal setting may produce better seals because there is less coarse clastic sediment input in quiet water, which leads to the deposition of clays during the maximum transgression of sea level. This is important because the coarse sediment provides a framework to prevent the pore throat diameters from collapsing. A clay rich rock, which has less coarse material is more likely to compact, thus collapsing the pore networks.
4. How does this rock fit into the overall sequence or parasequence?
 - In general, the best seals are located in the upper parts of the TST deposits. This sometimes occurs within the condensed section but also occurs below the condensed section.
5. How does the integrity and/or position of the seal change across the basin?
 - Seal occurrence is stratigraphically higher in depositional topographic high areas, such as at Turkey Creek for the Skull Creek Shale, and lower in areas that were topographically low at the time of deposition.

- This study was unable to determine how the integrity of the seal changed across the basin because both cores and outcrops were used, and the cores have greater seal integrity because the samples are unweathered.

11.1 Future Work Statement

Future work for the study of top seal development in marine shales should be geared toward developing better methods of analyzing the data. My study focused on data collection and preliminary analysis. Further research should be performed with geostatistical analysis to determine better classification schemes for the existing data.

Future top seal studies of marine shales should be focused in economical areas, as these will be the analogs for future oil/gas exploration projects. Larger packages of shale should be studied to see the variations over hundreds of feet. More specifically, the rock fabric of each sample should be analyzed in greater detail to provide information on grain orientation (size and shape) and grain packing.

An effort should be made to directly correlate academic research with actual well data. If possible core behind the outcrop to obtain un-weathered samples and run all possible wireline logs. These logs and any geophysical data should be correlated back to the physical or mechanical properties of the rock to make results more applicable to the exploration teams.

REFERENCES

- Allen, P.A., and Allen, J.R., 1990. Basin Analysis Principles and Applications. Blackwell Scientific Publications, Osney Mead, Oxford. pp. 451.
- Bohacs, K.M., 1993. Contrasting expressions of Depositional Sequences in Mudrocks from marine to non-marine Environs *in* Schieber, J., Zimmerle, W., Sethi, P.S. eds., Shales and Mudstones I: Basin Studies, Sedimentology and Paleontology. E. Schweizerbart'sche Verlagsbuchhandlung, Stuttgart, vol. I, p. 33-78.
- Cobban, W.A., Merewether, E.A., Fouch, T.D., and Obradovich, J.D., 1994. Some Cretaceous shorelines in the Western Interior of the U.S. *in* Caputo, M.V., Peterson, J.A. and Francyk, K.J., eds., Mesozoic Systems of the Rocky Mountain Region, U.S.A: Rocky Mountain Section SEPM, p. 393-428.
- Dewhurst, D.N., and Aplin, A.C., 1998. Compaction-driven evolution of porosity and permeability in natural mudstones: An experimental study. *Journal of Geophysical Research*, vol. 103, p. 651-661.
- Dolson, J.C., 1985. Lower Cretaceous Dakota Group *in* Macke, D.L. and Maughan, E.K., eds. Rocky Mountain Section Field Trip Guide. RMS-AAPG and RMS-SEPM, Denver, CO p. 2-30.
- Dolson, J.C., Muller, D., Evetts, M. J., and Stein, J.A., 1991. Regional paleotopographic trends and production, Muddy sandstone (Lower Cretaceous), Central and Northern Rocky Mountains. *AAPG Bulletin*, vol. 75, p. 409-435.
- Dolson, J.C., and Weimer, R.J., 1992. Examples of Unconformities of Related Systems Tracts, Cretaceous through Precambrian Strata, Front Range (Colorado) and Wyoming *in* Flores, R.M., eds. Mesozoic of the Western Interior Field Guidebook. Rocky Mountain Section SEPM, Fort Collins, CO p. 55-74.
- Espitalie, J., Laporte, J.L., Madec, M., Marquis, F., Leplat, P., Poulet, J., and Bouteffeu, A., Methode rapide de caracterisation des roches meres de leur potentiel petrolier et de leur degre d'evolution. *Revue de l'Institut Francais du Petrole*, 32:23-42.
- Galloway, W.E., 1989. Genetic stratigraphic sequences in basin analysis. 1: Architecture and genesis of flooding-surface bounded depositional units. *AAPG Bulletin* vol. 73, p. 125-142.
- Graham, J., and Ethridge, F.G., 1995. Sequence stratigraphy implications of gutter casts in the Skull Creek shale, Lower Cretaceous, Northern Colorado. *RMAG*, vol. 32, p. 95-106.

- Higley, D.K., Cox, D.O., and Weimer, R.J., submitted to AAPG Bulletin, 1999. Reservoir geologic and engineering properties of the Wattenberg Basin-Center gas field, Denver Basin, CO.
- Higley, D.K., and Schmoker, J.W., 1989. Influence of depositional environment and diagenesis on regional porosity trends in the Lower Cretaceous "J" sandstone, Denver Basin, CO. *in* Ed Coalson, ed., Sandstone Reservoirs of the Rocky Mountains. Rocky Mtn. Assoc. of Geol. Special publication p. 183-196.
- International Centre for Diffraction Data. 1993. Mineral powder diffraction file databook. ICDD, Swarthmore, PA.
- Jennings, J.B., 1987. Capillary pressure techniques: applications to exploration and development geology. AAPG Bulletin, vol. 71, p. 1196-1209.
- Katz, B.J., 1983. Limitations of 'Rock-Eval' pyrolysis for typing organic matter. *Org. Geochem.*, vol. 4, p. 195-199.
- Loutit, T.S., Hardenbol, J., Vail, P.R., and Baum, G.R., 1988. Condensed sections: the key to age dating and correlations of continental margin sequences *in* Wilgus, C.K., Hastings, B.S., Kendall, C.G.St.C., Posamentier, H.W., Ross, C.A., Van Wagoner, J.C., eds., Sea-Level Changes: An Integrated Approach. Society of Paleontologists and Mineralogists Special Publication No. 42, p. 183-213.
- MacKenzie, D.B., 1971. Post-Lytle Dakota Group on west flank of Denver Basin, Colorado. *The Mountain Geologist*, vol. 8, p.91-133.
- Mitchum, R.M., 1977. Seismic stratigraphy and global changes of sea level, Part 1. glossary of terms in seismic stratigraphy *in* Payton, C.E., eds., Seismic stratigraphy—Applications to Hydrocarbon Exploration. Association of Petroleum Geologists Memoir, vol. 26, p. 205-212.
- Moore, D.M. and Reynolds, R.C., Jr. 1997. X-ray diffraction and the Identification and Analysis of Clay Minerals. Oxford University Press, New York. pp. 378.
- Pietraszek-Mattner, S., 1995. Source Rock Analysis of the Graneros shale, Denver Basin, Colorado related to depositional environment, generative potential and primary migration: M.Sc. thesis, Colorado School of Mines.
- Potter, P.E., Maynard, J.B., and Pryor, W.A., 1980. *The Sedimentology of Shale*. Springer-Verlag, New York. pp. 303.
- Reading, H.G., 1996. *Sedimentary Environments: Processes, Facies and Stratigraphy*. Third Edition, Blackwell Science, Dept. of Earth Sciences, University of Oxford.
- Reynolds, R.C. Jr., 1985. NEWMOD[®] A Computer Program for the Calculation of One-

Dimensional Diffraction Patterns of Mixed-Layered Clays. R.C. Reynolds, 8
Brook Rd., Hanover, NH, 03755.

- Reynolds, R.C. Jr., 1989. Principles and Technologies of Quantitative Analysis of Clay Minerals by X-ray Powder Diffraction, CMS Workshop Lectures Vol.1 Chapter 4, Quantitative Mineral Analysis of Clays, D.R. Pevear and F.A. Mumpton Editors p. 4-36.
- Schultz, L.G. 1964. Quantitative interpretation of mineralogical composition from x-ray and chemical data for the Pierre shale, Geological Survey Professional Paper 391-C.
- Schutter, S.R., 1998. Characteristics of Shale Deposition in Relation to Stratigraphic Sequence Systems Tracts in Schieber, J., Zimmerle, W., Sethi, P.S. eds., Shales and Mudstones I: Basin Studies, Sedimentology and Paleontology. E. Schweizerbart'sche Verlagsbuchhandlung, Stuttgart, vol. I, p. 79-108.
- Slatt, R.M., Borer, J., Al-Siyabi, H., Horn, B., and Pietraszek, S.R., 1995. Outcrop gamma-ray logging applied to subsurface geology. The Mountain Geologist, vol. 2, p. 81-94.
- Sneider, R.M., Sneider, J.S., Bolger, G.W., and Neasham, J.W., 1997. Comparison of seal capacity determinations: conventional cores vs. cuttings *in* Surdam, R.C. eds., Seals, traps and the petroleum system: AAPG Memoir 67, p.1-12.
- Sneider, R.M., 1987. Practical petrophysics for exploration and development. AAPG Education short course notes, variously paginated.
- Sorby, H.C., 1980. On the applications of quantitative methods to the study of the structure and history of rocks. Quart. Geol. Soc. London, vol. 64, p. 171-233.
- Van Wagoner, J.C., 1985. Reservoir facies distribution as controlled by sea-level change. Abstract and Poster session, Society of Economic Paleontologists and Mineralogists Mid-Year meeting, Golden, CO, p. 91-92 *in* Wilgus, C.K., Hastings, B.S., Kendall, C.G.St.C., Posamentier, H.W., Ross, C.A., Van Wagoner, J.C., eds., Sea-Level Changes: An Integrated Approach. Society of Paleontologists and Mineralogists Special Publication No. 42, p. 39-46.
- Van Wagoner, J.C., Mitchum, R.M., Jr., Vail, P.R., Sarg, J.F., Loutit, T.S., and Hardenbol, J., An overview of the fundamentals of sequence stratigraphy and key definitions *in* Wilgus, C.K., Hastings, B.S., Kendall, C.G.St.C., Posamentier, H.W., Ross, C.A., Van Wagoner, J.C., eds., Sea-Level Changes: An Integrated Approach. Society of Paleontologists and Mineralogists Special Publication No. 42, p. 39-46.

- Vavra, C.L., Kaldi, J.G., and Sneider, R.M., 1992. Geological applications of capillary pressure: A review. AAPG Bulletin, vol. 76, p. 840-850.
- Wardlaw, N.C., 1976. Pore geometry of carbonate rocks as revealed by pore casts and capillary pressure. AAPG Bulletin, vol. 60, p. 245-257.
- Wardlaw, N.C., and Taylor, R.P., 1976. Mercury capillary pressure curves and the interpretation of pore structures and capillary behavior in reservoir rocks. Bulletin of Canadian Petroleum Geology, vol. 24, p. 225-262.
- Watts, N.L., 1987. Theoretical aspects of cap-rock and fault seals for single- and two-phase hydrocarbon columns. Marine and Petroleum Geology, vol. 4, p. 274-307.
- Weimer, R.J., 1991. Sequence Stratigraphy of the Muddy (Viking) Sandstone (Lower Cretaceous), Rocky Mountain Region, USA. Submitted to Sequence Stratigraphy Seminar, Banff, Alberta, August 26-30, 1991.
- Weimer, R.J., and Sonnenburg, S.A., 1994. Sequence stratigraphy and petroleum geology of the Central Denver Basin. AAPG annual meeting field guide #8, sponsored by the Rocky Mountain Assoc. of Geologists.
- Weimer, R.J., 1996. Guide to the petroleum geology and Laramide Orogeny, Denver Basin and Front Range, CO. Colorado Geological Survey, Dept. of Natural Resources.
- Yang, Y., and Aplin, A.C., 1998. Influence of lithology and compaction on the pore size distribution and modeled permeability of some mudstones from the Norwegian margin. Marine and Petroleum Geology 15, p. 163-175.

APPENDIX A

SOLDIER CANYON DAM OUTCROP

SKULL CREEK SHALE

THIN SECTION PHOTOMICROGRAPHS

Figure A1.
 HSC015 (42 R)- Facies B
 Medium magnification (PPL) thin section photomicrograph of carbonaceous mudstone. Dark-grayish brown, moderately well sorted, compact matrix includes clay minerals and siliceous detrital grains (quartz, feldspar, rock fragments). This matrix appears to be slightly mottled or burrowed without root fragments. The matrix appears to be slightly mottled or burrowed without root fragments. The presence of well-developed laminae. The large dark colored particles are carbonaceous debris. Small amounts of siderite may be replacing some of the clay minerals. *Siderite porosity is not evident.*

Figure A2.
 HSC015 (42 R)- Facies B
 High magnification (PPL) thin section photomicrograph of same carbonaceous mudstone as pictured in Figure A1. Sub-rounded quartz grains appear to be "floating" in the clay rich matrix. *Wavy laminations of organic matter are visible in high magnification.* The arrow is pointing to a small dark red rod-like that is probably siderite. *No matrix porosity is noted.*

Figure A1.

BSC015 (42 ft)- Facies K

Medium magnification (PPL) thin section photomicrograph of carbonaceous mudstone. Dark-grayish brown, moderately well sorted, compacted matrix includes clay minerals and silt-size detrital grains (quartz, feldspars, sedimentary rock fragments). This matrix appears to be slightly mottled or burrowed without the presence of well-developed laminations. The large dark colored particles are carbonaceous debris. Small amounts of siderite may be replacing some of the clay minerals. Matrix porosity is not evident.

Figure A2.

BSC015 (42 ft)- Facies K

High magnification (PPL) thin section photomicrograph of same carbonaceous mudstone as pictured in Figure A1. Sub-rounded quartz grains appear to be "floating" in the clay rich matrix. Wispy laminations of organic matter are visible at high magnification. The arrow is pointing to a small dark red nodule that is probably siderite. No matrix porosity is noted.

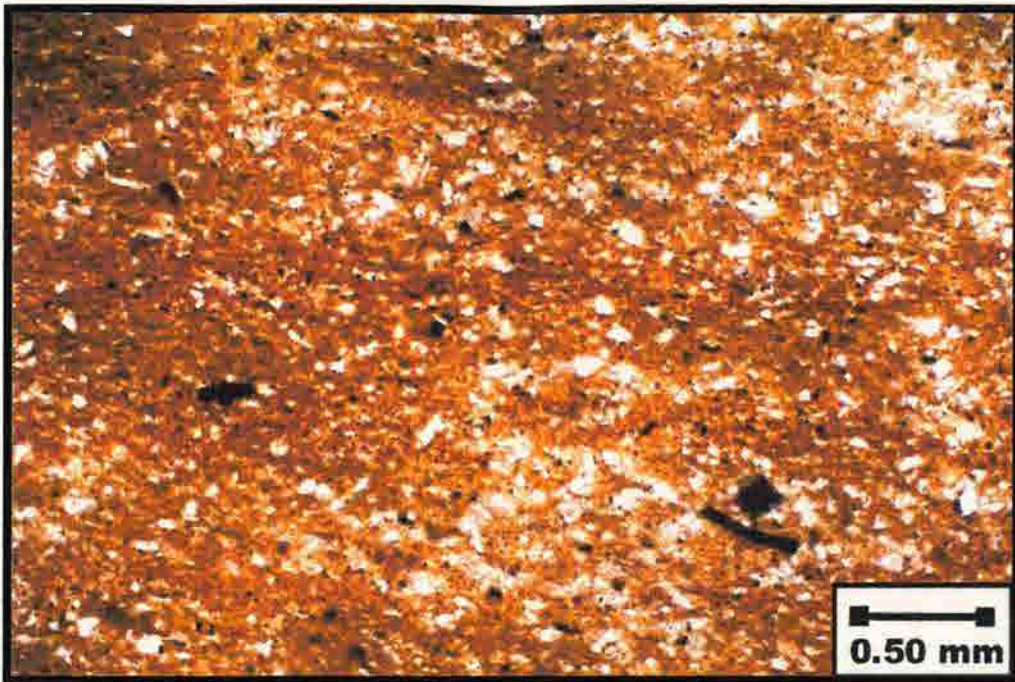


Figure A1.

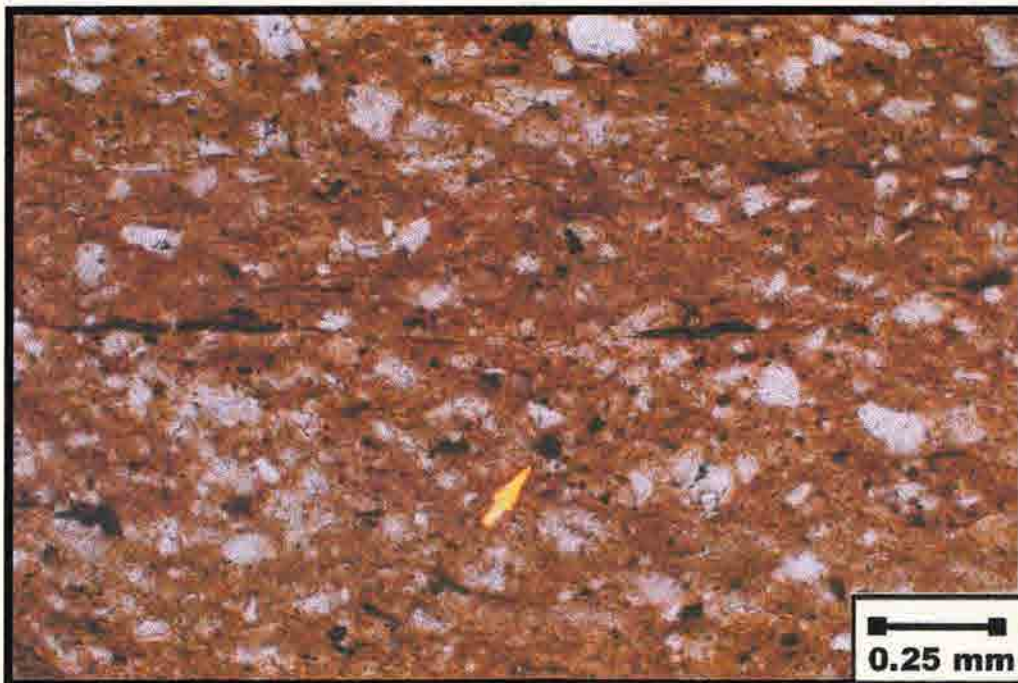


Figure A2.

Figure A3.
 SC004 (24 ft) - Facies K
 Low magnification (PPL) of thin-section photomicrograph of carbonaceous silt shale. Strongly compact, well-sorted matrix contains clay minerals and silt size detrital grains (quartz, feldspar, mica), with an occasional fine-grained sand particle. This shale is well laminated with discontinuous beds of silt and wavy laminations of organic matter. Matrix porosity is not evident.

Figure A4.
 SC004 (24 ft) - Facies K
 Medium magnification (PPL) of thin-section photomicrograph of same carbonaceous silt shale as Figure A3. This shale has wavy laminations of dark colored organic matter in addition to the larger scale silt laminations. Accessory components include authigenic (framboidal) pyrite (opaque nodules) and subangular carbonate (colorful, dolomite nodules). It is difficult to distinguish the more high level carbonate minerals from the clay in this photo. Siderite may be replacing some of the clay minerals. No visible porosity is detected.

Figure A3.

SC004 (54 ft)- Facies K

Low magnification (PPL) of thin-section photomicrograph of carbonaceous silty shale. Strongly compacted, well-sorted matrix contains clay minerals and silt size detrital grains (quartz, feldspar, mica), with an occasional fine-grained sand particle. This shale is well laminated with discontinuous lens of silt and wispy laminae of organic matter. Matrix porosity is not evident.

Figure A4.

SC004 (54 ft)- Facies K

Medium magnification (PPL) of thin-section photomicrograph of same carbonaceous silty shale in Figure A3. This shale has wispy laminations of dark colored, organic matter in addition to the larger scale silt laminations. Accessory components include authigenic framboidal pyrite (opaque nodules) and authigenic carbonates (calcite, dolomite, siderite). It is difficult to distinguish the more high relief carbonate minerals from the clays in this photo. Siderite may be replacing some of the clay minerals. No visible porosity is detected.



Figure A3.

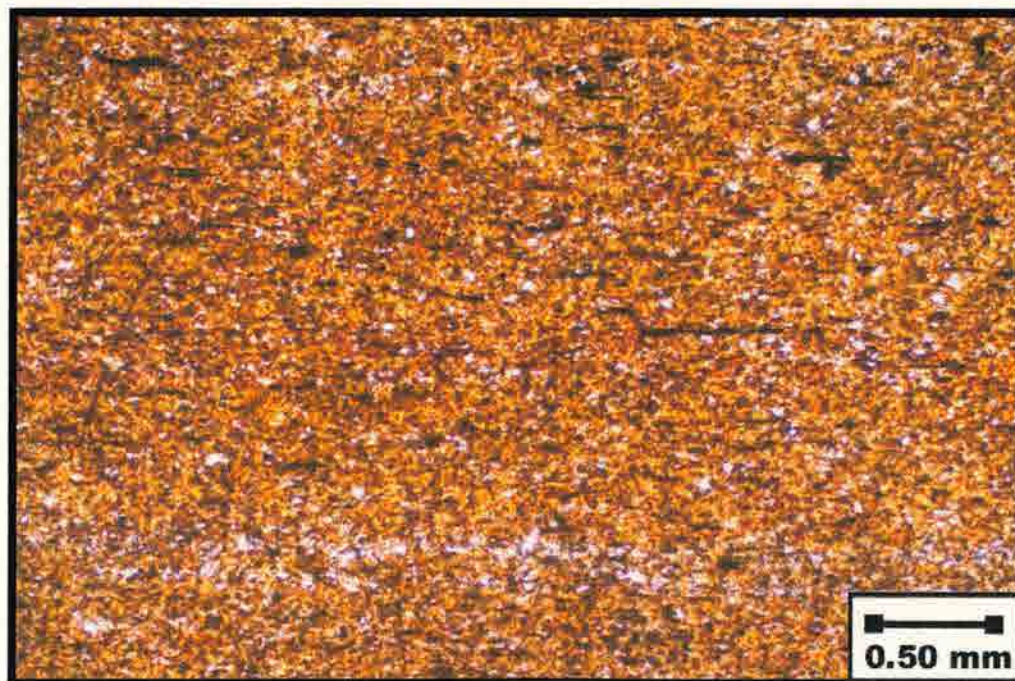


Figure A4.

Figure 22

SC009 (29 ft)-Facies A

Low magnification (X20) thin section photomicrograph of bentonite. Well-sorted matrix mainly contains clay minerals with a few silt size detrital grains (quartz, feldspar, mica), with an occasional fine-grained sand particle. The arrow is pointing to a feldspar grain that has been completely replaced by clay. Small amounts of siderite may be replacing some of the clay. No visible matrix porosity is detected.

Figure 23

SC009 (29 ft)-Facies A

High magnification (X200) thin section photomicrograph of same bentonite as Fig. 22. Under cross-polarized light and high magnification the clay minerals can be identified by their vibrant yellow color. They are interspersed with the dark colored organic matter, dark red siderite nodules and silt size detrital grains and feldspar grains. No laminae are present except for the wavy lens of organic matter. The arrow is pointing to a silt size detrital grain of feldspar that appears to be "floating" in the clay rich matrix. No matrix porosity is evident.

Figure A5.

SC009 (59 ft)- Facies A

Low magnification (XN) thin section photomicrograph of bentonite. Well-sorted matrix mainly contains clay minerals with a few silt size detrital grains (quartz, feldspar, mica), with an occasional fine-grained sand particle. The arrow is pointing to a feldspar grain that has been completely replaced by clay. Small amounts of siderite may be replacing some of the clays. No visible matrix porosity is detected.

Figure A6.

SC009 (59 ft)- Facies A

High magnification (XN) thin section photomicrograph of same bentonite in Fig. A5. Under cross-polarized light and high magnification the clay minerals can be identified by their vibrant yellow color. They are interspersed with the dark colored organic matter, dark red siderite nodules and silt size detrital quartz and feldspar grains. No laminations are present except for the wispy lens of organic matter. The arrow is pointing to a silt size detrital grain of feldspar that appears to be "floating" in the clay rich matrix. No matrix porosity is evident.

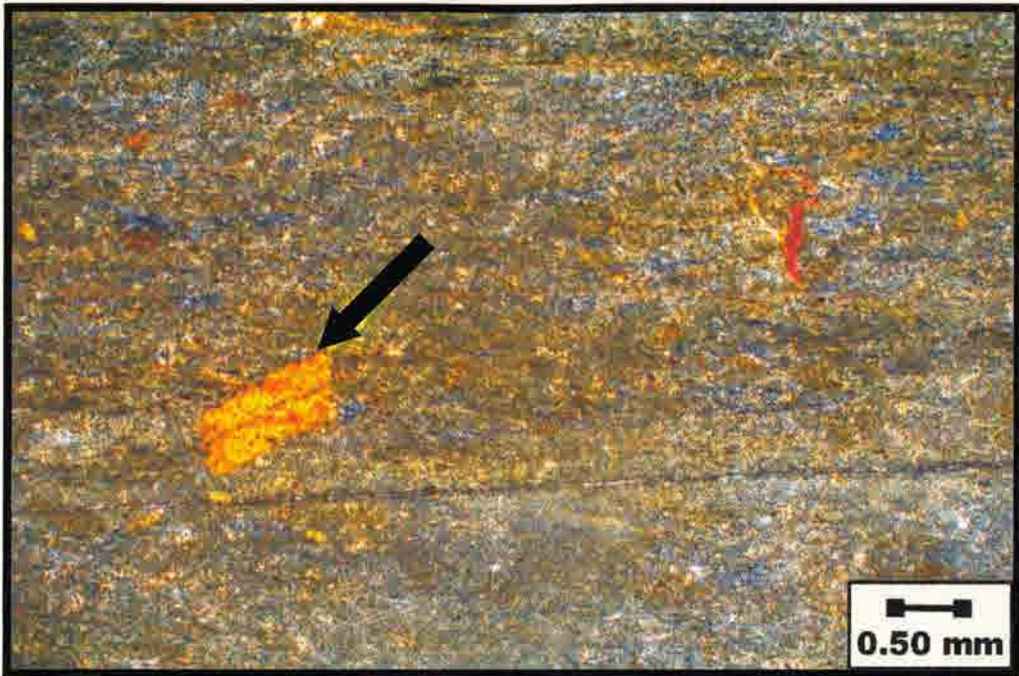


Figure A5.

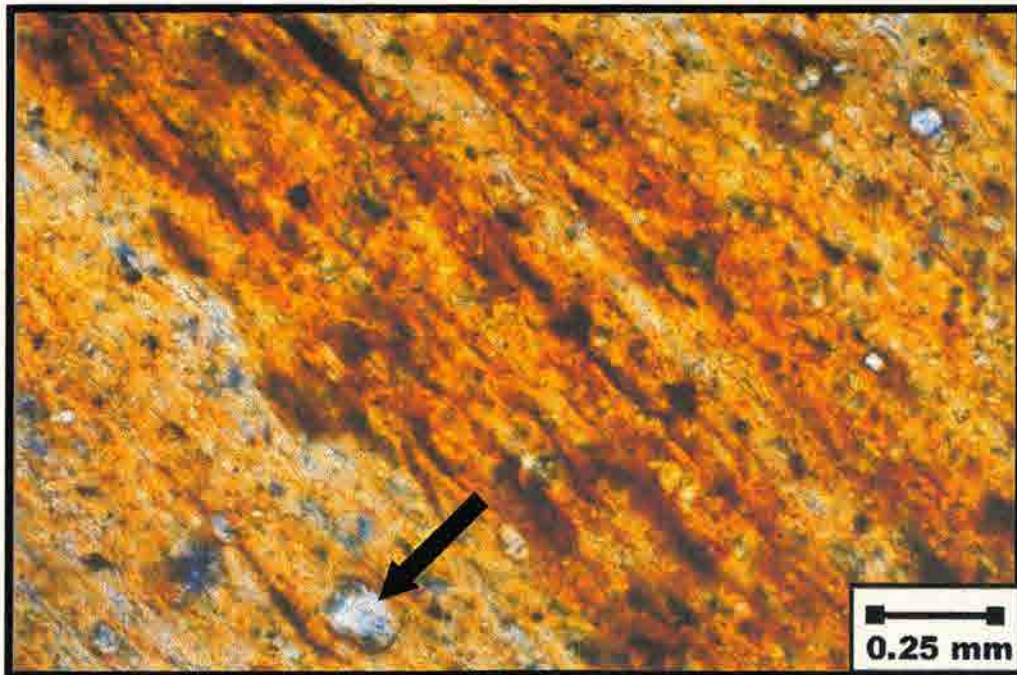


Figure A6.

Figure A7

Section 012 (a) - Figure A

Low magnification (PP1) thin section photomicrograph of a carbonaceous silt shale strongly compacted well-sorted matrix contains clay minerals and silt size detrital grains (quartz, feldspar, mica) with an occasional fine-grained sand particle. The shale has moderately-developed laminations of silt, clay and organic matter. Vialite matrix presence is not evident.

Figure A8

Section 012 (a) - Figure A

Medium magnification (PP1) thin section photomicrograph of same carbonaceous silt shale in Figure A7. Wavy laminations of organic matter and clay give the shale a lentic appearance. Accretionary masses include fibrous detrital grains and authigenic carbonates such as calcite, dolomite and siderite. These carbonates are present as cement and replacing some of the fossil fragments, which is easier to distinguish under higher power than present in this photo. Vialite matrix presence is not detected.

Figure A7.

SC012 (63 ft)- Facies A

Low magnification (PPL) thin section photomicrograph of a carbonaceous silty shale. Strongly compacted, well-sorted matrix contains clay minerals and silt size detrital grains (quartz, feldspar, mica), with an occasional fine-grained sand particle. This shale has moderately-developed laminations of silt, clays and organic matter. Matrix porosity is not evident.

Figure A8.

SC012 (63 ft)- Facies A

Medium magnification (PPL) thin section photomicrograph of same carbonaceous silty shale in Figure A7. Wispy laminations of organic matter and clays give this rock a fissile appearance. Accessory minerals include framboidal pyrite and authigenic carbonates such as calcite, dolomite and siderite. These carbonates are present as cement and replacing some of the fossil fragments, which is easier to distinguish under higher power than present in this photo. Visible matrix porosity is not detected.

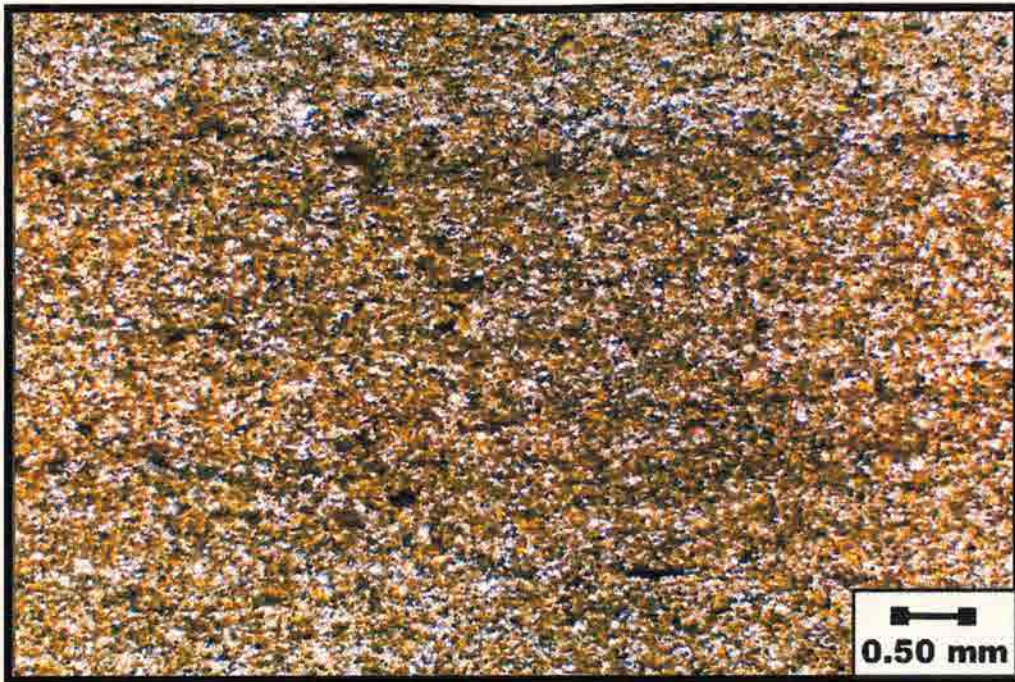


Figure A7.

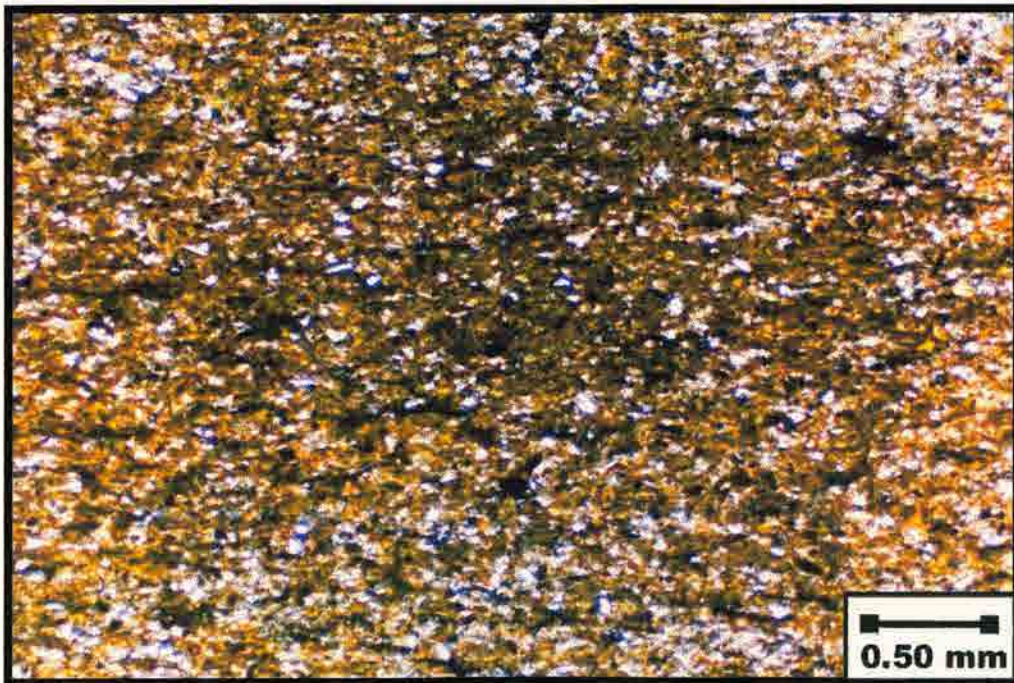


Figure A8.

Figure 49
 SC017 (62 ft) - Factor B
 Low magnification (10X) thin section photomicrograph of metamorphosed
 biotite limestone and shale. Strongly compacted, well-sorted matrix the shale
 portion in the lower half of the photo, contains clay minerals and siliceous detrital
 grains (quartz, feldspar, mica) with an occasional fine-grained sand particle. This
 shale is strongly intercalated with pelagically deposited shell biotite (locally
 thin form calcareous laminae in the top half of the photo. Accessory constituents
 include authigenic carbonates (calcite, dolomite and siderite) and authigenic
 hematite. Matrix porosity is not detected.

Figure 410
 SC018 (62 ft) - Factor B
 Medium magnification (10X) thin section photomicrograph of same
 metamorphosed biotite limestone and shale as Figure 49. The abundant
 intercalated pelagically deposited biotite is more pelagically deposited and
 authigenic carbonates (calcite, dolomite and siderite) provide a matrix for the
 biotite laminae. Very small amount of irregular porosity may be
 noted.

Figure A9.

SC015 (65 ft)- Facies B

Low magnification (PPL) thin section photomicrograph of interlaminated bioclastic limestone and shale. Strongly compacted, well-sorted matrix the shale pictured in the lower half of the photo, contains clay minerals and silt size detrital grains (quartz, feldspar, mica) with an occasional fine-grained sand particle. This shale is sharply interlaminated with pelecypod shell bioclasts (Inoceramid prisms) that form calcareous laminae in the top half of the photo. Accessory constituents include authigenic carbonates (calcite, dolomite and siderite) and authigenic framboidal pyrite. Matrix porosity is not detected.

Figure A10.

SC015 (65 ft)- Facies B

Medium magnification (PPL) thin section photomicrograph of same interlaminated bioclastic limestone and shale in Figure A9. The abundant Inoceramid prisms are more palpable at high power. Clay minerals and authigenic carbonates (calcite, dolomite and siderite) provide a matrix for the bioclastic limestone debris. Very small amounts of intergranular porosity may be noted.

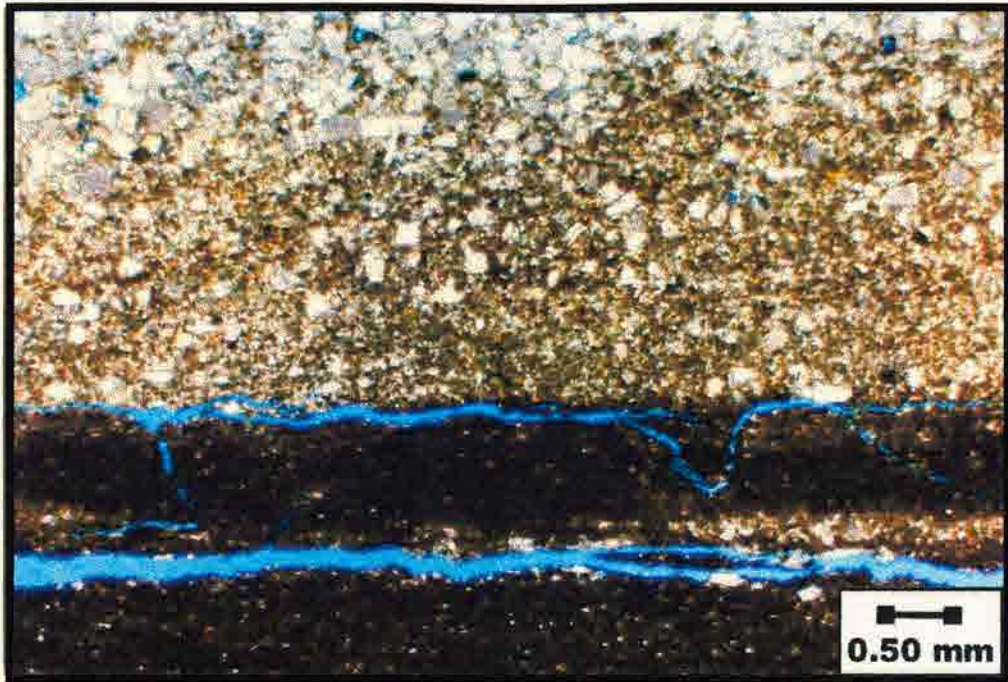


Figure A9.

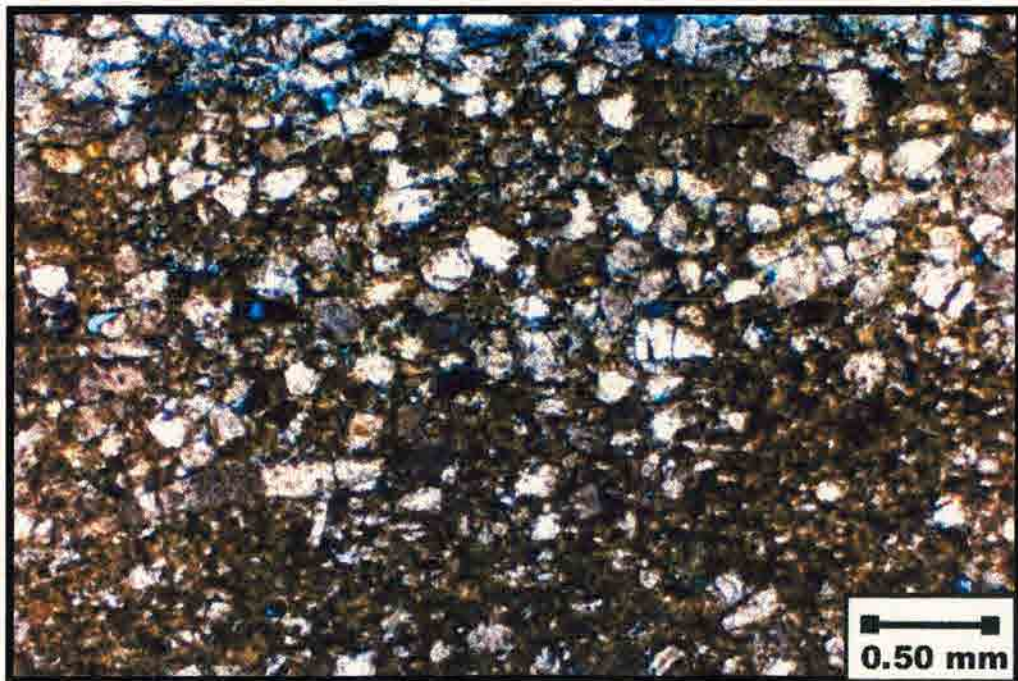


Figure A10.

Figure A11.
 SC030 (80 ft)-Facies B
 Low magnification (PPL) thin section photomicrograph of argillaceous siltstone. The irregular distribution of detrital silt size quartz and feldspar grains in the clay rich matrix gives a slight "mottled" texture that is typical of bioherms. The less rich matrix also has an irregular distribution. Accessory constituents include authigenic lamellar pyrite, authigenic carbonates and carbonaceous detritus. No visible matrix porosity is detected.

Figure A12.
 SC040 (100 ft)-Facies C
 Medium magnification (PPL) thin section photomicrograph of calcareous cemented quartzose siltstone. This well-sorted matrix contains clay minerals and silt size detrital grains (quartz, feldspar, mica) with an occasional fine-grained sand particle. Quartz grains are well rounded, spherulitic silt to medium-grained and rich. Accessory constituents include glauconitic (small green nodules) and authigenic pyrite (small opaque nodules). Carbonate (caliche dolomite and siliceous) is present as major cement and replacing some detrital grains. Visible matrix porosity is lacking.

Figure A11.

SC030 (80 ft)- Facies B

Low magnification (PPL) thin section photomicrograph of argillaceous siltstone. The irregular distribution of detrital silt size quartz and feldspar grains in the clay rich matrix gives a slight "mottled" texture that is typical of bioturbation. The lens of organic matter also have an irregular distribution. Accessory constituents include authigenic framboidal pyrite, authigenic carbonates and carbonaceous detritus. No visible matrix porosity is detected.

Figure A12.

SC040 (100 ft)- Facies C

Medium magnification (PPL) thin section photomicrograph of carbonate cemented quartzose siltstone. This well-sorted matrix contains clay minerals and silt size detrital grains (quartz, feldspar, mica) with an occasional fine-grained sand particle. Quartz grains are well rounded, spherical, silt to medium-grained sand size. Accessory constituents include glauconite (small green nodules) and authigenic pyrite (small opaque nodules). Carbonate (calcite, dolomite, and siderite) is present as major cement and replacing some detrital grains. Visible matrix porosity is lacking.

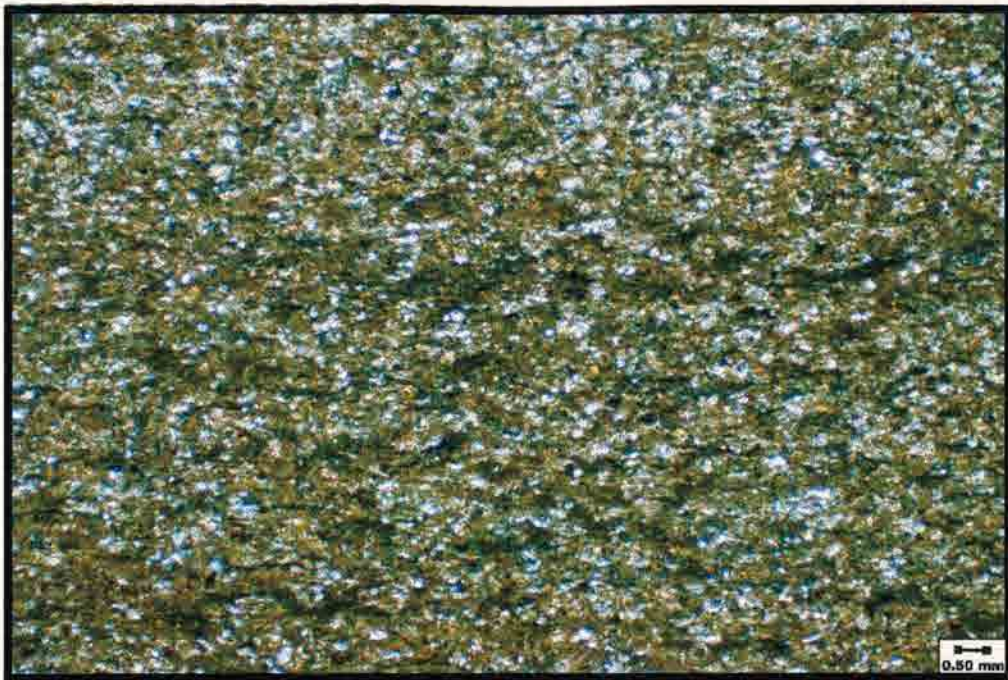


Figure A11.

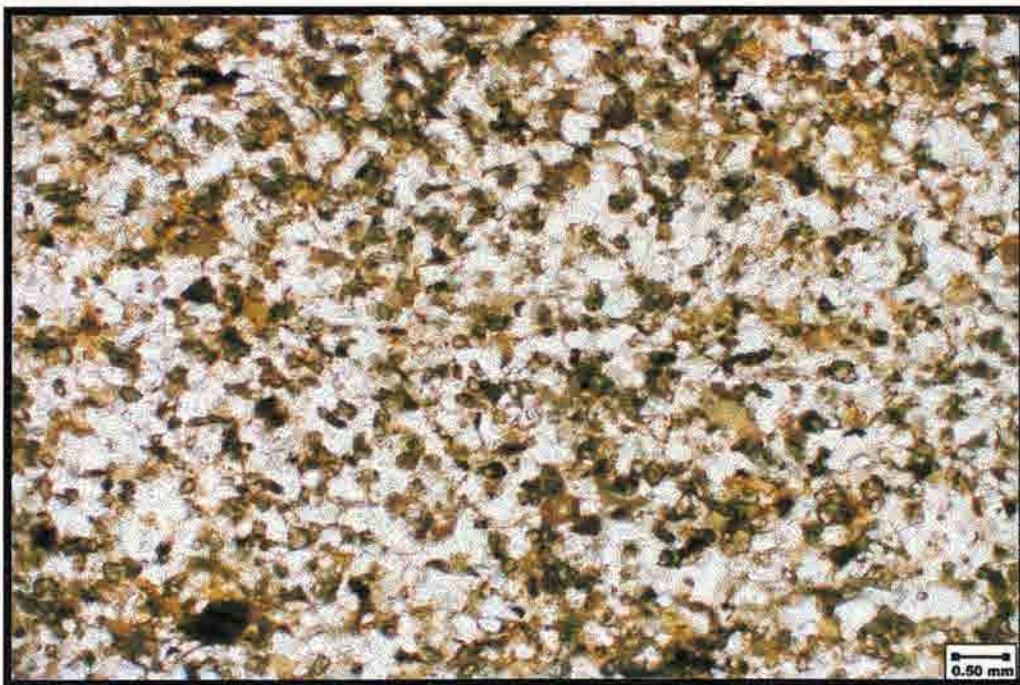


Figure A12.

APPENDIX B

SOLDIER CANYON DAM OUTCROP

SKULL CREEK SHALE

SEM PHOTOMICROGRAPHS

1. The first part of the document is a list of the names of the members of the committee who have been appointed to study the problem of the...
2. The second part of the document is a list of the names of the members of the committee who have been appointed to study the problem of the...

3. The third part of the document is a list of the names of the members of the committee who have been appointed to study the problem of the...
4. The fourth part of the document is a list of the names of the members of the committee who have been appointed to study the problem of the...

5. The fifth part of the document is a list of the names of the members of the committee who have been appointed to study the problem of the...
6. The sixth part of the document is a list of the names of the members of the committee who have been appointed to study the problem of the...

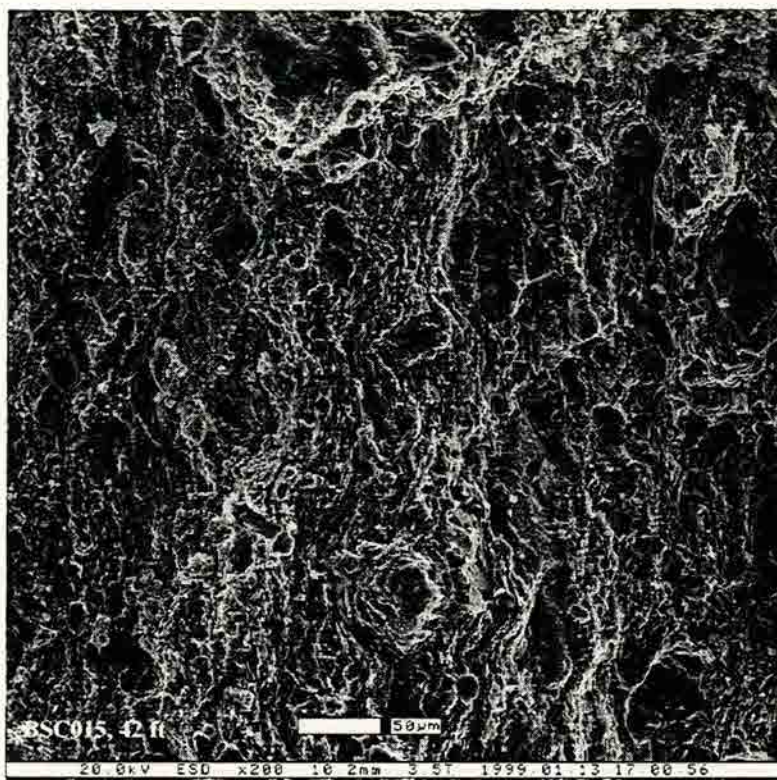
BSC015: 42 ft – Facies K

Top photo: Low Power (x200)

Bottom photo: High Power (x700)

At low magnification, the overall texture is a well-sorted, subangular to subrounded, framework supported silty shale. The framework particle size ranges from 10 to 30 μm and is homogeneously distributed throughout the bulk of this sample. The framework mineralogy primarily consists of detrital quartz grains with secondary amounts of feldspars. Quartz overgrowths are present and seem to be cut off by clay cementation.

At high magnification, the clay minerals are displayed primarily as grain coating but also as pore filling. Small kaolinite “books” can be distinguished. The sample exhibits a poorly developed intergranular macropore system and a poorly developed intergranular micropore system. Molds of plucked grains are found throughout this sample and probably an artifact of sample preparation.



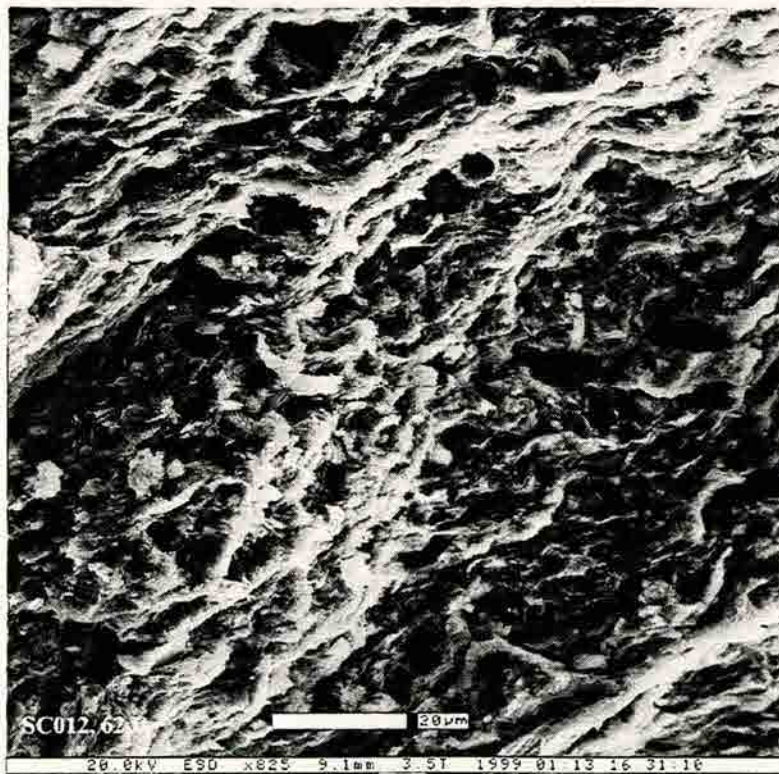
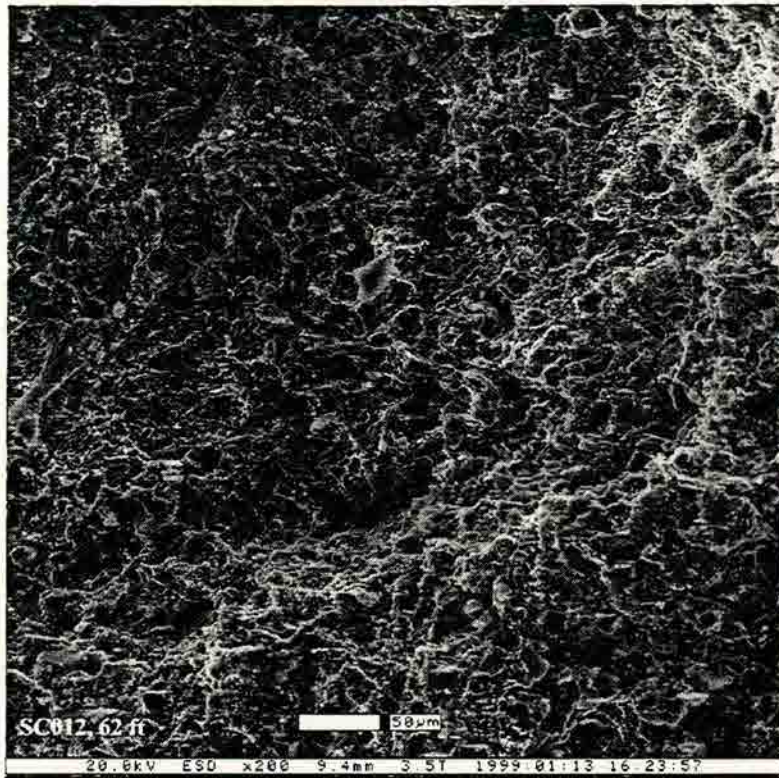
SC012: 62 ft – Facies A

Top photo: Low Power (x225)

Bottom photo: High Power (x825)

At low magnification, the overall texture is a well-sorted, subangular to subrounded, framework supported silty shale. The framework particle size ranges from 10 to 30 μm and is homogeneously distributed throughout the bulk of this sample. The framework mineralogy primarily consists of detrital quartz grains with secondary amounts authigenic carbonates and feldspars. Quartz overgrowths are present and seem to be cut off by clay cementation.

At high magnification, the grain coating nature of the clay minerals is evident. Small amounts of kaolinite in the form of “books” are present but hard to distinguish. The pore filling clays have a strong preferred orientation. The sample exhibits a poorly developed intergranular macropore system and a poorly developed intergranular micropore system. Grain plucking and fractured grains are an artifact of sample preparation.



1. The first part of the document is a letter from the author to the editor of the journal. The letter discusses the author's interest in the topic and the reasons for writing the paper. It also mentions the author's affiliation and contact information.

2. The second part of the document is the abstract of the paper. It provides a brief summary of the main findings and conclusions of the study. The abstract is followed by the introduction, which sets the context for the research and states the objectives of the study. The main body of the paper follows, where the author presents the methodology, results, and discussion. The paper concludes with a summary of the findings and a list of references.

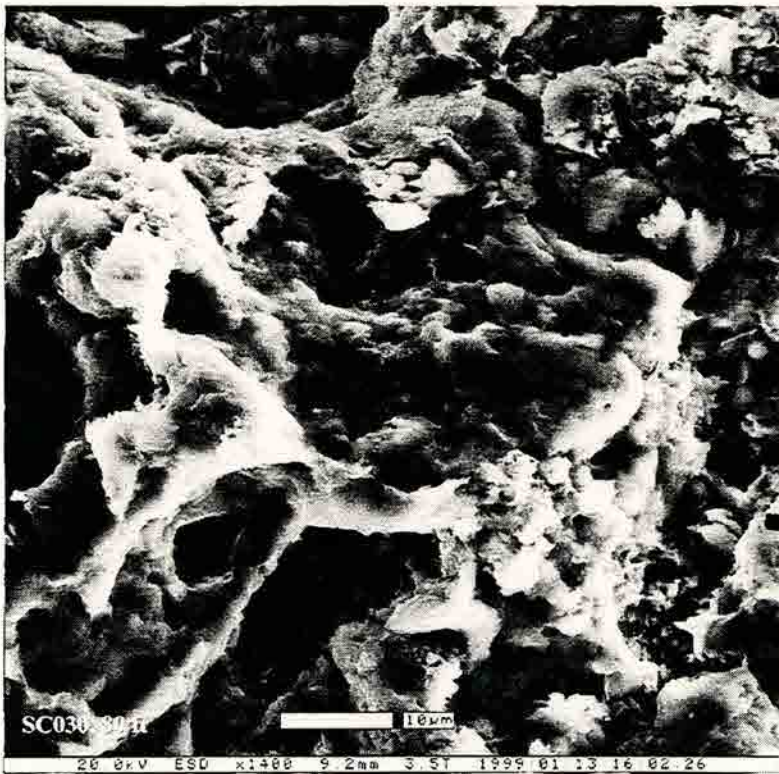
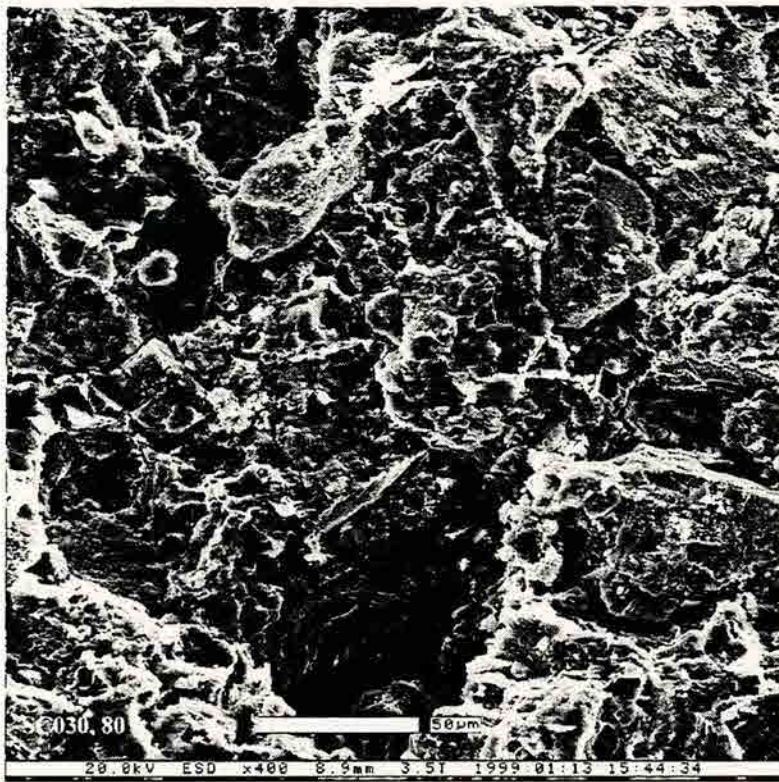
SC030: 80 ft – Facies B

Top photo: Low Power (x400)

Bottom photo: High Power (x2600)

At low magnification, the overall texture is a moderately sorted, angular to subrounded, framework-supported siltstone. The framework particle size ranges from 10 to 50 μm and comprises the bulk of this sample. The framework mineralogy primarily consists of detrital quartz grains with secondary amounts of carbonate and feldspars. Quartz overgrowths are present and seem to be cut off by clay cementation.

At high magnification, the clay minerals can be seen coating the detrital hard grains. Specific “books” of kaolinite are present. The sample exhibits a moderate-well developed intergranular macropore system and a moderate-well developed intergranular micropore system. This sample seems to have fractures or artifacts caused by sample preparation.



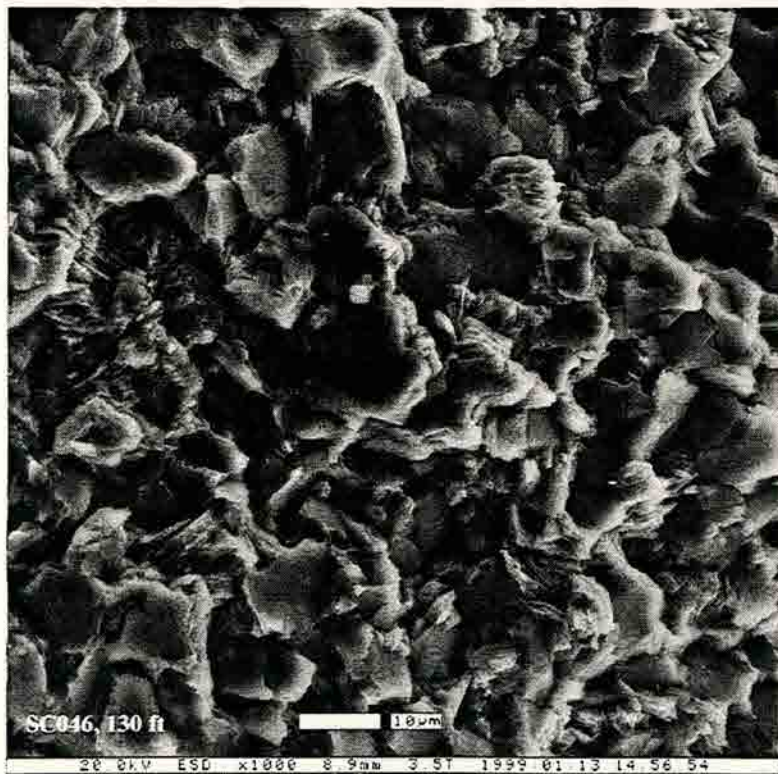
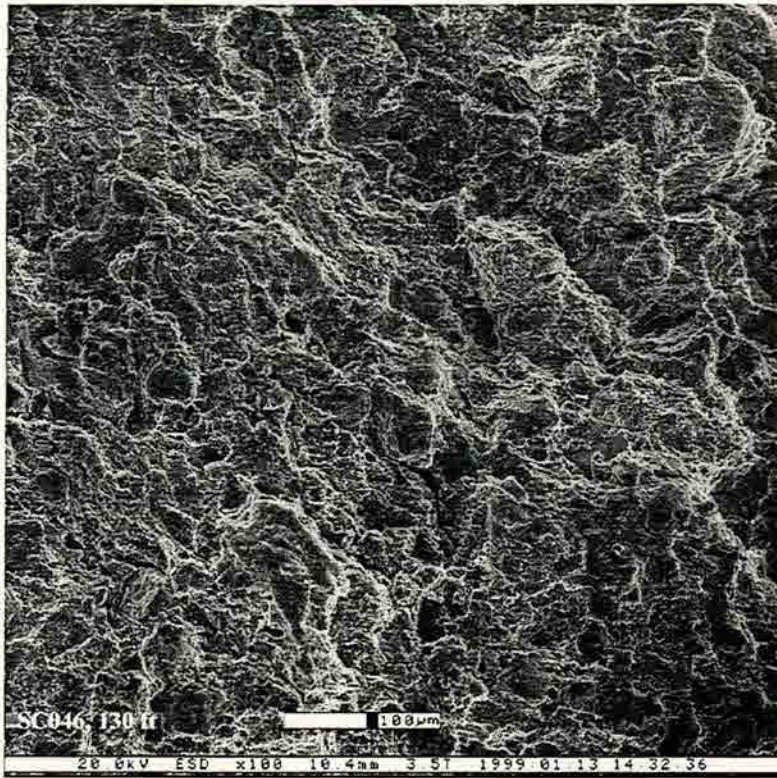
SC046: 62 ft – Facies C

Top photo: Low Power (x100)

Bottom photo: High Power (x1000)

At low magnification, the overall texture is a moderately sorted, subangular to subrounded, framework supported siltstone-sandstone. The framework particle size ranges from 10 to 30 μm and is homogeneously distributed throughout the bulk of this sample. The framework mineralogy primarily consists of detrital quartz grains with secondary amounts of authigenic carbonates and feldspars.

At high magnification, the kaolinite “books” are clearly distinguishable due to the cross-sectional views. Other clay minerals appear to be grain coating or pore-filling. The sample exhibits a poor to moderately developed intergranular macropore system and a poor to moderately developed intergranular micropore system. Molds of plucked grains are found throughout this sample. This sample seems to have fractures or artifacts caused by sample preparation.



APPENDIX C

SOLDIER CANYON DAM OUTCROP

SKULL CREEK SHALE

MICP GRAPHS

MICP table for Soldier Canyon Dam (Skull Creek shale)

Sample#	FT	Facies	Median PTD	Pore Volume %	Sorting Index
SCCS1	West 40	A	0.025	70	VW
SCCS2	West 30	A	0.03	60	W
			0.1	40	W-VW
SCCS3	West 20	A	0.03	100	VW
SCCS4	West 10	A	0.03	100	VW
SCCS5	East 10	A	0.03	100	VW
SCCS6	East 20	A	0.04	100	M
SCCS7	East 30	A	0.03	100	M
BSC-000	0	K	0.03	80	P-M
			0.1	20	W
BSC-004	20	K	0.025	100	M
BSC-007	26	K	0.2	40	VW
			0.05	40	P
			0.015	20	M
BSC-009	30	K	0.05	60	W
			0.015	40	M
BSC-011	34	K	0.015	80	W
			0.08	20	M
BSC-014	40	K	0.015	100	W
BSC-016	44	K	0.007	50	P
			0.02	30	M
			0.25	20	M
BSC-018	48	K	0.02	100	W
BSC-019	50	K	0.008	100	VW
SC-001	51	K	0.015	70	M
			0.06	30	VW
SC-004	54	K	0.02	70	M
			0.05	30	VW
SC-008	58	K	0.03	70	P-M
			0.2	30	W
SC-009	59	A	0.015	100	VW
SC-010	60	A	0.02	100	W
SC-011	61	A	0.02	60	W
			0.06	20	P-M
			0.15	10	M
SC-012	62	A	0.02	100	W
SC-013	63	A	0.05	50	M
			0.02	30	W
			0.2	20	VW
SC-014	64	A	0.06	60	P-M
			0.2	20	VW
			0.015	20	M
SC-015	65	B	0.06	50	VW
			0.25	30	P
			0.015	20	P-M

Sample#	FT	Facies	Median PTD	Pore Volume %	Sorting Index
SC-020	70	B	0.1	50	W
			0.2	30	M
			0.015	20	P-M
SC-025	75	B	0.4	40	VW
			0.1	40	P
			0.02	20	P
SC-028	78	B	0.1	60	P
			0.3	20	W
			0.02	20	P-M
SC-030	80	B	0.05	50	W
			0.5	30	P-M
			0.01	20	M
SC-031	82	C	0.2	50	VW
			1	40	P-M
			0.03	10	P-M
SC-035	90	C	0.1	50	P-M
			0.5	40	VW
			0.03	10	M
SC-038	96	C	0.1	50	P-M
			0.5	40	VW
			0.02	10	M
SC-040	100	C	0.08	50	P-M
			0.5	30	VW
			0.02	20	M
SC-042	104	C	0.2	50	VW
			0.7	30	P-M
			0.02	20	M
SC-043	124	C	0.08	50	P-M
			0.4	30	VW
			0.02	20	M
SC-045	128	C	0.08	50	P-M
			0.3	30	VW
			0.03	20	M
SC-046	130	C	1	40	P-M
			0.08	40	M
			0.02	20	M
SC-049	136	C	0.1	50	P-M
			0.6	30	VW
			0.02	20	M
SC-051	140	C	0.08	50	P-M
			0.3	30	VW
			0.02	20	M
SC-054	146	C	0.2	50	P-M
			0.8	30	VW
			0.02	20	M

Sample#	FT	Facies	Median	Pore Volume %	Sorting Index
			PTD (micron)		
SC-055	148	C	0.1	50	P-M
			0.8	30	VW
			0.02	20	M
SC-056	150	C	0.2	50	P-M
			0.9	30	VW
			0.03	20	M
SC-057	152	C	0.2	50	P-M
			0.9	30	VW
			0.02	20	M
SC-058	154	C	0.2	50	P-M
			0.9	30	VW
			0.02	20	P-M

LEGEND:

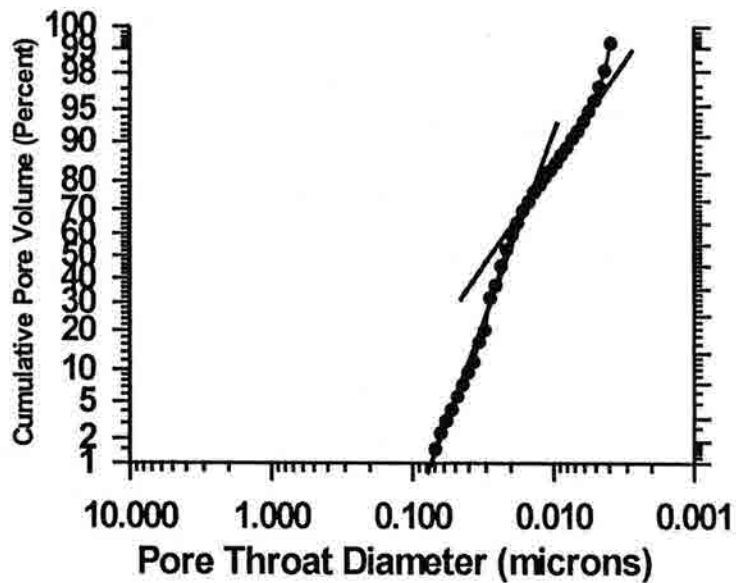
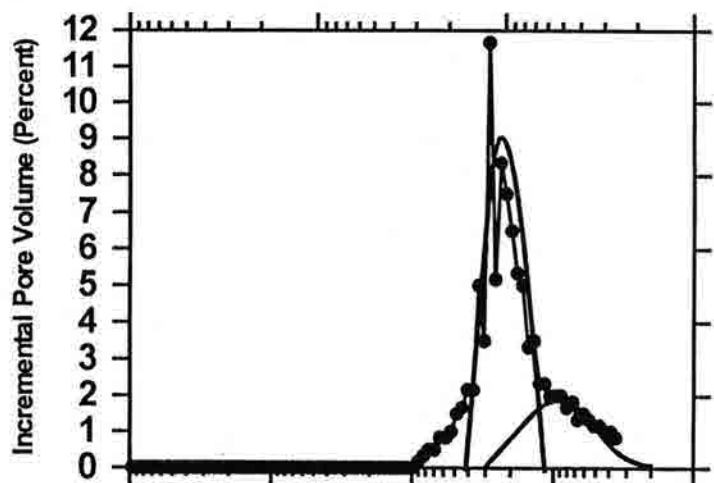
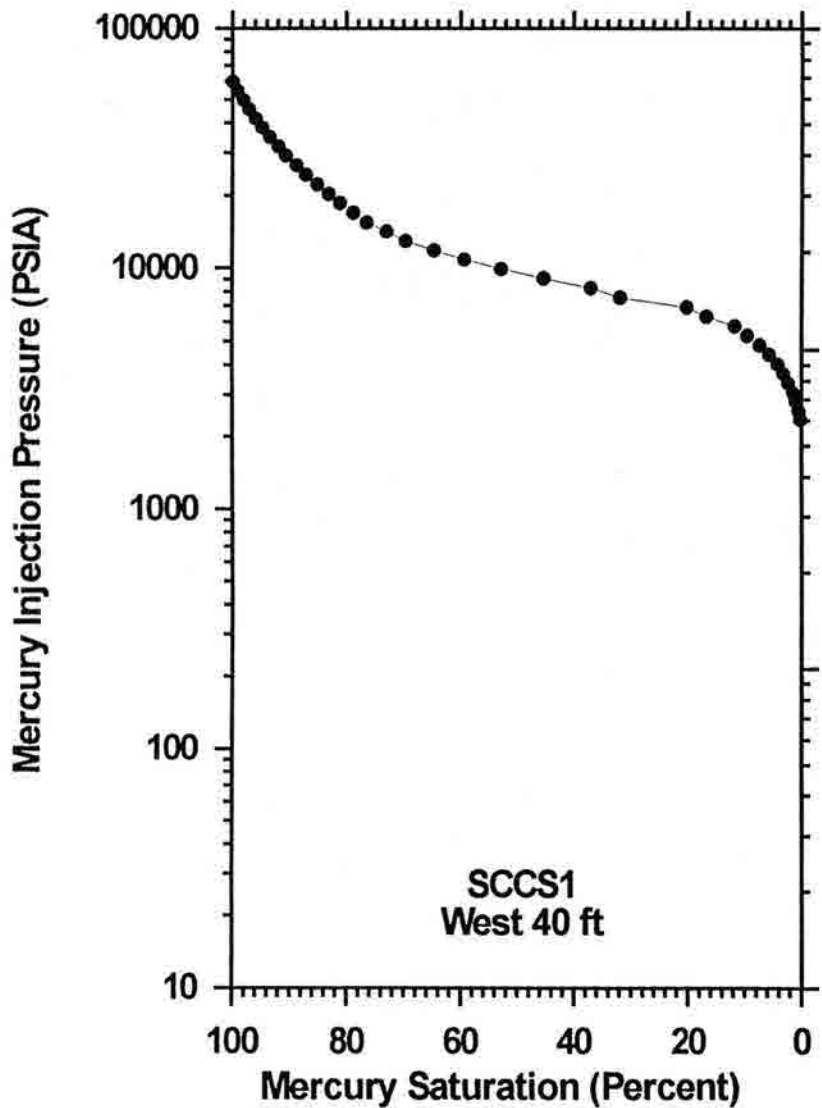
VW= Very Well sorted

W= Well sorted

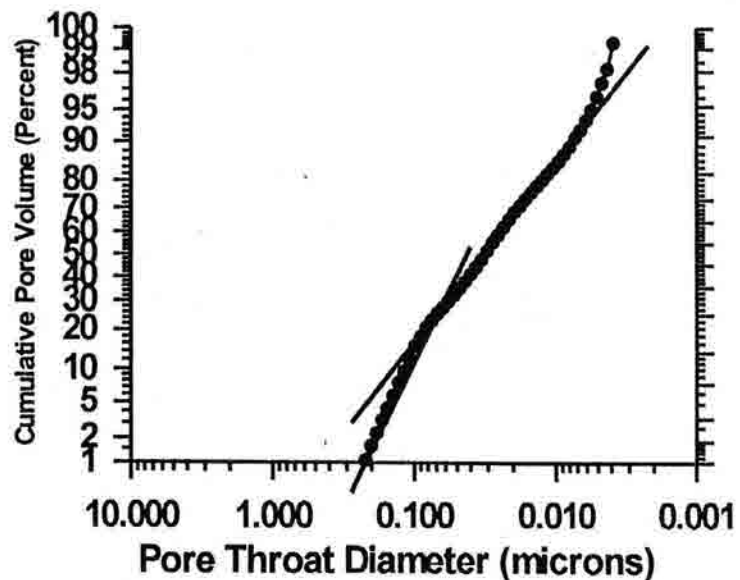
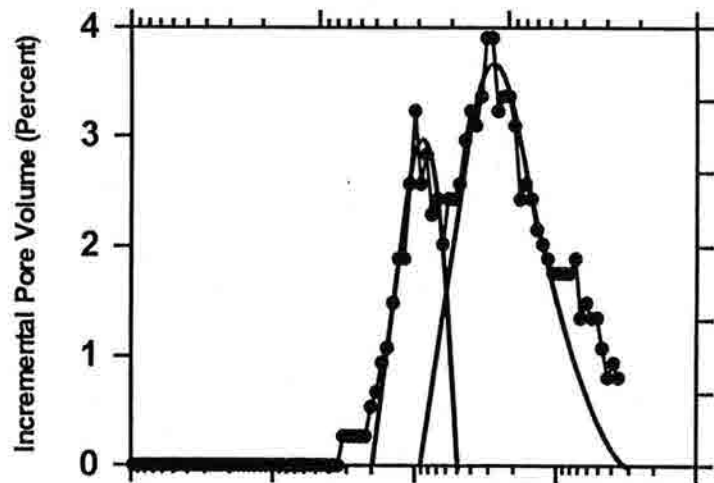
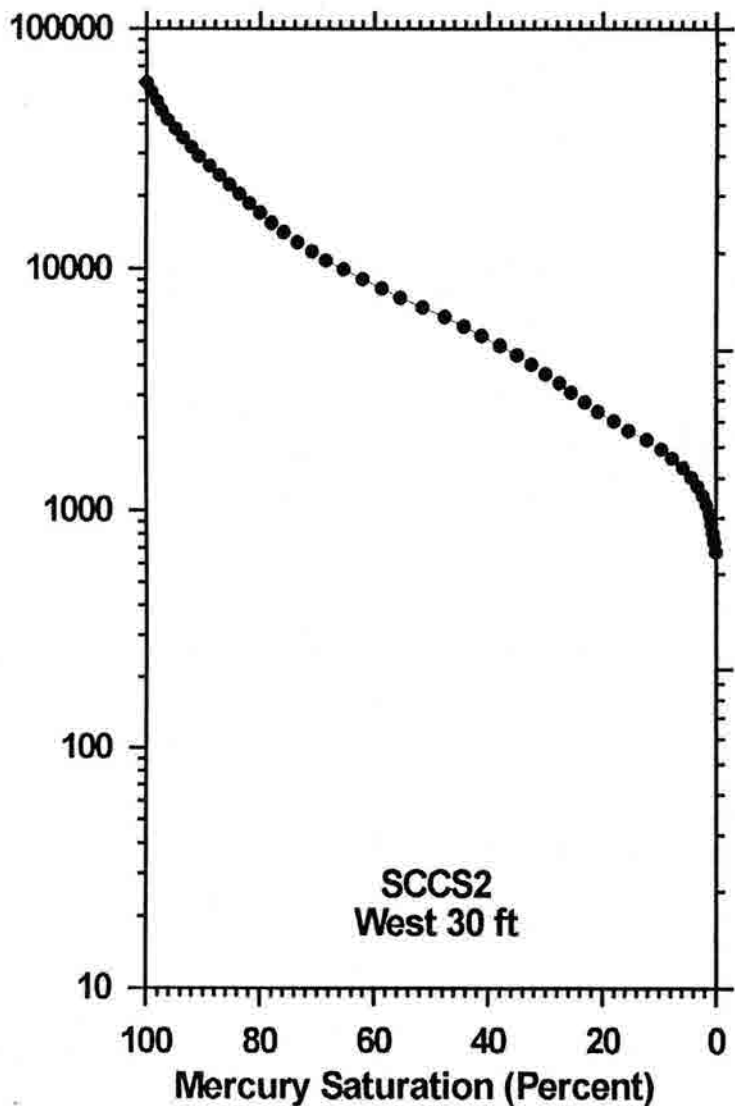
MW= Moderately-well sorted

M= Moderately sorted

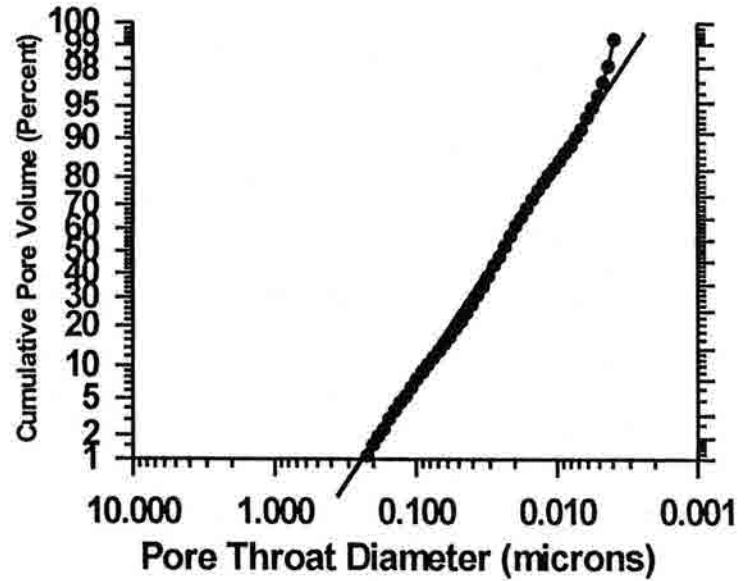
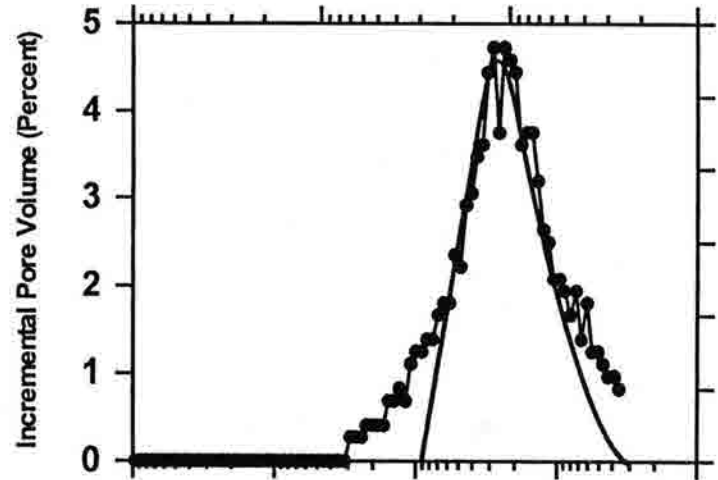
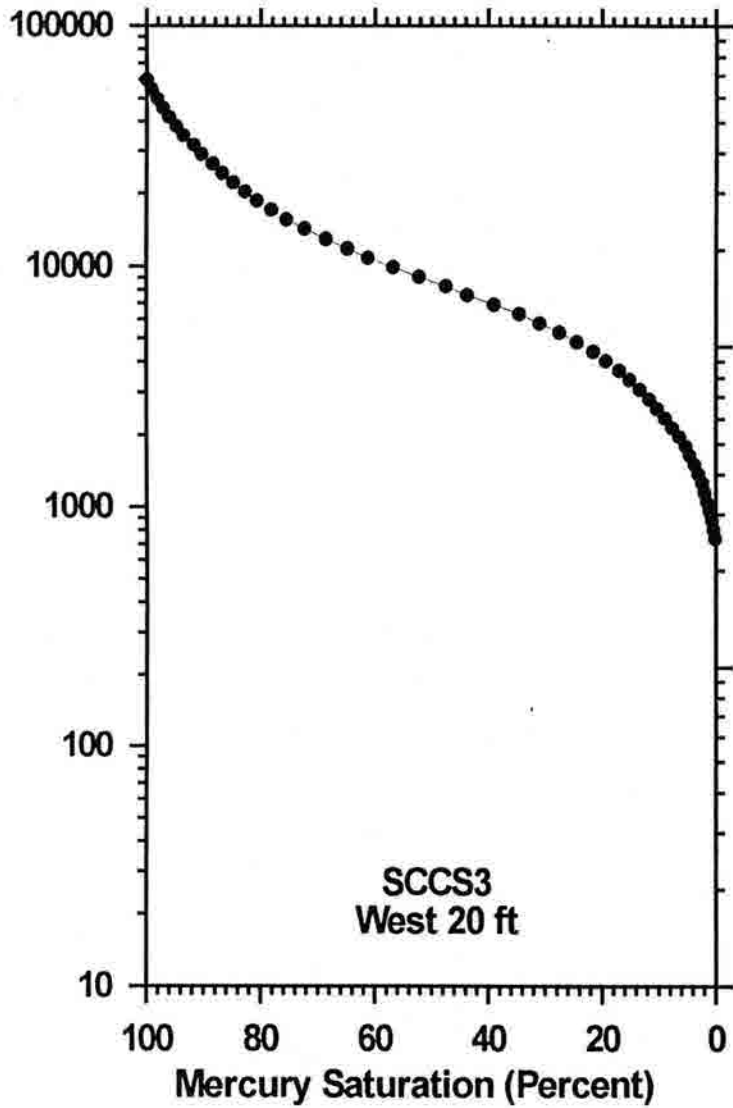
P= Poorly sorted



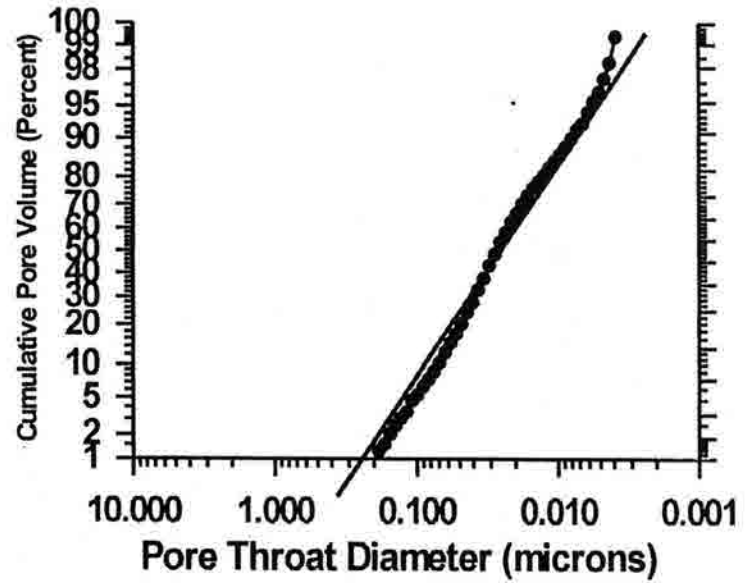
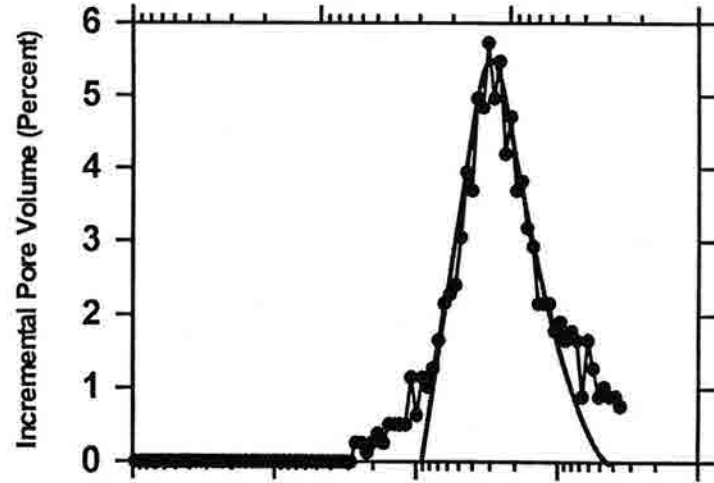
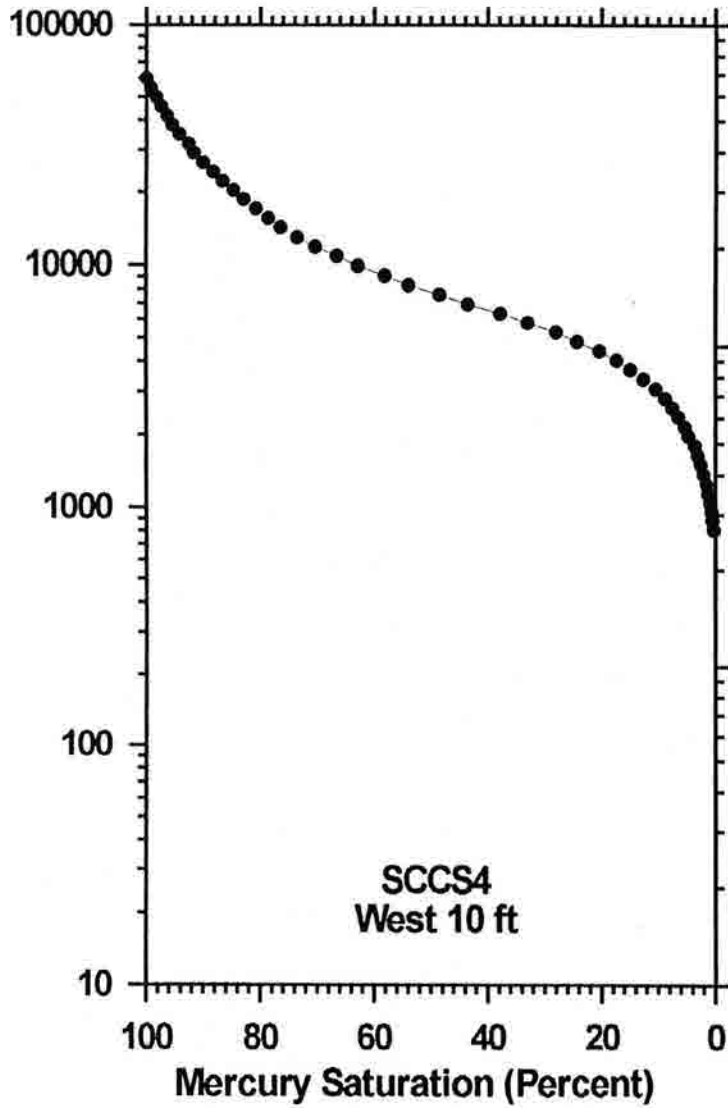
Mercury Injection Pressure (PSIA)



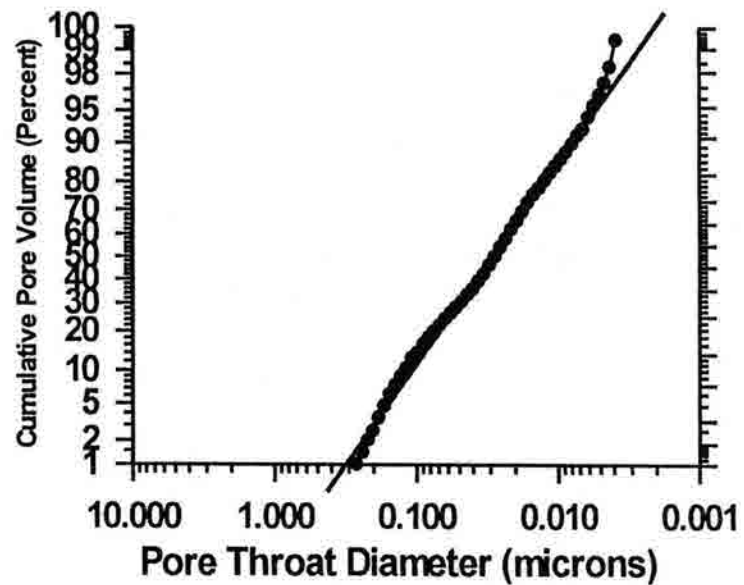
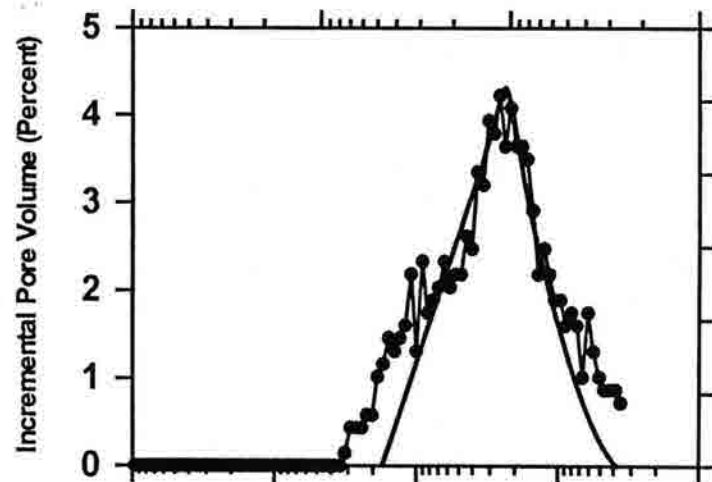
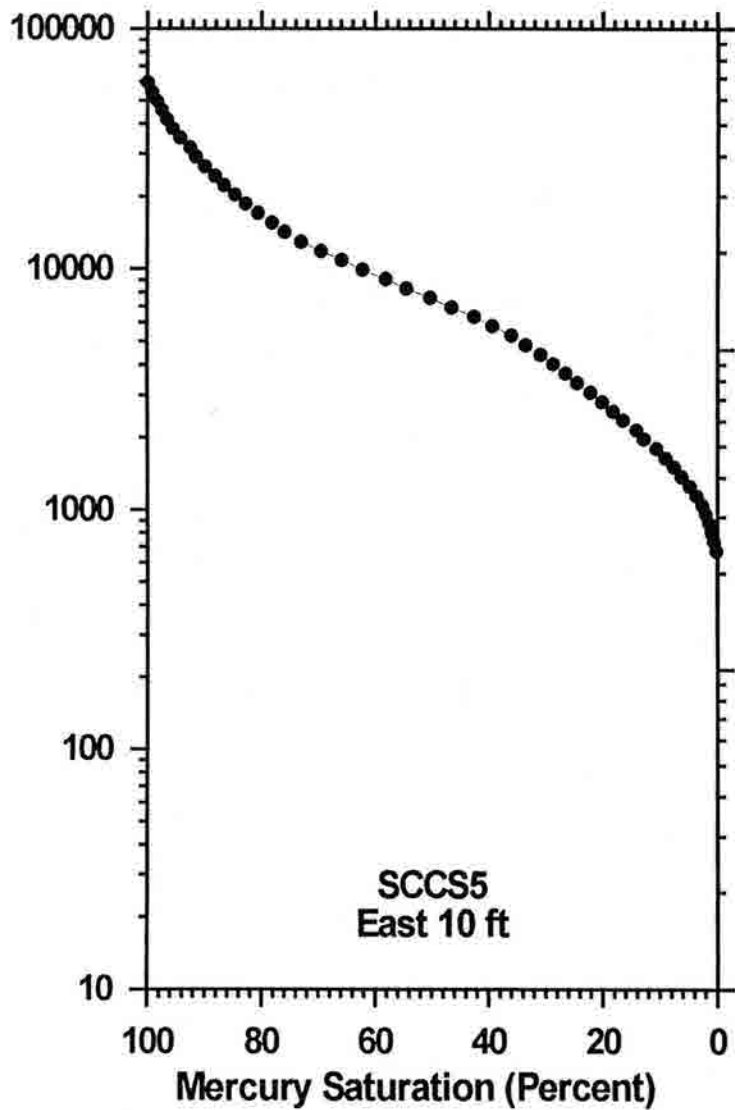
Mercury Injection Pressure (PSIA)



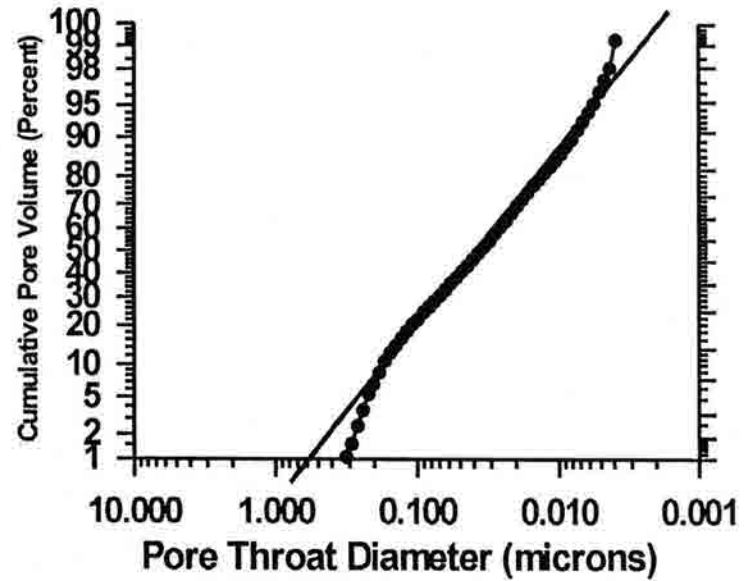
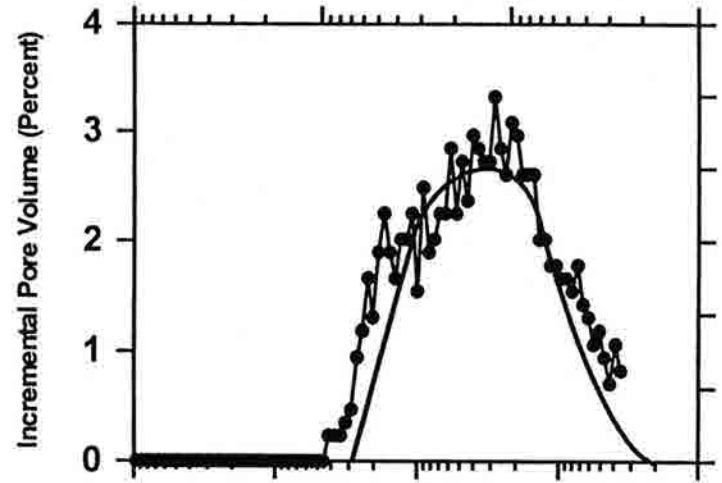
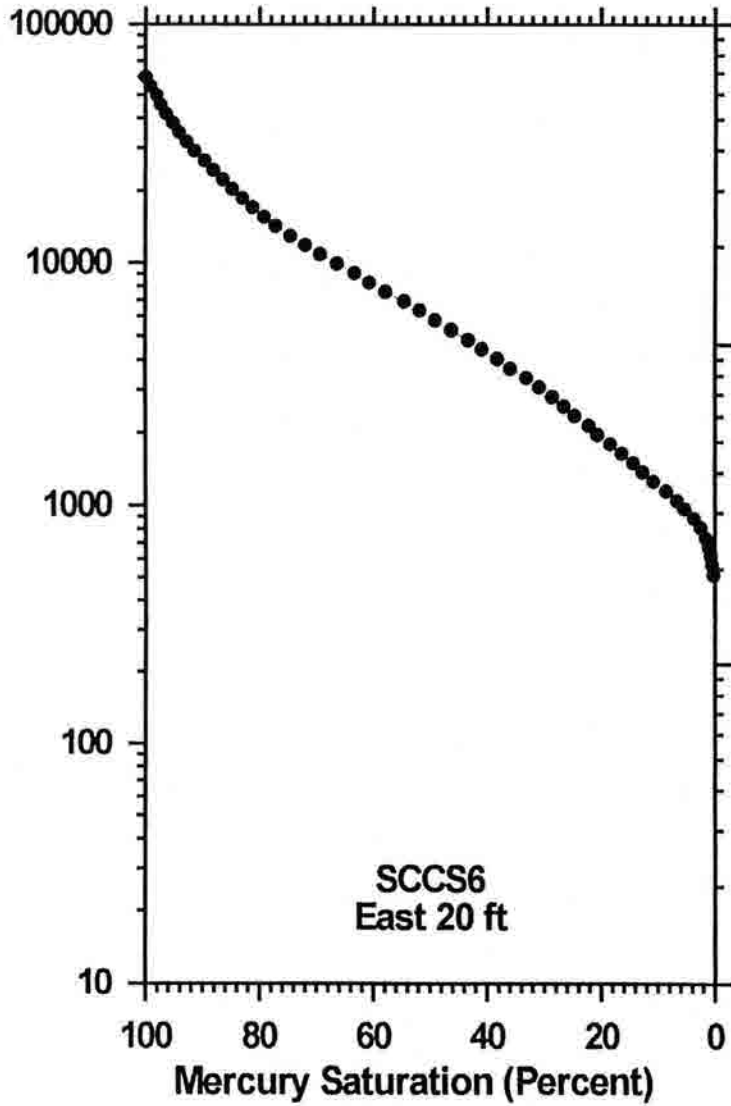
Mercury Injection Pressure (PSIA)

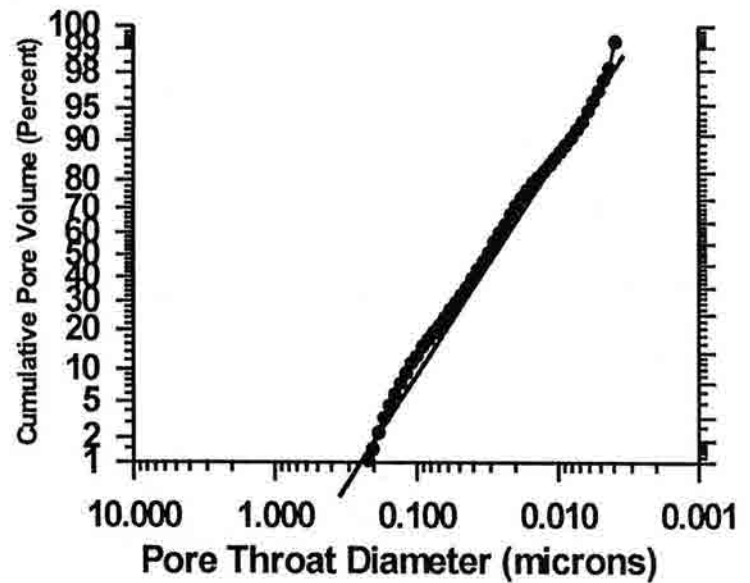
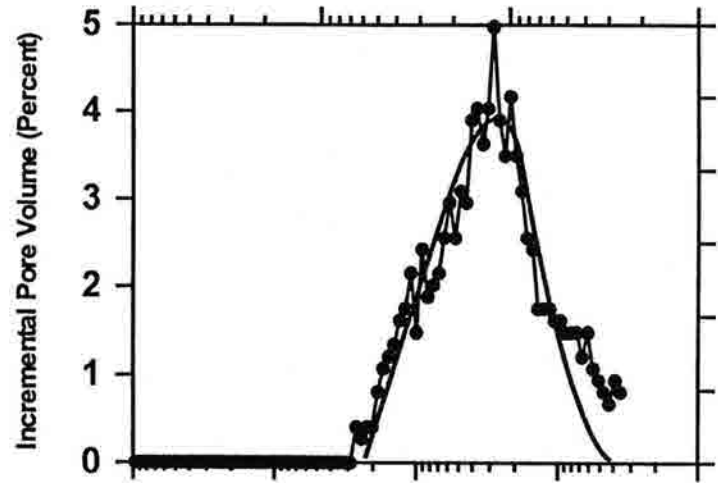
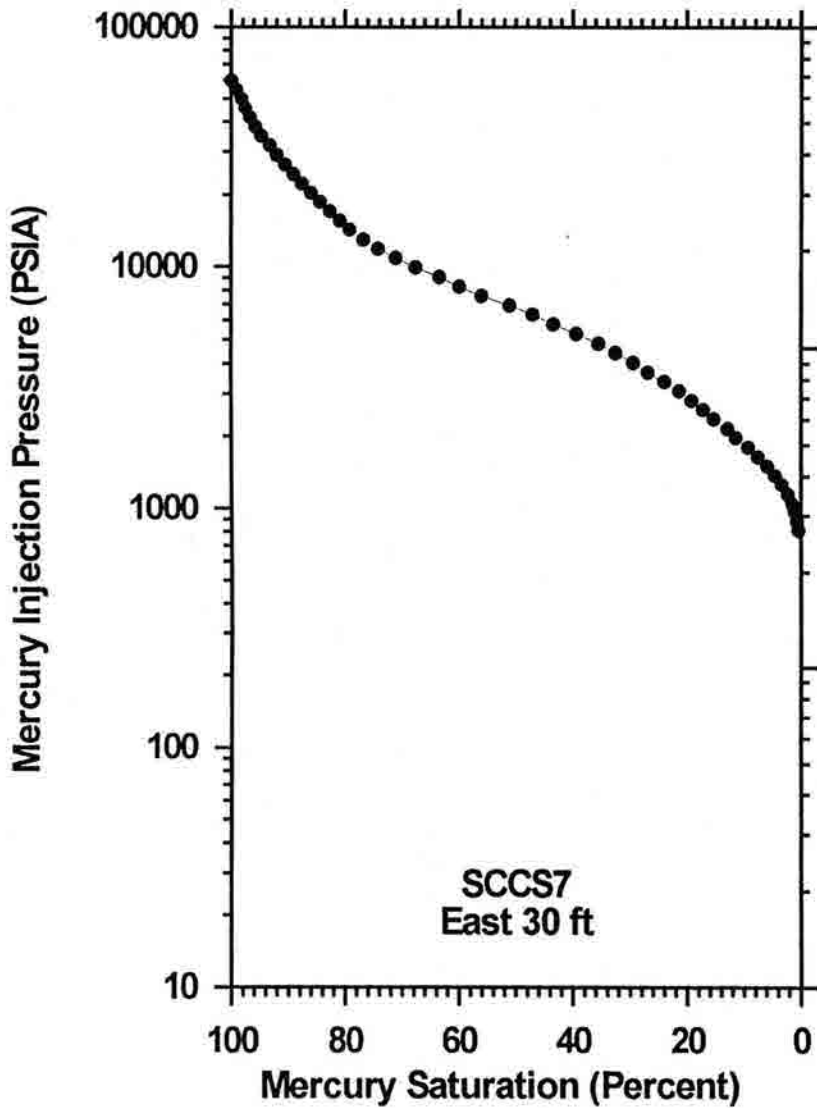


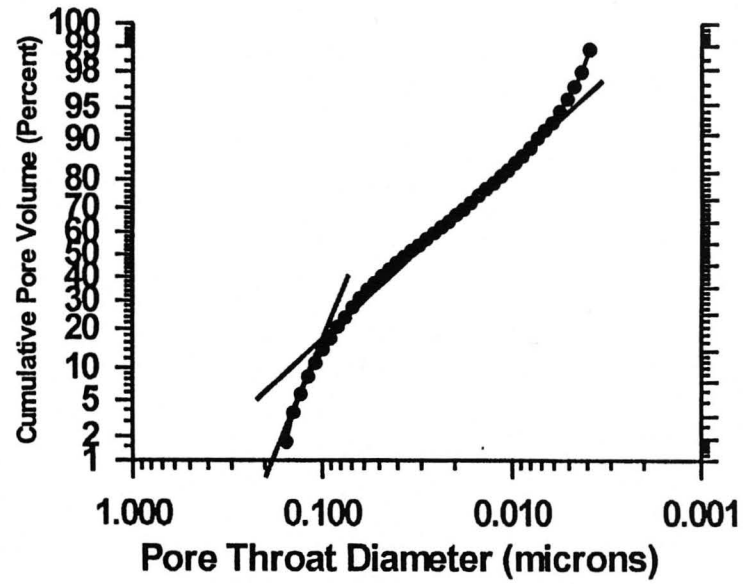
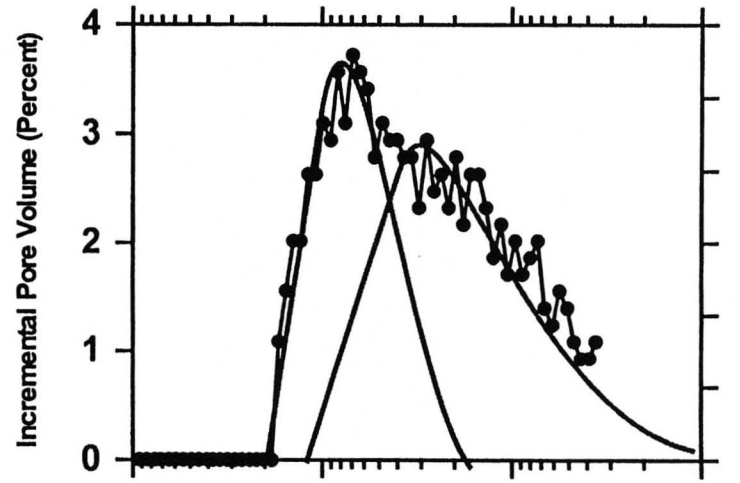
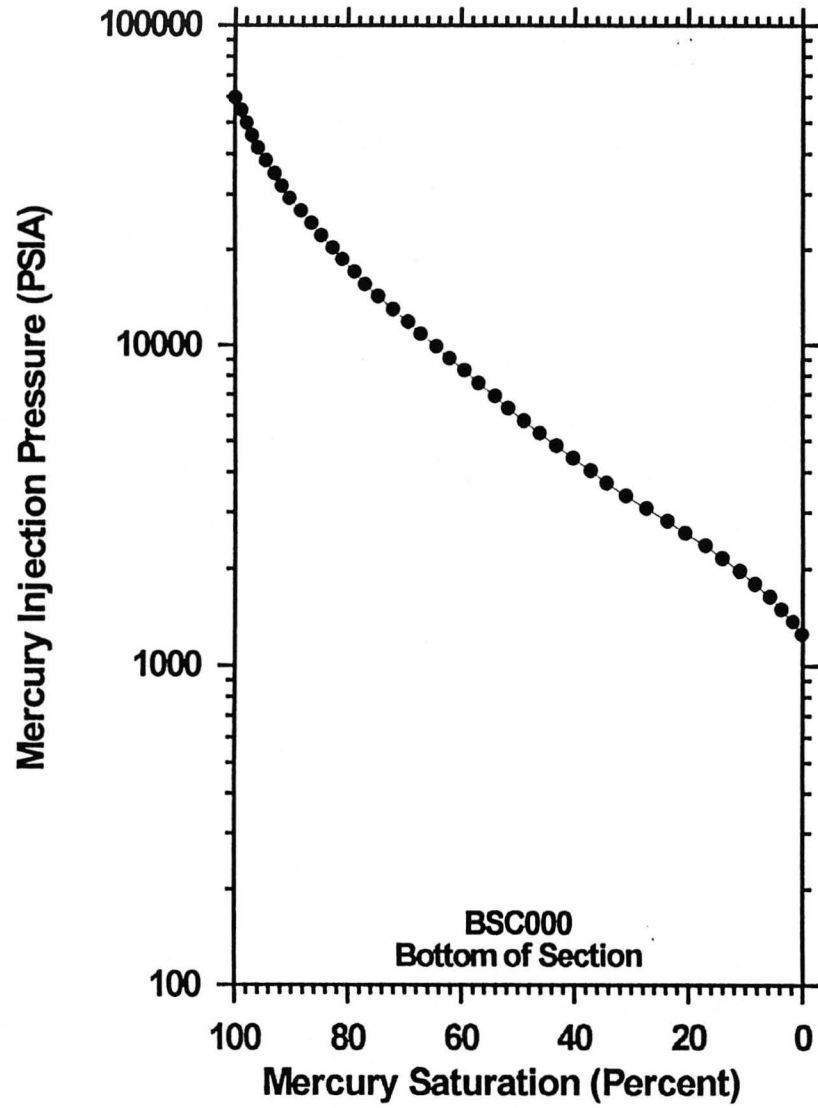
Mercury Injection Pressure (PSIA)



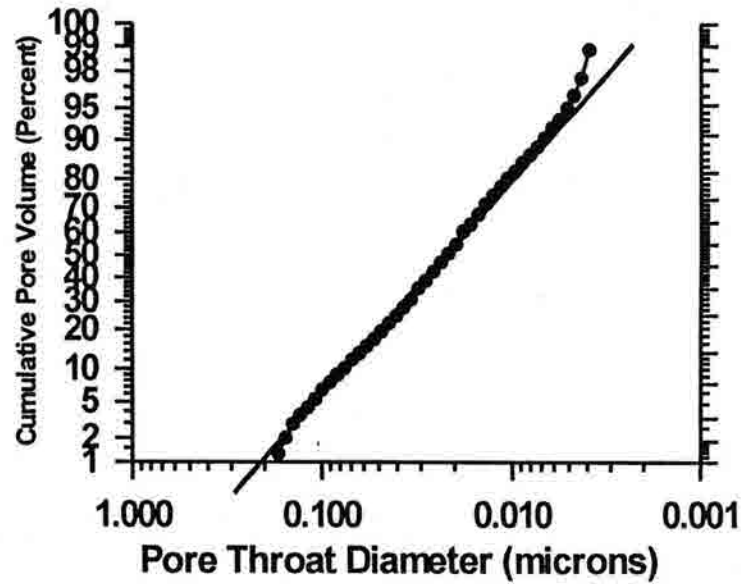
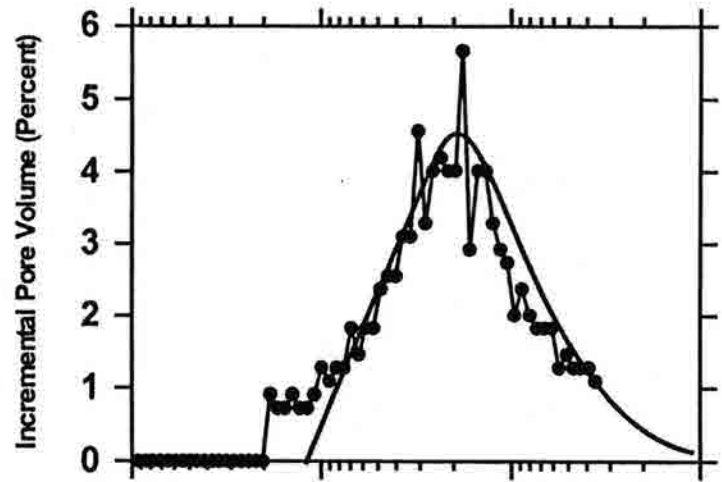
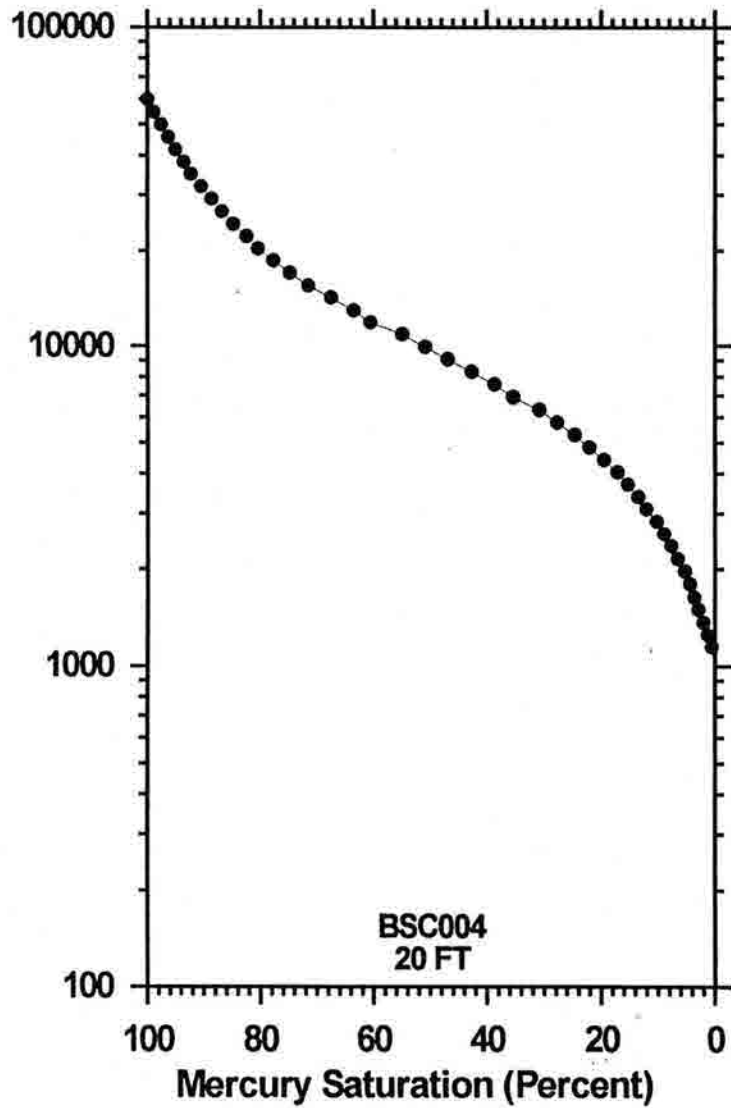
Mercury Injection Pressure (PSIA)

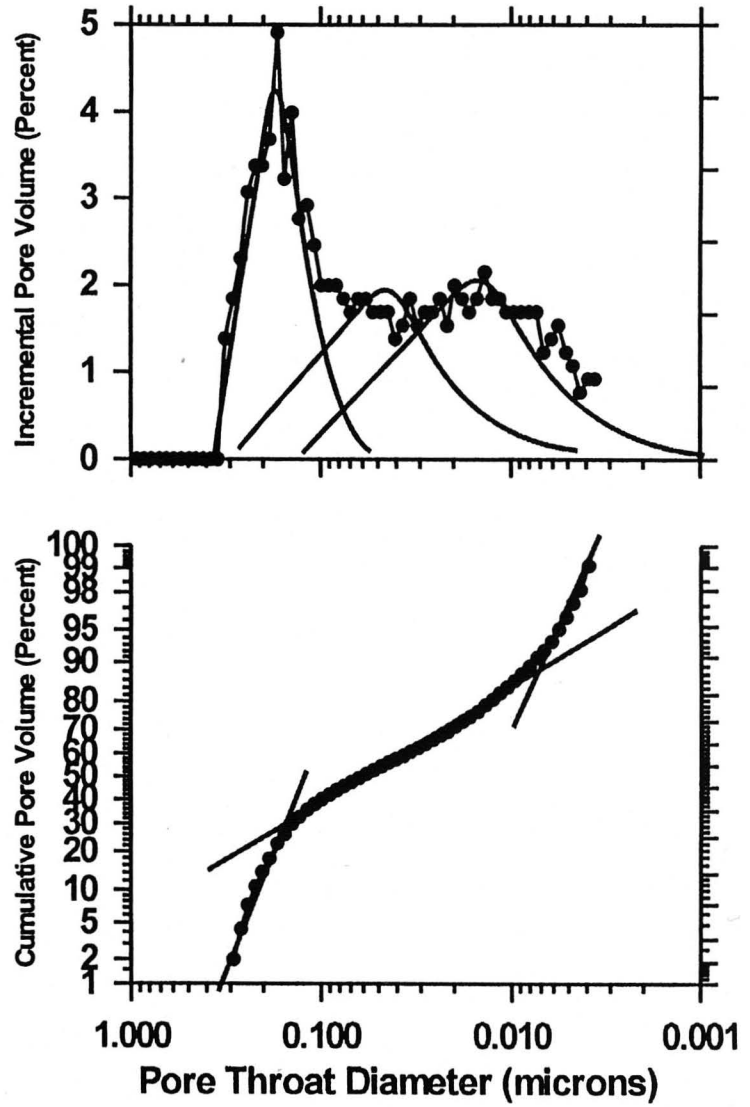
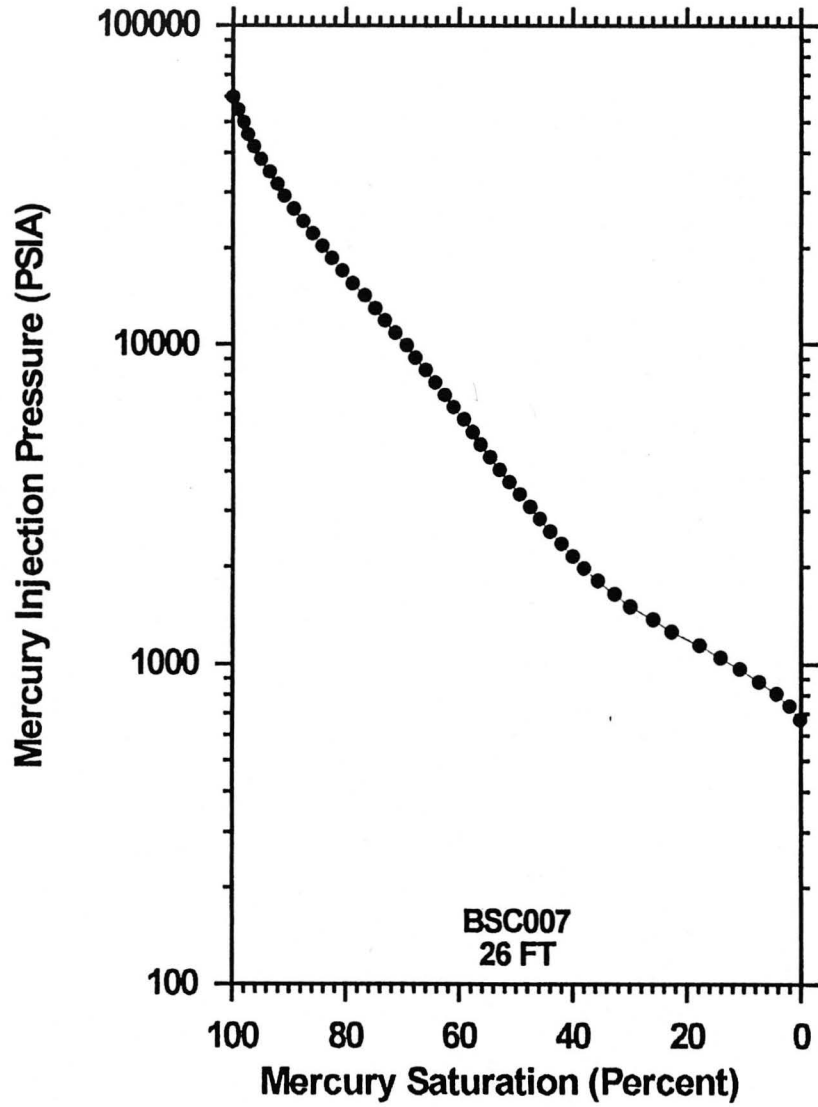


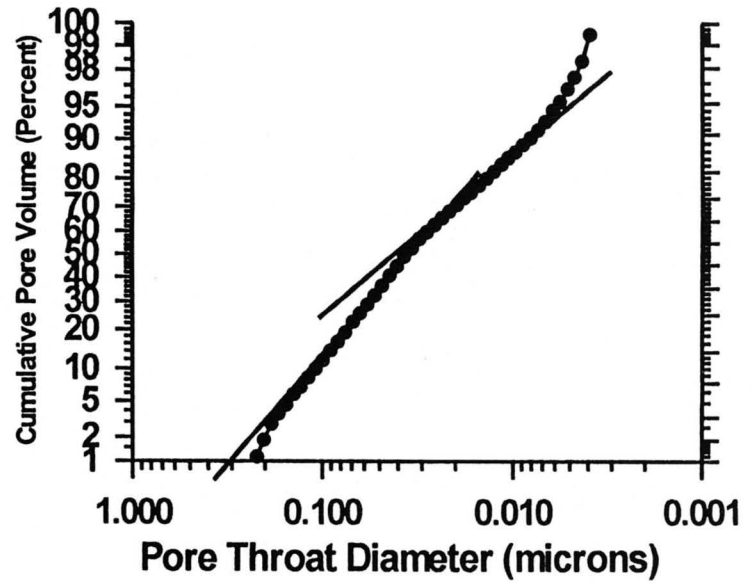
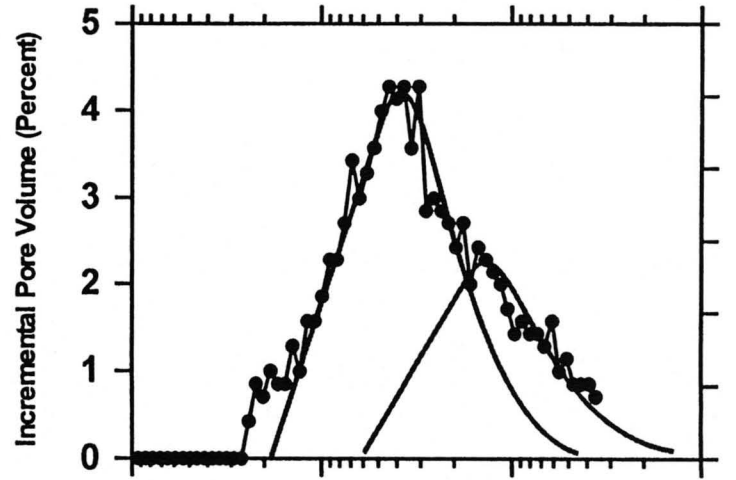
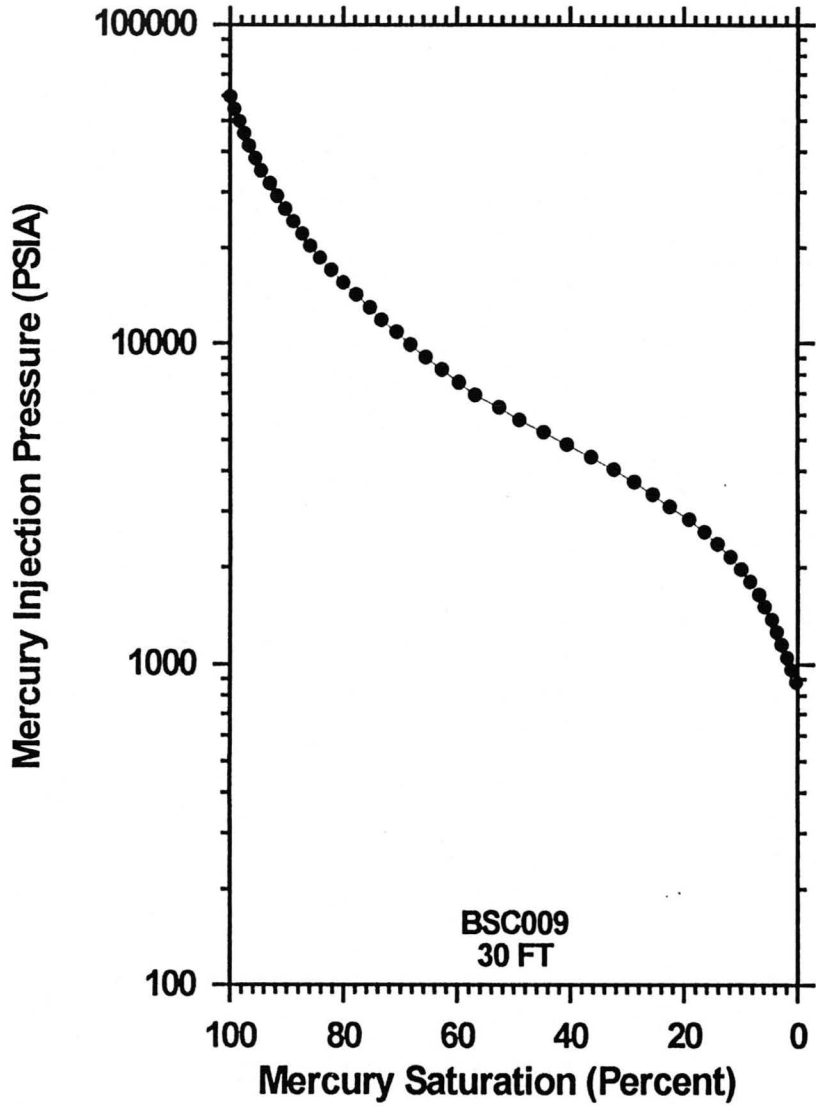


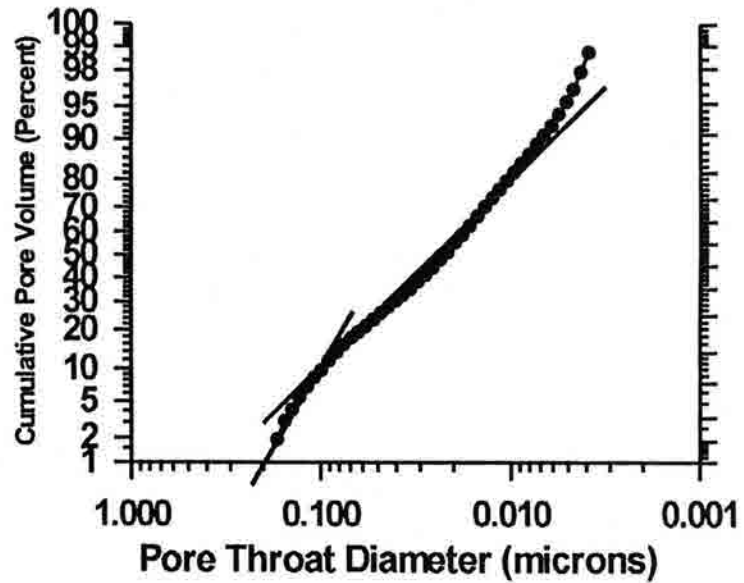
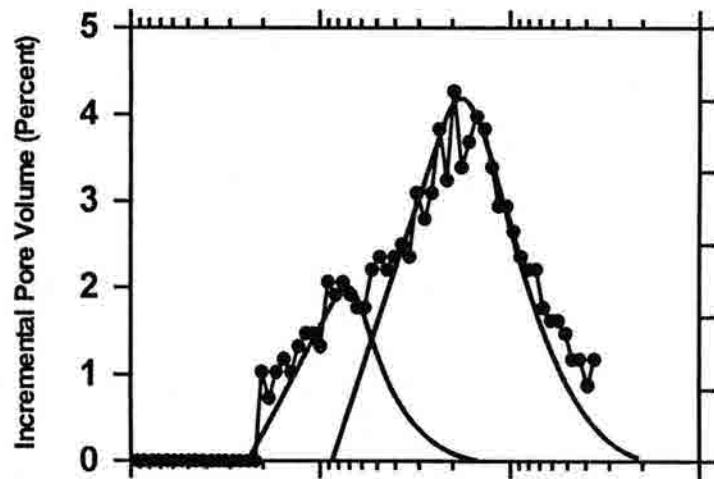
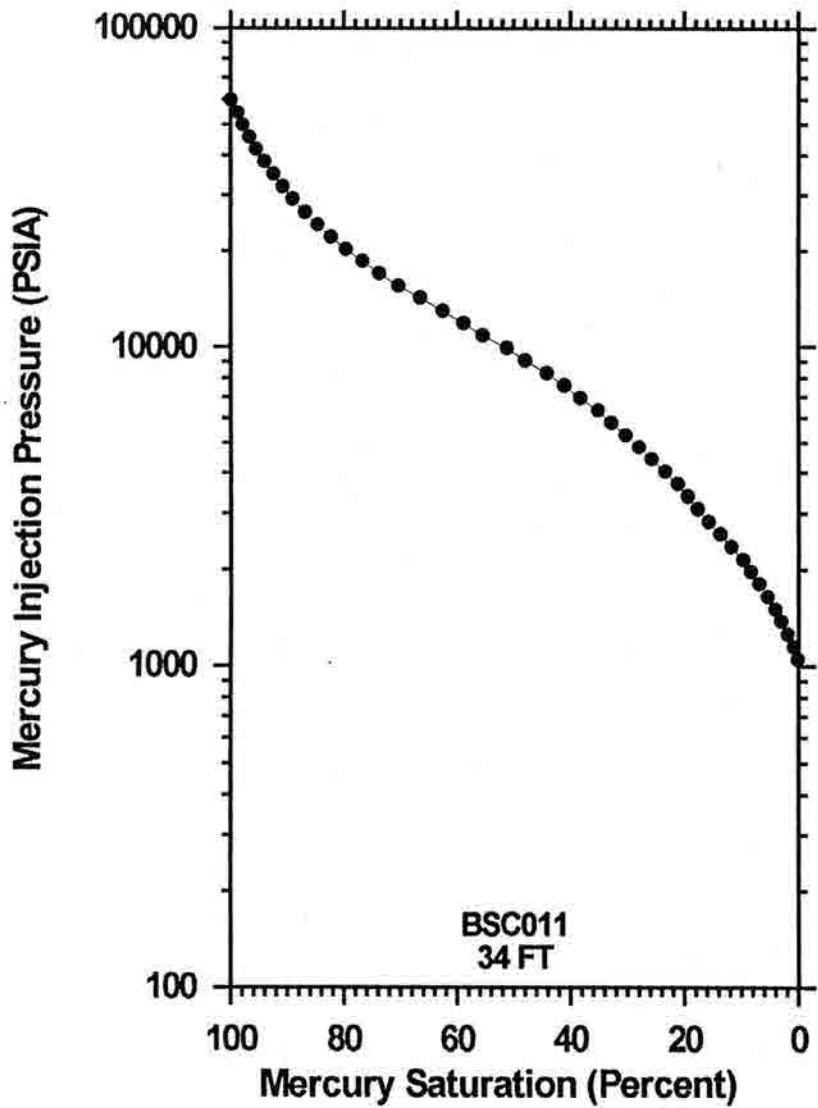


Mercury Injection Pressure (PSIA)

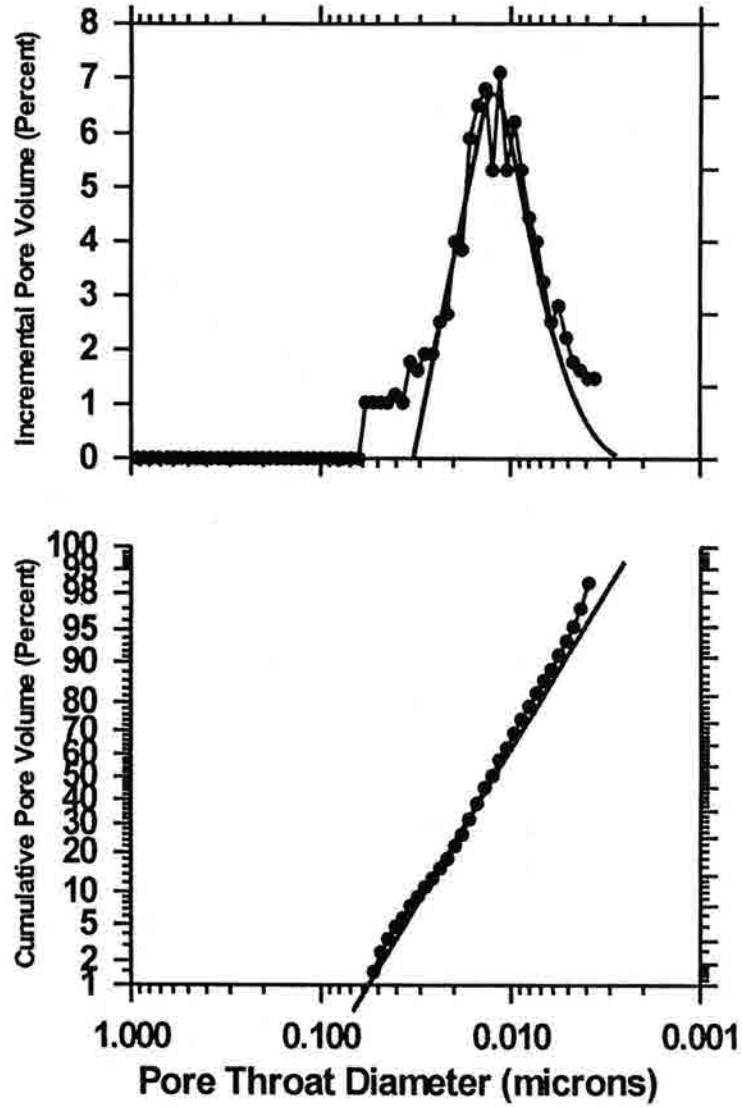
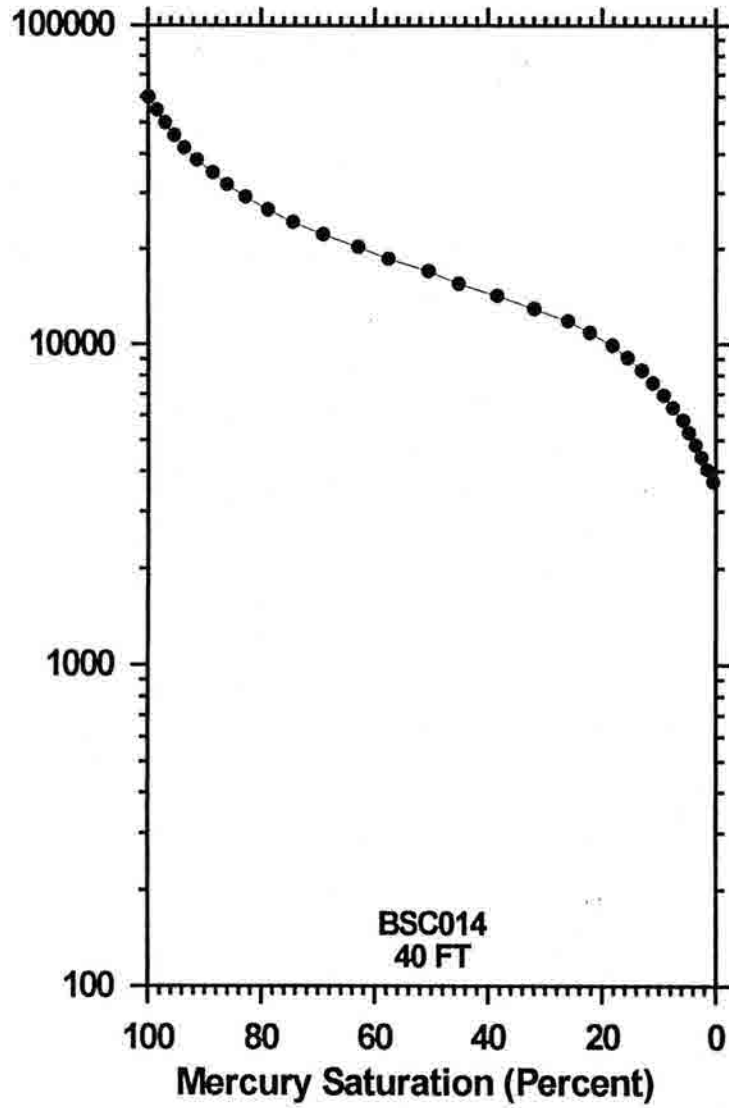


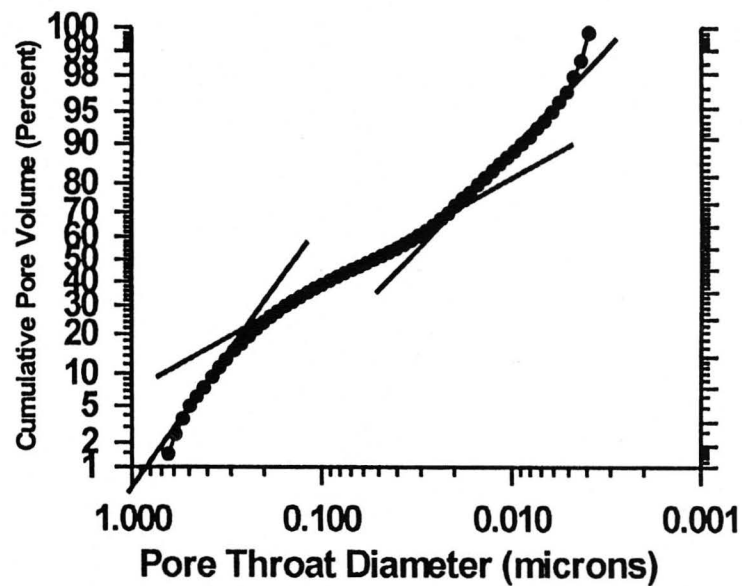
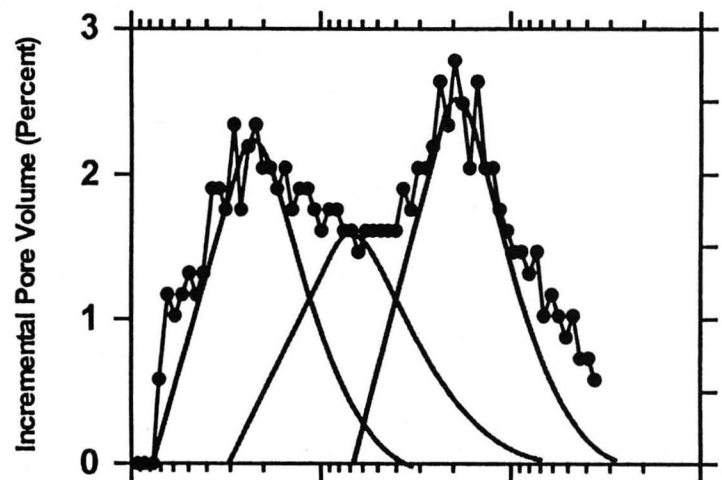
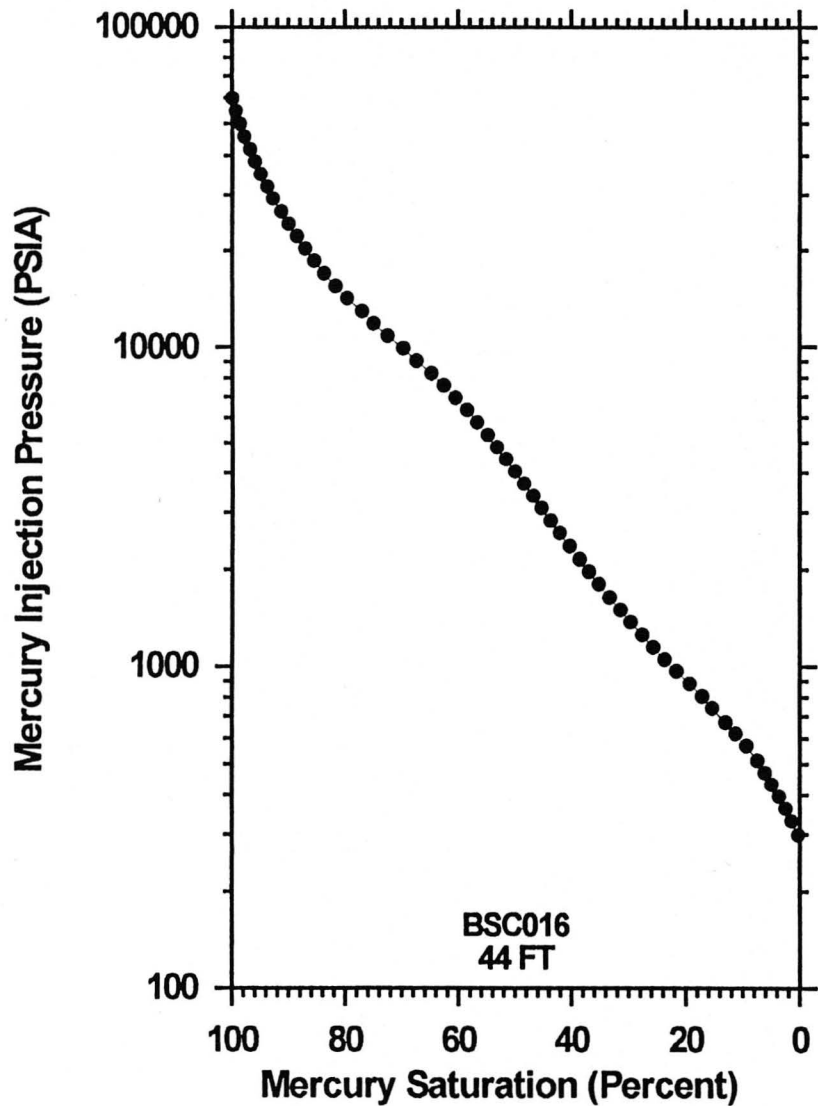


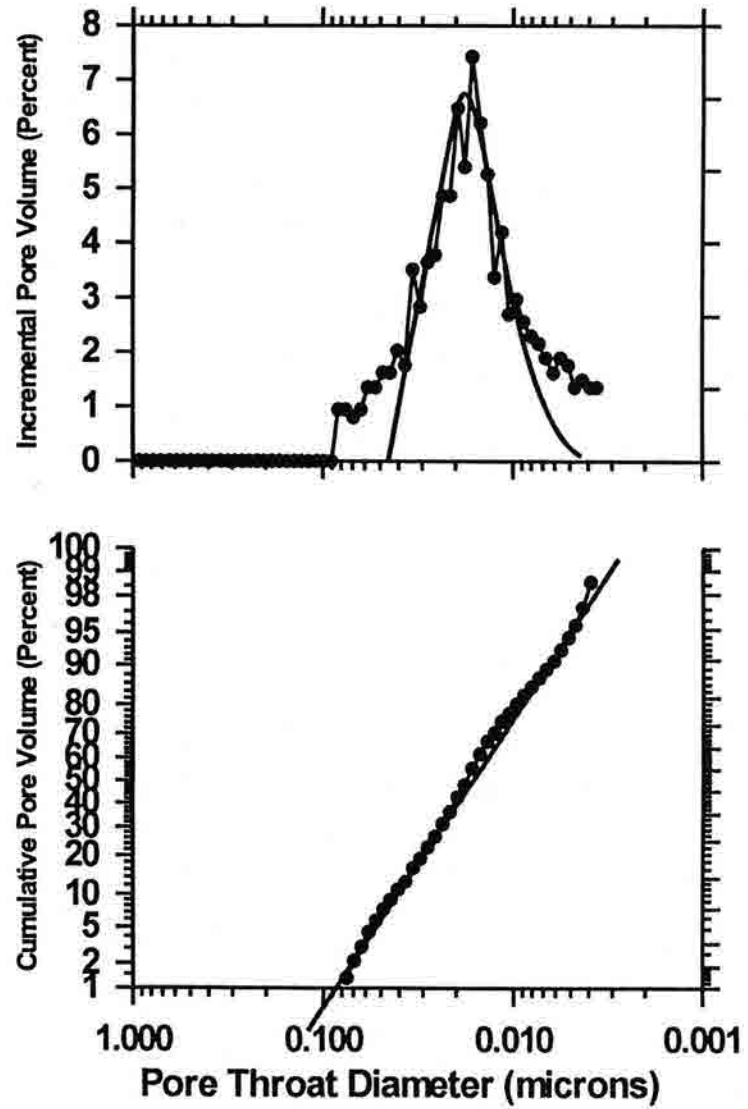
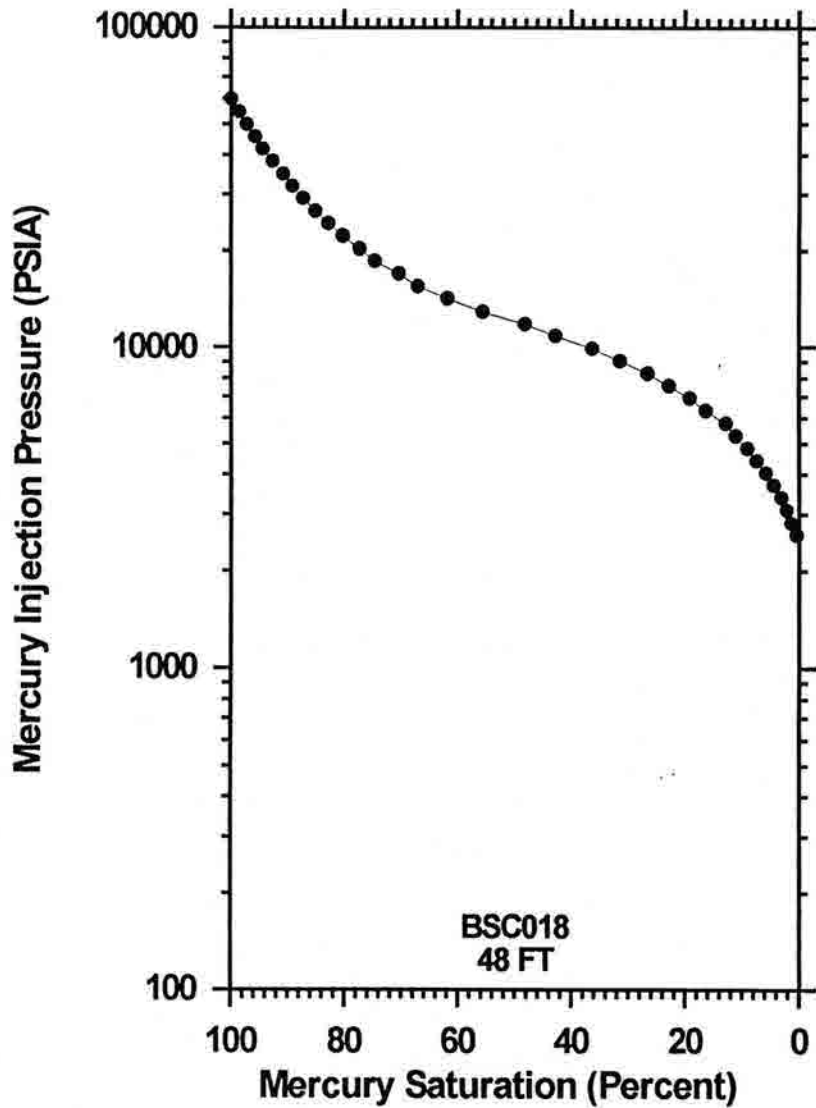


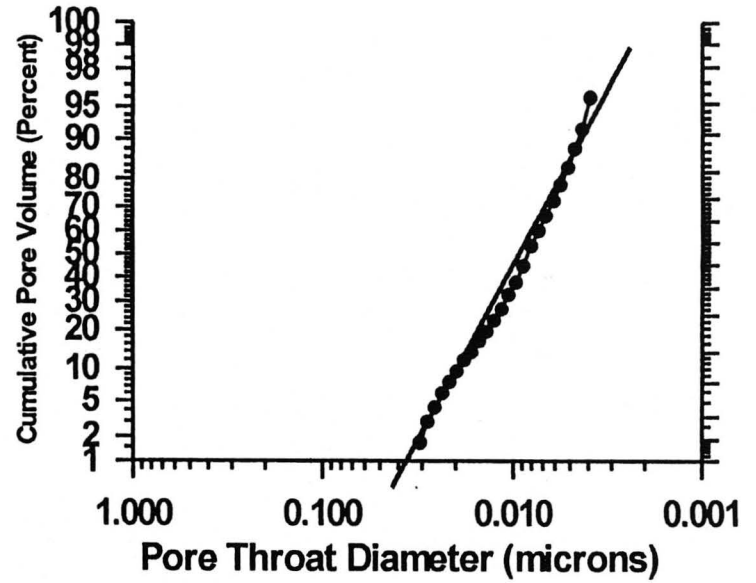
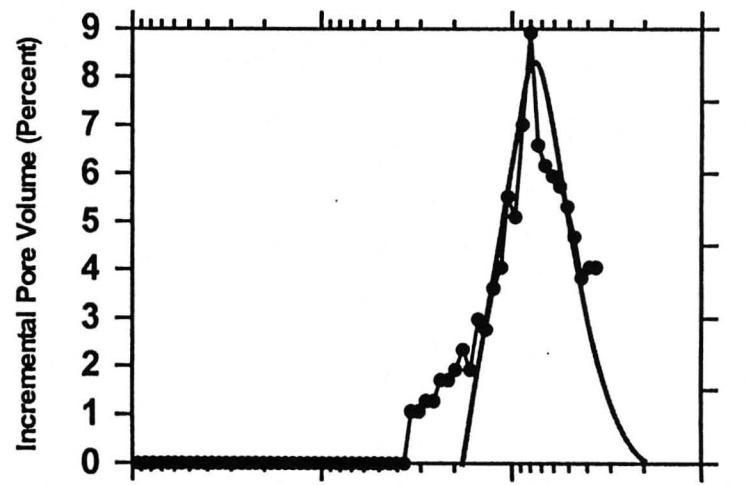
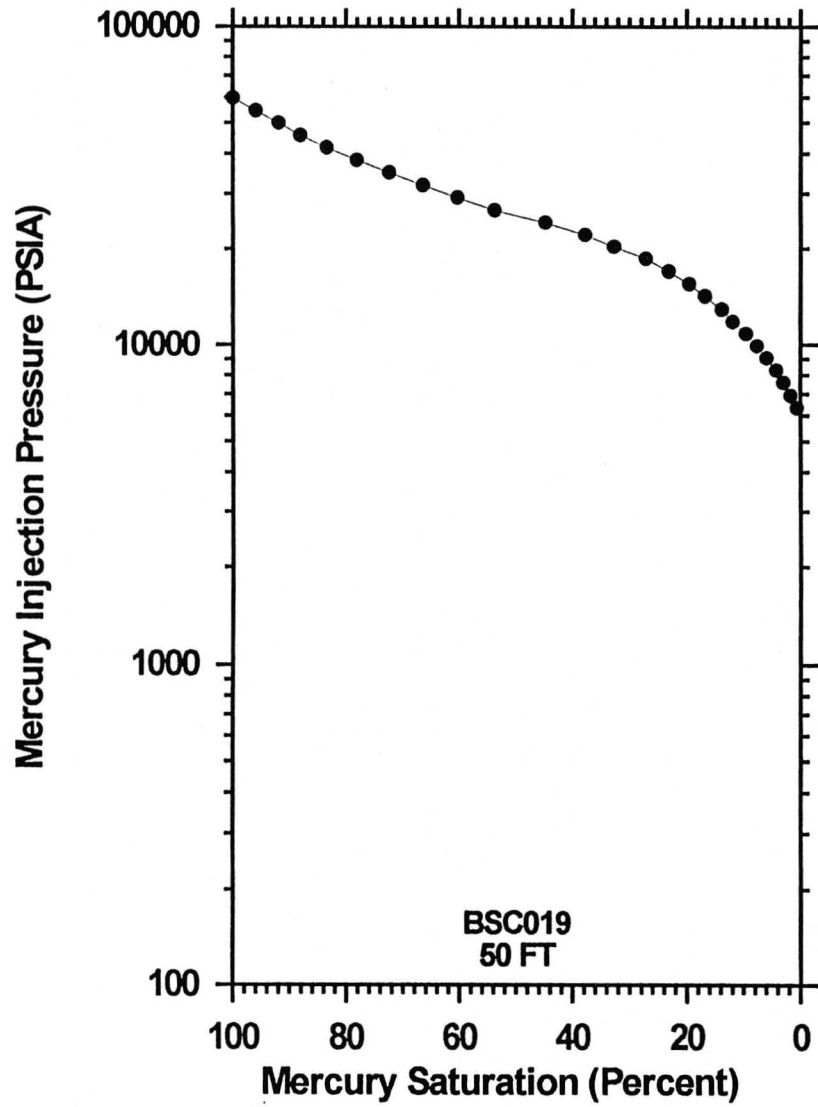


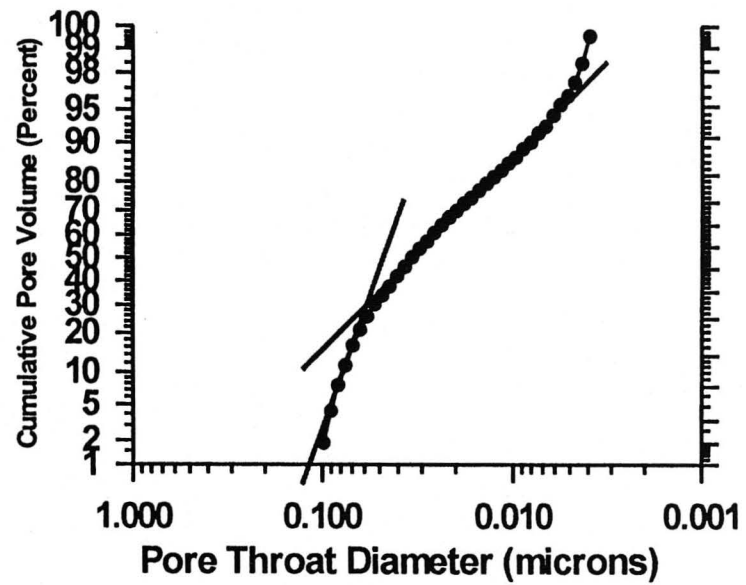
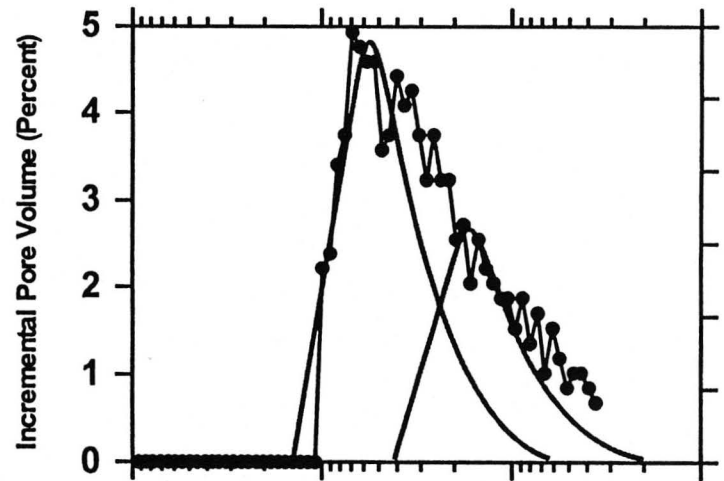
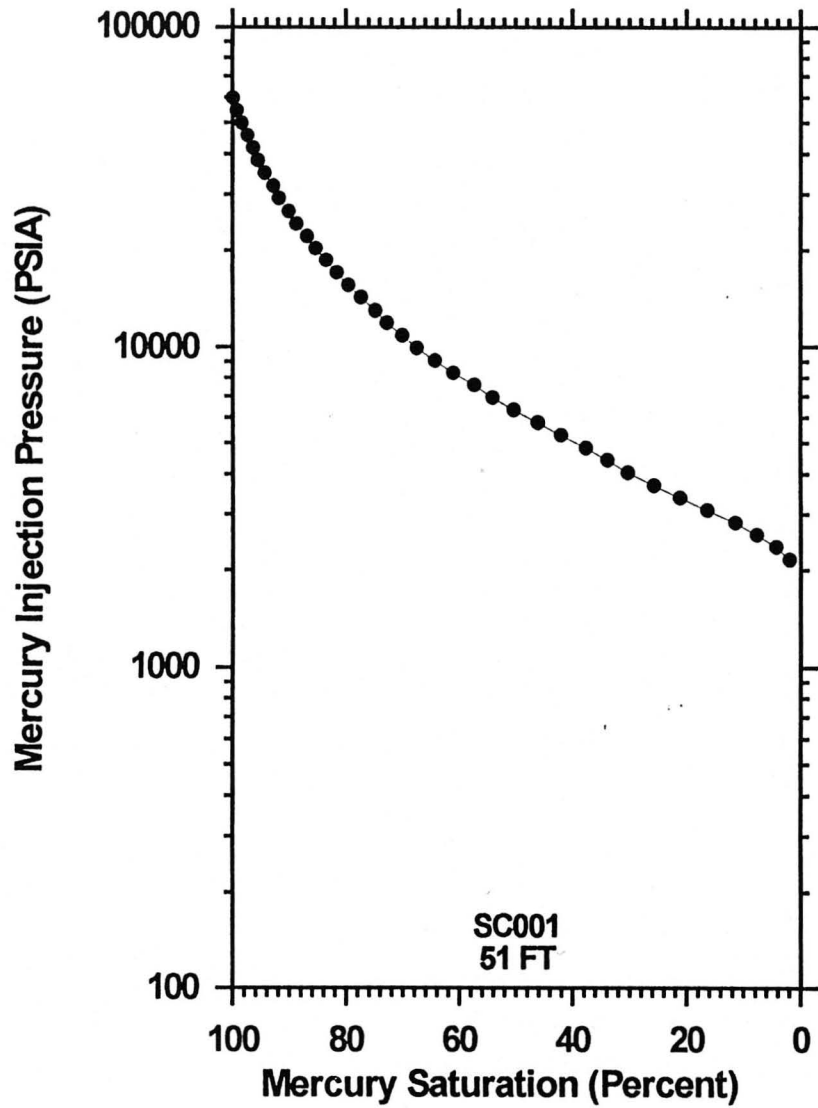
Mercury Injection Pressure (PSIA)



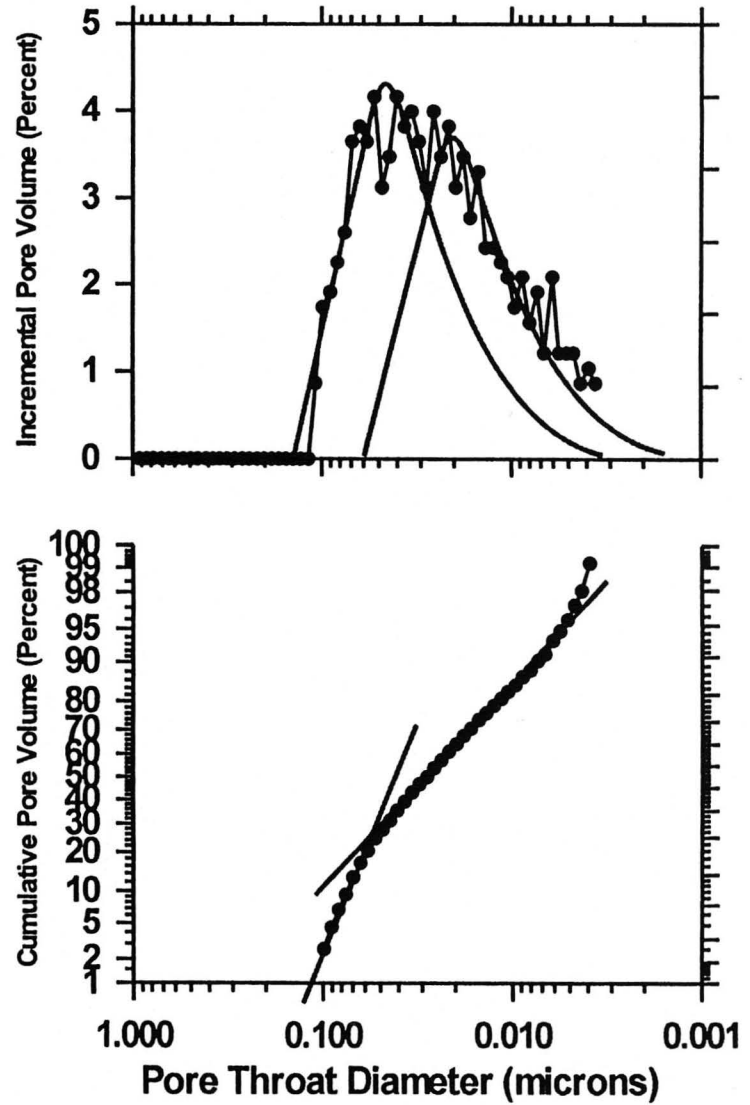
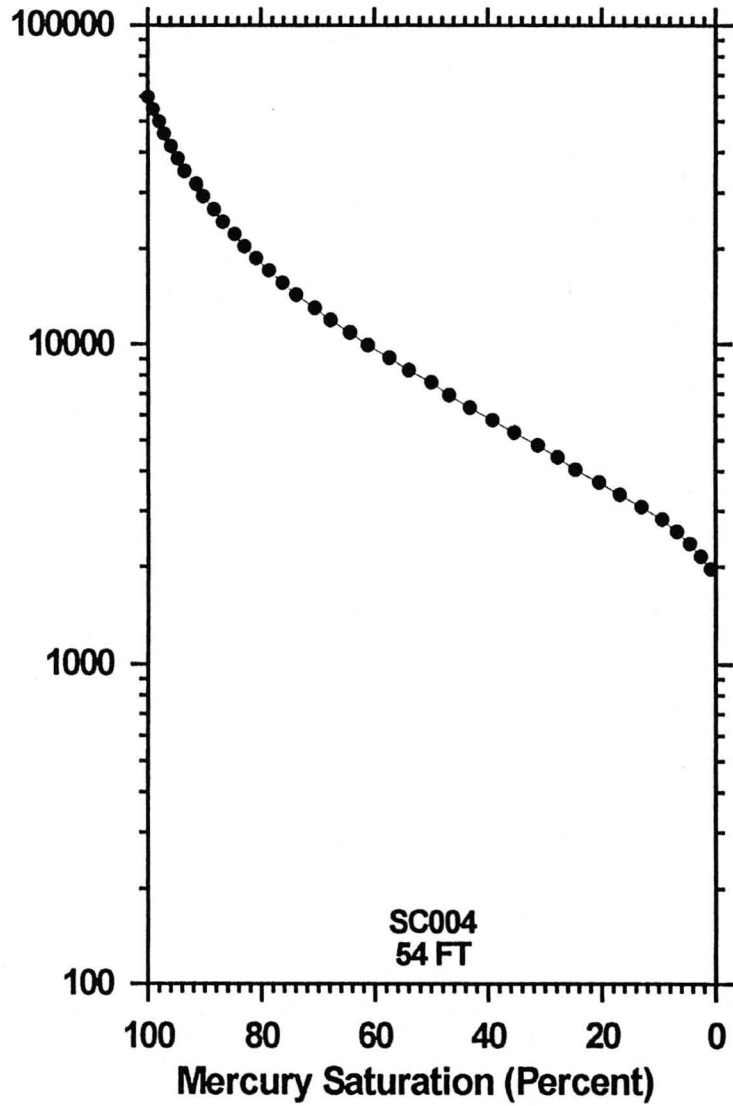


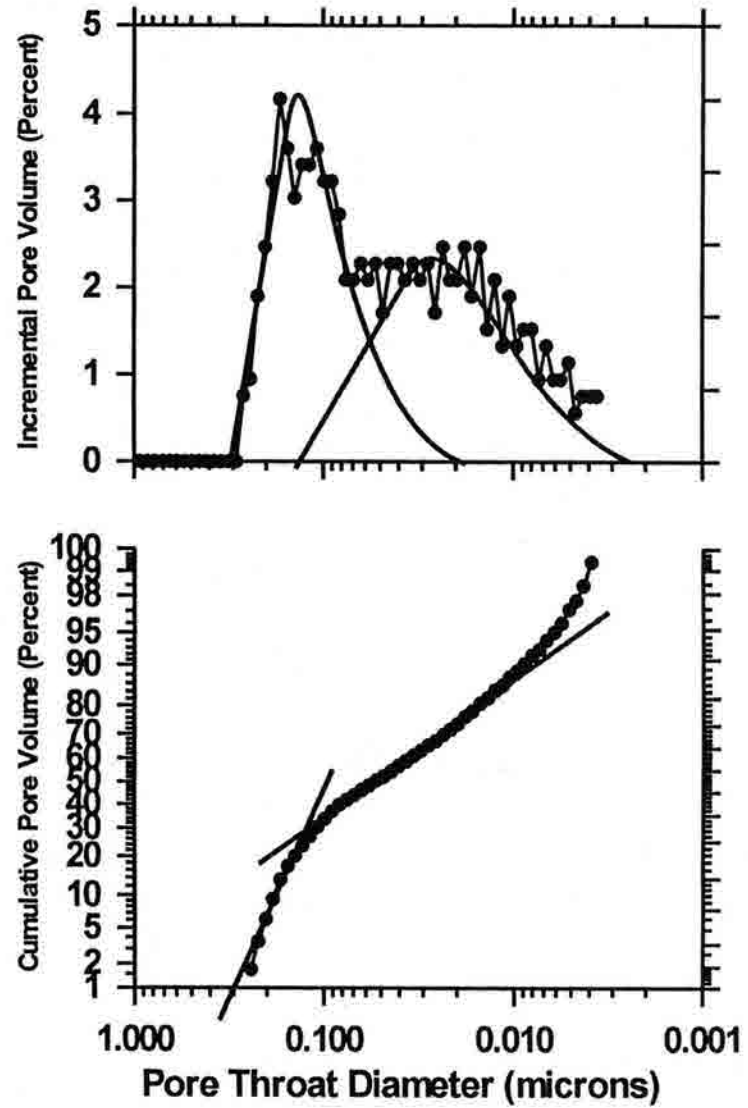
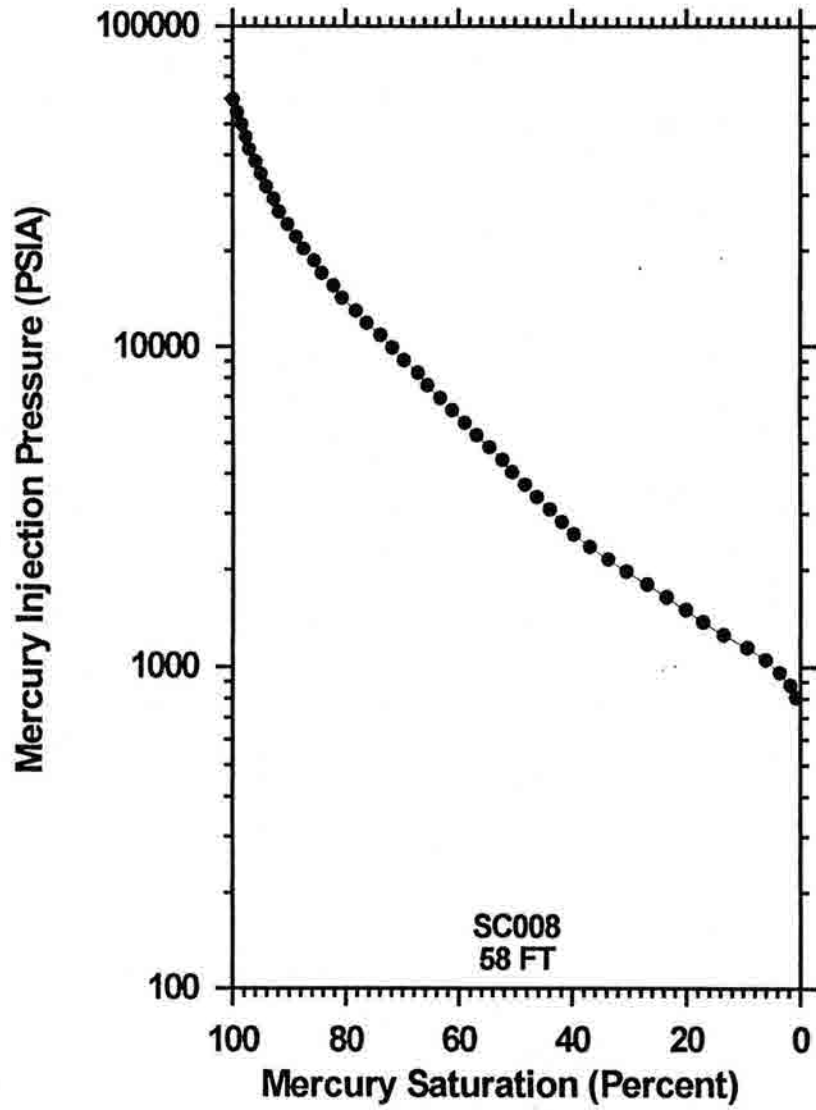


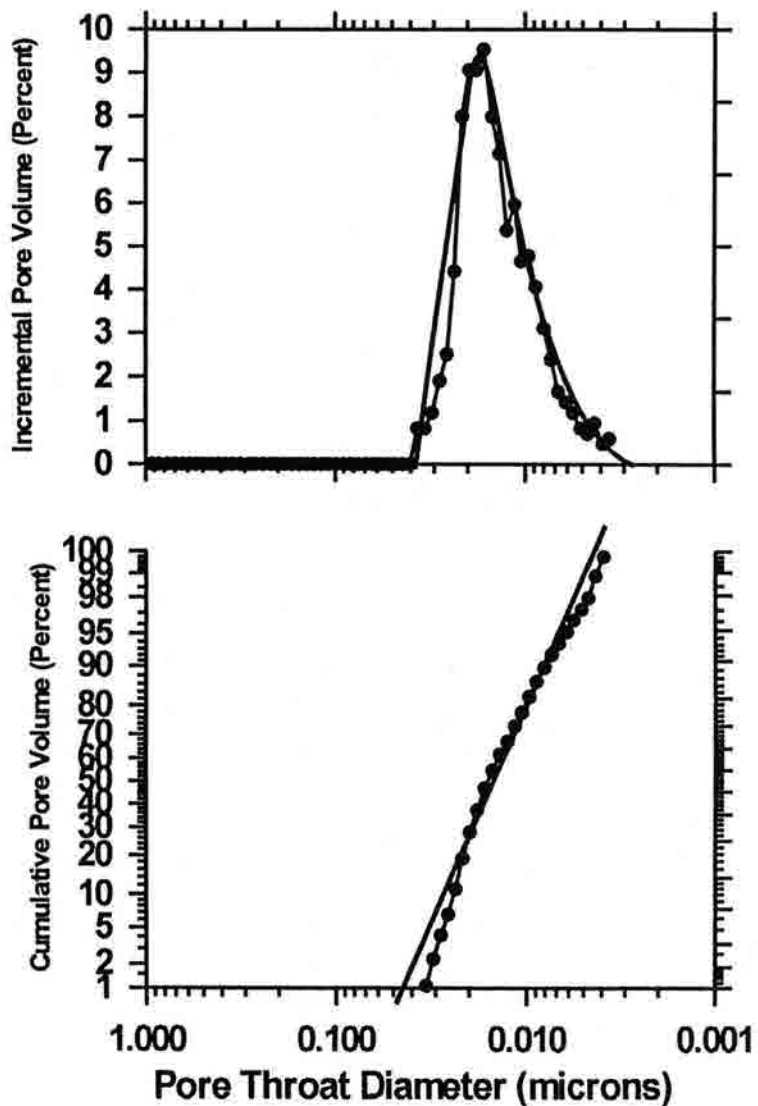
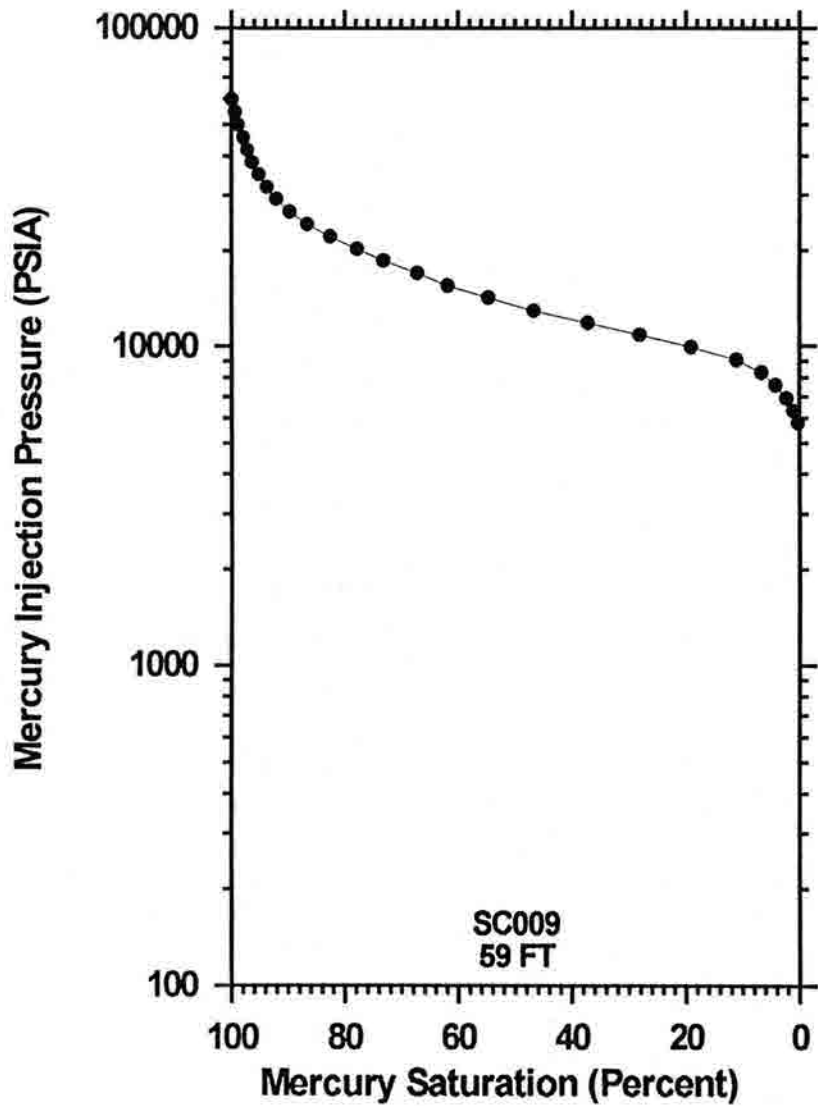


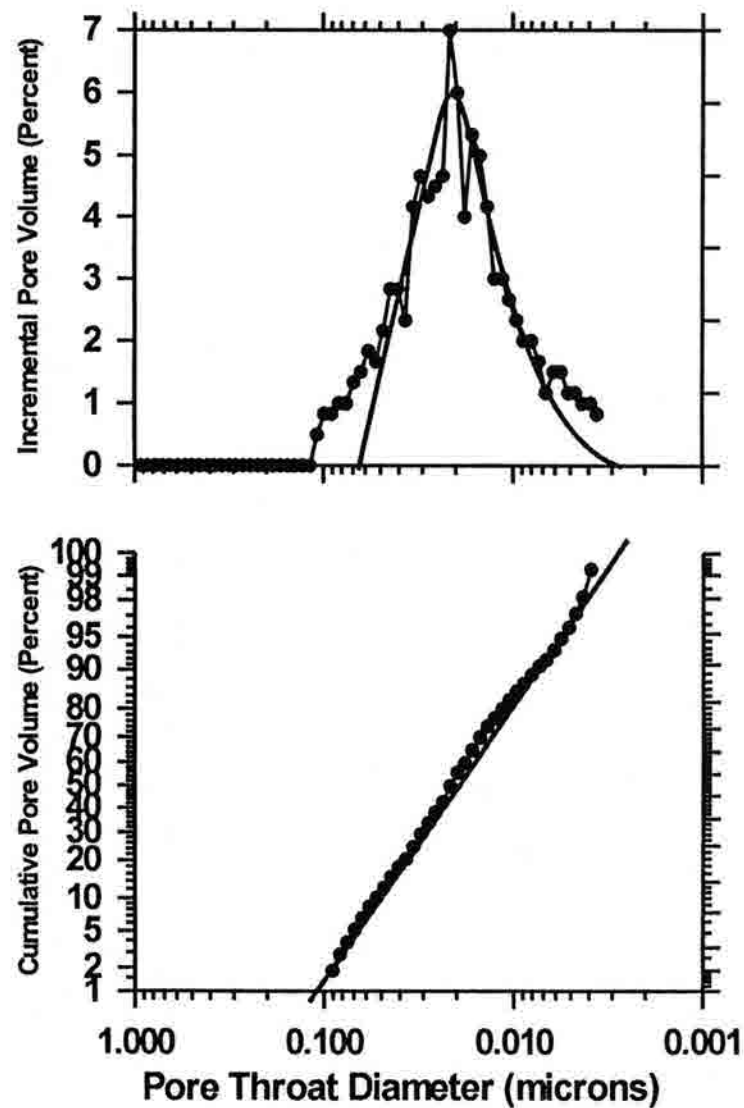
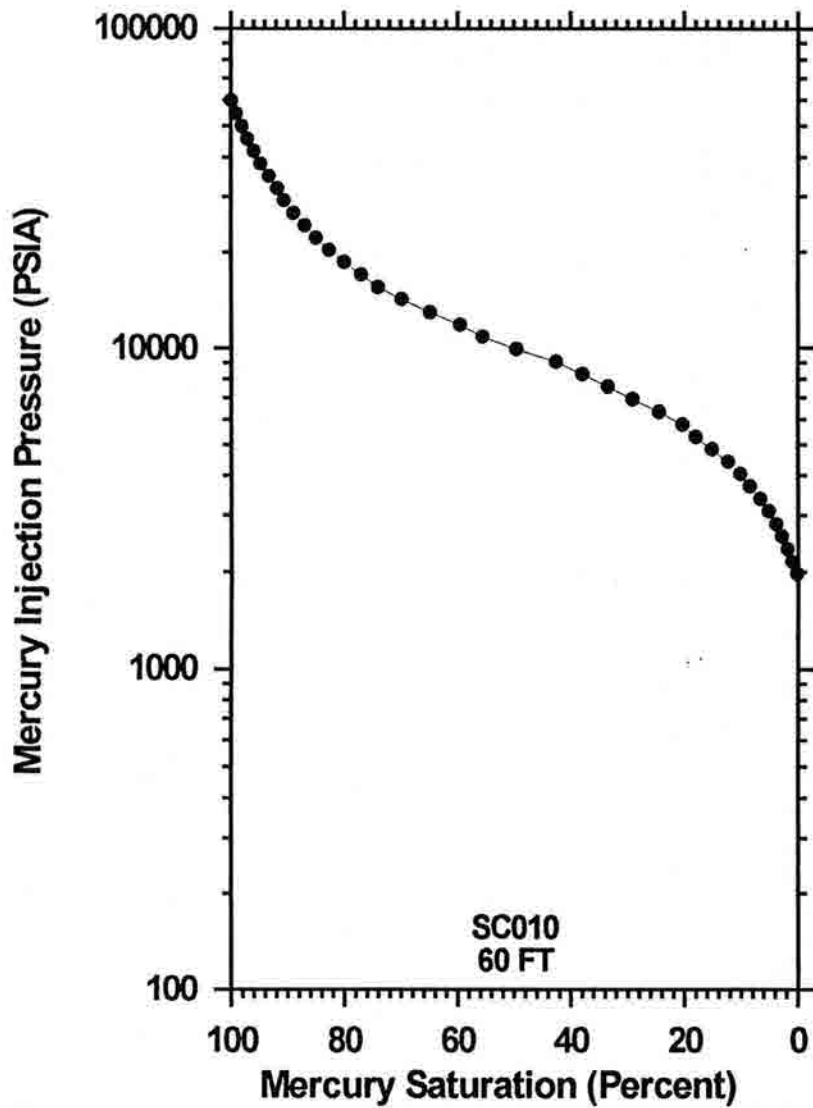


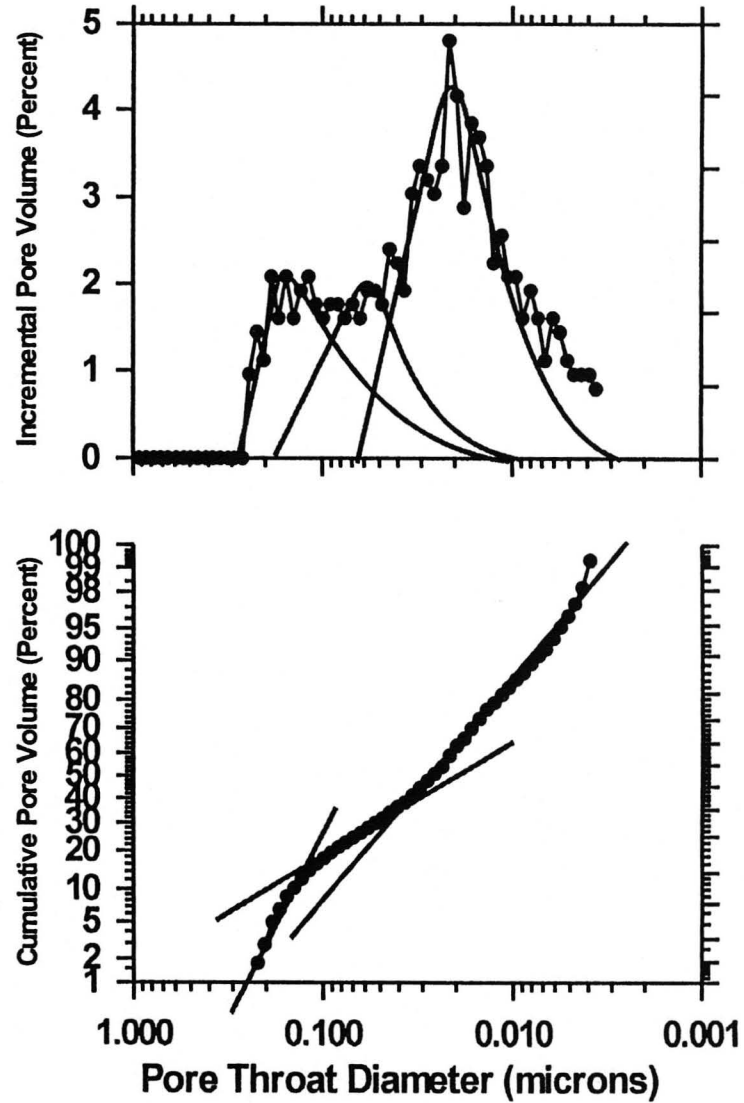
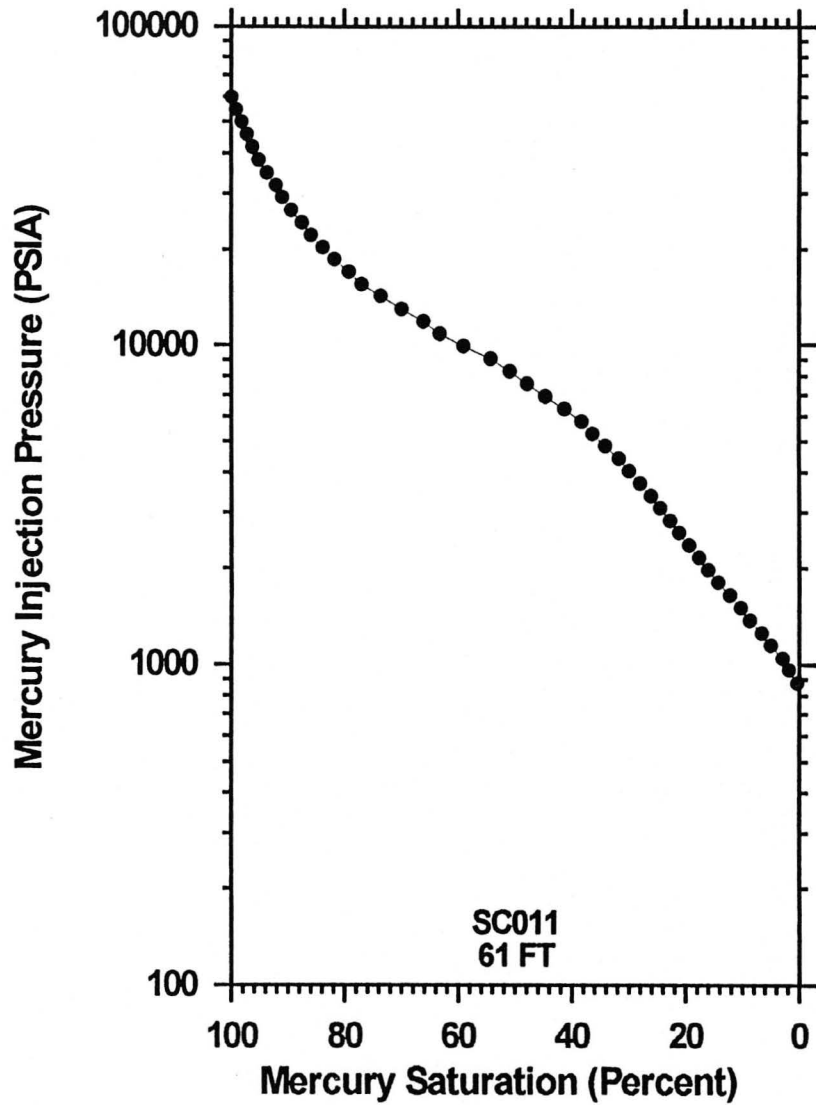
Mercury Injection Pressure (PSIA)



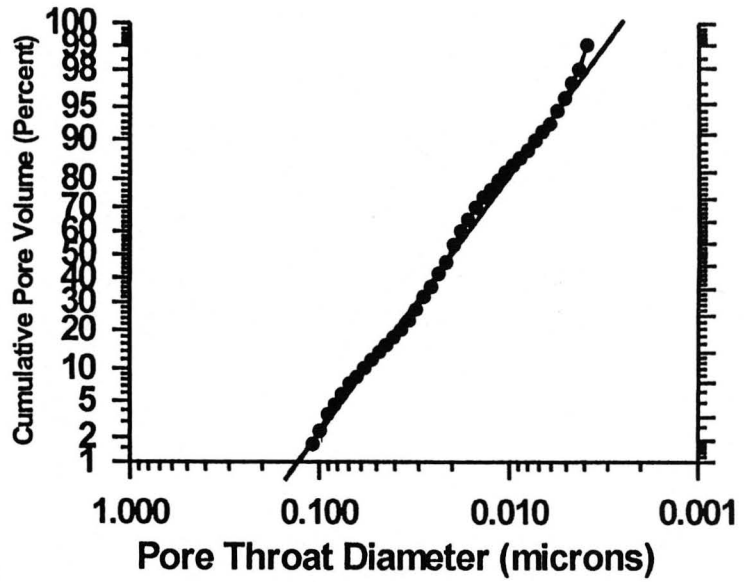
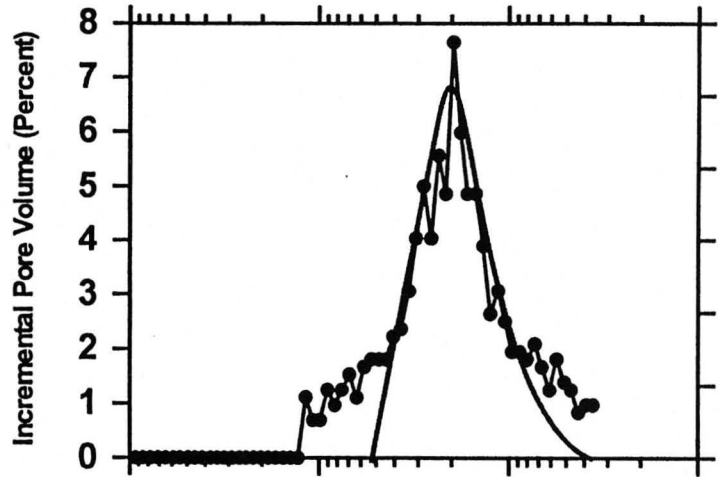
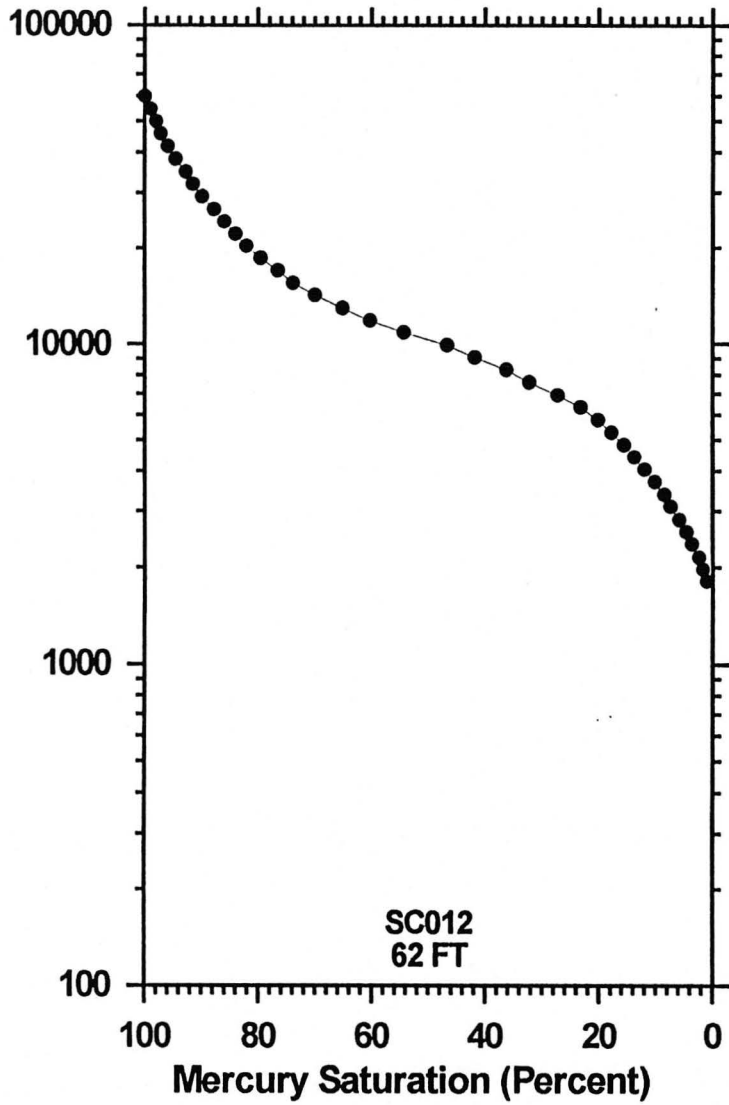


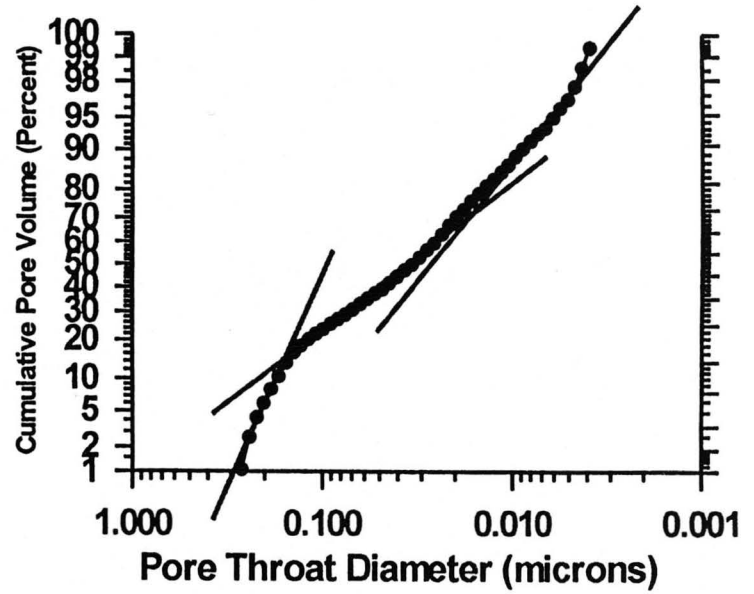
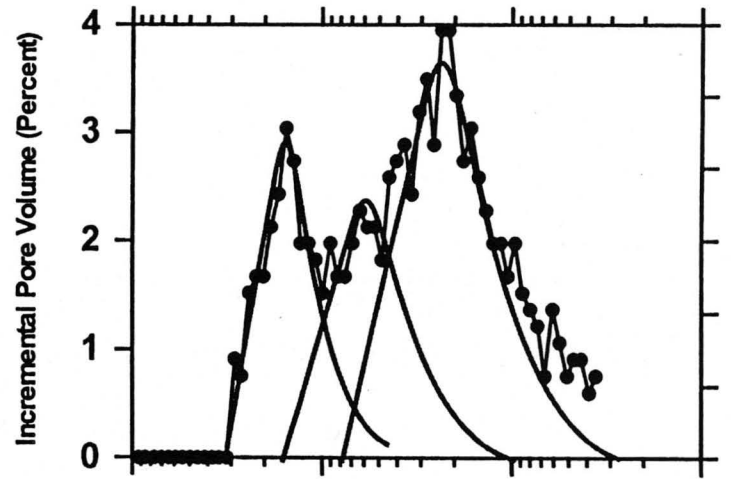
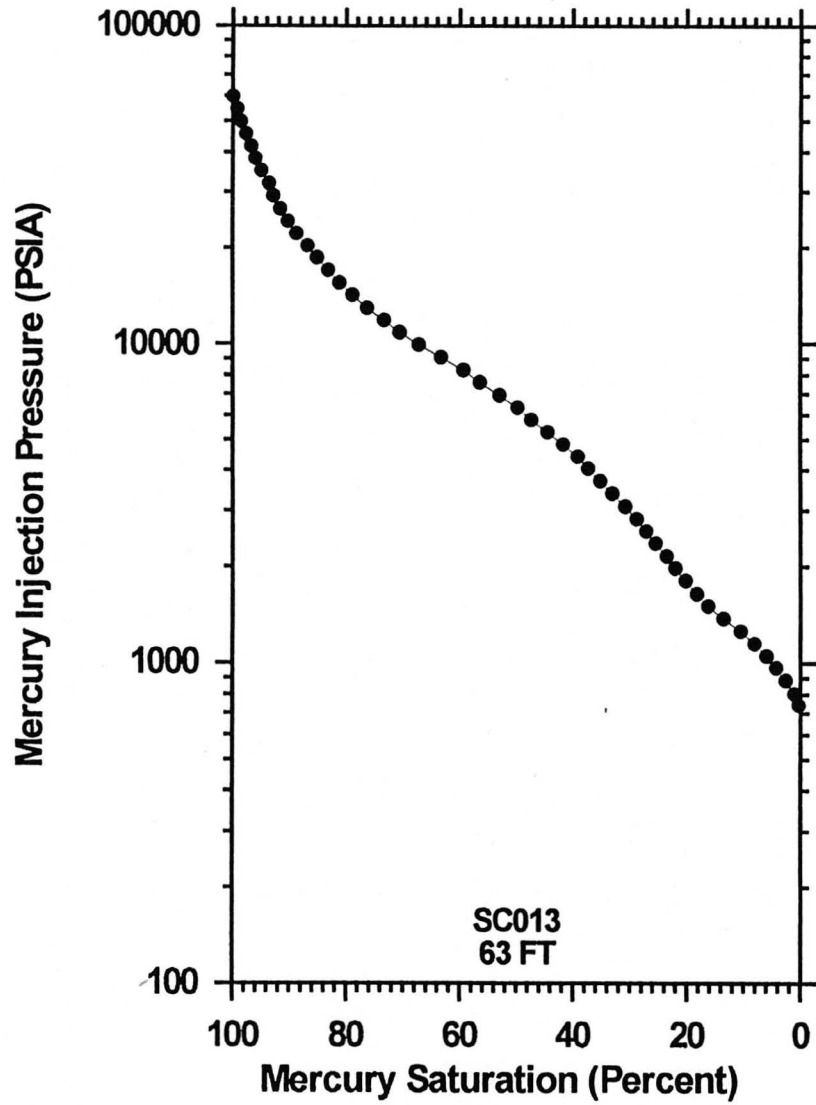




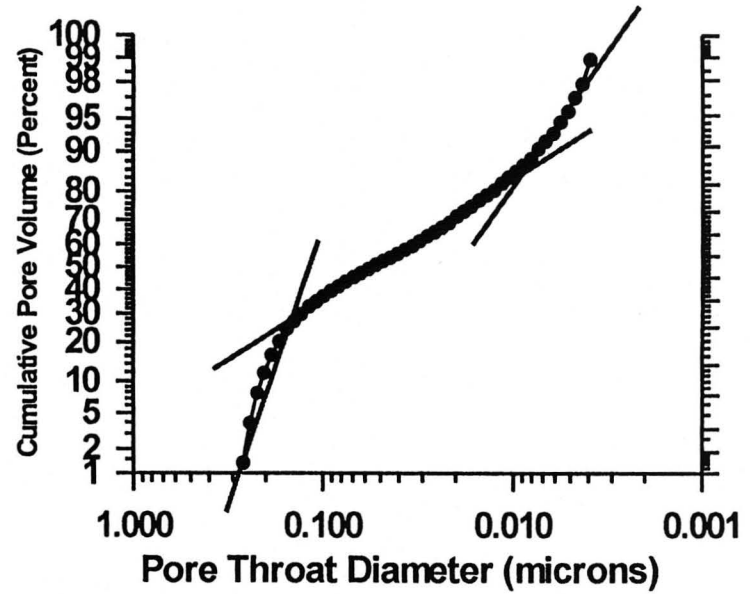
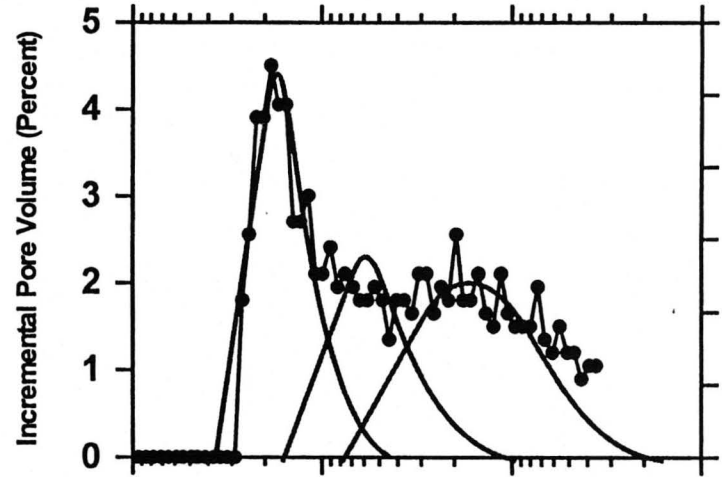
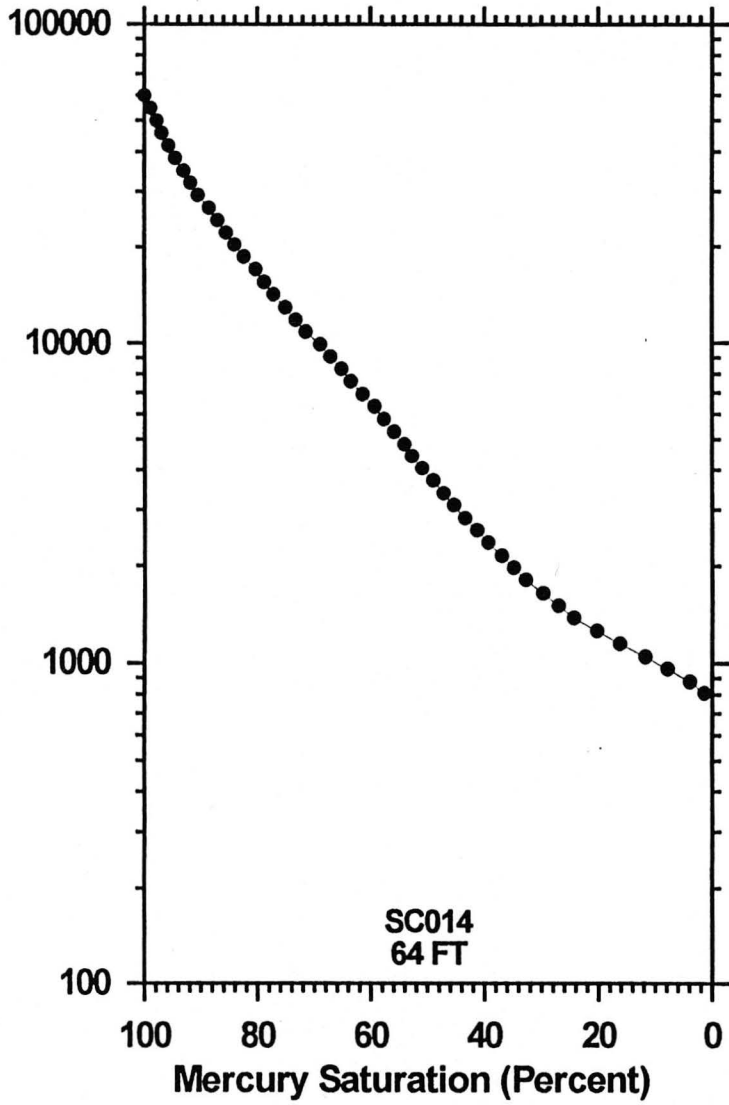


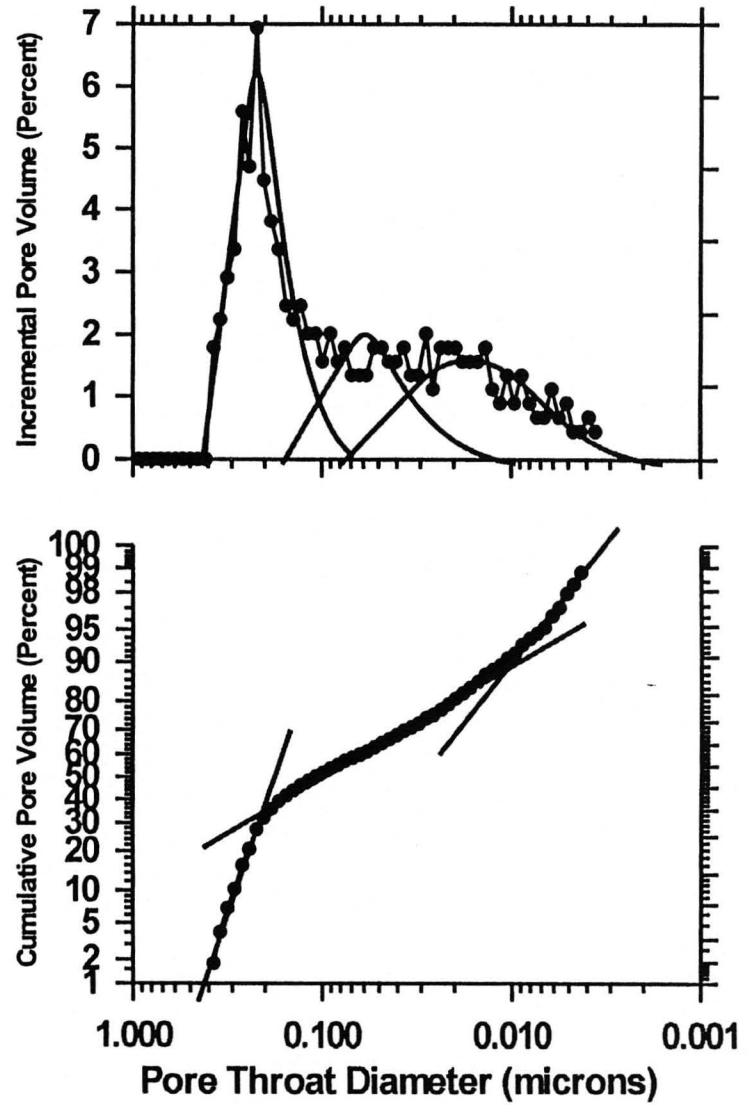
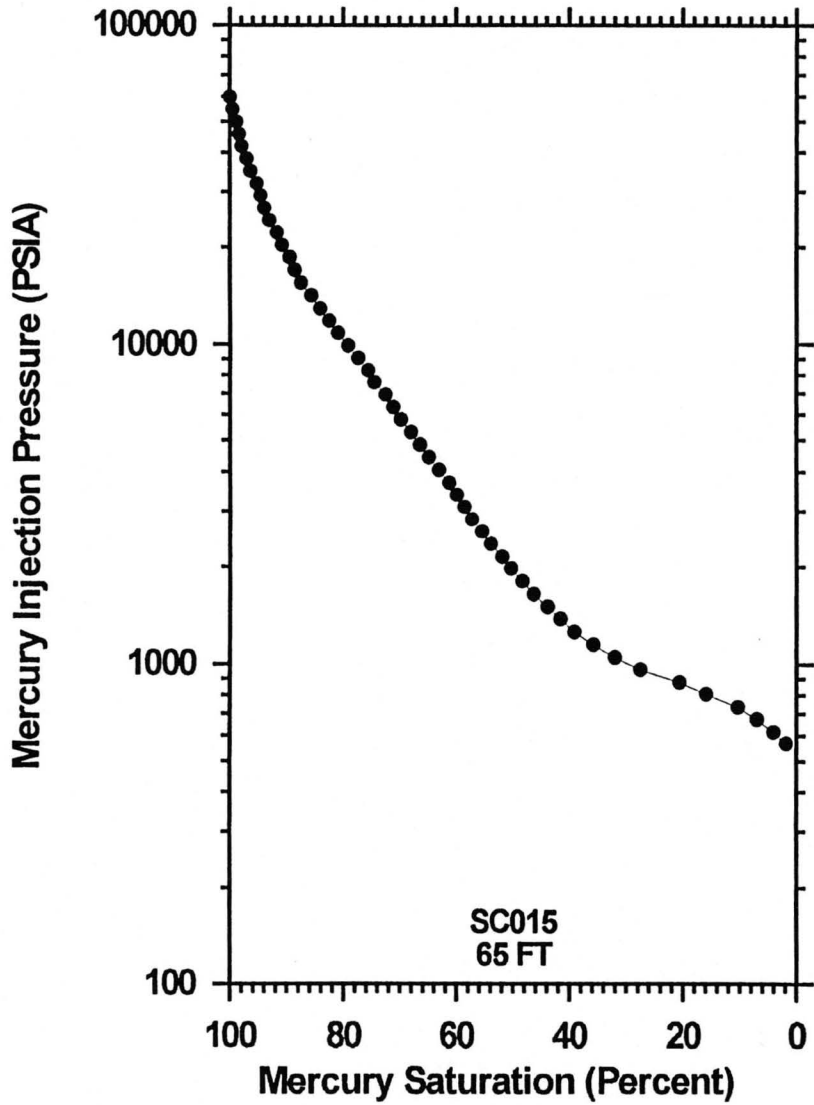
Mercury Injection Pressure (PSIA)

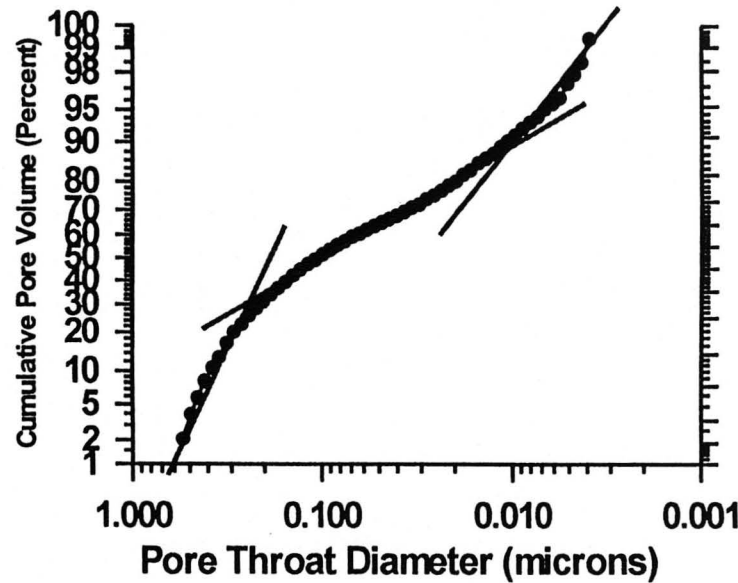
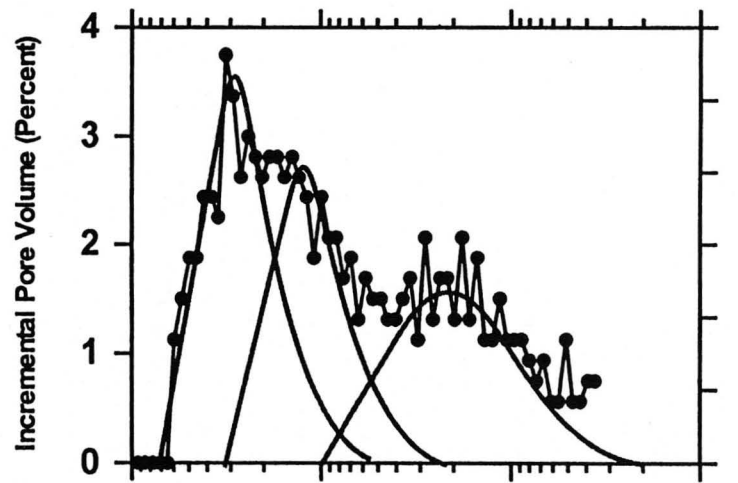
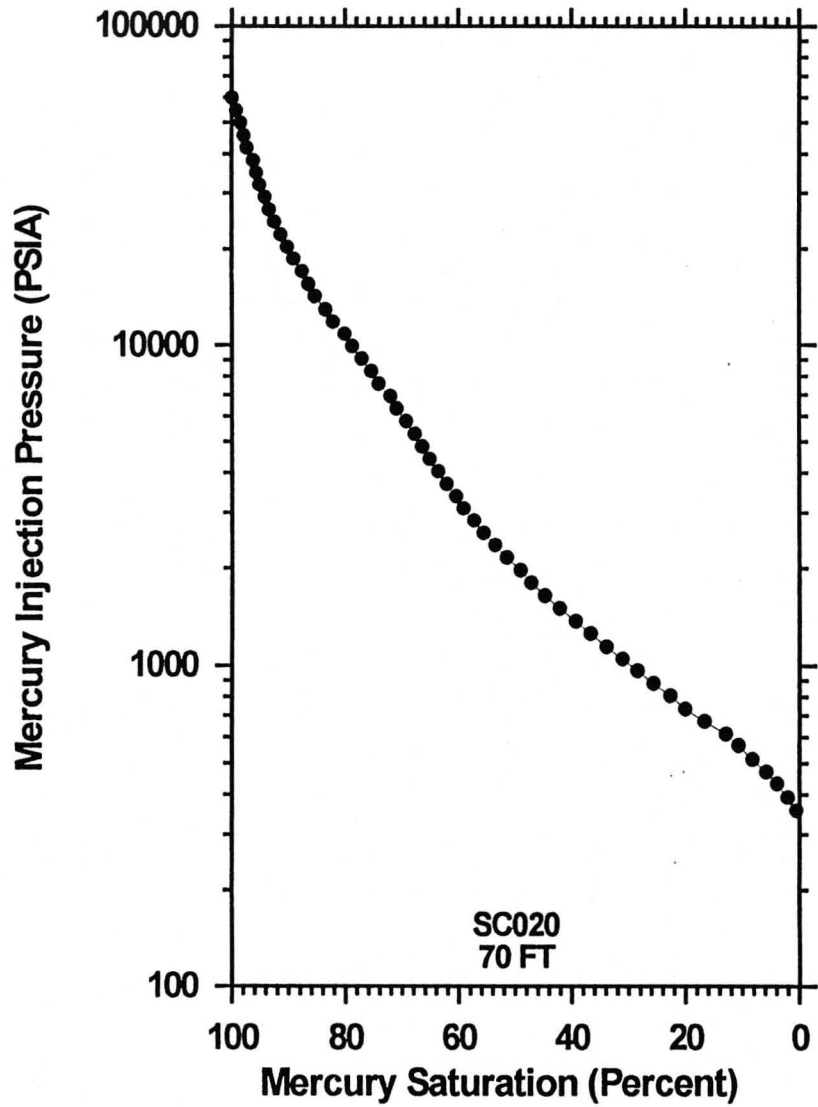




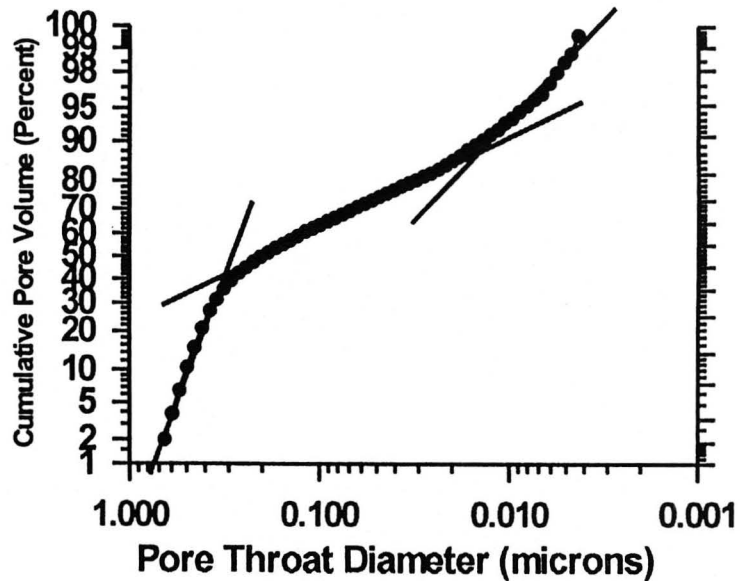
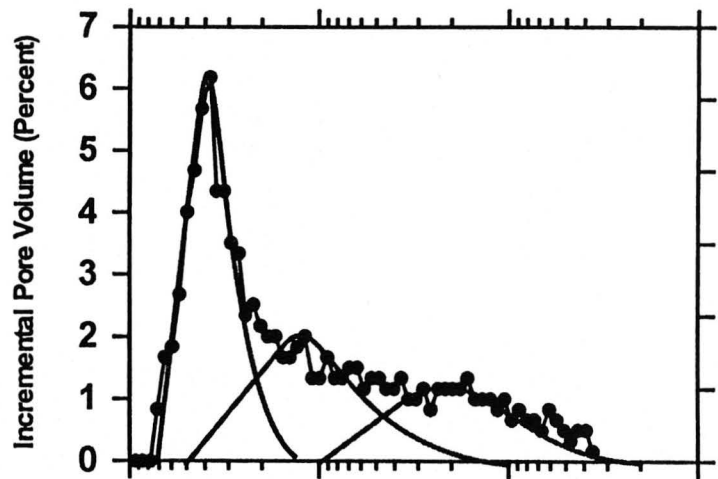
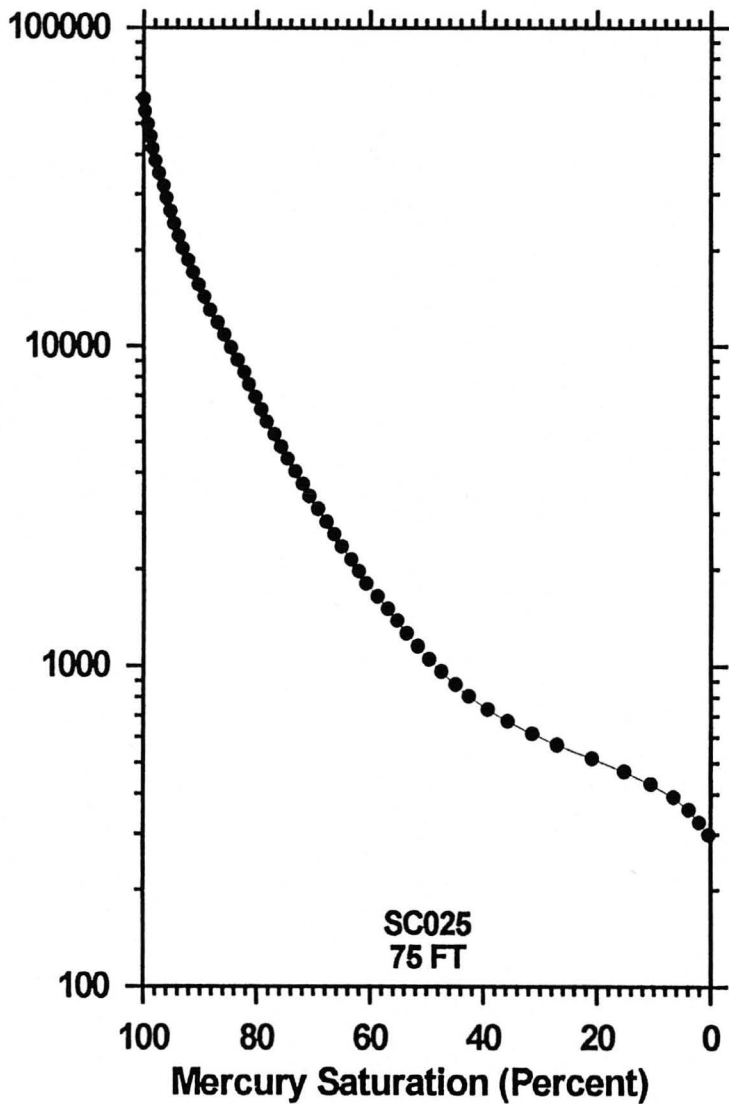
Mercury Injection Pressure (PSIA)

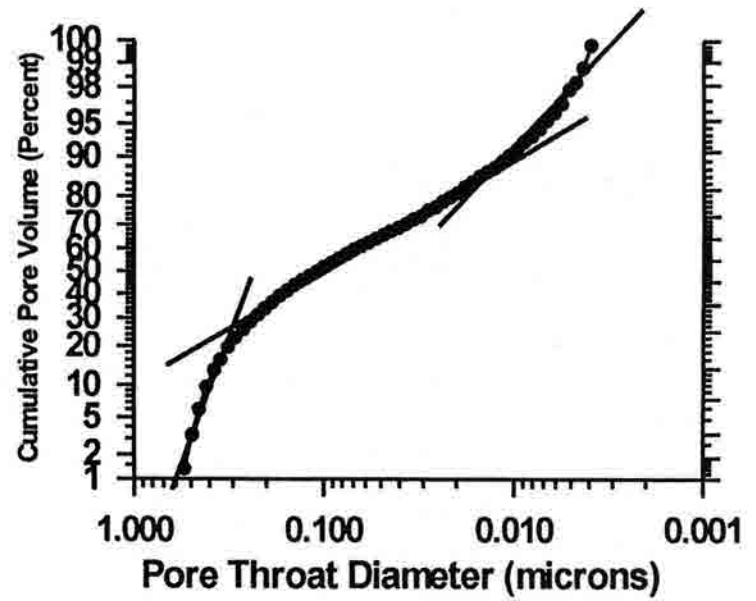
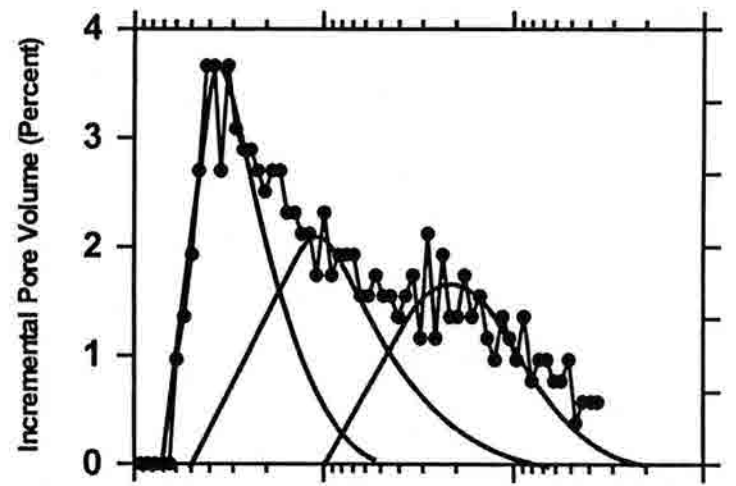
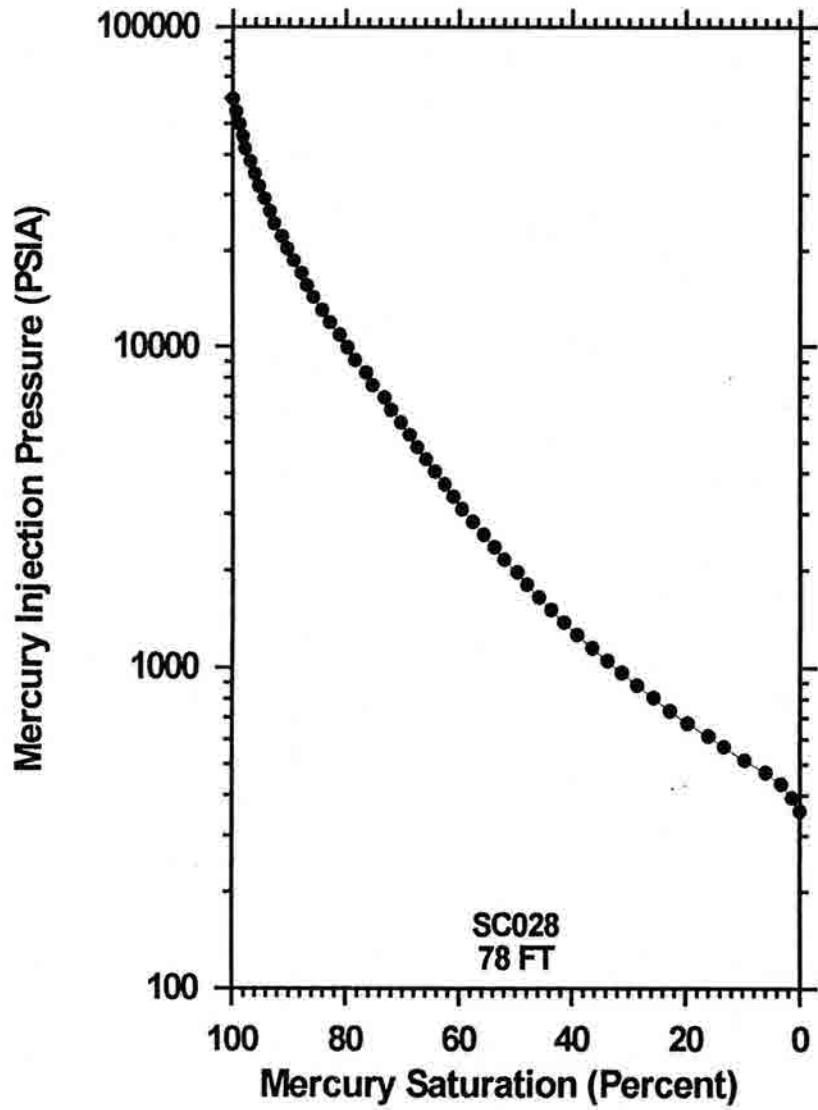


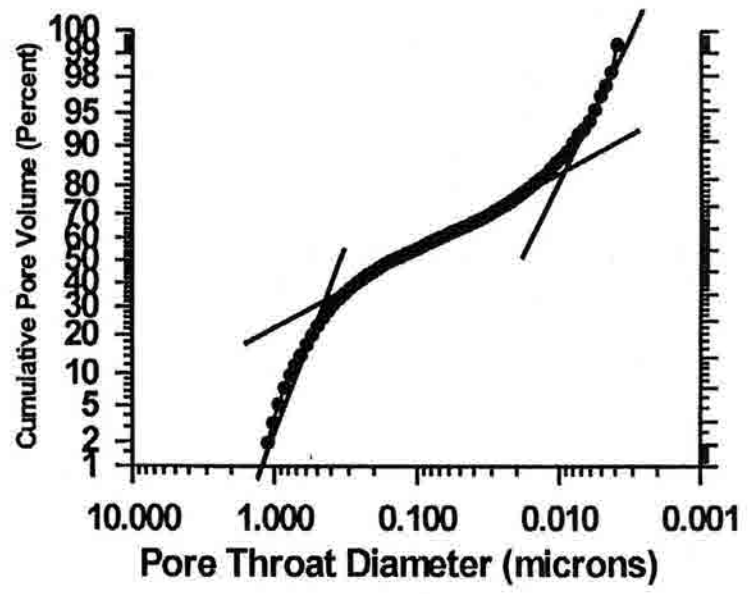
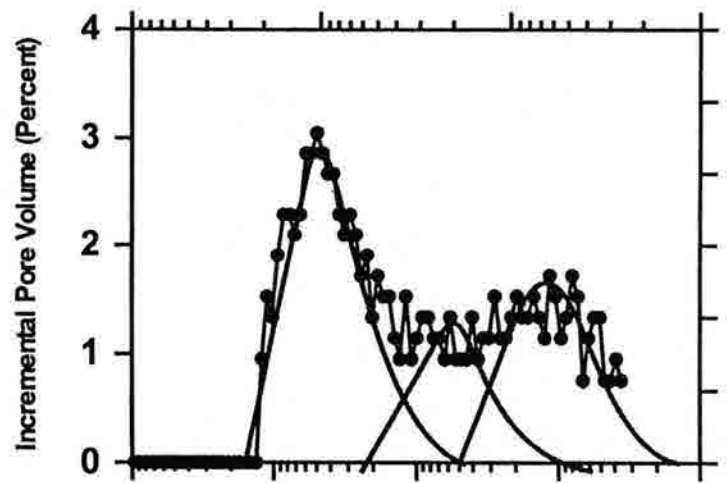
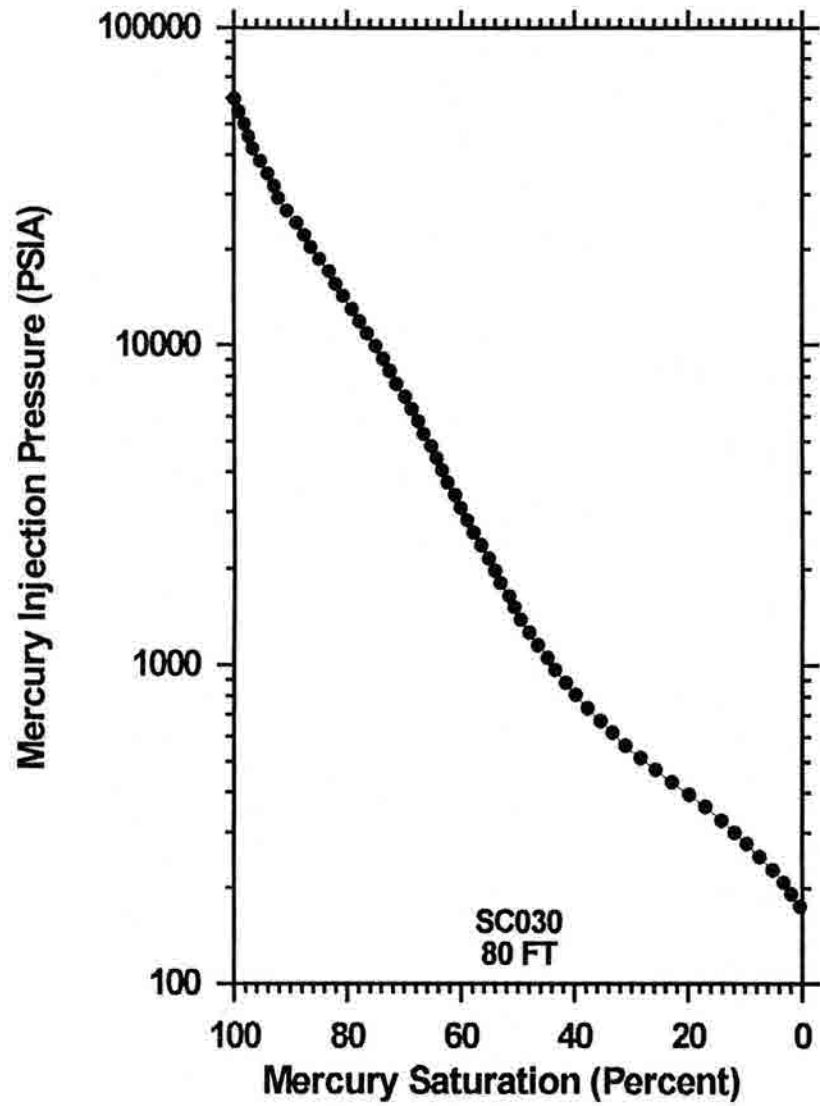


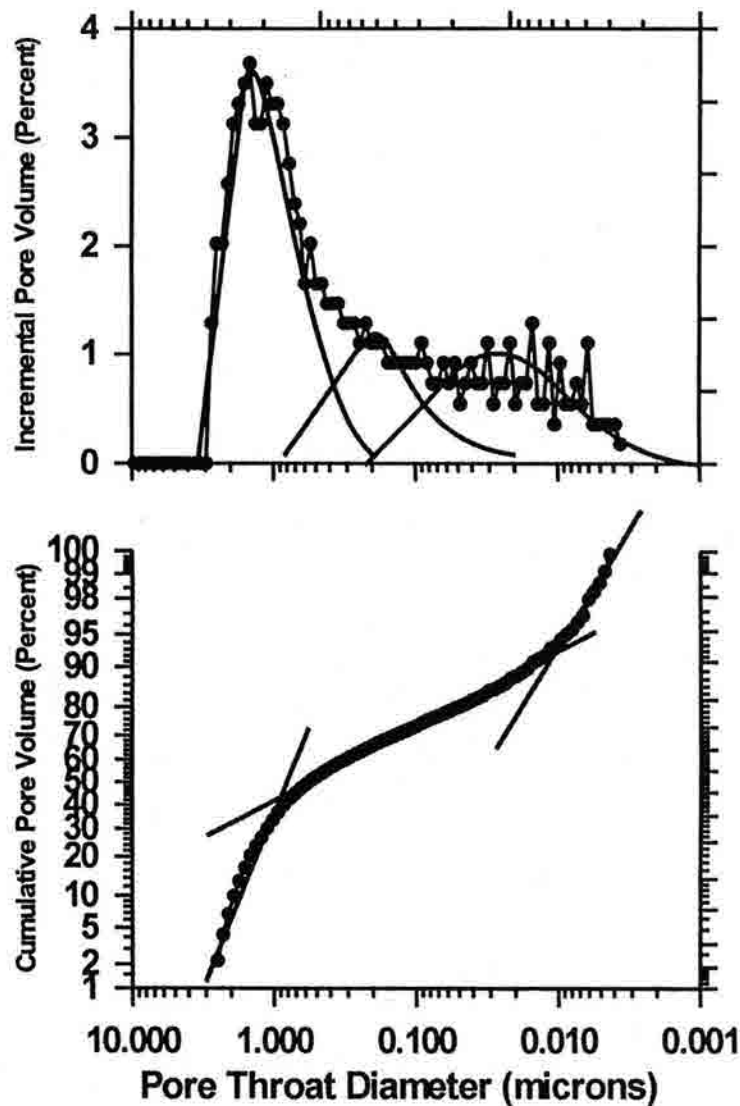
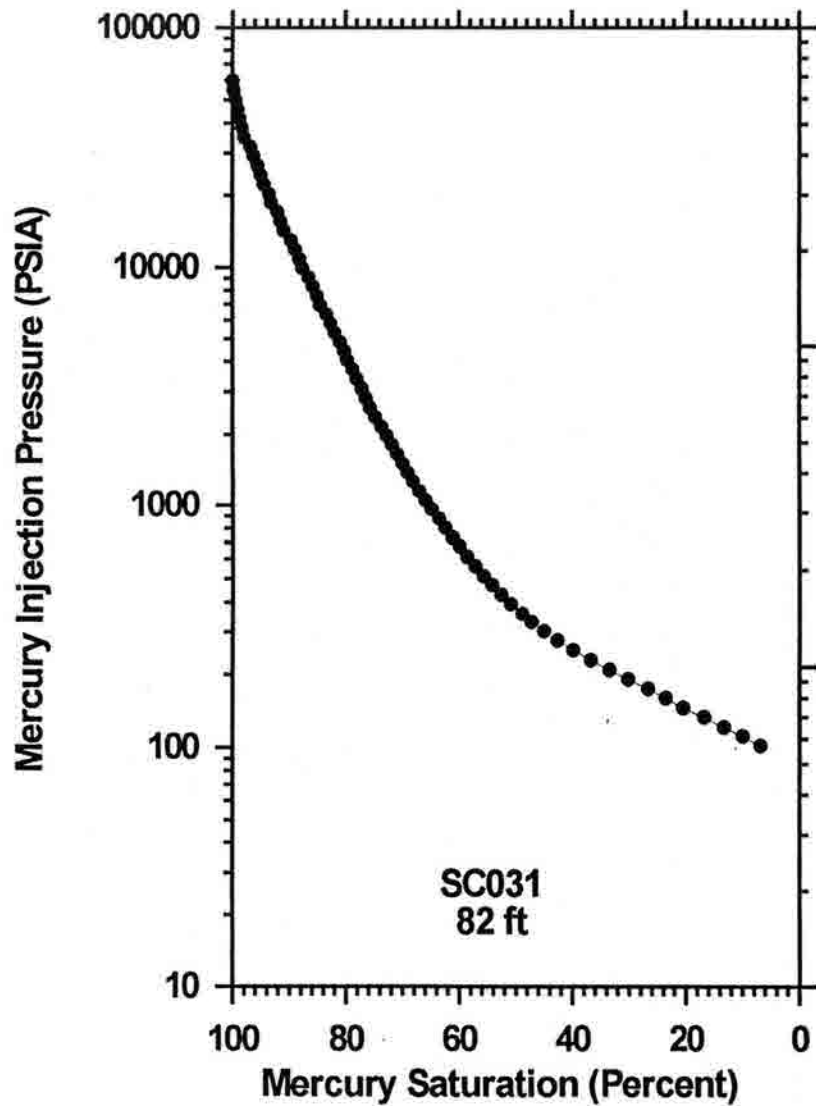


Mercury Injection Pressure (PSIA)

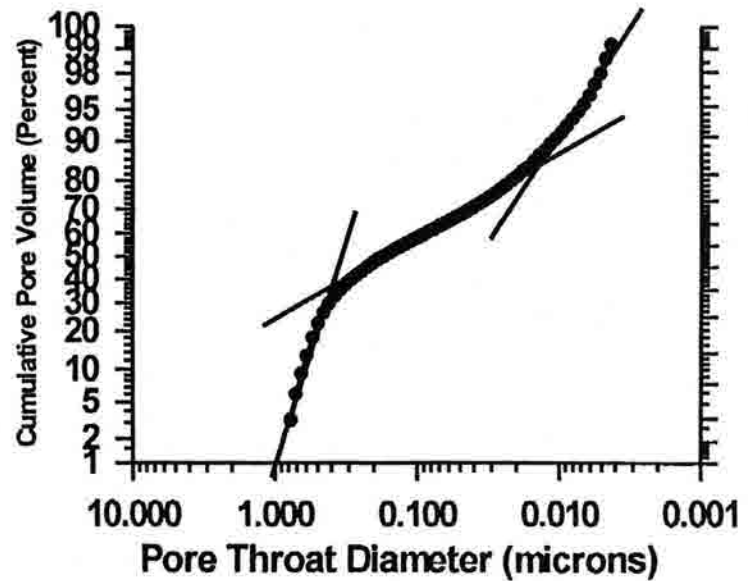
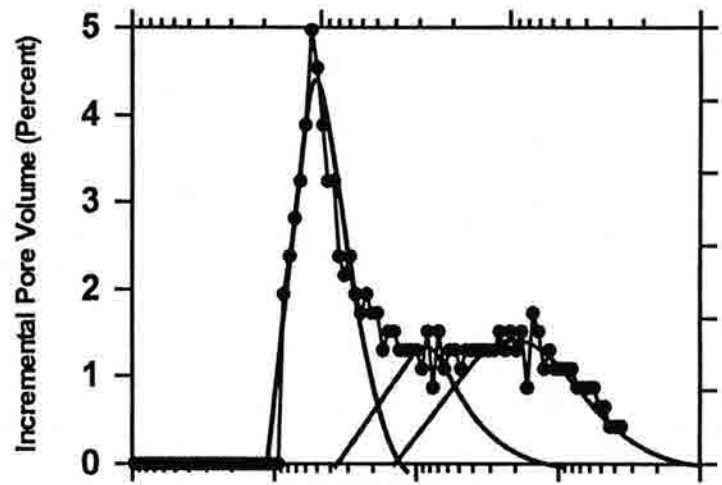
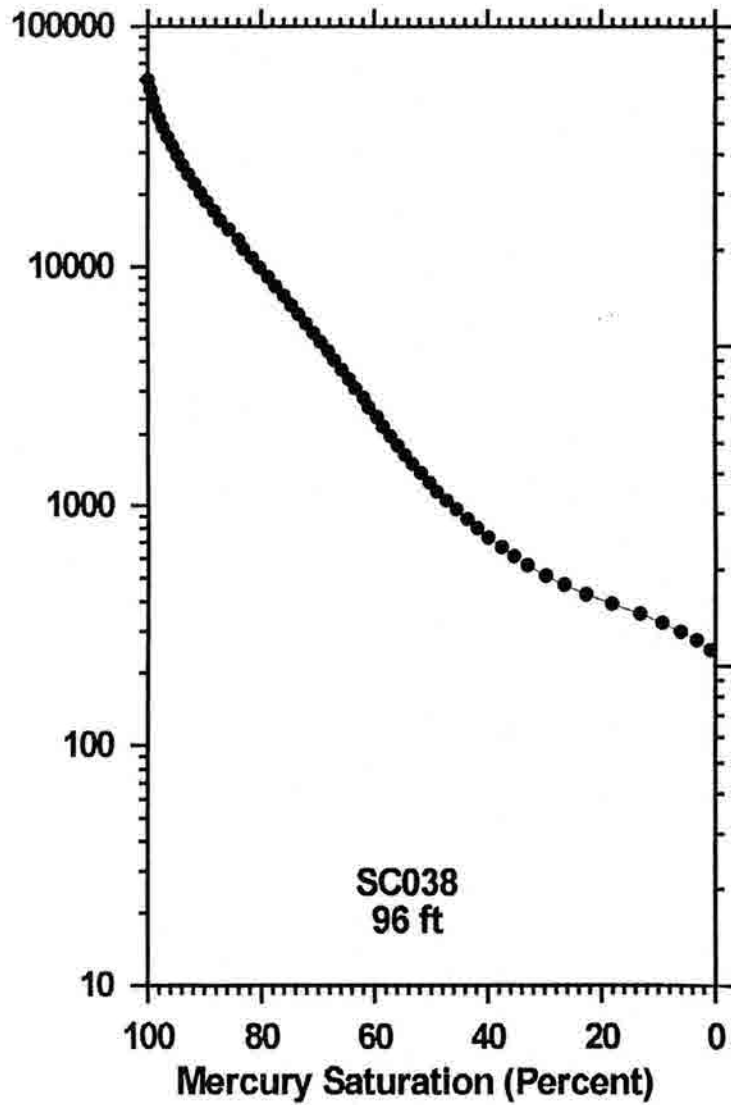


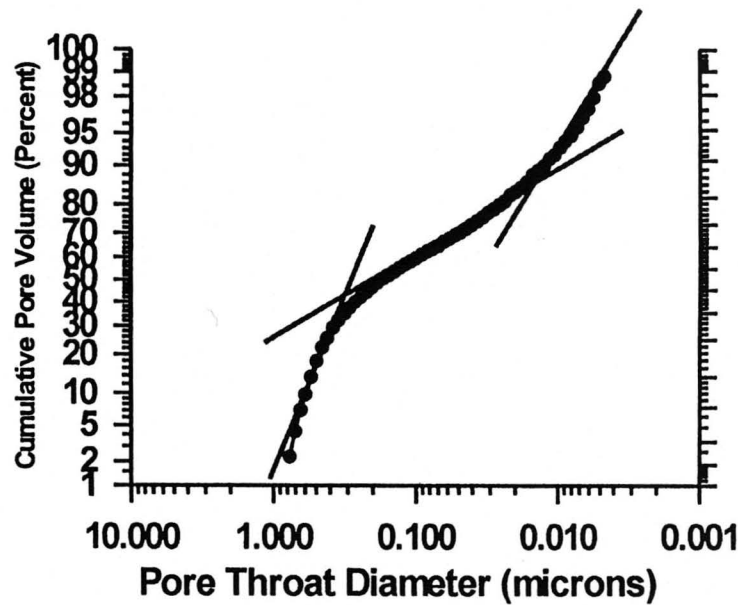
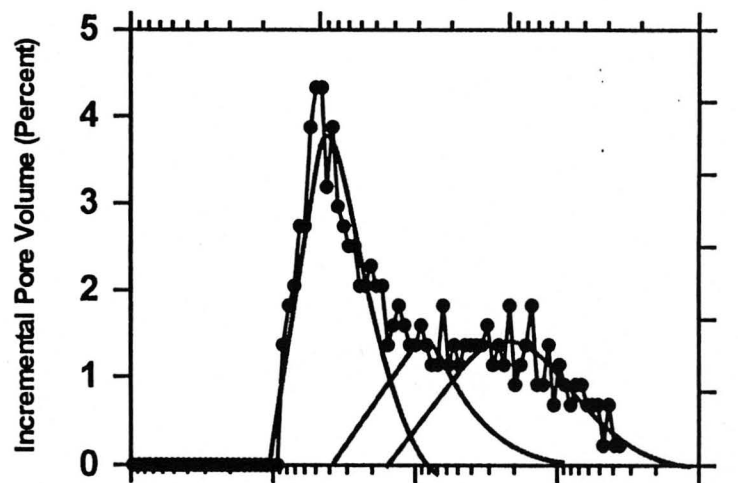
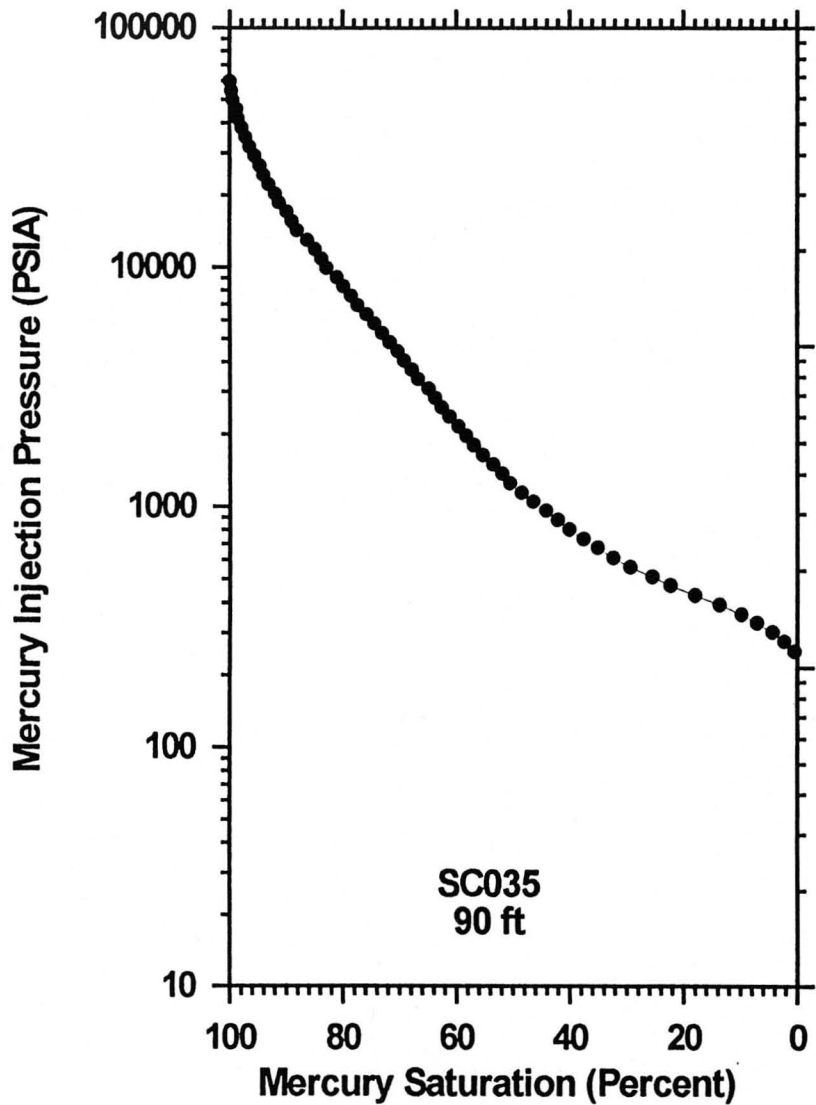




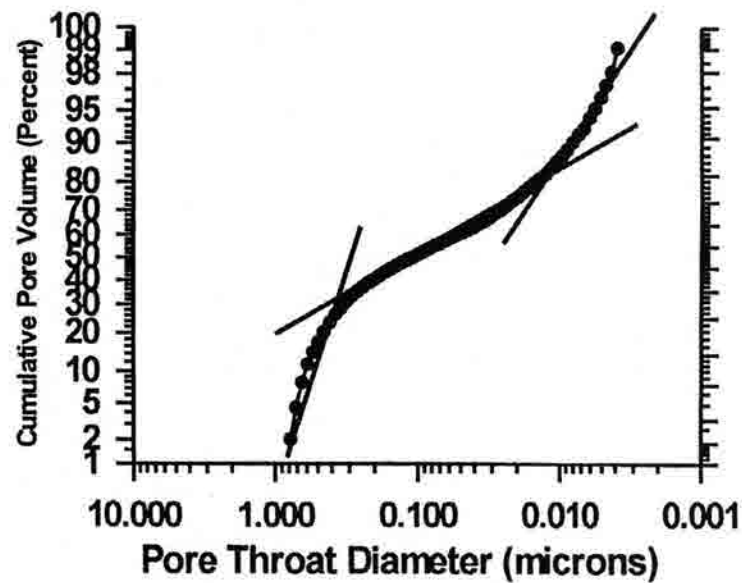
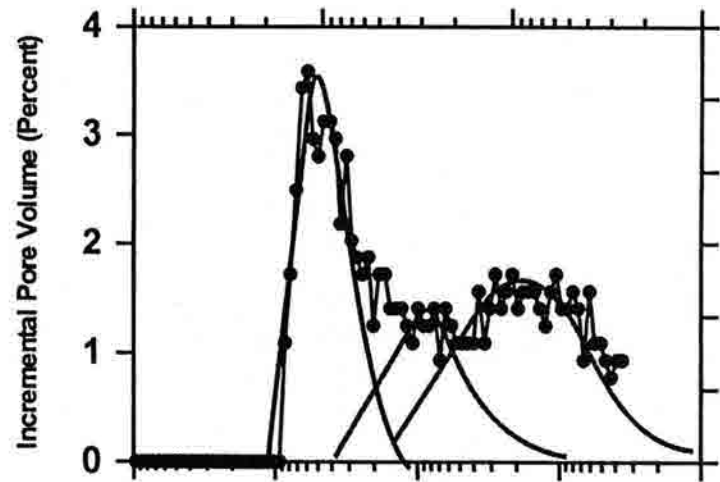
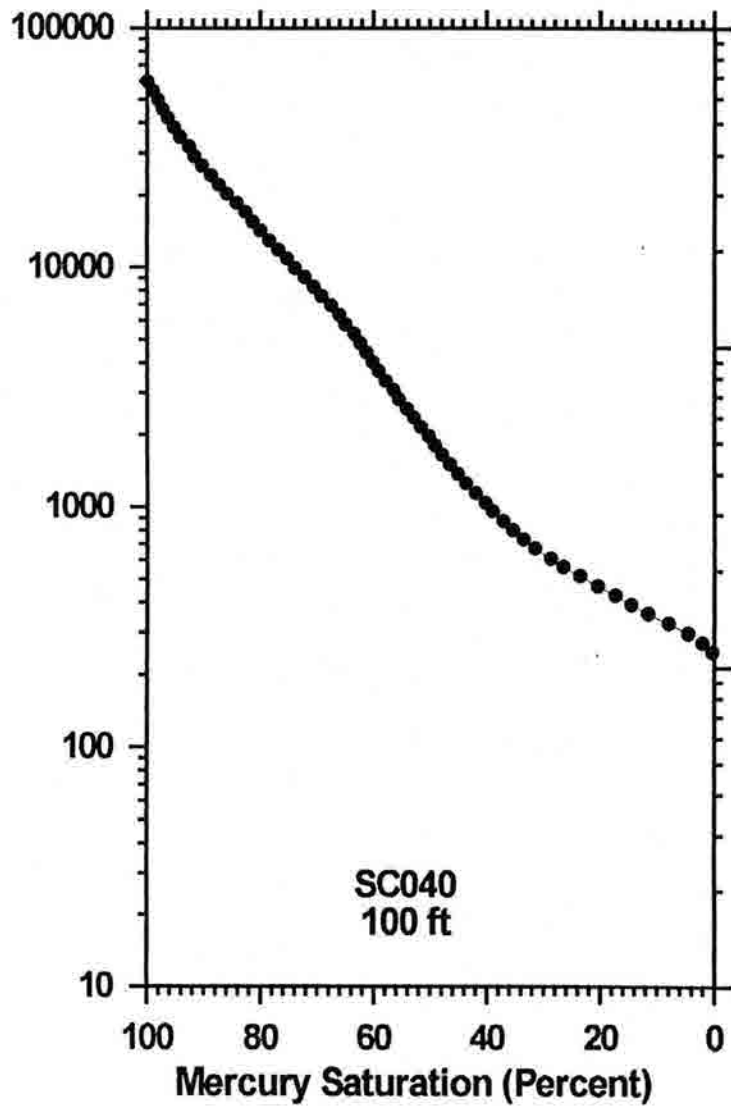


Mercury Injection Pressure (PSIA)

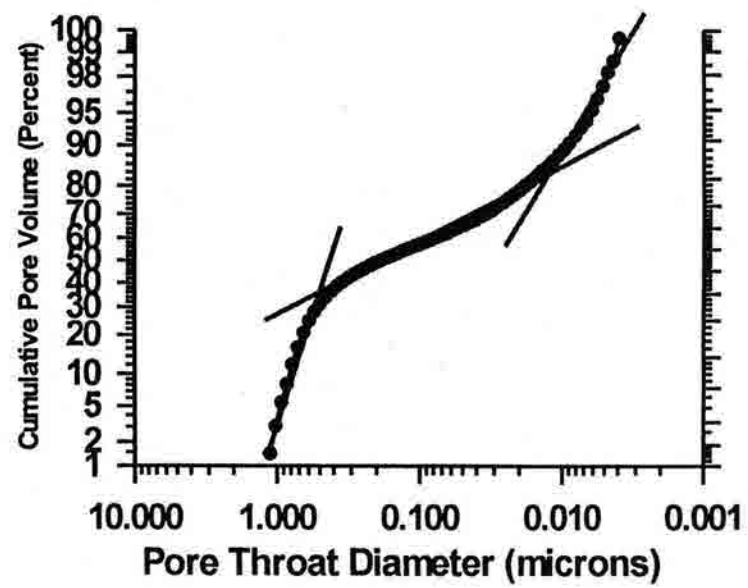
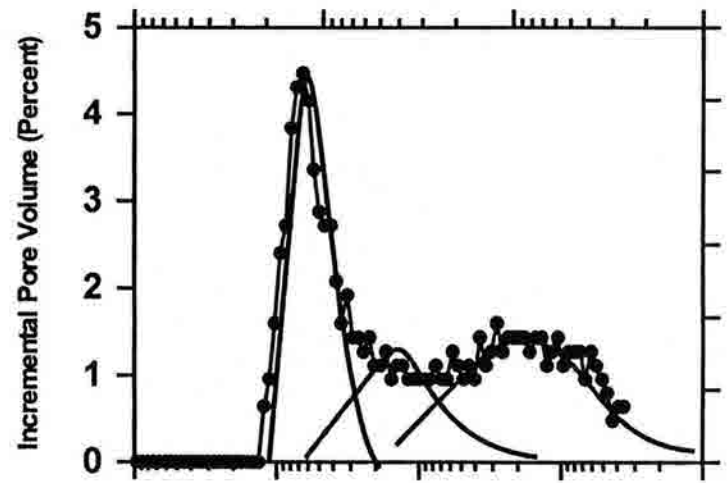
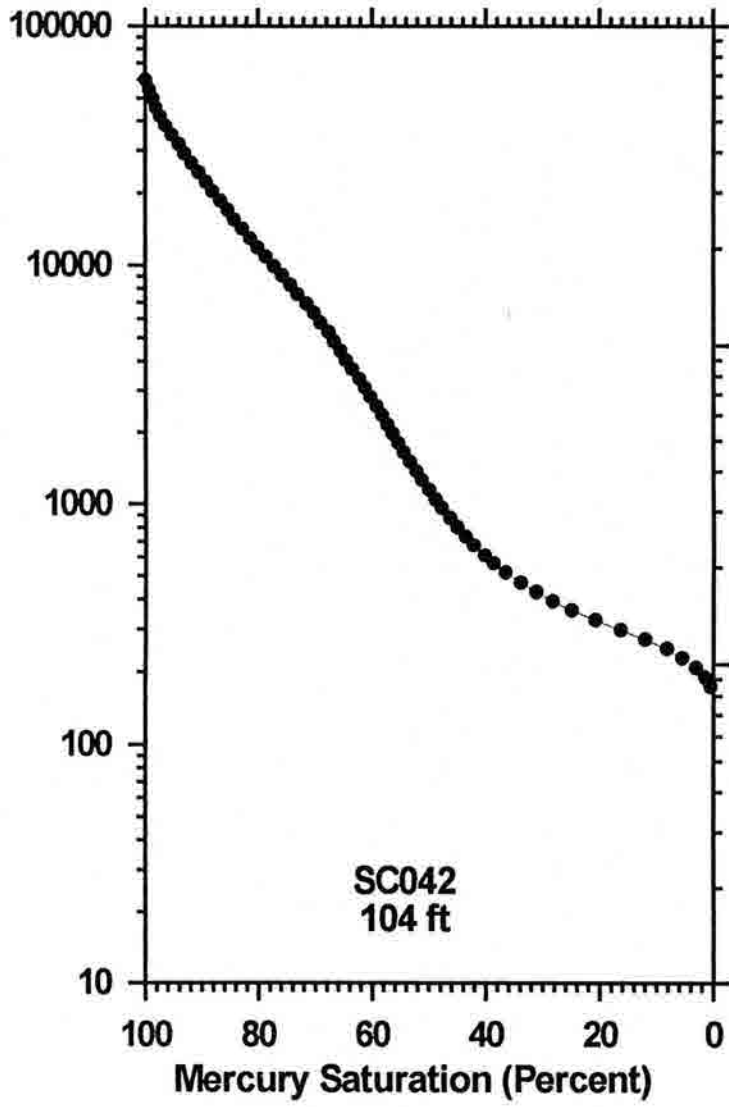


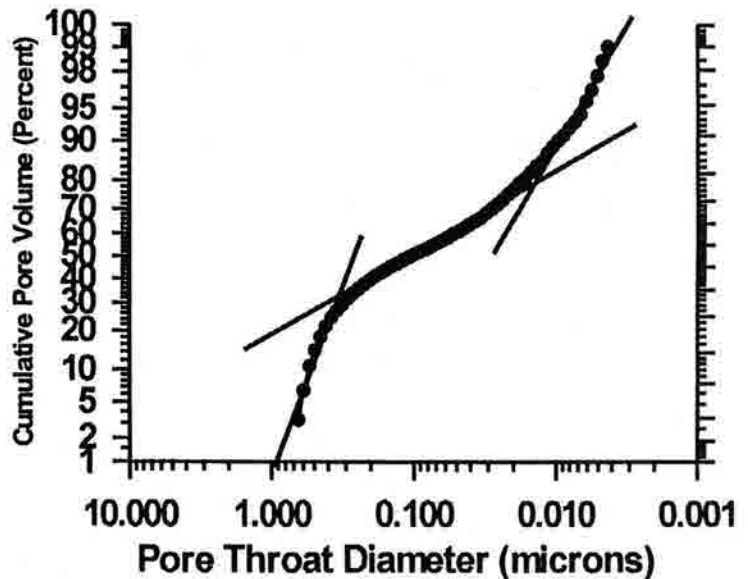
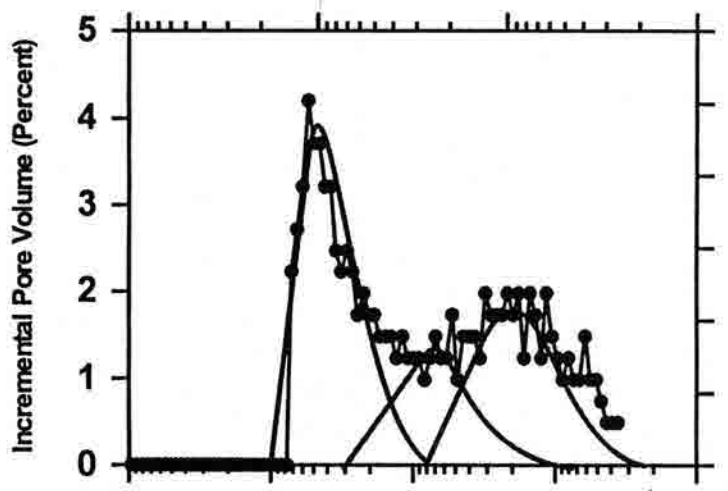
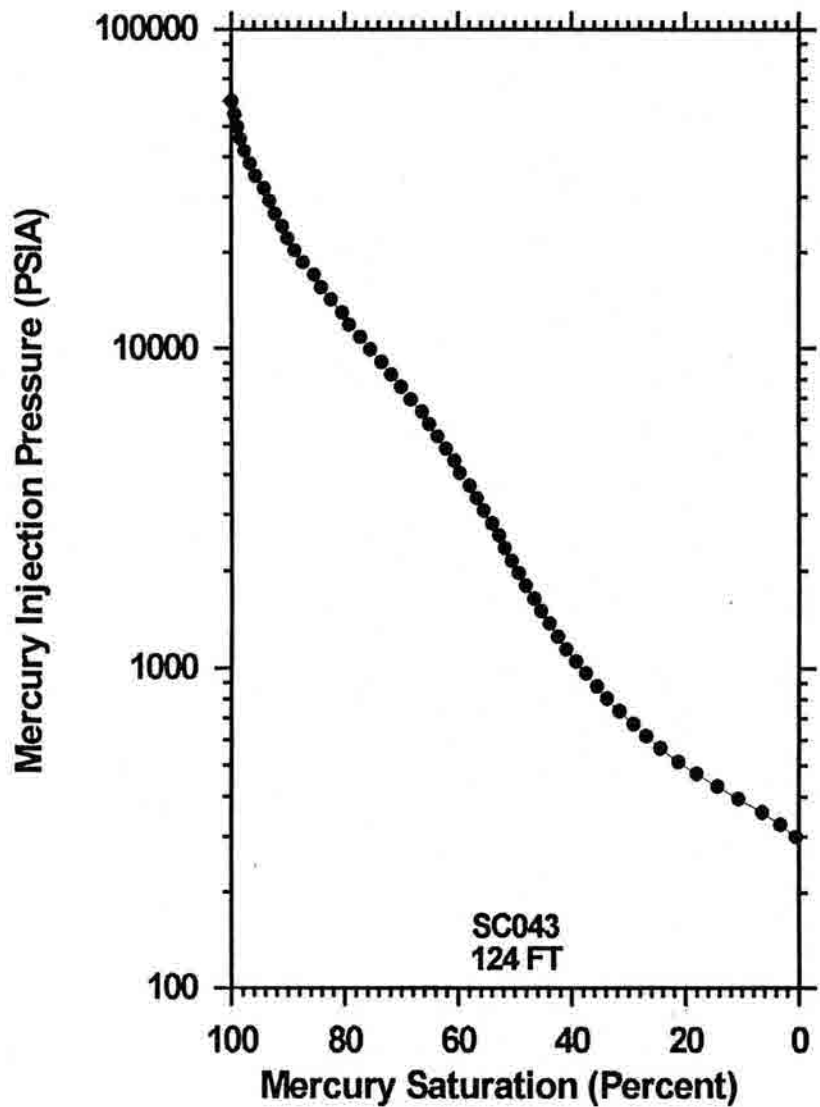


Mercury Injection Pressure (PSIA)

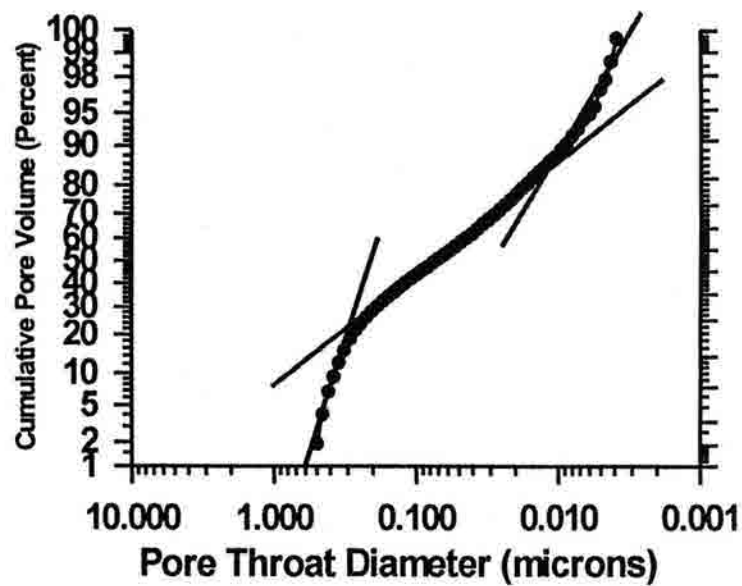
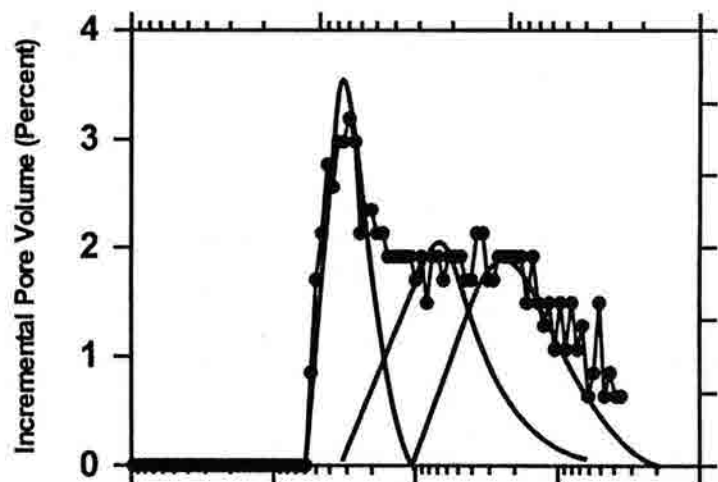
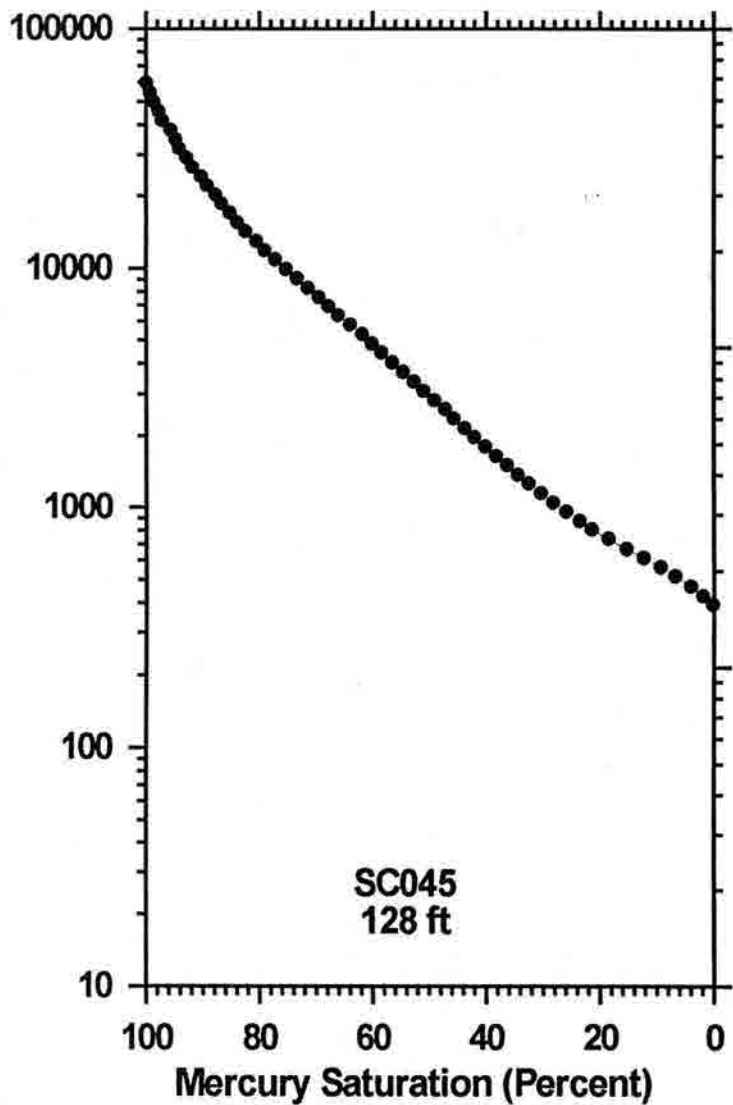


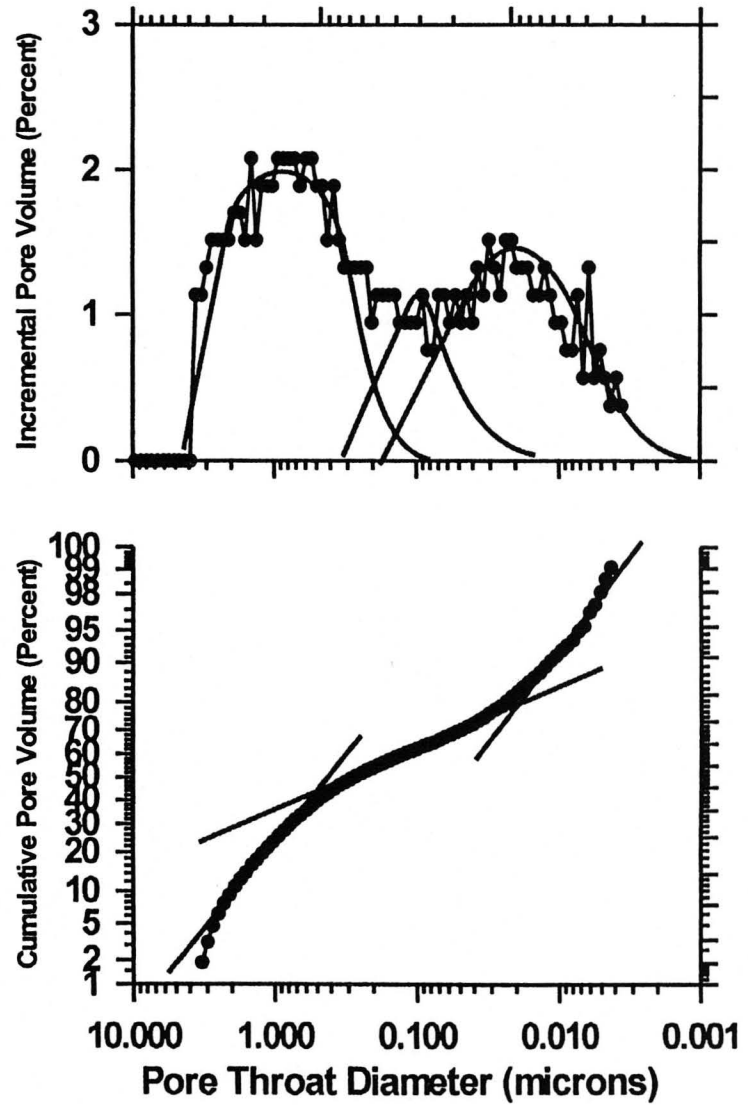
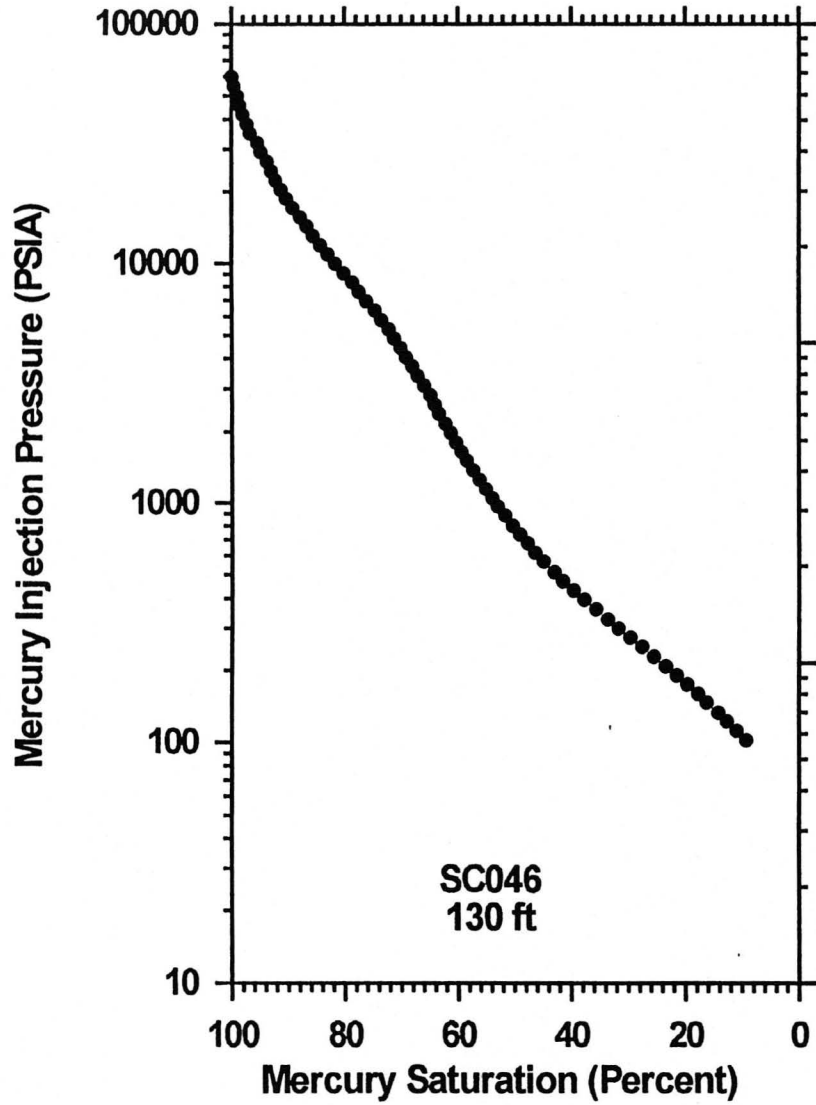
Mercury Injection Pressure (PSIA)



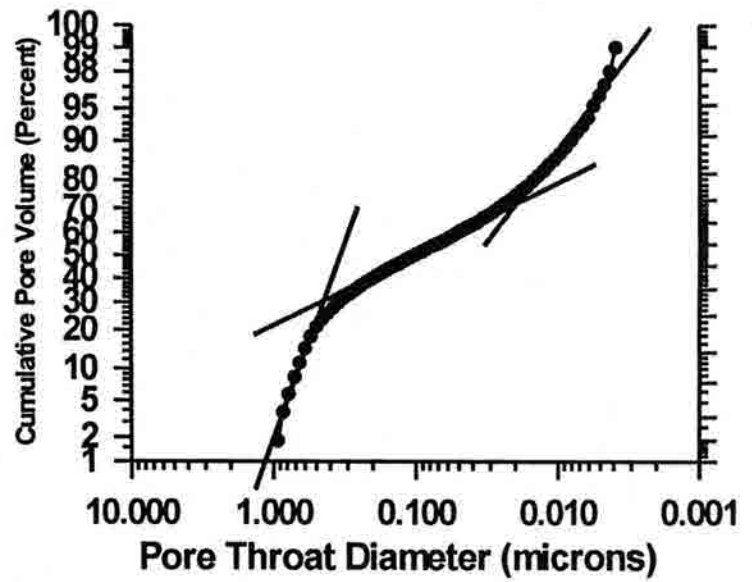
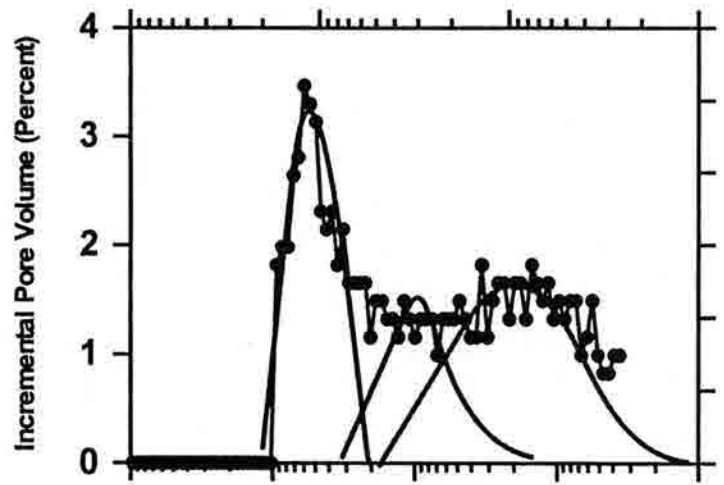
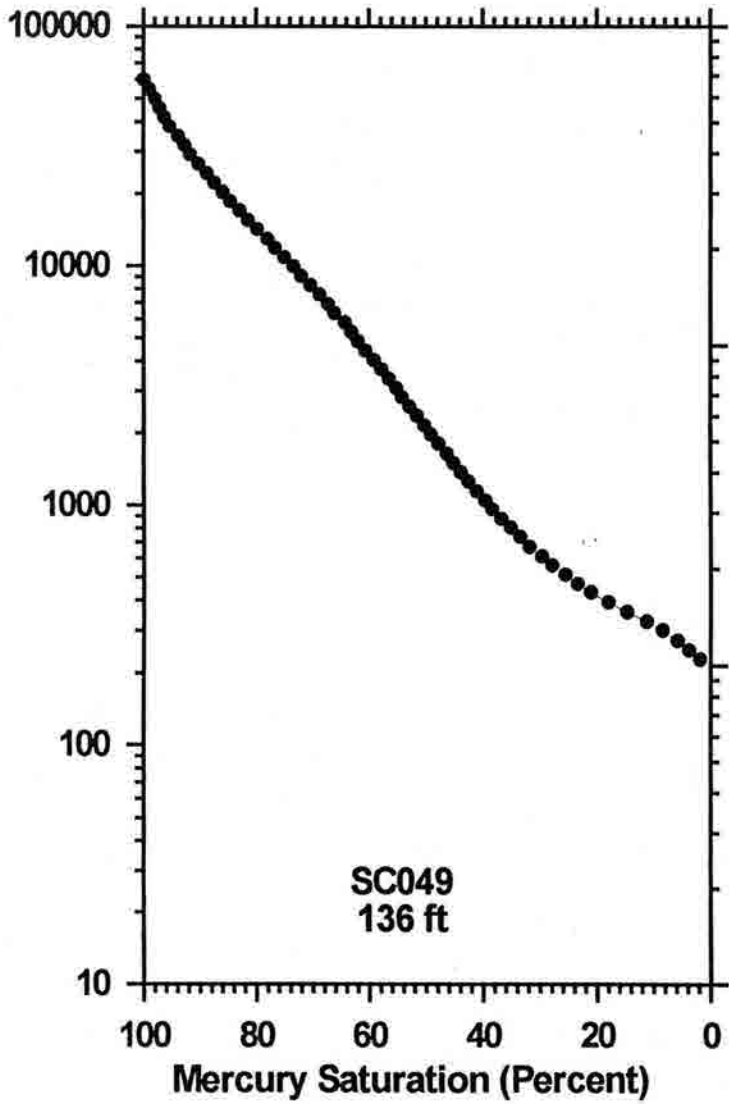


Mercury Injection Pressure (PSIA)

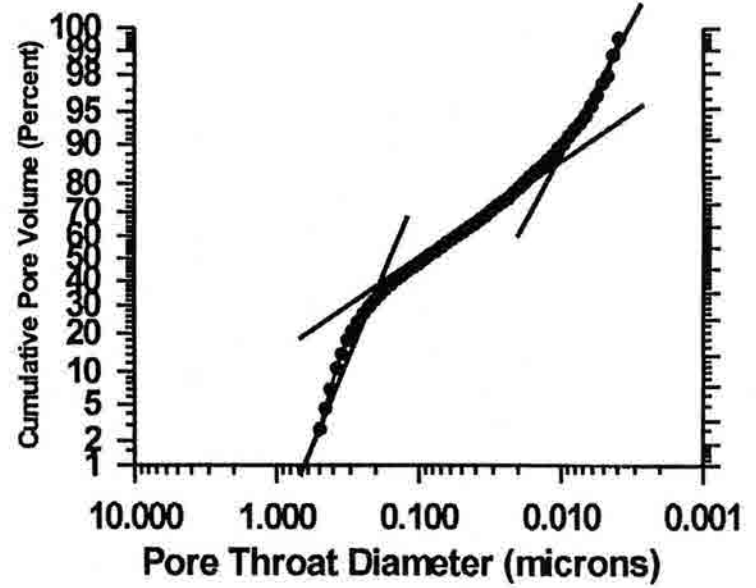
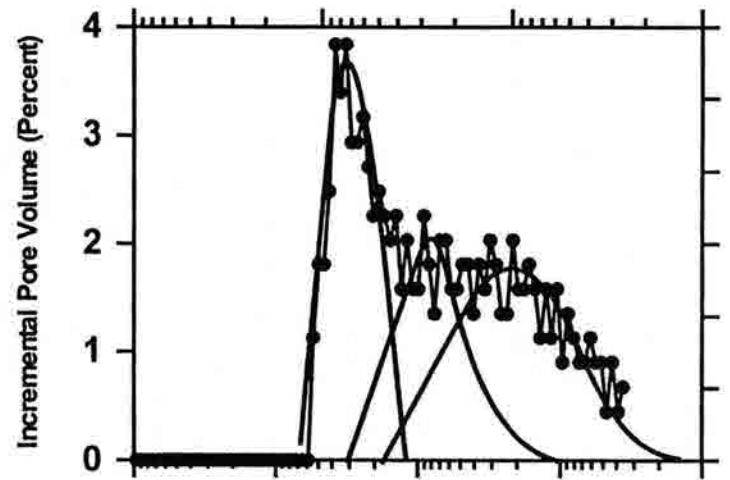
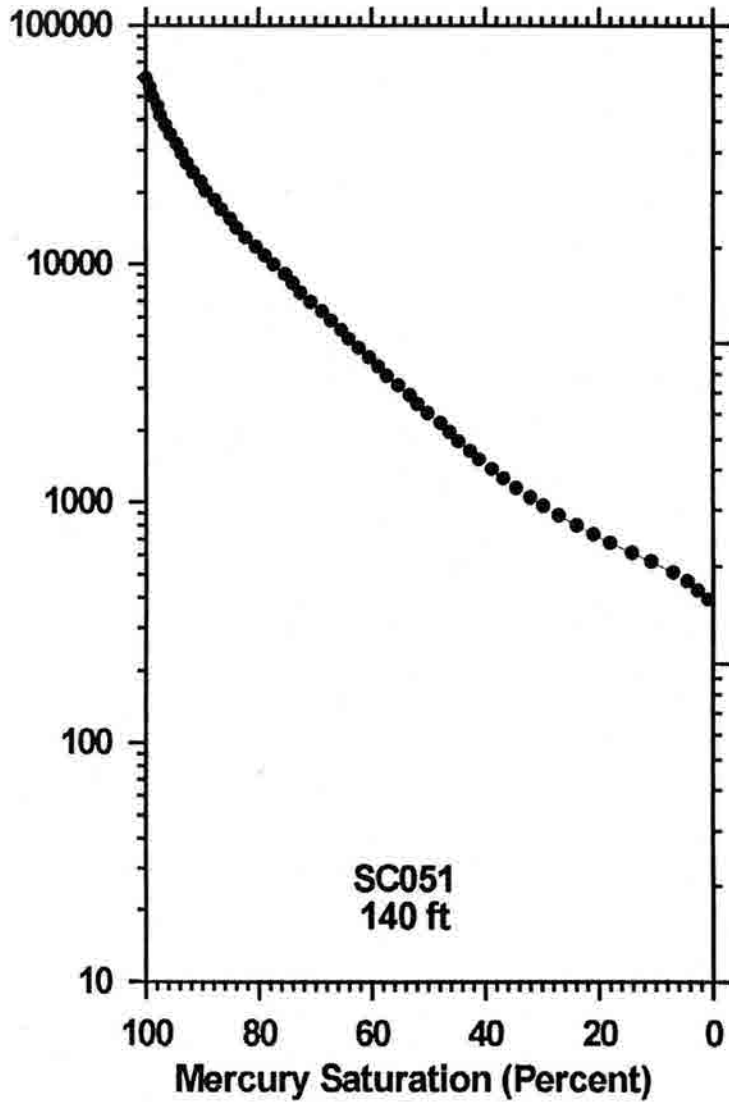




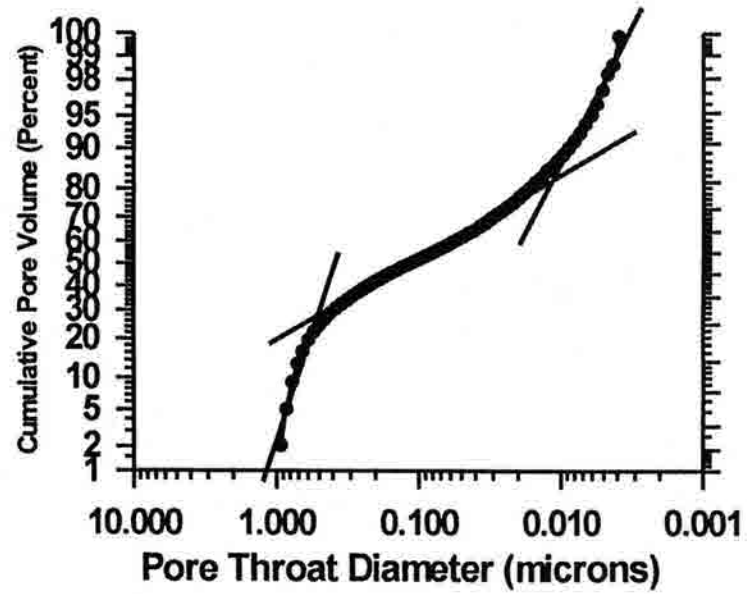
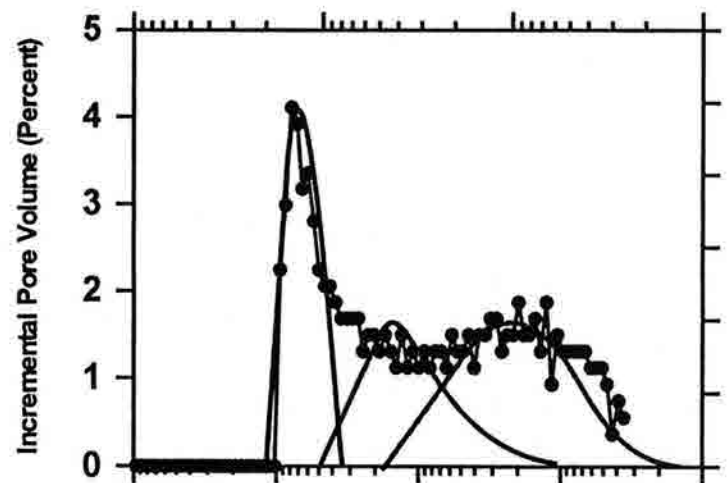
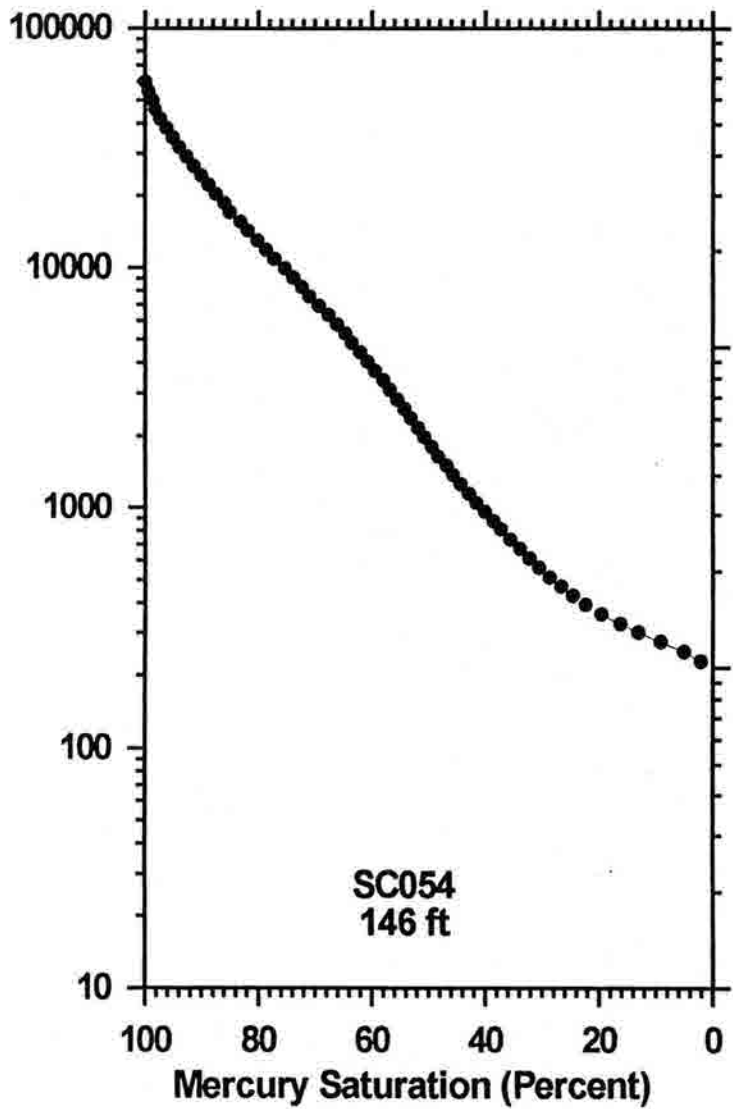
Mercury Injection Pressure (PSIA)



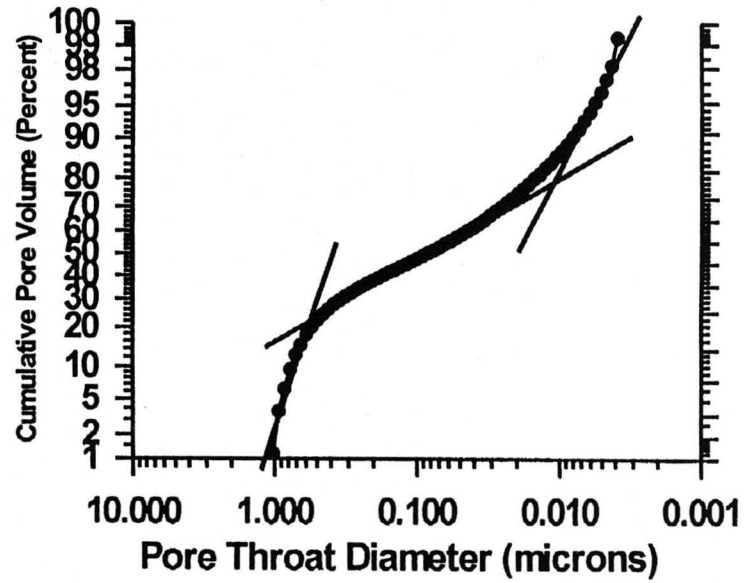
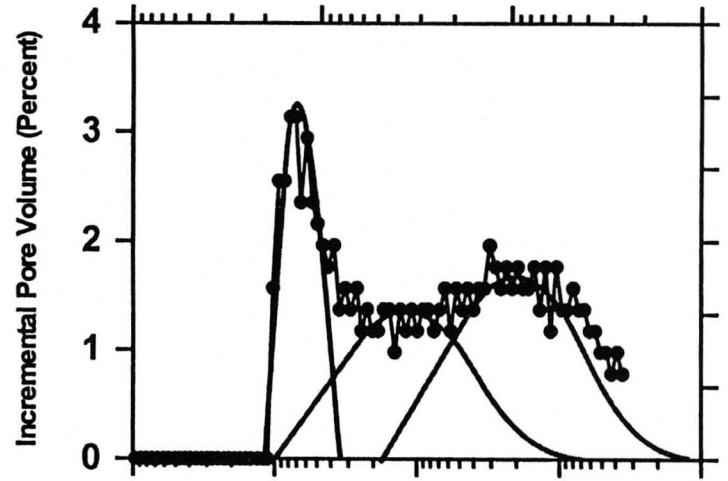
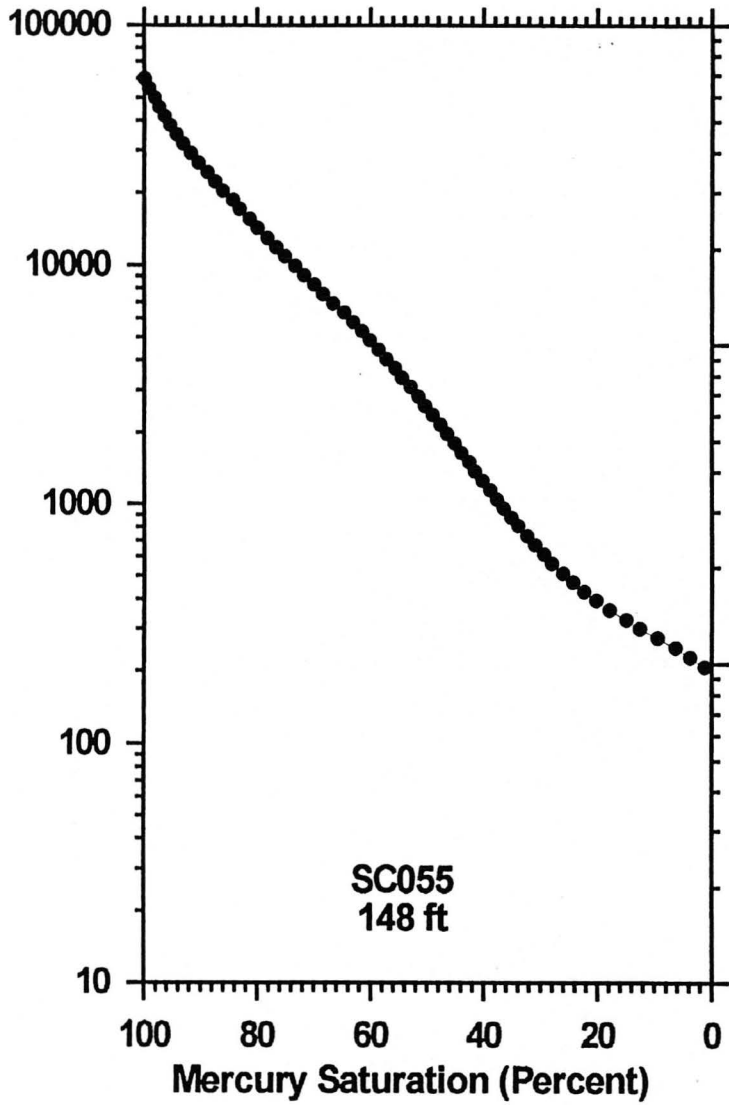
Mercury Injection Pressure (PSIA)

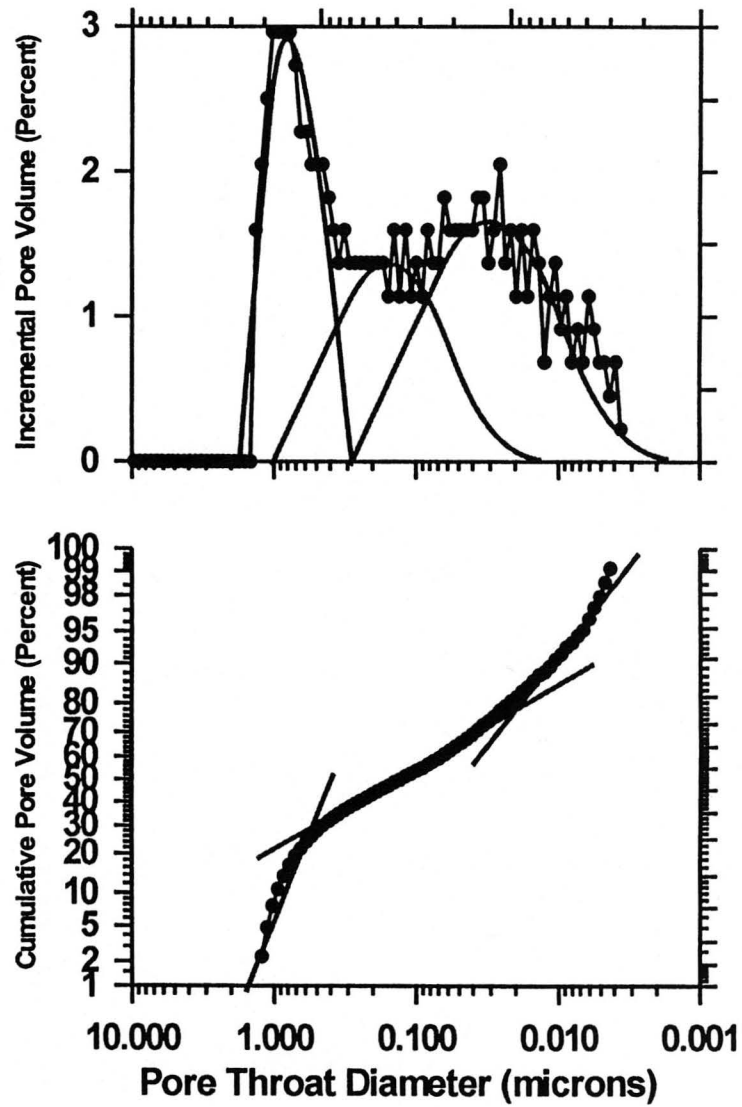
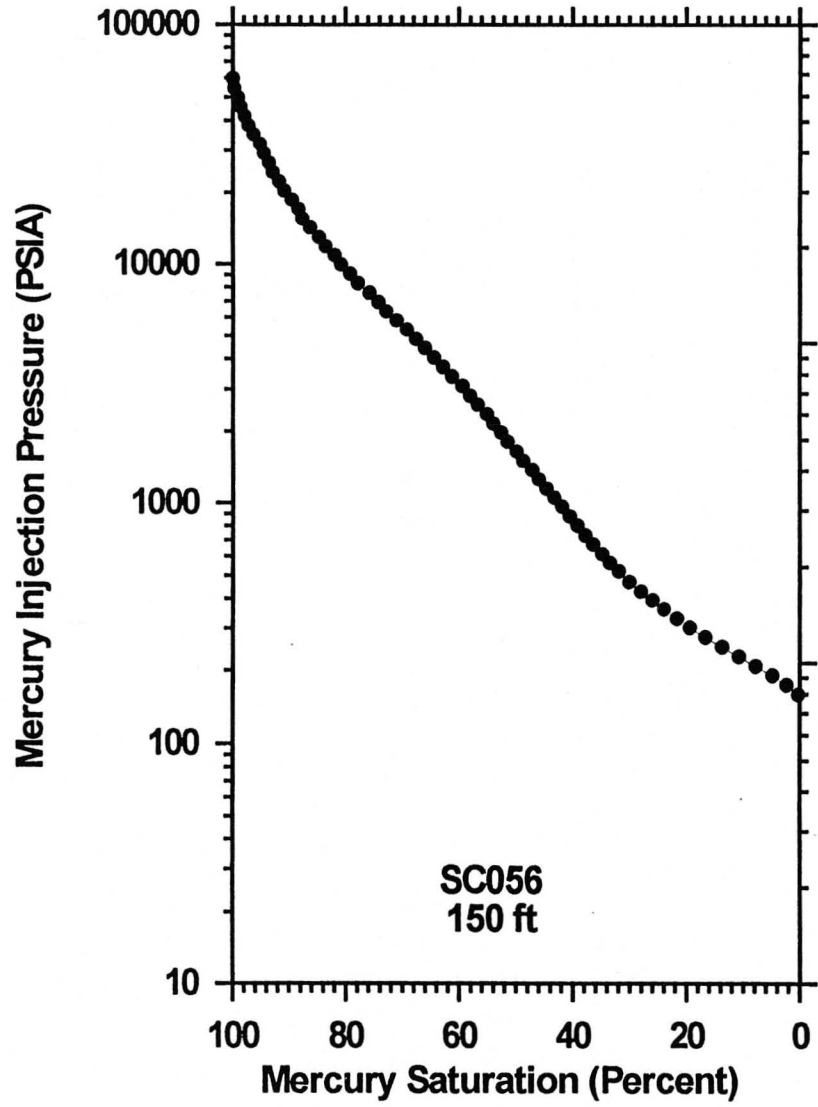


Mercury Injection Pressure (PSIA)

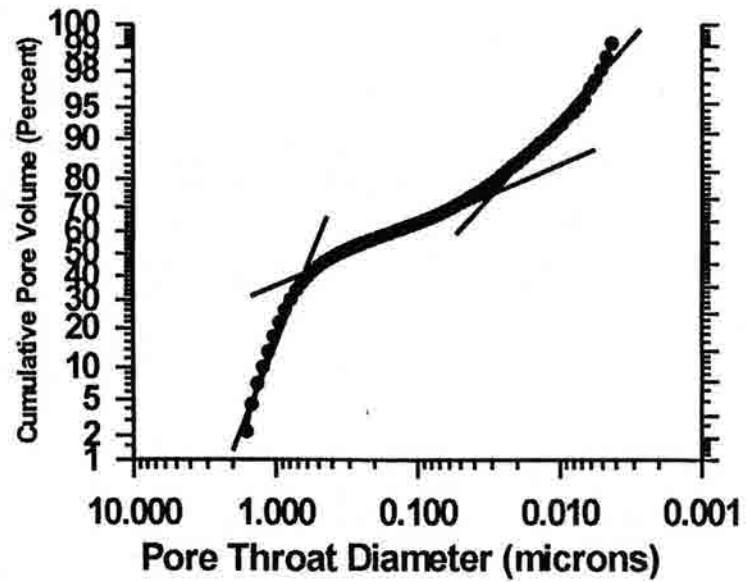
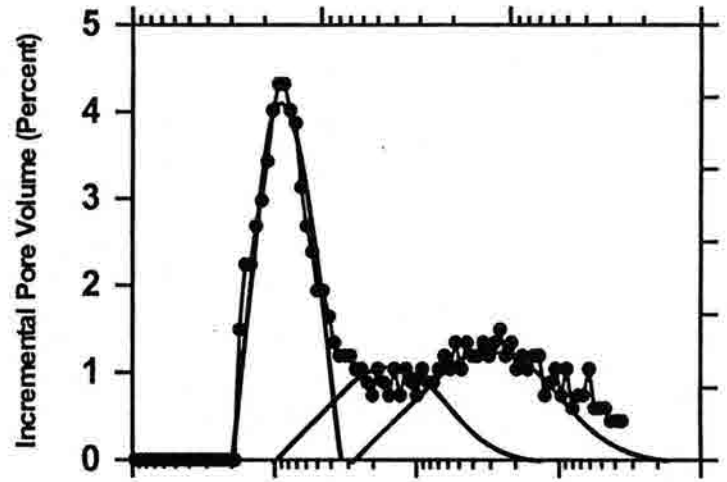
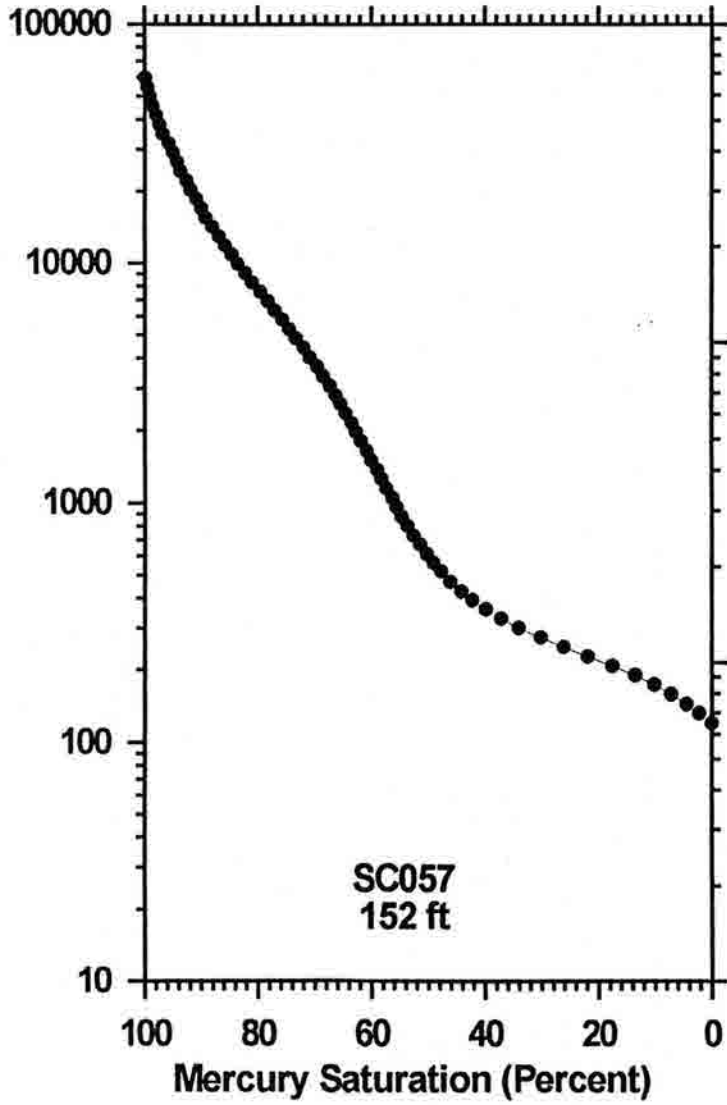


Mercury Injection Pressure (PSIA)

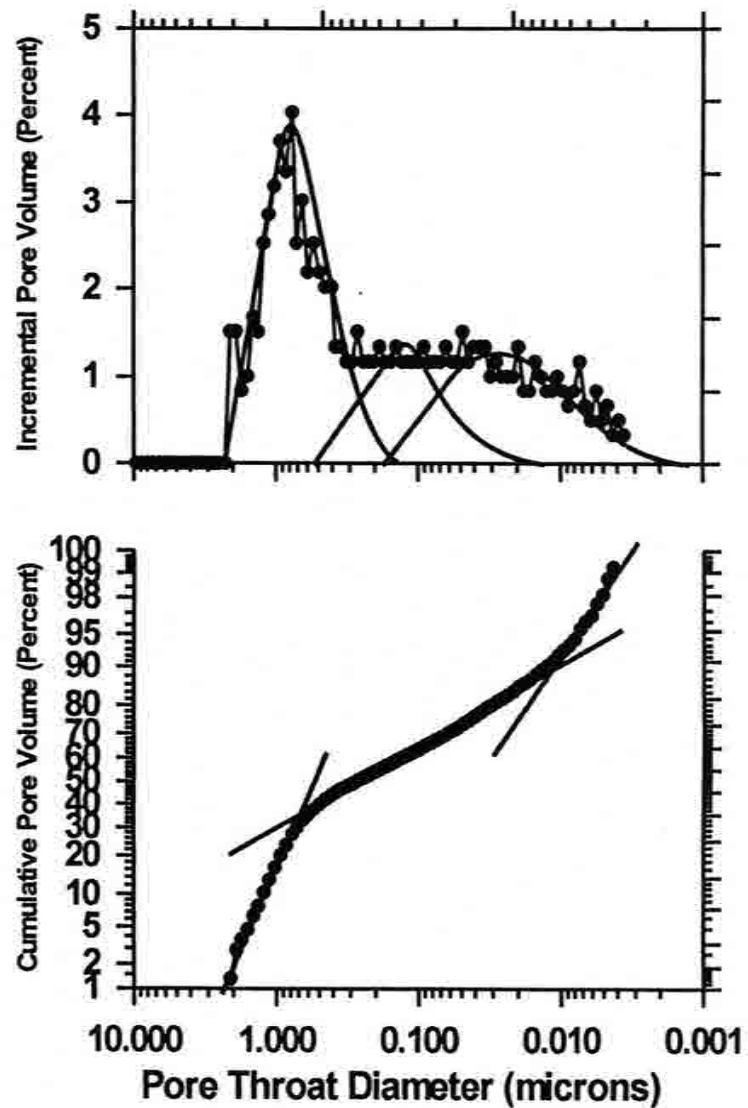
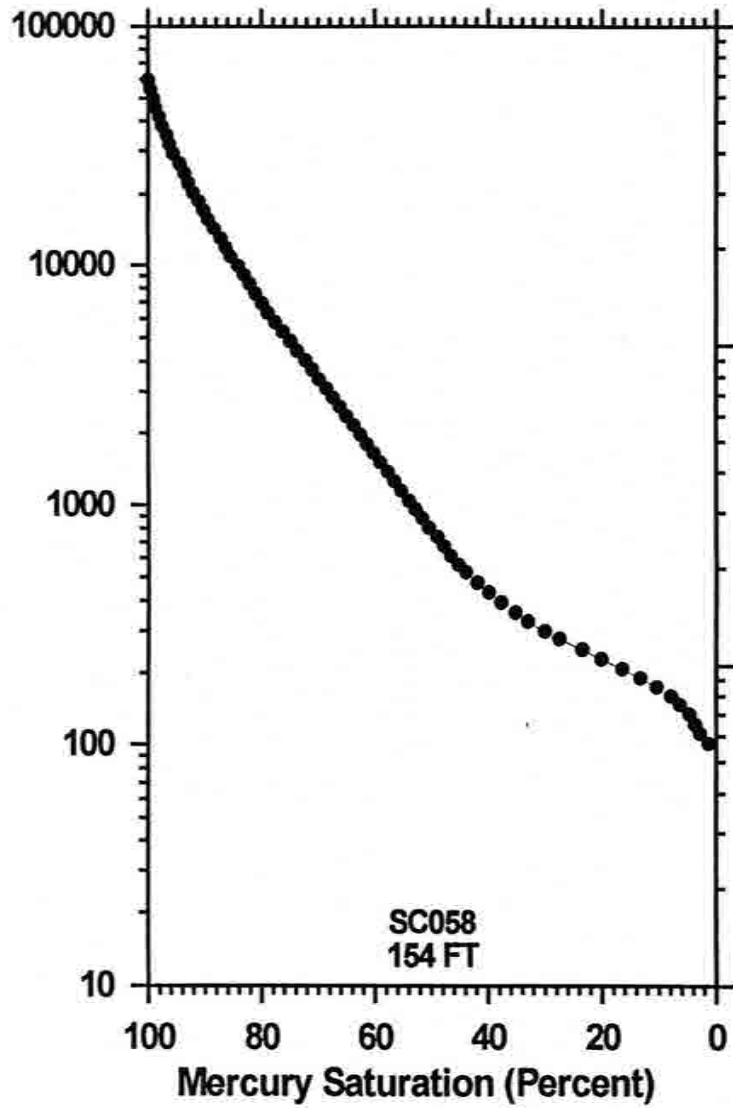




Mercury Injection Pressure (PSIA)



Mercury Injection Pressure (PSIA)



APPENDIX D

BELLEVUE OUTCROP

SKULL CREEK SHALE

THIN SECTION PHOTOMICROGRAPHS

Figure D1.

17003 (3 R)-Facies K

Low magnification (PPL) thin section photomicrograph of carbonaceous siltstone. Moderately well-sorted matrix contains clay minerals and illite-sized detrital hard grains. Occasional fine-grained sand particles. Accessory constituents include small opaque nodules that may be authigenic hematoidal ferrite or altered siderite. Dark red hematite staining is scattered throughout, giving an overall rusty appearance. No matrix porosity is detected.

Figure D2.

17003 (3 R)-Facies K

High magnification (PPL) thin section photomicrograph of same carbonaceous siltstone facies as in D1. Well-sorted matrix contains clay minerals and separated to elongate silt-sized detrital hard grains. The dark red mineral is hematite and is surrounding the quartz grains and replacing some of the clay minerals. Accessory constituents include very small amounts of authigenic carbonates with some of the small nodules being either authigenic hematoidal ferrite or altered siderite. Small amounts of dark colored organic matter are present as wispy laminations. No matrix porosity is detected.

Figure D1.

JY003 (3 ft)- Facies K

Low magnification (PPL) thin section photomicrograph of carbonaceous silty mudstone. Moderately well sorted matrix contains clay minerals and silt size detrital hard grains, with an occasional fine-grained sand particle. Accessory constituents include small opaque nodules that may be authigenic framboidal pyrite or altered siderite nodules. Dark red hematite staining is scattered throughout, giving an overall patchy appearance. No matrix porosity is detected.

Figure D2.

JY003 (3 ft)- Facies K

High magnification (PPL) thin section photomicrograph of same carbonaceous silty mudstone pictured in D1. Well-sorted matrix contains clay minerals and spherical to elongate, silt size, detrital hard grains. The dark red mineral is hematite and is surrounding the quartz grains and replacing some of the clay minerals. Accessory constituents include very small amounts of authigenic carbonates with some of the small nodules being either authigenic framboidal pyrite or altered siderite. Small amounts of dark colored organic matter are present as wispy laminations. No matrix porosity is detected.

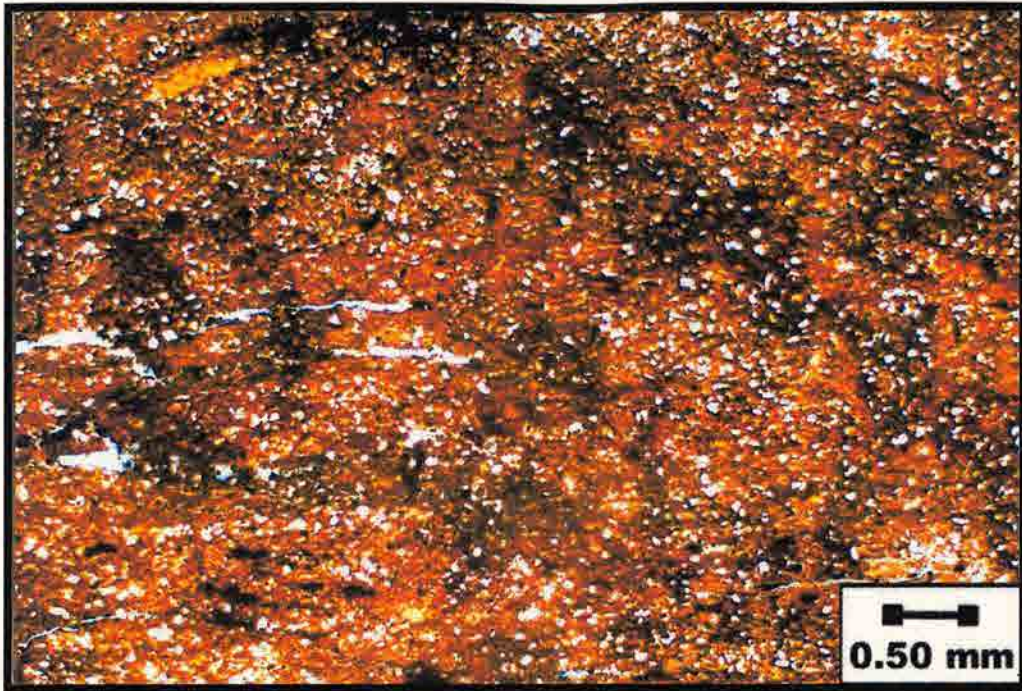


Figure D1.

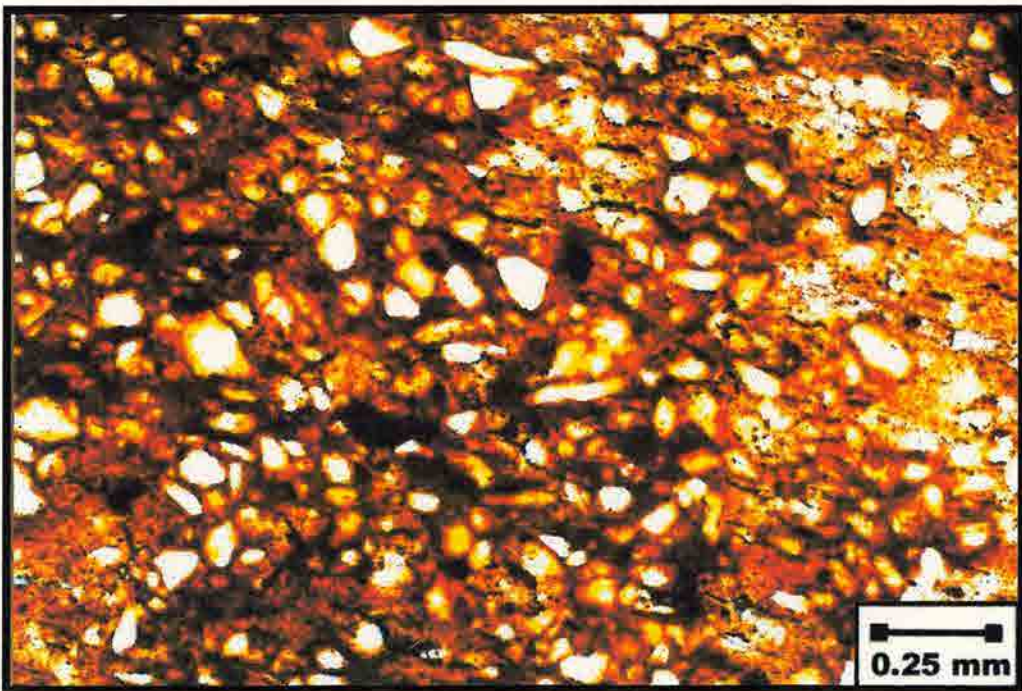


Figure D2.

Figure D3.

JYC005 (49 ft)- Facies K

Low magnification (PPL) thin section photomicrograph of carbonaceous silty shale. Strongly compacted, well-sorted matrix contains clay minerals and silt size detrital hard grains. This picture shows the transition of a silt bed in the lower half of the photo to the clay bed in the upper half. The upper half of shale has moderately developed laminations of organic matter. Accessory constituents are scattered throughout both beds and include small nodules of either authigenic framboidal pyrite or altered siderite nodules. No matrix porosity is present.

Figure D4.

JYC005 (49 ft)- Facies K

Medium magnification (PPL) thin section photomicrograph of same carbonaceous silty shale pictured in D3. Under higher magnification the boundary between the beds of silt and clay appear to be more gradational, as the silt content gradually decreases upward. Wispy laminations of organic matter are clearly seen in the upper half of the photo. The small opaque nodules are either authigenic framboidal pyrite or altered siderite nodules. No matrix porosity is present.

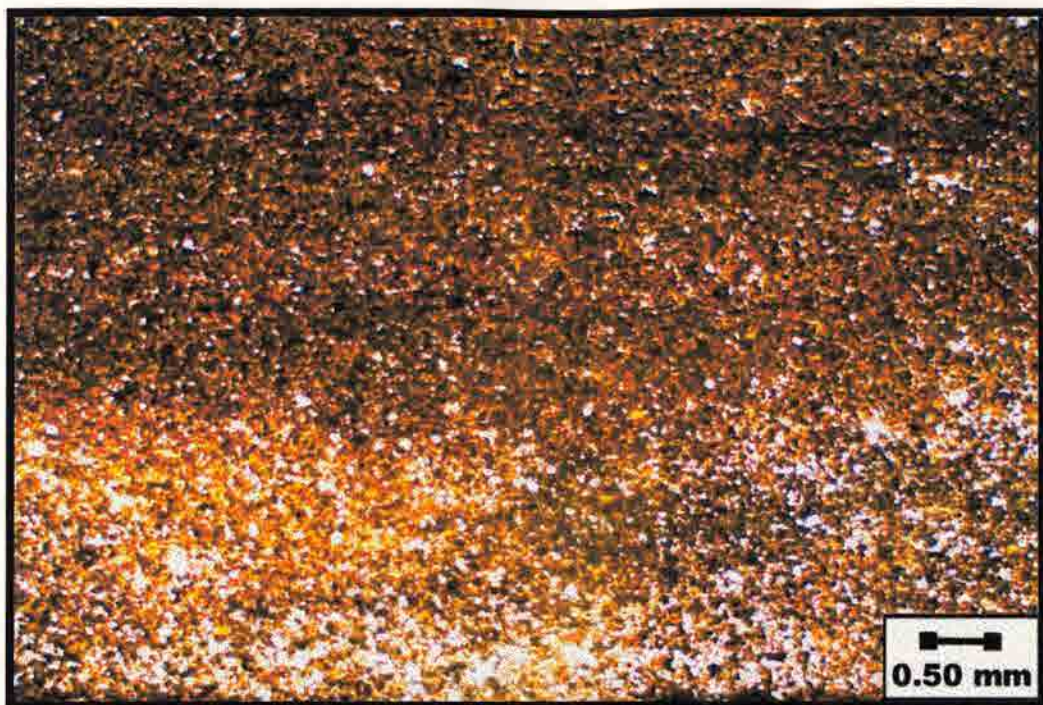


Figure D3.

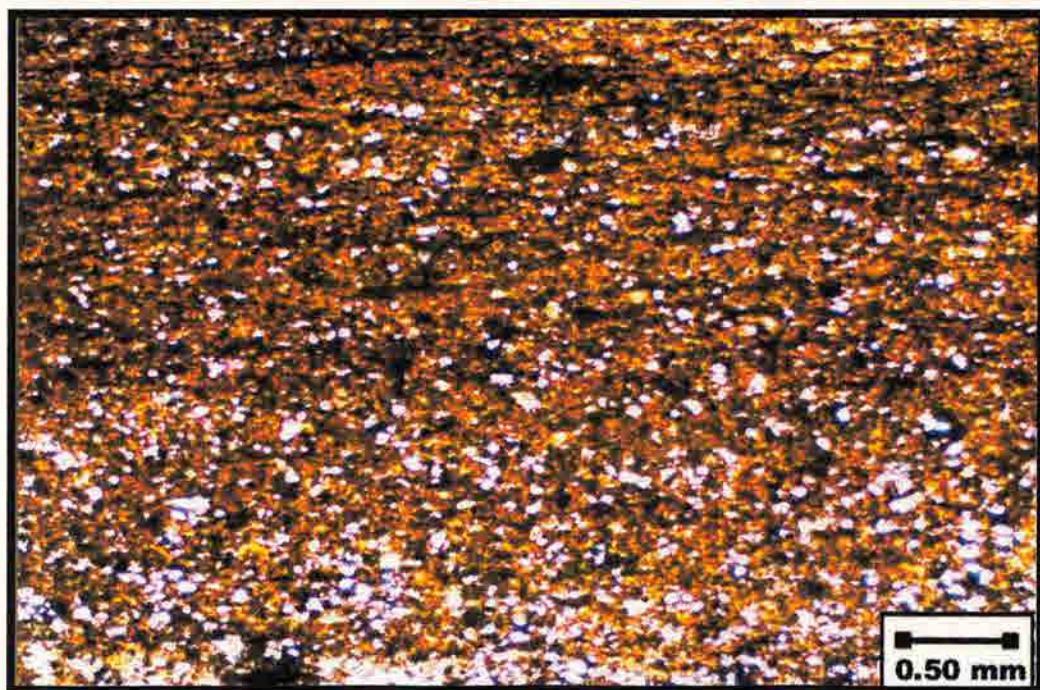


Figure D4.

Figure 102

LYC018 (89 B)-Facies A

Medium magnification (X15) thin section photomicrograph of carbonaceous silt shale. Strongly coarsened, well-sorted matrix contains clay crystals and silt size detrital (but granular) with an occasional fine-grained sand particle. This photo shows a gradational transition from a silt bed (in the lower right corner) to a clay bed (in the upper left corner). No matrix porosity is noted.

Figure 103

LYC018 (89 B)-Facies A

High magnification (X30) thin section photomicrograph of same carbonaceous silt shale. Detrital sand grains appear to "float" in the clay rich matrix. Wavy laminations of dark colored organic matter are present and delineated by the arrow. Other accessory minerals include opaque nodules of authigenic limonitic grains. Some of these large opaque particles may be altered siderite or hematite. No matrix porosity is detected.

Figure D5.

JYC015 (59 ft)- Facies A

Medium magnification (XN) thin section photomicrograph of carbonaceous silty shale. Strongly compacted, well-sorted matrix contains clay minerals and silt size detrital hard grains, with an occasional fine-grained sand particle. This photo shows a gradational transition from a silt bed (in the lower right corner) to a clay bed (in the upper left corner). No matrix porosity is noted.

Figure D6.

JYC015 (59 ft)- Facies A

High magnification (XN) thin section photomicrograph of same carbonaceous silty shale pictured in D5. Detrital hard grains appear to "float" in the clay rich matrix. Wispy laminations of dark colored organic matter are present and delineated by the arrow. Other accessory minerals include opaque nodules of authigenic framboidal pyrite. Some of these large opaque particles may be altered siderite or hematite. No matrix porosity is detected.

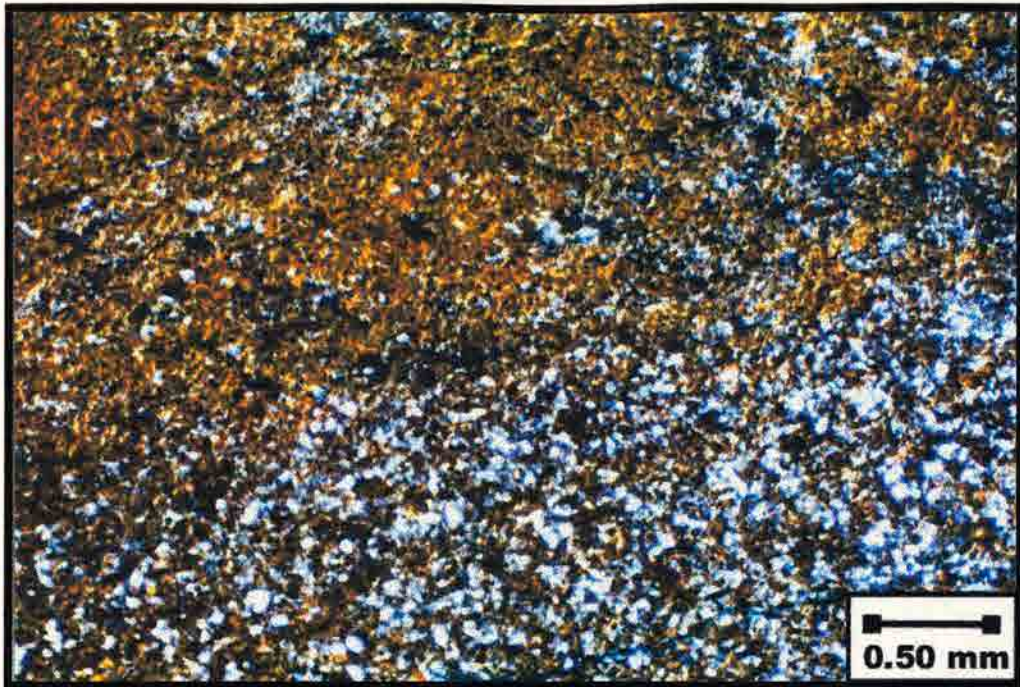


Figure D5.

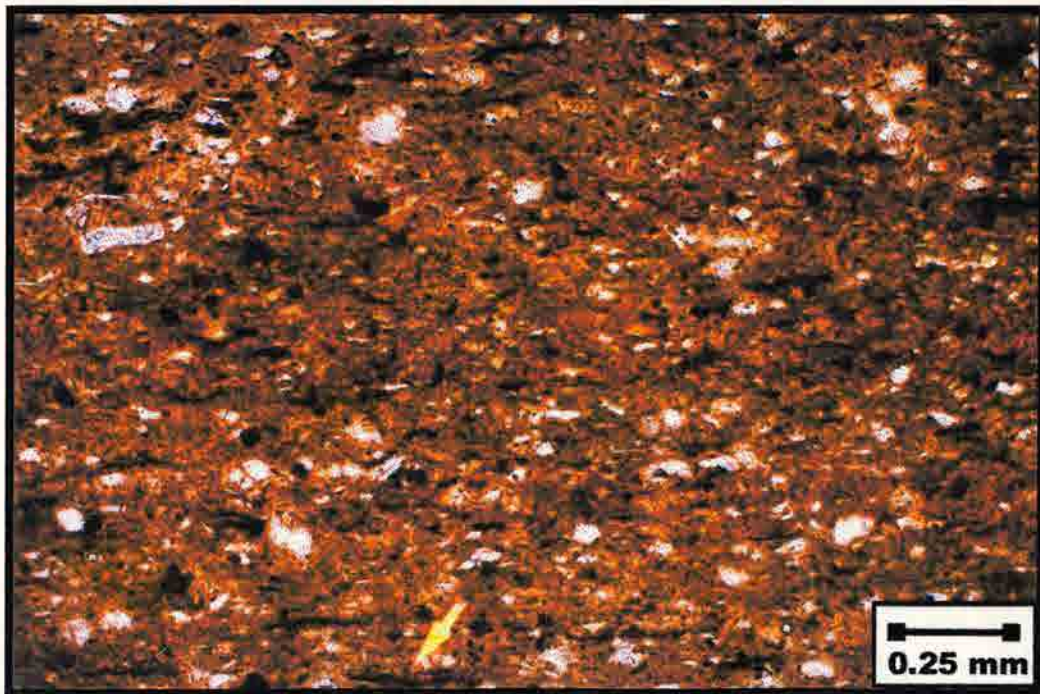


Figure D6.

Figure 17.

17042 (02 H) - Factor B

Low magnification (X1) thin section photomicrograph of interbedded carbonaceous siltstone and shale. This picture shows well-developed beds of silt and clay. Within each bed, the matrix is well sorted. The matrix is pointing to the top of a clay bed that appears to be a rounded surface, which has been filled in with silt. Organic matter is present as wavy laminae within the clay beds. No matrix porosity is observed.

Figure 18.

17042 (02 H) - Factor B

High magnification (X10) thin section photomicrograph of same interbedded carbonaceous siltstone and shale as 17042 (02 H). Quartz grains are sub-rounded, spherical and silt size. At higher power the necessary components are easier to distinguish and include fibrous material, small siltstone nodules and siltstone from weathered siltstone. The arrow is pointing to an siltstone hard grain, siltstone or fibrous, which appears to be "pinned" into the clay matrix, disrupting the organic matter laminae. No matrix porosity is observed.

Figure D7.

JY045 (69 ft)- Facies B

Low magnification (PPL) thin section photomicrograph of interbedded carbonaceous siltstone and shale. This picture shows well-developed beds of silt and clay. Within each bed, the matrix is well sorted. The arrow is pointing to the top of a clay bed that appears to be a scoured surface, which has been filled in with silt. Organic matter is present as wispy laminae within the clay beds. No matrix porosity is detected.

Figure D8.

JY045 (69 ft)- Facies B

High magnification (XN) thin section photomicrograph of same interbedded carbonaceous siltstone and shale in D7. Quartz grains are sub-rounded, spherical, and silt size. At higher power the accessory constituents are easier to distinguish and include phosphatic material, small siderite nodules and sericite from weathered feldspars. The arrow is pointing to an altered hard grain, either quartz or feldspar, which appears to be "pushed" into the clay matrix, disrupting the organic matter lamination. No matrix porosity is detected.

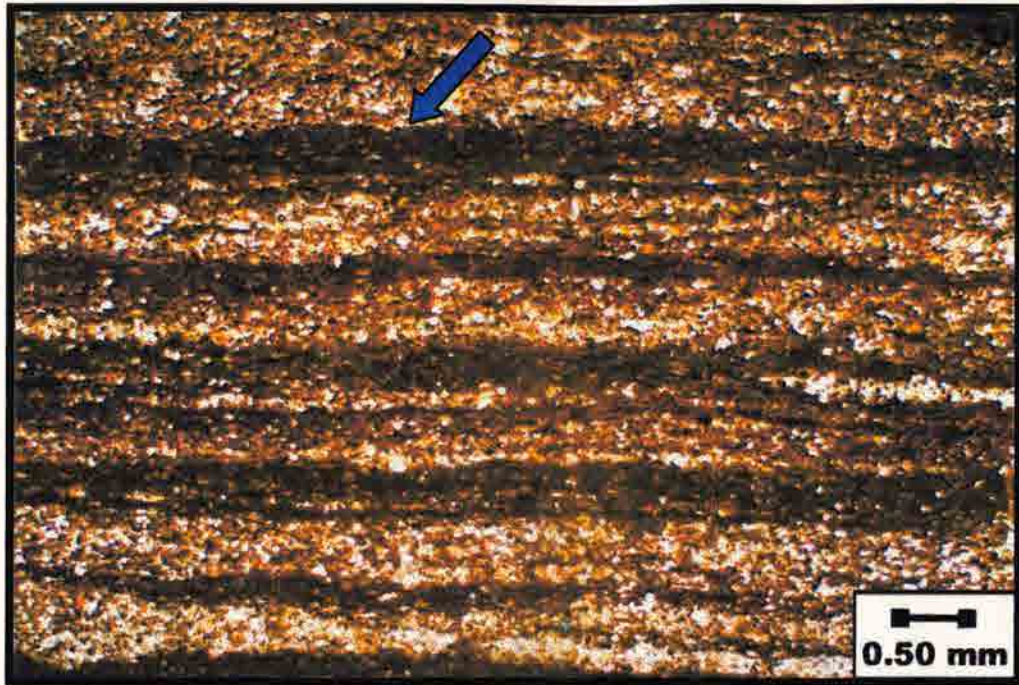


Figure D7.

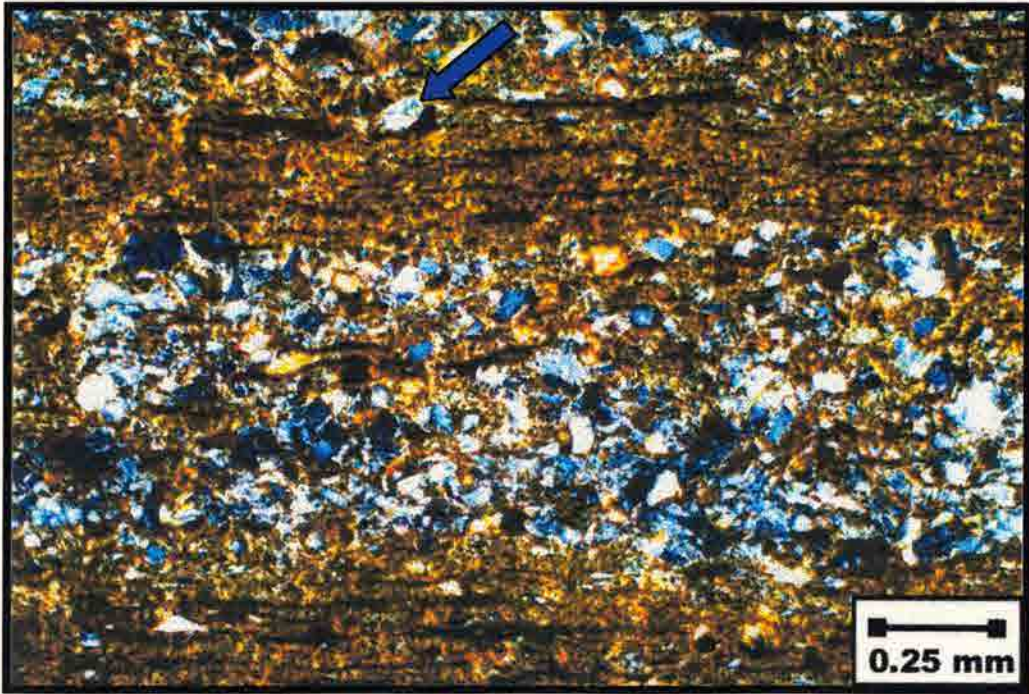


Figure D8.

APPENDIX E

BELLEVUE OUTCROP

SKULL CREEK SHALE

SEM PHOTOMICROGRAPHS

JYC006: 50 ft – Facies A

Top left: Low Power (x110)

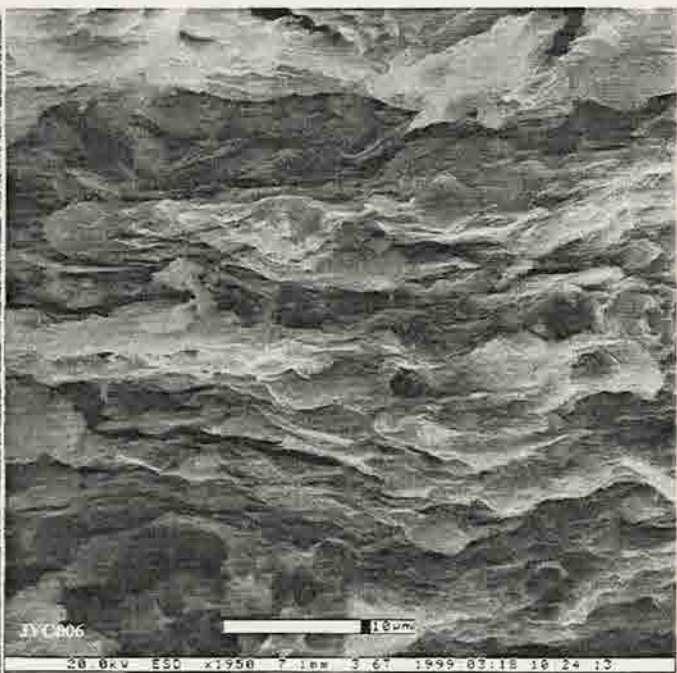
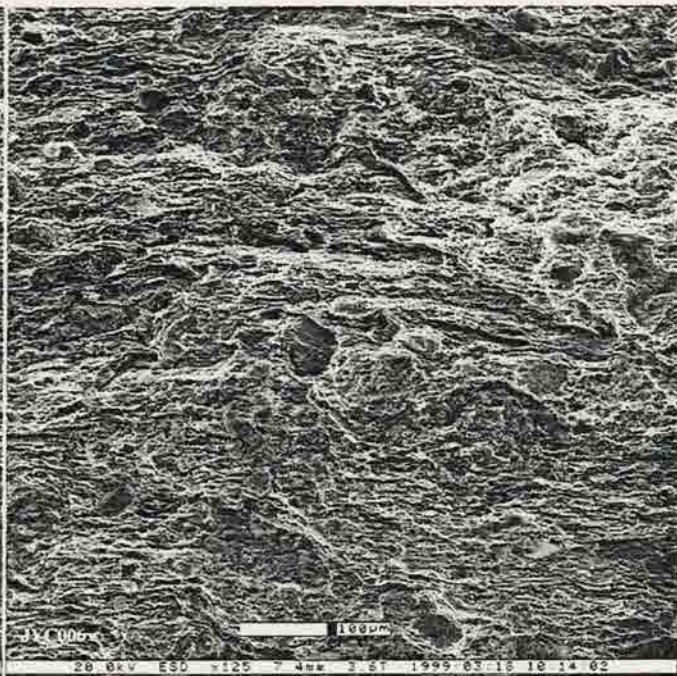
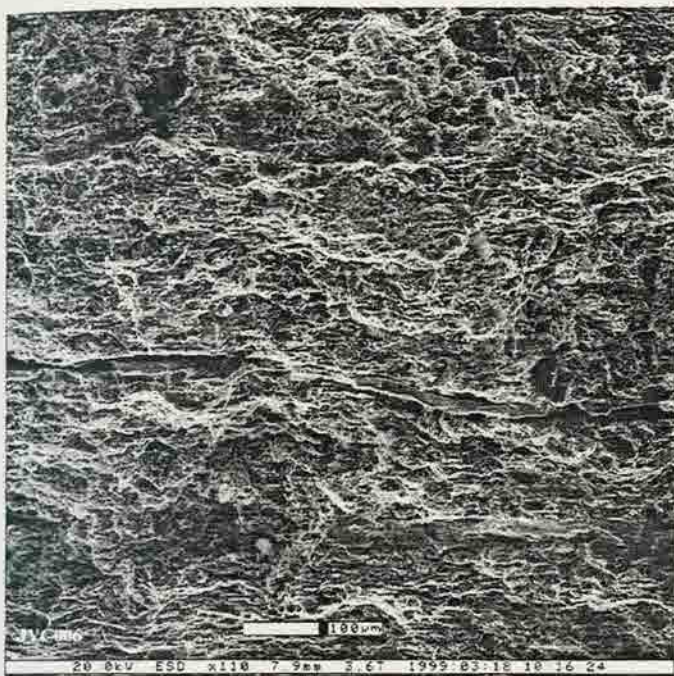
Top right: Low Power (x125)

Bottom left: High Power (x870)

Bottom right: High Power (x1950)

At low magnification, the overall texture is a moderately sorted, angular to subrounded, framework supported, silty shale. The framework particle size ranges from 30 to 50 μm and composes the bulk of this sample. The framework mineralogy primarily consists of detrital quartz grains with secondary amounts of feldspars and authigenic carbonates. Quartz overgrowths are present and seem to be cut off by clay cementation.

At high magnification, the “flake-like” nature of discrete illite is clearly displayed. The clay minerals show strong preferred orientation with well-developed laminations. The clays “bend” around the hard grains as seen in the bottom left picture. The sample exhibits a poorly developed intergranular macropore system and a poorly developed intergranular micropore system. Molds of plucked grains are found throughout this sample and an artifact of sample preparation.



THE UNIVERSITY OF CHICAGO
DEPARTMENT OF POLITICAL SCIENCE
1100 EAST 58TH STREET
CHICAGO, ILLINOIS 60637
(773) 936-3300

The University of Chicago is a leading center of research and learning in the social sciences, humanities, and natural sciences. It is a place where the most brilliant minds in the world come to study and to work. The University is committed to the highest standards of academic excellence and to the advancement of knowledge for the benefit of all.

The University of Chicago is a place where the most brilliant minds in the world come to study and to work. The University is committed to the highest standards of academic excellence and to the advancement of knowledge for the benefit of all. The University of Chicago is a place where the most brilliant minds in the world come to study and to work. The University is committed to the highest standards of academic excellence and to the advancement of knowledge for the benefit of all.

JYC016: 60 ft – Facies B

Top left: Low Power (x130)

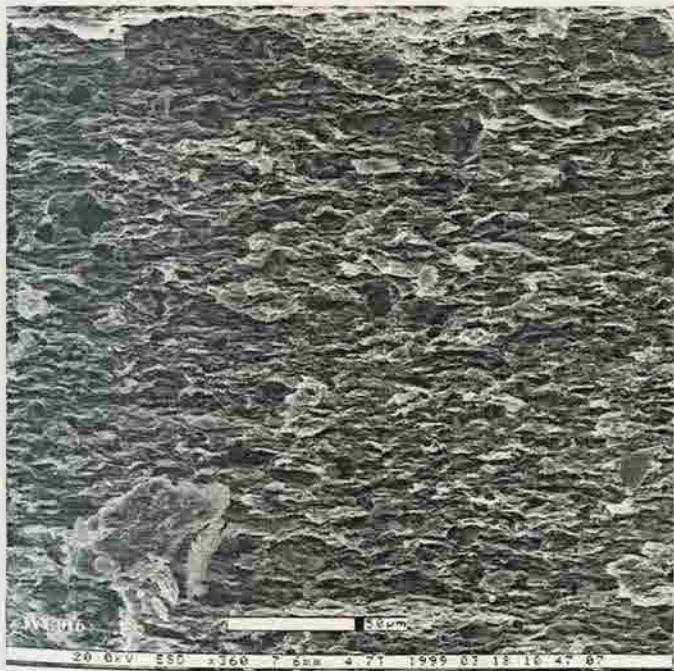
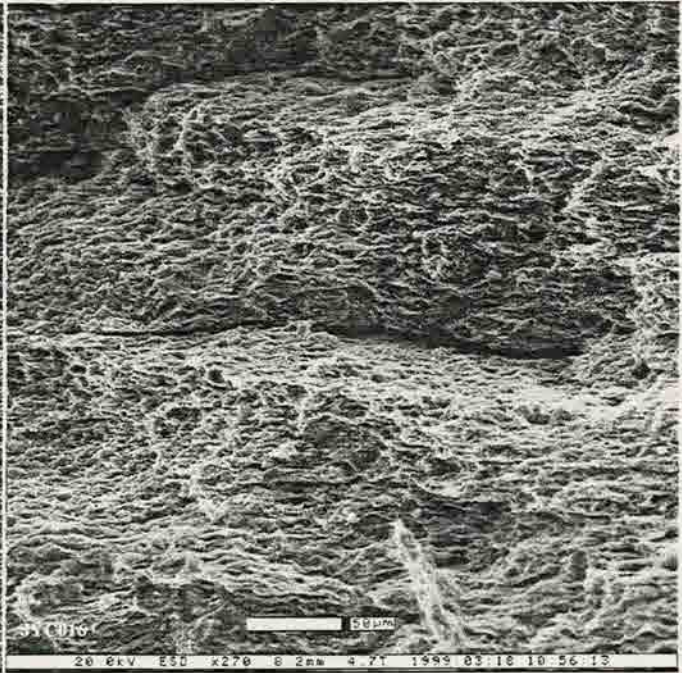
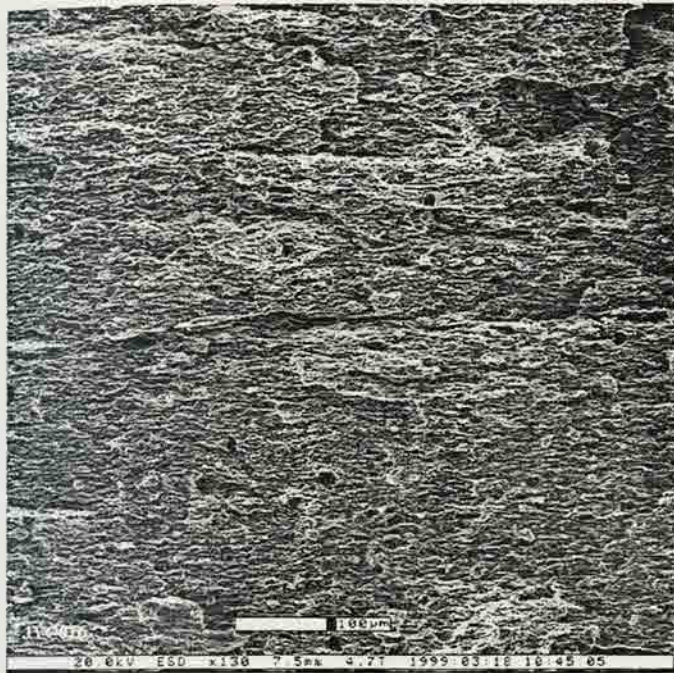
Top right: Low Power (x270)

Bottom left: Low Power (x360)

Bottom right: High Power (x1100)

At low magnification, the overall texture is a well sorted, subangular to subrounded, framework supported, silty shale. The framework particle size ranges from 10 to 30 μm and is homogeneously distributed throughout the bulk of this sample. The framework mineralogy primarily consists of detrital quartz grains with secondary amounts of authigenic carbonates and feldspars. Quartz overgrowths seem to be cut off by clay cementation.

At high magnification, the clays are to be coating the detrital hard grains. Discrete illite is shown as the light-colored, “flake-like” clay mineral. Small “books” of kaolinite may also be distinguished. The clays in this sample are primarily grain coating but are also pore filling. The sample exhibits a moderately developed intergranular macropore system and a poorly developed intergranular micropore system. Molds of plucked grains and fractured grains are an artifact of sample preparation.



JY045: 69 ft – Facies B

Top left: Low Power (x115)

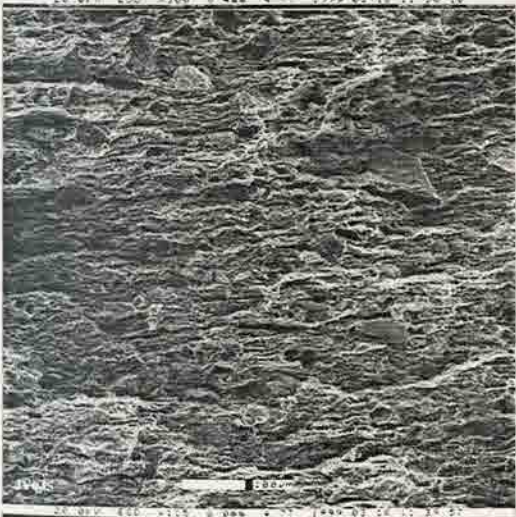
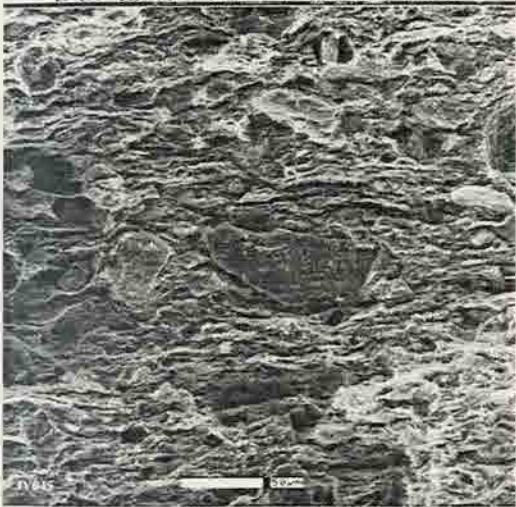
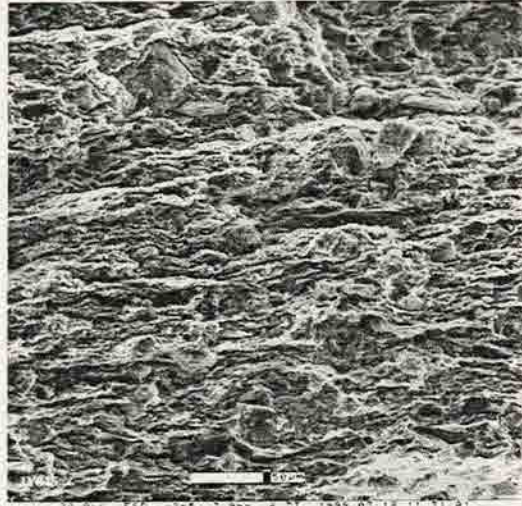
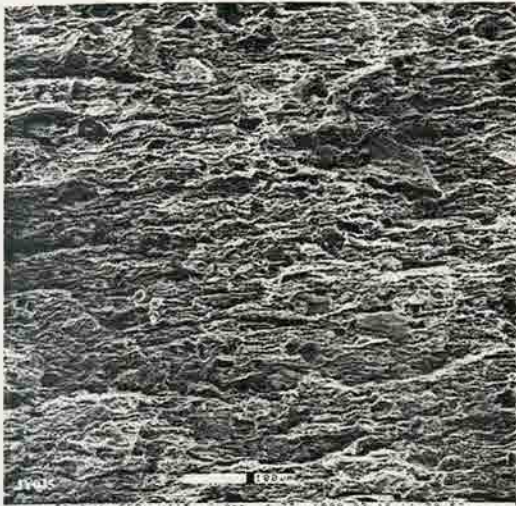
Top right: Low Power (x265)

Bottom left: Low Power (x300)

Bottom right: High Power (x605)

At low magnification, the overall texture is a moderate to well sorted, subangular to subrounded, framework supported silty shale. The framework particle size ranges from 10 to 30 μm and is homogeneously distributed throughout the bulk of this sample. The framework mineralogy primarily consists of detrital quartz with secondary amounts of authigenic carbonates, pyrite, and feldspars.

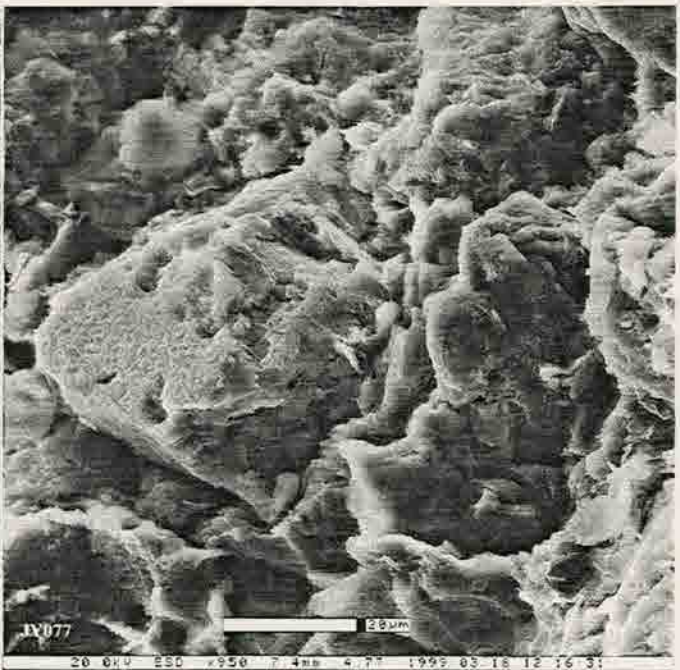
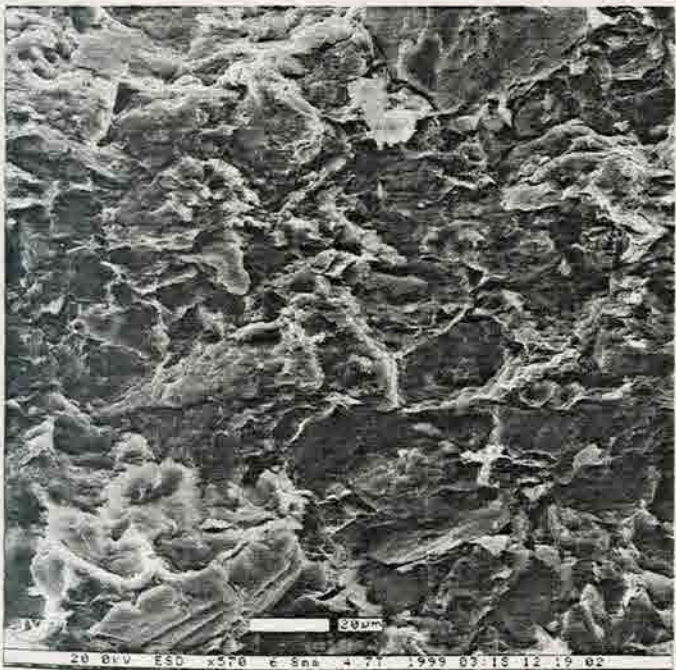
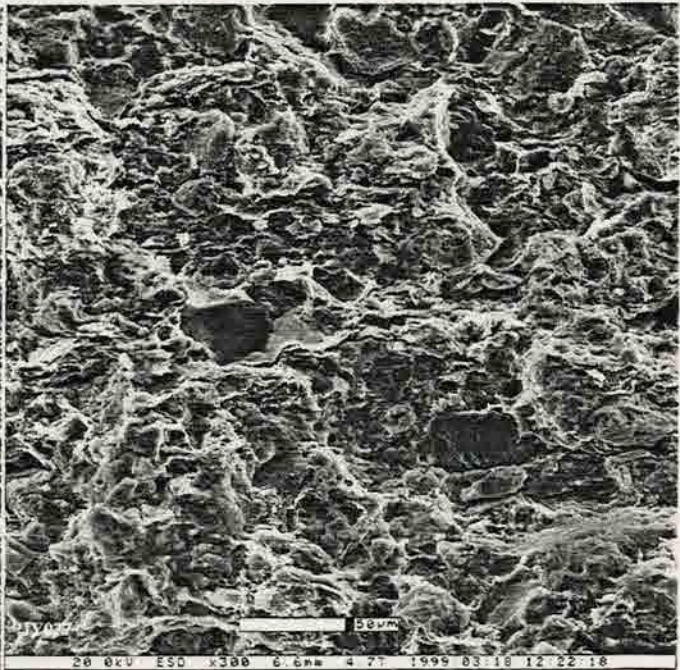
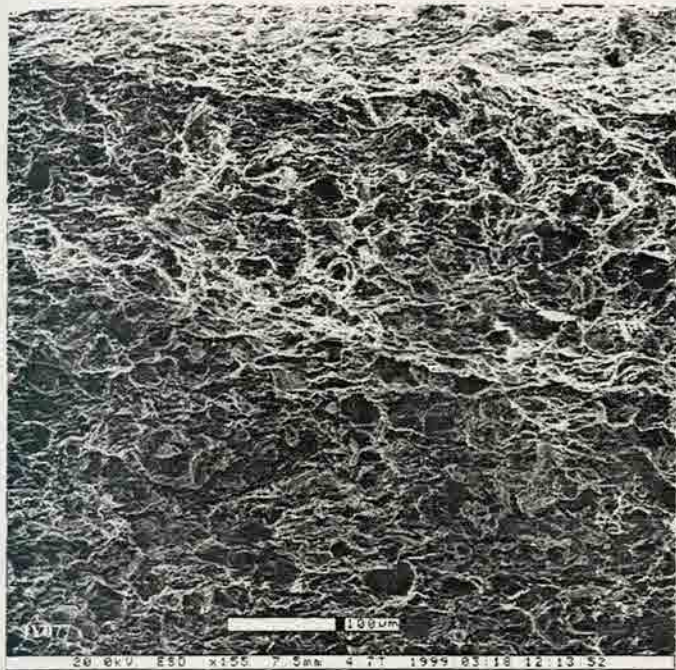
At high magnification, the clay minerals show a strong preferred orientation and well-developed laminations. The sample exhibits a moderately developed intergranular macropore system and a poorly developed intergranular micropore system. Some of the plucked grains and fractures are an artifact of sample preparation.



JY077: 108 ft – Facies C
Top left: Low Power (x155)
Top right: Low Power (x300)
Bottom left: High Power (x570)
Bottom right: High Power (x950)

At low magnification, the overall texture is a moderate to well sorted, subrounded, matrix supported paleosol. The framework particle size ranges from 30 to 50 μm and is homogeneously distributed. The framework mineralogy primarily consists of detrital quartz with secondary amounts of authigenic carbonates, pyrite, and feldspars.

At high magnification, the clays display grain-coating and pore-filling properties. Small “books” of kaolinite can be distinguished. The sample exhibits a moderate to well-developed intergranular macropore system and a moderately developed intergranular micropore system.



JY088: 130 ft – Facies C

Top left: Low Power (x120)

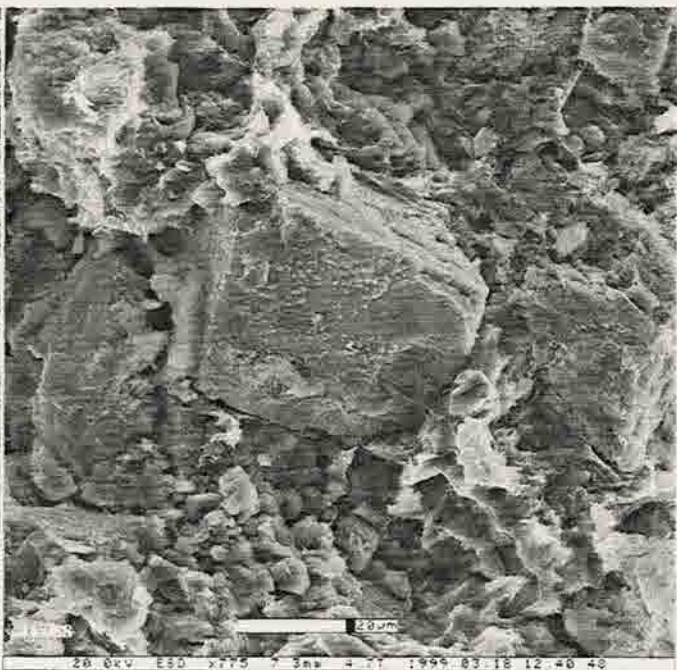
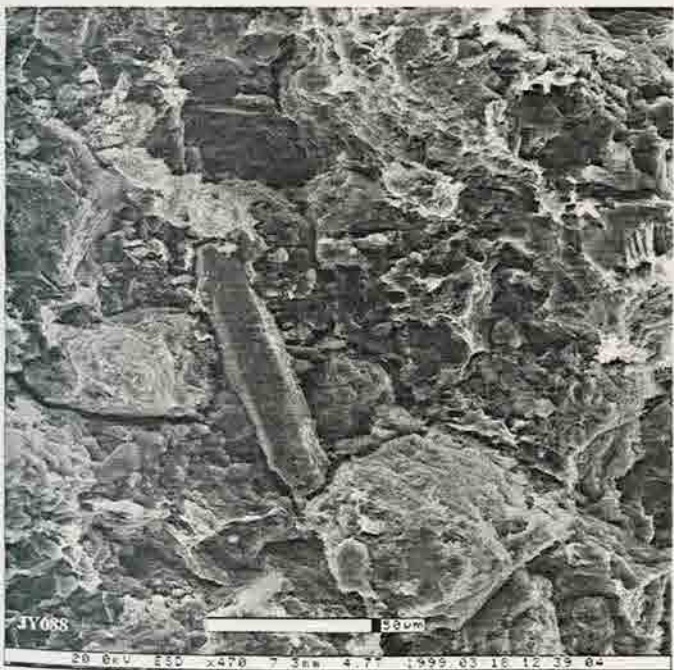
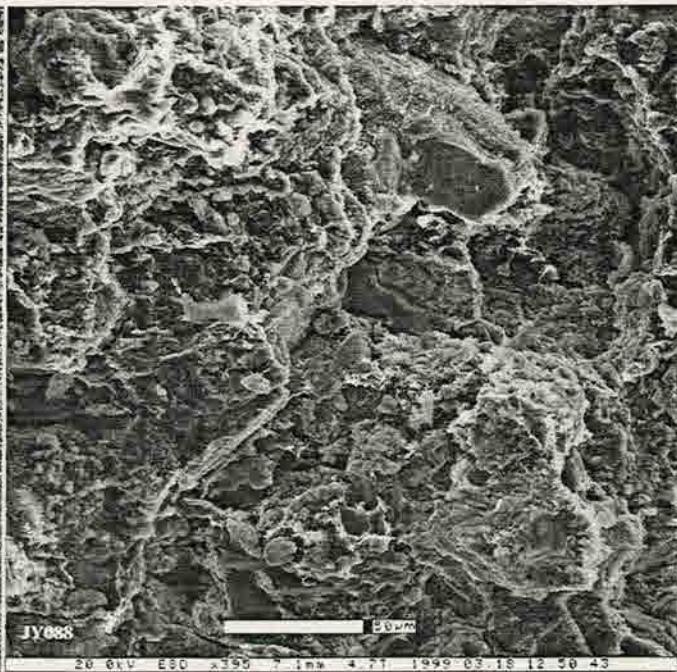
Top right: Low Power (x395)

Bottom left: High Power (x470)

Bottom right: High Power (x775)

At low magnification, the overall texture is a moderately sorted, subangular to subrounded, framework supported silty shale. The framework particle size ranges from 10 to 40 μm and is homogeneously distributed throughout the bulk of this sample. The framework mineralogy primarily consists of detrital quartz grains with secondary amounts of authigenic carbonate, pyrite, and feldspars.

At high magnification, large (40 μm) carbonate minerals can be distinguished due to their rhombic shape. These clays occur primarily as grain coating and pore filling interstitial fines with a strong preferred orientation. Small “books” of kaolinite are visible. The white flake-like clay mineral is discrete illite. The sample exhibits a moderately developed intergranular macropore system and a moderately developed intergranular micropore system. Molds of plucked grains are found throughout this sample and probably an artifact of sample preparation.



APPENDIX F

BELLEVUE OUTCROP

SKULL CREEK SHALE

MICP GRAPHS

MICP table for Bellevue Outcrop (Skull Creek shale)

Sample#	FT	Facies	Median PTD	Pore Volume %	Sorting Index
JY-004	4	K	0.02	60	W
			0.008	20	M
			0.05	20	M
JY-009	9	K	0.01	60	W
			0.025	40	M
JY-014	14	K	0.015	50	M-W
			0.03	40	P-M
			0.15	10	W
JY-020	20	K	0.03	70	M
			0.09	30	M
JY-025	25	K	0.045	60	M
			0.01	40	P-M
JY-030	30	K	0.045	50	M
			0.015	50	P-M
JY-036	36	K	0.02	50	W
			0.06	50	M
JY-040	40	K	0.025	70	W
			0.1	30	P-M
JY-044	44	K	0.3	40	VW
			0.1	40	P
			0.015	20	P-M
JYC-005	49	K	0.09	50	M
			0.3	30	P-M
			0.02	20	M
JYC-010	54	A	0.015	60	M
			0.07	40	M-W
JYC-015	59	B	0.06	60	W
			0.02	40	P-M
JYC-021	65	B	0.3	50	W
			0.08	50	P-M
JY-046	70	B	0.45	60	VW
			0.1	20	P
			0.015	20	P-M
JY-051	75	B	0.02	60	P
			0.05	30	M
			0.007	10	M
JY-056	80	B	0.05	50	M
			0.01	50	P-M
JY-061	85	B	0.2	40	VW
			0.04	40	P
			0.1	20	M
JY-074	102	B	0.2	40	M
			0.03	50	P
			0.01	10	P-M
JY-080	114	C	0.1	40	VW
			1	30	P
			0.02	30	M
JY088	130	C	0.09	50	VW
			0.2	30	P-M
			0.02	20	M

LEGEND:

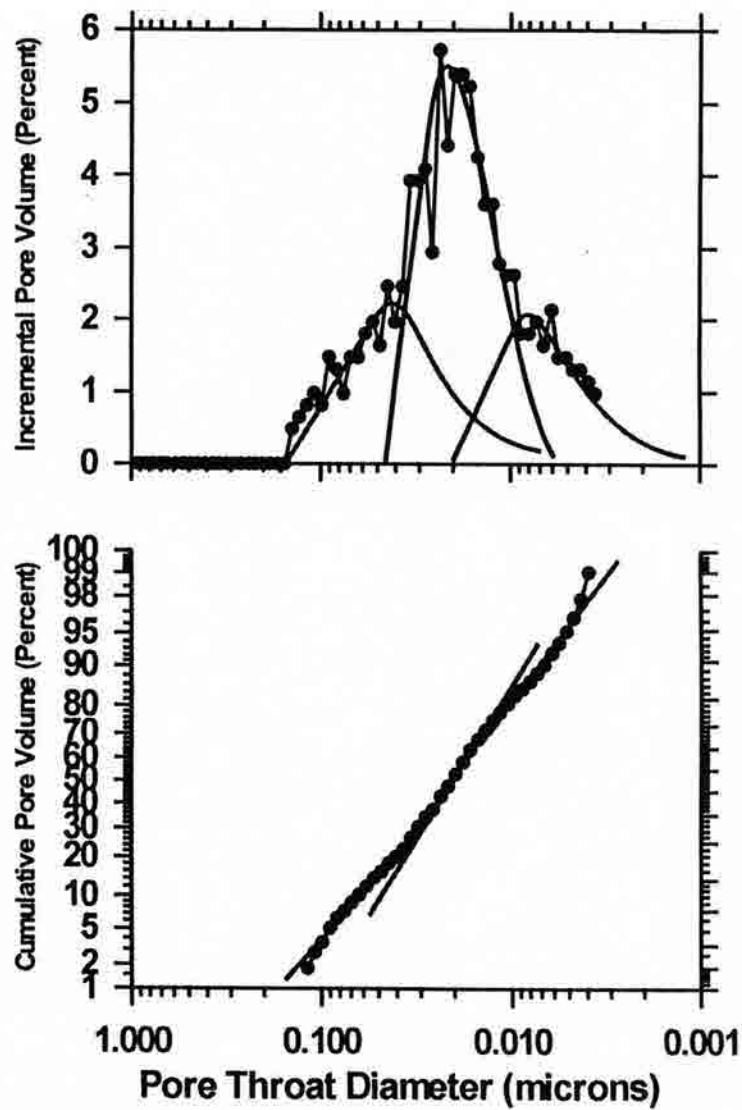
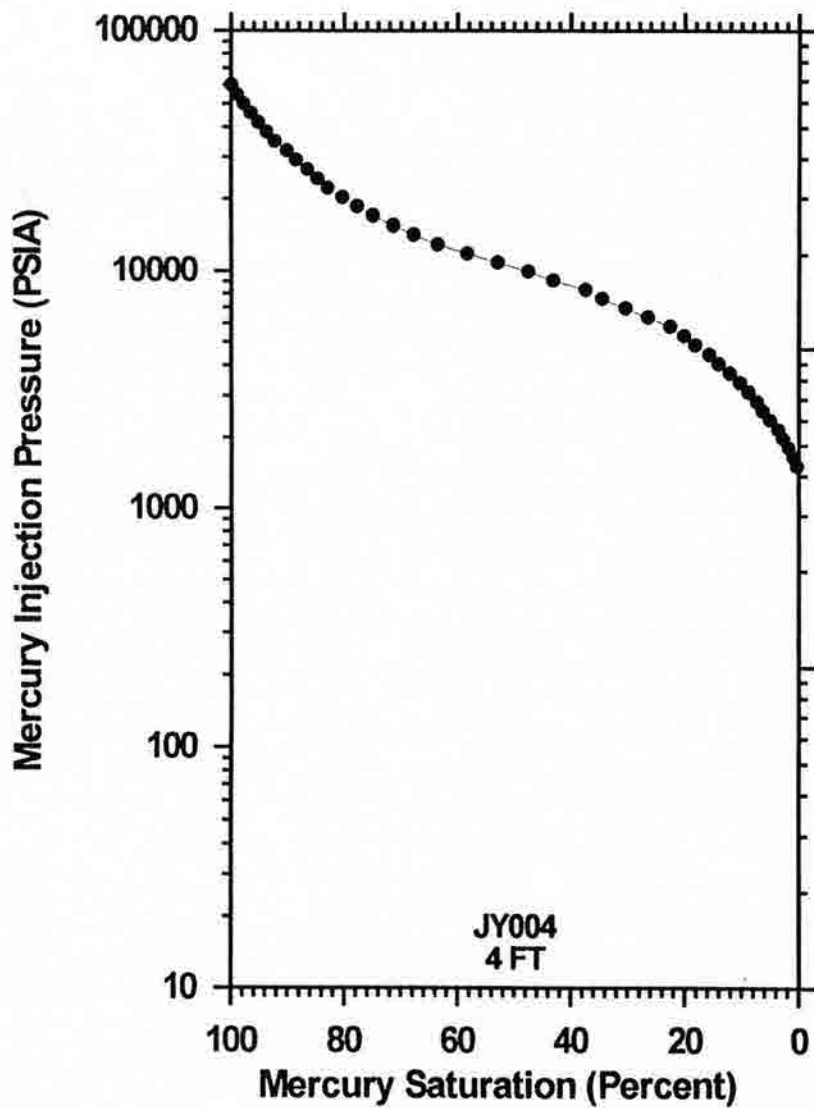
VW= Very Well sorted

W= Well sorted

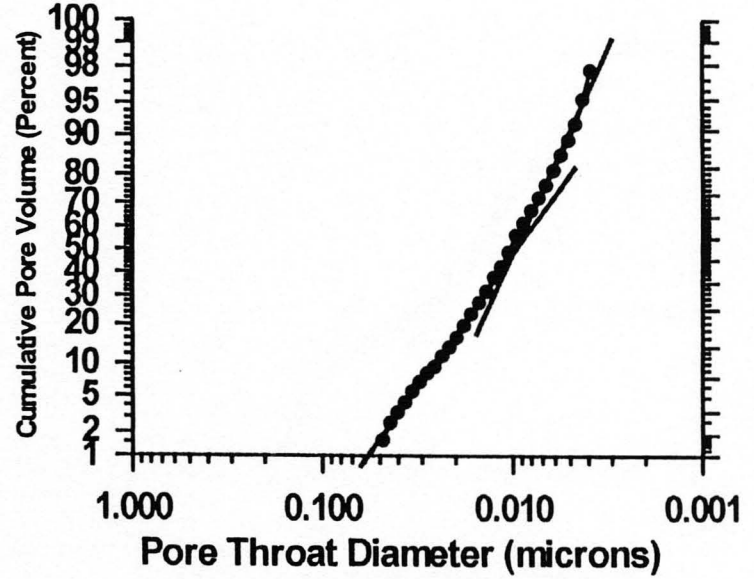
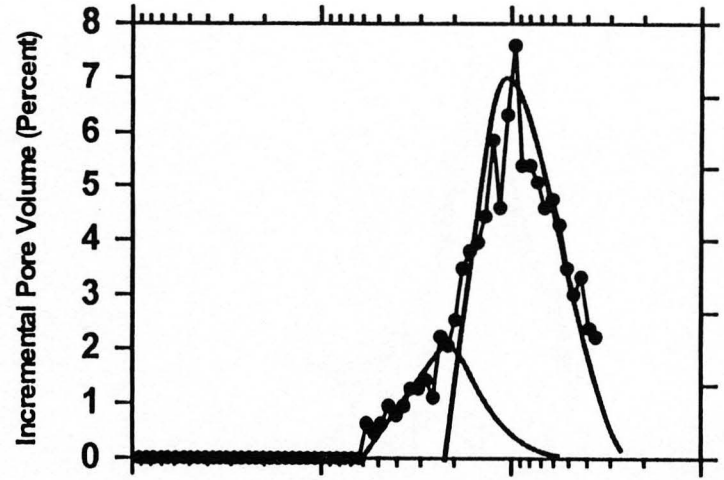
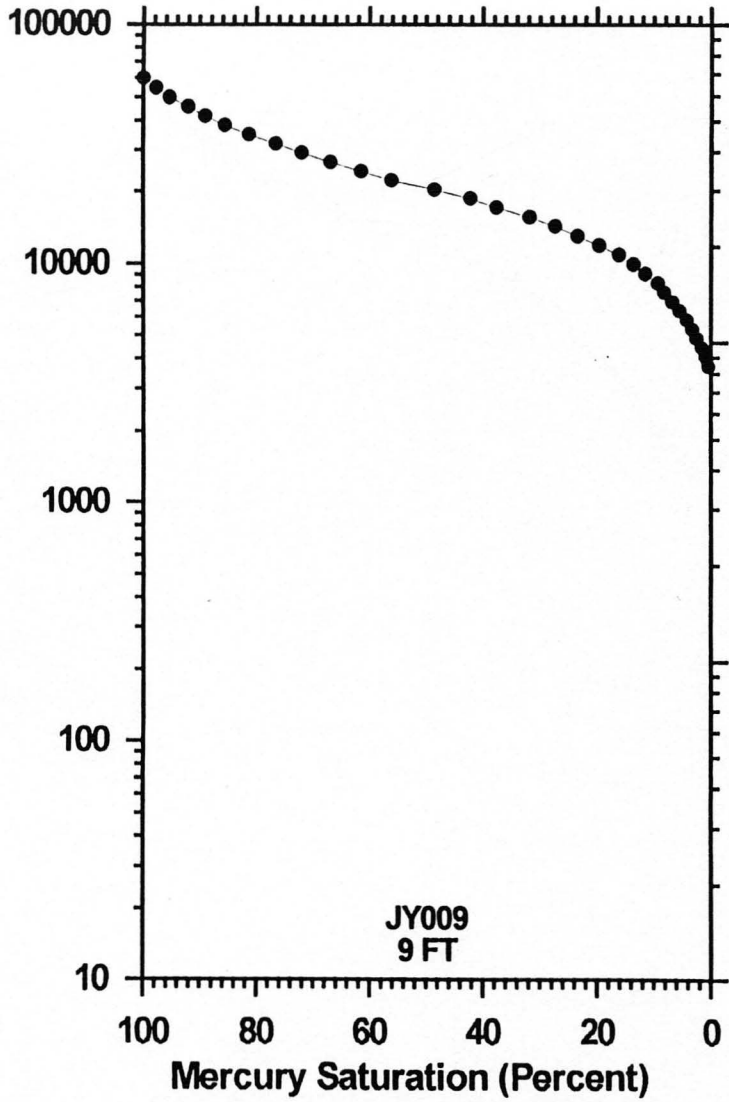
MW= Moderately-well sorted

M= Moderately sorted

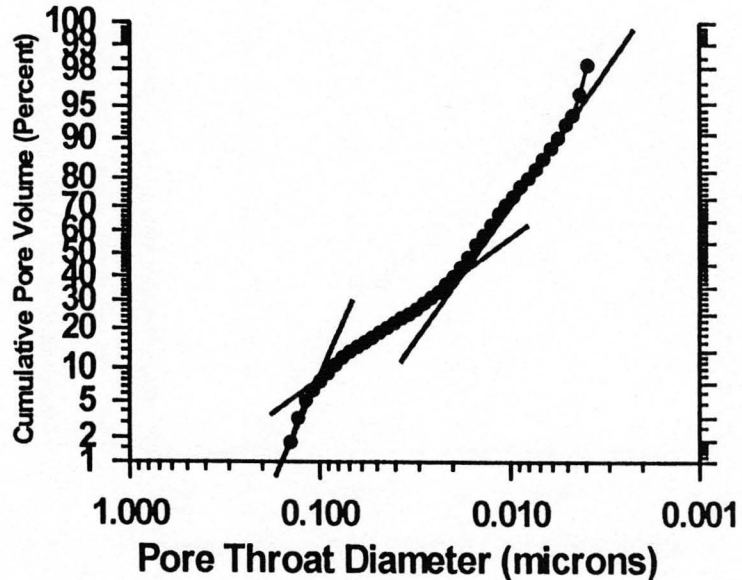
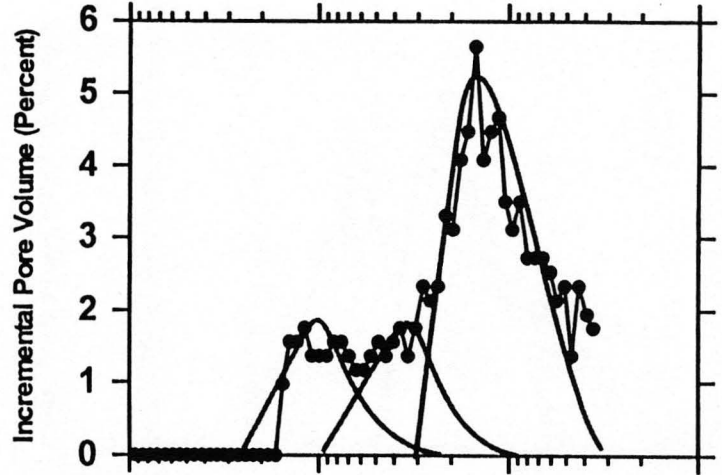
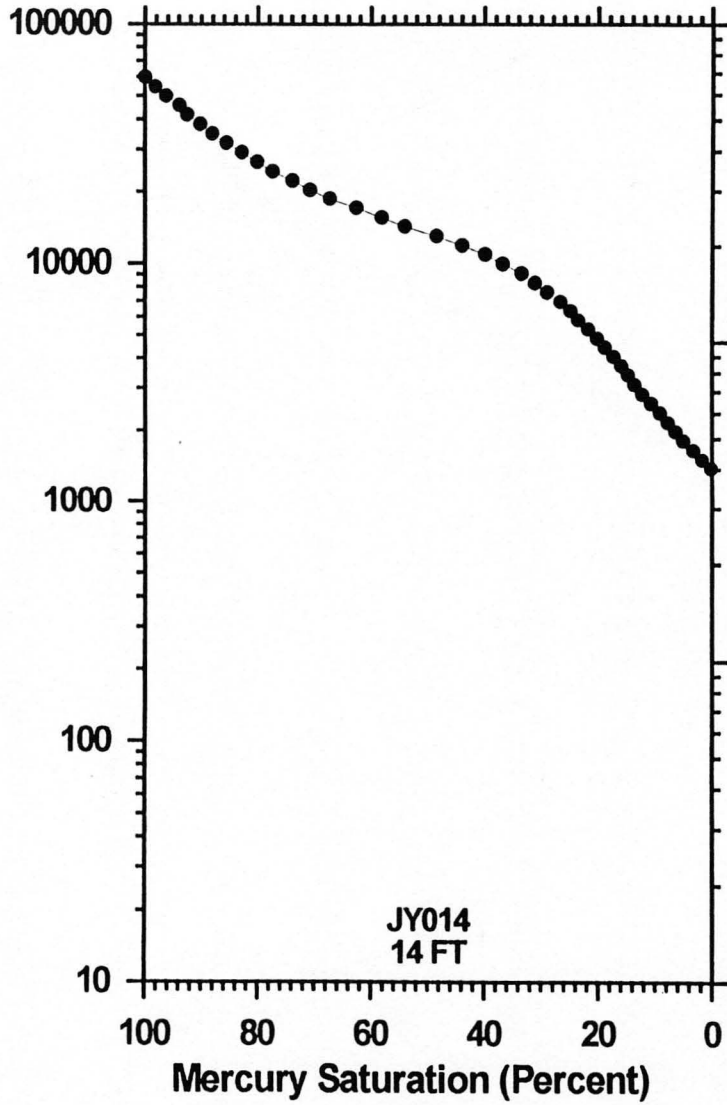
P= Poorly sorted



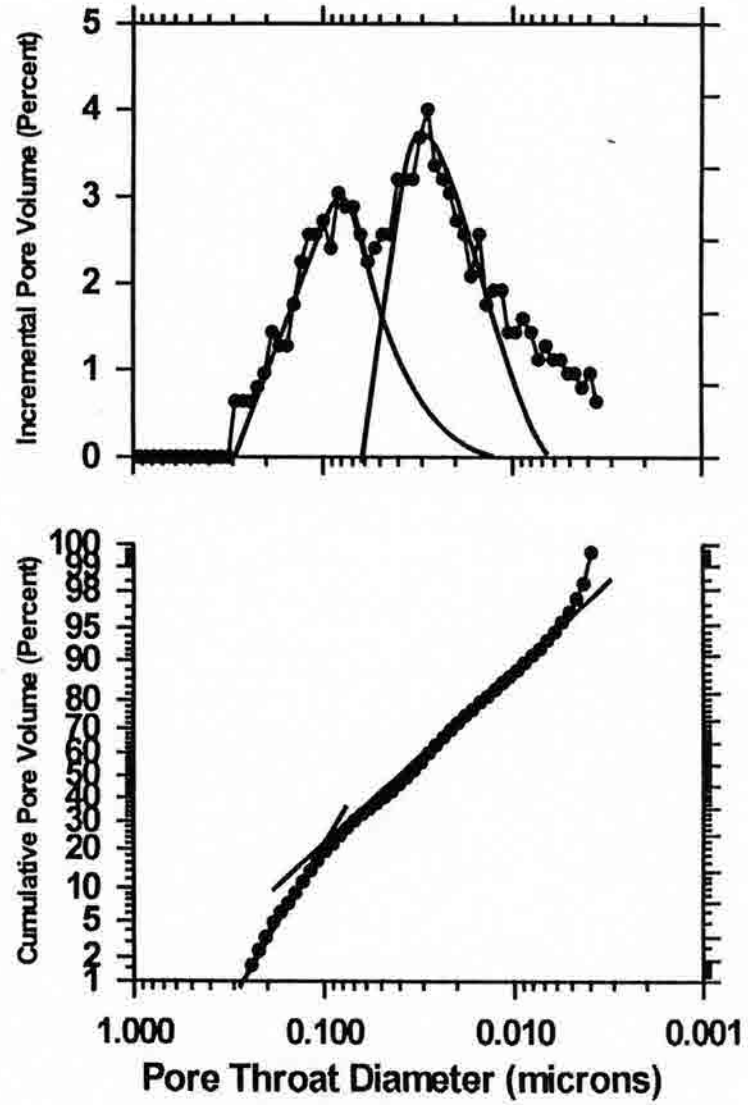
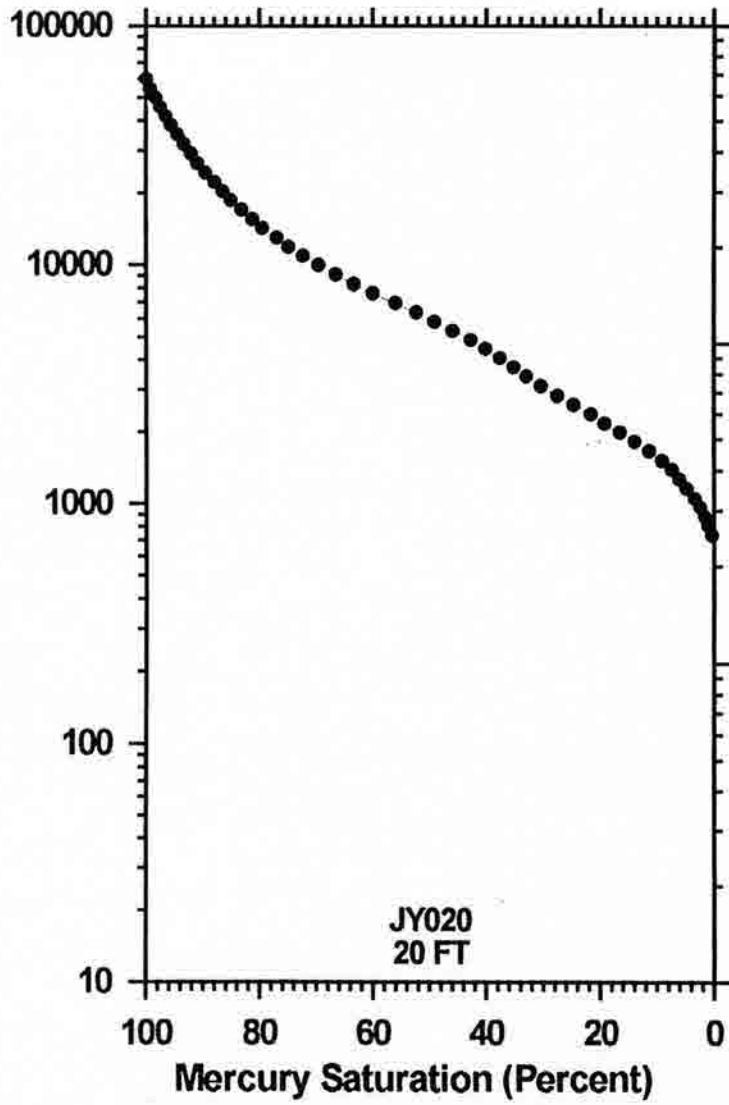
Mercury Injection Pressure (PSIA)



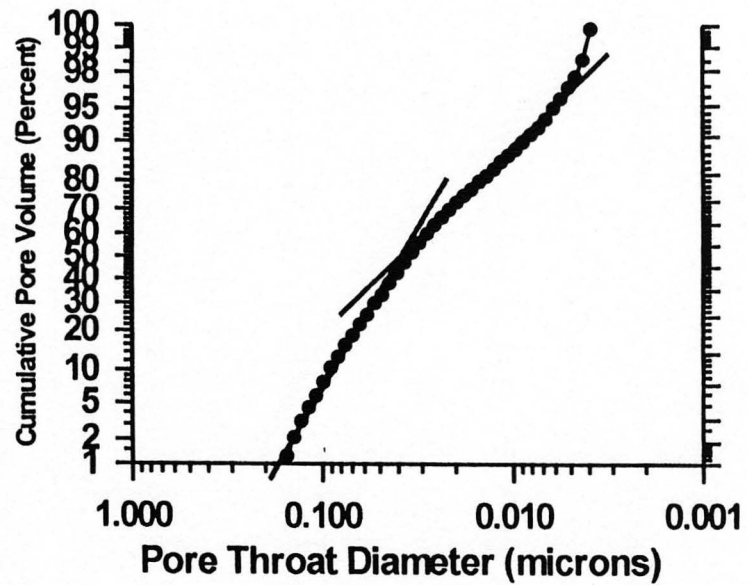
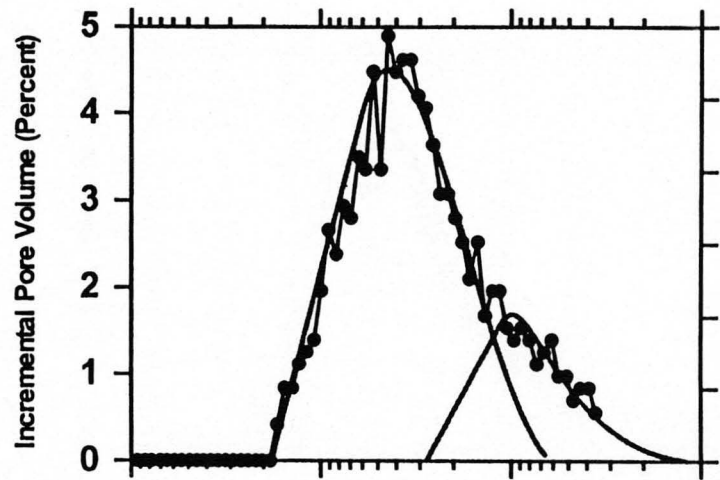
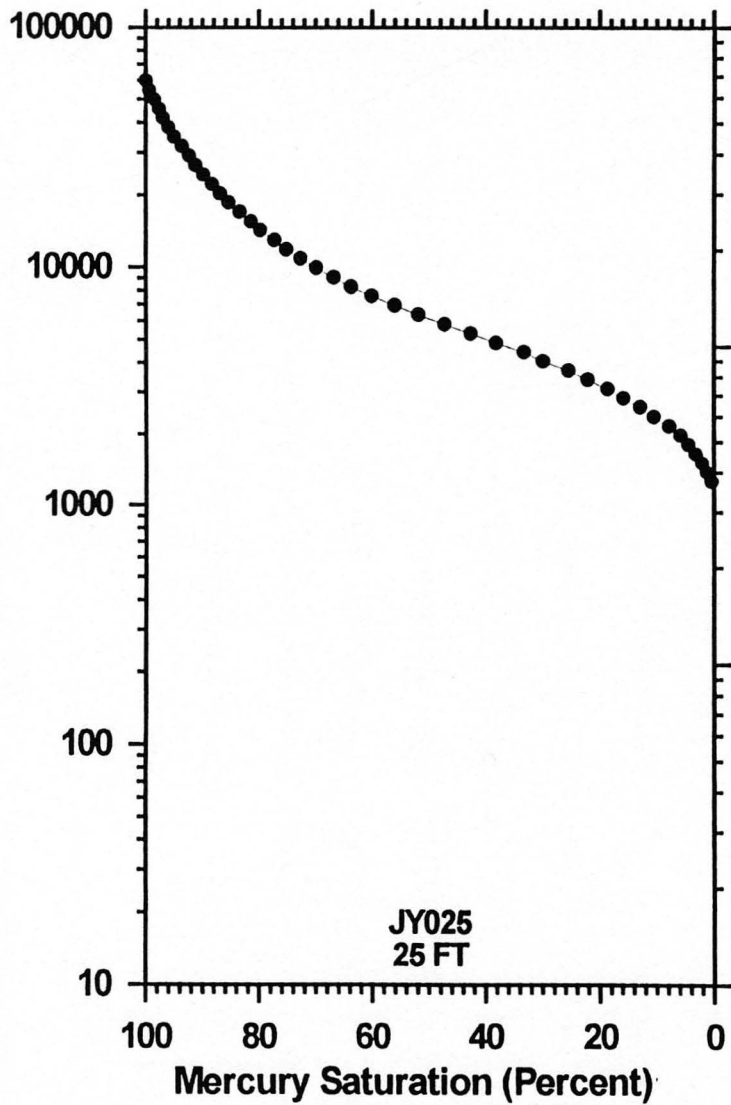
Mercury Injection Pressure (PSIA)

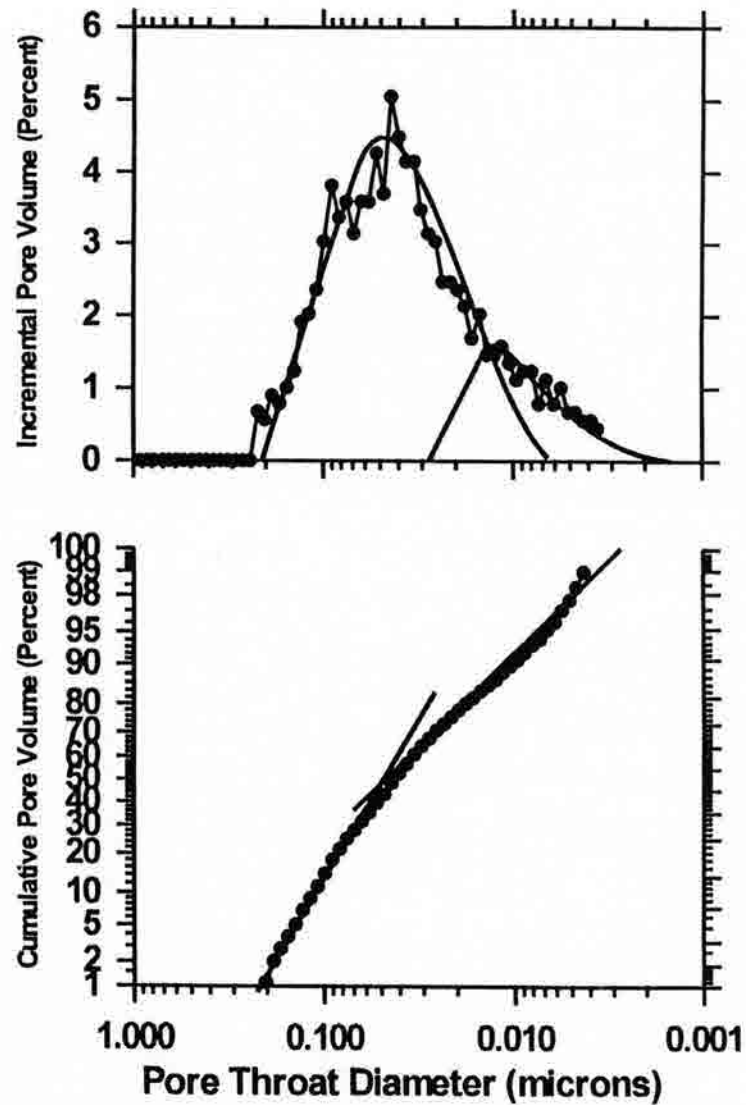
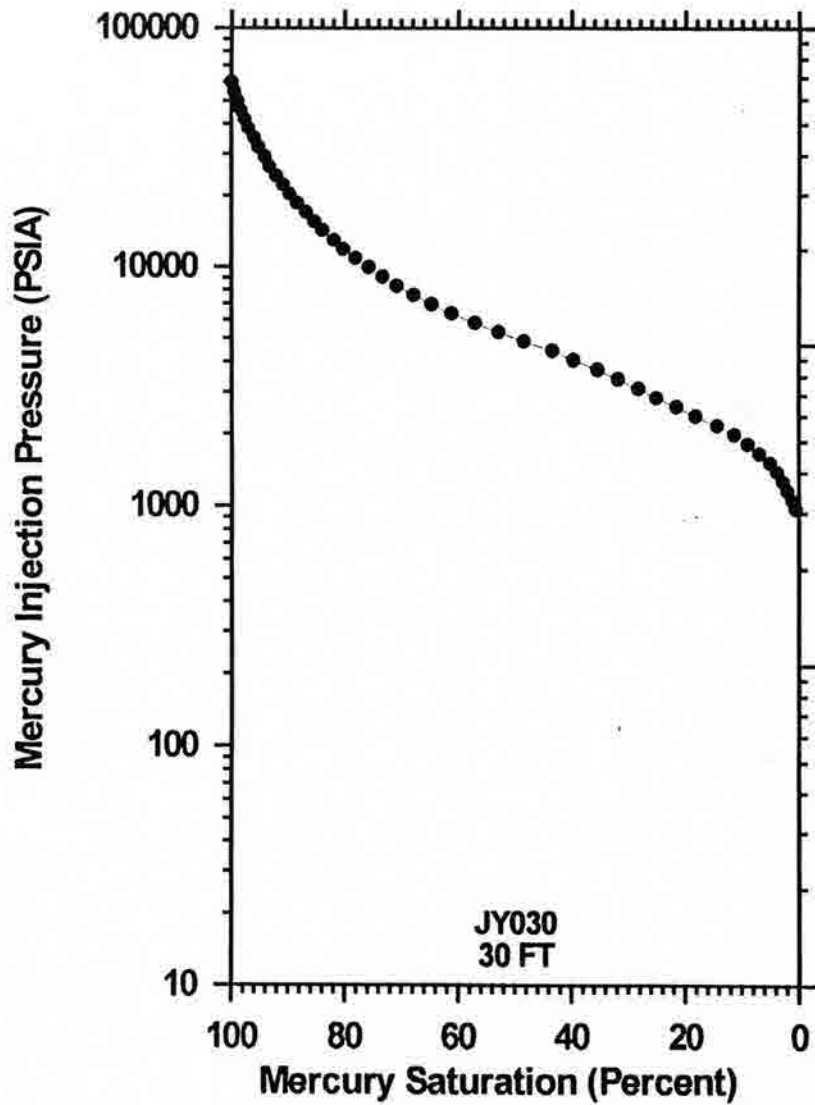


Mercury Injection Pressure (PSIA)

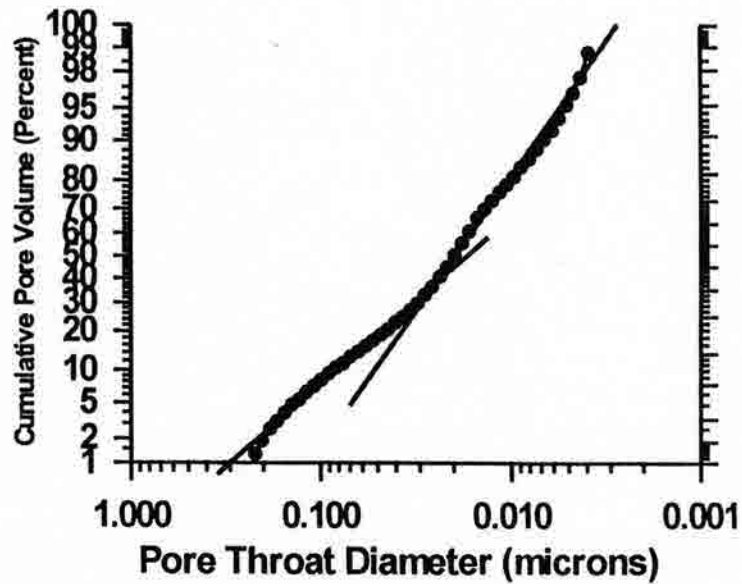
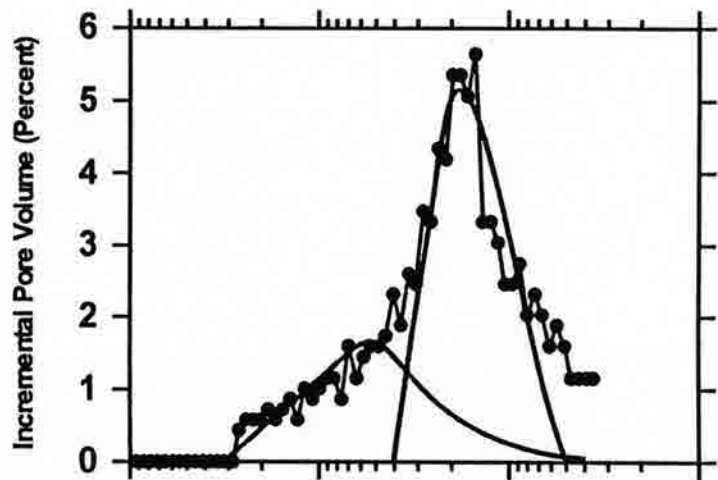
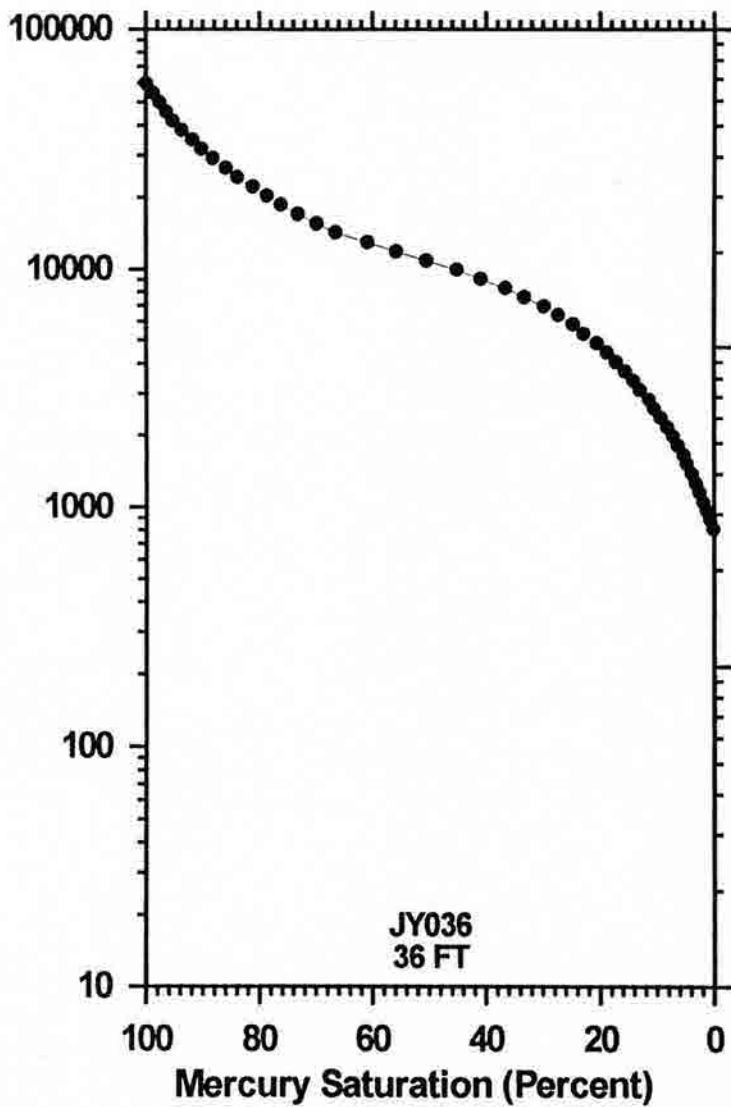


Mercury Injection Pressure (PSIA)

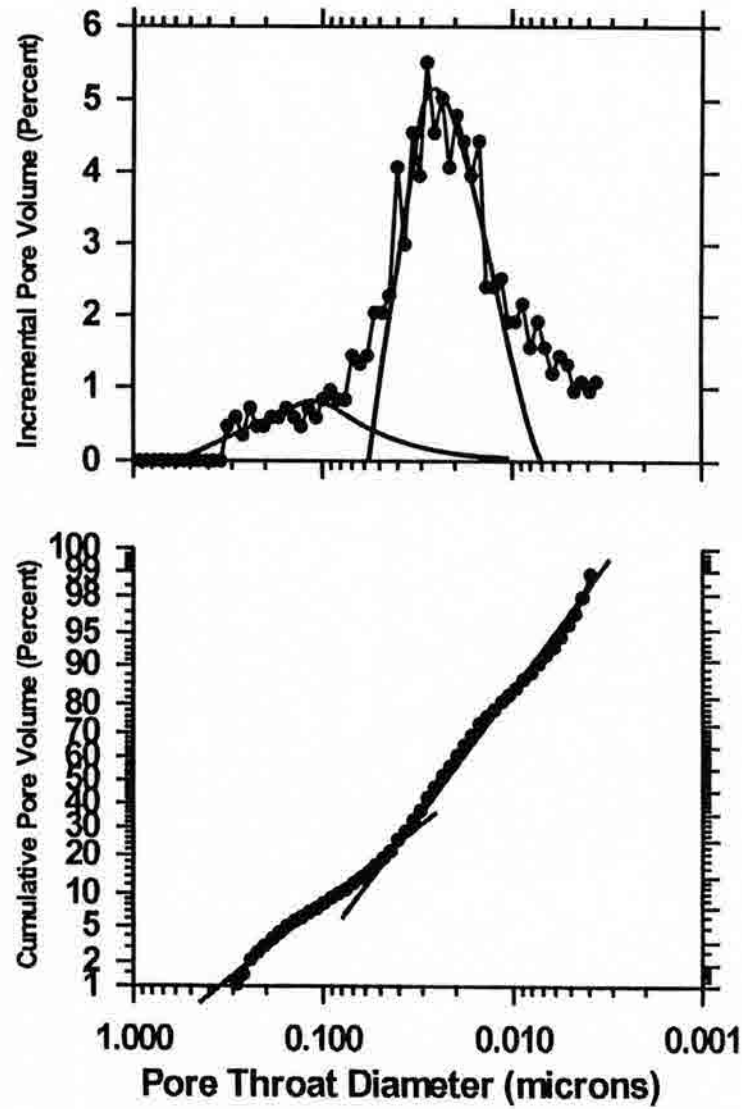
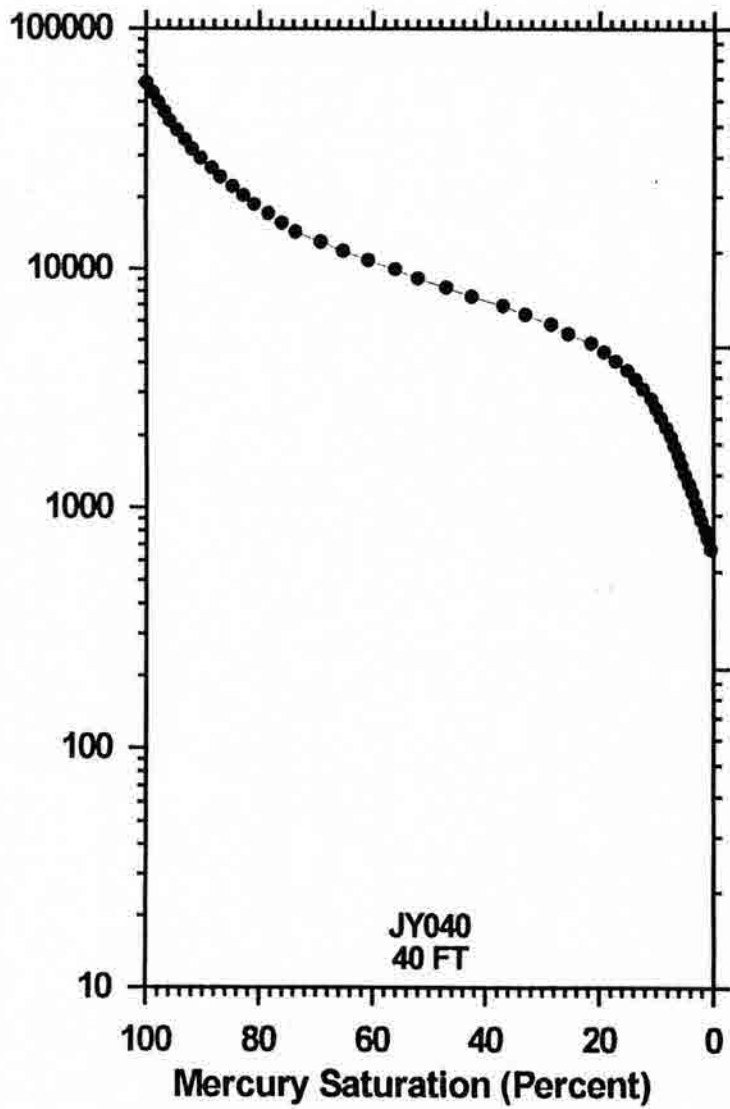


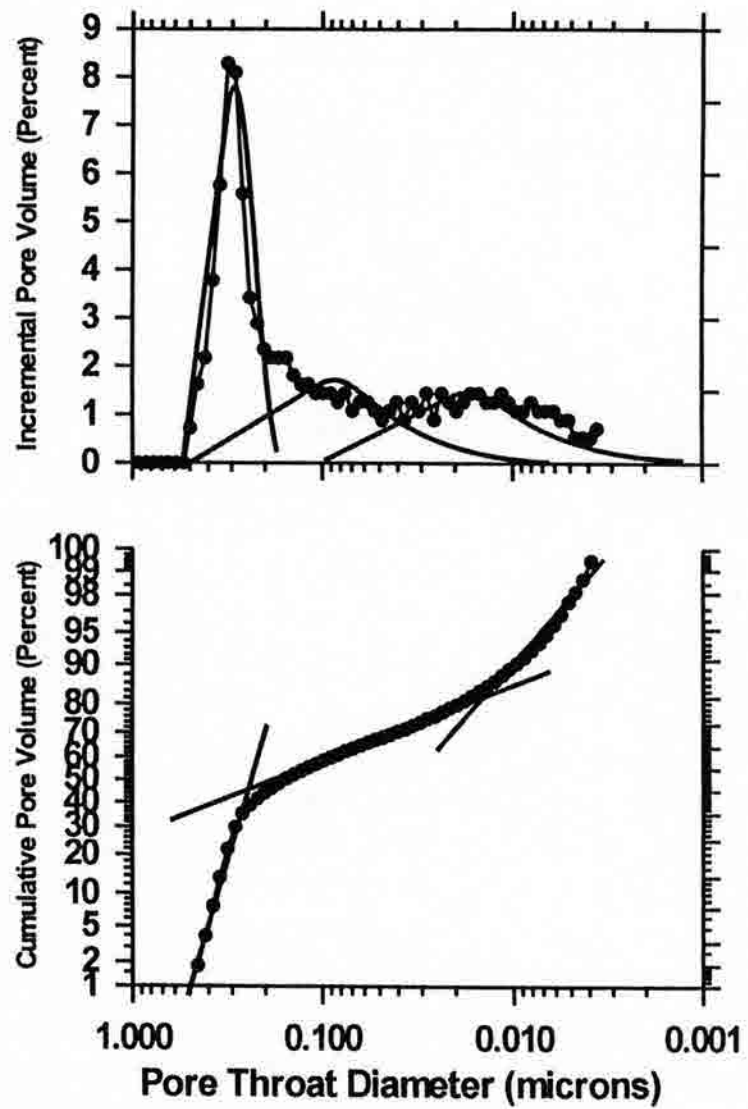
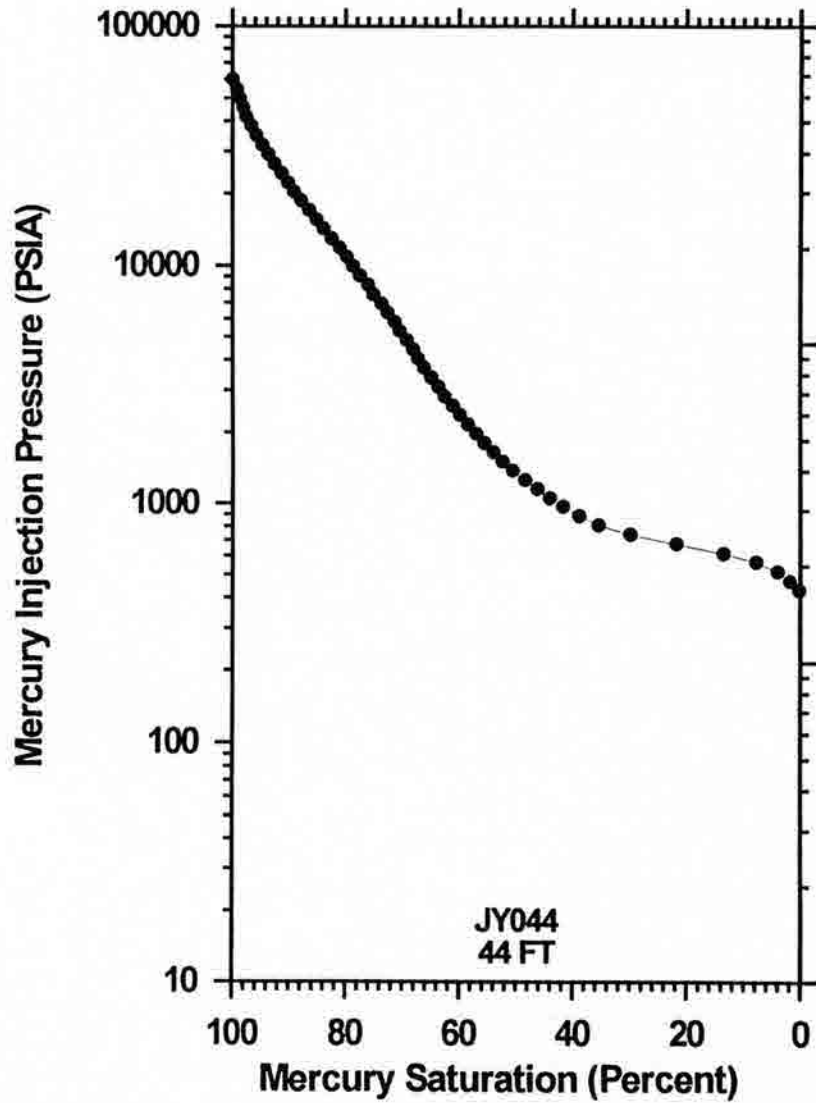


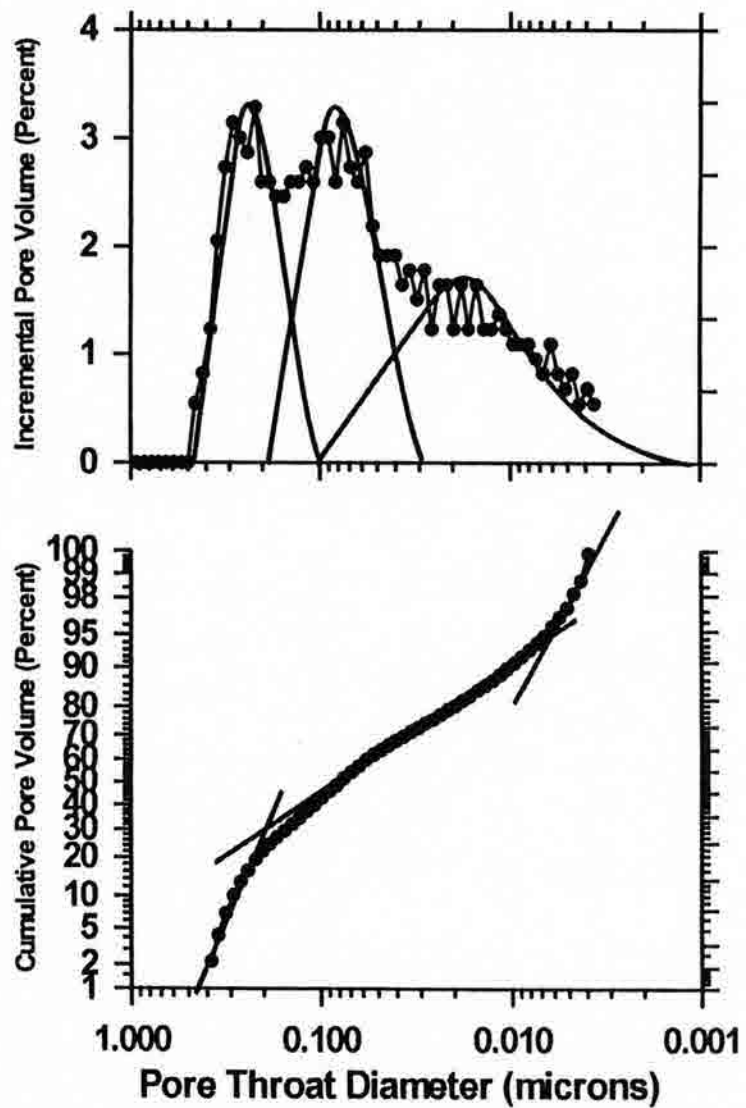
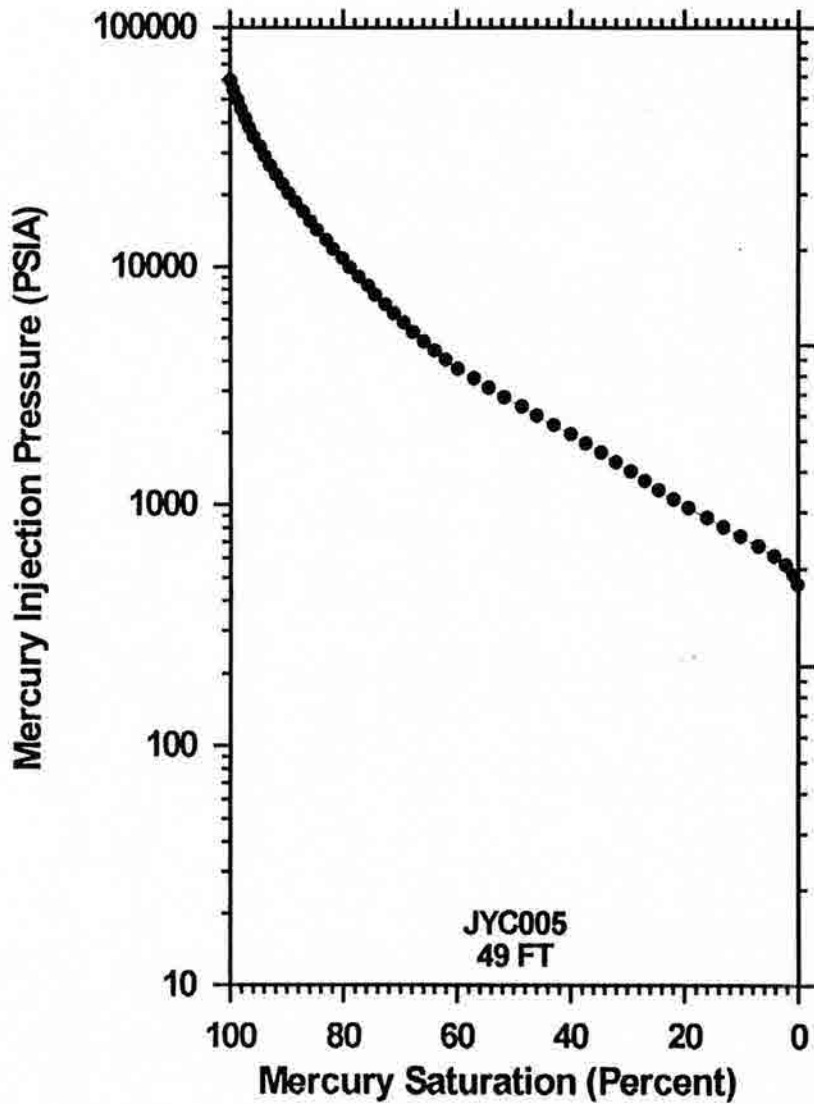
Mercury Injection Pressure (PSIA)

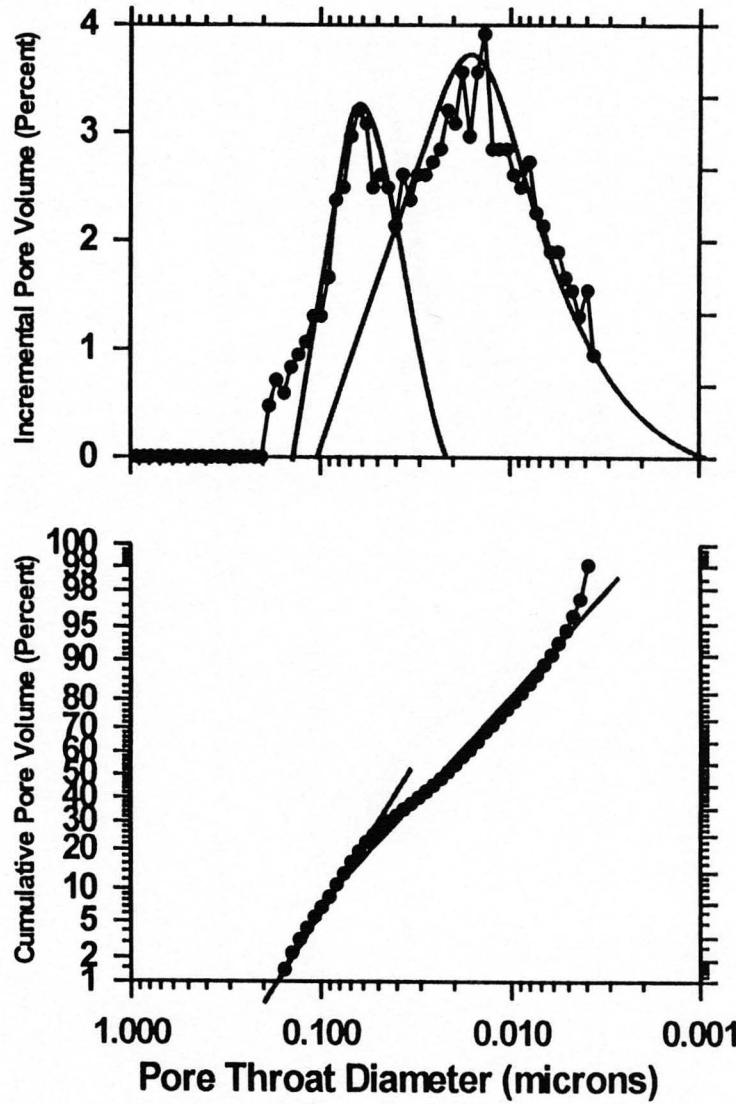
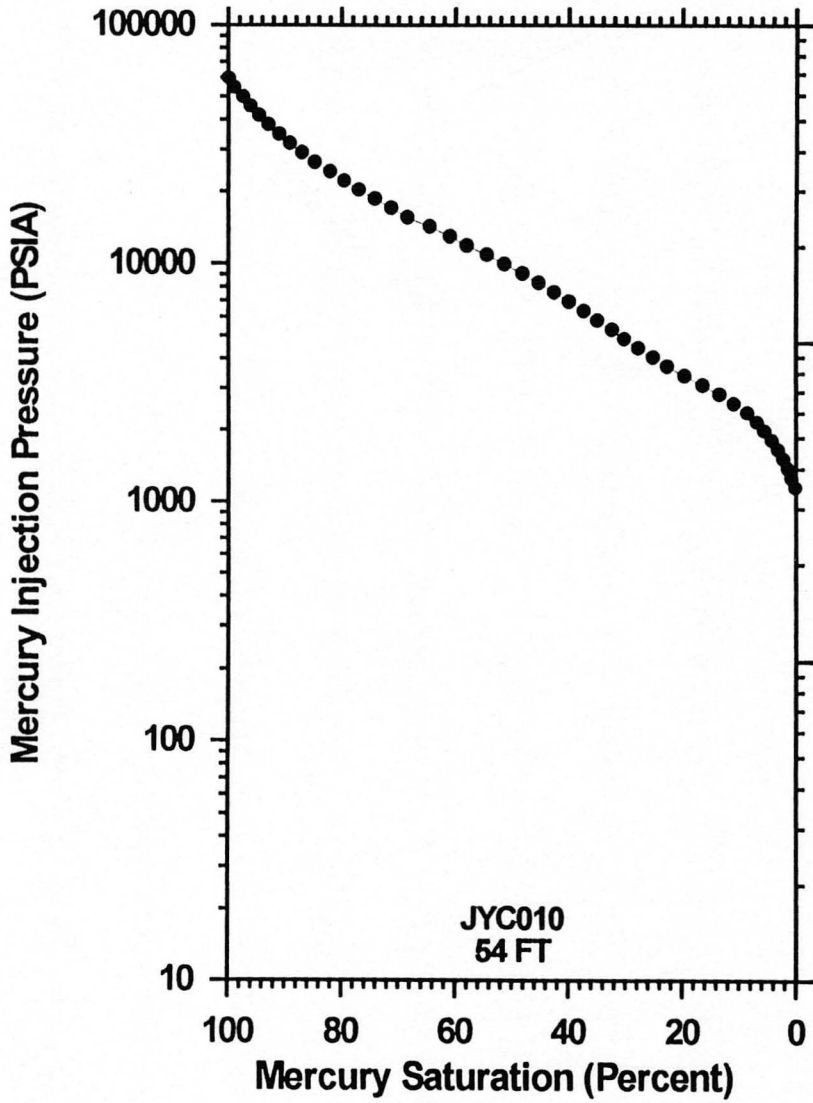


Mercury Injection Pressure (PSIA)

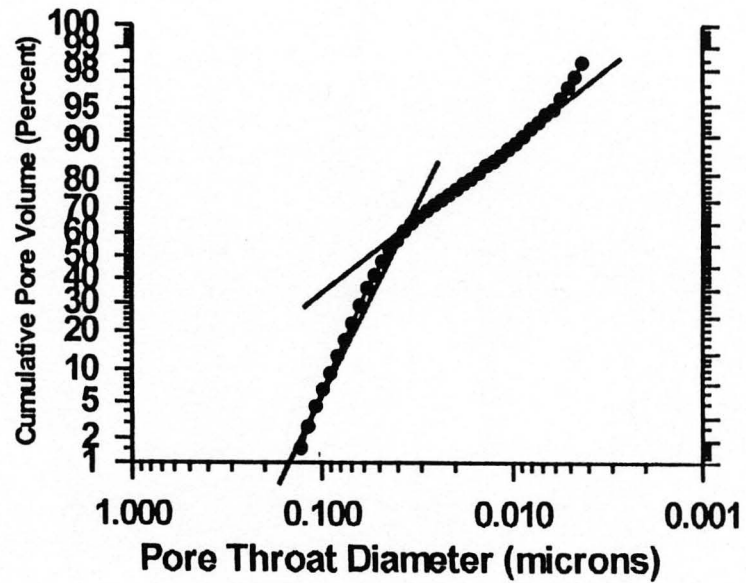
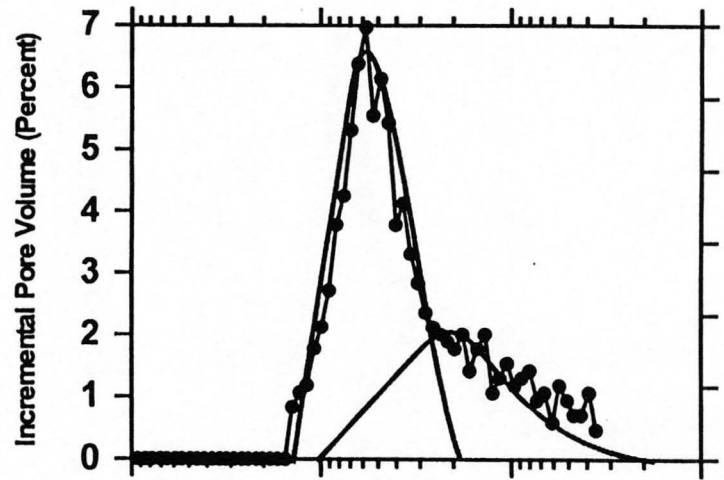
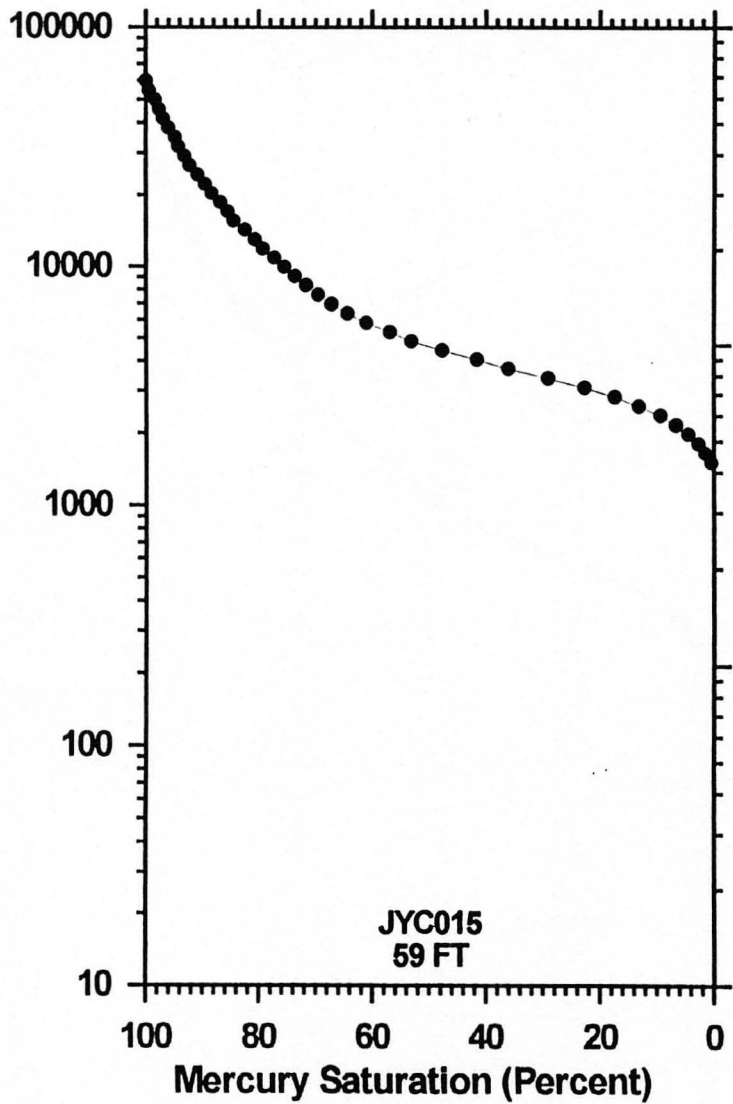




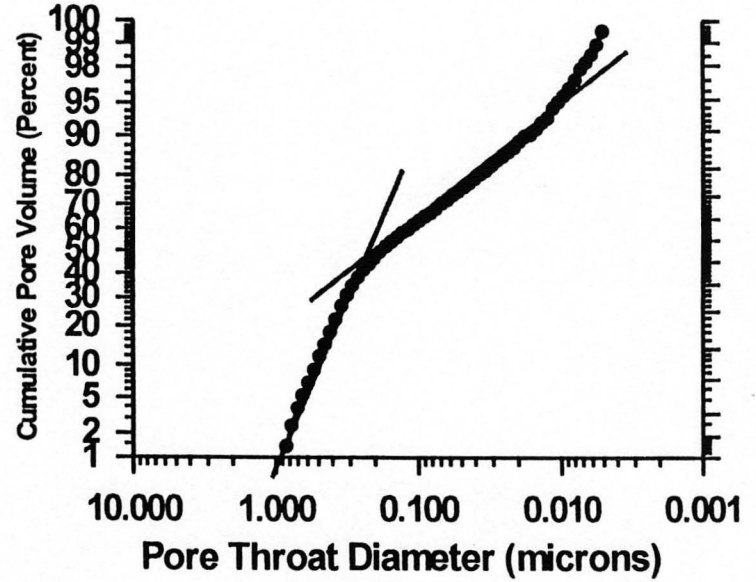
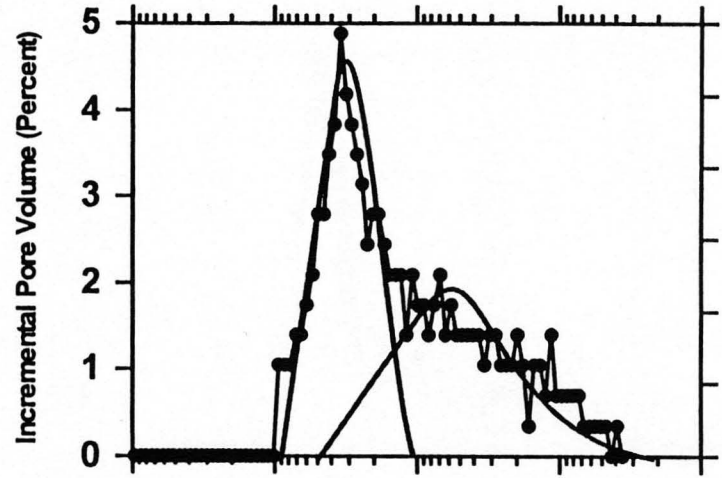
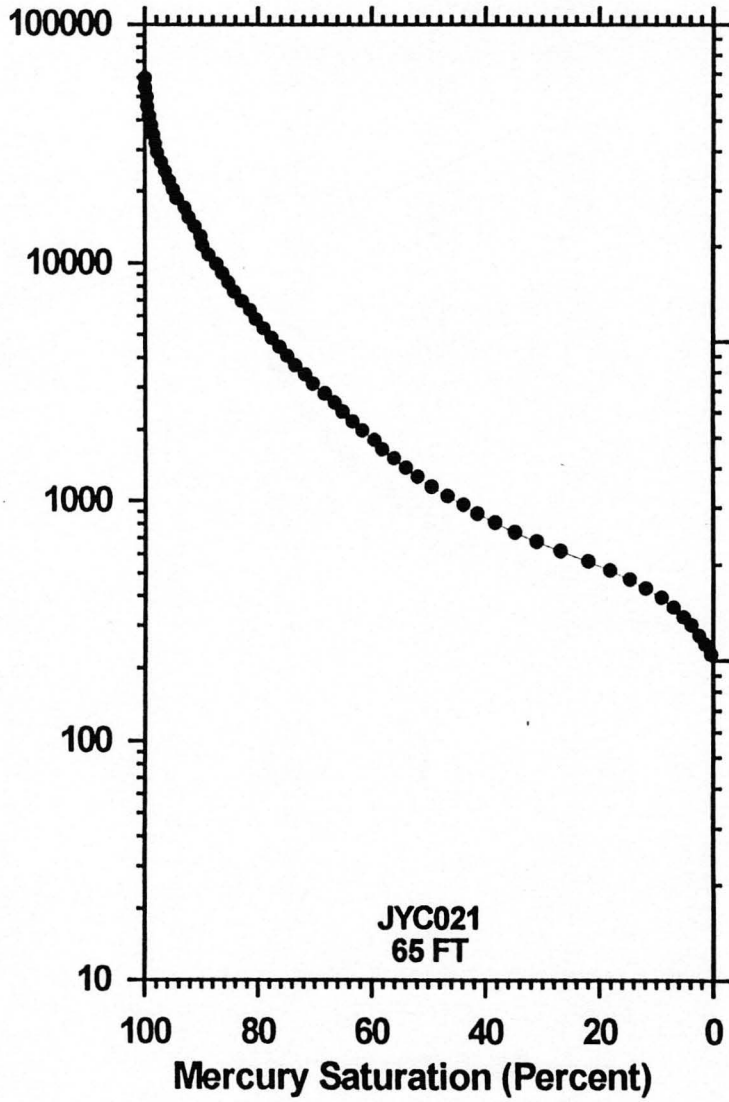


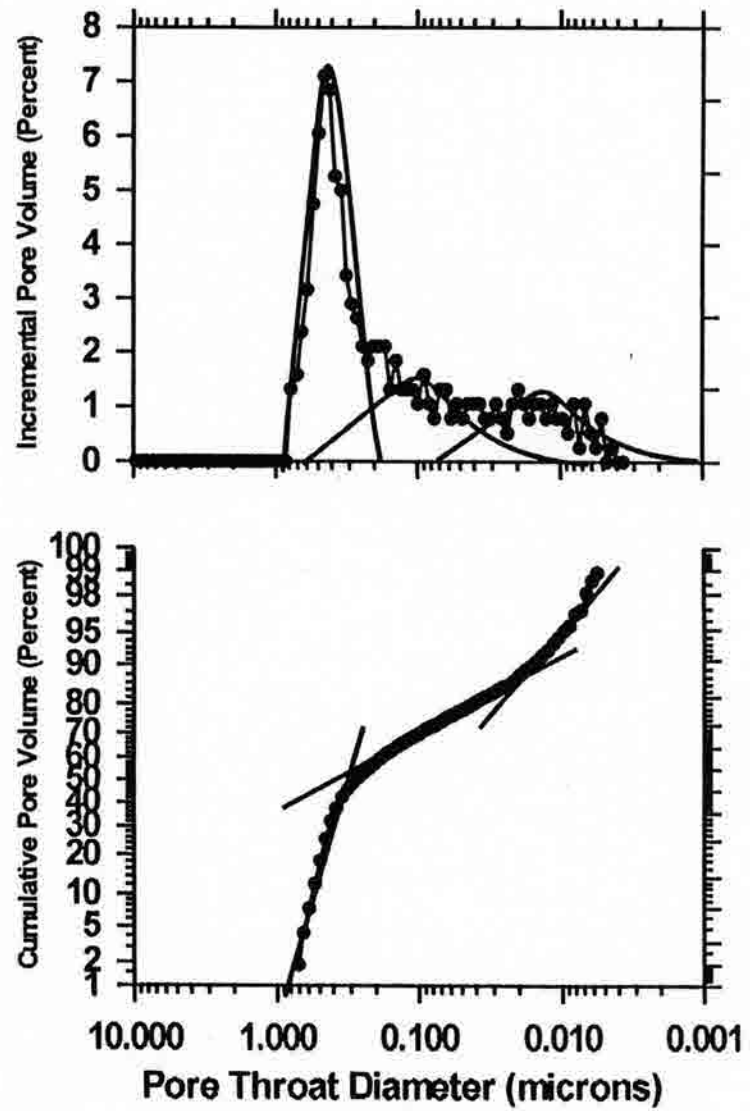
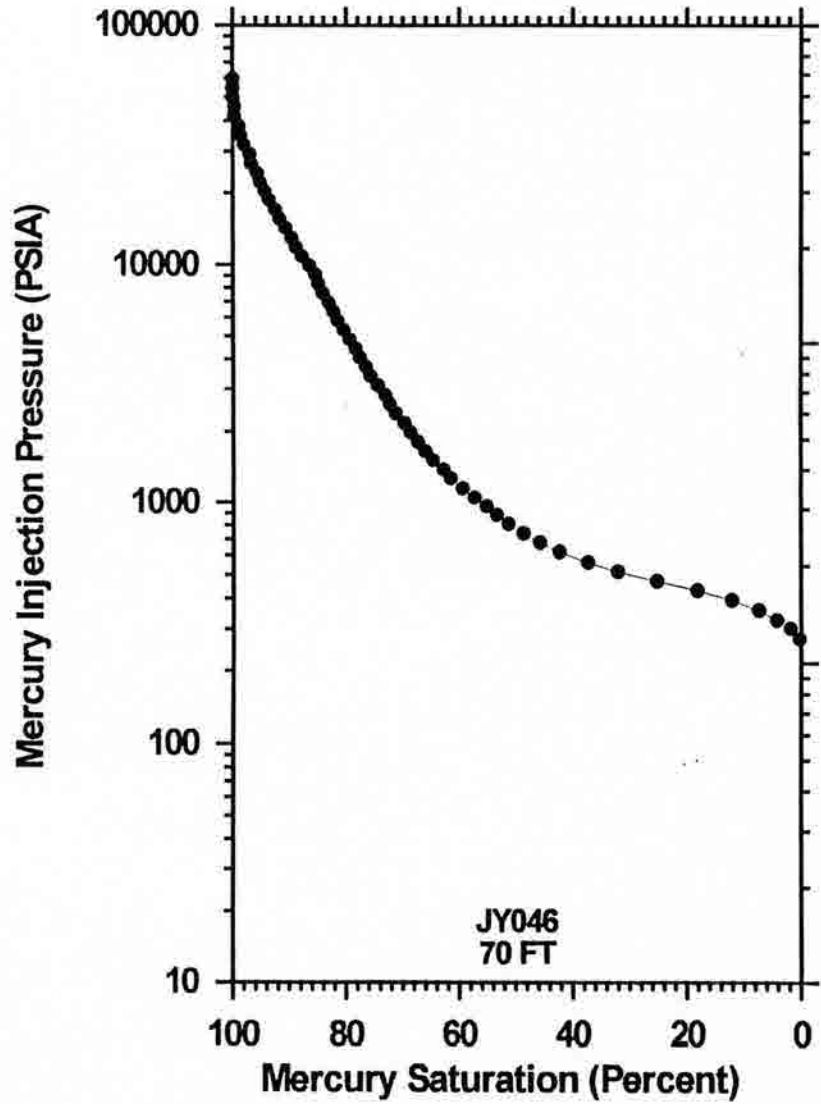


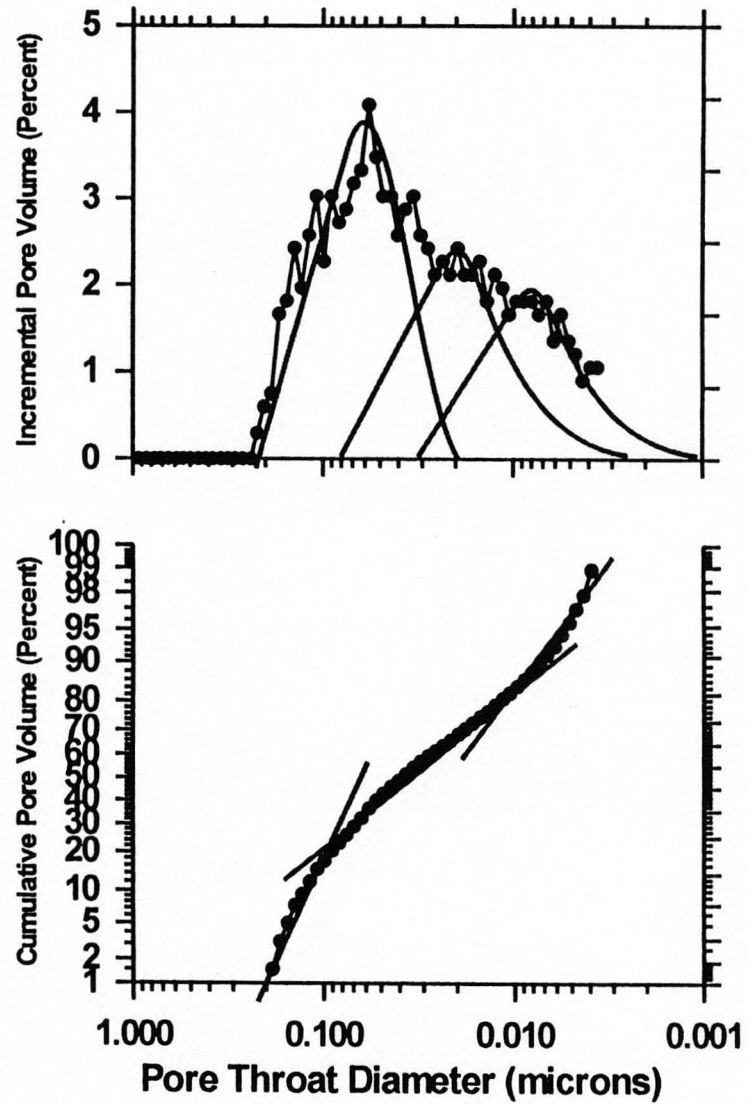
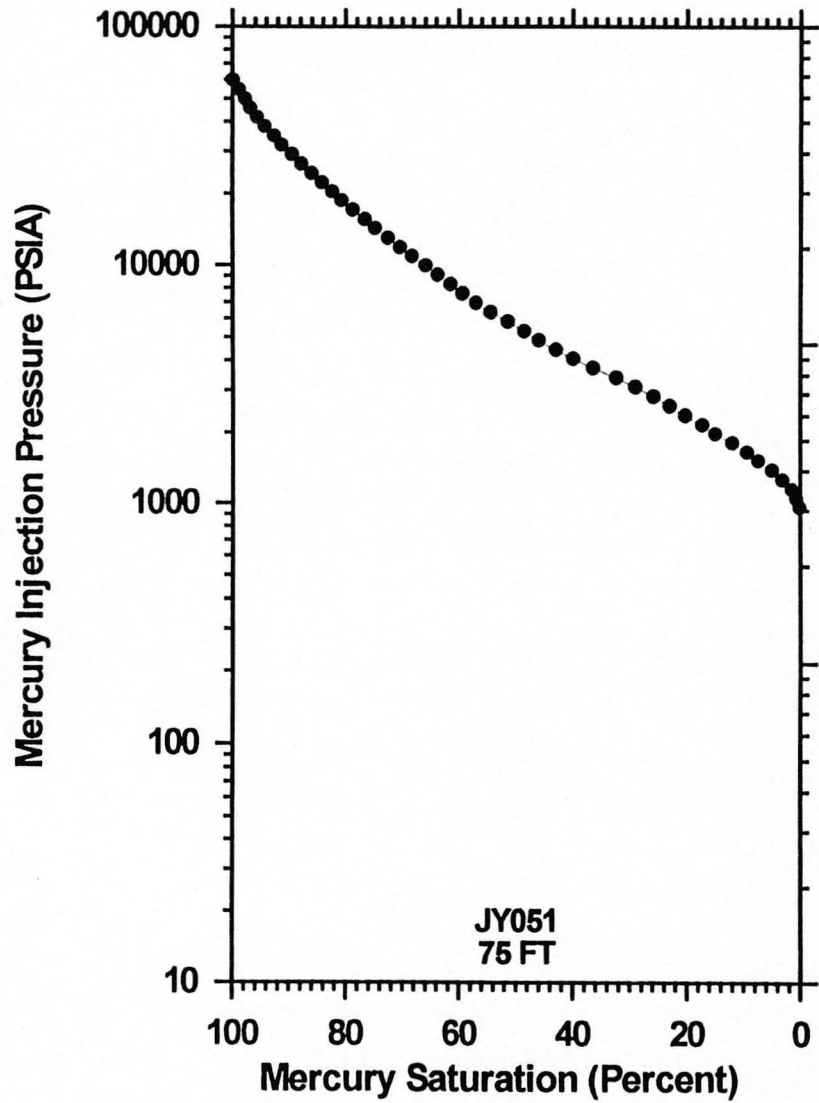
Mercury Injection Pressure (PSIA)

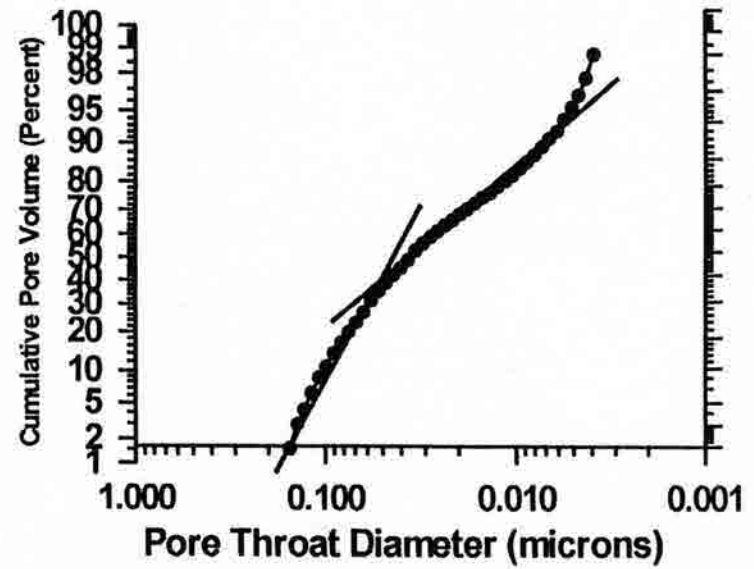
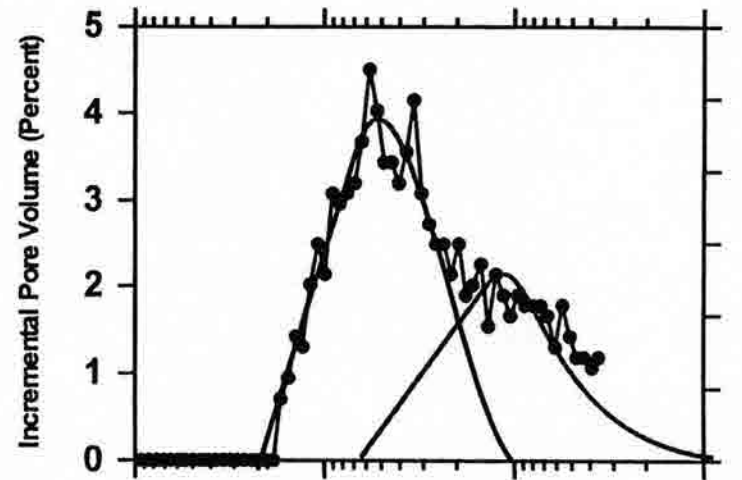
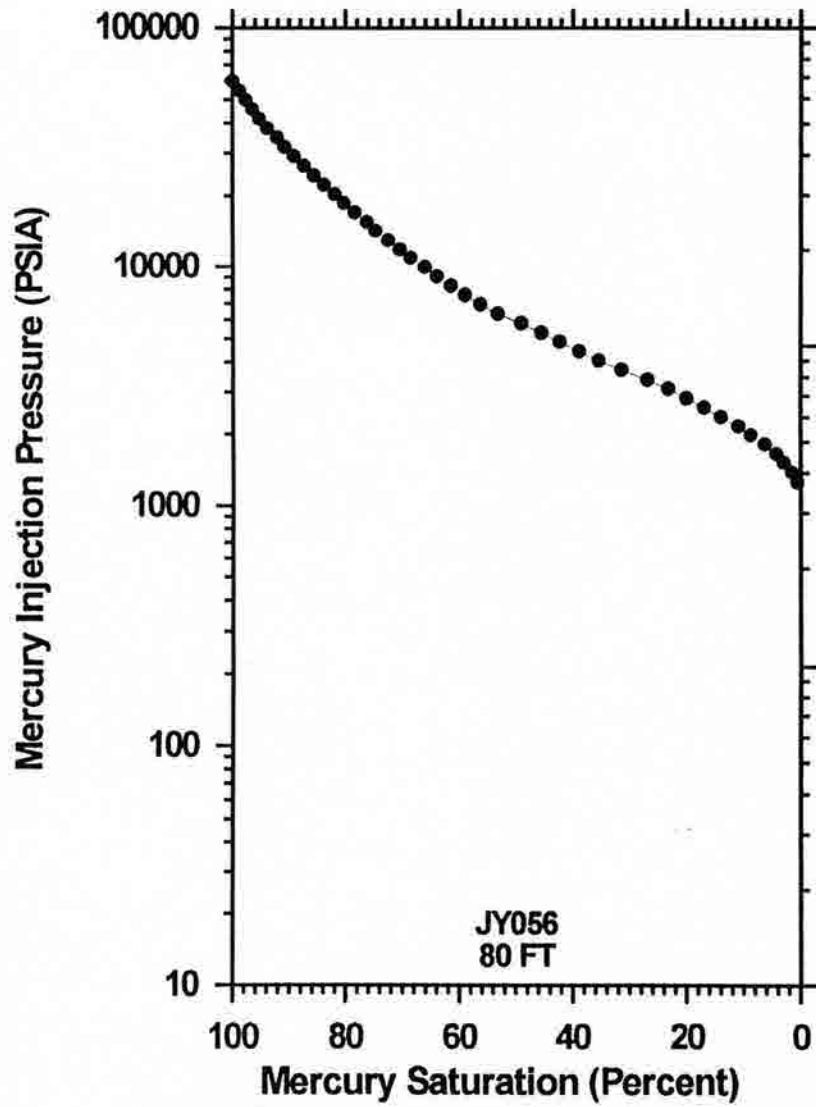


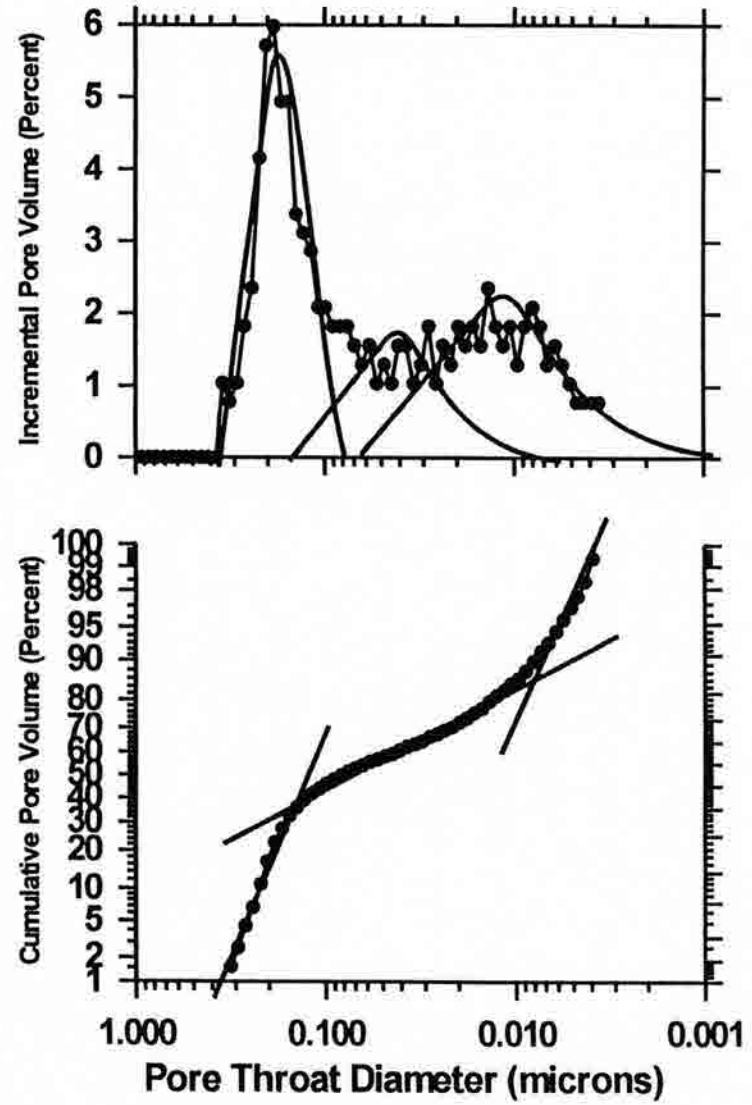
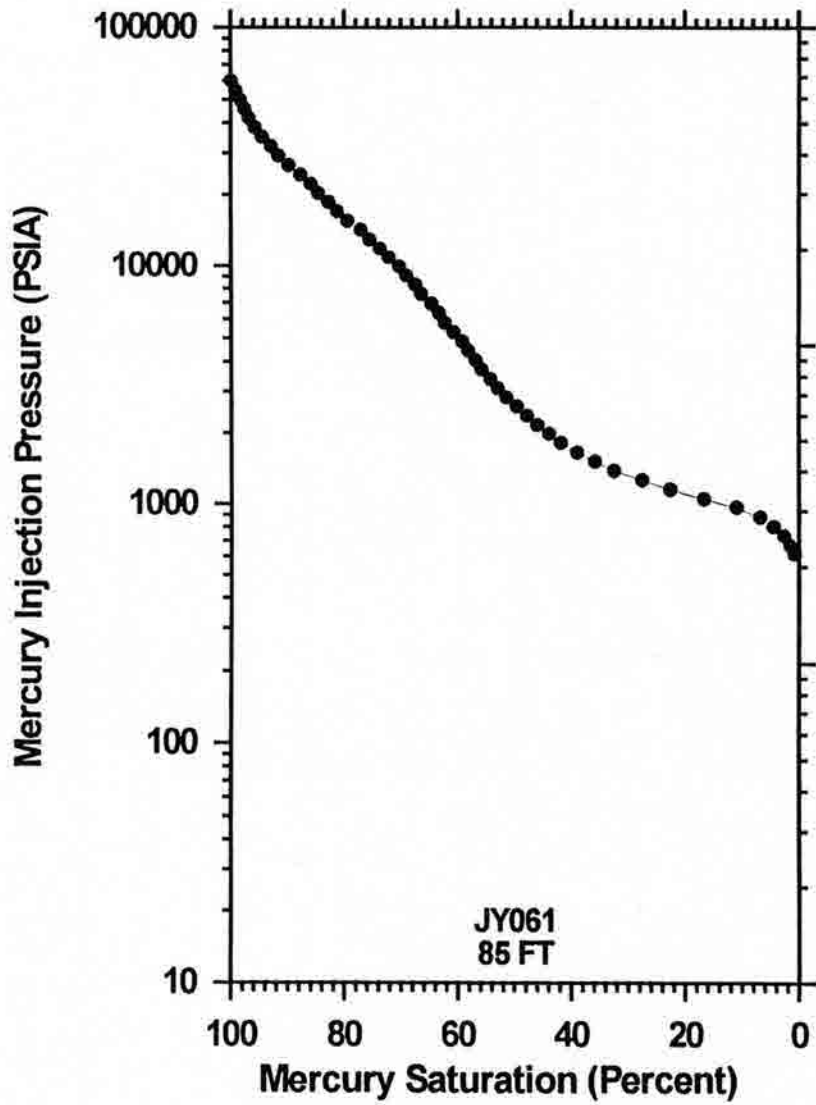
Mercury Injection Pressure (PSIA)

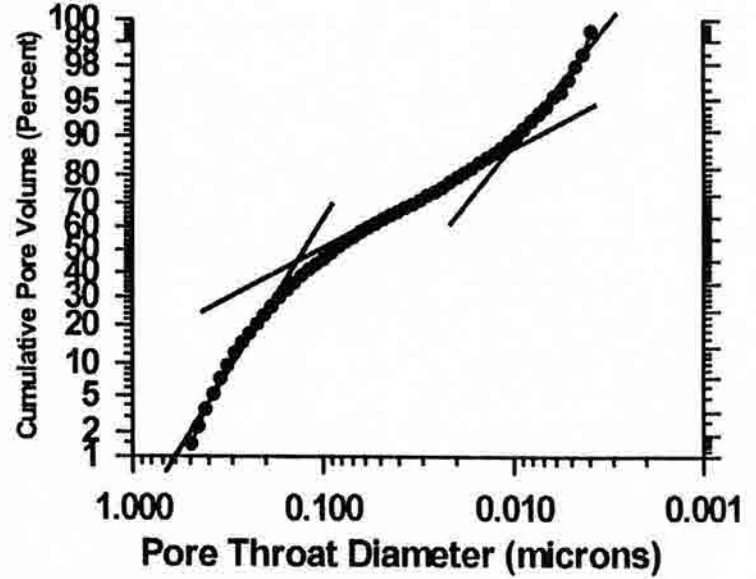
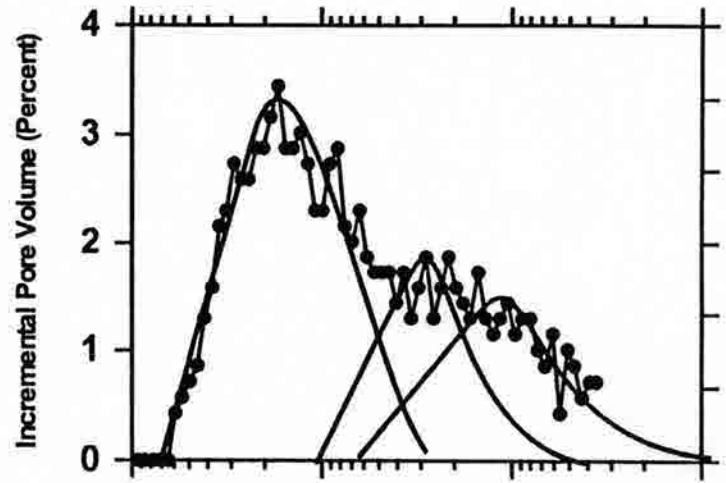
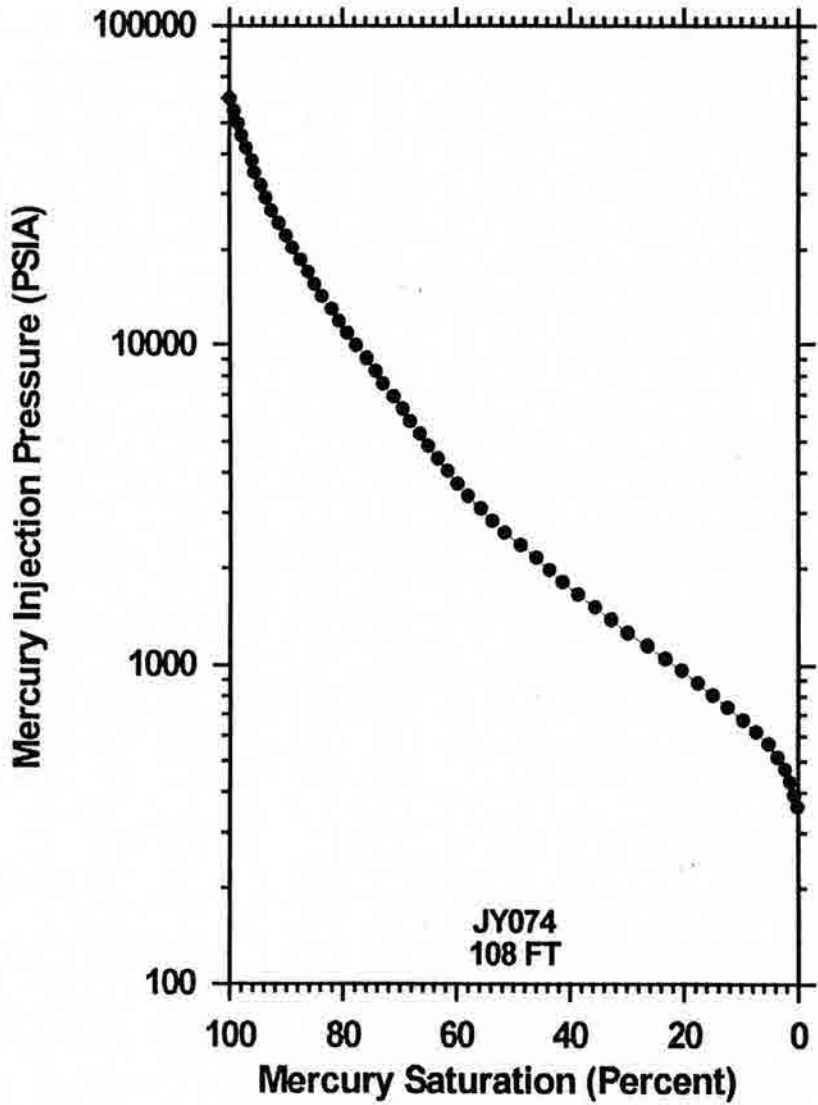


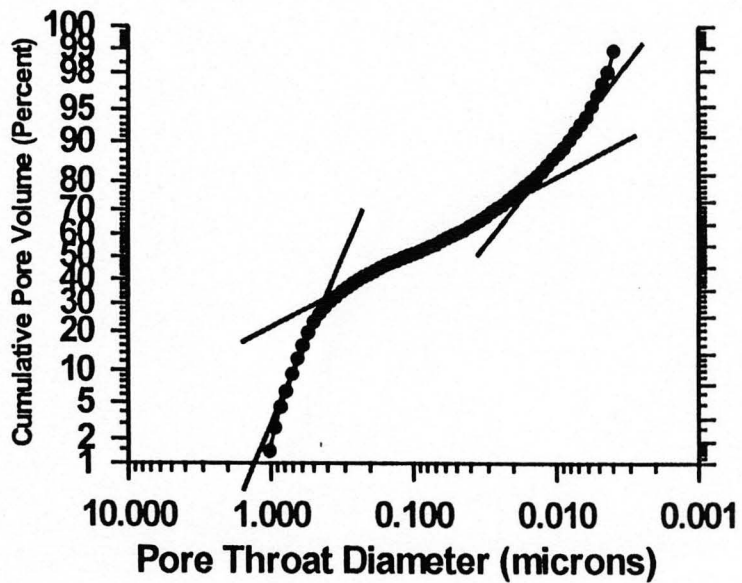
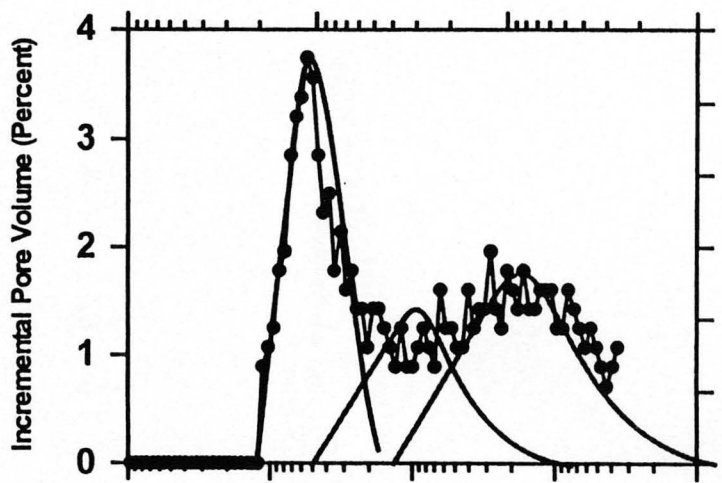
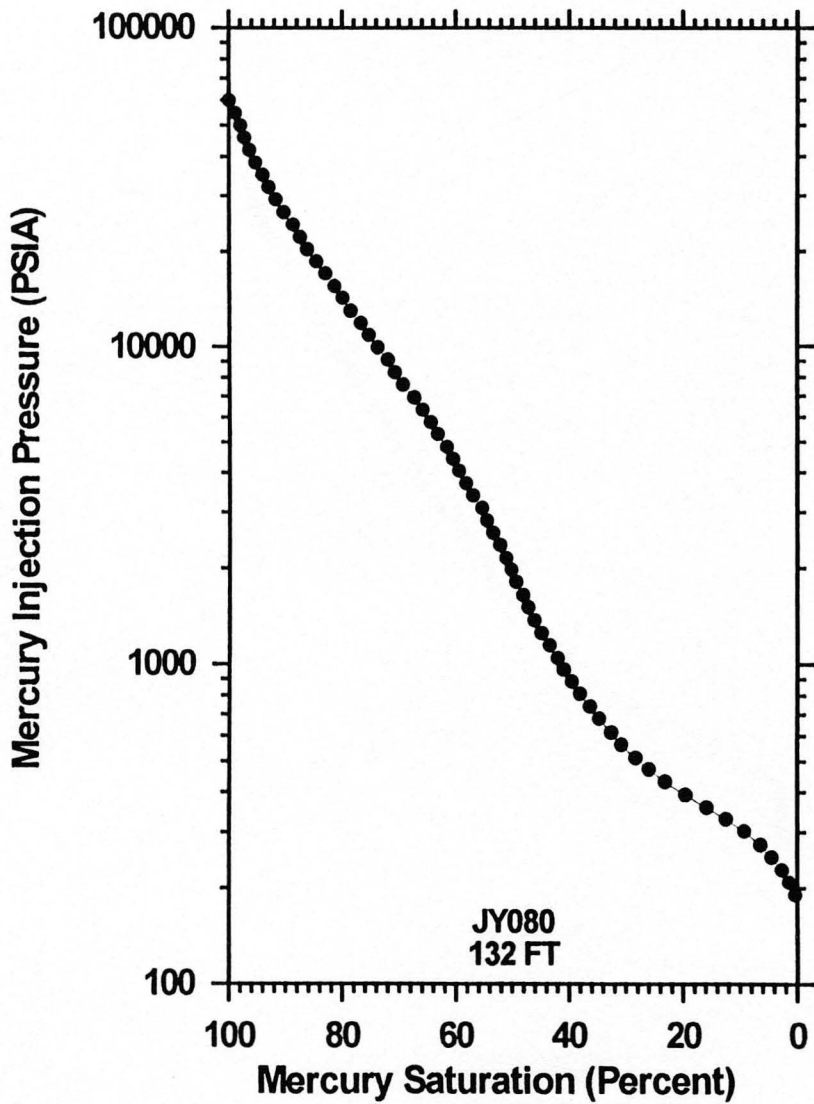


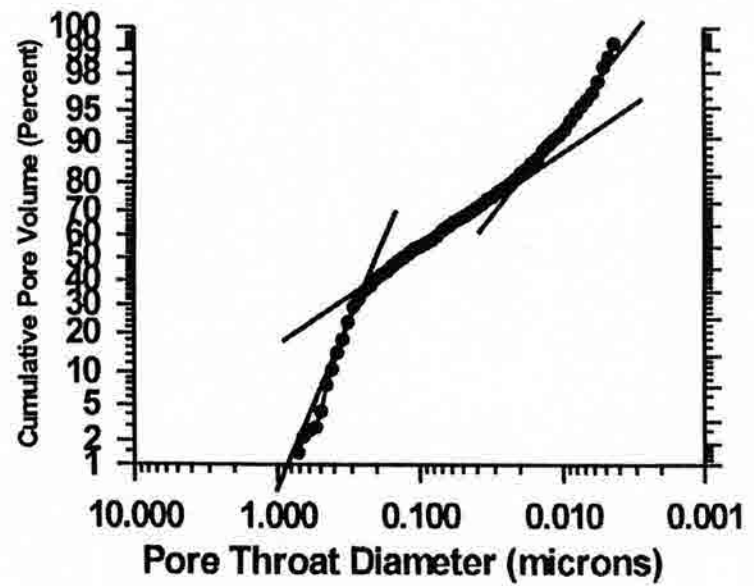
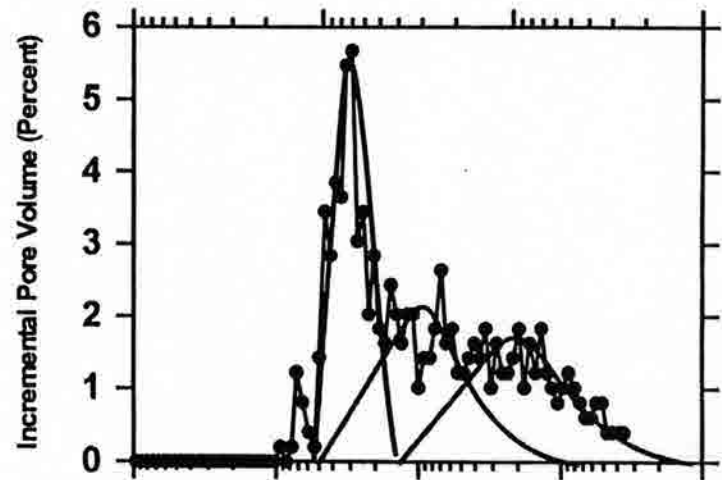
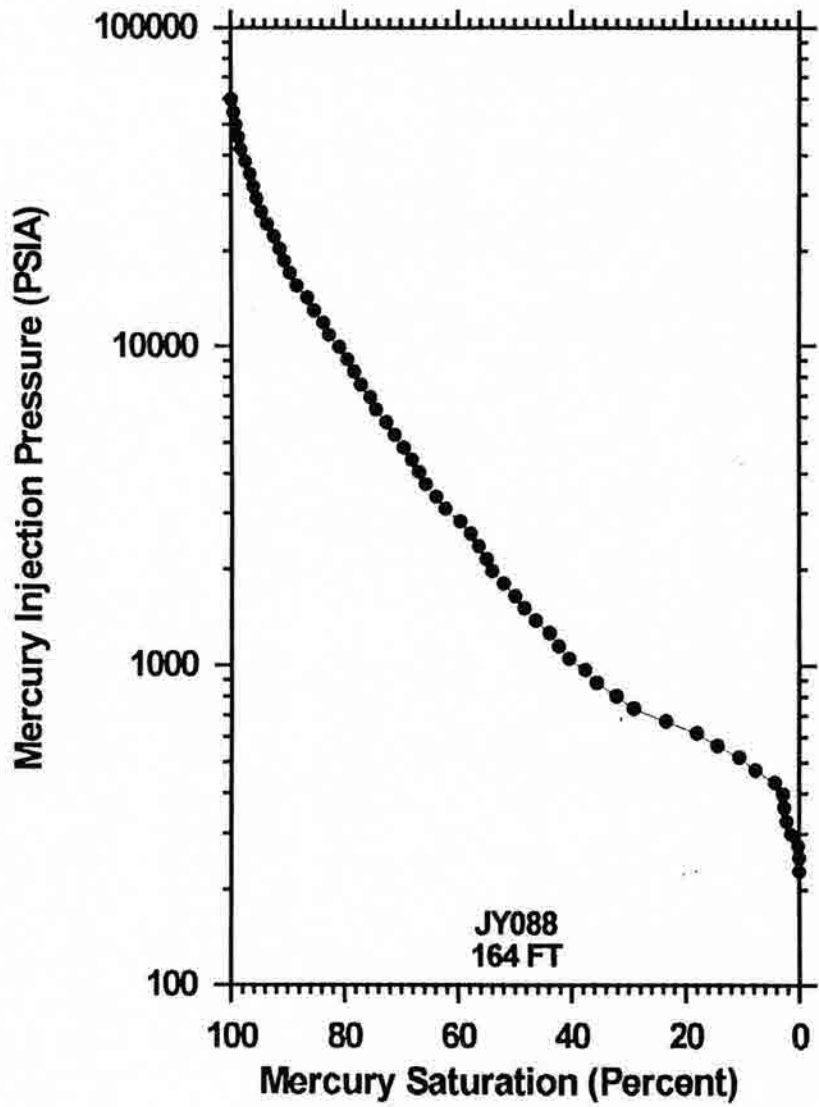












APPENDIX G

TURKEY CREEK OUTCROP

SKULL CREEK SHALE

THIN SECTION PHOTOMICROGRAPHS

Figure C1.

TC010 (20 ft) - Factor C

Low magnification (75X) thin section photomicrograph of an argillaceous siltstone. Strongly compacted, poorly sorted matrix contains clay minerals and silt size detrital grains (quartz, feldspar, mica) with an occasional fine-grained sand particle. Staining is common throughout, concentrated around the organic matter. The bedding in this shale has been destroyed by extensive bioturbation, noted by the discontinuous line of organic and clay. Sarcosites is forming from the dissolution of feldspar. This selective dissolution has produced the intergranular porosity.

Figure C2.

TC010 (20 ft) - Factor C

Medium magnification (150X) thin section photomicrograph of same argillaceous siltstone pictured in C1. Strongly compacted, poorly sorted matrix contains clay minerals and silt size detrital grains (quartz, feldspar, mica). At higher magnification, it is easier to distinguish the clays from the organic matter. The bright yellow clay mineral is sarcosites. This selective dissolution has produced the intergranular porosity.

Figure G1.

TC020 (20 ft)- Facies C

Low magnification (PPL) thin section photomicrograph of an argillaceous siltstone. Strongly compacted, poorly sorted matrix contains clay minerals and silt size detrital grains (quartz, feldspar, mica) with an occasional fine-grained sand particle. Siderite staining is common throughout, concentrated around the organic matter. The bedding in this shale has been destroyed by extensive bioturbation, noted by the discontinuous lens of organics and clays. Sericite is forming from the dissolution of feldspar. This selective dissolution has produced 5% intergranular porosity.

Figure G2.

TC020 (20 ft)- Facies C

Medium magnification (PPL) thin section photomicrograph of same argillaceous siltstone pictured in G1. Strongly compacted, poorly sorted matrix contains clay minerals and silt size detrital grains (quartz, feldspar, mica). At higher magnification, it is easier to distinguish the clays from the organic matter. The bright yellow clay mineral is sericite. This selective dissolution has produced 5% intergranular porosity.

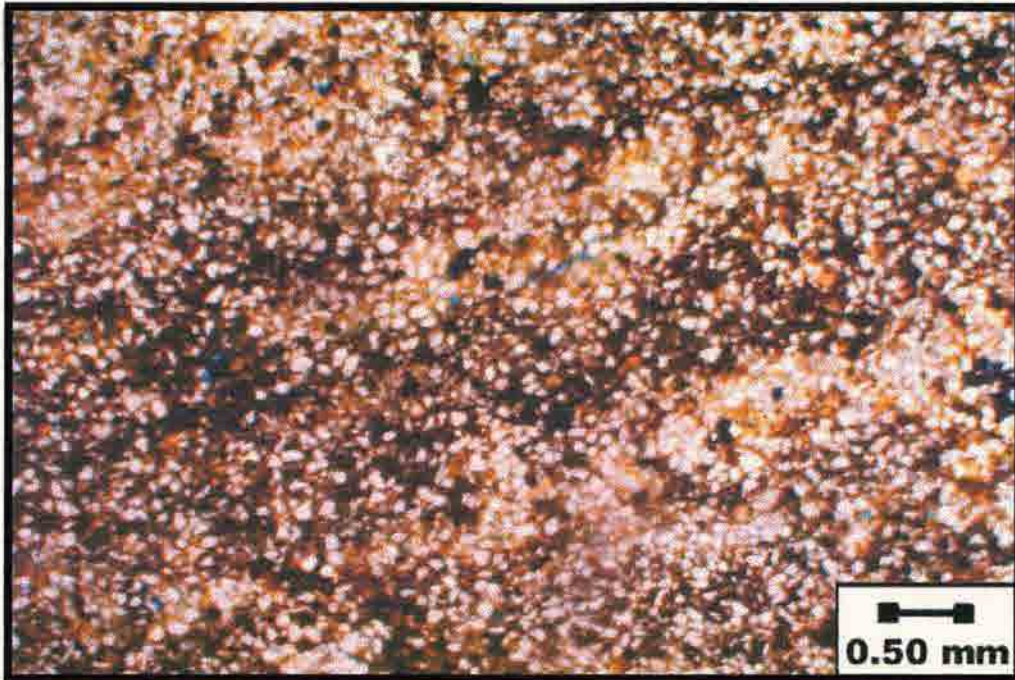


Figure G1.

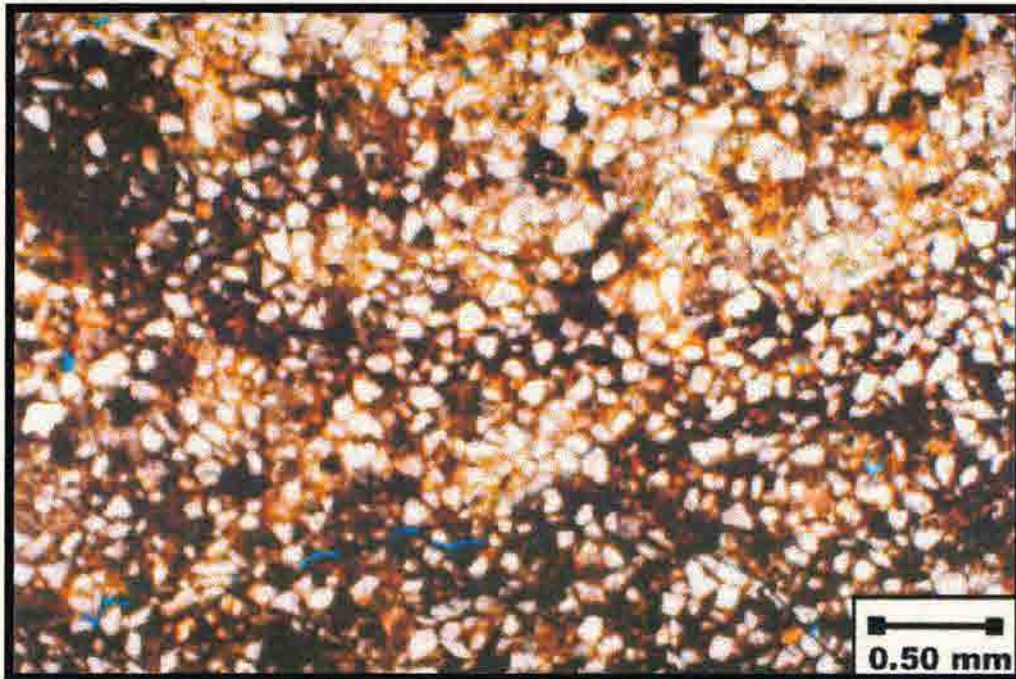


Figure G2.

Figure G3.

TC040 (40 ft)-Factor A

Low magnification (PM) thin section photomicrograph of carbonaceous silt shale. Strongly compacted, well-sorted matrix contains clay minerals and silt size detrital grains (quartz, feldspar, mica). Authigenic cements (calcite, dolomite and siderite) are present as cement that surrounds the sand grains and gives them the appearance of "floating". Well-developed laminations of clay and organics are present, in addition to the distinct graded bedding. Imbrication or matrix porosity is not visible.

Figure G4.

TC040 (40 ft)-Factor A

Low magnification (XN) thin section photomicrograph of same carbonaceous silt shale pictured in G3. Strongly compacted, well-sorted matrix contains clay minerals and silt size detrital grains (quartz, feldspar, mica). The partly light colored cement consists of authigenic cements (calcite, dolomite and siderite). Well-developed laminations of clay and organics are present, in addition to the distinct graded bedding. No matrix porosity is detected.

Figure G3.

TC040 (40 ft)- Facies A

Low magnification (PPL) thin section photomicrograph of carbonaceous silty shale. Strongly compacted, well-sorted matrix contains clay minerals and silt size detrital grains (quartz, feldspar, mica). Authigenic carbonates (calcite, dolomite and siderite) are present as cement that surrounds the hard grains and gives them the appearance of "floating". Well-developed laminations of clays and organics are present, in addition to the distinct graded bedding. Intergranular or matrix porosity is not visible.

Figure G4.

TC040 (40 ft)- Facies A

Low magnification (XN) thin section photomicrograph of same carbonaceous silty shale pictured in G3. Strongly compacted, well-sorted matrix contains clay minerals and silt size detrital grains (quartz, feldspar, mica). The patchy light colored cement consists of authigenic carbonates (calcite, dolomite and siderite). Well-developed laminations of clays and organics are present, in addition to the distinct graded bedding. No matrix porosity is detected.

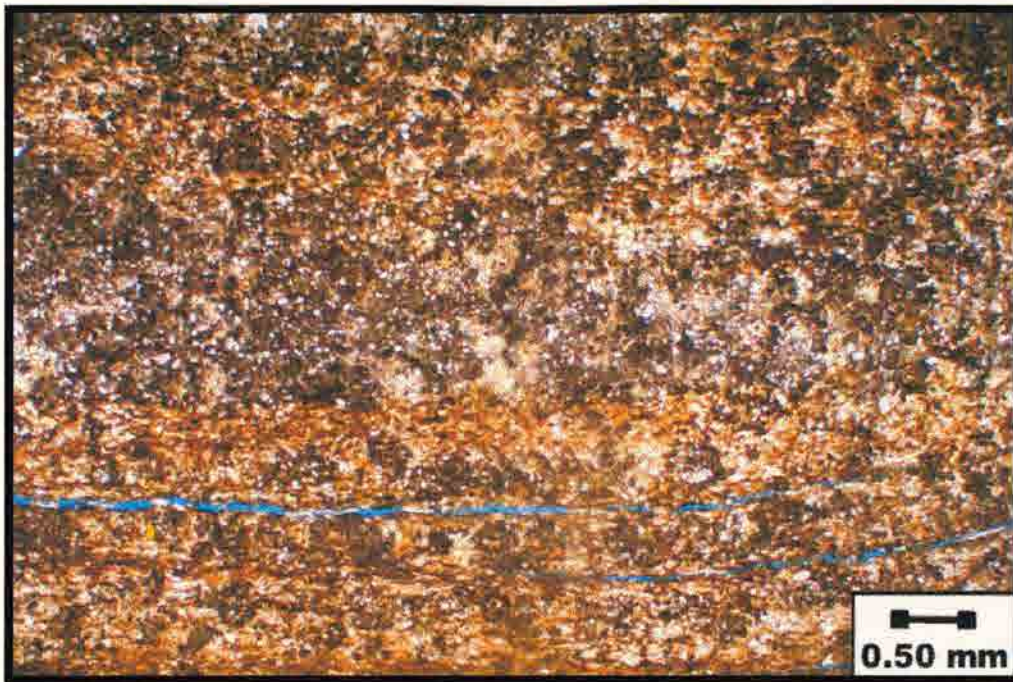


Figure G3.

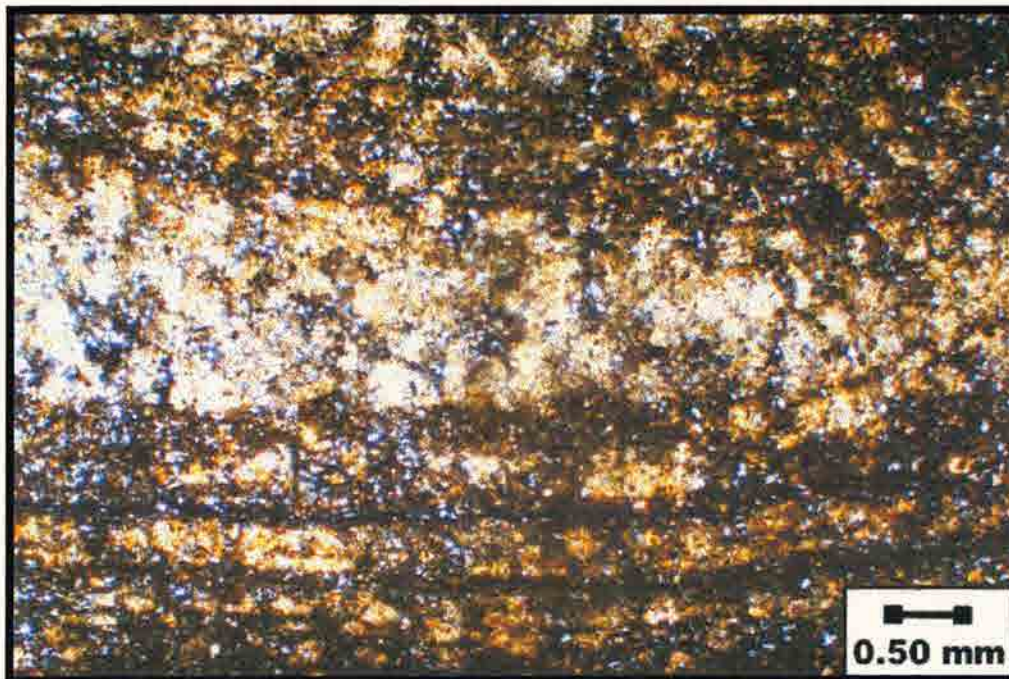


Figure G4.

Figure 68

TC045 (42 ft) - Factor A

Low magnification (95x) thin section photomicrograph of a carbonaceous silt shale. Strongly compacted, well-sorted matrix contains clay minerals and silt size detrital grains (quartz, feldspar, mica) with occasional fine-grained sand particles. Accessory minerals include siderite and authigenic pyrite nodules. Thin laminae of organic matter and silt are present in the overall homogeneous matrix. No matrix porosity is evident.

Figure 69

TC045 (42 ft) - Factor A

Medium magnification (291x) thin section photomicrograph of same carbonaceous silt shale pictured in 68. Strongly compacted, well-sorted matrix contains clay minerals and silt size detrital grains (quartz, feldspar, mica) with occasional fine-grained sand particles. At higher magnification, the silt and organic matter laminae are easier to distinguish. The large organic nodules are authigenic laminated pyrite. Authigenic carbonates (siderite, calcite, and dolomite) accentuate the mineralogy of the shale. No matrix porosity is detected.

Figure G5.

TC045 (45 ft)- Facies A

Low magnification (PPL) thin section photomicrograph of a carbonaceous silty shale. Strongly compacted, well-sorted matrix contains clay minerals and silt size detrital grains (quartz, feldspar, mica) with occasional fine grained sand particles. Accessory minerals include siderite and authigenic pyrite nodules. Faint laminations of organic matter and silt are present in the overall homogeneous matrix. No matrix porosity is evident.

Figure G6.

TC045 (45 ft)- Facies A

Medium magnification (PPL) thin section photomicrograph of same carbonaceous silty shale pictured in G5. Strongly compacted, well-sorted matrix contains clay minerals and silt size detrital grains (quartz, feldspar, mica) with occasional fine-grained sand particles. At higher magnification, the silt and organic matter laminations are easier to distinguish. The large opaque nodules are authigenic framoidal pyrite. Authigenic carbonates (siderite, calcite, and dolomite) accessorize the mineralogy of this shale. No matrix porosity is detected.



Figure G5.

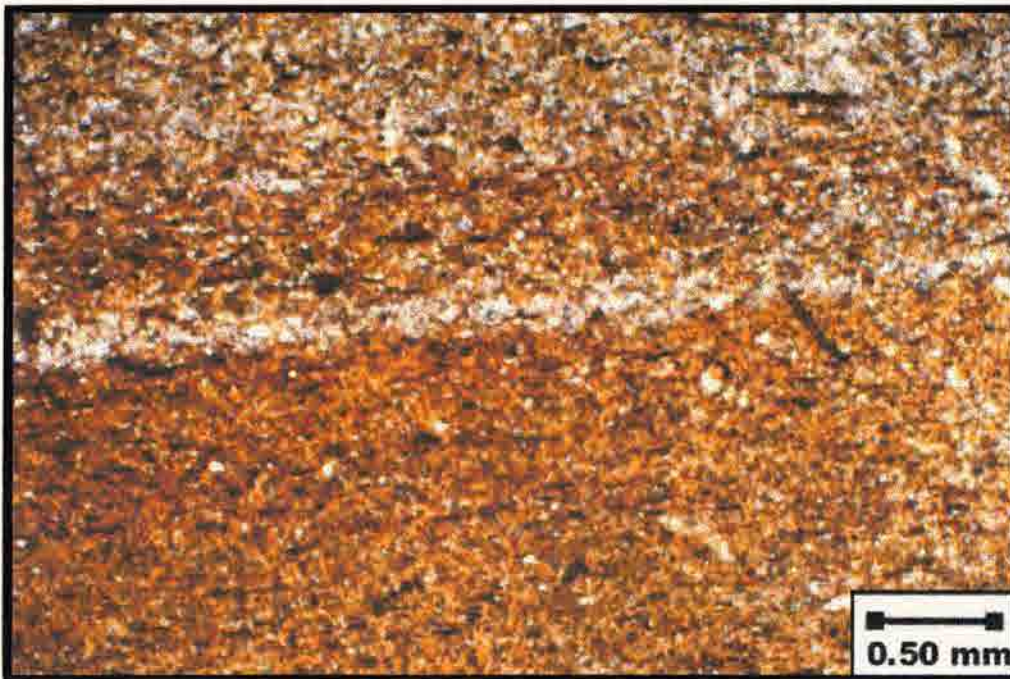


Figure G6.

Figure 67.

TC063 (63 ft) - Facies B

Low magnification (11X) thin section photomicrograph of an argillaceous siltstone. Strongly compacted, moderately well sorted matrix contains clay minerals and silty to very silty sand size detrital grains (quartz, feldspar, mica). Authigenic carbonates (calcite, dolomite, siderite) provide the cement in this framework with small amounts of authigenic framboidal pyrite. Well-developed laminations of clay and organic are present in addition to the distinct graded bedding and minor burrowing. No matrix porosity is evident.

Figure 68.

TC070 (70 ft) - Facies C

Medium magnification (11X) thin section photomicrograph of an argillaceous siltstone. Strongly compacted, moderately well sorted matrix contains clay minerals and silty sand size detrital grains (quartz, feldspar, mica). Authigenic carbonates (calcite, dolomite, siderite) provide the cement in this framework with small amounts of authigenic framboidal pyrite. The bedding has been destroyed by dissolution. No matrix porosity is visible.

Figure G7.

TC063 (63 ft)- Facies B

Low magnification (PPL) thin section photomicrograph of an argillaceous siltstone. Strongly compacted, moderately well sorted matrix contains clay minerals and silt to very fine sand size detrital grains (quartz, feldspar, mica). Authigenic carbonates (calcite, dolomite, siderite) provide the cement in this framework with small amounts of authigenic framboidal pyrite. Well-developed laminations of clays and organics are present in addition to the distinct graded bedding and minor burrowing. No matrix porosity is evident.

Figure G8.

TC070 (70 ft)- Facies C

Medium magnification (PPL) thin section photomicrograph of an argillaceous siltstone. Strongly compacted, moderately well sorted matrix contains clay minerals and silt size detrital grains (quartz, feldspar, mica). Authigenic carbonates (calcite, dolomite, siderite) provide the cement in this framework with small amounts of authigenic framboidal pyrite. The bedding has been destroyed by bioturbation. No matrix porosity is visible.

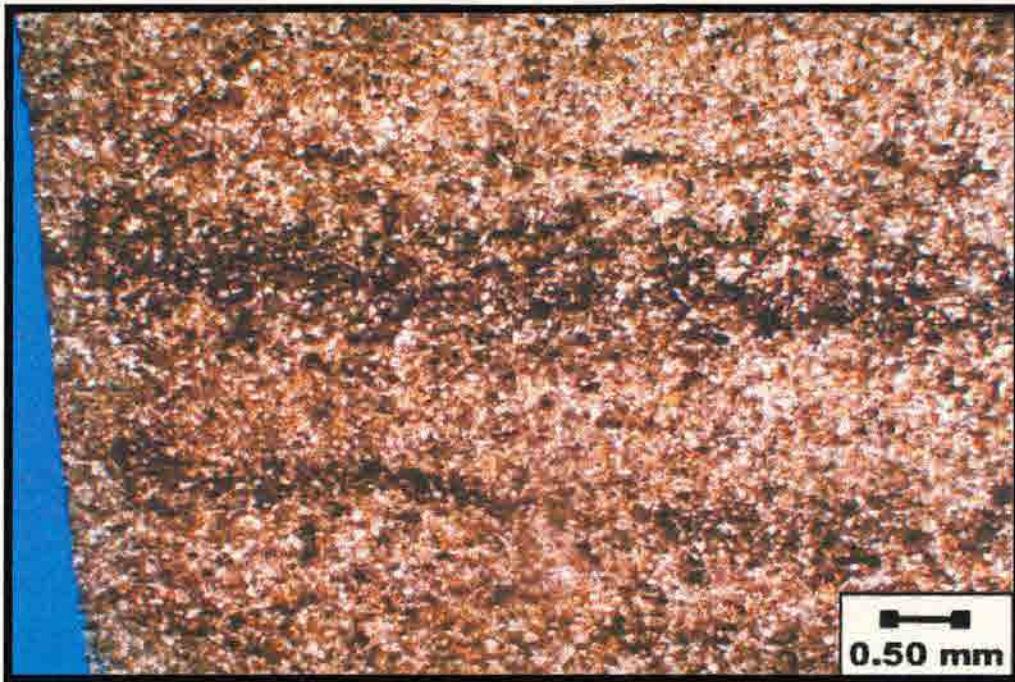


Figure G7.

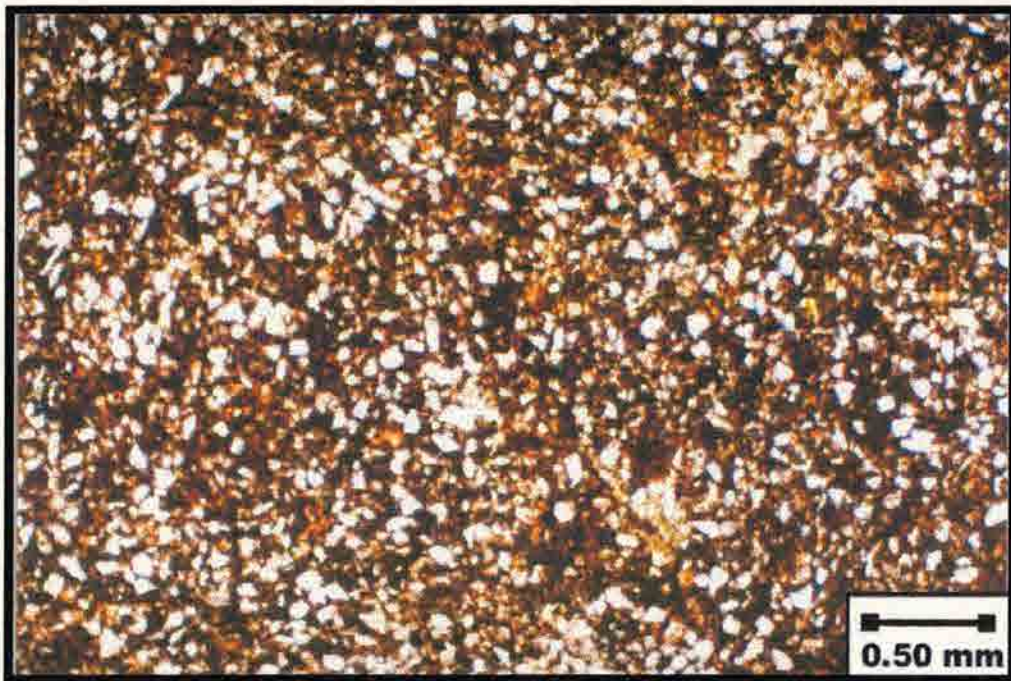


Figure G8.

APPENDIX H

TURKEY CREEK OUTCROP

SKULL CREEK SHALE

MICP GRAPHS

MICP table for Turkey Creek (Skull Creek shale)

Sample#	FT	Facies	Median PTD	Pore Volume %	Sorting Index
TC-000	0	C	0.06	50	P-M
			0.02	50	P-M
TC-010	10	C	0.04	60	M
			0.2	40	P-M
TC-020	20	C	0.2	60	P
			0.04	40	P-M
TC-030	30	B	0.025	90	VW
			0.007	10	M
TC-035	35	B	0.0125	70	VW
			0.03	30	M
TC-040	40	A	0.0075	70	VW
			0.02	30	M
TC-045	45	A	0.015	90	W
			0.045	10	M
TC-063	63	B	0.07	70	W
			0.01	30	M
TC-070	70	B	0.055	60	VW
			0.008	40	M
TC-078	78	C	0.055	80	VW
			0.008	20	M
TC-083	90	C	0.08	70	W
	0.7		20	P-M	
	7		10	P	

LEGEND:

VW= Very Well sorted

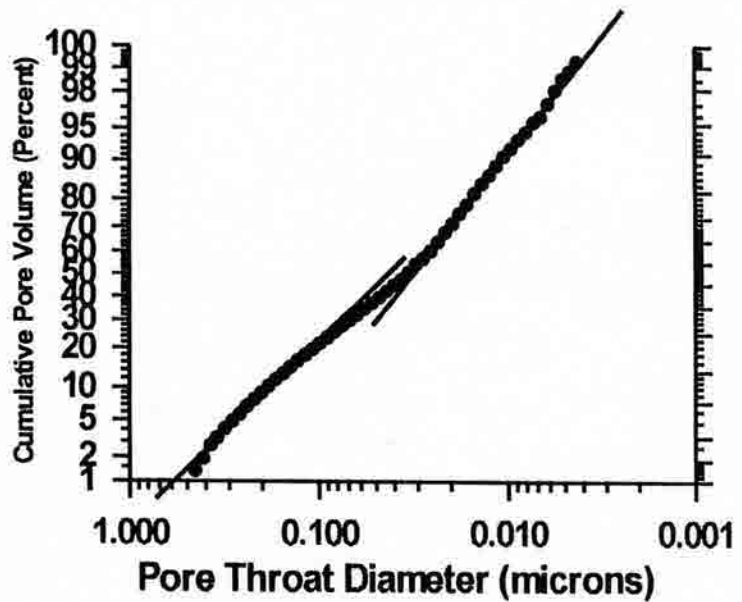
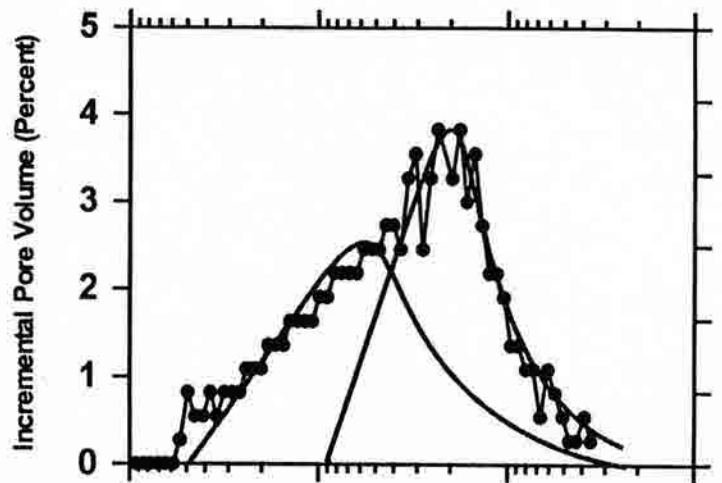
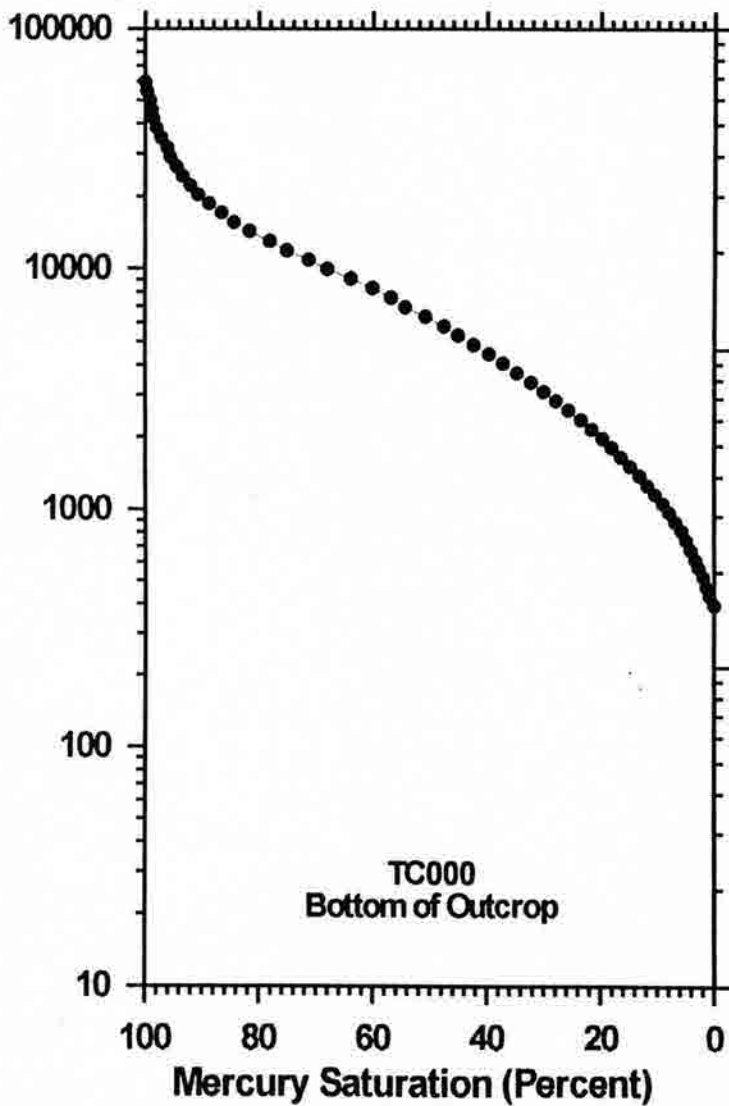
W= Well sorted

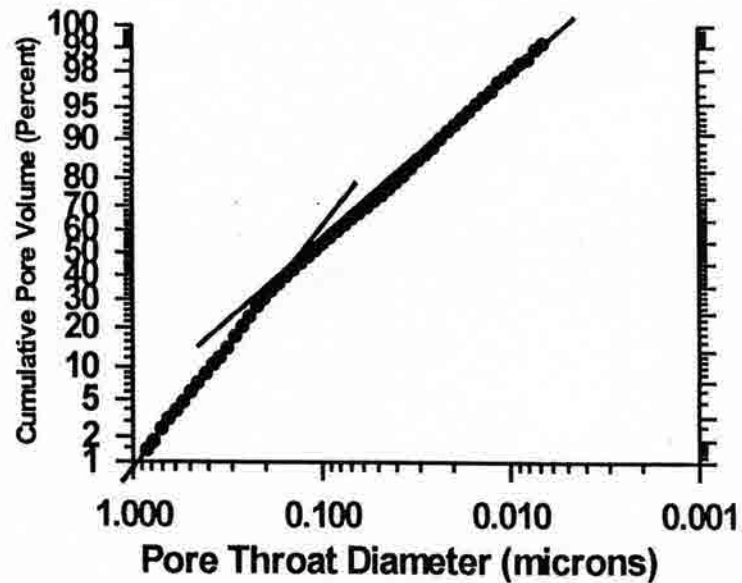
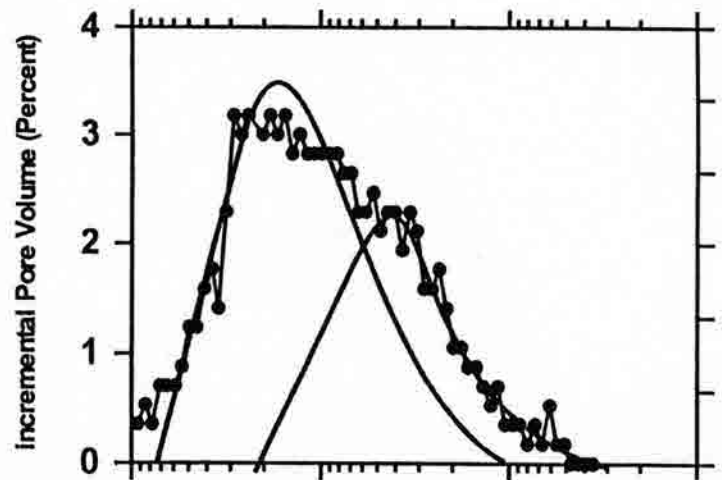
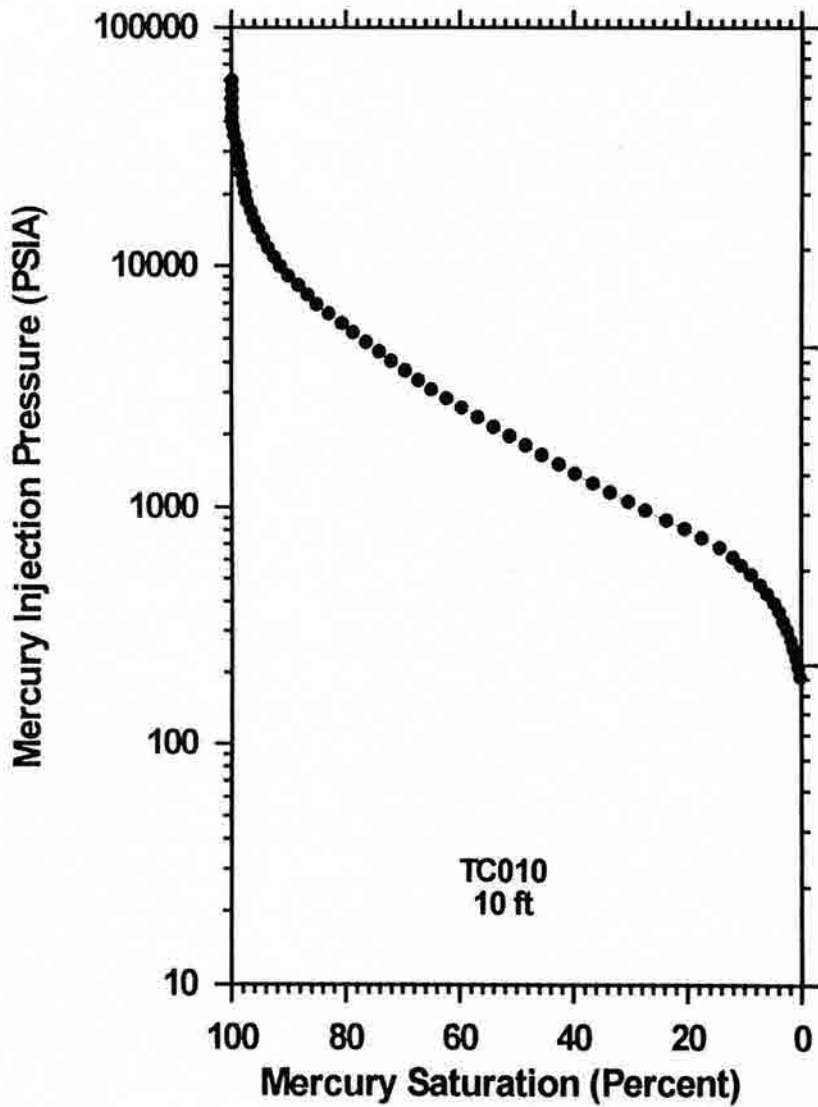
MW= Moderately-well sorted

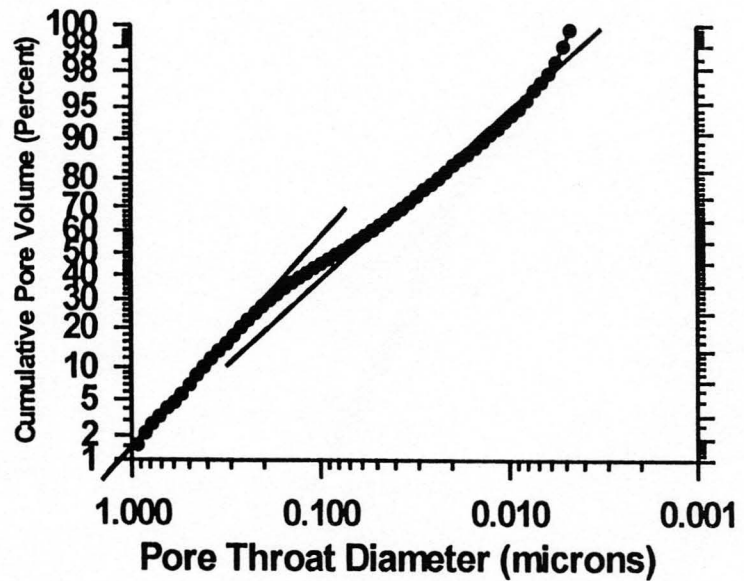
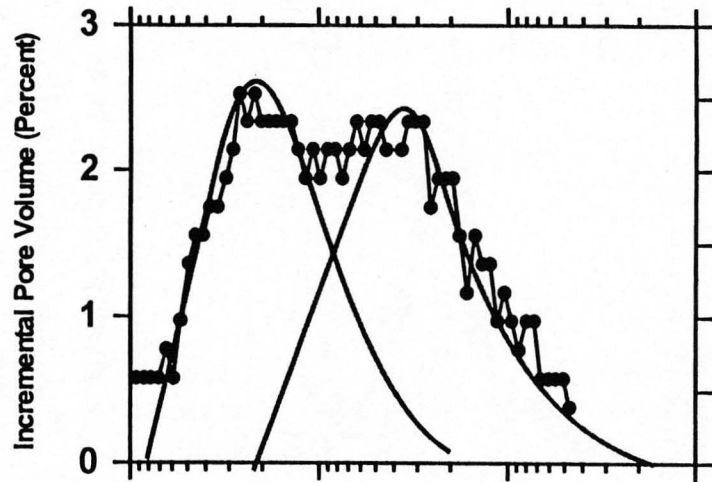
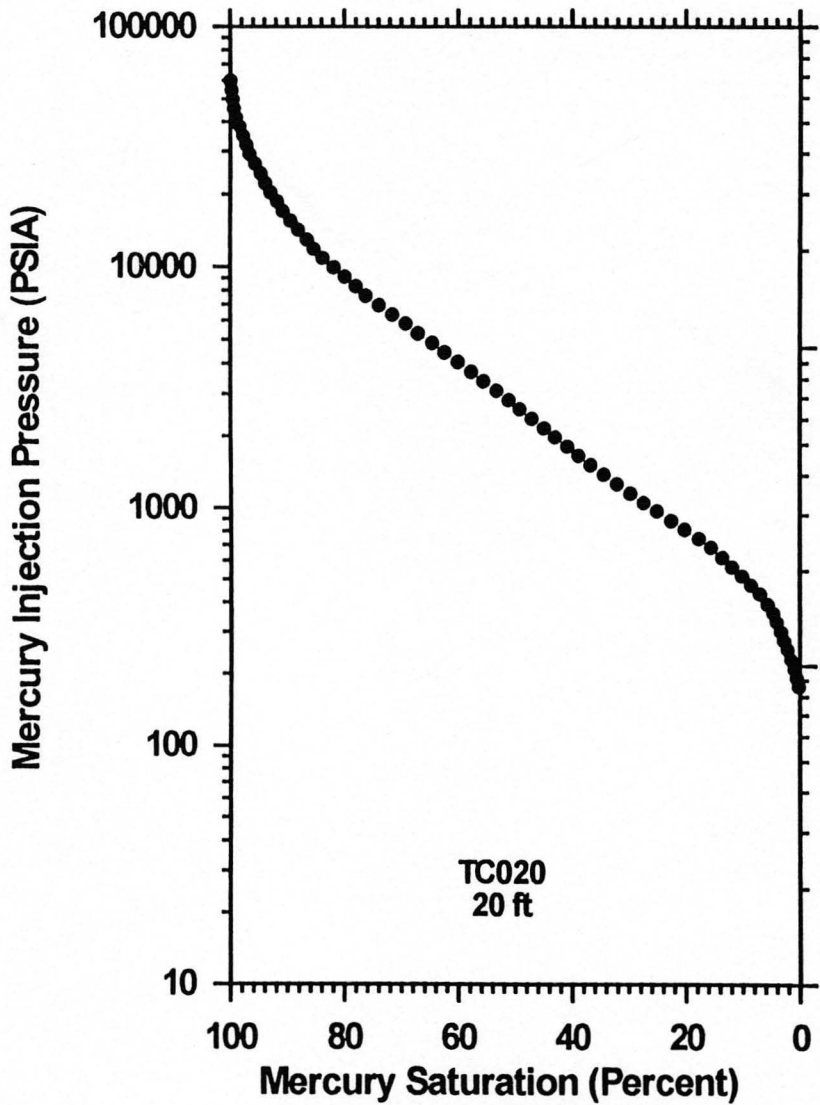
M= Moderately sorted

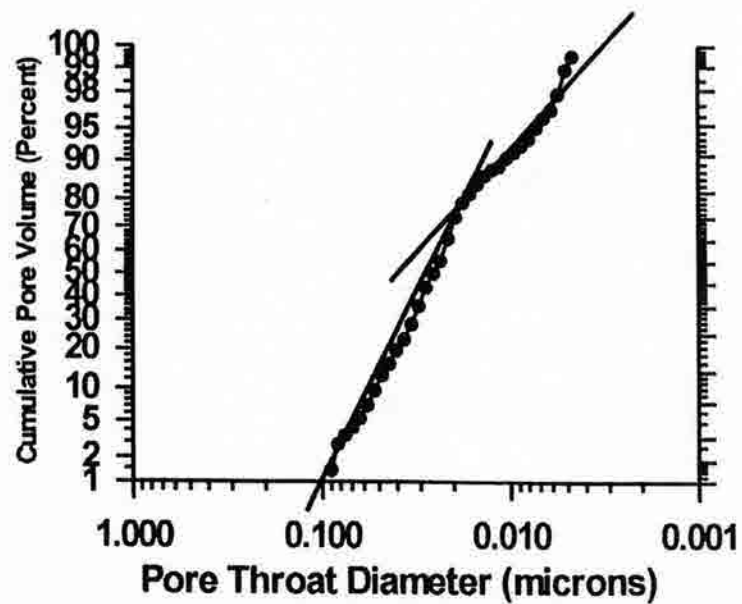
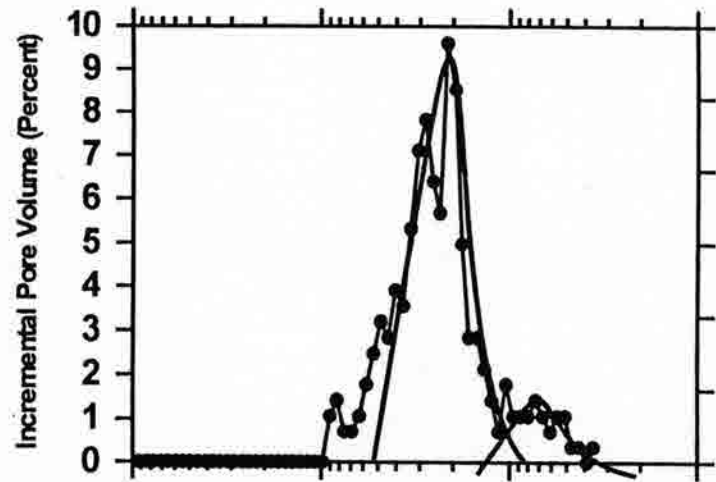
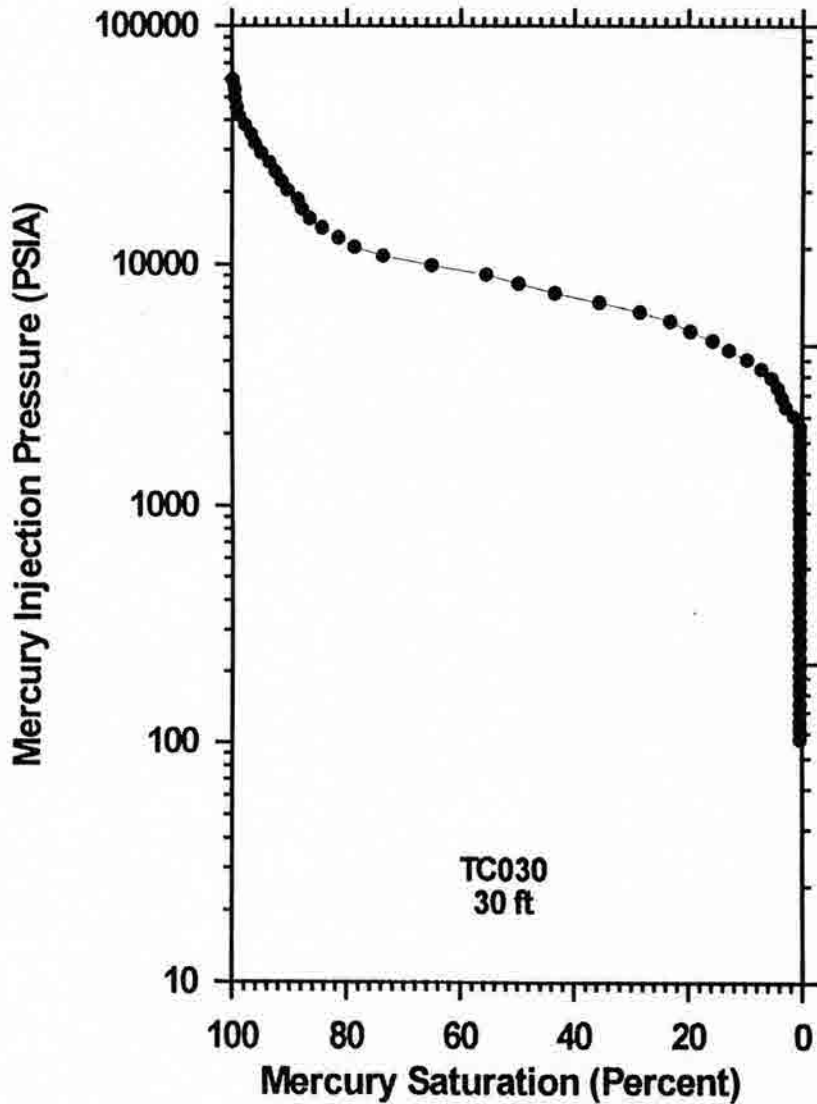
P= Poorly sorted

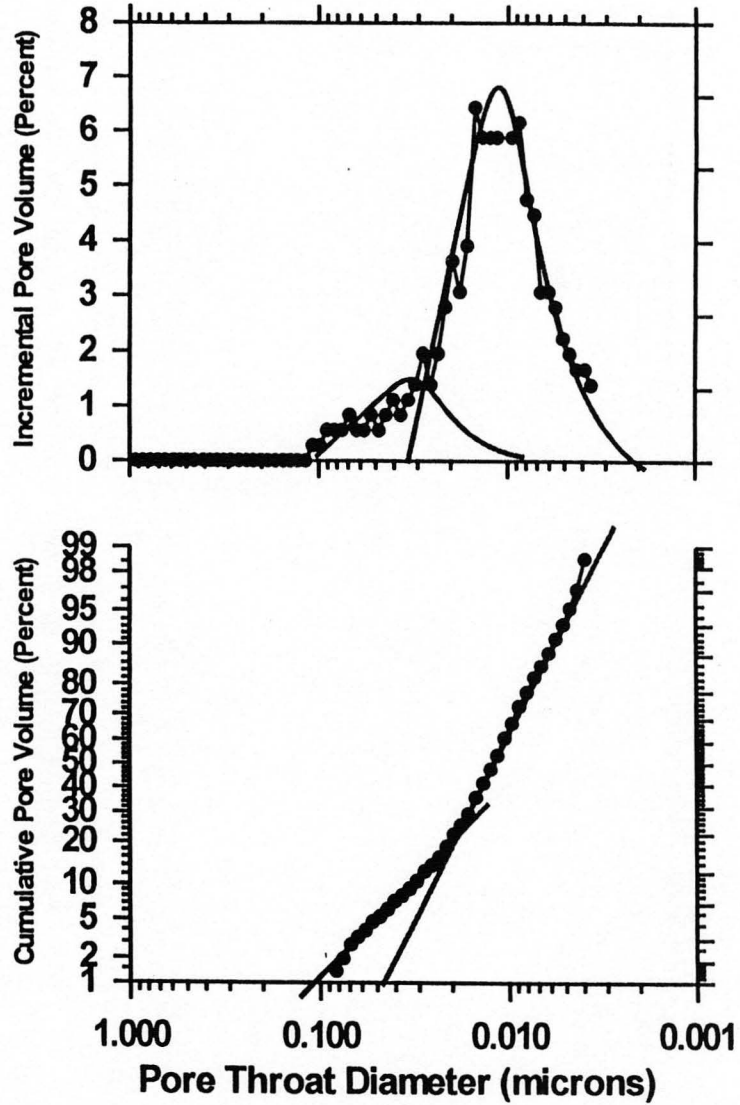
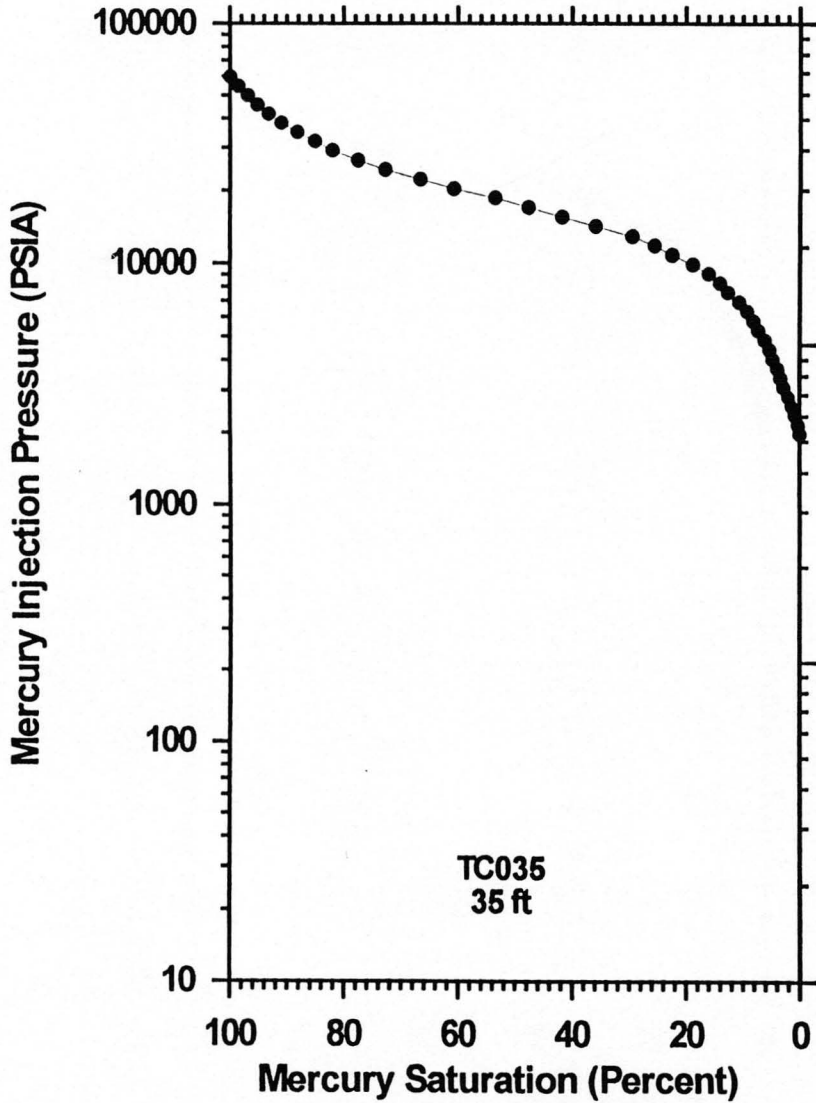
Mercury Injection Pressure (PSIA)

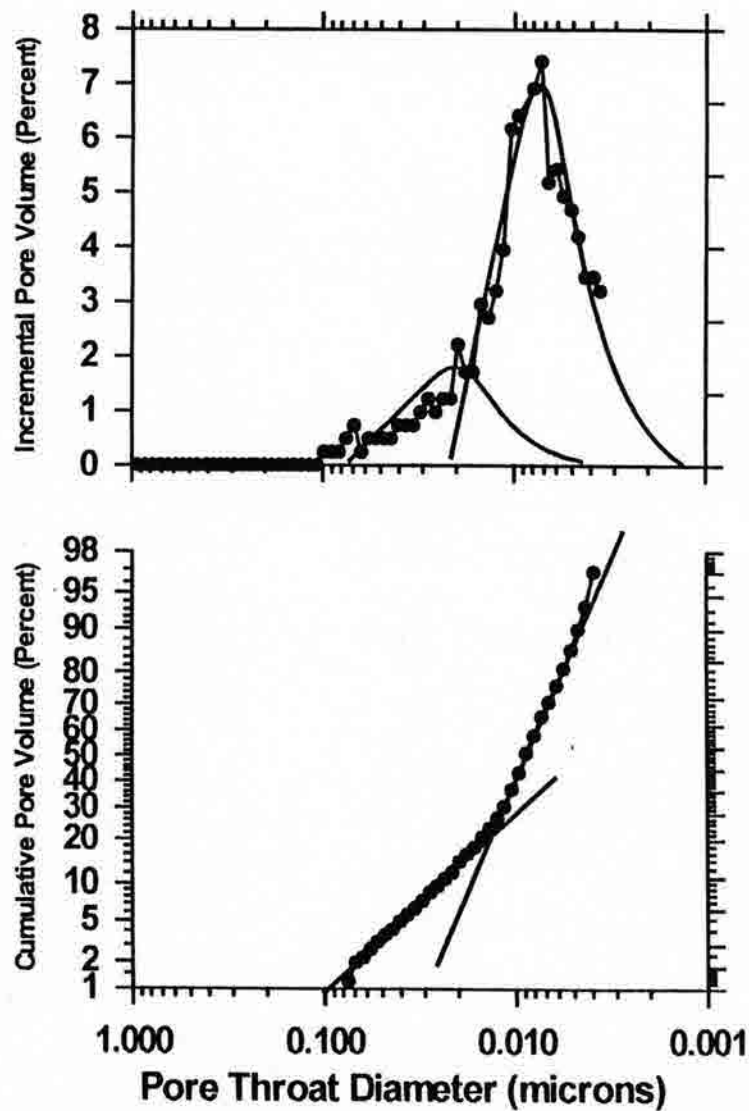
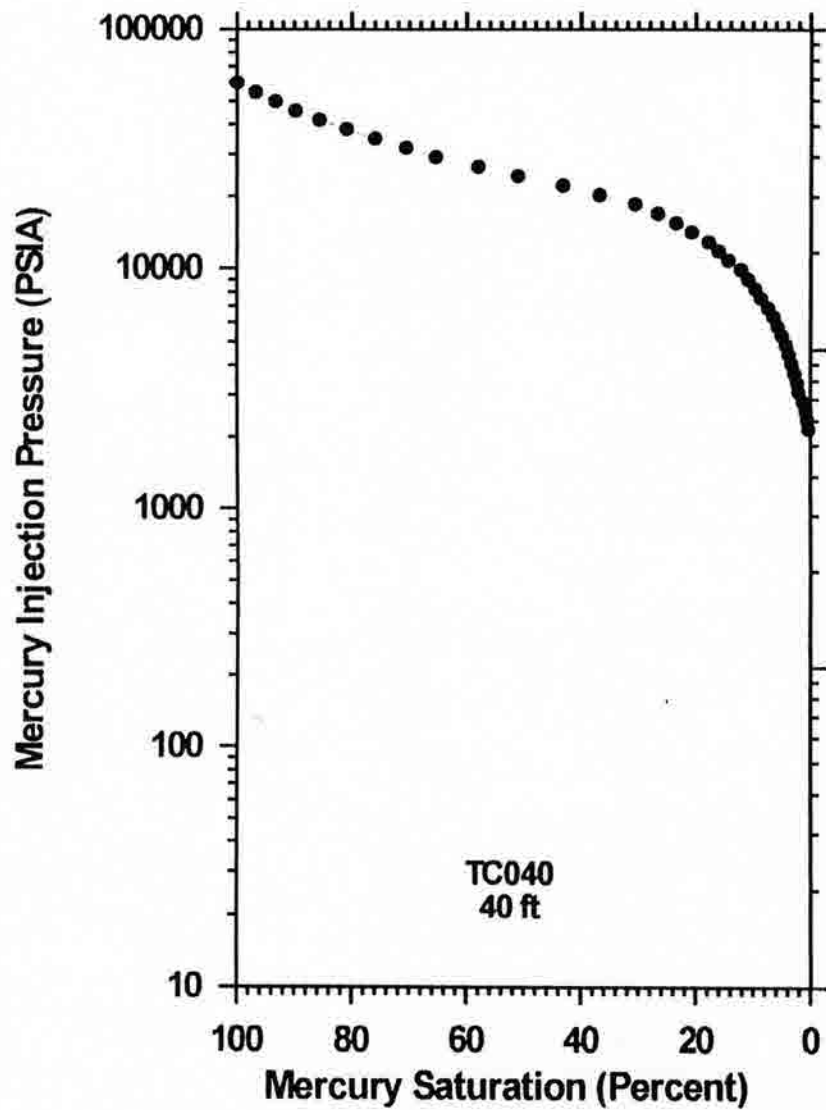


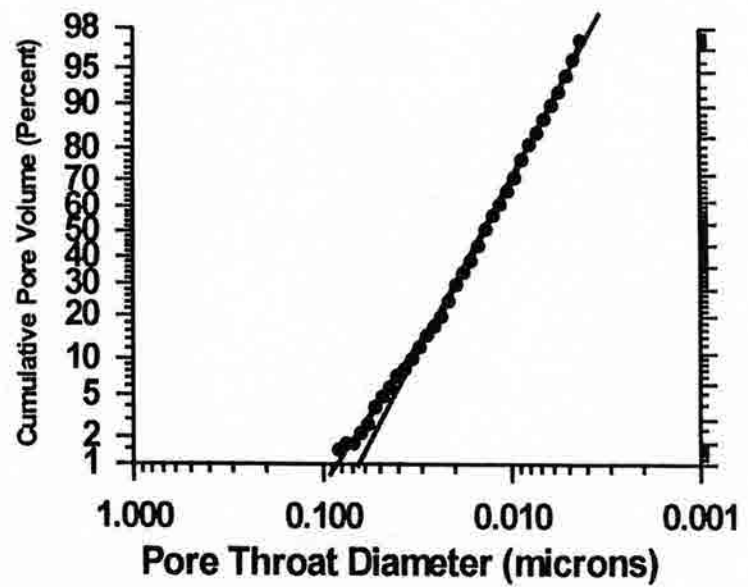
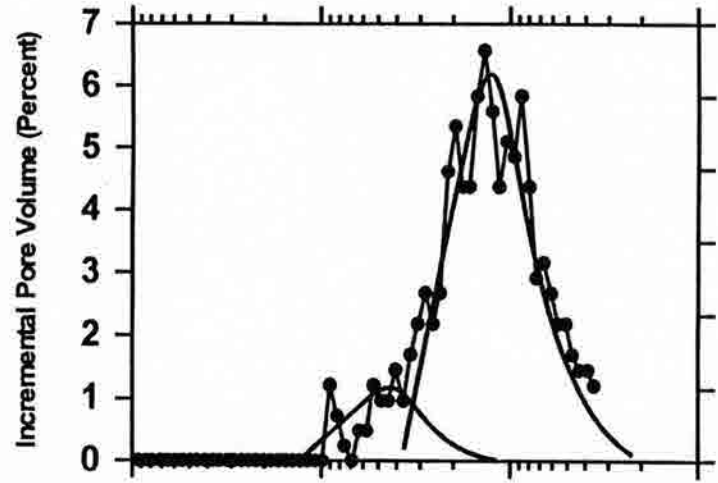
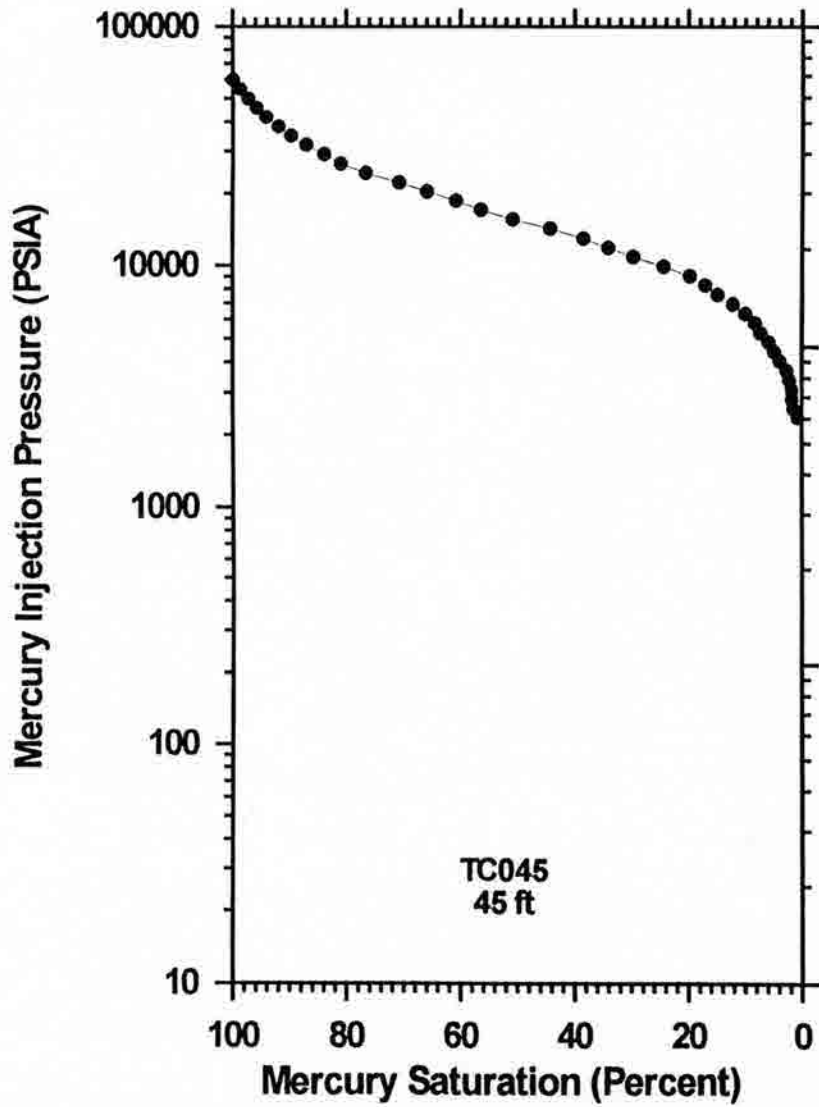


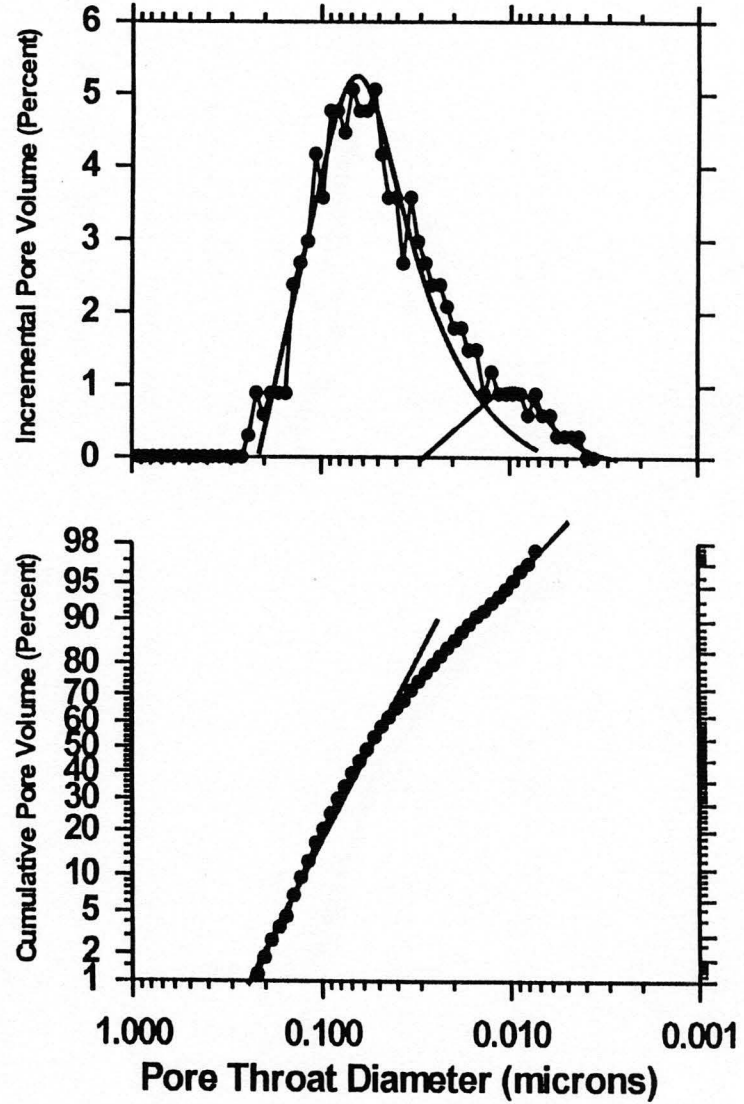
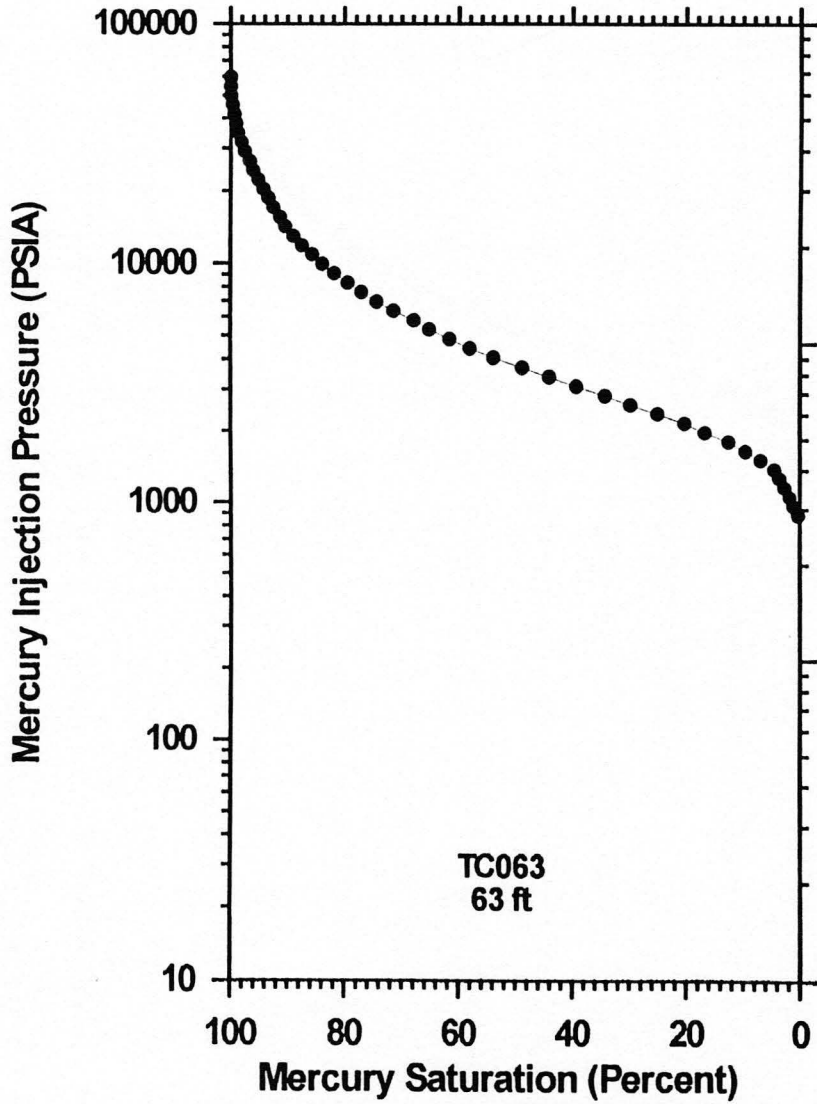


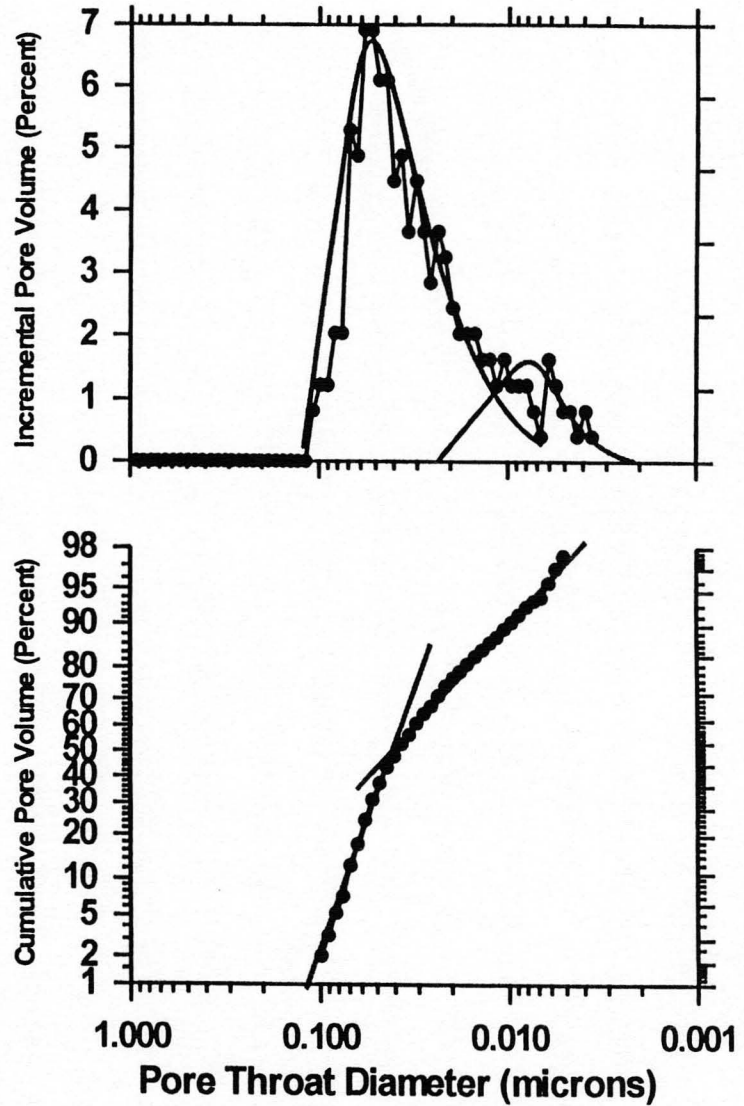
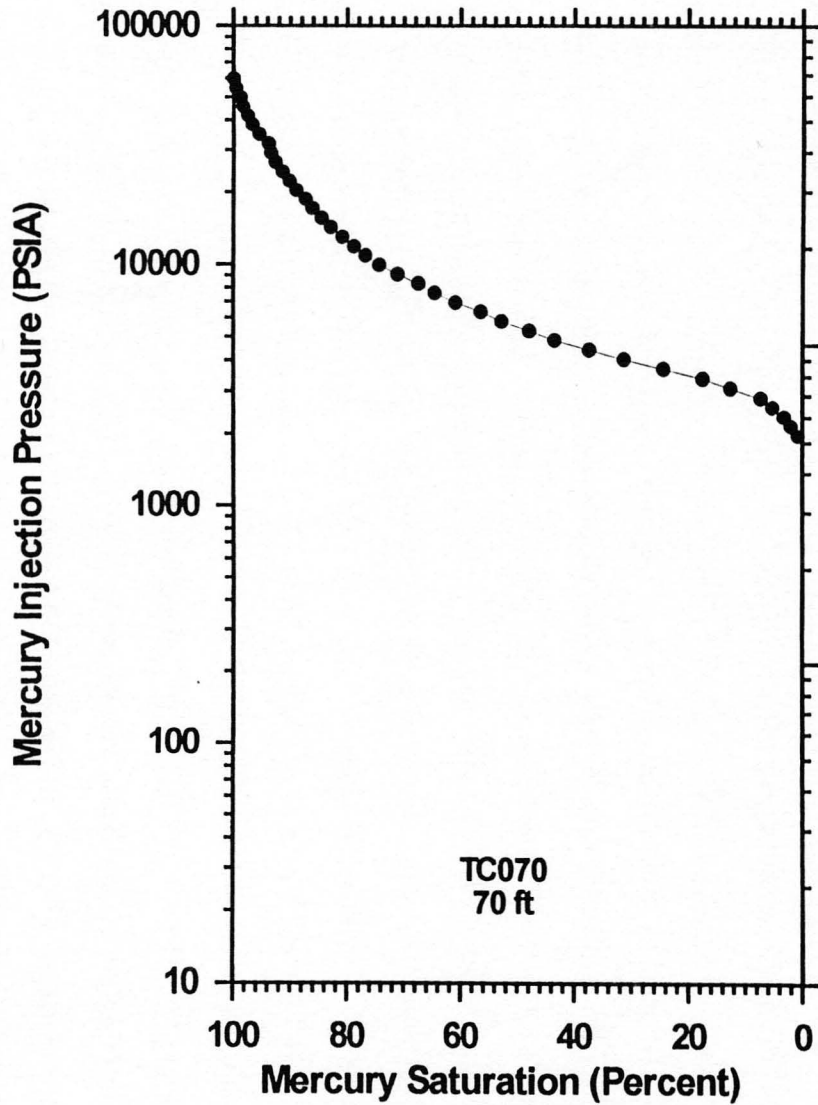


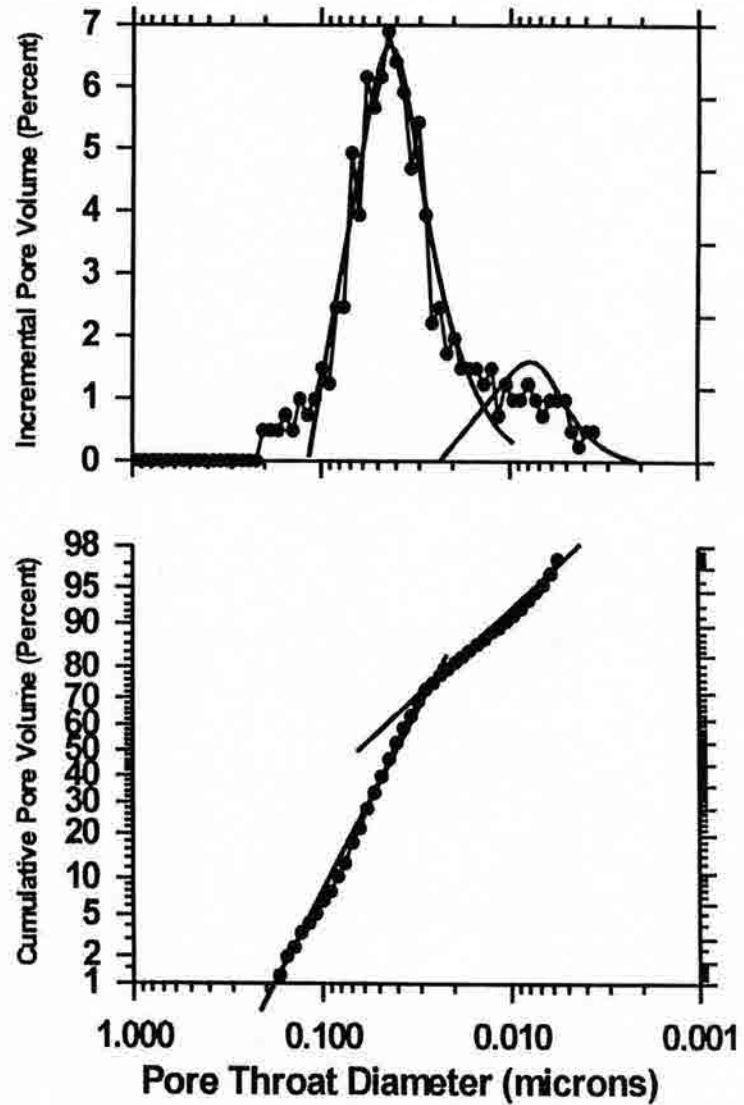
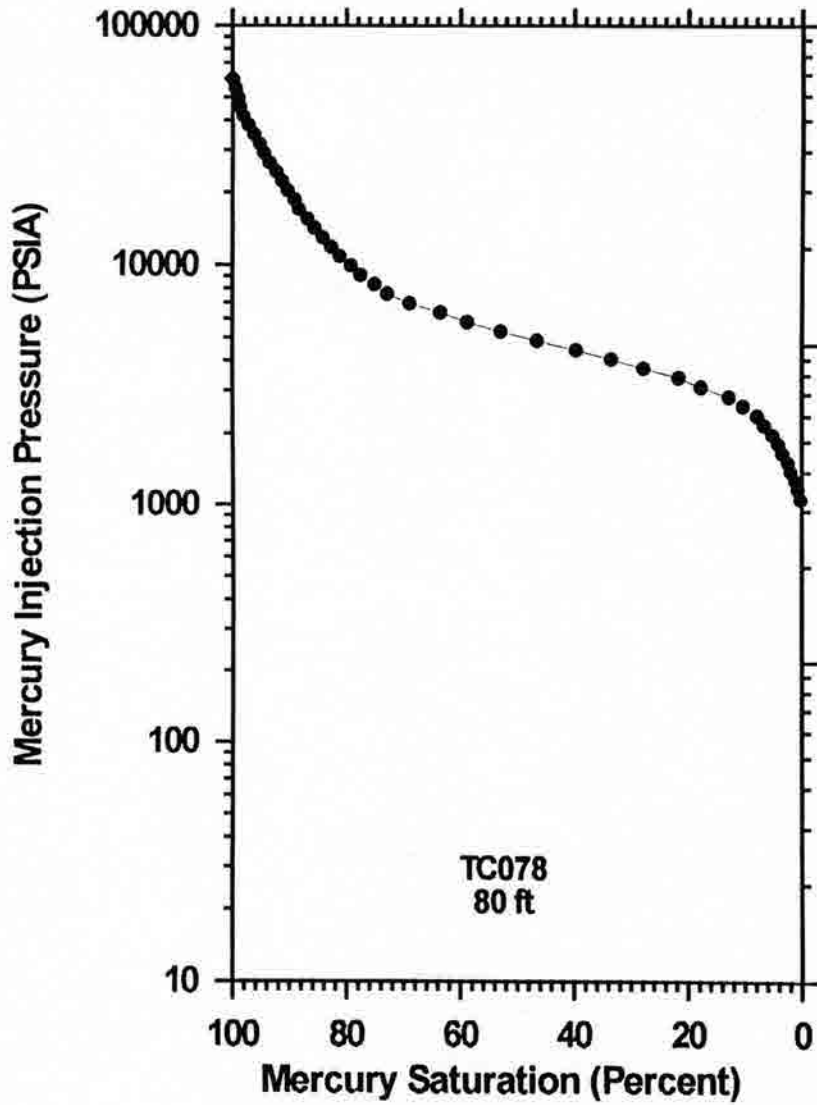


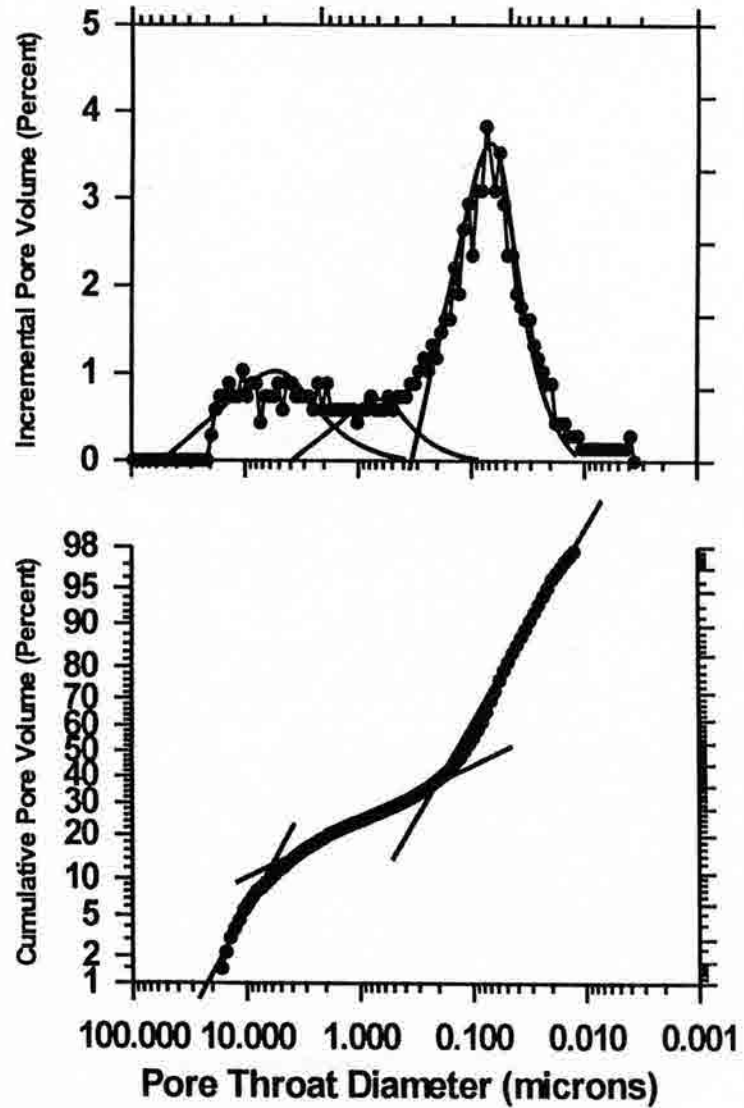
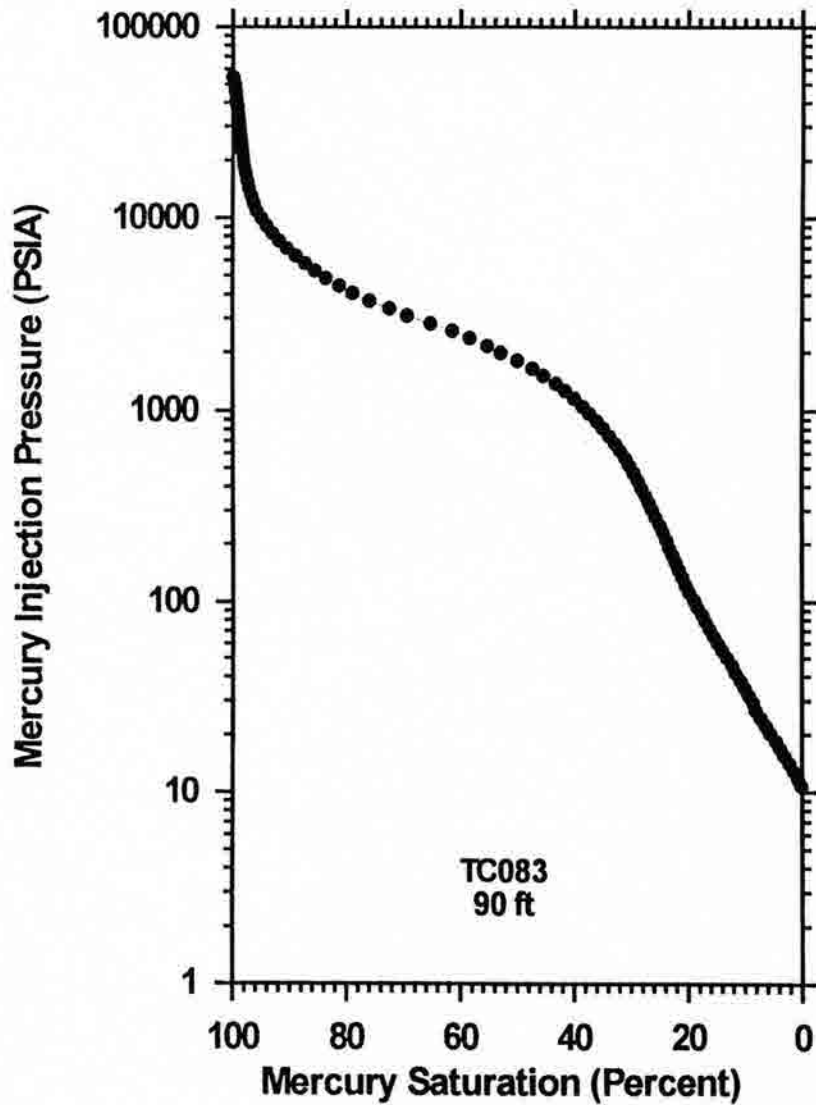












APPENDIX I

MEADOW SPRINGS CORE

SKULL CREEK SHALE

THIN SECTION PHOTOMICROGRAPHS

Figure 11.

Z18000 (7937 ft) - Table A

Low magnification (PL) thin section photomicrograph of carbonaceous silt shale. Strongly compacted, well-sorted matrix contains clay minerals and silt size detrital grains. Accessory constituents include authigenic framboidal pyrite and phosphatic debris. This shale is well laminated with alternating layers of silt and clay with wavy laminations of organic matter. A sharp erosional contact has been recognized over the clay rich matrix and filled in with silt. Carbonate (dolomite, dolonite, and siderite) is present as cement. No matrix porosity is detected.

Figure 12.

Z18000 (7937 ft) - Table A

Low magnification (PL) thin section photomicrograph interbedded silt and siltstone. Strongly compacted, well-sorted matrix contains clay minerals and silt size detrital grains. Accessory constituents include authigenic framboidal pyrite and phosphatic debris. The bottom one-third of this photo is a mineral protuberance of some silt size origin. The bottom one-third of this photo is a carbonaceous siltstone with phosphatic debris that contains wavy laminations in the underlying clay laminae, which suggests the matrix has been compacted. It forms a sharp contact with the shale at the top third of this photo that contains wavy laminations of organic matter. Carbonate (dolomite, dolonite, and siderite) is present as cement. No matrix porosity is evident.

Figure I1.

MS000 (7944 ft)- Facies A

Low magnification (PPL) thin section photomicrograph of carbonaceous silty shale. Strongly compacted, well-sorted matrix contains clay minerals and silt size detrital grains (quartz, feldspar, mica). Accessory constituents include authigenic framboidal pyrite and phosphatic debris. This shale is well laminated with alternating layers of silt and clay with wispy laminations of organic matter. A sharp erosional contact has been scoured into the clay rich matrix and filled in with silt material. Carbonate (calcite, dolomite, and siderite) is present as cement. No matrix porosity is detected.

Figure I2.

MS005 (7939 ft)- Facies A

Low magnification (PPL) thin section photomicrograph interbedded shale and siltstone. Strongly compacted, well-sorted matrix contains clay minerals and silt size detrital grains. Accessory constituents include authigenic framboidal pyrite and phosphatic material probably of bone or fish scale origin. The bottom two-thirds of this photo is a carbonaceous siltstone with phosphatic debris that correlates with an irregularity in the underlying clay lamination, which suggests this matrix has been compacted. It forms a sharp contact with the shale in the top third of this photo that contains wispy laminations of organic matter. Carbonate (calcite, dolomite, and siderite) is present as cement. No matrix porosity is evident.

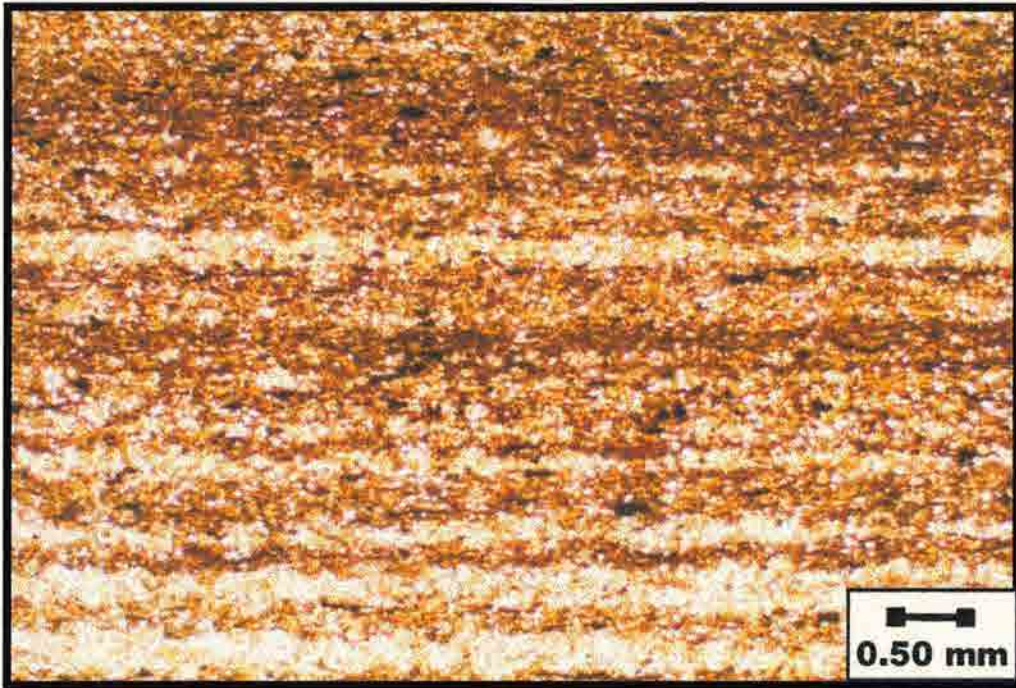


Figure I1.



Figure I2.

Figure 13.

212000 (7078 ft) - Facies A

Low magnification (PL) thin section photomicrograph of carbonaceous silt shale. Strongly compacted, well-sorted matrix contains clay minerals and silt size detrital grains (quartz, feldspar, mica) with an occasional fine-grained sand particle. This finely laminated silt has alternating layers of silt and clay with wavy laminations of organic matter. Carbonate (calcite, dolomite, siderite) is present as cement with minor amounts of subhedral fibrous. Visible matrix porosity is not evident.

Figure 14.

212000 (7078 ft) - Facies A

High magnification (PL) thin section photomicrograph of same carbonaceous silt shale depicted in 13. Strongly compacted, well-sorted matrix contains clay minerals and silt size detrital grains. Accessory constituents include subhedral fibrous pyrite and phosphate nodules. Wavy laminations of organic matter are present. Carbonate (calcite, dolomite, siderite) is present as cement. Visible matrix porosity is not evident.

Figure I3.

MS006 (7938 ft)- Facies A

Low magnification (PPL) thin section photomicrograph of carbonaceous silty shale. Strongly compacted, well-sorted matrix contains clay minerals and silt size detrital grains (quartz, feldspar, mica) with an occasional fine-grained sand particle. This finely laminated shale has alternating layers of silt and clay with wispy laminations of organic matter. Carbonate (calcite, dolomite, siderite) is present as cement with minor amounts of authigenic framboidal pyrite. Visible matrix porosity is not evident.

Figure I4.

MS006 (7938 ft)- Facies A

High magnification (PPL) thin section photomicrograph of same carbonaceous silty shale pictured in I3. Strongly compacted, well-sorted matrix contains clay minerals and silt size detrital grains. Accessory constituents include authigenic framboidal pyrite and phosphatic nodules. Wispy laminations of organic matter are prevalent. Carbonate (calcite, dolomite, siderite) is present as cement. Visible matrix porosity is not evident.

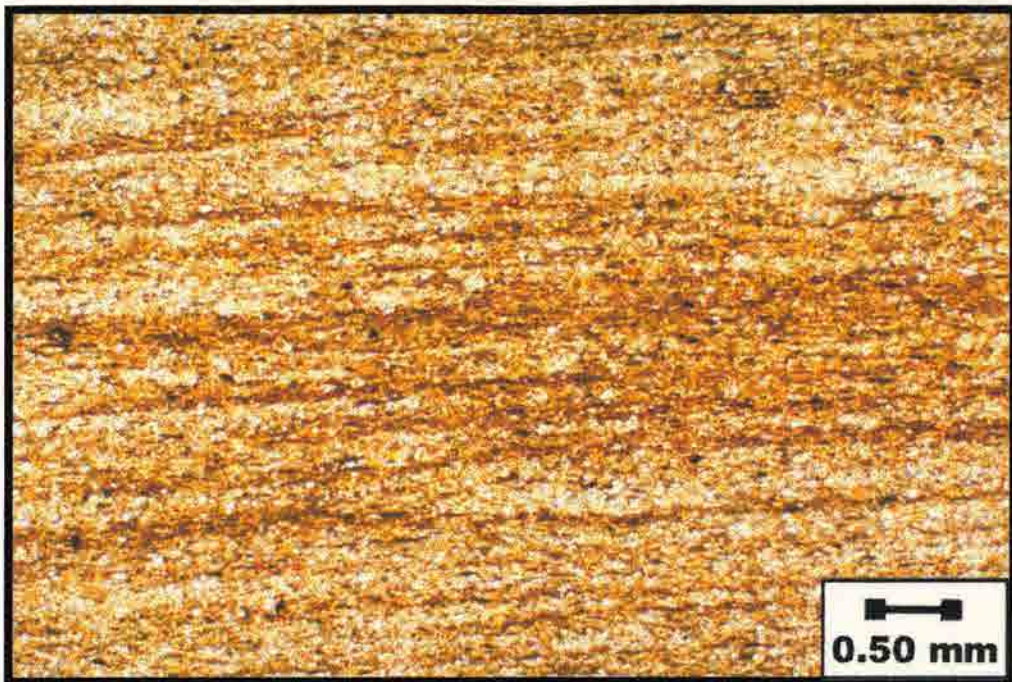


Figure I3.

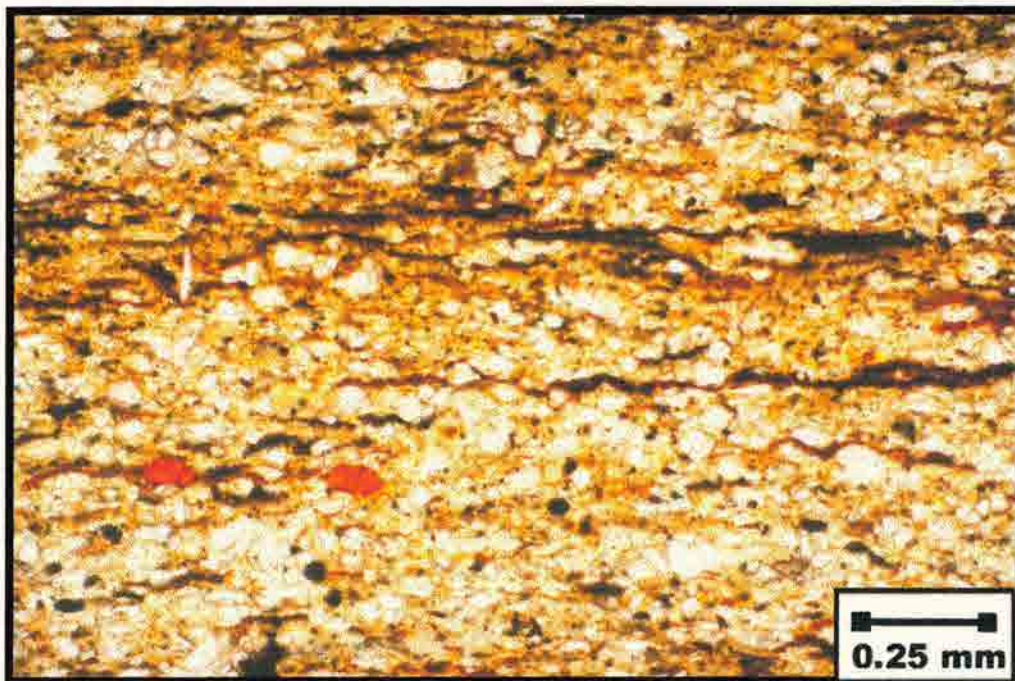


Figure I4.

Figure 13.

215013 (7930 ft) - Facies II

Low magnification (PPL) thin section photomicrograph of carbonaceous silt shale. Strongly compressed, well-sorted matrix contains clay minerals and fine detrital grains (quartz, feldspar, mica). Abundant concentric radial nodular pyrite. This shale is well-laminated with alternating layers of silt and clay with wavy laminations of organic matter. Calcite, dolomite, and siderite is present as cement. No matrix porosity is detected.

Figure 14.

215014 (7930 ft) - Facies II

Medium magnification (PPL) thin section photomicrograph of sand carbonaceous silt shale. Strongly compressed, well-sorted matrix contains clay minerals and fine detrital grains. The well-laminated shale has minor burrowing that has disturbed some of the laminations. Calcite, dolomite, and siderite is present as cement with minor amounts of anhedral fibroblastic pyrite. No matrix porosity is noted.

Figure I5.

MS014 (7930 ft)- Facies B

Low magnification (PPL) thin section photomicrograph of carbonaceous silty shale. Strongly compacted, well-sorted matrix contains clay minerals and silt size detrital grains (quartz, feldspar, mica). Accessory constituents include authigenic framboidal pyrite. This shale is well-laminated with alternating layers of silt and clay with wispy laminations of organic matter. Carbonate (calcite, dolomite, and siderite) is present as cement. No matrix porosity is detected.

Figure I6.

MS014 (7930 ft)- Facies B

Medium magnification (PPL) thin section photomicrograph of same carbonaceous silty shale pictured in I5. Strongly compacted, well-sorted matrix contains clay minerals and silt size detrital grains. The well-laminated shale has minor burrowing that has disturbed some of the laminations. Carbonate (calcite, dolomite, and siderite) is present as cement with minor amounts of authigenic framboidal pyrite. No matrix porosity is noted.

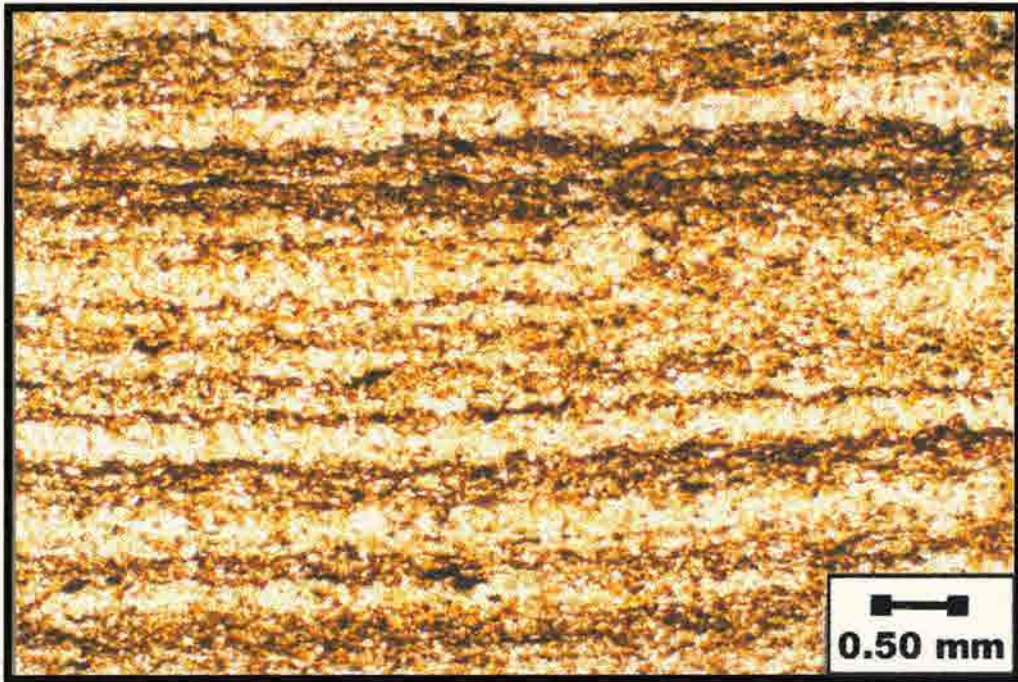


Figure I5.

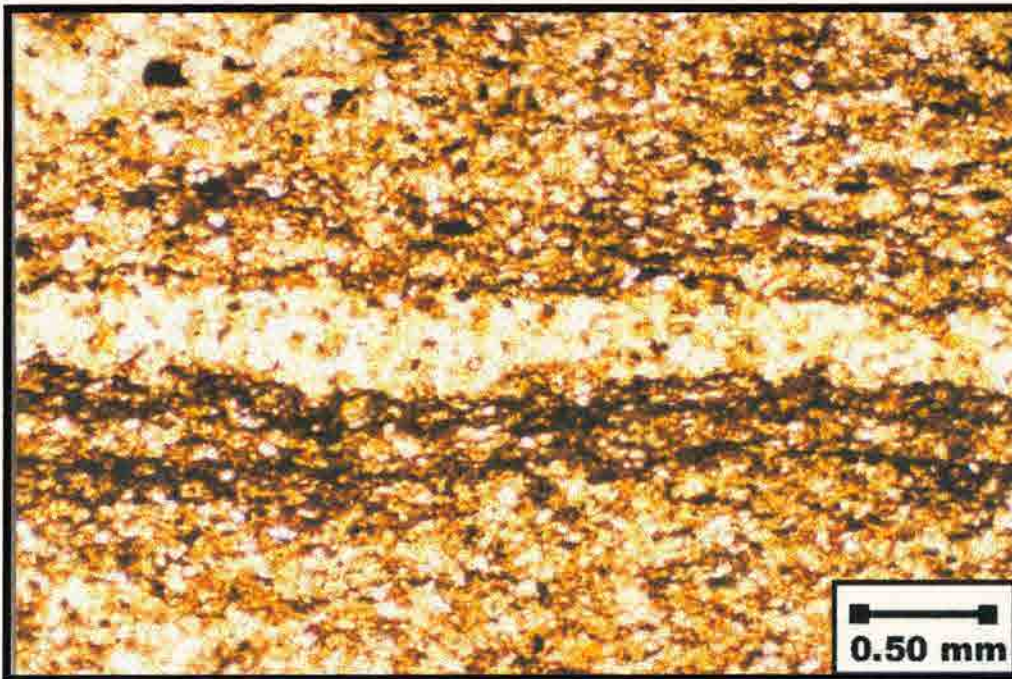


Figure I6.

Figure 17.

MR029 (7918 ft)-Factor C

Low magnification (PM) thin section photomicrograph of the grainoid carbonaceous silty shale (strongly compacted, moderately well sorted matrix contains clay minerals and silty fine detrital grains (quartz, feldspar, mica) with occasional very fine-grained sand particles. This shale has alternating layers of silt and clay with wavy laminations of organic matter that has been disrupted by burrowing. Carbonate (calcite, dolomite, siderite) is present as cement with minor amounts of zoogenic fibroblastic pyrite. No matrix porosity is evident.

Figure 18.

MR029 (7918 ft)-Factor C

Medium magnification (PM) thin section photomicrograph of same fine-grained carbonaceous silty shale (strongly compacted, moderately well sorted matrix contains clay minerals and silty fine detrital grains (quartz, feldspar, mica) with occasional very fine-grained sand particles. Accretionary concretions include subigneous (amorphous) pyrite. This shale has alternating layers of silt and clay that have been disrupted by burrowing. Organic matter is present as wavy laminations. Carbonate (calcite, dolomite, siderite) is present as a cement. Matrix porosity is not evident.

Figure I7.

MS029 (7915 ft)- Facies C

Low magnification (PPL) thin section photomicrograph of fine grained, carbonaceous siltstone. Strongly compacted, moderately well sorted matrix contains clay minerals and silt size detrital grains (quartz, feldspar, mica) with occasional very fine-grained sand particles. This shale has alternating layers of silt and clay with wispy laminations of organic matter that has been disrupted by burrowing. Carbonate (calcite, dolomite, siderite) is present as cement with minor amounts of authigenic framboidal pyrite. No matrix porosity is evident.

Figure I8.

MS029 (7915 ft)- Facies C

Medium magnification (PPL) thin section photomicrograph of same fine-grained, carbonaceous siltstone pictured in I7. Strongly compacted, moderately well sorted matrix contains clay minerals and silt size detrital grains (quartz, feldspar, mica) with occasional very fine-grained sand particles. Accessory constituents include authigenic framboidal pyrite. This shale has alternating layers of silt and clay that have been disrupted by burrowing. Organic matter is present as wispy laminations. Carbonate (calcite, dolomite, siderite) is present as a cement. Matrix porosity is not evident.



Figure I7.

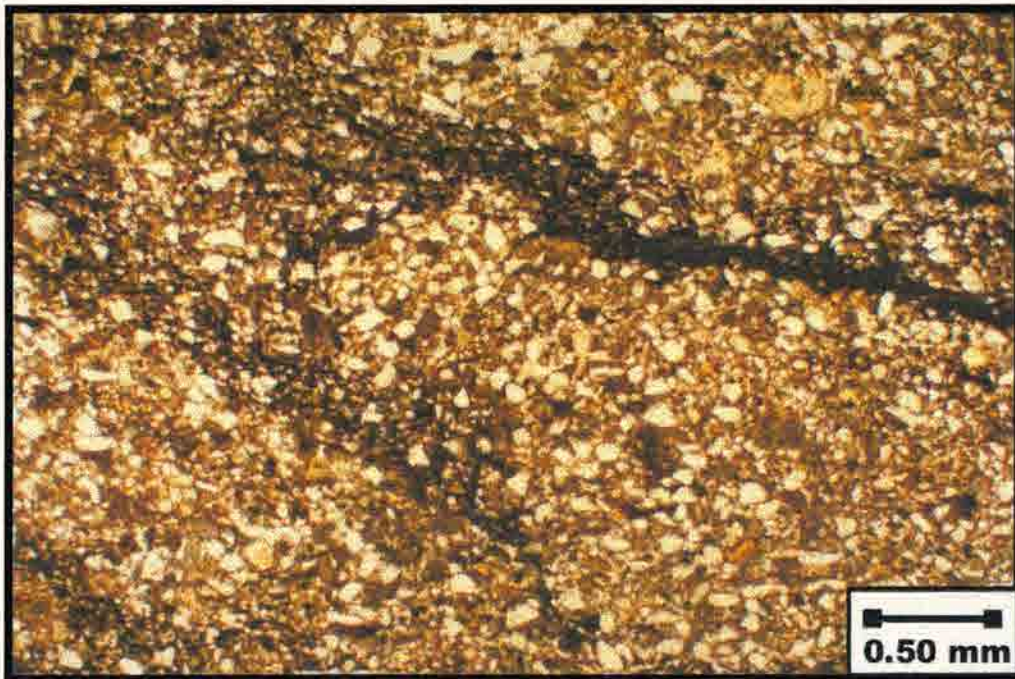


Figure I8.

Figure 18.

M5034 (7910 B)-Factor C

Medium magnification (PPL) thin section photomicrograph of fine grained calcareous siltstone. Compacted, moderately sorted matrix contains clay minerals and fine to medium grained quartz (black, oblique, minor) with fine grained sand particles. Secondary cementation includes authigenic (anhedral) pyrite. This shale has a heterogeneous distribution of hard grains with distinct laminae of clay and organic matter, which is a common feature of (shale, dolomite, calcite, dolomite, calcite) is present as a major cement. No matrix porosity is evident.

Figure 19.

M5035 (7884 B)-matrix

Low magnification of (PPL) thin section photomicrograph of a clay-rich interval. The dominantly clay rich matrix has poor to moderately sorted, very fine sand and silt sized quartz grains. The clay matrix is not laminated or burrowed, but does show some evidence of root traces with Fe staining along with some phosphate mineral. There is no porosity evident except for the indistinct traces of sample preservation.

Figure I9.

MS034 (7910 ft)- Facies C

Medium magnification (PPL) thin section photomicrograph of fine grained, carbonaceous siltstone. Compacted, moderately sorted matrix contains clay minerals and silt size detrital grains (quartz, feldspar, mica) with fine grained sand particles. Accessory constituents include authigenic framboidal pyrite. This shale has a homogeneous distribution of hard grains with disturbed laminations of clay and organic matter, which is a common burrowing feature. Carbonate (calcite, dolomite, siderite) is present as a major cement. No matrix porosity is evident.

Figure I10.

MS055 (7884 ft)- paleosol

Low magnification of (PPL) thin section photomicrograph of a clay-rich paleosol. The dominantly clay rich matrix has poor to moderately sorted, very fine sand size detrital quartz grains. The clay matrix is not laminated or burrowed, but does show some evidence of root traces with Fe staining along with some phosphate material. There is no porosity evident except for the induced fractures by sample preparation.

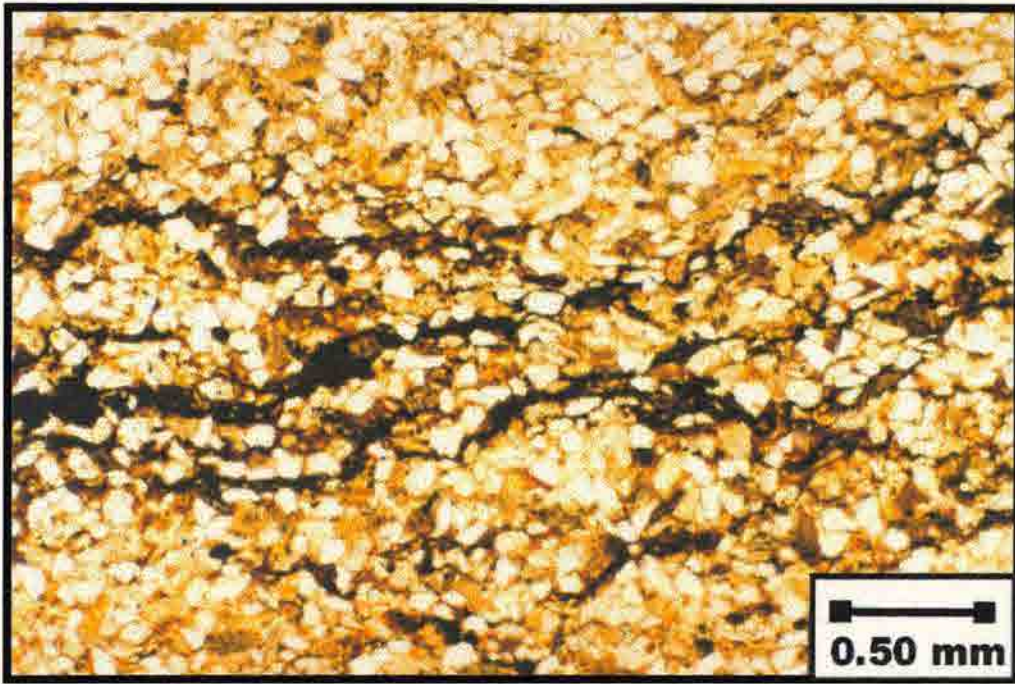


Figure I9.



Figure I10.

APPENDIX J

MEADOW SPRINGS CORE

SKULL CREEK SHALE

SEM PHOTOMICROGRAPHS

1950-1951 - 1951
1952-1953 - 1953
1954-1955 - 1955

The first step in the development of a new product is the identification of a market need. This is done by conducting market research, which involves gathering information about the target market's needs, preferences, and buying behavior. The next step is to develop a product concept that addresses the identified need. This concept is then refined through prototyping and testing to ensure it meets the market requirements. Finally, the product is launched into the market, and its performance is monitored to make necessary adjustments.

As the product moves through the development process, it is important to maintain a focus on the customer. This involves regular communication with the target market to gather feedback and ensure the product remains relevant and valuable. Additionally, it is crucial to manage the product's lifecycle, including monitoring sales, profitability, and market trends. This allows the company to make informed decisions about when to discontinue or update the product, ensuring it remains competitive in the market.

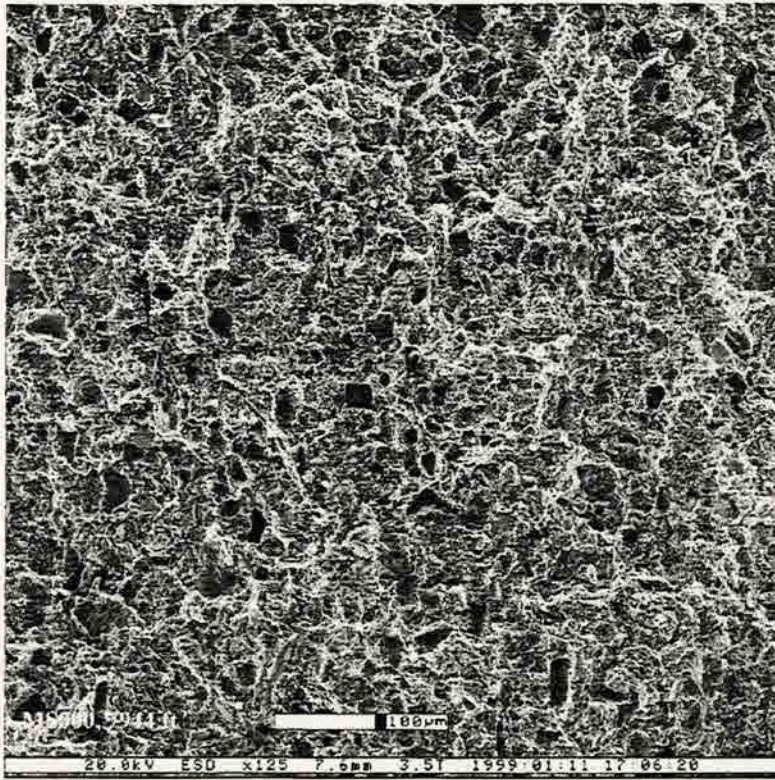
MS000: 7944 ft – Facies A

Top Photo: Low Power (x125)

Bottom Photo: High Power (x1200)

At low magnification, the overall texture is a moderately sorted, angular to subrounded, framework supported, silty shale. The framework particle size ranges from 10 to 50 μm and composes the bulk of this sample. The framework mineralogy primarily consists of detrital quartz grains with significant amounts of authigenic framboidal pyrite and authigenic carbonates with secondary amounts of feldspars. Quartz overgrowths are present and seem to be cut off by clay cementation.

At high magnification, authigenic framboidal pyrite is clearly distinguishable. Discrete illite is shown by the white flakelike clay minerals that are primarily coating grains. In addition to grain coating, the clays are also pore filling. The sample exhibits a poorly developed intergranular macropore system and a poorly developed intergranular micropore system. Molds of plucked grains (pyrite and quartz) are found throughout this sample and an artifact of sample preparation.



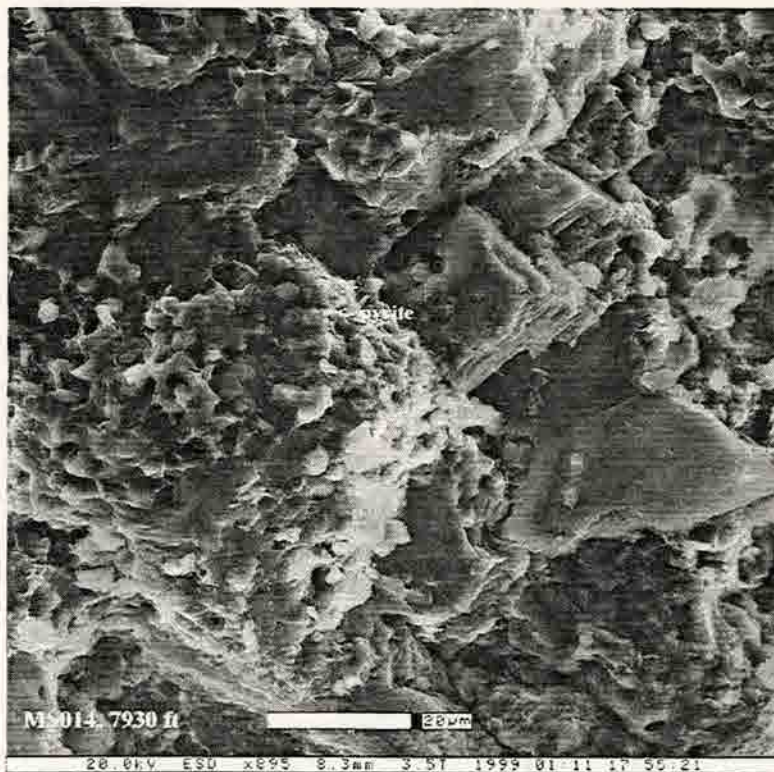
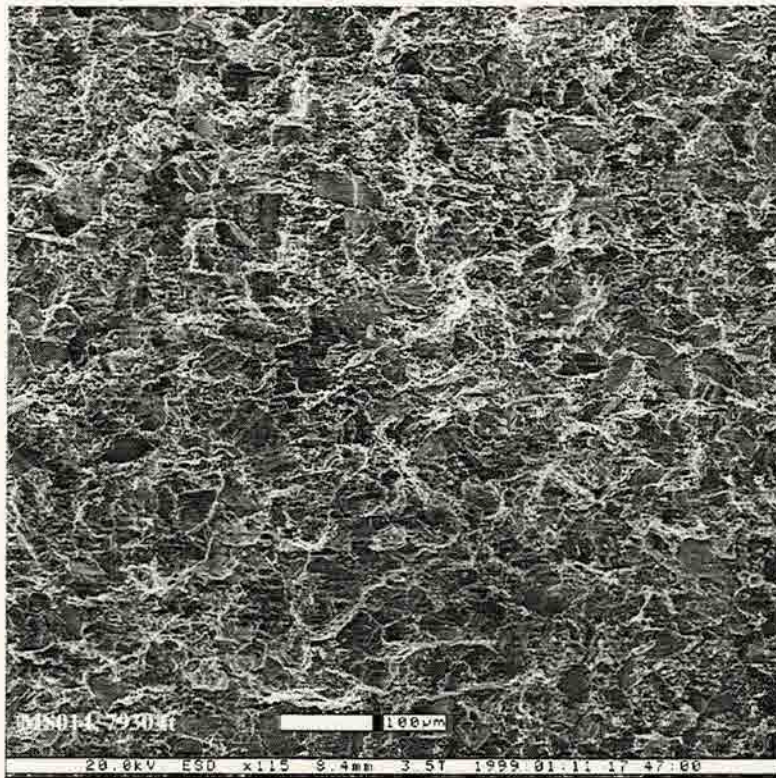
MS014: 7930 ft – Facies B

Top photo: Low Power (x115)

Bottom photo: High Power (x895)

At low magnification, the overall texture is a moderate to well sorted, subangular to subrounded, framework supported, silty shale. The framework particle size ranges from 10 to 50 μm and is homogeneously distributed throughout the bulk of this sample. The framework mineralogy primarily consists of detrital quartz grains with significant amounts of authigenic framboidal pyrite and authigenic carbonates with secondary amounts of feldspars. Quartz overgrowths seem to be cut off by this clay cementation.

At high magnification, the authigenic framboidal pyrite is clearly visible and appears to be coated by clay minerals. Discrete illite is shown as the whitish, flake-like clay mineral. The clays in this sample are primarily grain coating but are also pore-filling. The sample exhibits a poorly developed intergranular macropore system and a poorly developed intergranular micropore system. Molds of plucked grains (pyrite and quartz) and fractured grains are artifacts of sample preparation.



1870-1871
1872-1873
1874-1875

The first of these is the fact that the
second is the fact that the
third is the fact that the
fourth is the fact that the
fifth is the fact that the
sixth is the fact that the
seventh is the fact that the
eighth is the fact that the
ninth is the fact that the
tenth is the fact that the

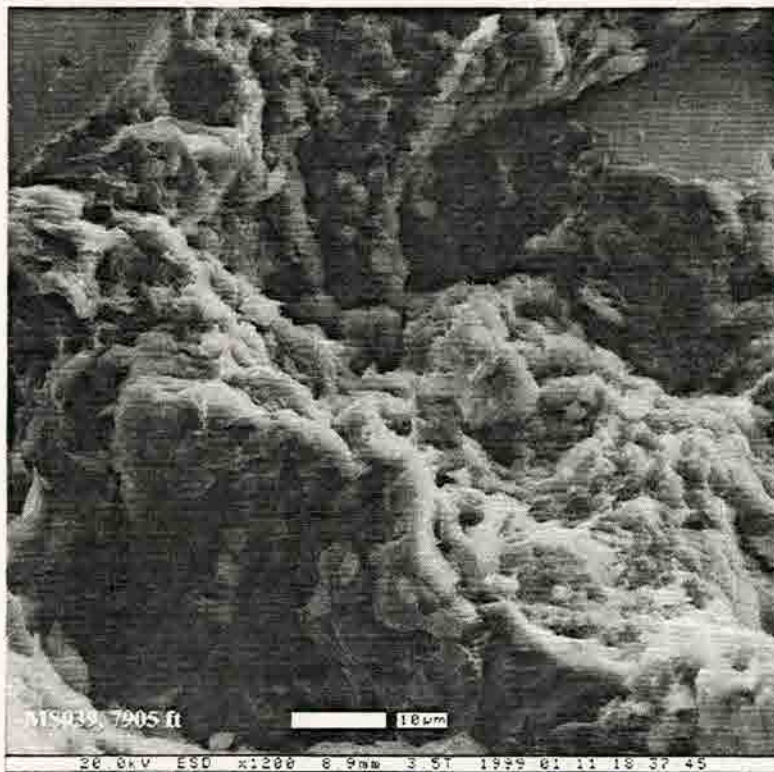
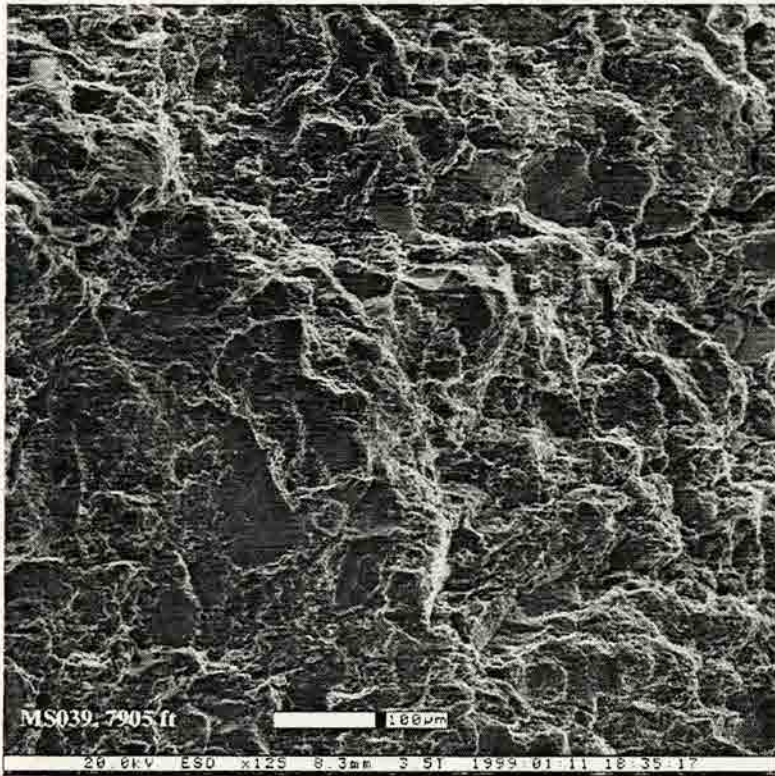
MS039: 7905 ft – Facies C

Top photo: Low Power (x125)

Bottom photo: High Power (x1200)

At low magnification, the overall texture is a moderate to well sorted, subangular to subrounded, framework supported silty shale. The framework particle size ranges from 20 to 50 μm and is homogeneously distributed throughout the bulk of this sample. The framework mineralogy primarily consists of detrital quartz with secondary amounts of feldspars.

At high magnification, the clay minerals are displayed as pore filling interstitial fines and coating detrital hard grains. The sample exhibits a poor to moderate developed intergranular macropore system and a poorly developed intergranular micropore system.



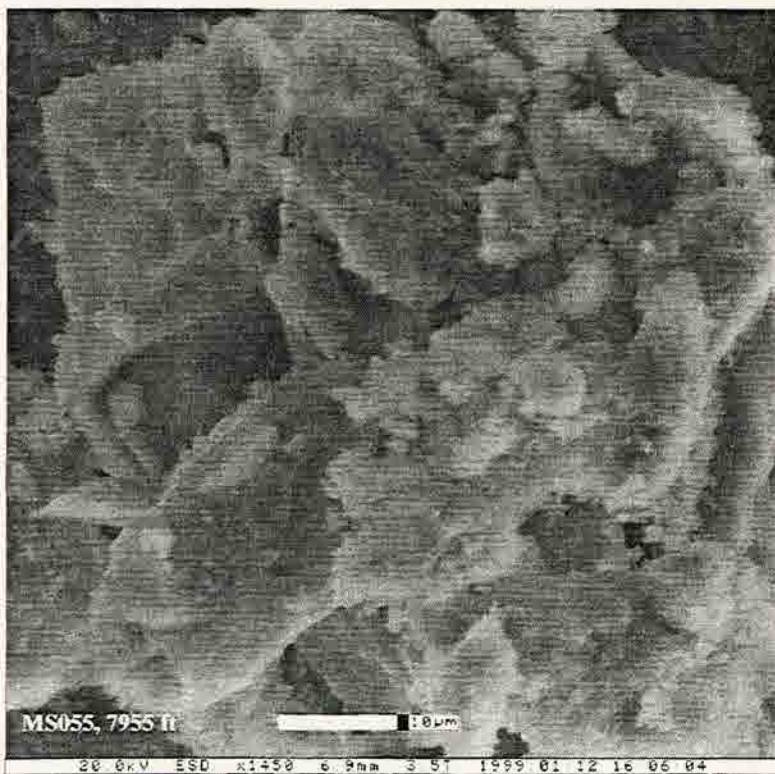
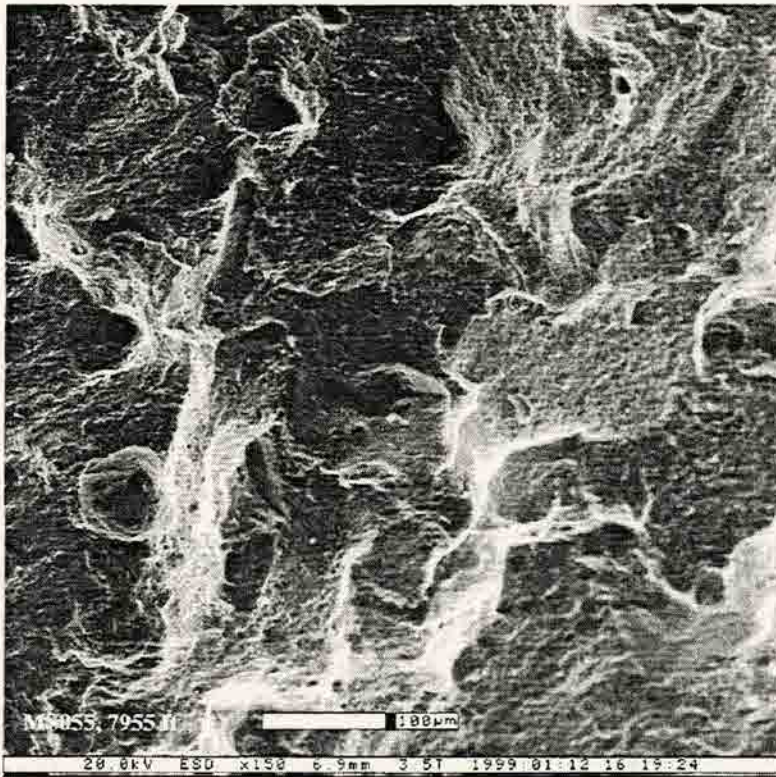
MS055: 7955 ft – Paleosol

Top photo: Low Power (x150)

Bottom photo: High Power (x1450)

At low magnification, the overall texture is a moderate to well sorted, subrounded, matrix supported paleosol. The framework particle size ranges from 30 to 50 μm and is sparsely distributed. The framework mineralogy primarily consists of detrital quartz with secondary amounts of feldspars.

At high magnification, small “books” of kaolinite can be distinguished. The remaining clay minerals compose the bulk of this sample. The sample exhibits a poorly developed intergranular macropore system and a poorly developed intergranular micropore system. Any fractured grains are an artifact of sample preparation.



Journal of the
Royal Society of
Medicine

The following is a summary of the
main points of the paper. The author
discusses the importance of the
subject and the need for further
research. He also discusses the
methodology used in the study and
the results obtained. The author
concludes that the findings of the
study are significant and that
further research is needed in this
area.

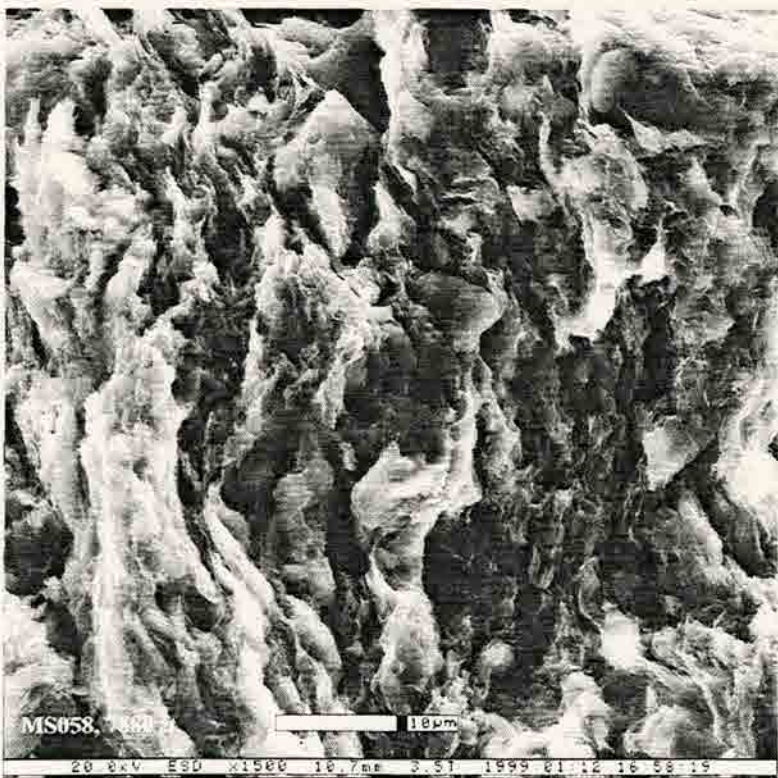
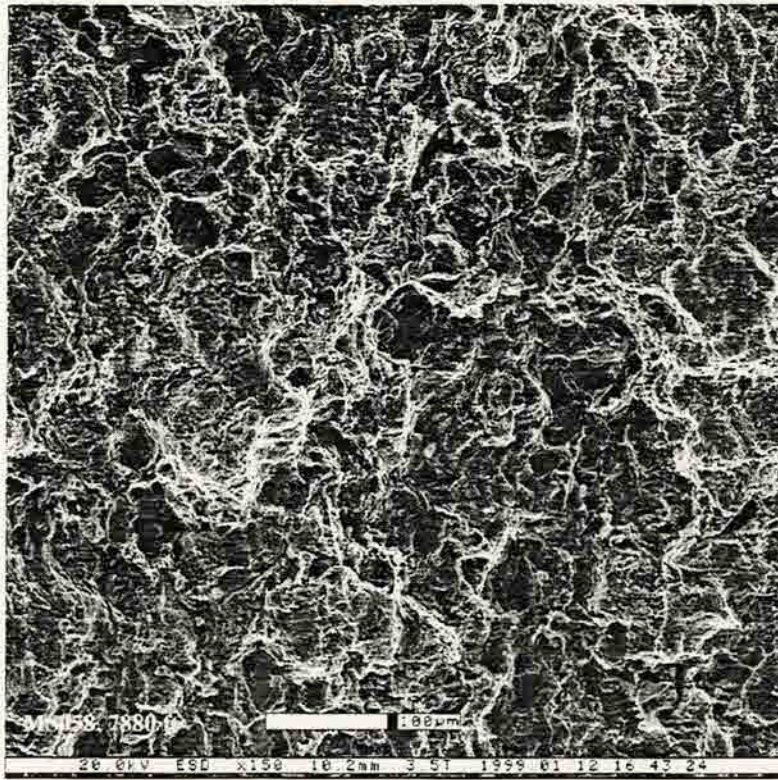
MS058: 7880 ft – Facies E

Top photo: Low Power (x150)

Bottom photo: High Power (x1500)

At low magnification, the overall texture is a moderately sorted, subangular to subrounded, framework supported silty shale. The framework particle size ranges from 10 to 50 μm and is homogeneously distributed throughout the bulk of this sample. The framework mineralogy primarily consists of detrital quartz grains and secondary amounts of feldspars.

At high magnification, the laminations of clay minerals are predominantly displayed. These clays occur primarily as grain coating and pore filling interstitial fines with a strong preferred orientation. The white flake-like clay mineral is discrete illite. The sample exhibits a moderately developed intergranular macropore system and a moderately developed intergranular micropore system. Molds of plucked grains are found throughout this sample and probably an artifact of sample preparation.



APPENDIX K

MEADOW SPRINGS CORE

SKULL CREEK SHALE

MICP GRAPHS

MICP table for Meadow Springs core (Skull Creek shale)

Sample#	FT	Facies	Median PTD	Pore Volume %	Sorting Index
MS000	7944	A	0.01	100	W
MS006	7938	A	0.007	100	W
MS014	7930	B	0.01	100	W
MS024	7920	B	0.0175	100	M-W
MS034	7910	C	0.0175	80	M-W
			0.15	20	VW
MS044	7900	D	0.1	80	M
			0.3	20	W
MS055	7884	PALEO	0.005	100	VW
MS058	7880	E	0.01	50	M
			0.04	50	M
MS066	7864	Mowry	0.005	100	W

LEGEND:

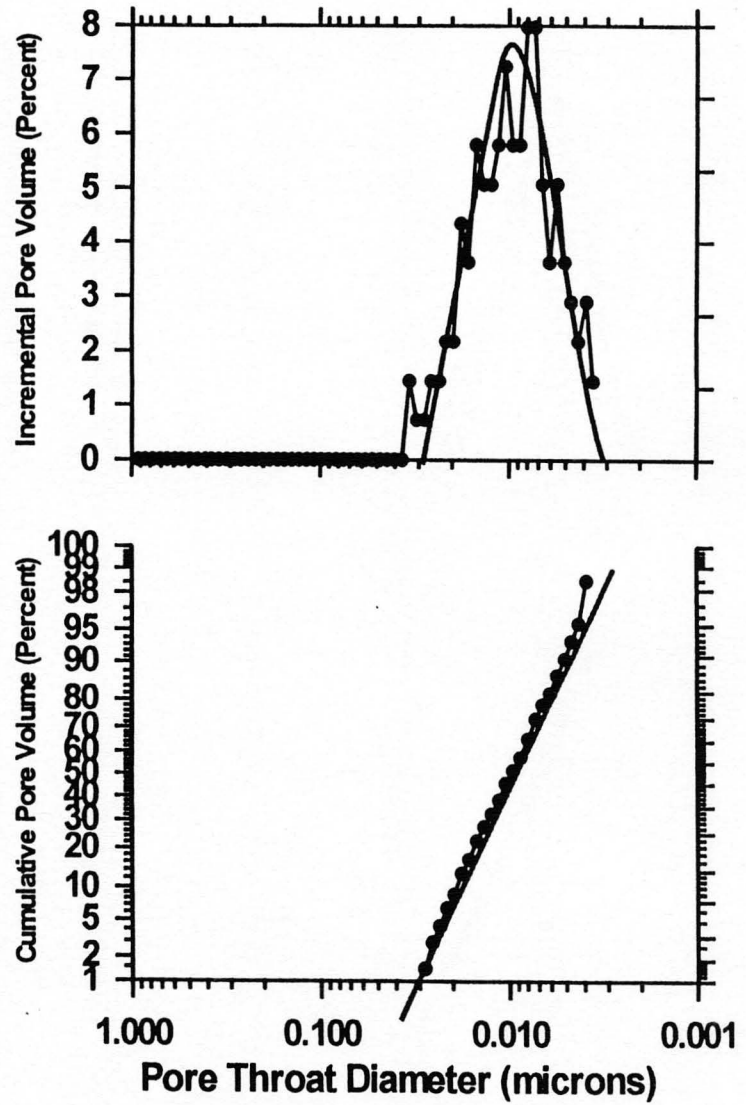
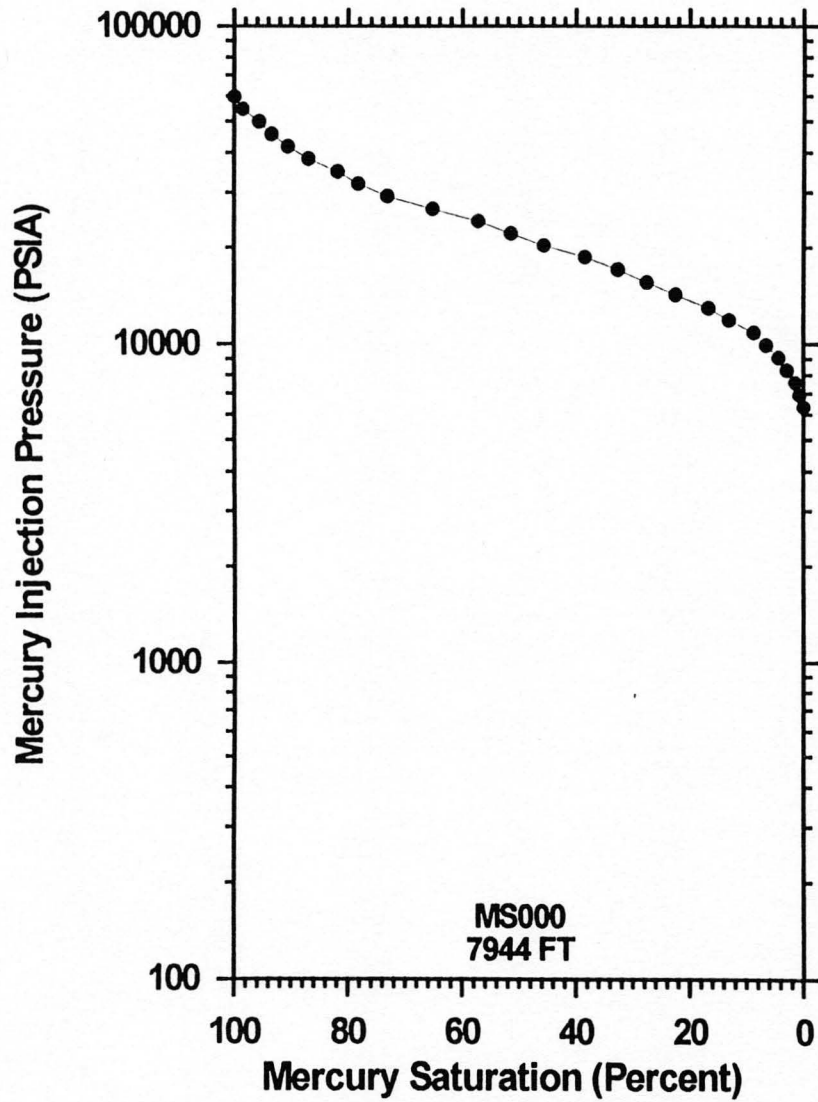
VW= Very Well sorted

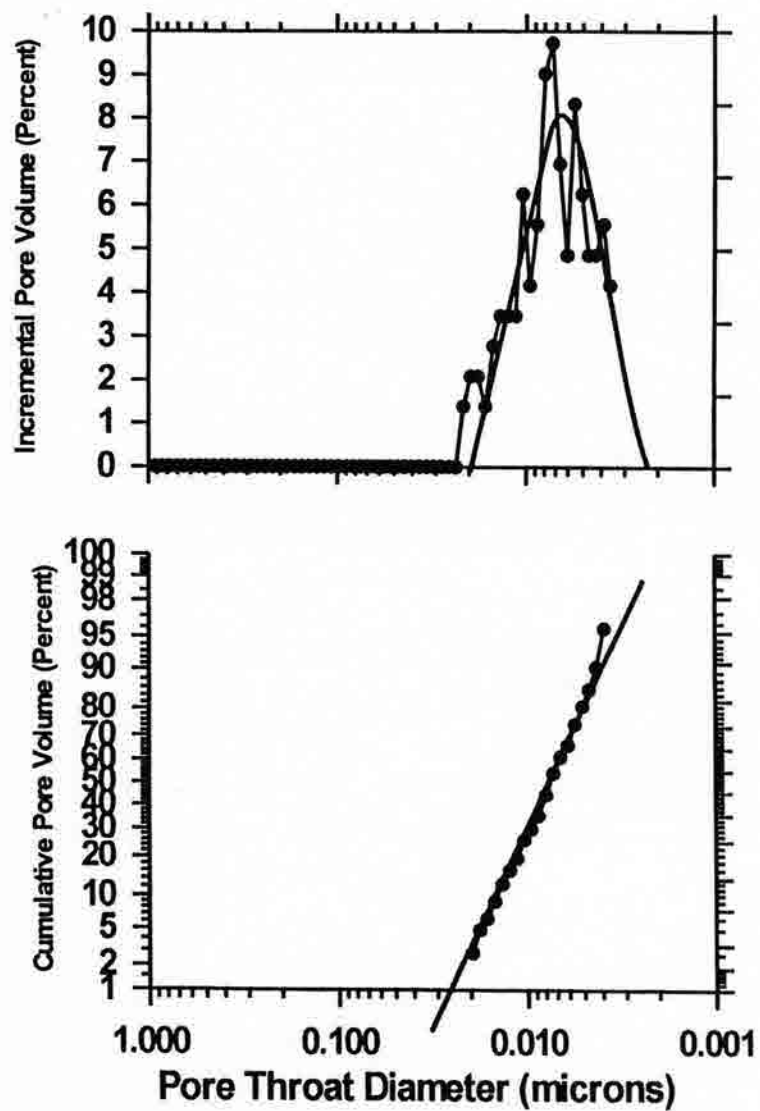
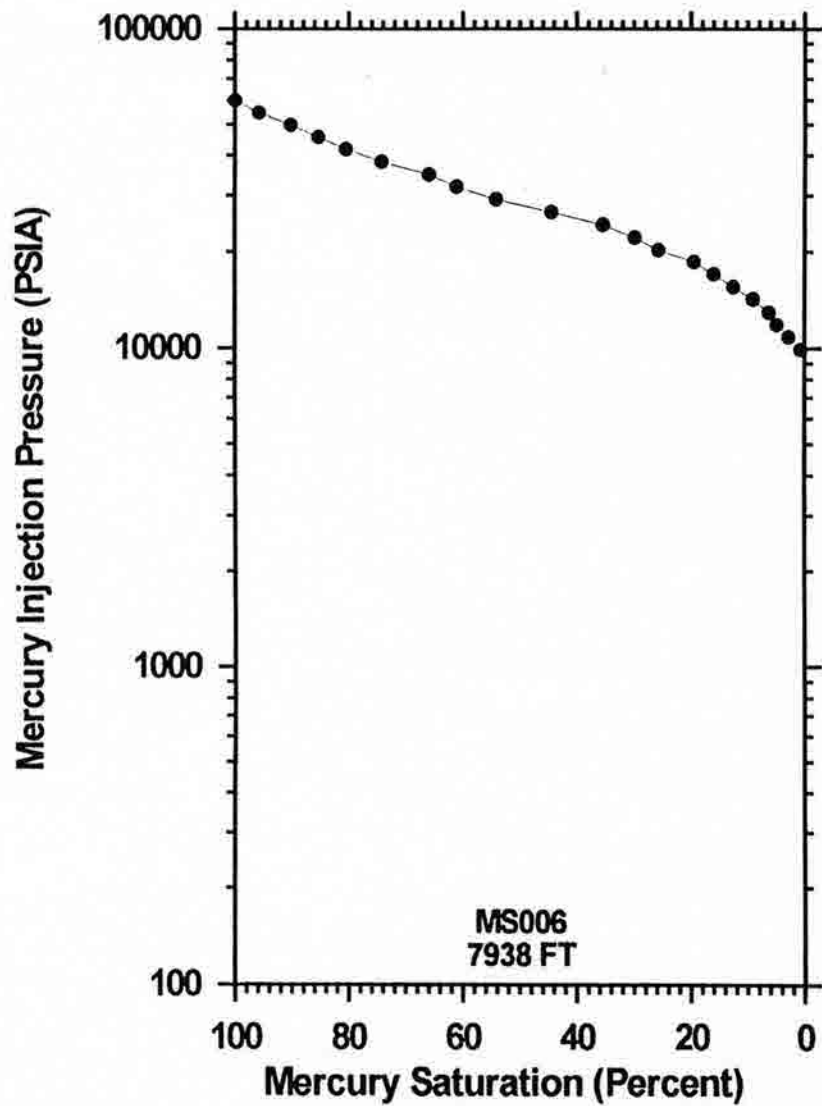
W= Well sorted

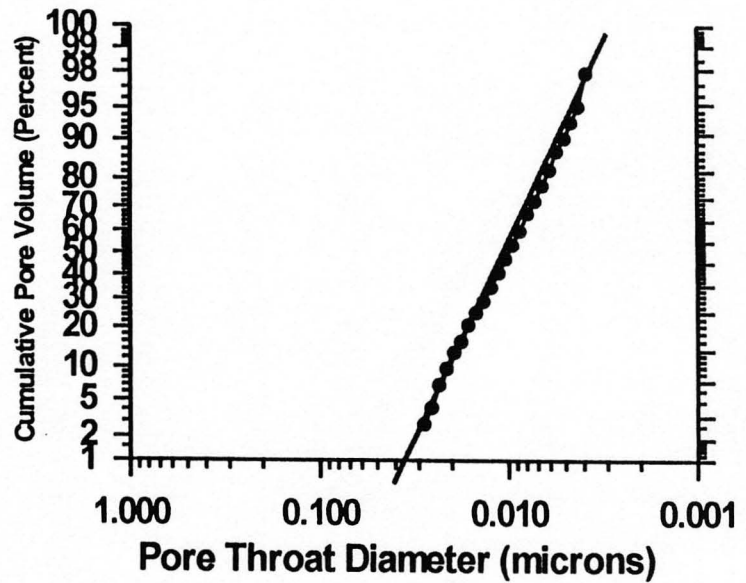
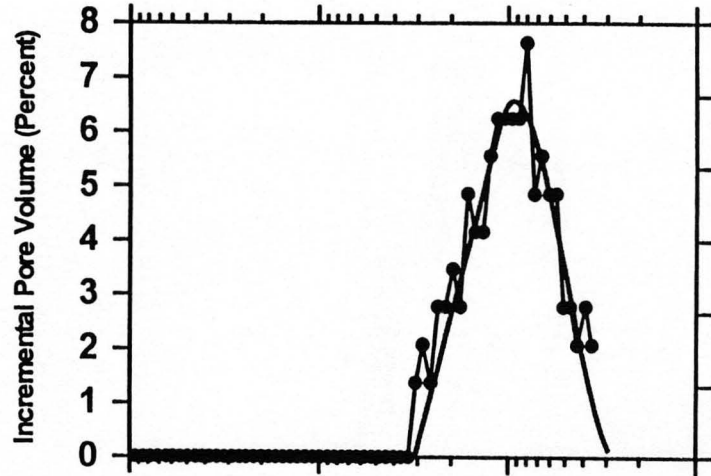
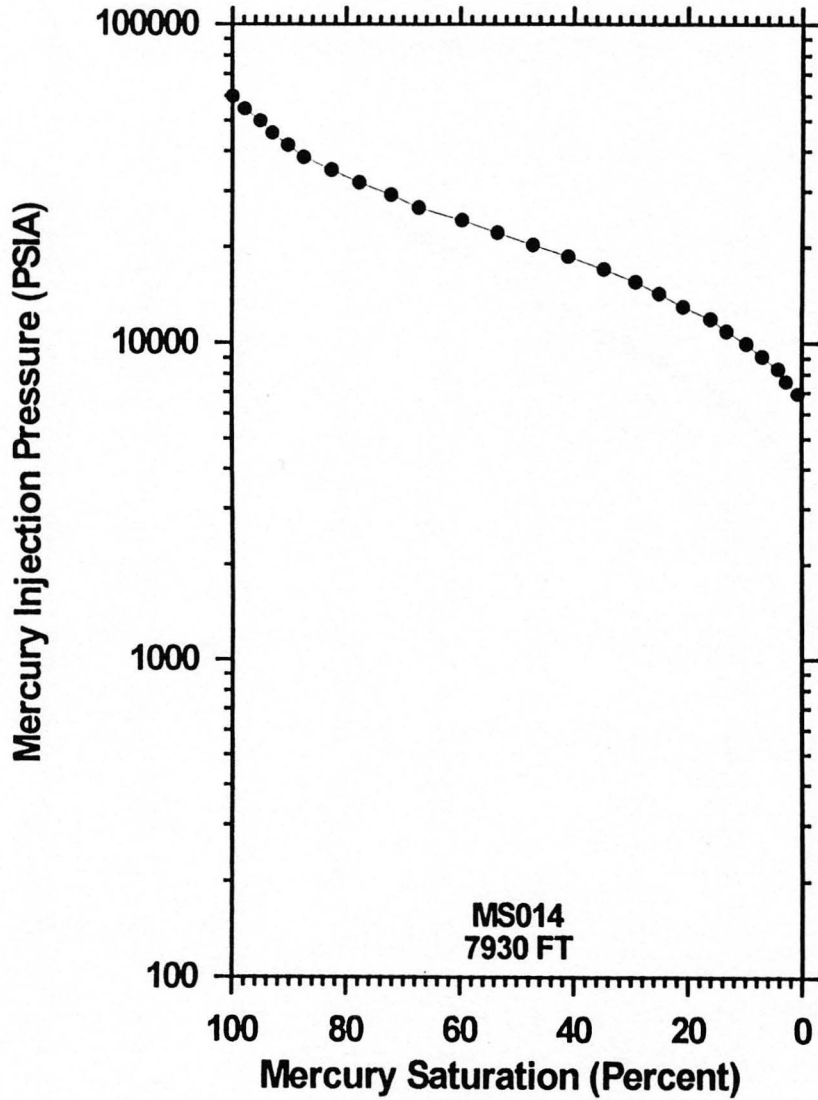
MW= Moderately-well sorted

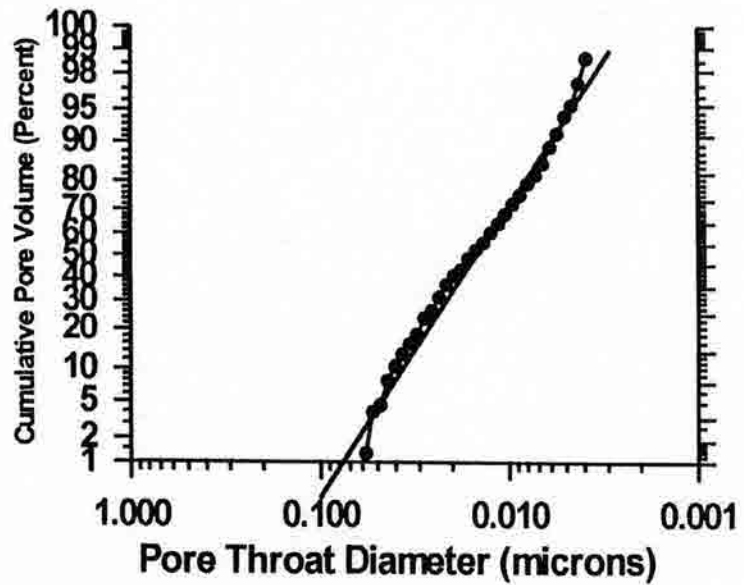
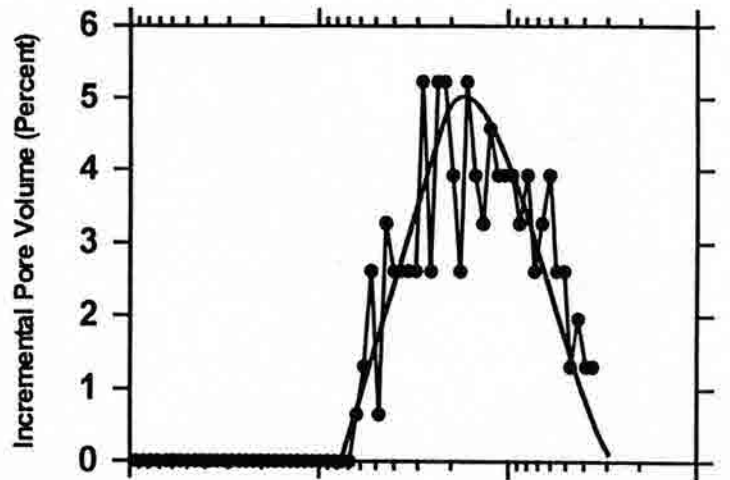
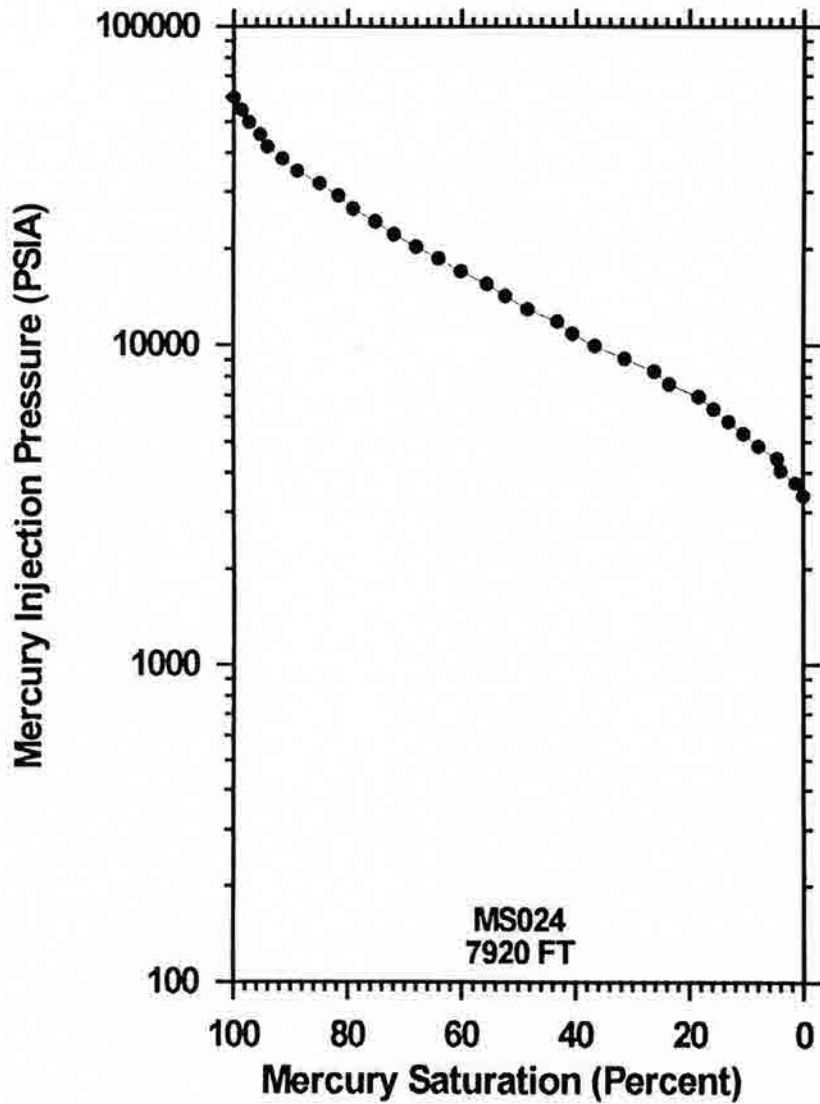
M= Moderately sorted

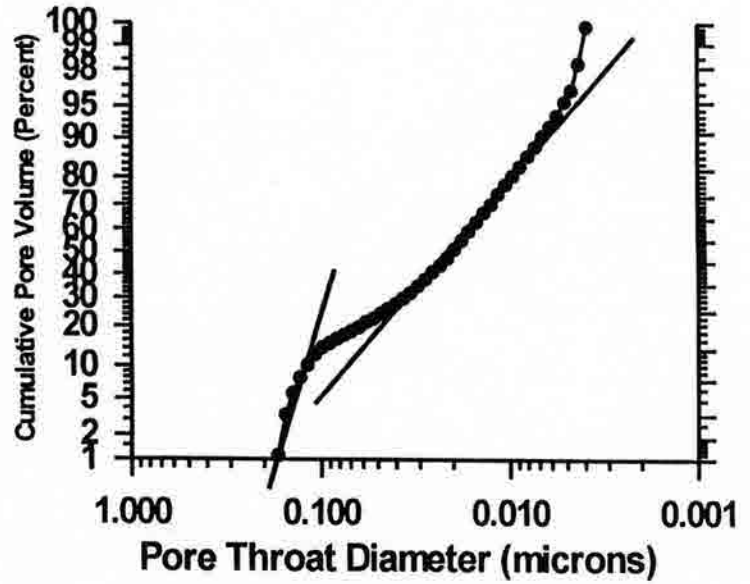
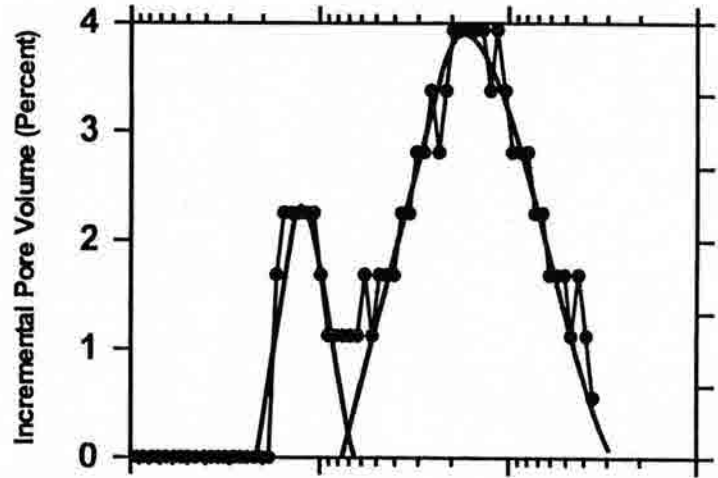
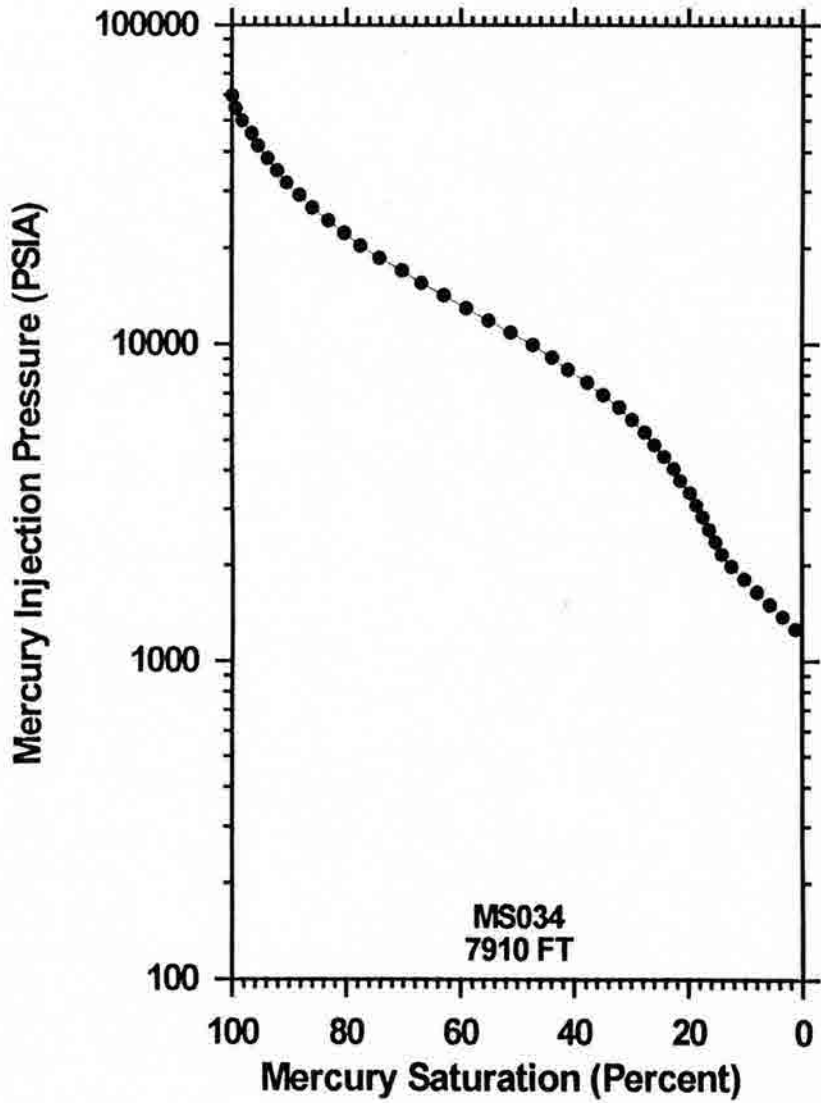
P= Poorly sorted

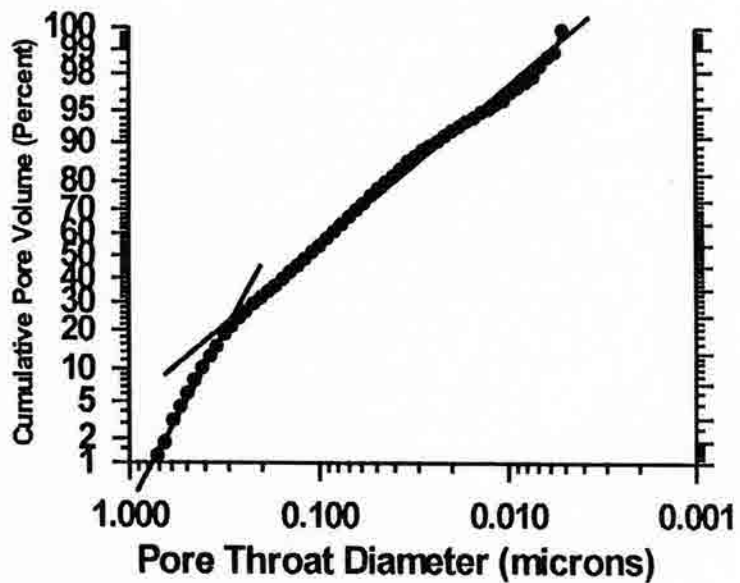
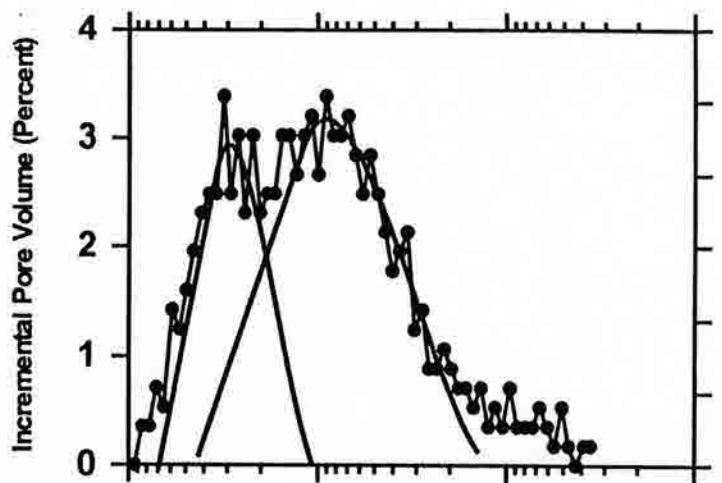
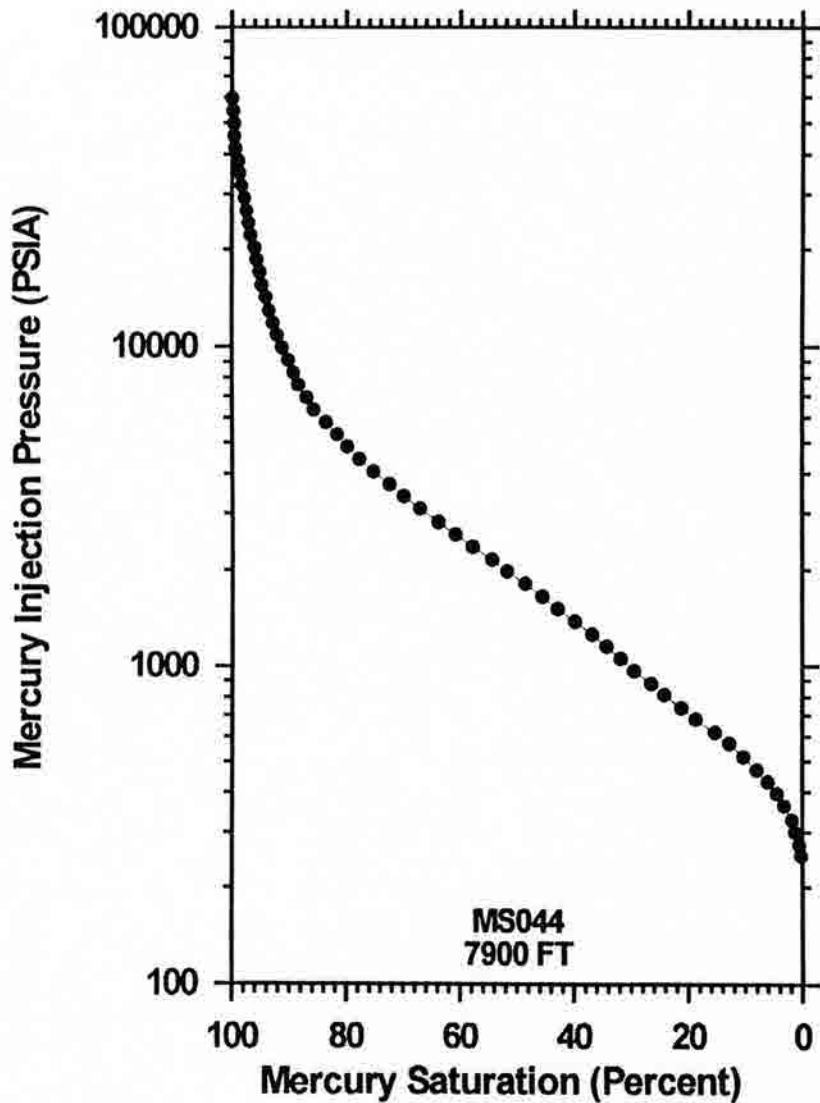


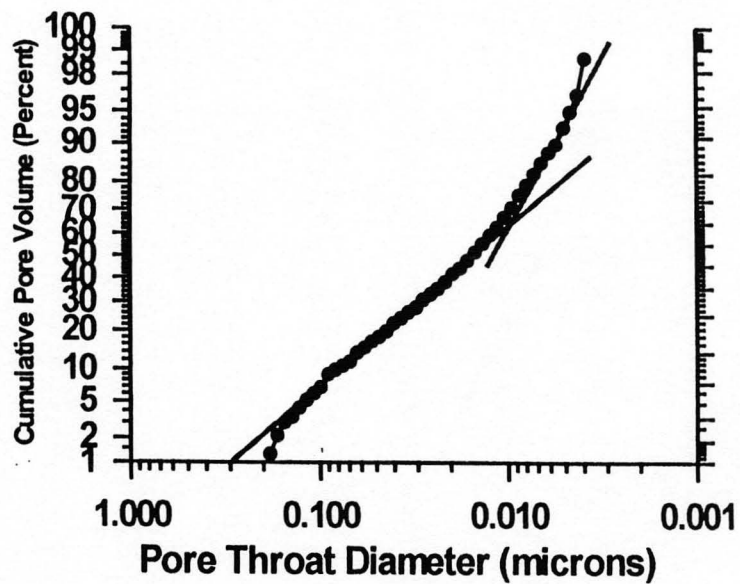
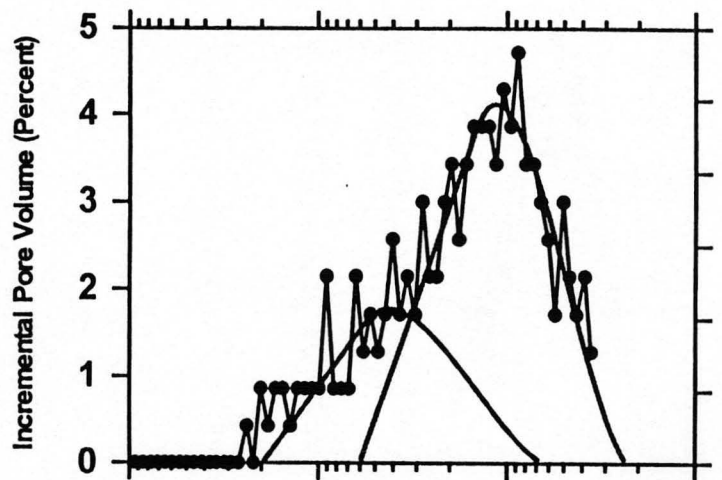
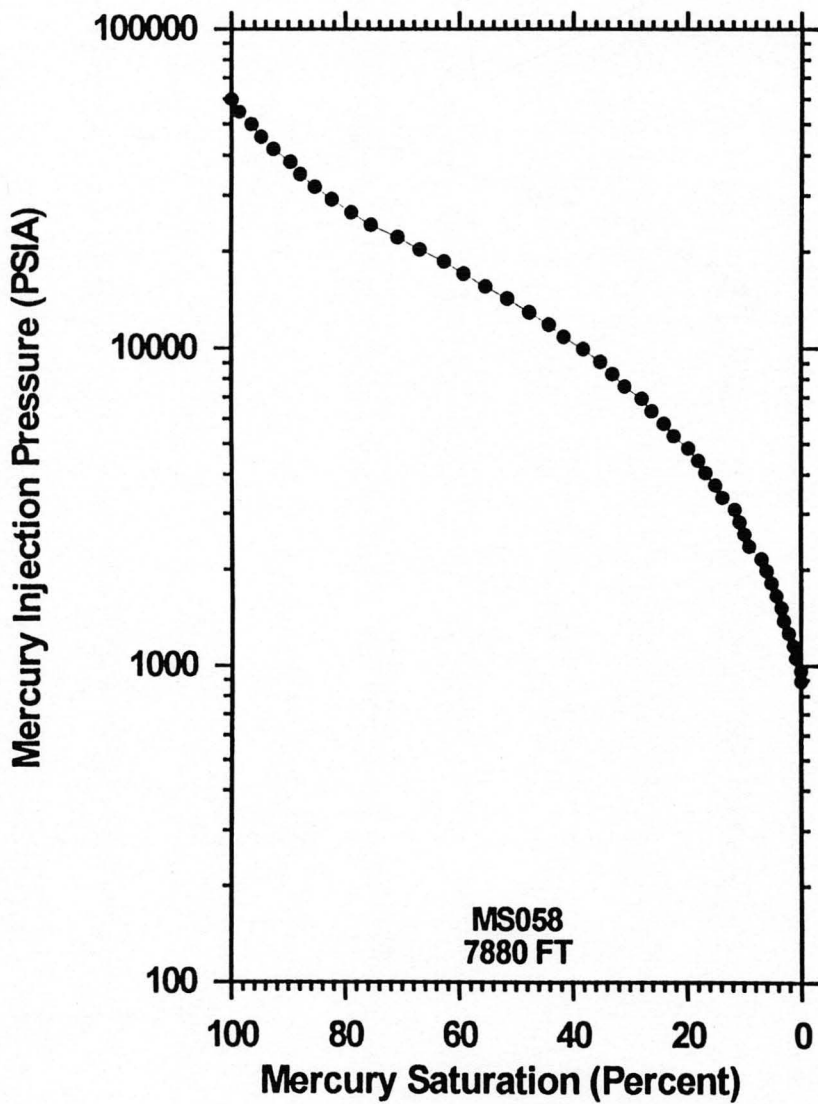


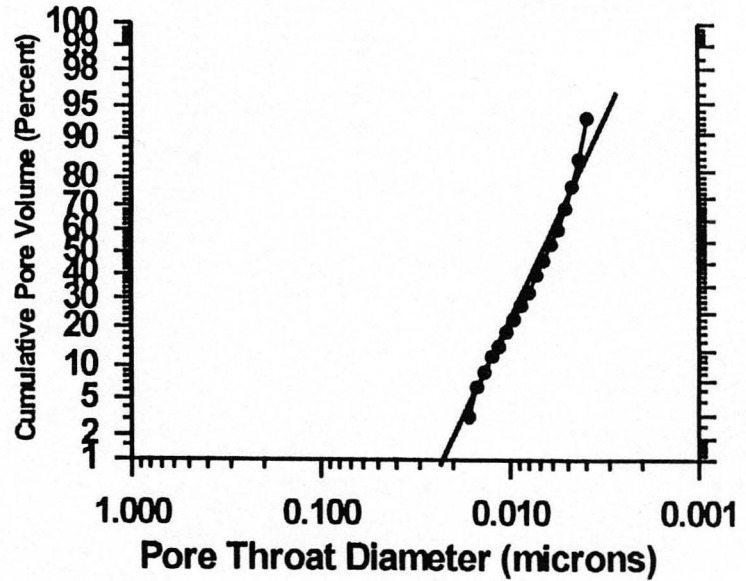
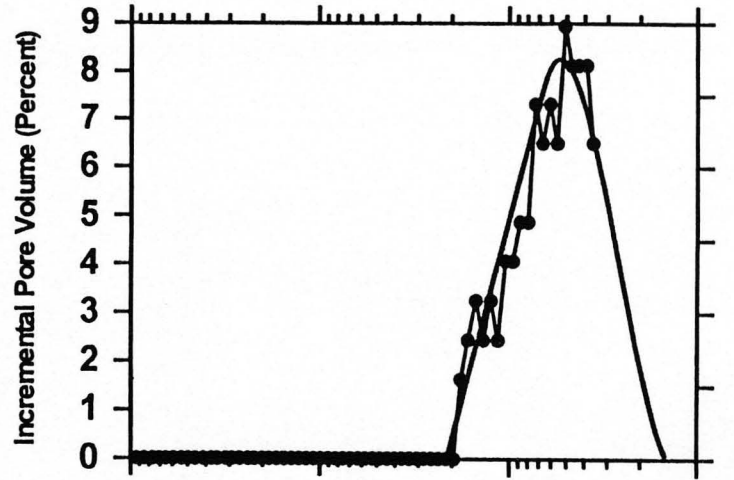
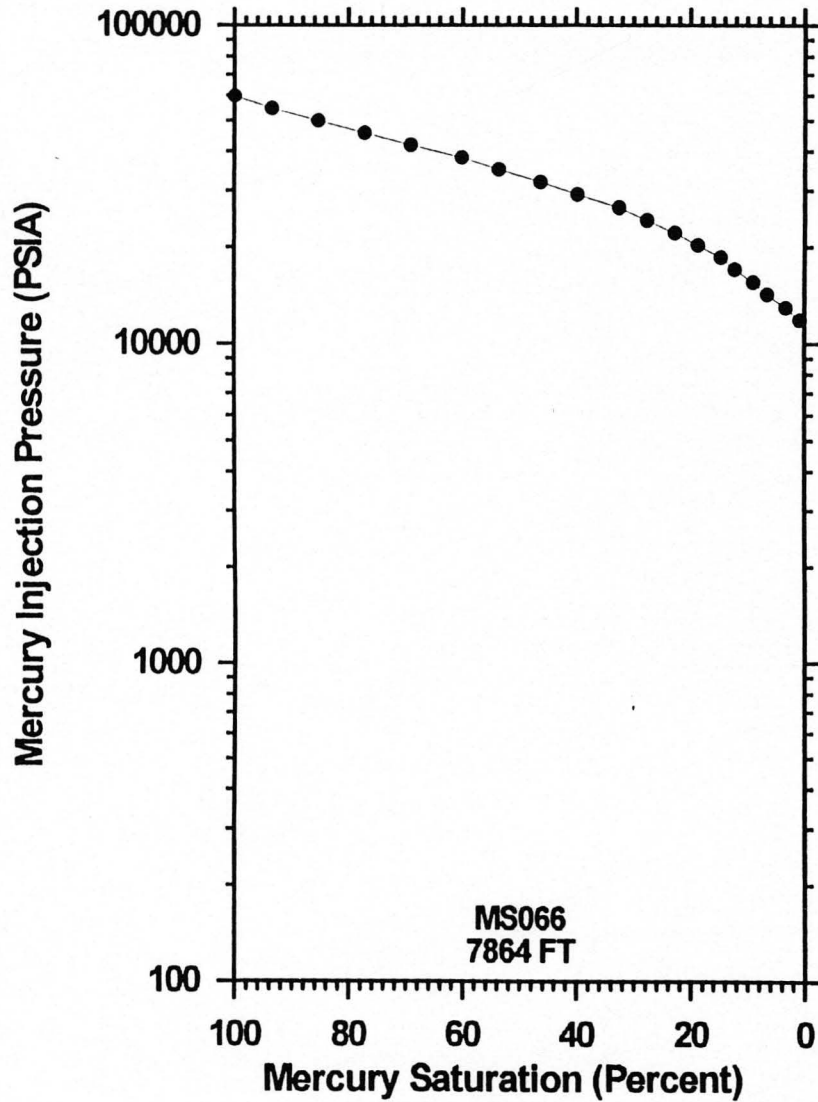












APPENDIX L

ROONEY RANCH OUTCROP

GRANEROS SHALE

THIN SECTION PETROGRAPHY

Figure 11.
 (100) (4 0) Factor X
 Low magnification (LM) thin-section photomicrograph of Fe-rich amphibole gneiss. The clay-rich matrix contains well sorted, dark, hornblende quartz grains. Numerous rounded, yellow mineral grains (epidote, hornblende, and quartz) are visible. Pyrite (small orange nodules), hematite (small dark red nodules), and plagioclase (large bright orange nodules with high relief). Visible matrix porosity is not evident.

Figure 12.
 (100) (4 0) Factor X
 Medium magnification (MM) thin-section photomicrograph of same Fe-rich amphibole gneiss as in Figure 11. Large nodules of hematite and pyrite replace the clay-rich matrix. This photo shows a nodule of hematite (dark red mineral) surrounded by a bright colored alteration ring. This ring could be interpreted as either iron in the hematite "bleeding out" into the surrounding matrix or a transition into siderite. No matrix porosity is visible.

Figure L1.

GR093 (4 ft)- Facies X

Low magnification (PPL) thin-section photomicrograph of Fe-rich argillaceous siltstone. The clay-rich matrix contains well sorted, silt size, detrital quartz grains. Accessory minerals include siderite (patchy yellow mineral with high relief), authigenic framboidal pyrite (small opaque nodules), hematite (small dark red nodules) and phosphatic debris (bright orange nodule with high relief). Visible matrix porosity is not evident.

Figure L2.

GR093 (4 ft)- Facies X

Medium magnification (PPL) thin-section photomicrograph of same Fe-rich argillaceous siltstone pictured in L1. Large nodules of hematite and/or pyrite replace the clay rich matrix. This photo shows a nodule of hematite (dark red mineral) surrounded by a bright colored alteration ring. This ring could be interpreted as either iron in the hematite "bleeding out" into the surrounding matrix or a transition into siderite. No matrix porosity is notable.



Figure L1.



Figure L2.

Figure 1.3.

(14088 (14 R)-Factor 2

Low magnification (WPI) thin-section photomicrograph of siltstone. The contacted shale has a clay-rich matrix that contains well-sorted, sub-parallel quartz (yellow, and some) and mica. Wavy laminae of organic matter and clay are visible. Some quartz appear to be elongated in the direction of the laminae. The arrow is pointing to a bright orange, high relief, granular texture. Matrix porosity is not detected.

Figure 1.4.

(14088 (14 R)-Factor 2

Medium magnification (WPI) thin-section photomicrograph of same siltstone contact as in 1.3. The image clearly portrays the Fe-rich, organic mineral laminae surrounding the quartz grains. The smaller, rounded, and bright yellow, high relief, granular texture is evident. The smaller, rounded, and bright yellow, high relief, granular texture is evident. Matrix porosity is evident.

Figure L3.

GR088 (14 ft)- Facies X

Low magnification (PPL) thin-section photomicrograph of silty shale. This compacted shale has a clay-rich matrix that contains well sorted, silt size detrital grains (quartz, feldspar, and mica). Wispy laminations of organic matter and clays enhance the fissile texture. Some quartz grains appear to be elongated in the direction of the laminations. The arrow is pointing to a bright orange, high relief phosphatic nodule. Matrix porosity is not detected.

Figure L4.

GR088 (14 ft)- Facies X

Medium magnification (PPL) thin-section photomicrograph of same silty shale pictured in L3. This photo clearly portrays the Fe-rich accessory minerals. Surrounding the quartz grains are abundant dark red nodules of hematite and patchy yellow high relief minerals of siderite. The smaller opaque nodules are authigenic framboidal pyrite. No matrix porosity is evident.

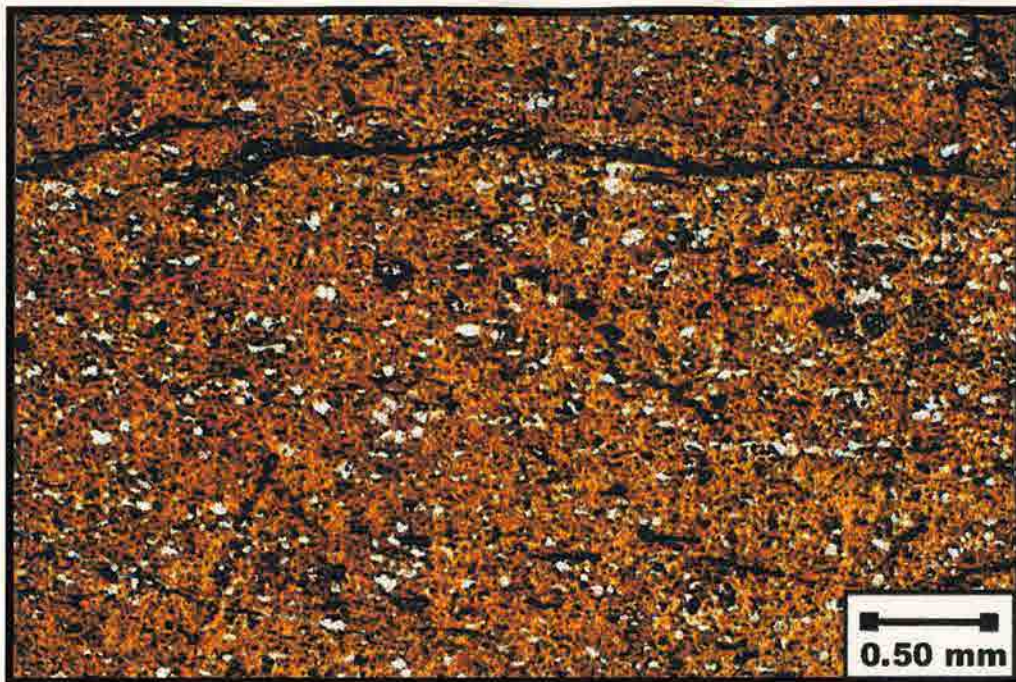


Figure L3.

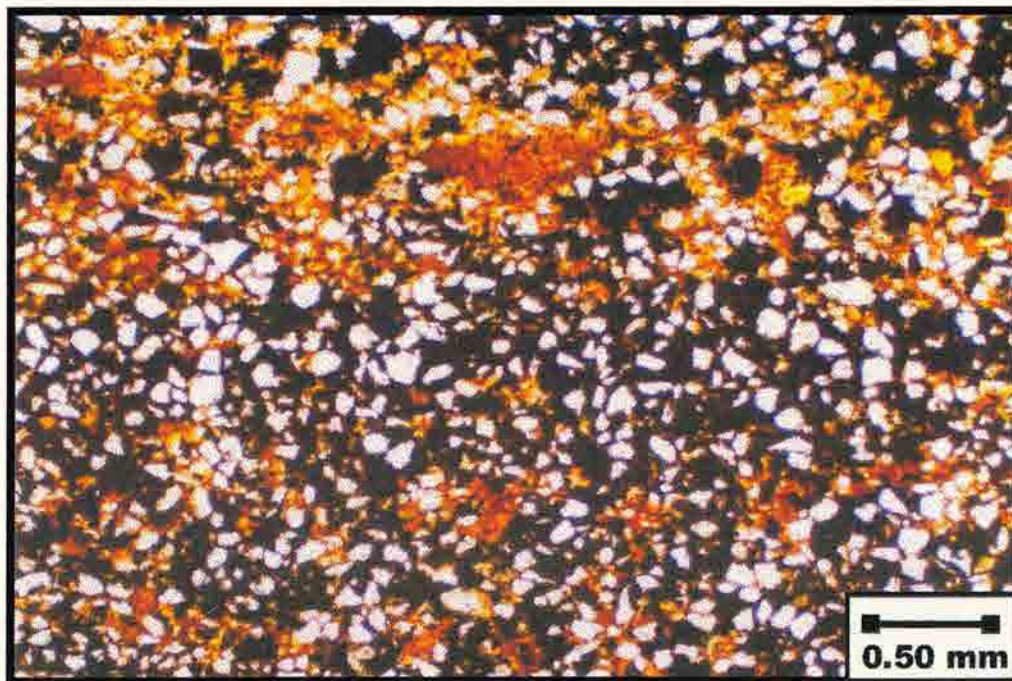


Figure L4.

Figure 1

Figure 1 (continued)

The following table shows the results of the regression analysis. The dependent variable is the natural logarithm of the number of employees. The independent variables are the natural logarithm of sales, the natural logarithm of assets, and the natural logarithm of the industry's sales. The results show that sales, assets, and industry sales are all positively related to the number of employees.

Figure 2

Figure 2 (continued)

The following table shows the results of the regression analysis. The dependent variable is the natural logarithm of the number of employees. The independent variables are the natural logarithm of sales, the natural logarithm of assets, and the natural logarithm of the industry's sales. The results show that sales, assets, and industry sales are all positively related to the number of employees.

Figure L5.

GR078 (34 ft)- Facies Lower Y

Low magnification (PPL) thin-section photomicrograph of silty shale. The clay-rich matrix contains well sorted, silt size detrital grains (quartz, feldspar, and mica). Wispy laminations of organic matter and clays give a "micro-styolitic" appearance. Notice the light colored area to the right is oblique to laminations. No matrix porosity is detected.

Figure L6.

GR078 (34 ft)- Facies Lower Y

Medium magnification (PPL) thin-section photomicrograph of same silty shale pictured in L5. The secondary mineralogy is more palpable at high power. It includes authigenic framboidal pyrite (small opaque nodules), phosphatic debris (bright orange high relief nodule), and siderite replacement (patchy high relief yellow mineral). Matrix porosity is not evident.

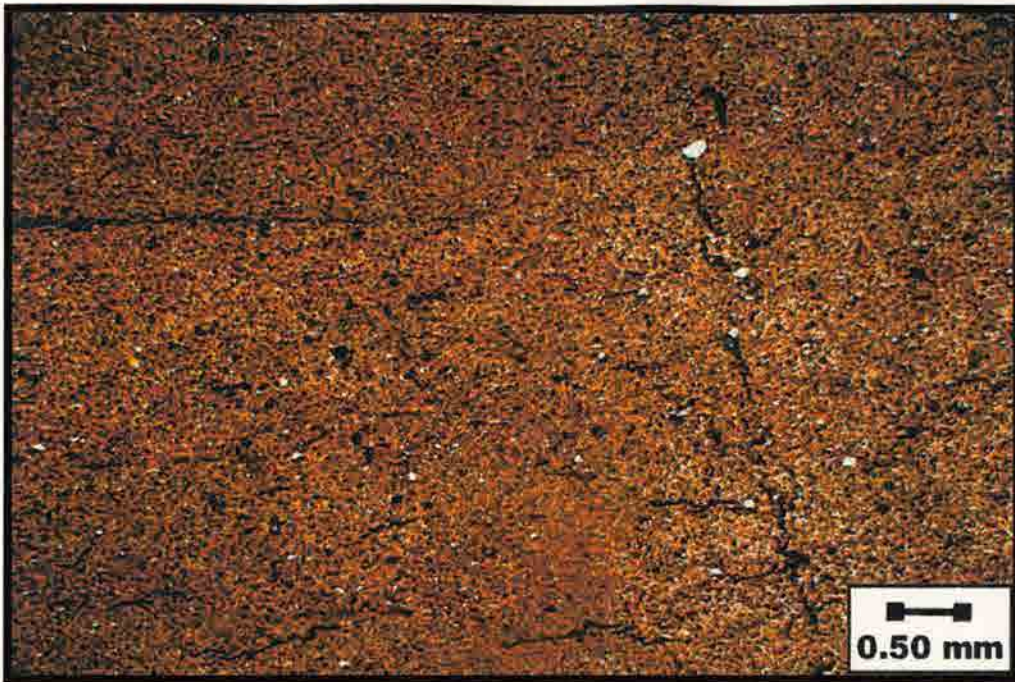


Figure L5.



Figure L6.

Figure L7.

GR024 (94 ft)- Facies Upper Y

Medium magnification (PPL) thin-section photomicrograph of silty shale/argillaceous siltstone. This shale is interbedded with continuous layers of silt to very fine sand size quartz grains. Accessory components include authigenic framboidal pyrite (small opaque nodules), hematite (dark red nodules) and siderite replacement of feldspar grains. No matrix porosity is visible.

Figure L8.

GR024 (94 ft)- Facies Upper Y

Medium magnification (XN) thin-section photomicrograph of same silty shale/argillaceous siltstone pictured in L7. Under cross-polarized light the siderite (bright yellow, patchy, high relief mineral) is easier to detect. Again, the accessory components include pyrite and hematite. The stage has been rotated so the layers of silt are diagonal to accentuate the laminated texture. Visible matrix porosity is not evident.

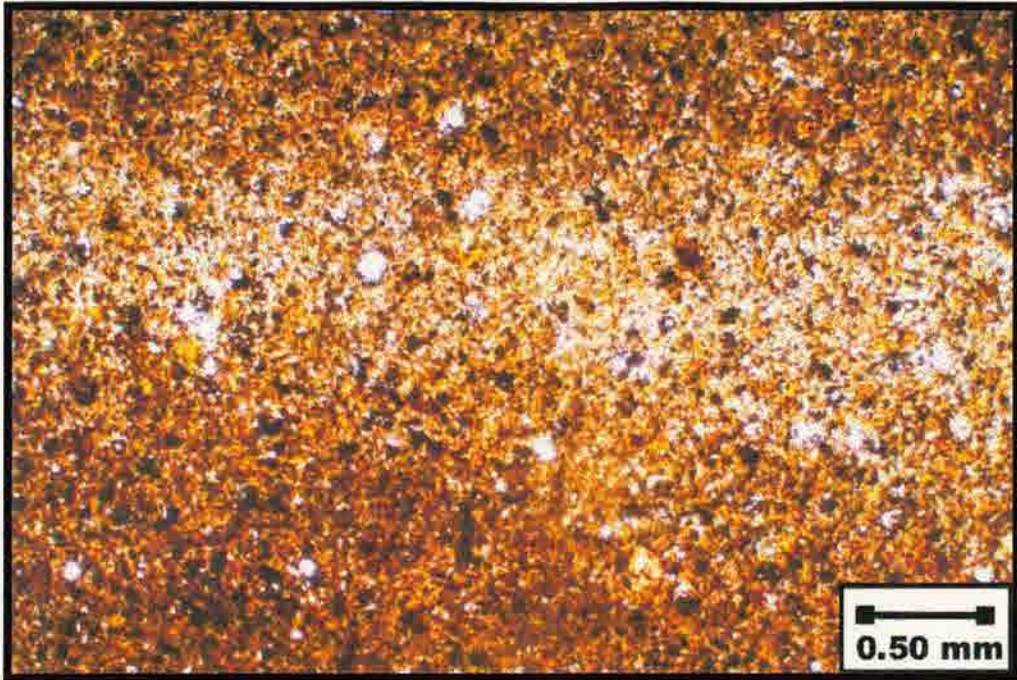


Figure L7.

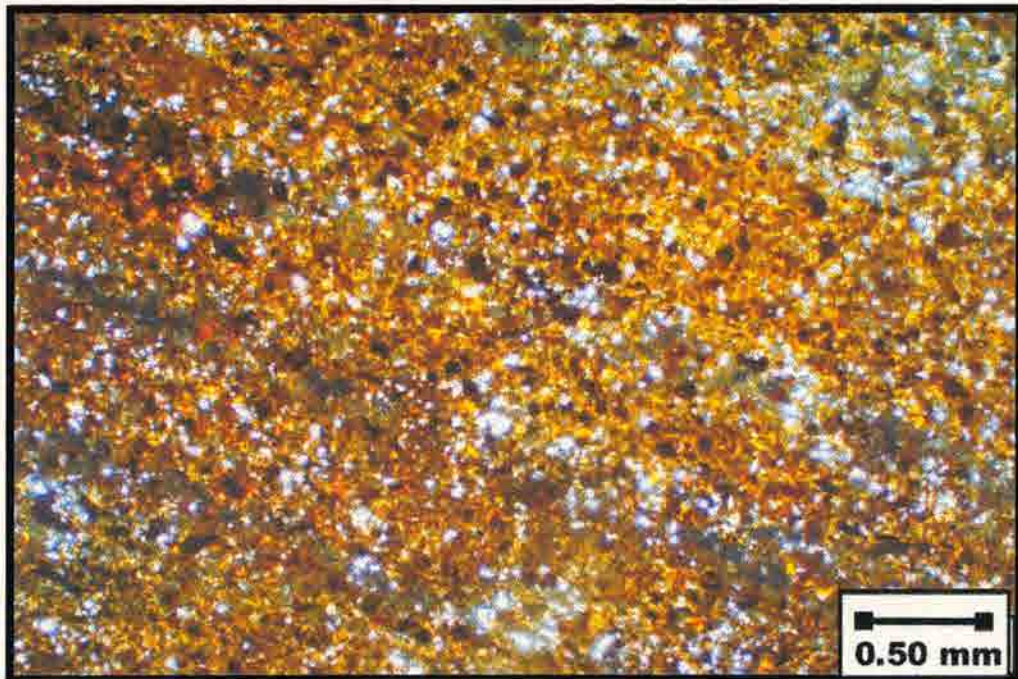


Figure L8.

Figure 13.

GR010 (14 B)- Facies Layer Y

Microscopic photomicrograph of silty sand. The clay-rich matrix contains well sorted, all size detrital grains (quartz, feldspar, and mica). Accessory constituents include subangular to subrounded (small opaque nodules), fibrous debris (bright orange high relief nodules), laminae (dark red nodules) and small amounts of siderite. No matrix porosity is detected.

Figure 14.

GR010 (14 B)- Facies Layer Y

High magnification (20x) thin-section photomicrograph of sand siltstone bedded as a thin cross-bedded light tan to light brown silty sand. The long opaque grains in the matrix are dark colored organic matter. It is surrounded by yellow to light gray clay minerals with some siderite replacement and all size quartz grains.

Figure L9.

GR010 (114 ft)- Facies Upper Y

Medium magnification (PPL) thin-section photomicrograph of silty shale. The clay-rich matrix contains well sorted, silt size detrital grains (quartz, feldspar, and mica). Accessory components include authigenic framboidal pyrite (small opaque nodules), phosphatic debris (bright orange high relief nodule), hematite (dark red nodules) and small amounts of siderite. No matrix porosity is detected.

Figure L10.

GR010 (114 ft)- Facies Upper Y

High magnification (XN) thin-section photomicrograph of same silty shale pictured in L9. Under cross-polarized light the separate laminations of clays, organic matter and quartz are more obvious. The long opaque lenses in the middle are dark colored organic matter. It is surrounded by yellow ductile clay minerals with some siderite replacement and silt size quartz grains.

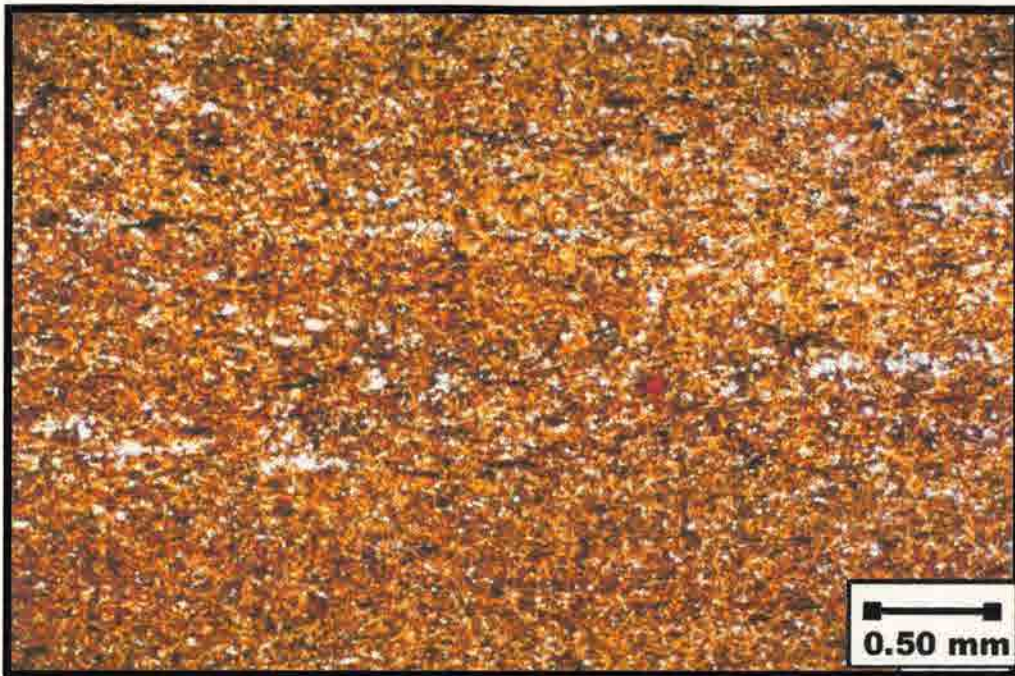


Figure L9.

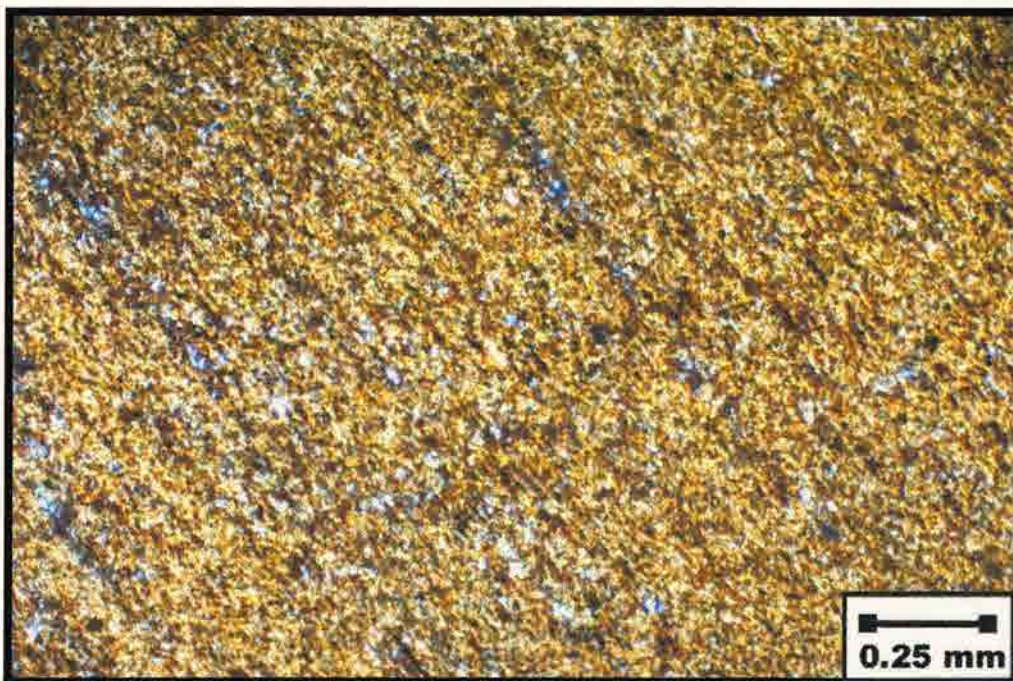


Figure L10.

Figure E11.

(18029 (89 0) - Figure X

Low magnification (PL) thin-section photomicrograph of silt shale. The clay-rich matrix contains well sorted, silt size detrital grains (quartz, feldspar, and mica). Discontinuous beds of organic matter and clay are prominent and provide a typical appearance. A large phosphate nodule is noted in the center of the picture. No matrix porosity is observed.

Figure E12.

(18029 (89 0) - Figure X

Medium magnification (PL) thin-section photomicrograph of same silt shale pictured in E11. The clay-rich matrix contains well sorted, silt size detrital grains (quartz, feldspar, and mica). The elongation of quartz grains parallels the lamination. The majority of the grains have a strong preferred orientation. No matrix porosity is visible.

Figure L11.

GR059 (59 ft)- Facies Z

Low magnification (PPL) thin-section photomicrograph of silty shale. The clay-rich matrix contains well sorted, silt size detrital grains (quartz, feldspar, and mica). Discontinuous lens of organic matter and clays are prominent and provide a fissile appearance. A large phosphatic nodule is noted in the center of this picture. No matrix porosity is detected.

Figure L12.

GR059 (59 ft)- Facies Z

Medium magnification (PPL) thin-section photomicrograph of same silty shale pictured in L11. The clay-rich matrix contains well sorted, silt size detrital grains (quartz, feldspar, and mica). The elongation of quartz grains parallels the laminations. The majority of the grains have a strong preferred orientation. No matrix porosity is visible.



Figure L11.

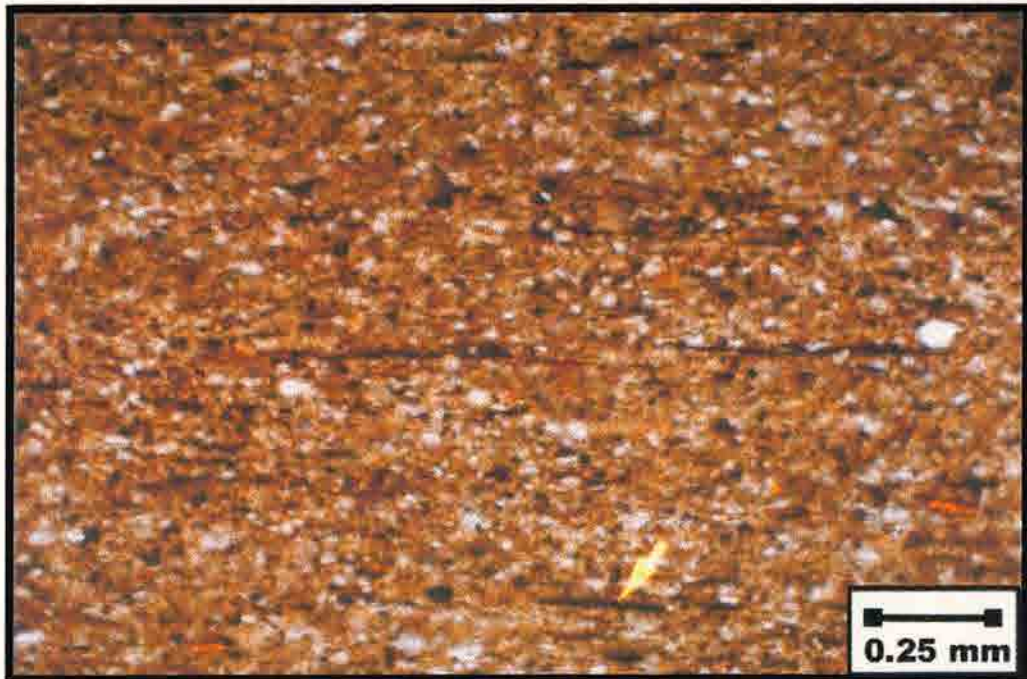


Figure L12.

Figure L13.

GR059 (59 ft)- Facies Z

Medium magnification (XN) thin-section photomicrograph of same silty shale pictured in L11 and L12. Under cross-polarized light the bright yellowish-green clay minerals are easier to distinguish from the dark colored organic matter. Organic matter forms the discontinuous dark colored laminations. Authigenic framboidal pyrite (opaque nodules) is highest in this facies as shown in this thin section. No matrix porosity is evident.

Figure L14.

GR059 (59 ft)- Facies Z

High magnification (PPL) thin-section photomicrograph of same silty shale pictured in L11, L12 and L13. The arrow is pointing to a lamination of organic matter. Other constituents include phosphatic debris, hematite nodules, authigenic framboidal pyrite along with very small amounts of siderite replacement. No porosity is visible.

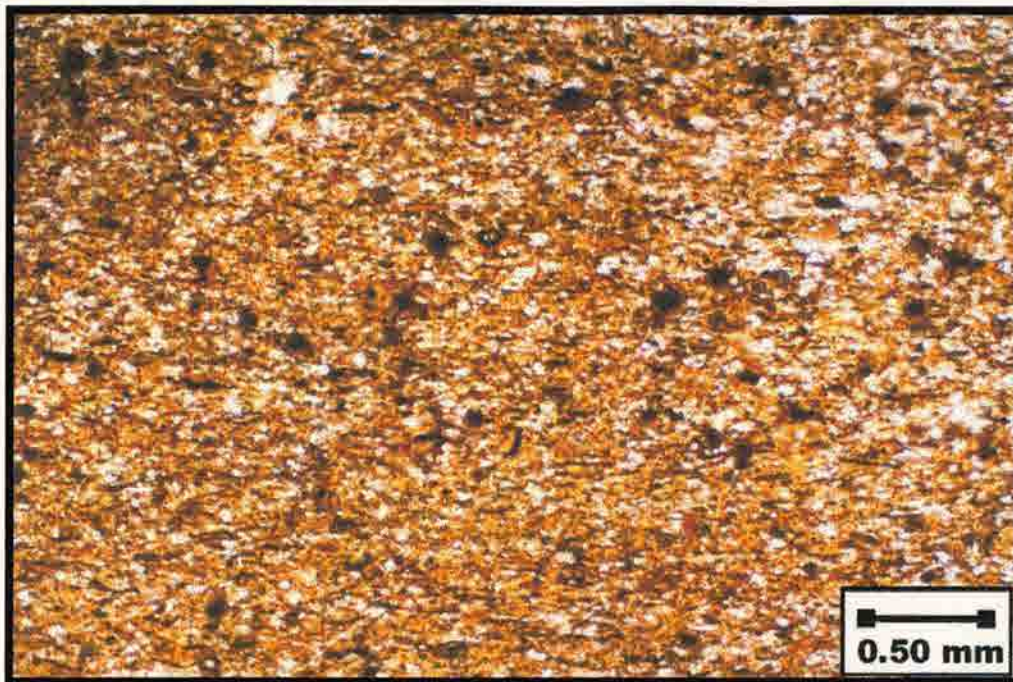


Figure L13.

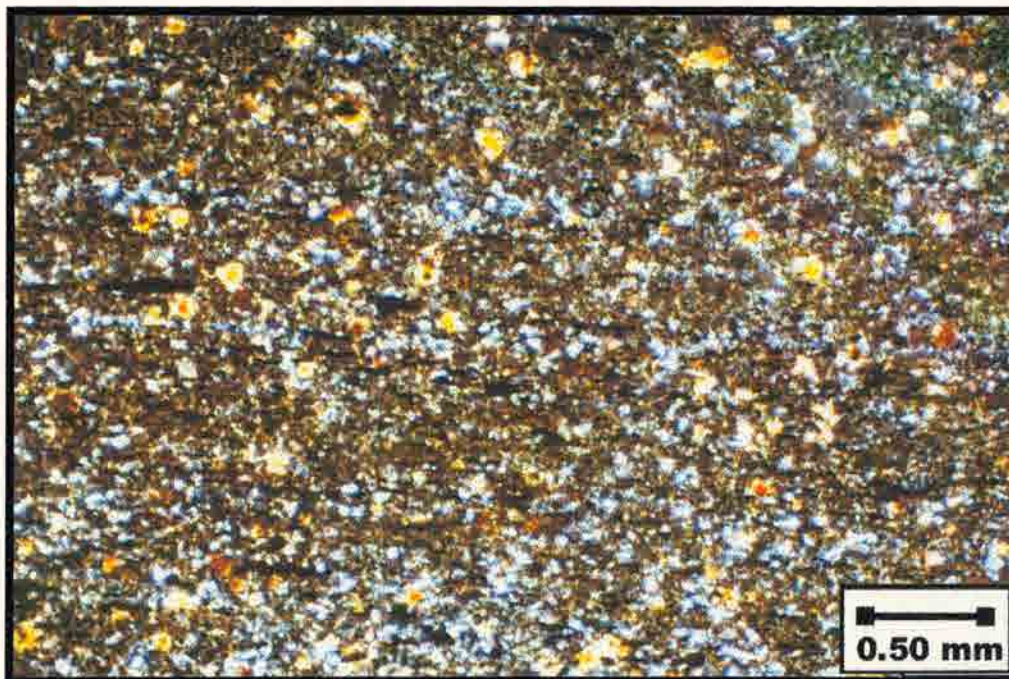


Figure L14.

APPENDIX M

ROONEY RANCH OUTCROP

GRANEROS SHALE

MICP GRAPHS

MICP table for Rooney Ranch (Graneros shale)

Sample#	FT	Facies	Median PTD	Pore Volume %	Sorting Index
GR093	4	X	0.025	70	VW
			0.008	20	M
			0.09	10	M
GR088	14	X	0.015	90	VW
			0.025	10	M
GR083	24	X	0.02	80	VW
			0.008	20	M
GR081	28	X	0.015	90	VW
			0.02	10	M
GR078	34	Y	0.015	50	VW
			0.15	30	M
			0.045	20	P
GR073	44	Y	0.0175	70	VW
			0.04	10	M
GR069	49	Y	0.006	65	W
			0.015	35	P
GR064	54	Z	0.0175	60	VW
			0.03	30	P
			0.006	10	P
GR059	59	Z	0.01	90	VW
			0.025	10	M
GR050	68	Z	0.0055	70	VW
			0.015	30	M
GR044	74	Z	0.0125	90	VW
			0.025	10	M
GR037	81	Z	0.009	70	W
			0.025	30	P-M
GR034	84	Z	0.0125	80	W
			0.04	20	M
GR031	87	Z	0.0095	80	W
			0.02	20	P
GR028	90	Z	0.0095	80	W
			0.02	20	P
GR027	91	Y	0.01	60	M
			0.03	40	P-M
GR024	94	Y	0.07	70	M
			0.02	20	M
			0.25	10	P
GR022	96	Y	0.025	70	M
			0.1	30	P
GR020	104	Y	0.02	70	M
			0.07	30	W
GR014	110	Y	0.008	70	W
			0.02	20	VW
			0.03	10	M
GR010	114	Y	0.03	70	VW
			0.009	30	M
GR006	118	Y	0.02	60	VW
			0.004	20	M
			0.4	10	M
GR002	122	Y	0.015	60	W
			0.03	10	P-M
			0.005	30	P-M
GR000	124	Y	0.03	70	VW
			0.01	30	M

LEGEND:

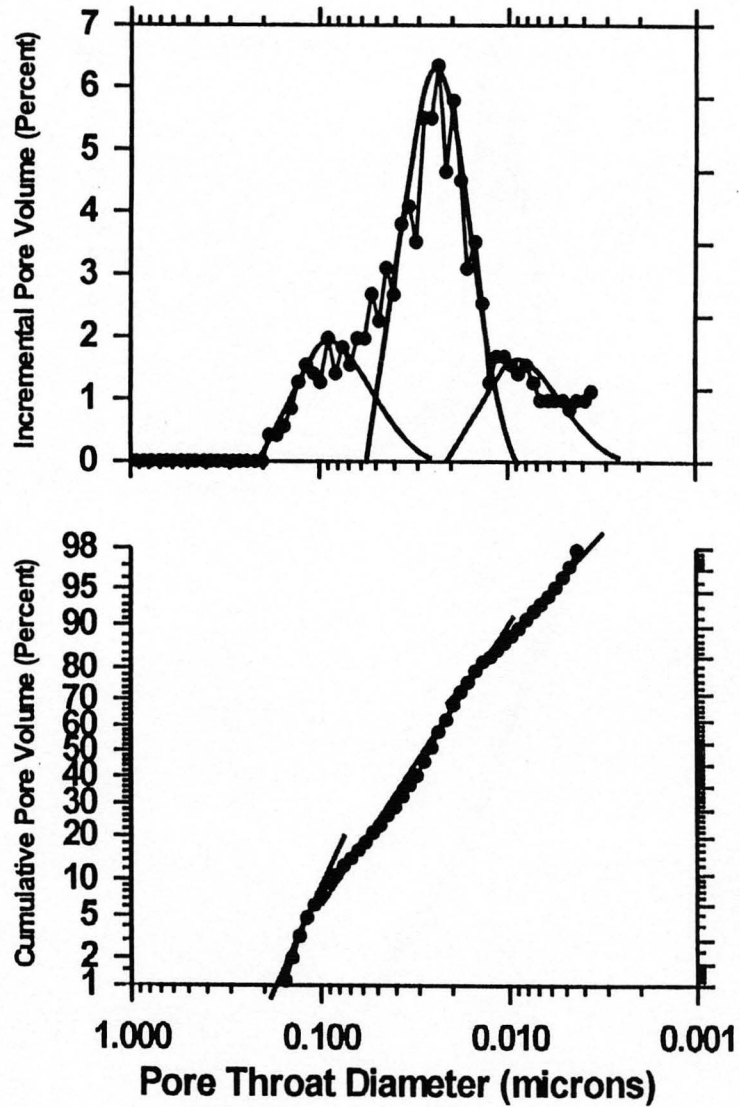
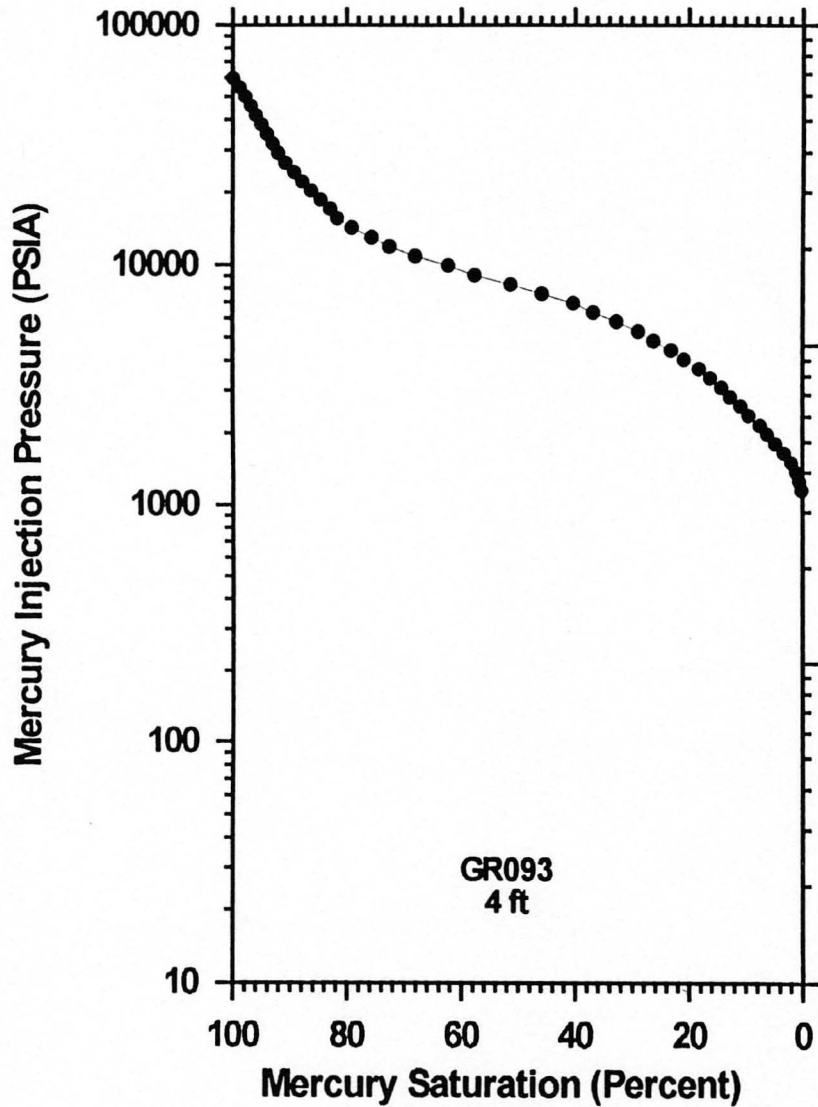
VW= Very Well sorted

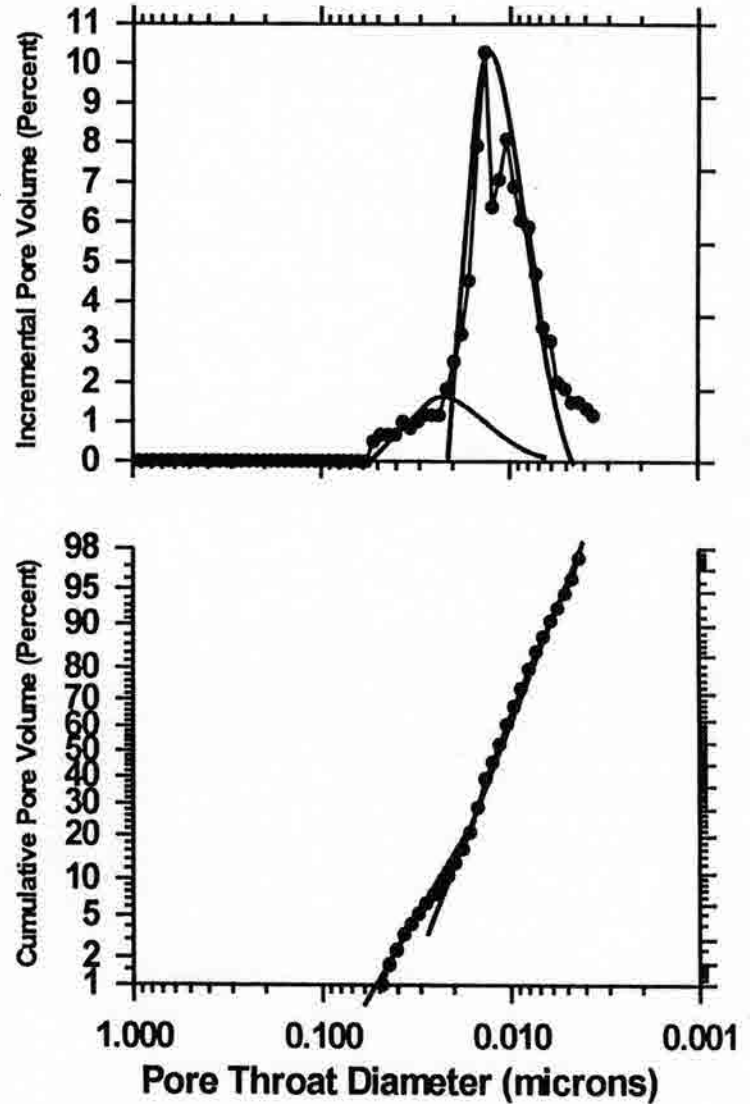
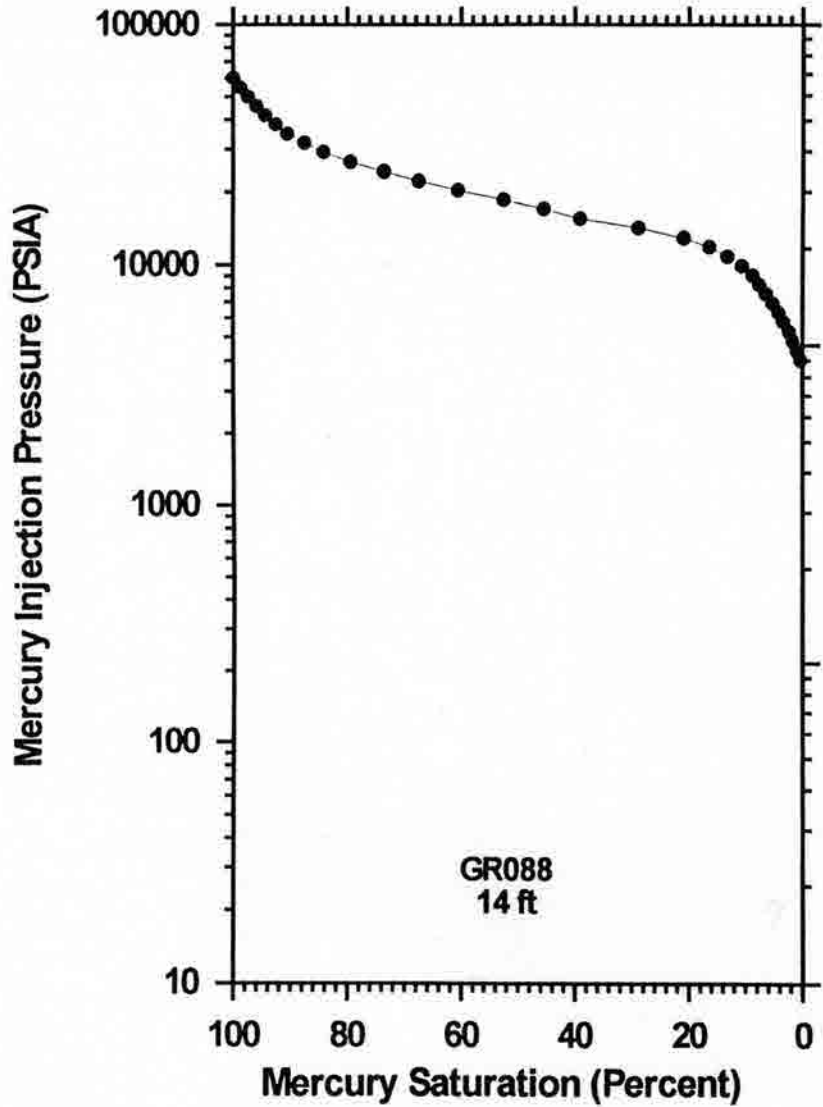
W= Well sorted

MW= Moderately-well sorted

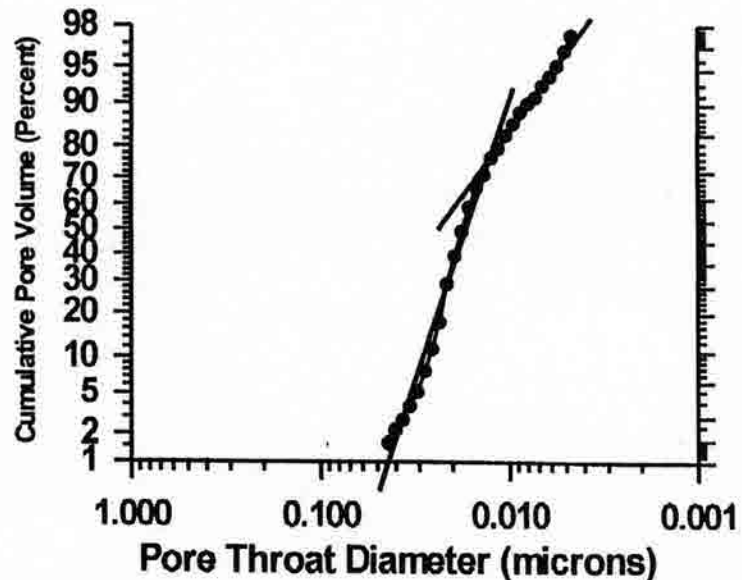
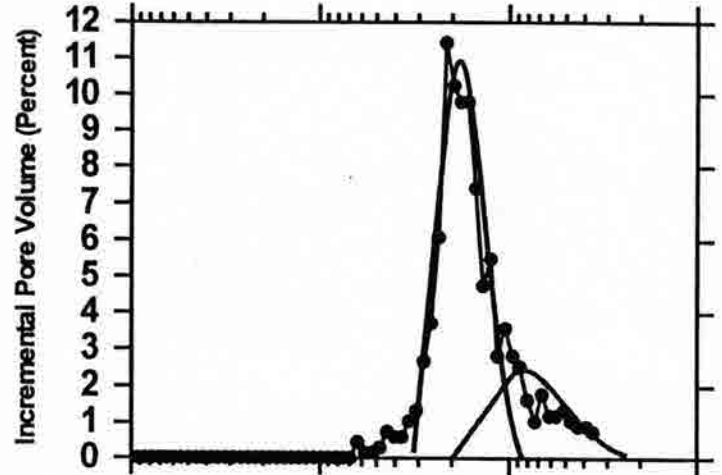
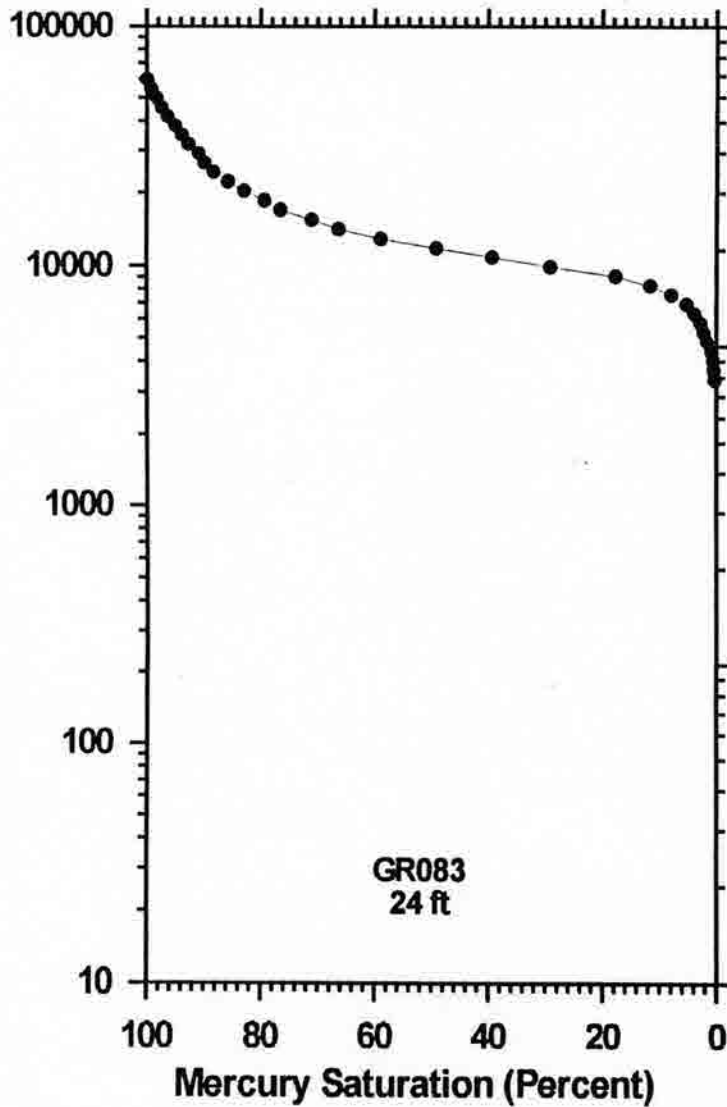
M= Moderately sorted

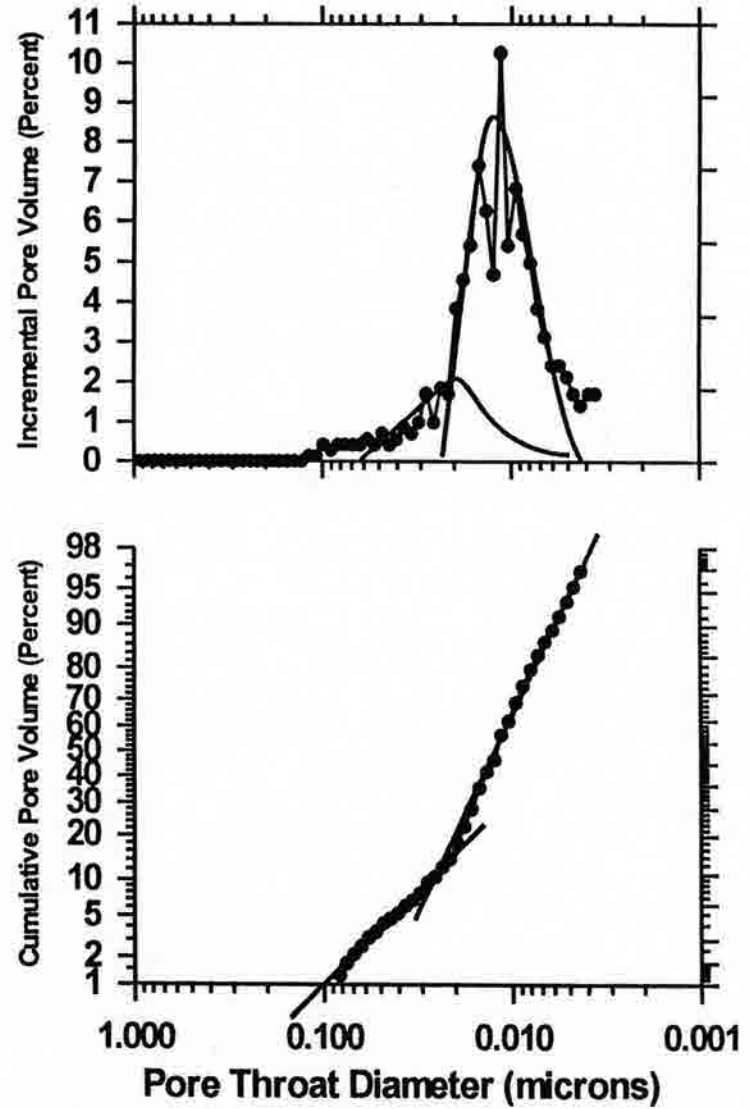
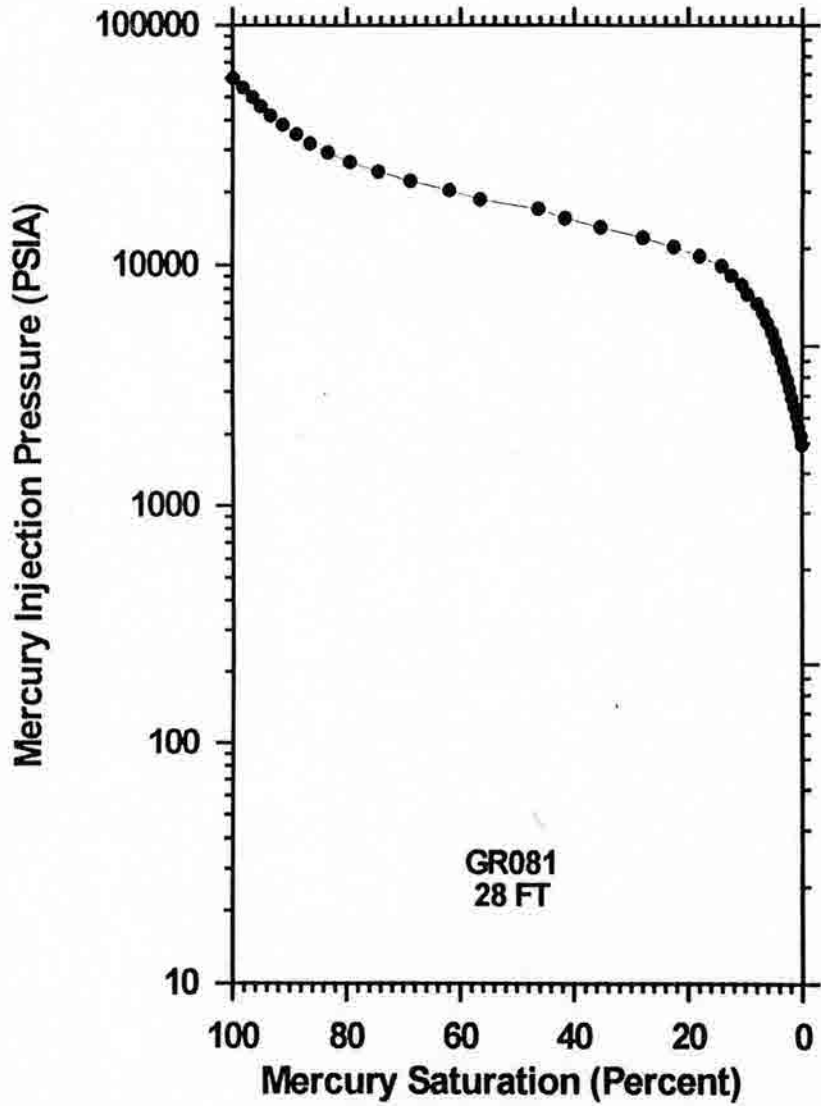
P= Poorly sorted

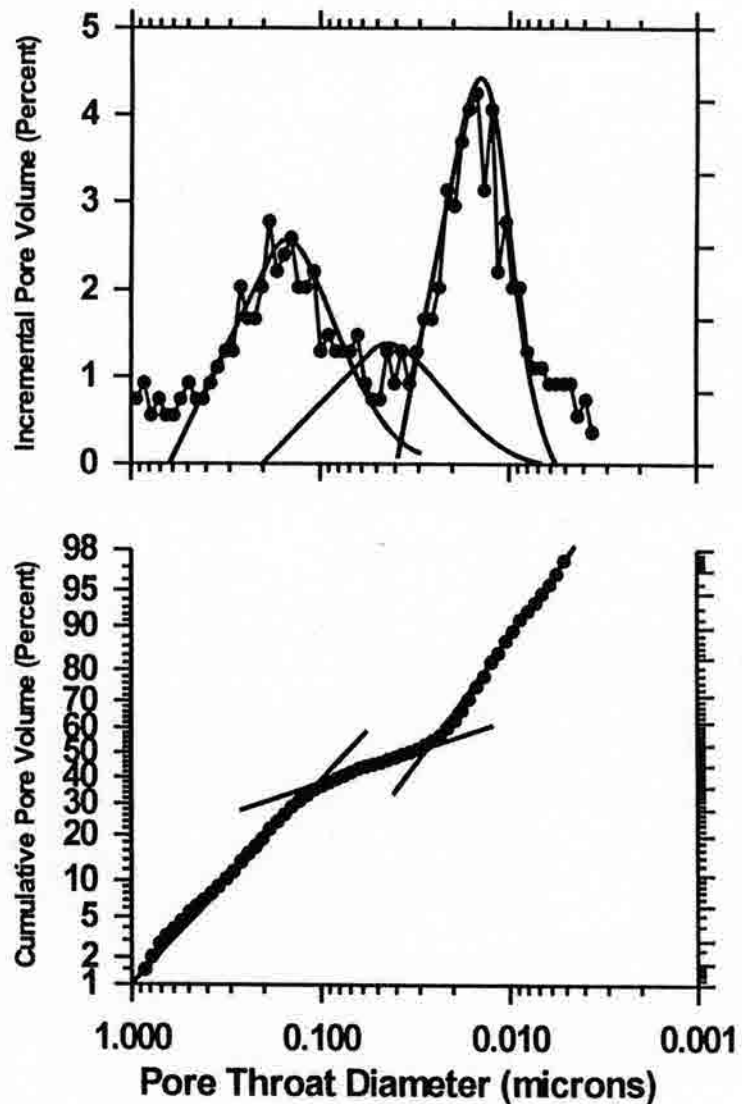
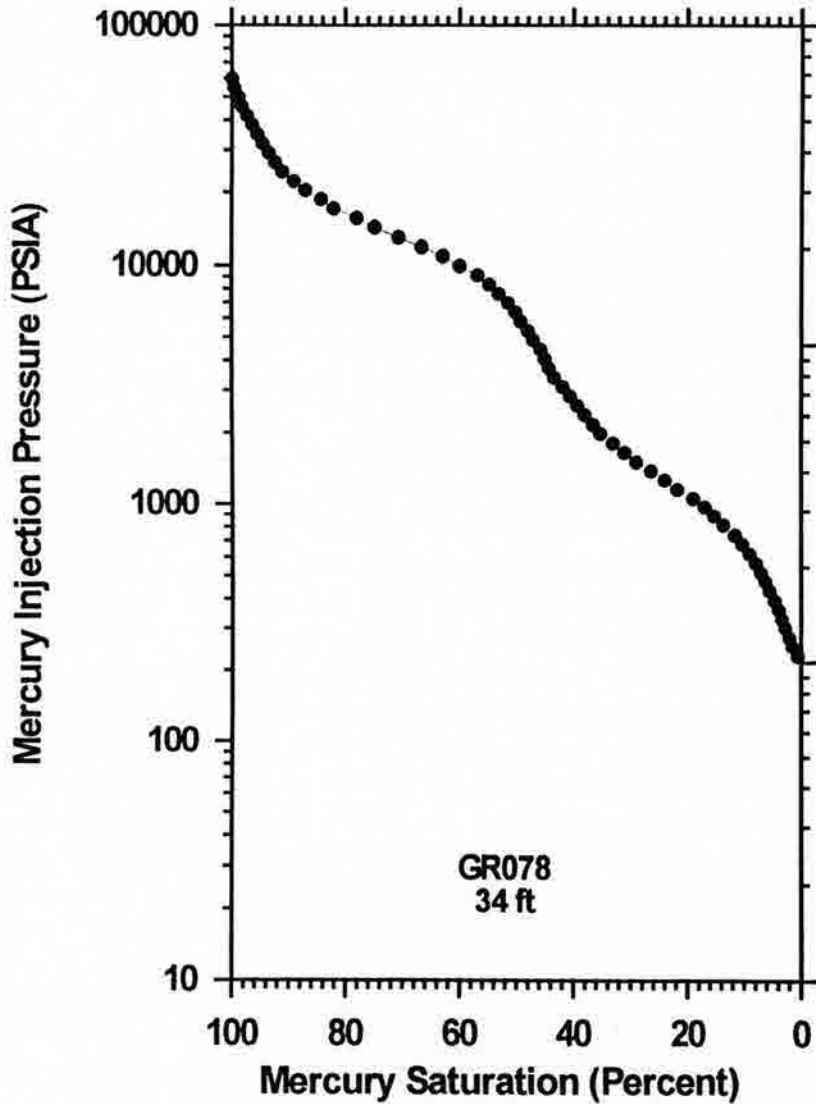


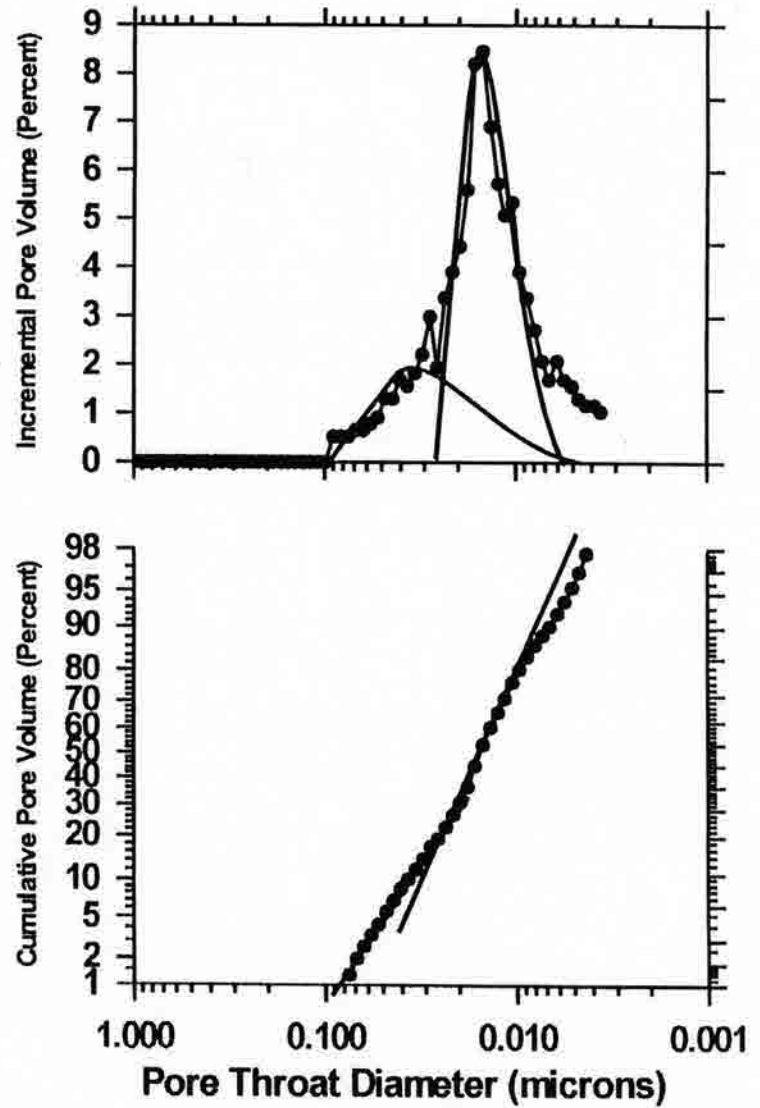
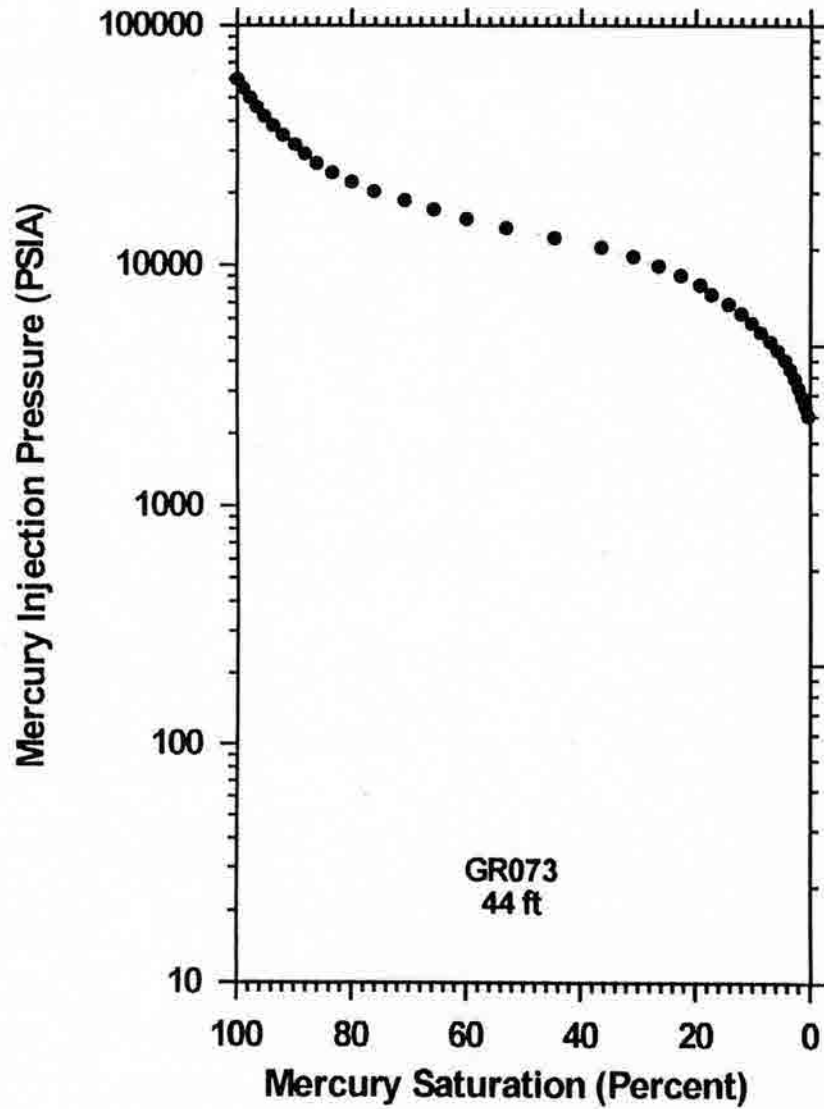


Mercury Injection Pressure (PSIA)

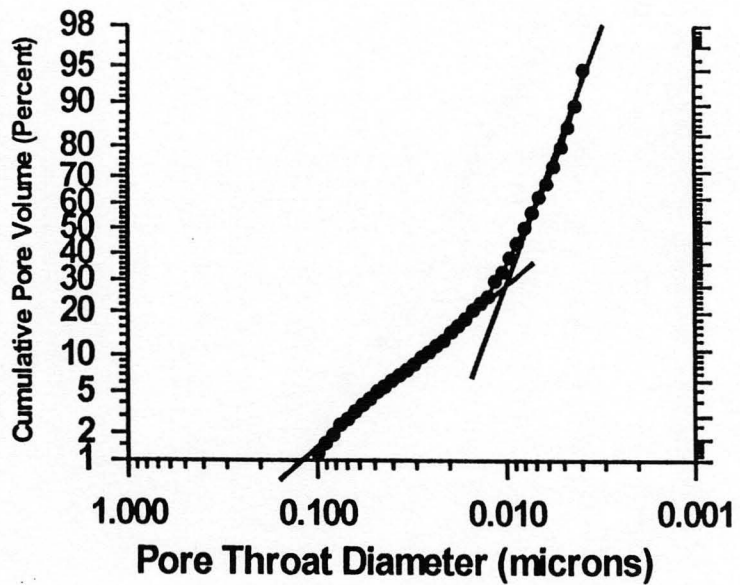
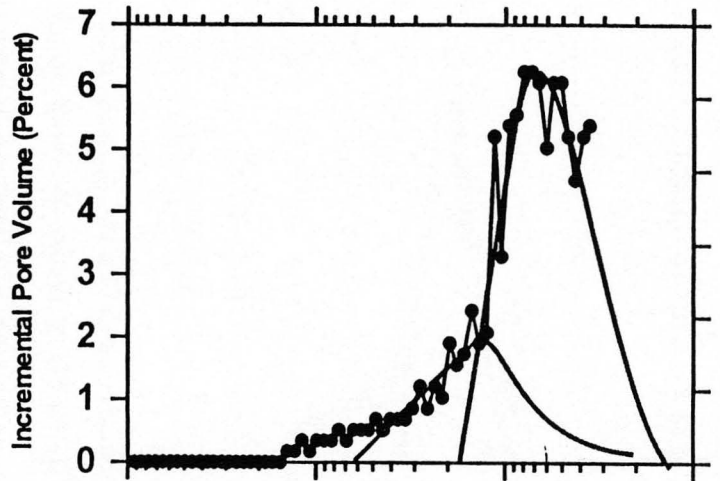
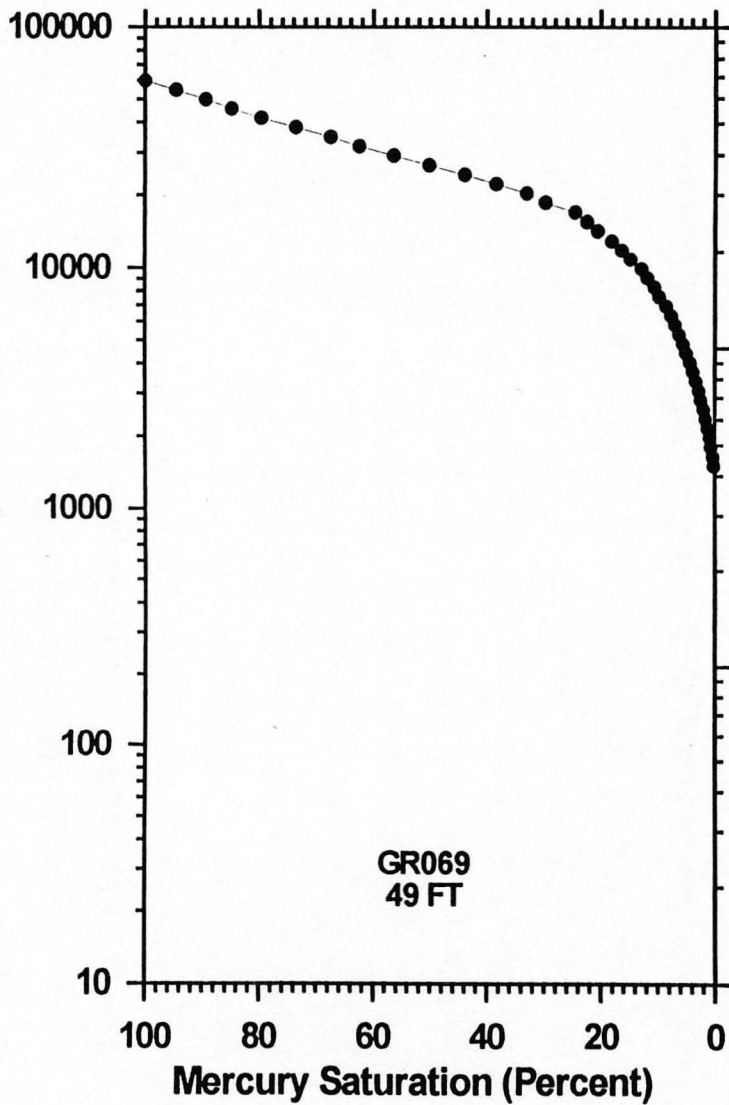


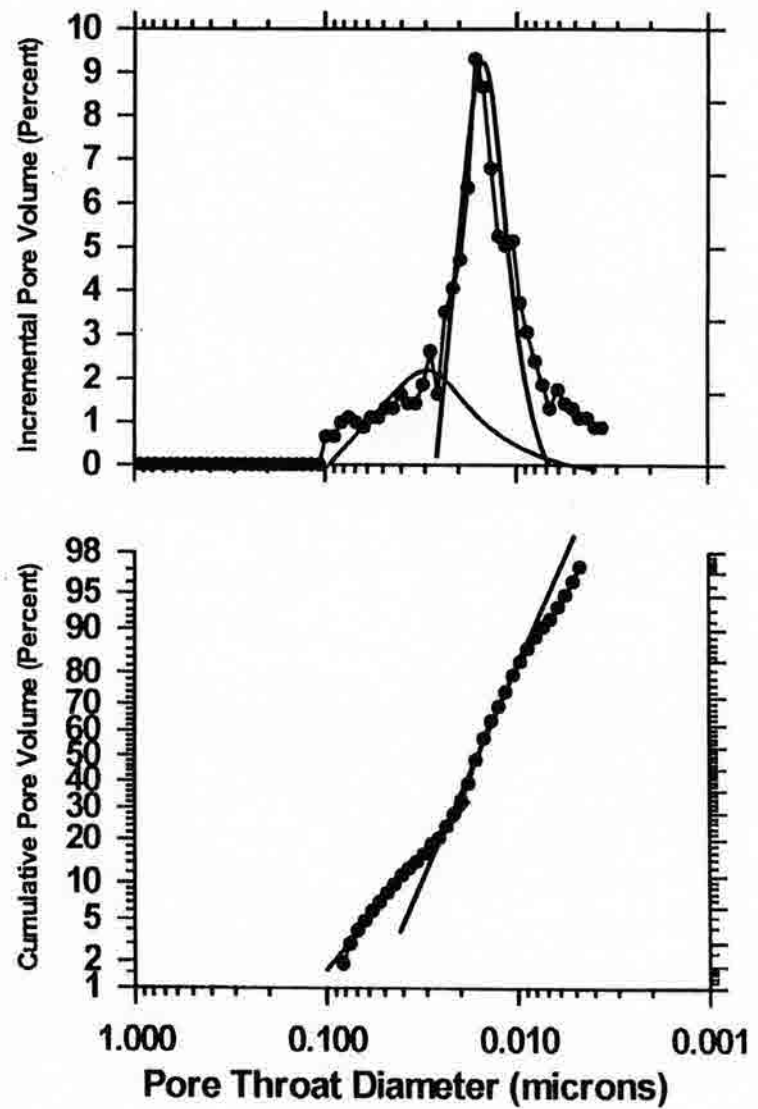
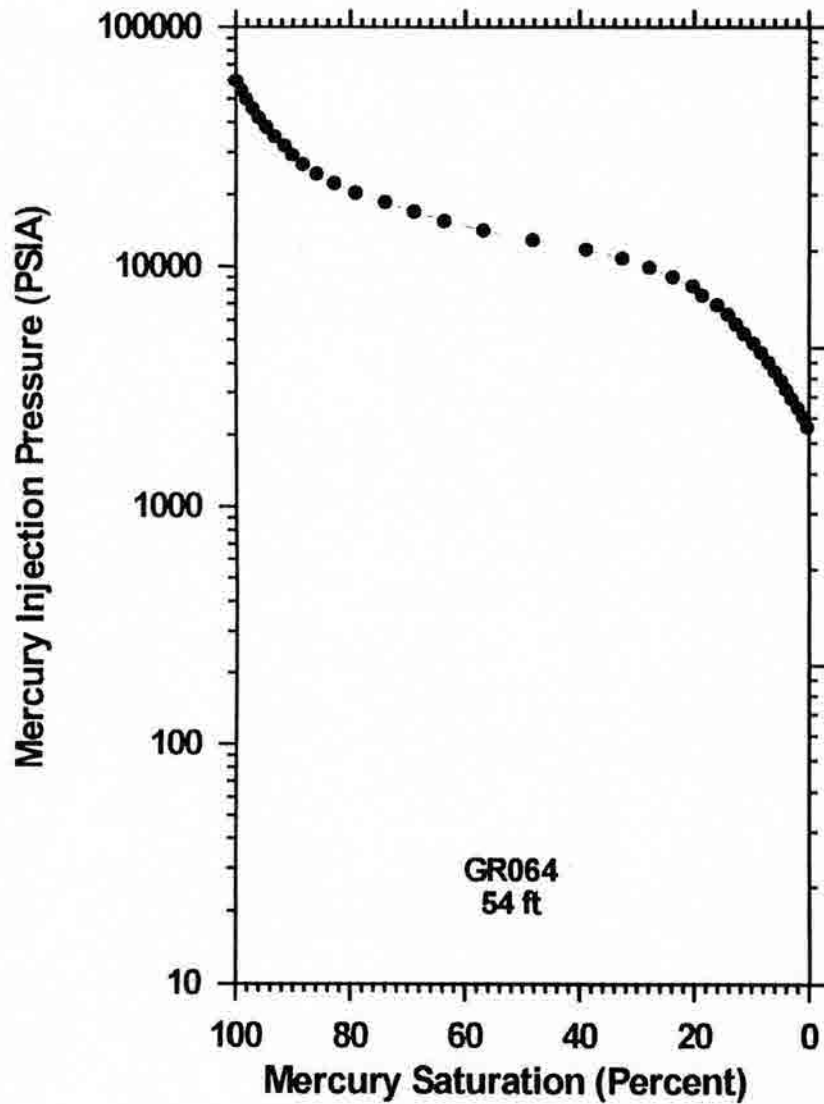


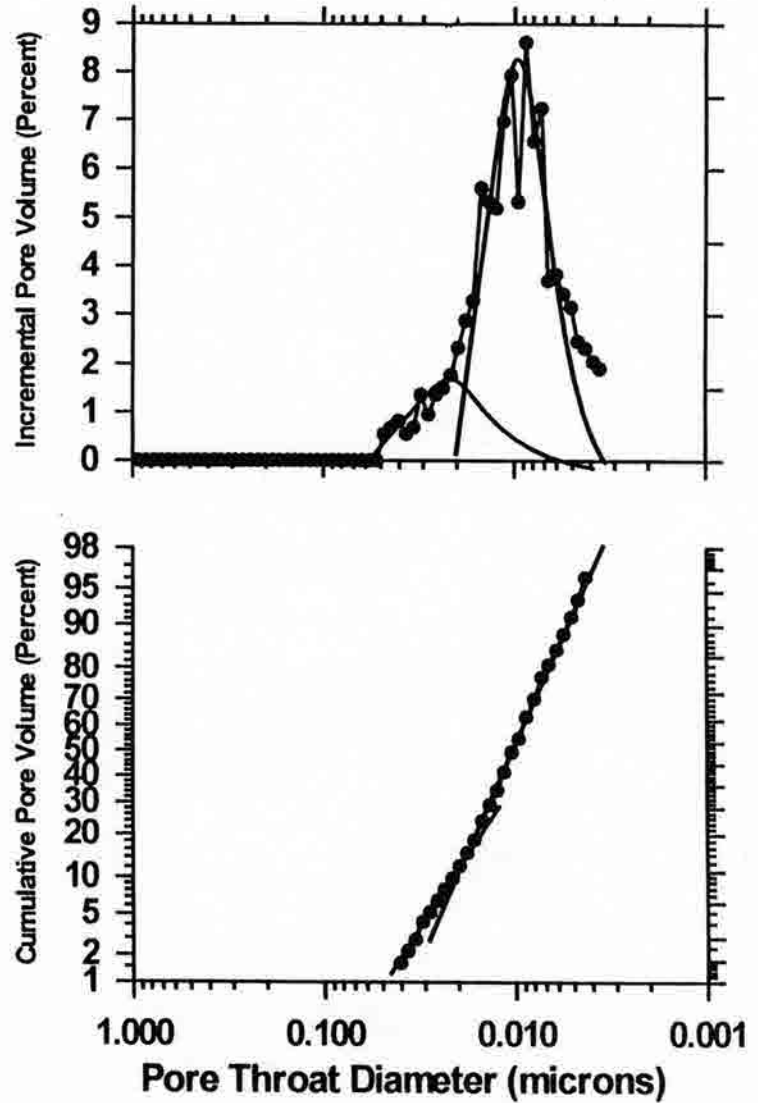
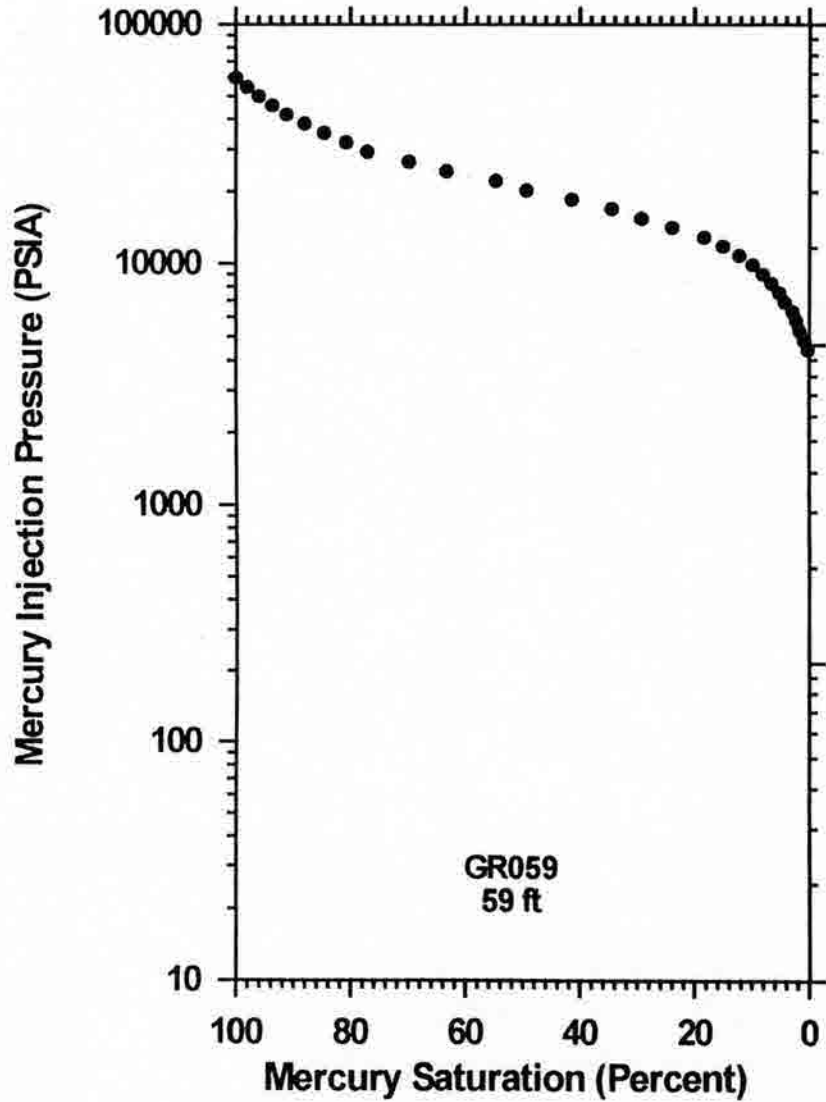


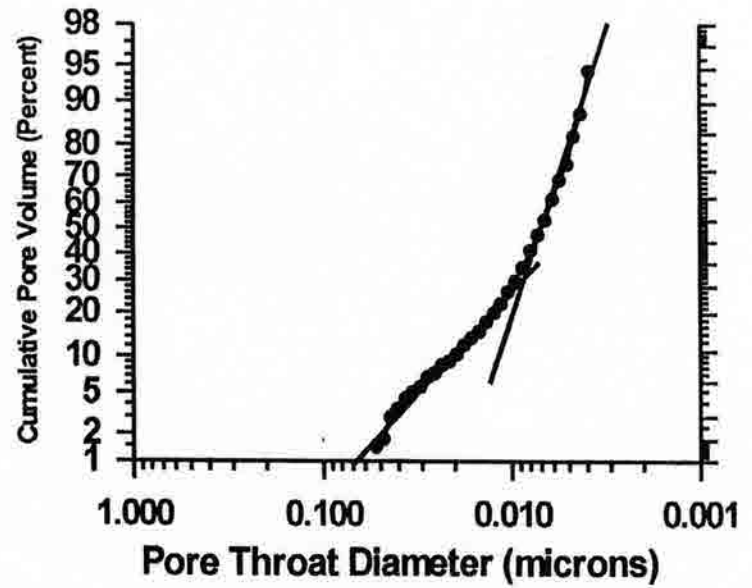
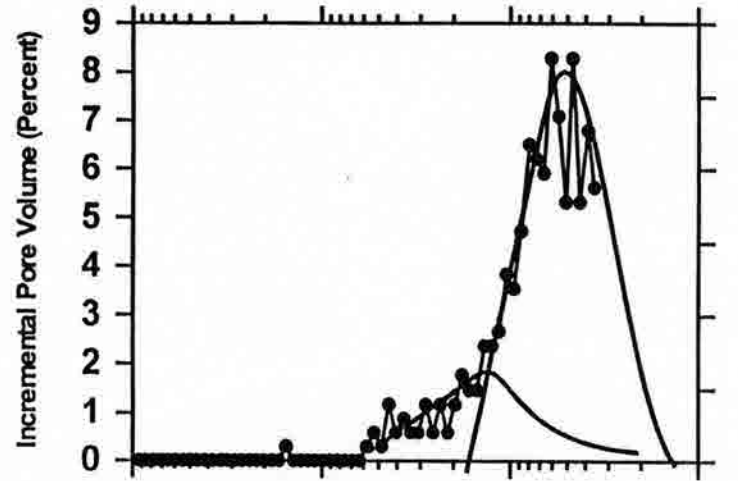
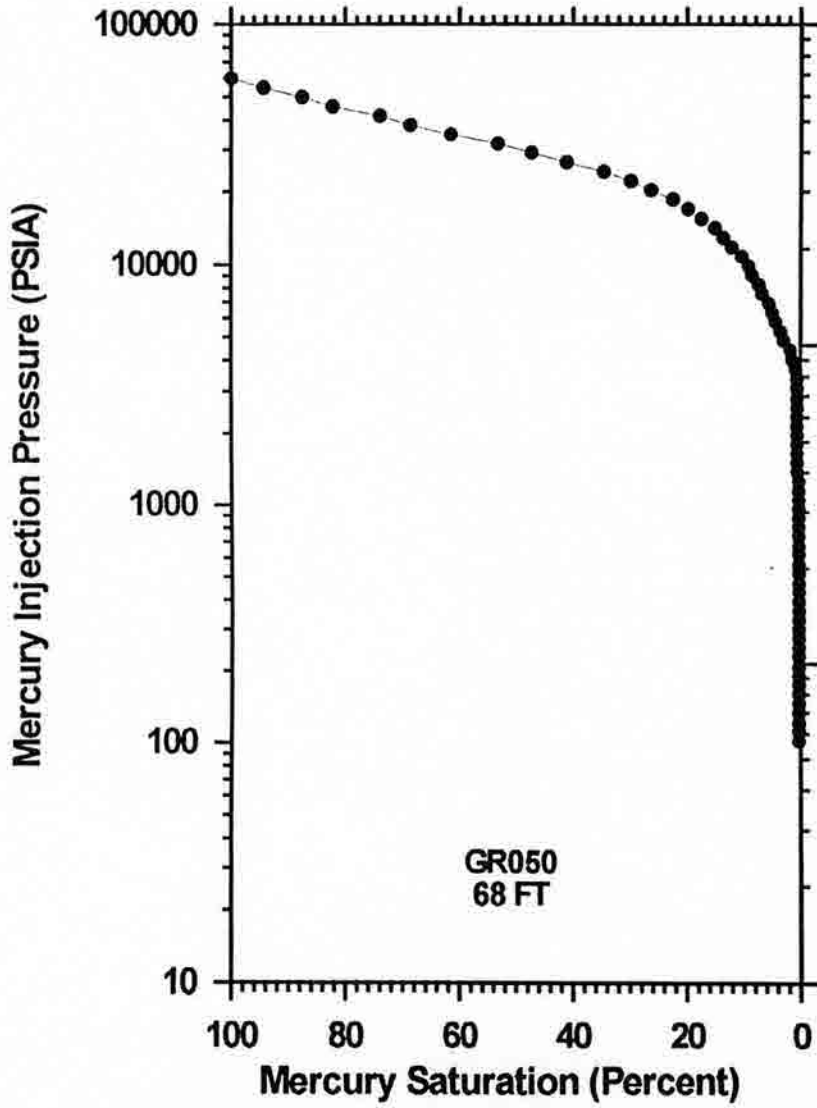


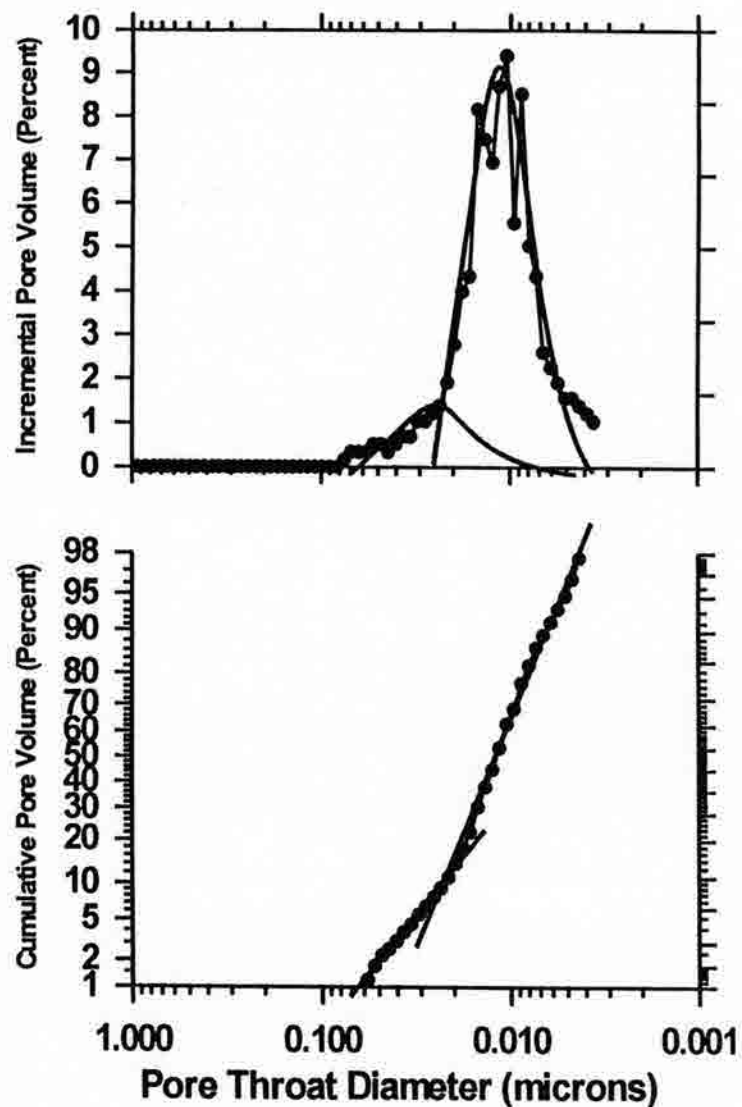
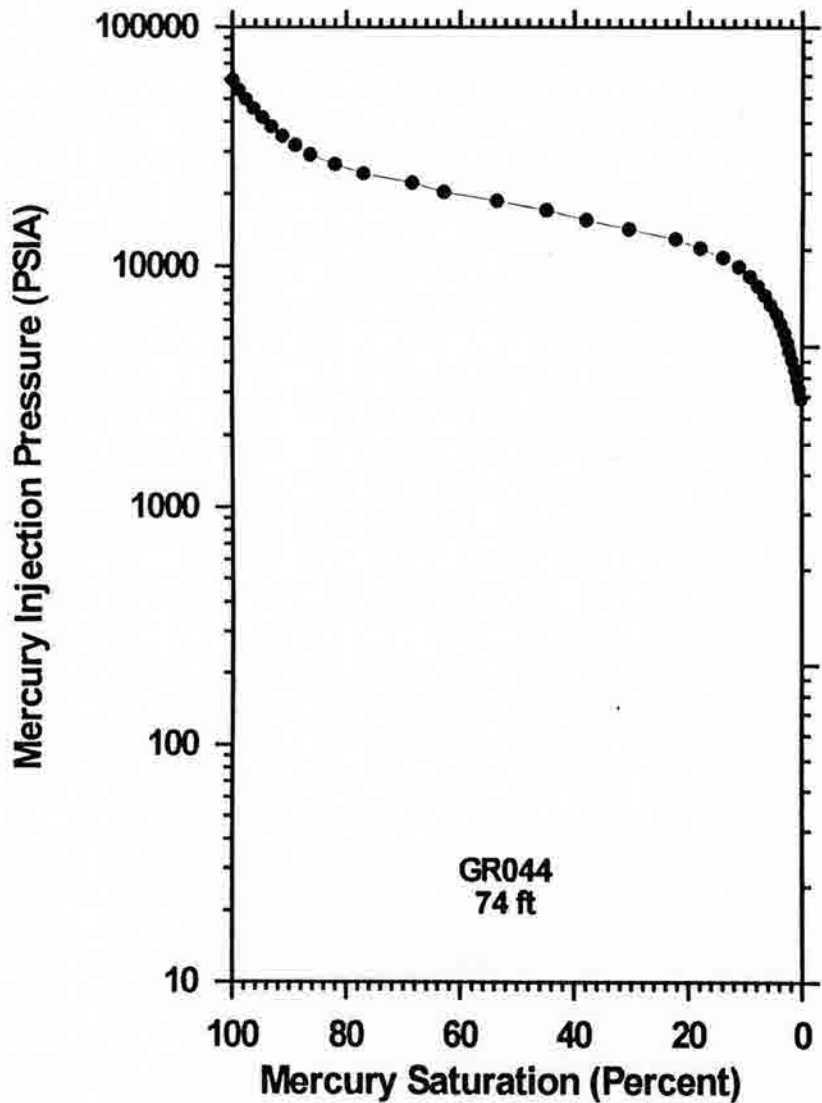
Mercury Injection Pressure (PSIA)

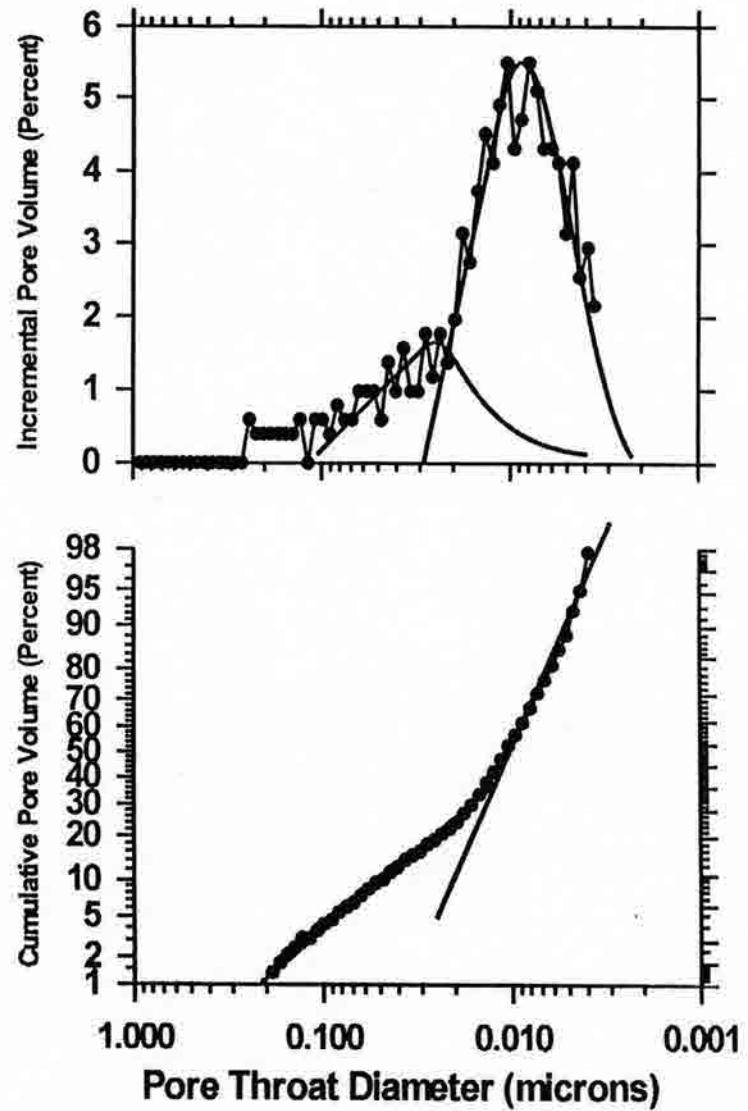
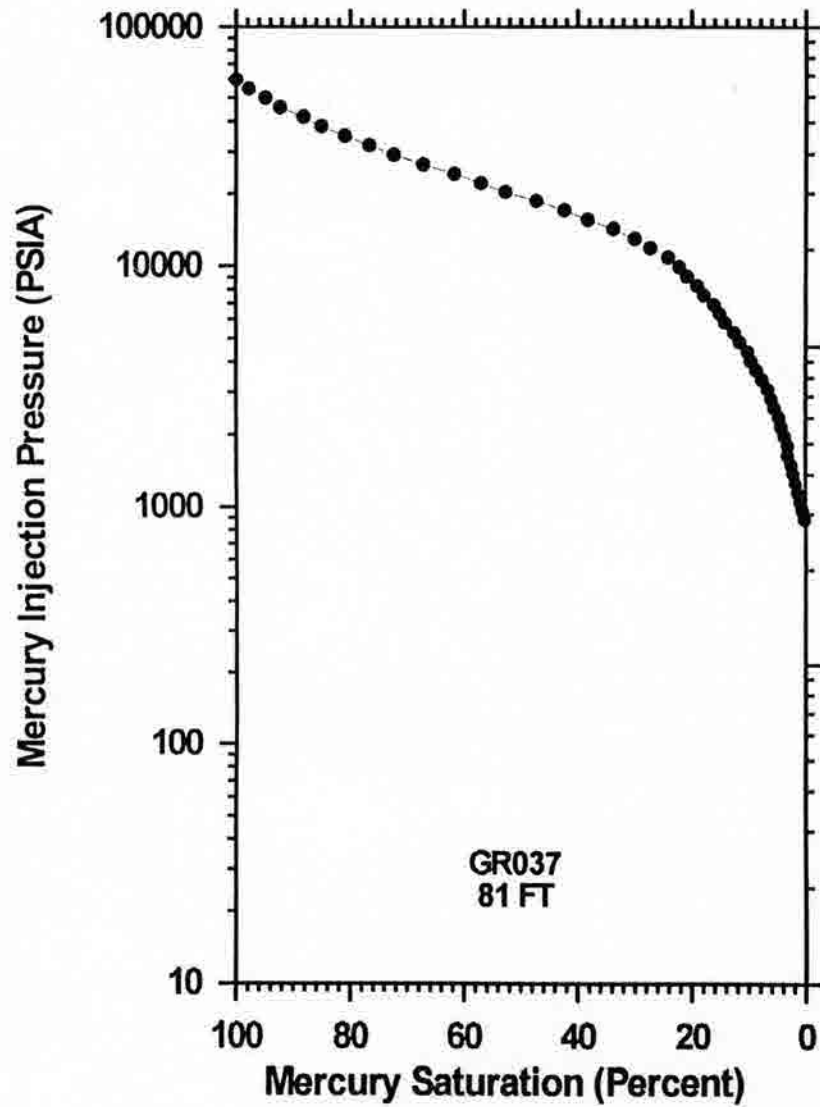


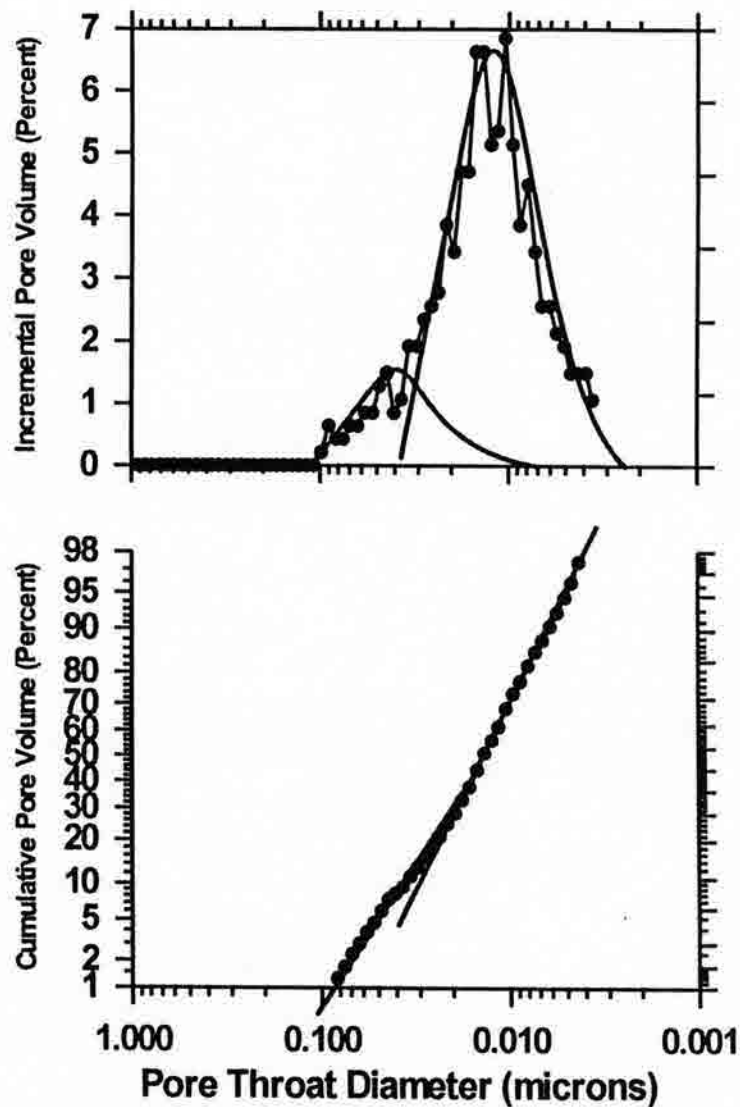
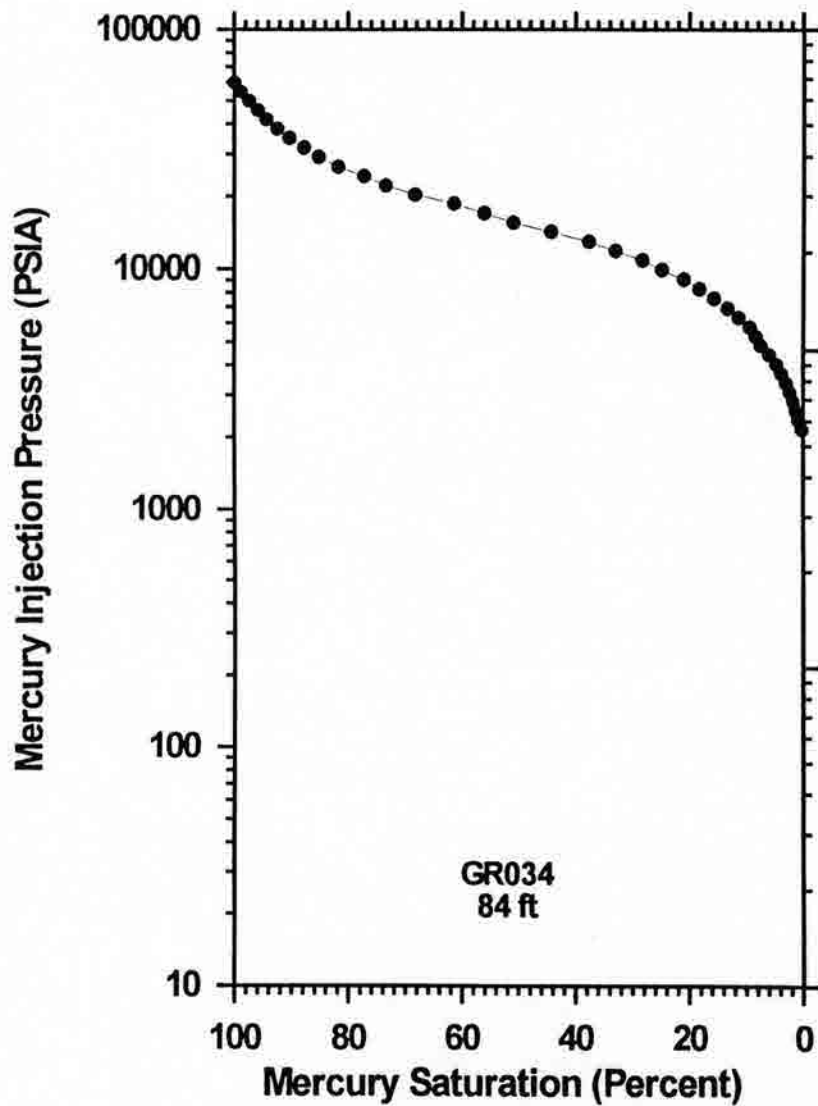


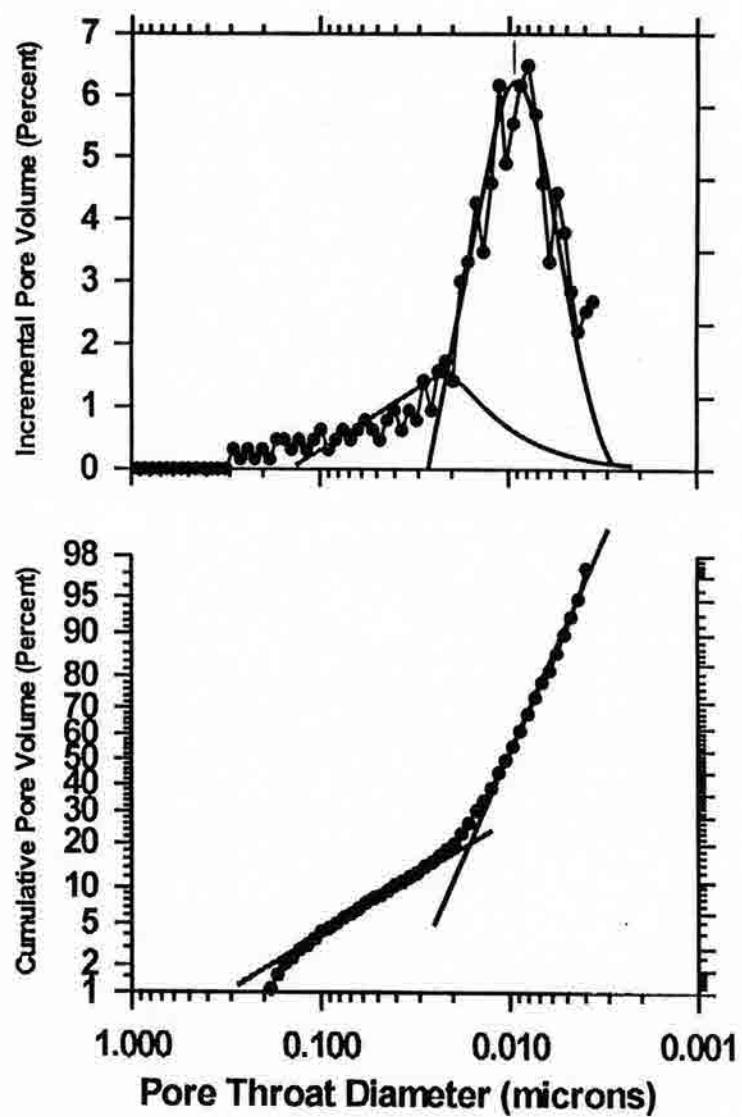
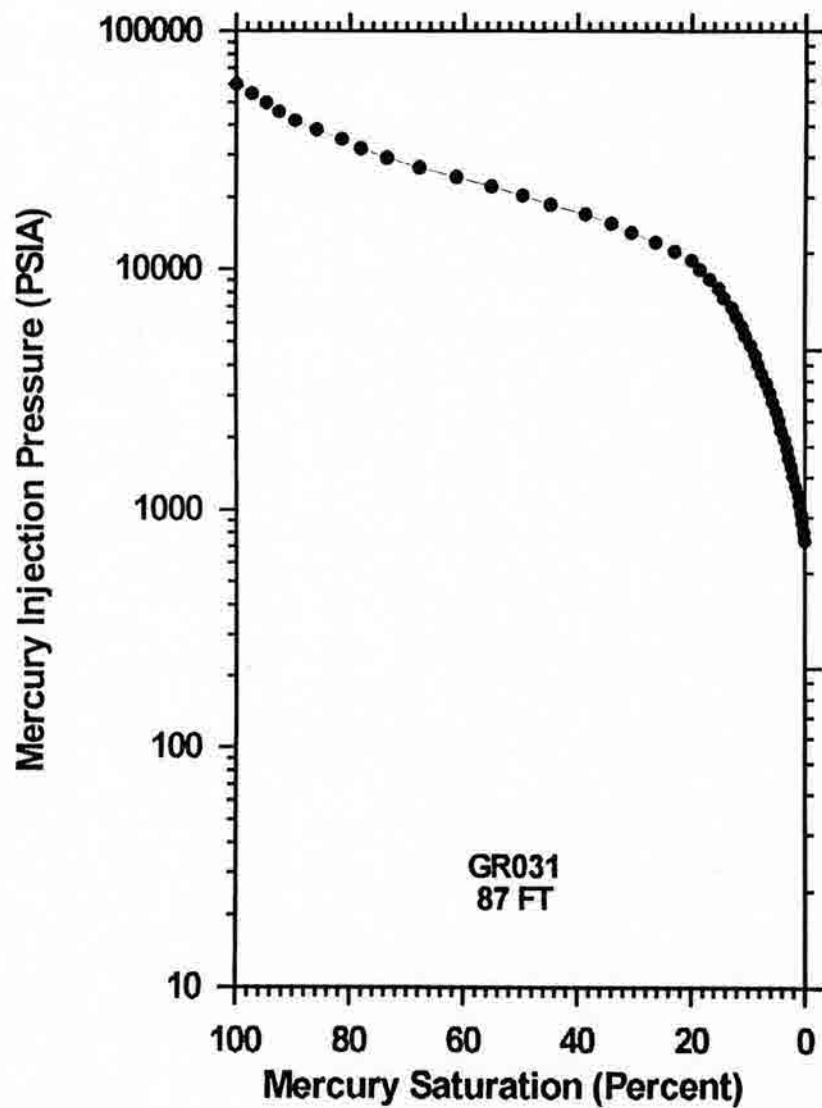


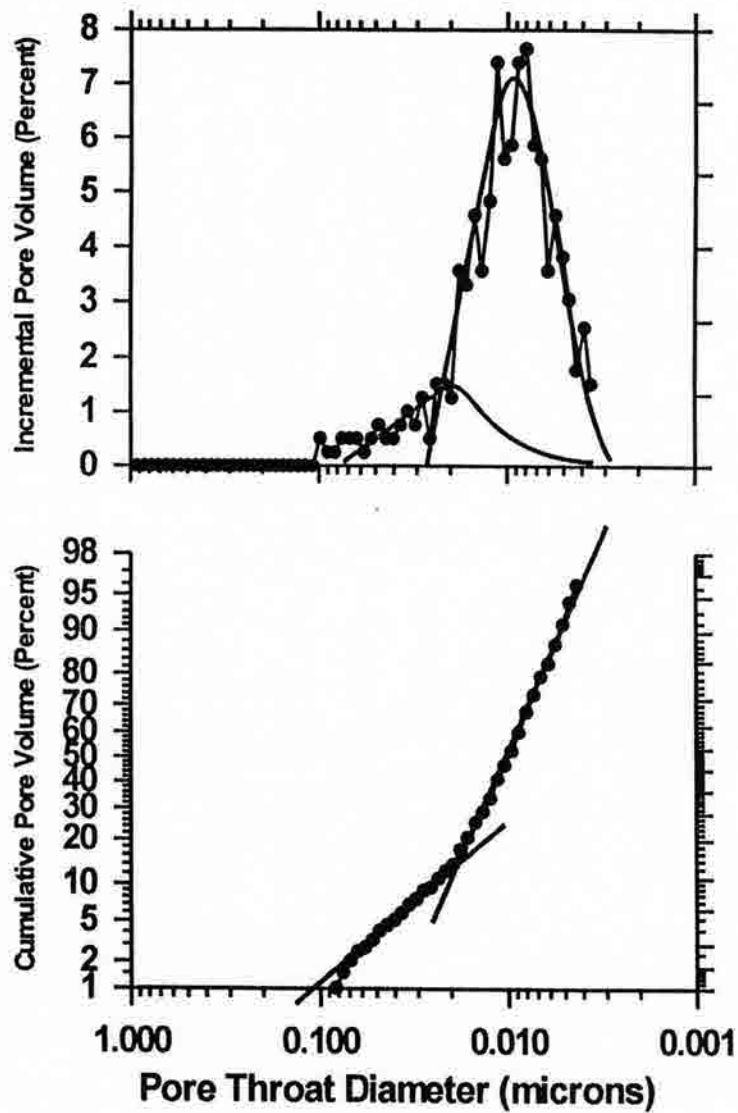
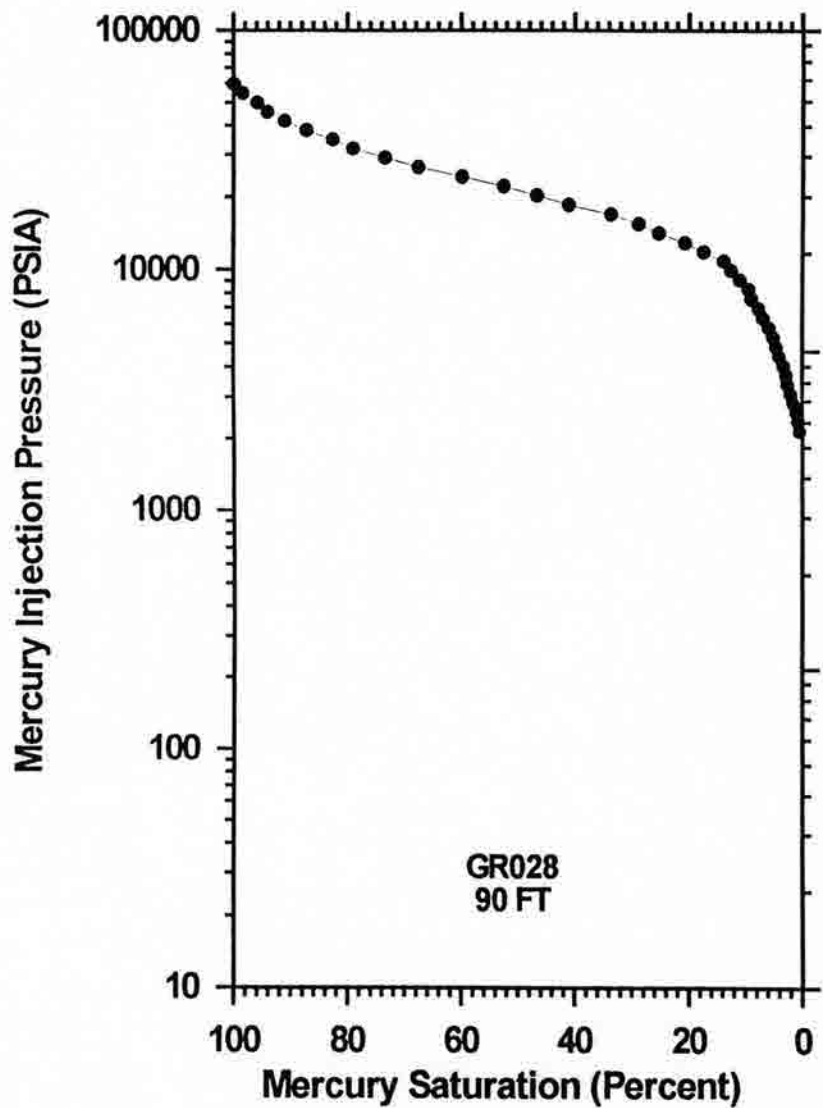


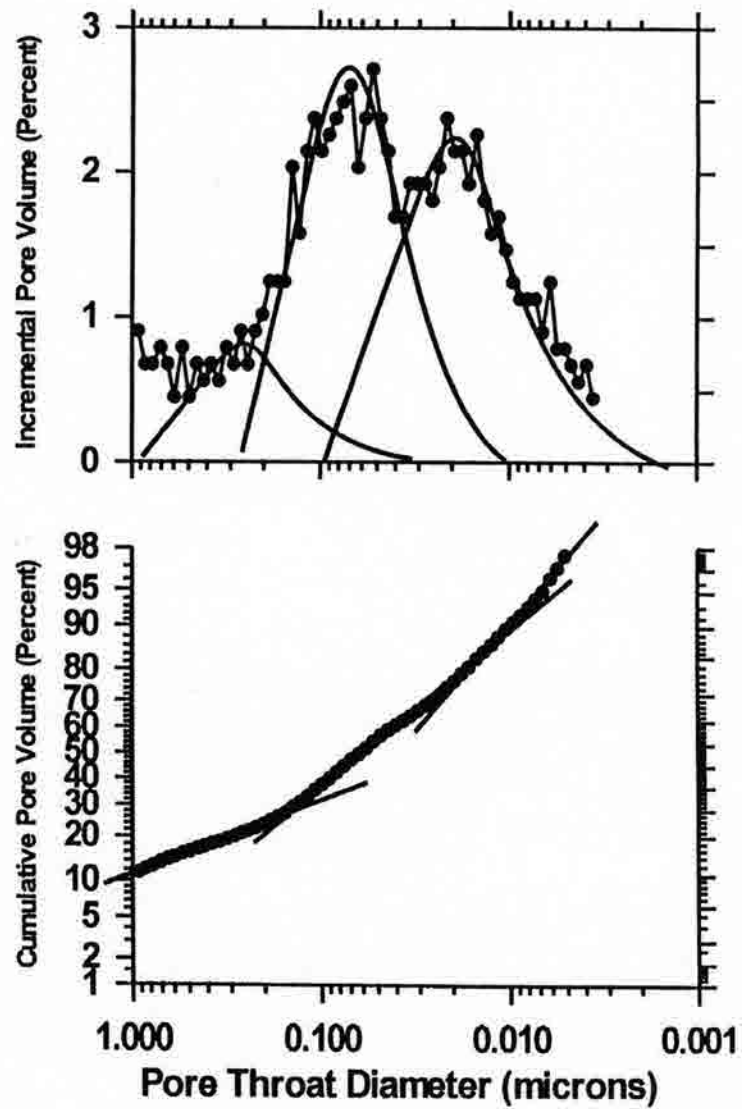
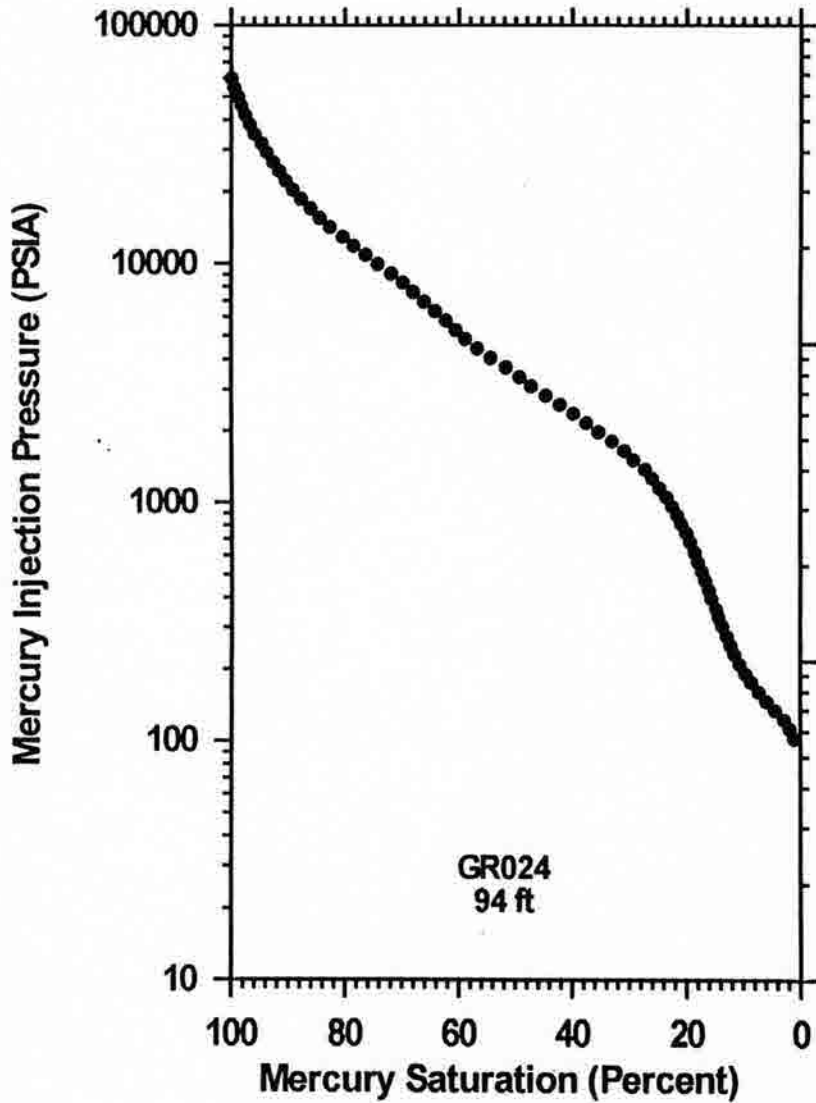


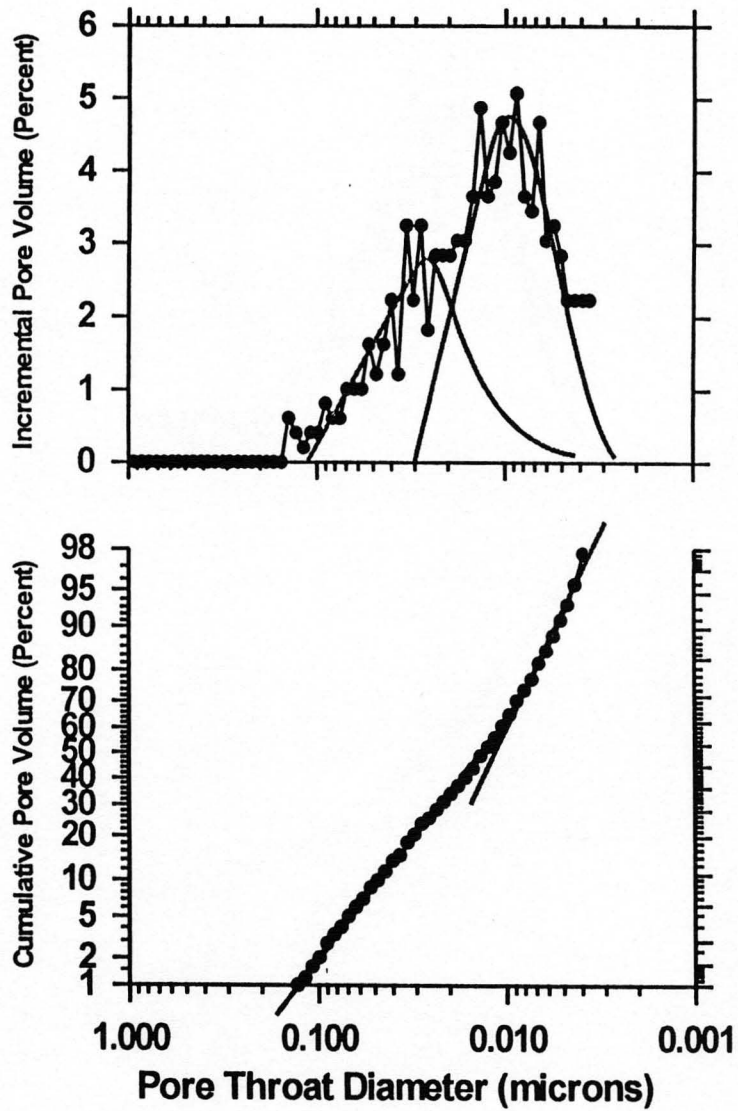
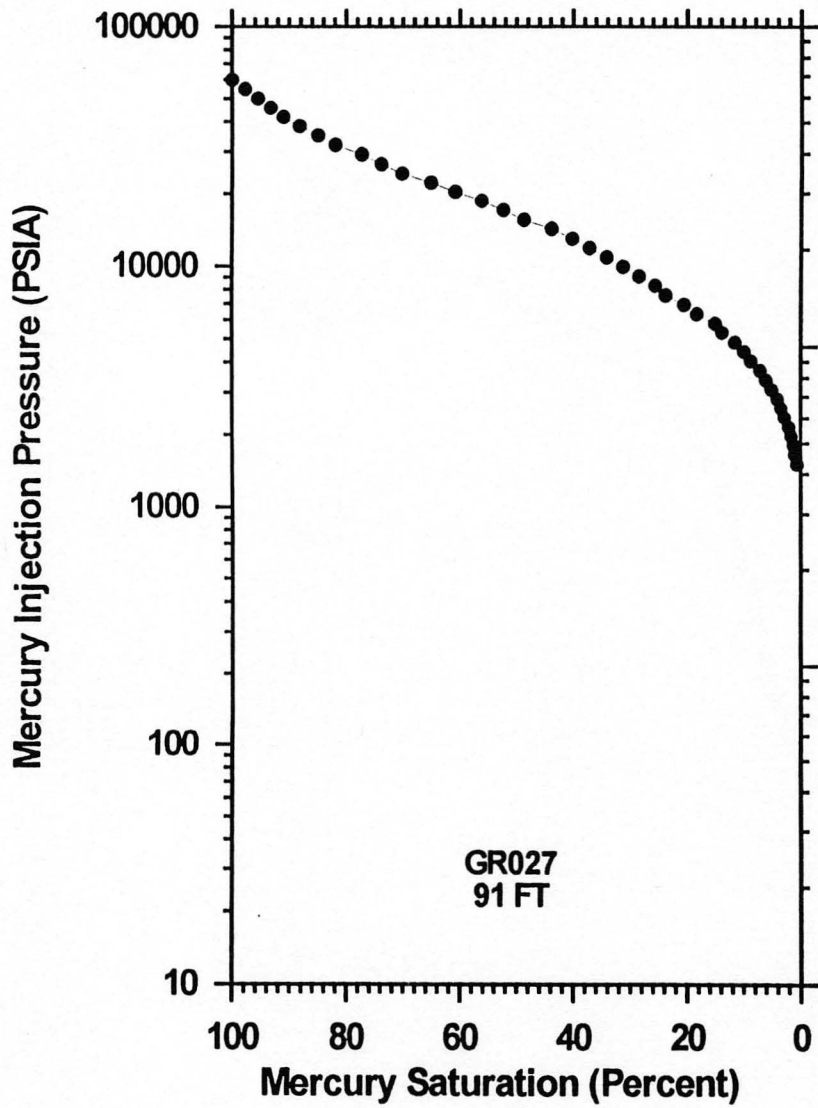




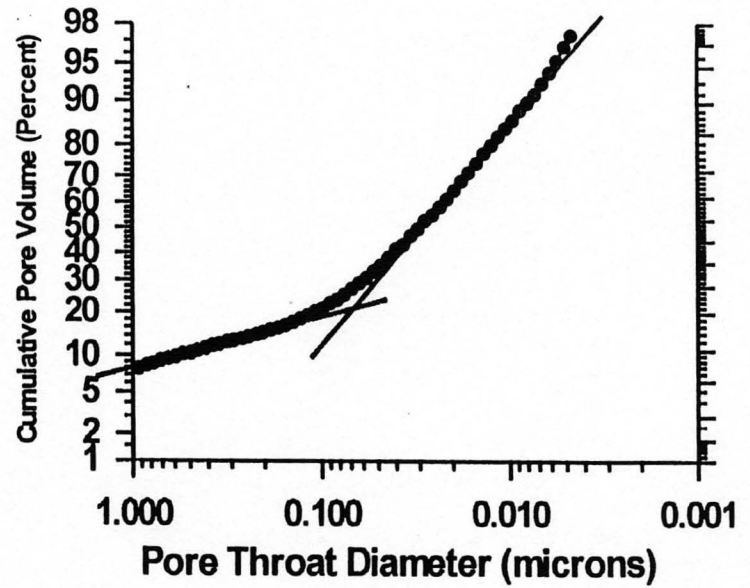
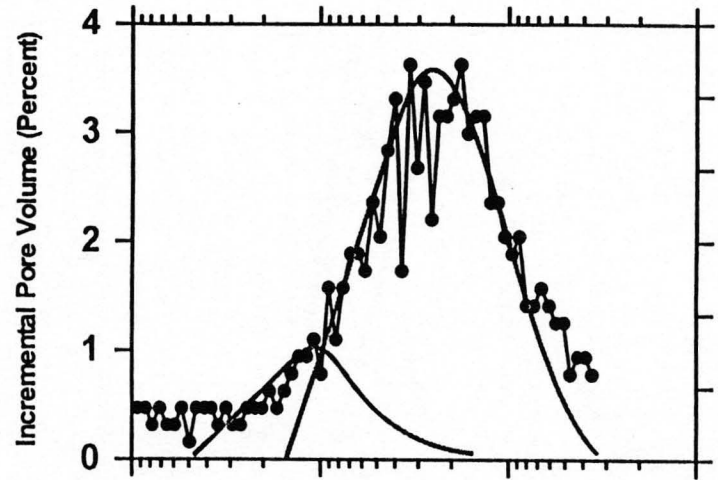
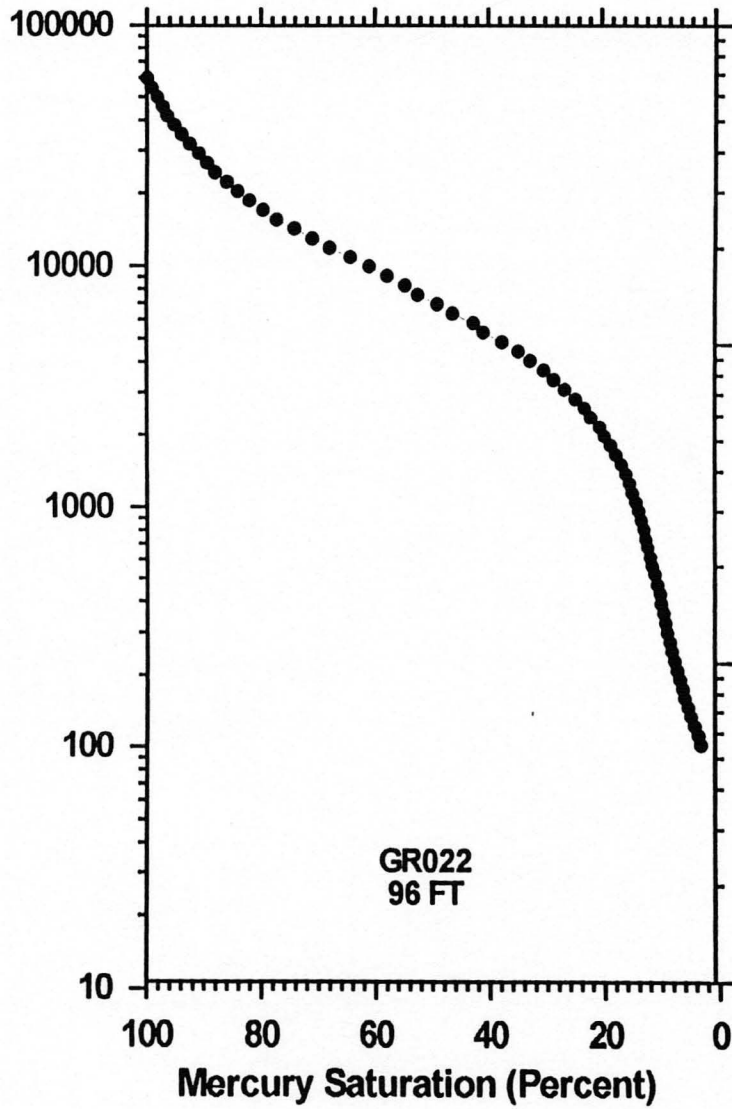


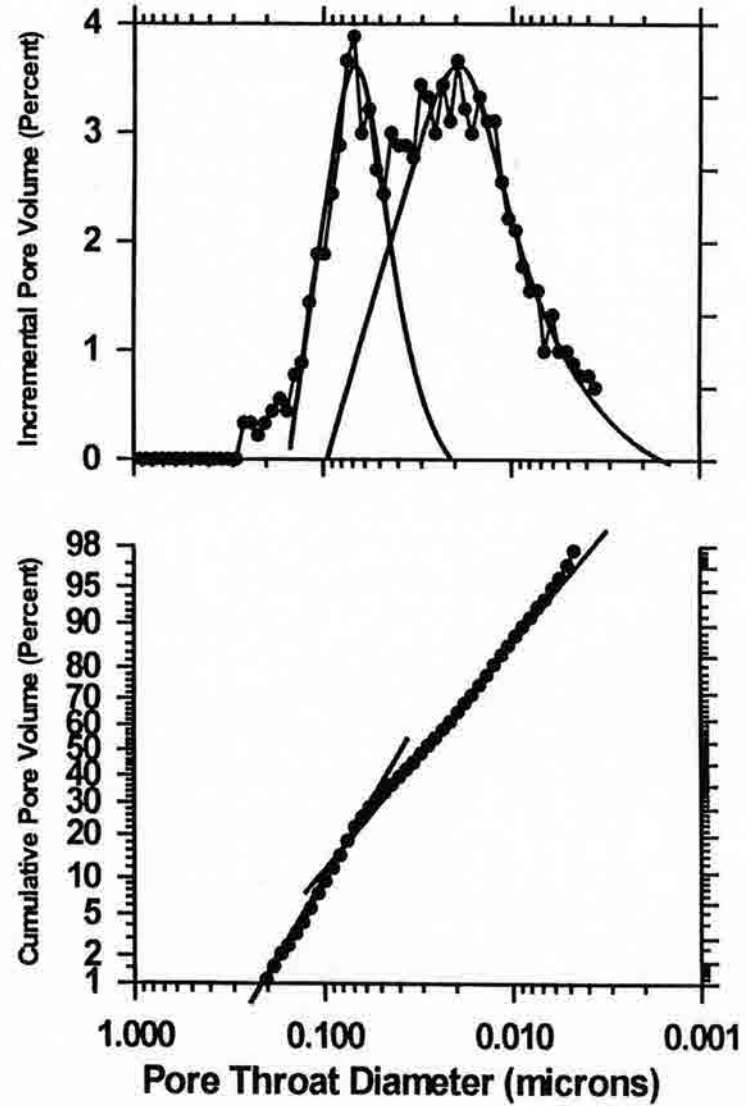
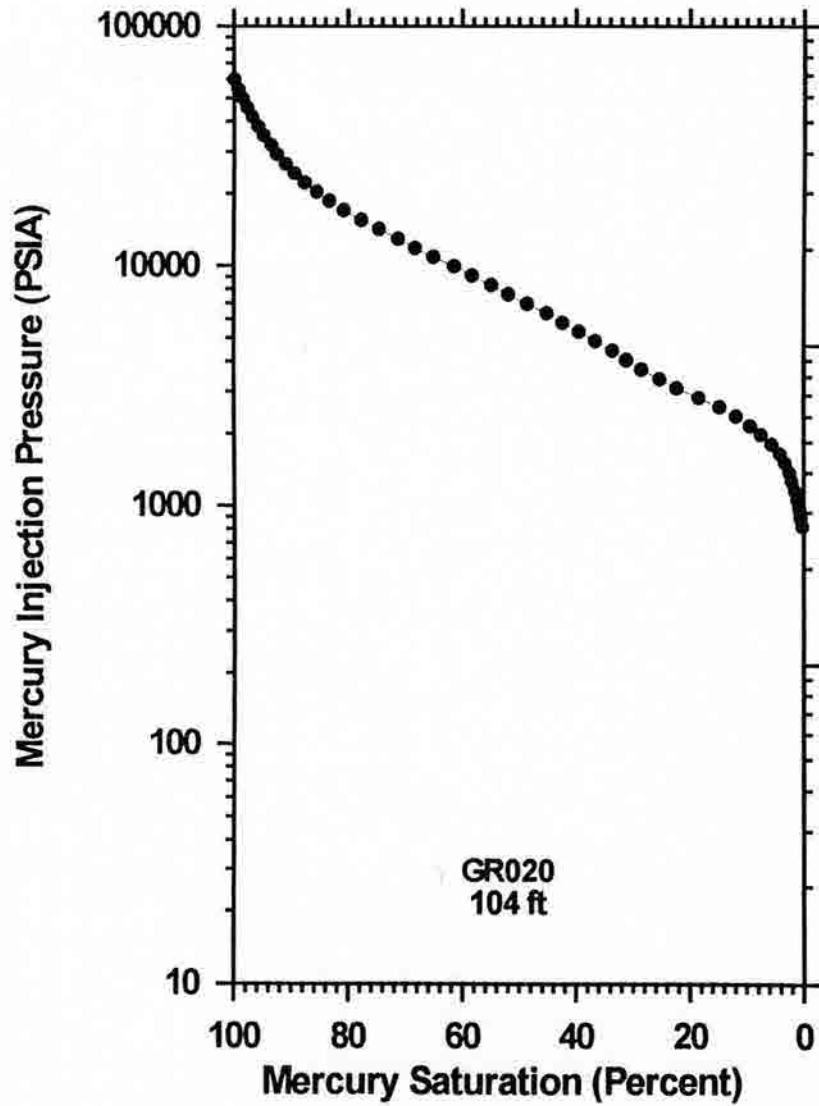


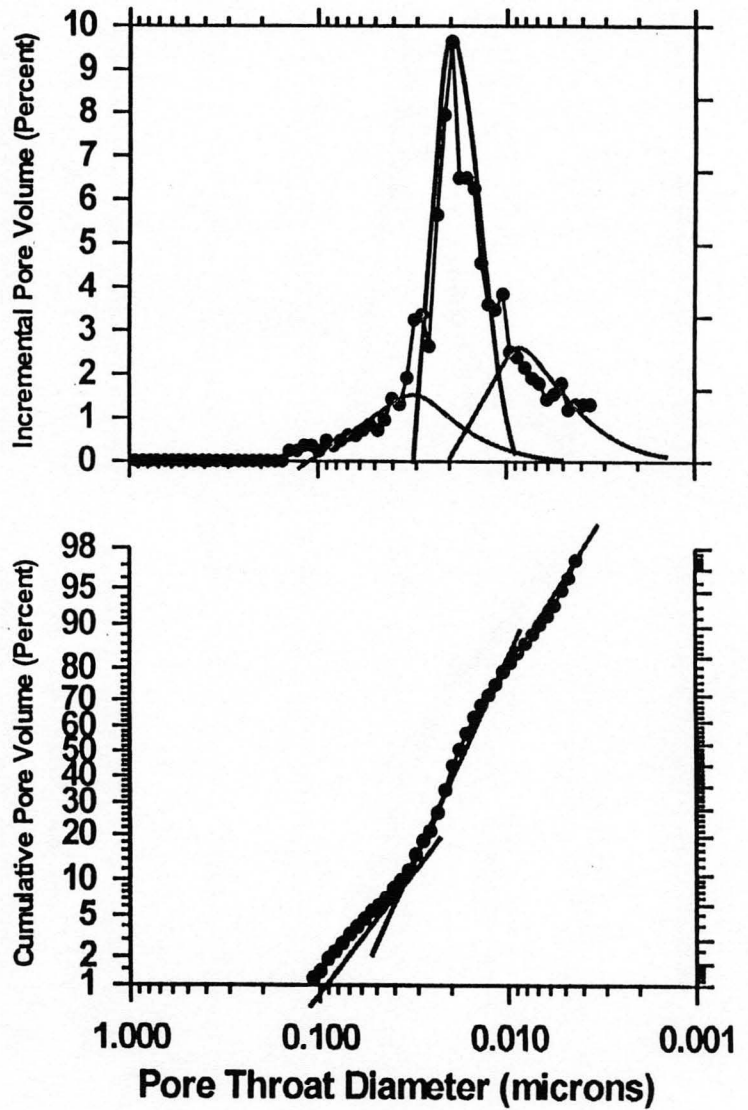
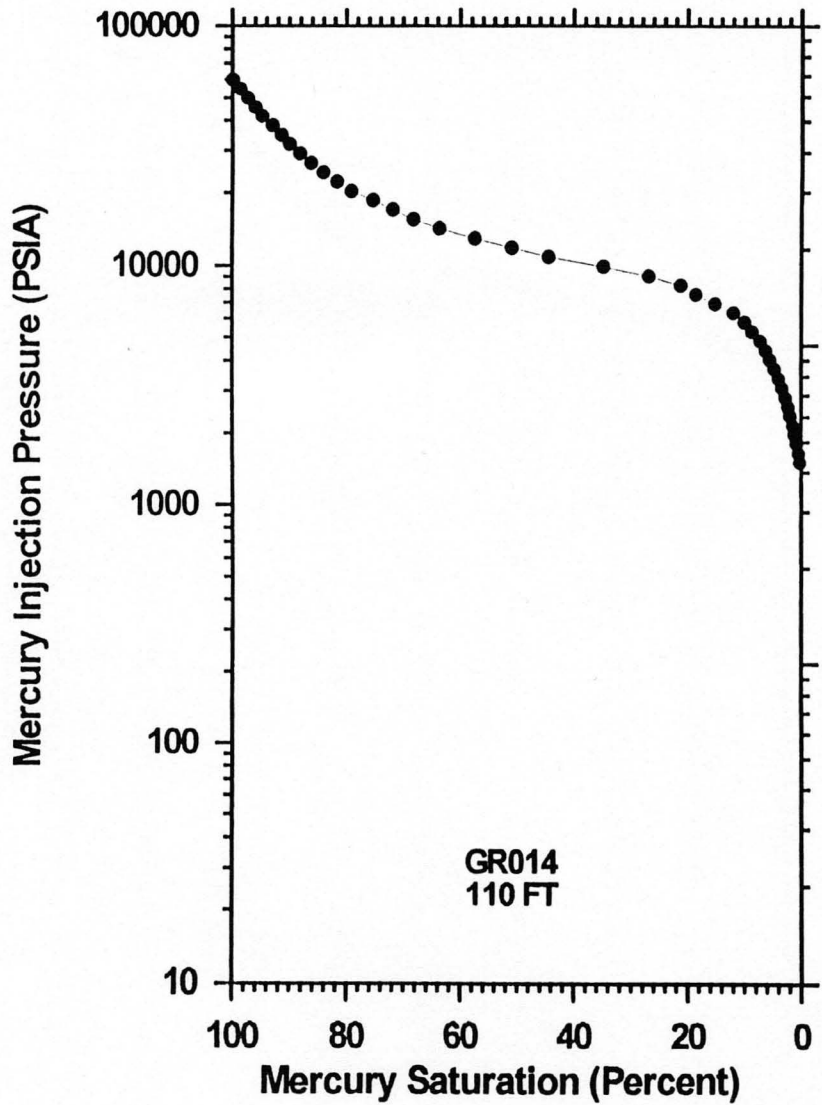


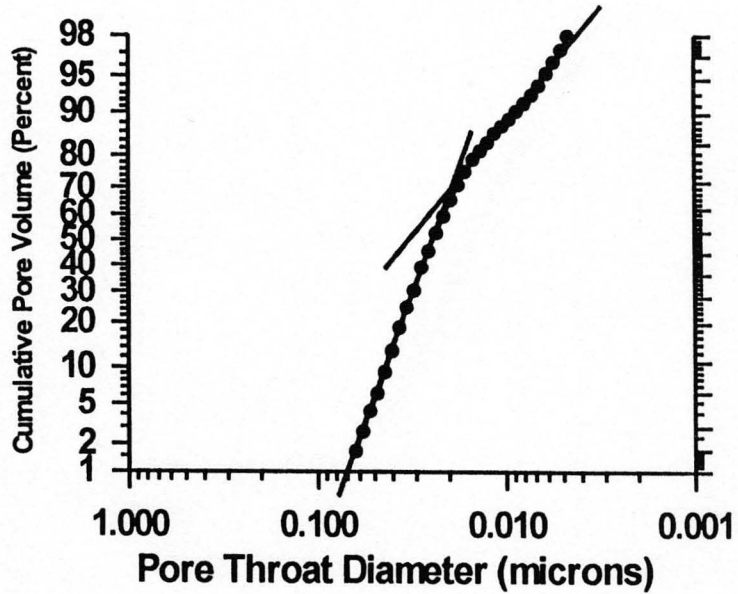
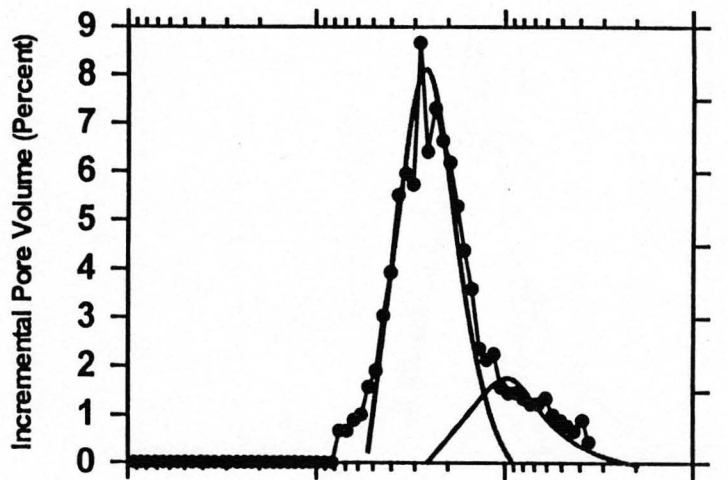
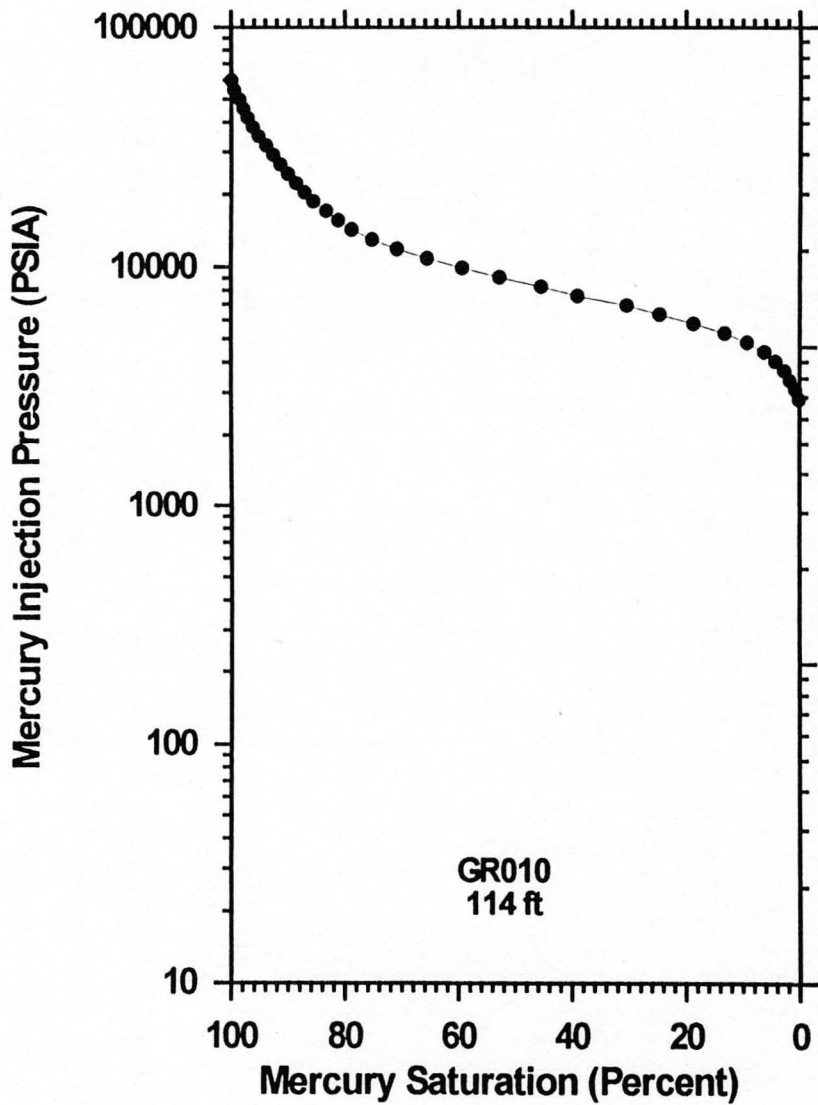


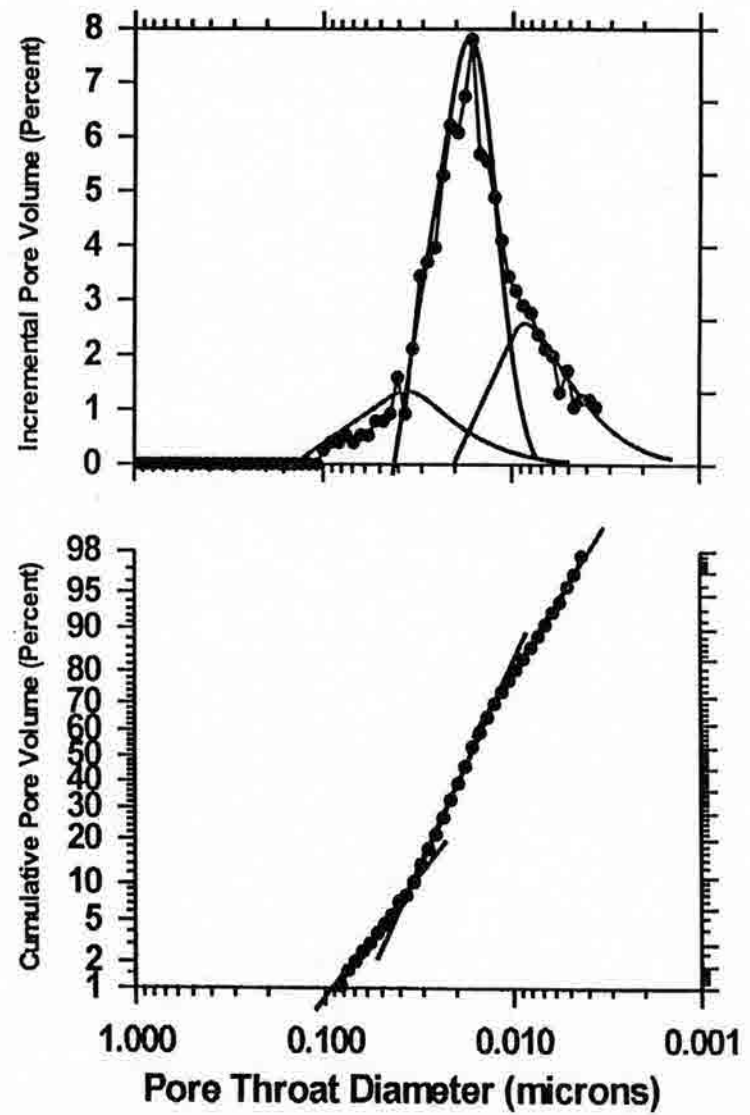
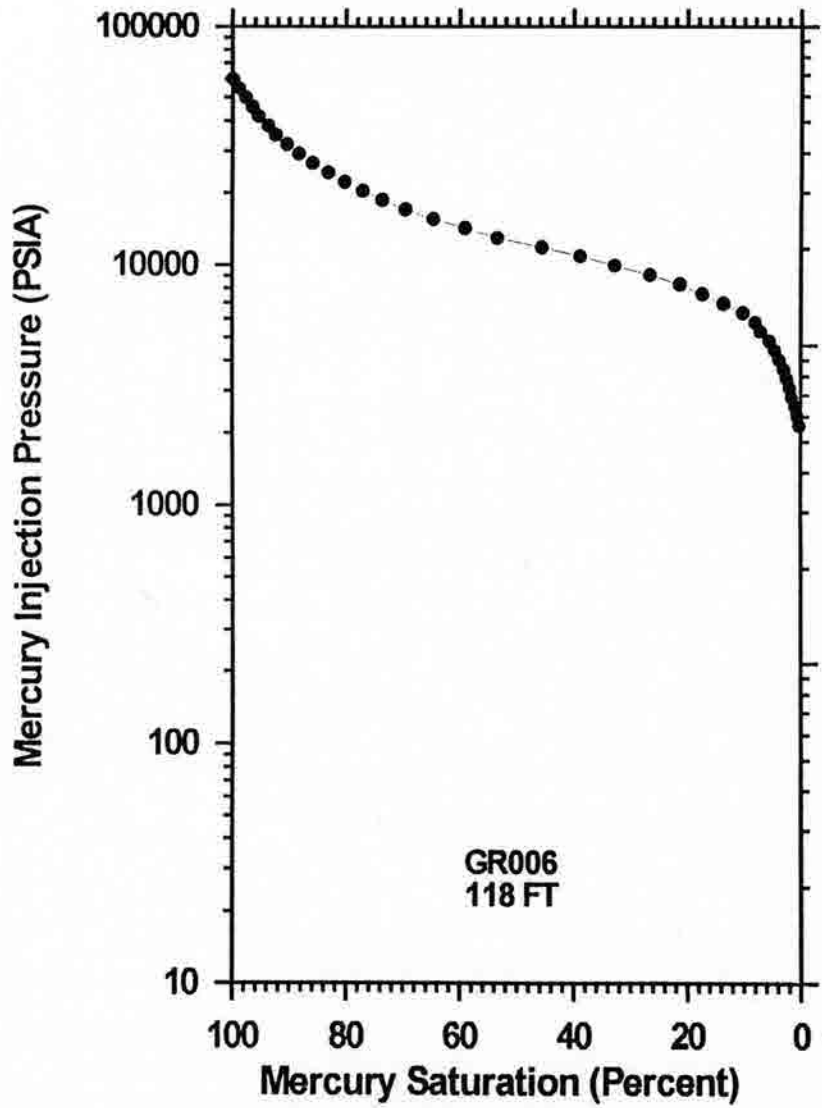
Mercury Injection Pressure (PSIA)

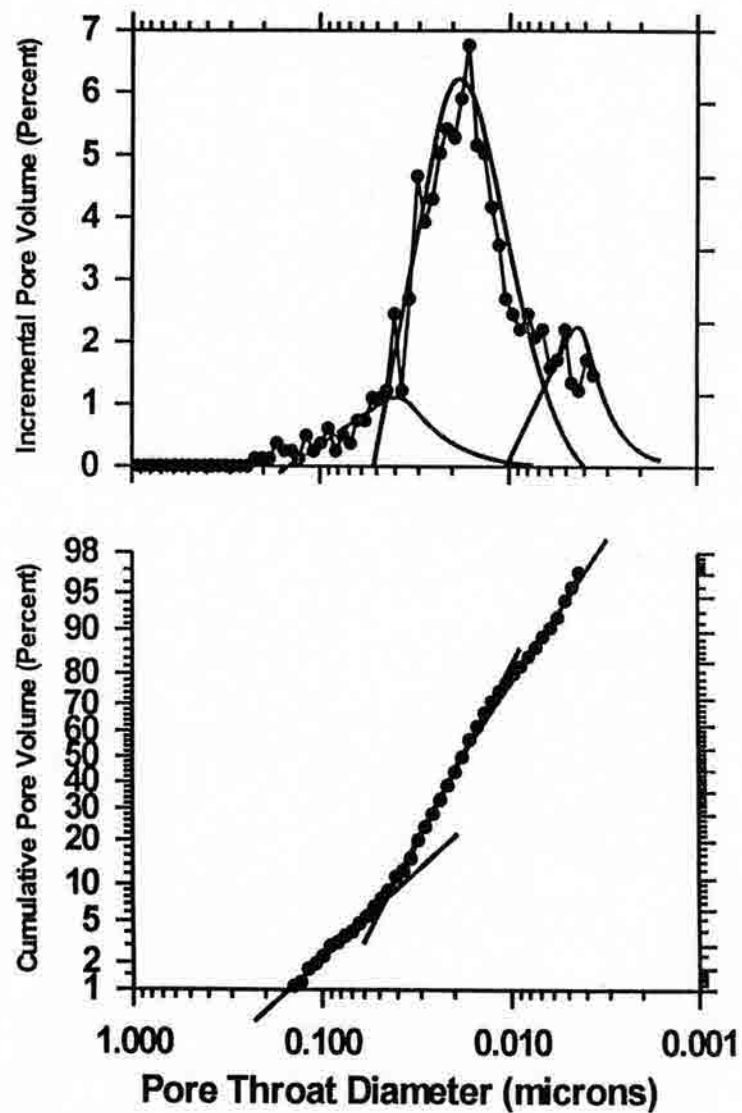
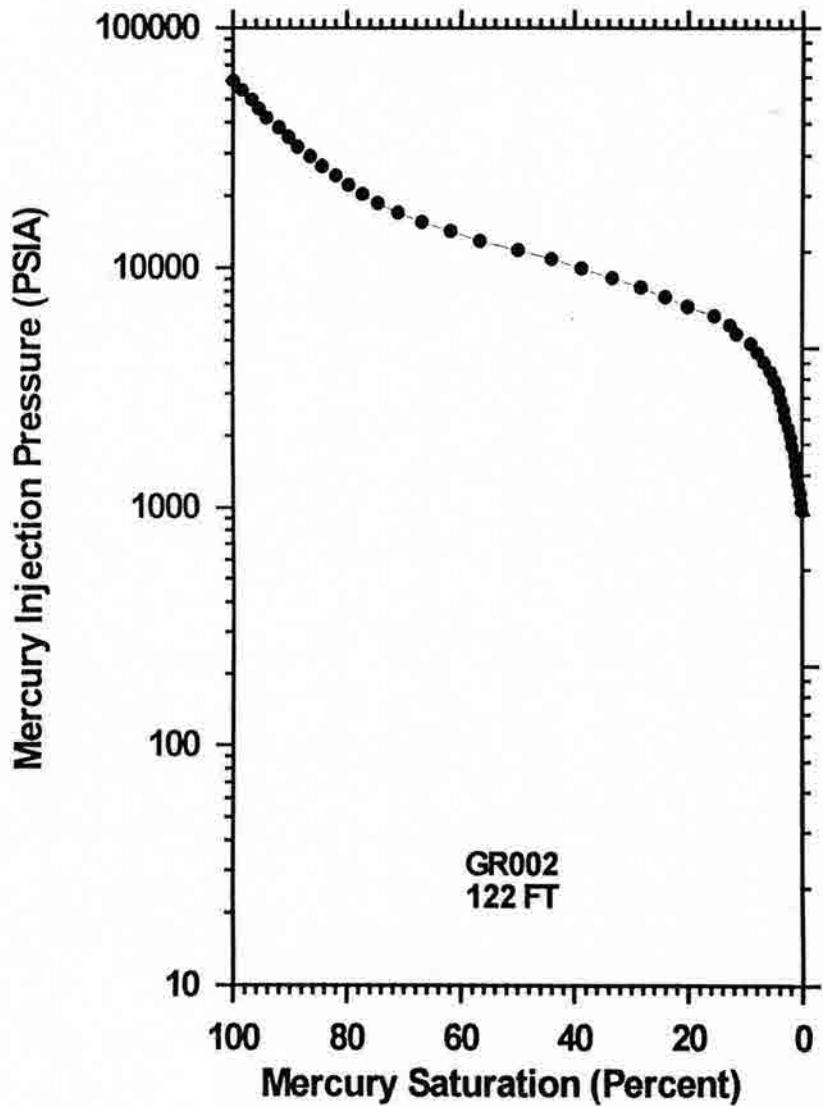


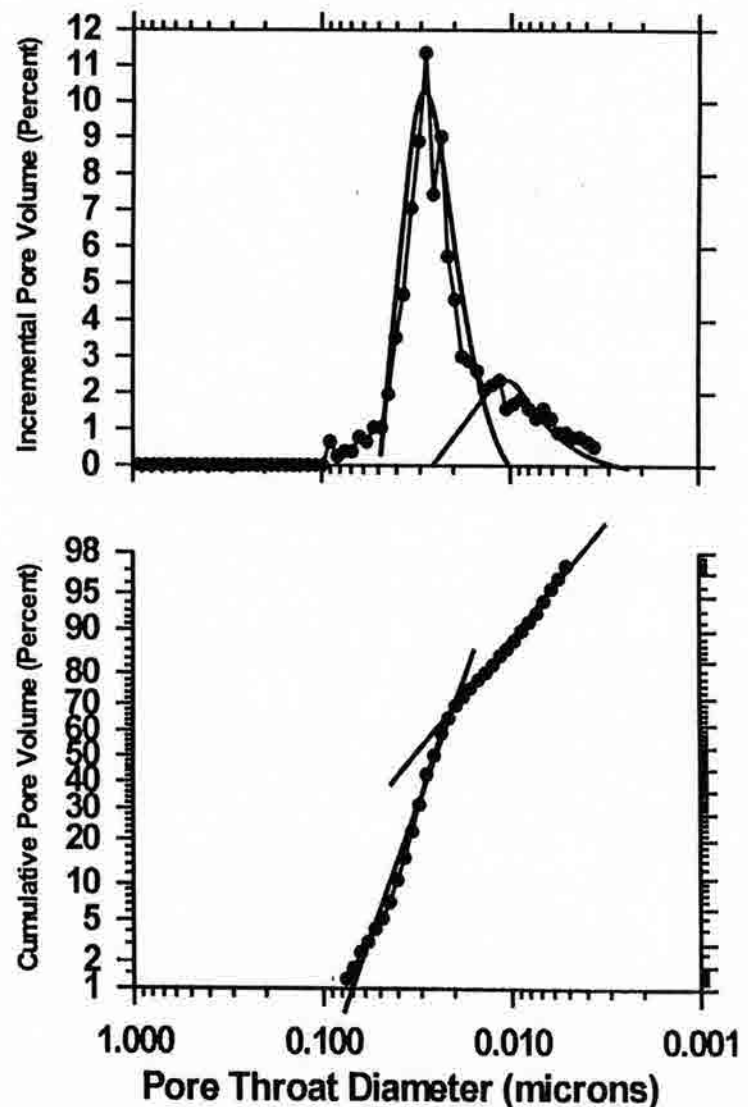
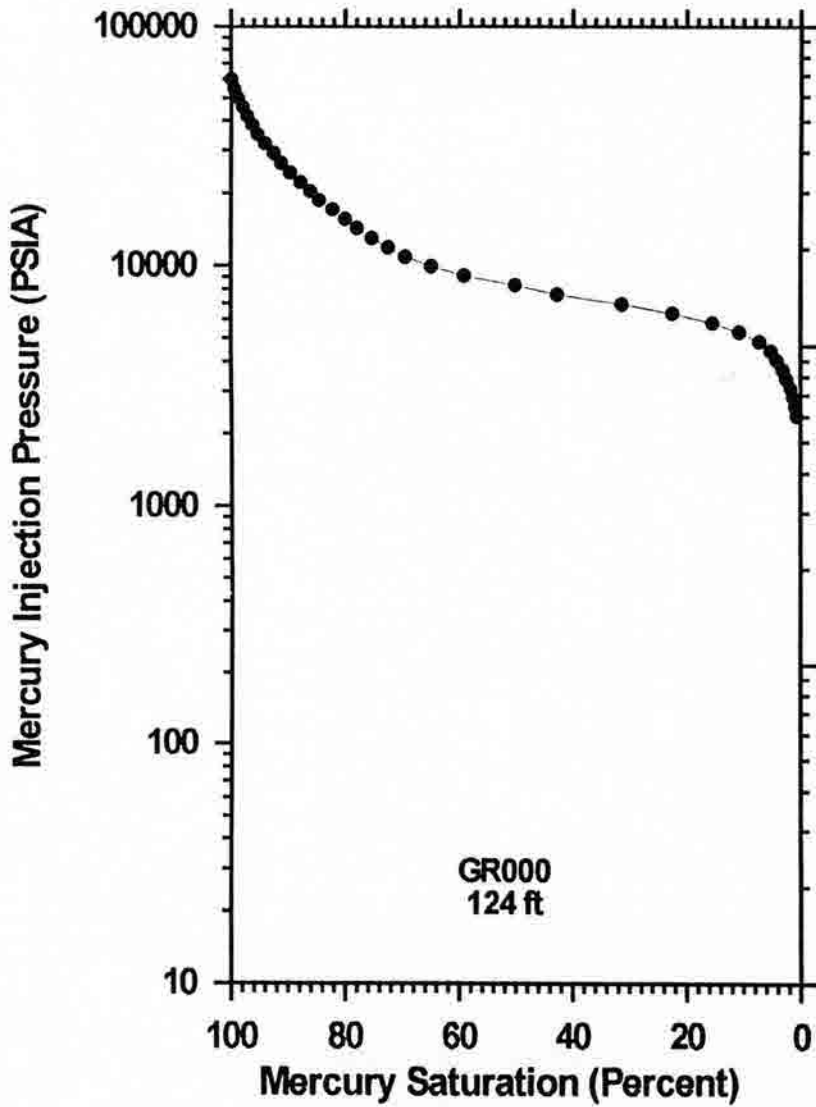












APPENDIX N

YOUNGS CORE

GRANEROS SHALE

THIN SECTION PETROGRAPHY

Figure 21.
Y018 (5790 ft)

Low magnification (PP) thin-section photomicrograph of silty shale. The coarse-grained matrix contains well sorted, oil size detrital grains (quartz, feldspar, mica). The detrital grains have a strong preferred grain orientation in addition to the well-developed laminations of clay and organic matter. Accessory minerals include authigenic hematite grains (small opaque nodules). In the lower left corner, bright orange phosphatic debris is noticeable. Visible matrix porosity is not evident.

Figure 22.
Y018 (5790 ft)

High magnification (PP) thin-section photomicrograph of same silty shale pictured in 01. At high magnification, the light orange colored laminations of organic matter are conspicuous. Clay minerals significantly add to the matrix and surround the oil size detrital quartz grains so they appear to be floating. The small opaque nodules of authigenic hematite provide a notable secondary mineralogy. No matrix porosity is observed.

Figure N1.

Y018 (5790 ft)

Low magnification (PPL) thin-section photomicrograph of silty shale. This compacted, clay-rich matrix contains well sorted, silt size detrital grains (quartz, feldspar, mica). The detrital grains have a strong preferred grain orientation in addition to the well-developed laminations of clays and organic matter. Accessory minerals include authigenic framboidal pyrite (small opaque nodules). In the lower left corner, bright orange phosphatic debris is noticeable. Visible matrix porosity is not evident.

Figure N2.

Y018 (5790 ft)

High magnification (PPL) thin-section photomicrograph of same silty shale pictured in O1. At high magnification, the light orange colored laminations of organic matter are conspicuous. Clay minerals significantly add to this matrix and surround the silt size detrital quartz grains so they appear to be "floating". The small opaque nodules of authigenic pyrite provide a notable secondary mineralogy. No matrix porosity is detected.

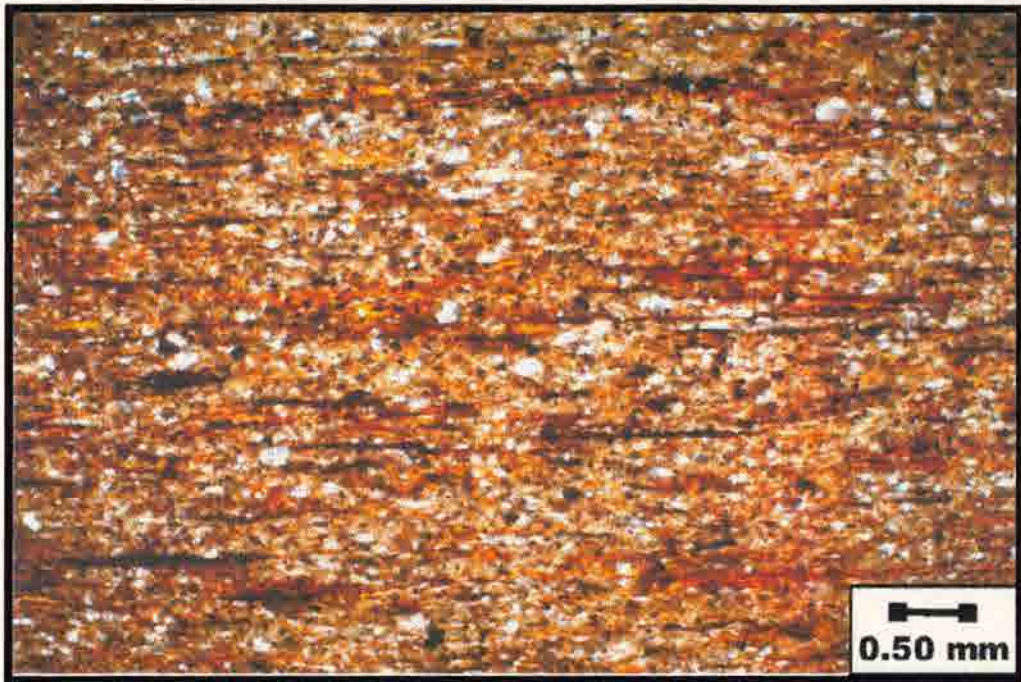


Figure N1.



Figure N2.

Figure 23
Y028 (3780 ft)

High magnification (HP) thin-section photomicrograph of silty shale. This compared clay-rich matrix contains well sorted, six sided detrital grains (quartz, mica, feldspar). The quartz grains are spherical and subangular with some preferred grain orientation. The shale has well-developed laminae of clay and organic matter. A secondary component includes amphiprotic lamellar pyrite and very small amounts of calcite. No matrix porosity is visible.

Figure 24
Y028 (3780 ft)

High magnification (HP) thin-section photomicrograph of some silty shale found in O1. This compared clay-rich matrix contains well sorted, six sided detrital grains (quartz, mica, feldspar). Most of the detrital grains have a strong preferred grain orientation. The middle of the picture shows a continuous layer of clay minerals. Wavy laminae of dark colored organic matter are present throughout. No matrix porosity is visible.

Figure N3.

Y028 (5780 ft)

High magnification (PPL) thin-section photomicrograph of silty shale. This compacted, clay-rich matrix contains well sorted, silt size detrital grains (quartz, mica, feldspars). The quartz grains are spherical and subangular with some preferred grain orientation. The shale has well-developed laminations of clays and organic matter. Accessory components include authigenic framboidal pyrite and very small amounts of carbonate cement. No matrix porosity is visible.

Figure N4.

Y028 (5780 ft)

High magnification (PPL) thin-section photomicrograph of same silty shale pictured in O3. This compacted, clay-rich matrix contains well sorted, silt size detrital grains (quartz, mica, feldspars). Most of the detrital grains have a strong preferred grain orientation. The middle of this picture shows a continuous layer of clay minerals. Wispy laminations of dark colored organic matter are present throughout. No matrix porosity is evident.



Figure N3.



Figure N4.

Figure 22
YPLM (2769 B)

Low magnification (17X) thin-section photomicrograph of silt shale. The compact shale has a clay-rich matrix that contains well-sorted, silt size detrital grains (quartz, feldspar, mica). The components of the shale have a strong preferred grain orientation and well-developed imbrication. Accessory minerals include authigenic lamellar pyrite (small opaque nodules) and phosphate debris. No matrix porosity is detected.

Figure 26
YPLM (2769 B)

Medium magnification (39X) thin-section photomicrograph of same silt shale pictured in 155. In the center of the picture is preserved fish fossil. The large piece appears to be a cross-section of a bone. The matrix of the shale is well sorted with many laminae of organic matter. Matrix porosity is not evident.

Figure N5.

Y039 (5769 ft)

Low magnification (PPL) thin-section photomicrograph of silty shale. This compacted shale has a clay-rich matrix that contains well-sorted, silt size detrital grains (quartz, feldspar, mica). The components of this shale have a strong preferred grain orientation and well-developed laminations. Accessory minerals include authigenic framboidal pyrite (small opaque nodules) and phosphatic debris. No matrix porosity is detected.

Figure N6.

Y039 (5769 ft)

Medium magnification (PPL) thin-section photomicrograph of same silty shale pictured in O5. In the center of the picture is preserved fish fossils. The large piece appears to be a cross-section of a bone. The matrix of this shale is well sorted with wispy laminations of organic matter. Matrix porosity is not evident.



Figure N5.



Figure N6.

Figure 27.
Y044 (8704 ft)

Low magnification (10X) thin-section photomicrograph of silt shale. This well
compacted shale has a clay-rich matrix that contains well sorted, silty silt and clay grains
(quartz, feldspar, mica). Wavy laminations of organic matter and clay are prominent
throughout. A concentration of silt grains is in the upper left corner, and appears to be a
silt-filled burrow. Accessory minerals include subhedral hematite (small
opaque nodules) and phosphatic debris (bright orange high relief nodules). No matrix
porosity is observed.

Figure 28.
Y044 (8704 ft)

Low magnification (10X) thin-section photomicrograph of silt and clay shale. This
shale shows large scale alternating laminations of silt and clay, with smaller
wavy laminations of organic matter. Phosphatic material has been well preserved. No
matrix porosity is evident.

Figure N7.

Y044 (5764 ft)

Low magnification (PPL) thin-section photomicrograph of silty shale. This well compacted shale has a clay-rich matrix that contains well sorted, silt size detrital grains (quartz, feldspar, mica). Wispy laminations of organic matter and clays are prominent throughout. A concentration of silt grains is in the upper left corner, and appears to be a silt filled burrow. Accessory minerals include authigenic framboidal pyrite (small opaque nodules) and phosphatic debris (bright orange high relief nodules). No matrix porosity is detected.

Figure N8.

Y044 (5764 ft)

Low magnification (PPL) thin-section photomicrograph of same silty shale pictured in O7. This picture shows large scale alternating laminations of silt and clays, with smaller wispy laminations of organic matter. Phosphatic material has been well preserved. No matrix porosity is evident.



Figure N7.



Figure N9.

Figure 10
Y044 (2704 ft)

High magnification (PPL) thin section photomicrograph of some silty shale partings in O2 and O3. The picture shows large scale alternating laminae of silt and clay, with smaller scale laminae of organic matter. Muscovite debris has been well preserved in what appears to be a well filled pore that is typical of the laminae. No matrix porosity is evident.

Figure 11
Y044 (2704 ft)

High magnification (PPL) thin-section photomicrograph of some silty shale partings in O2, O3 and O4. The shale has been heavily compacted due to the strong preferred grain orientation of the detrital grains and well-developed laminae of clay and organic matter. No matrix porosity is evident.

Figure N9.

Y044 (5764 ft)

Medium magnification (PPL) thin-section photomicrograph of same silty shale pictured in O7 and O8. This picture shows large scale alternating laminations of silt and clays, with smaller wispy laminations of organic matter. Phosphatic debris has been well preserved in what appears to be a silt filled burrow that is oblique to the laminations. No matrix porosity is evident.

Figure N10.

Y044 (5764 ft)

High magnification (PPL) thin-section photomicrograph of same silty shale pictured in O7, O8, and O9. This shale has been heavily compacted due to the strong preferred grain orientation of the detrital grains and well-developed laminations of clays and organic matter. No matrix porosity is evident.

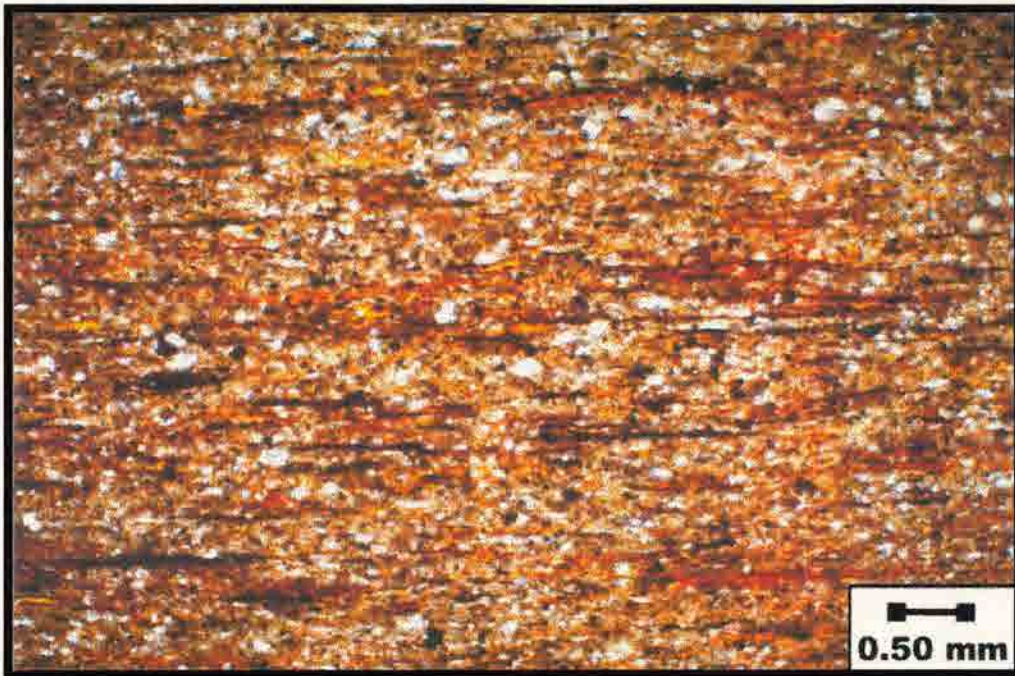


Figure N9.



Figure N10.

APPENDIX O

YOUNGS CORE
GRANEROS SHALE
MICP GRAPHS

MICP table for Youngs Core (Graneros shale)

Sample#	FT	Facies	Median PTD (micron)	Pore Volume %	Sorting Index
YO-000	5808	D	1	60	VW
			0.15	40	P
YO-004	5804	Z	0.0045	100	VW
YO-008	5800	Z	0.0055	70	VW
			0.015	30	M
YO-013	5795	Z	0.005	70	VW
			0.015	30	M
YO-018	5790	Z	0.0045	70	VW
			0.015	30	M
YO-023	5785	Z	0.0045	100	MW-W
YO-028	5780	Z	0.0045	100	MW-W
YO-033	5775	Z	0.006	100	MW-W
YO-039	5769	Z	0.006	100	MW-W
YO-044	5764	Z	0.007	100	MW-W

LEGEND:

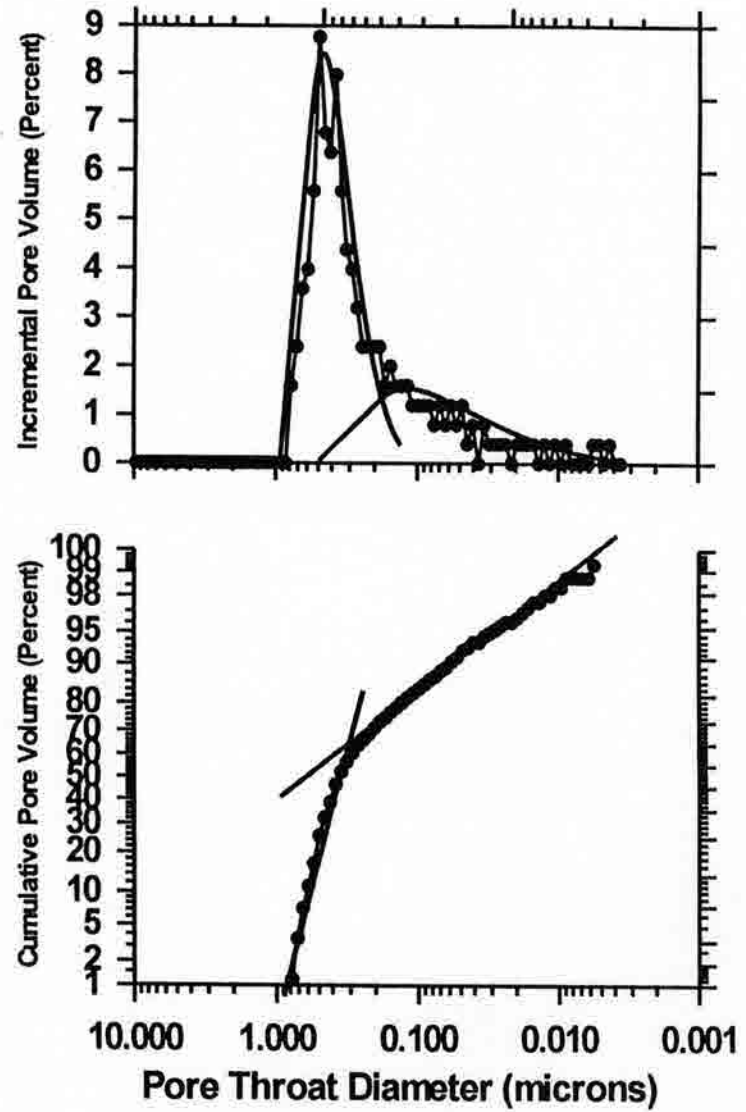
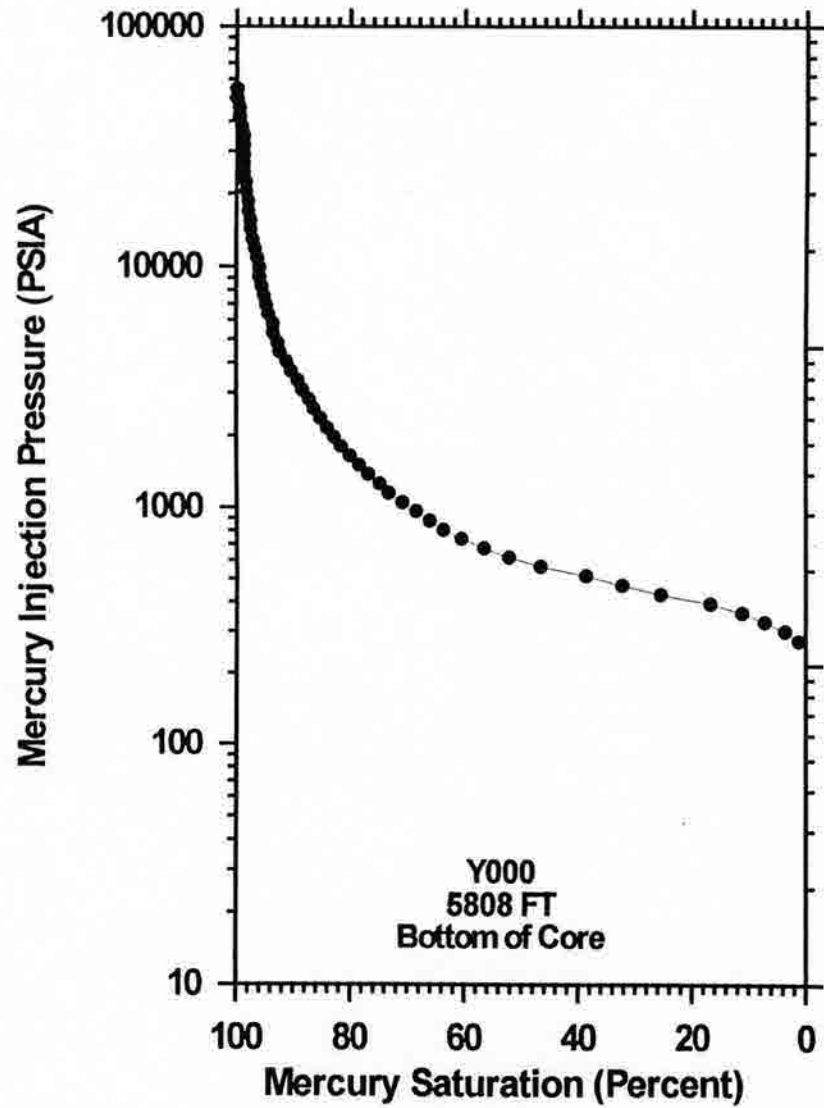
VW= Very Well sorted

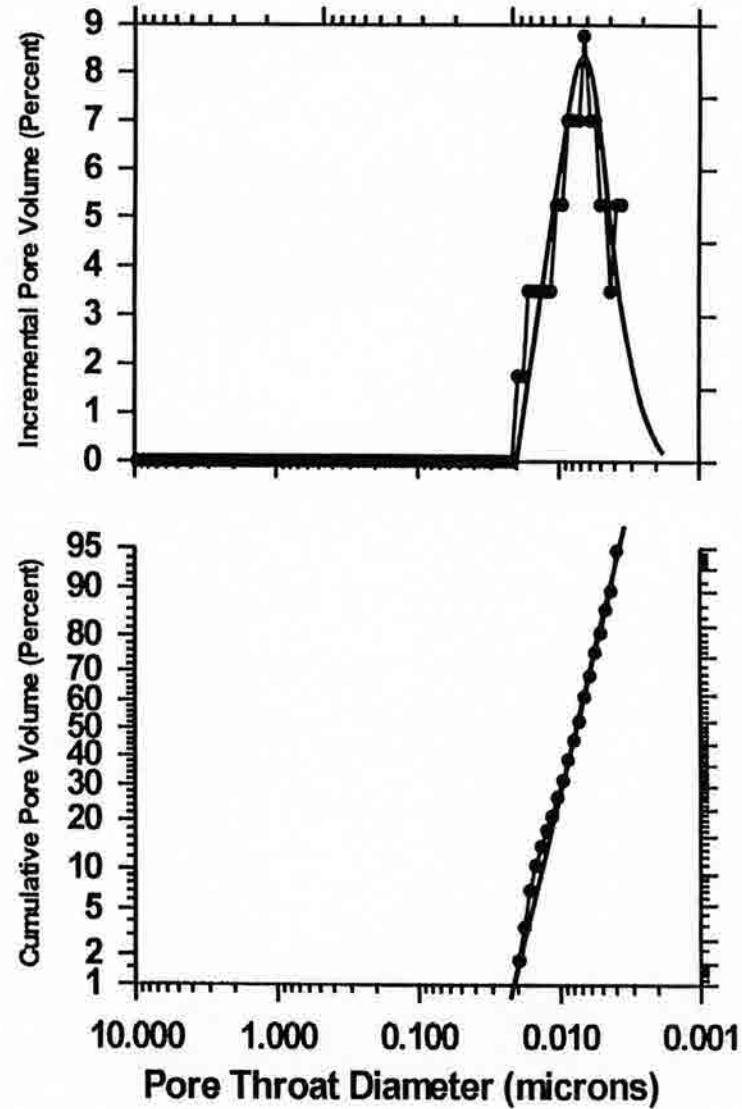
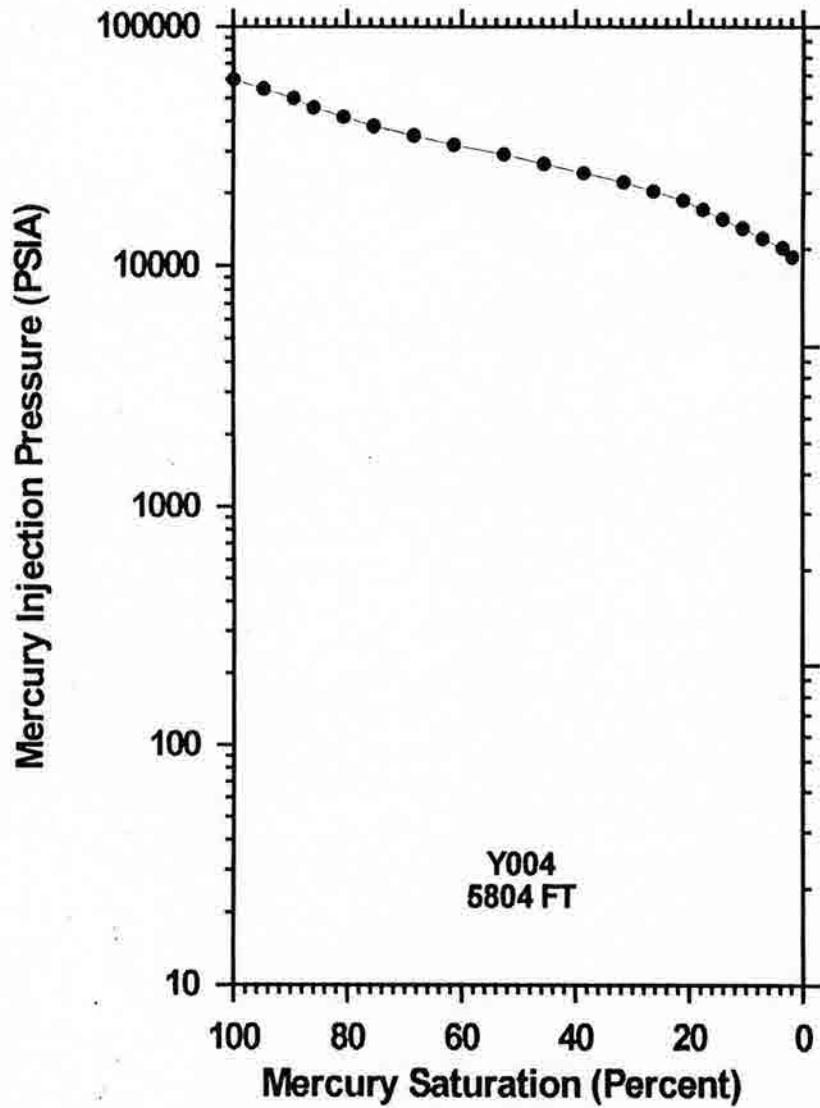
W= Well sorted

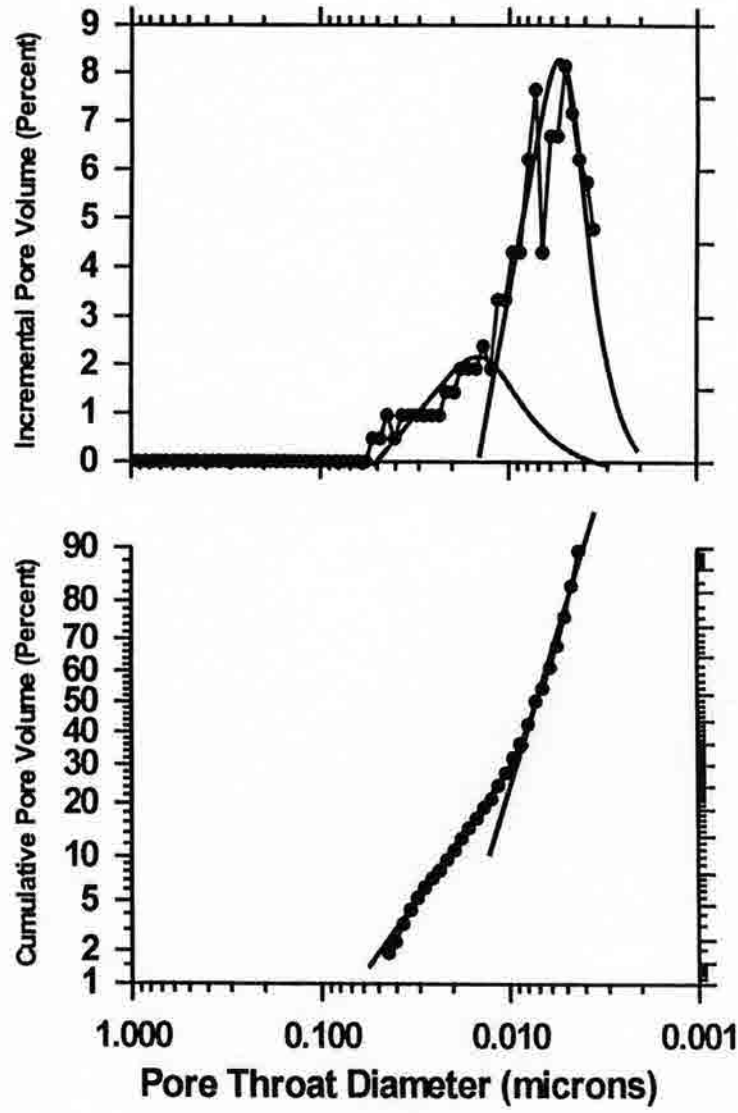
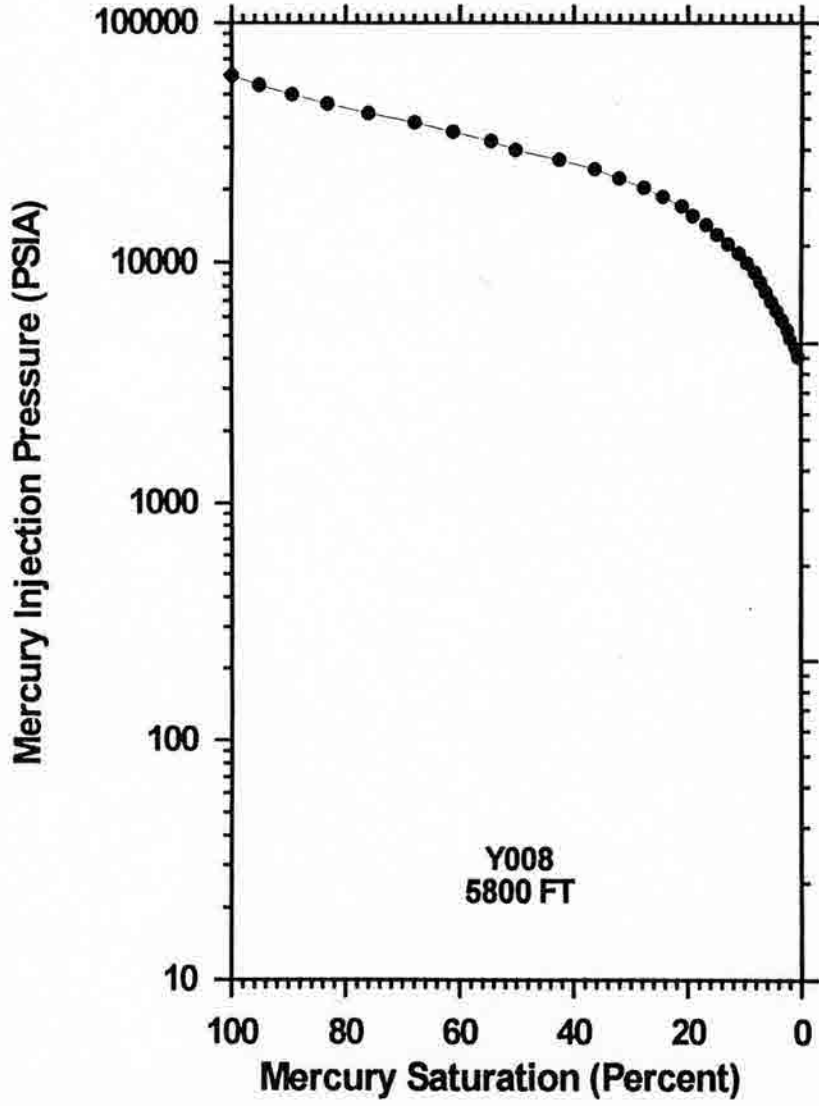
MW= Moderately-well sorted

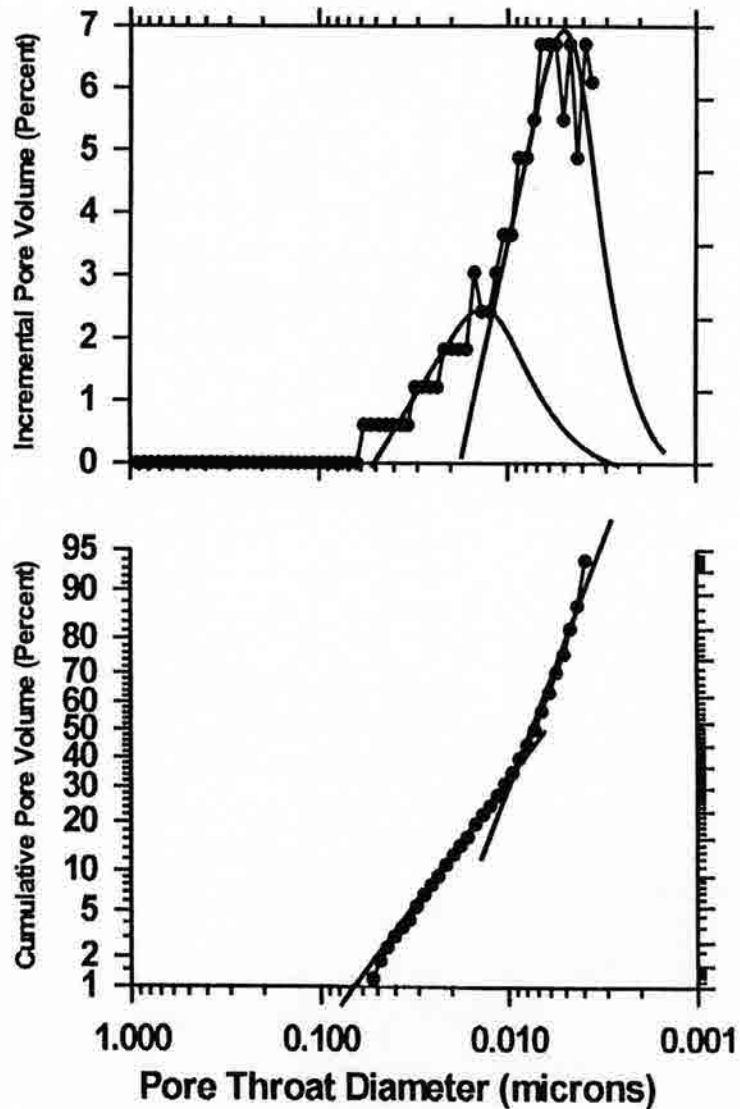
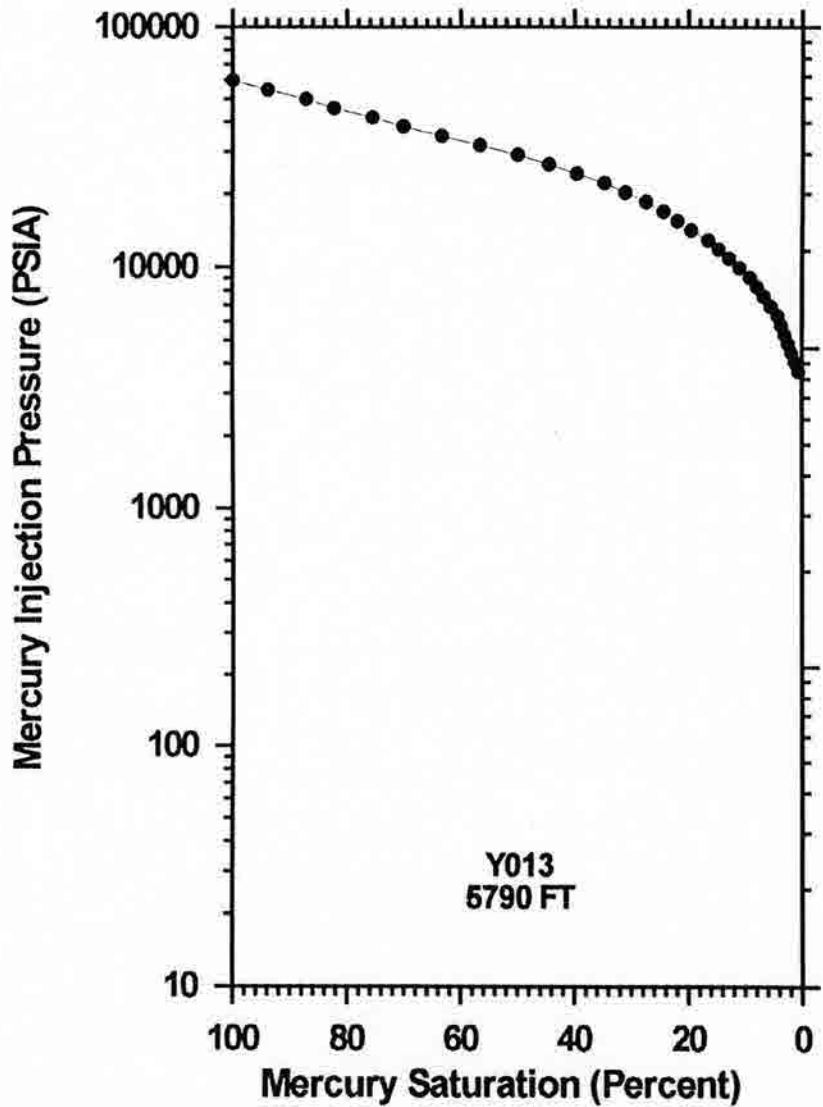
M= Moderately sorted

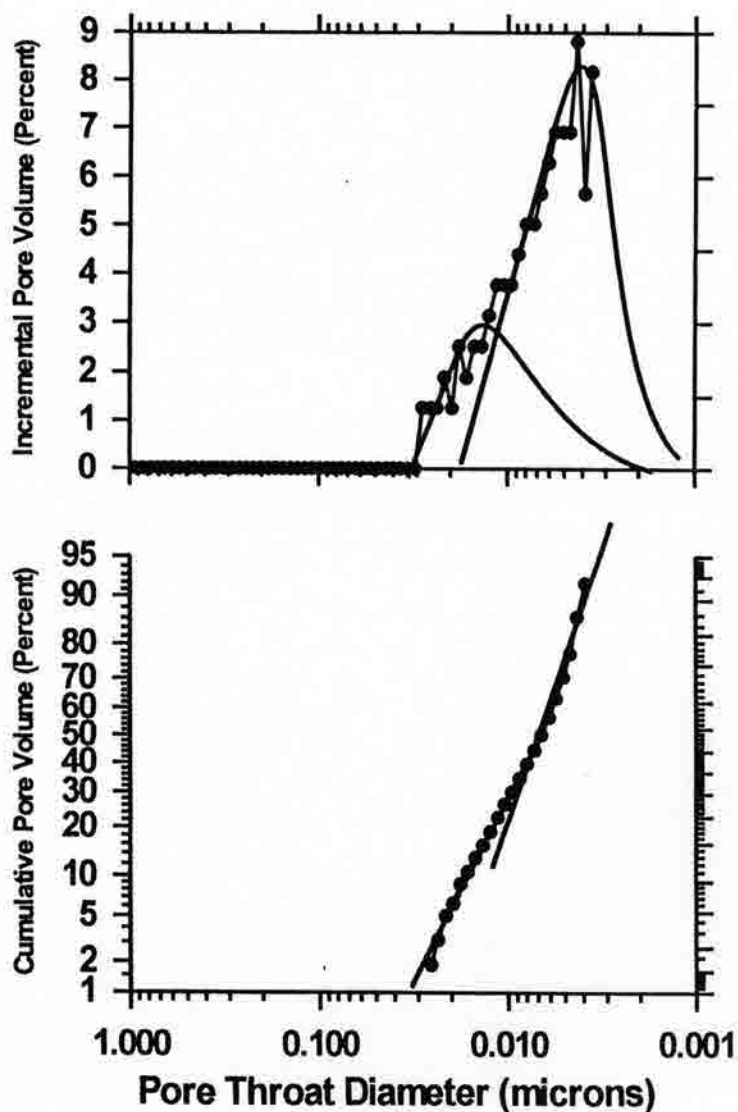
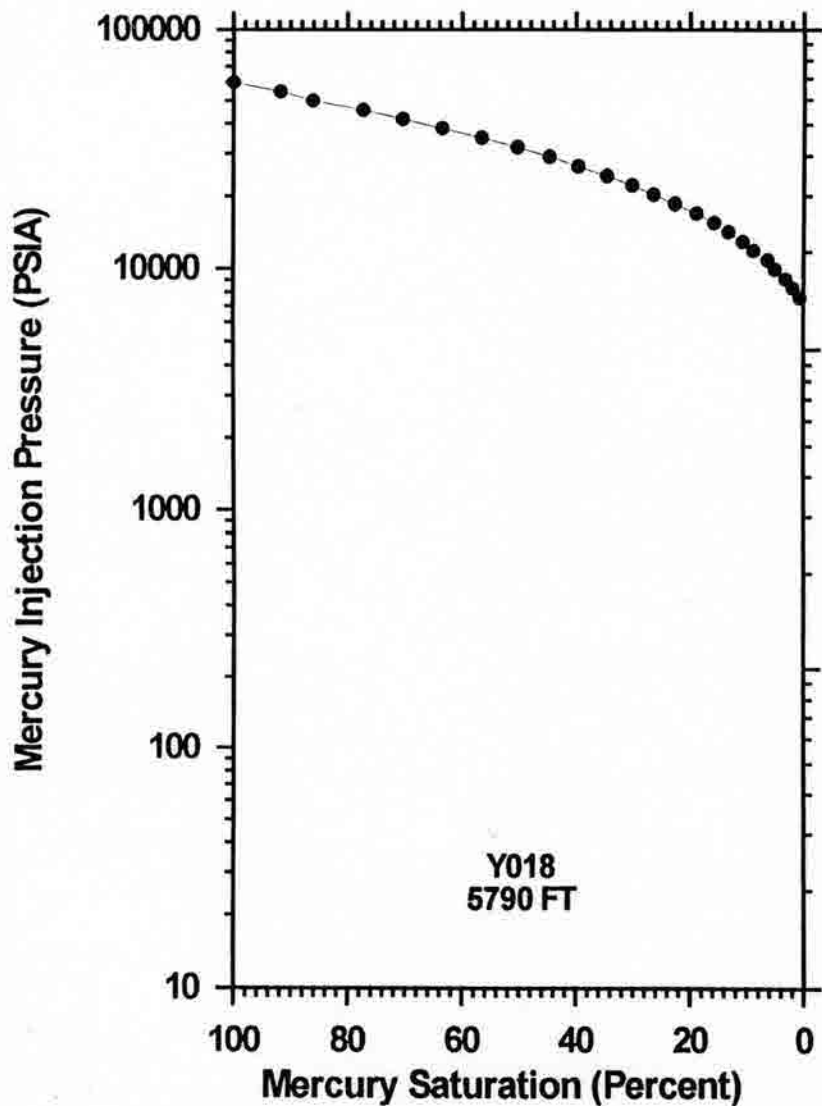
P= Poorly sorted



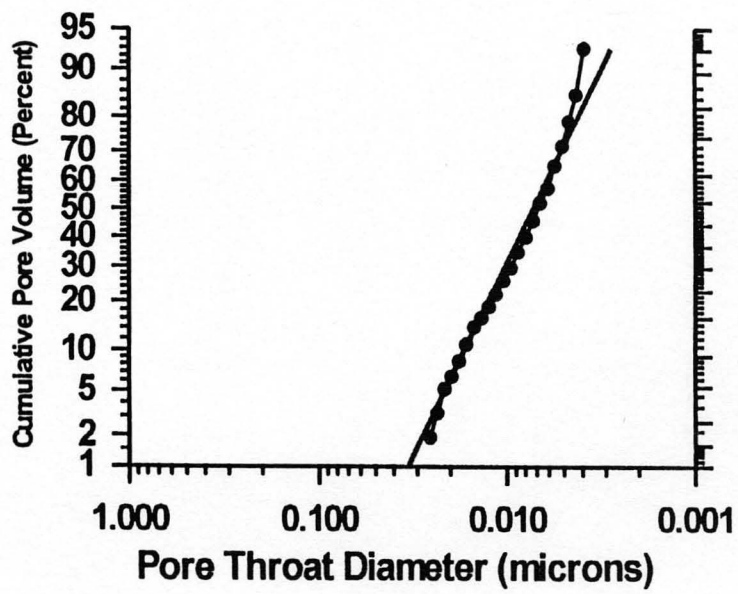
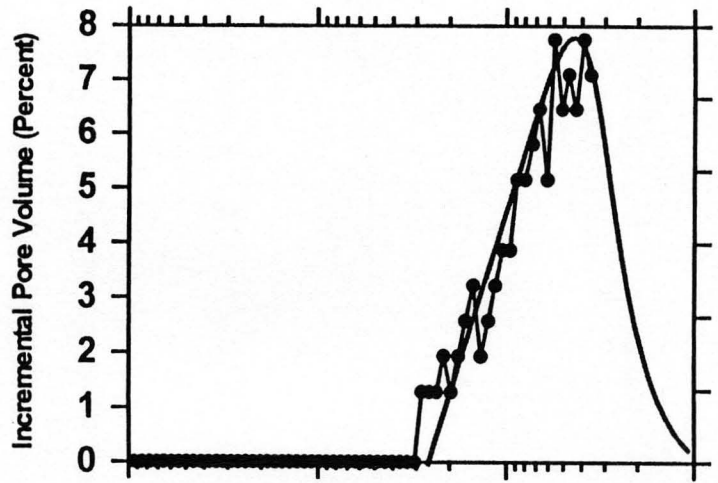
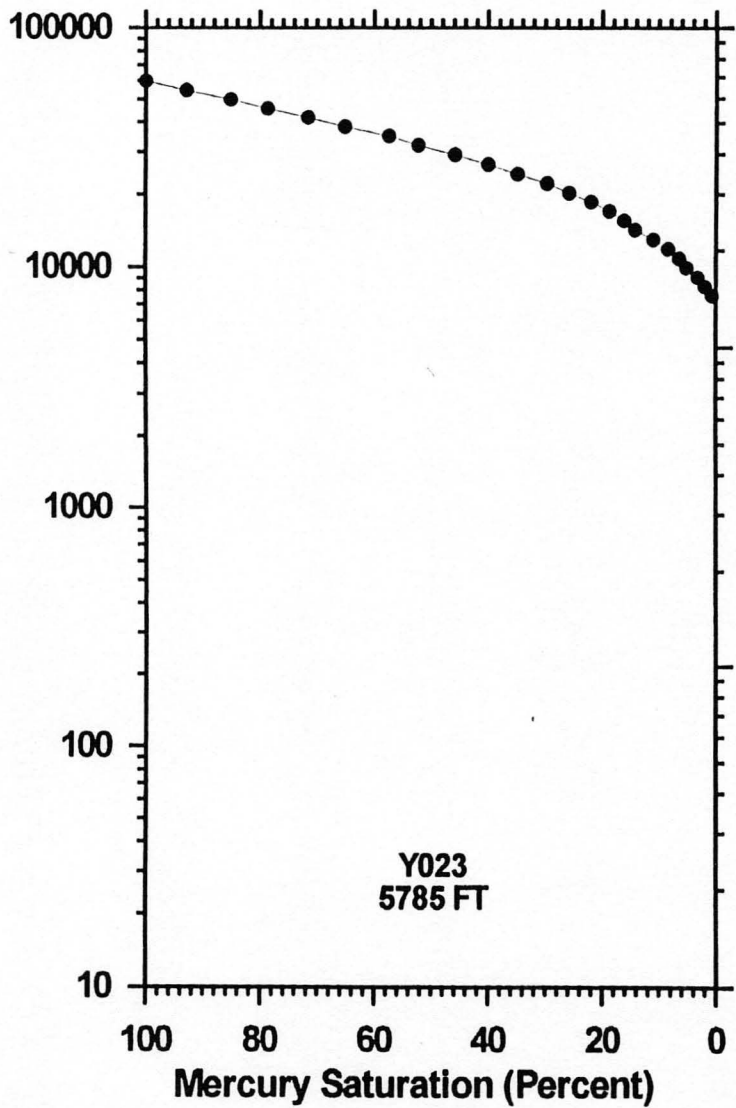




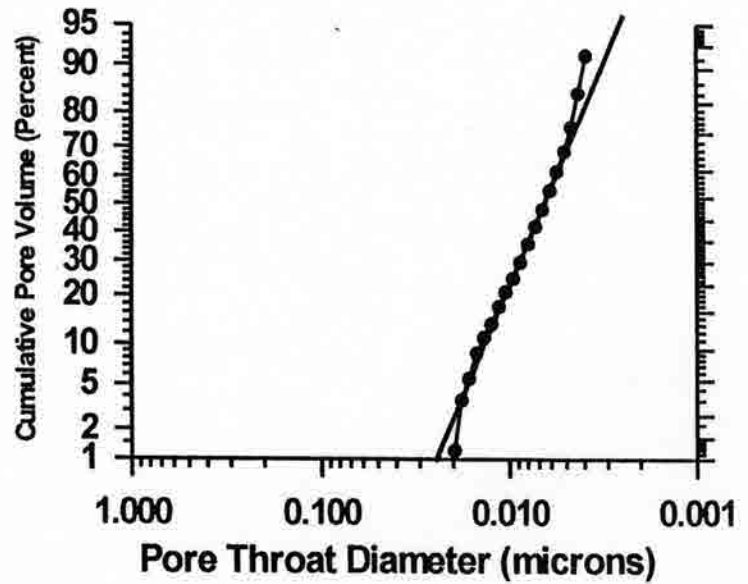
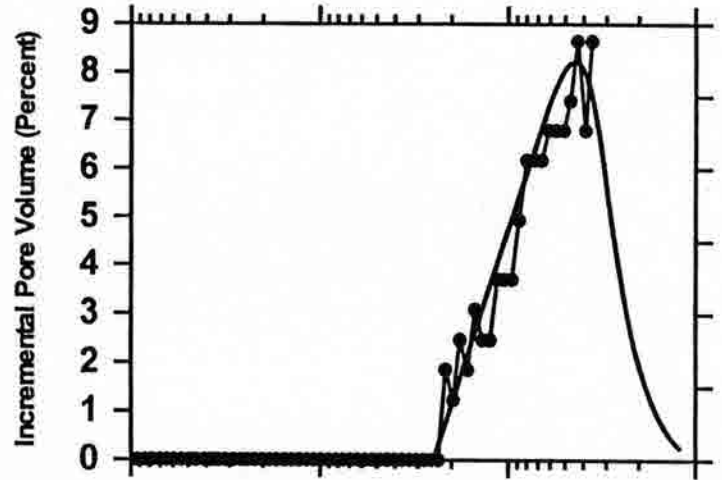
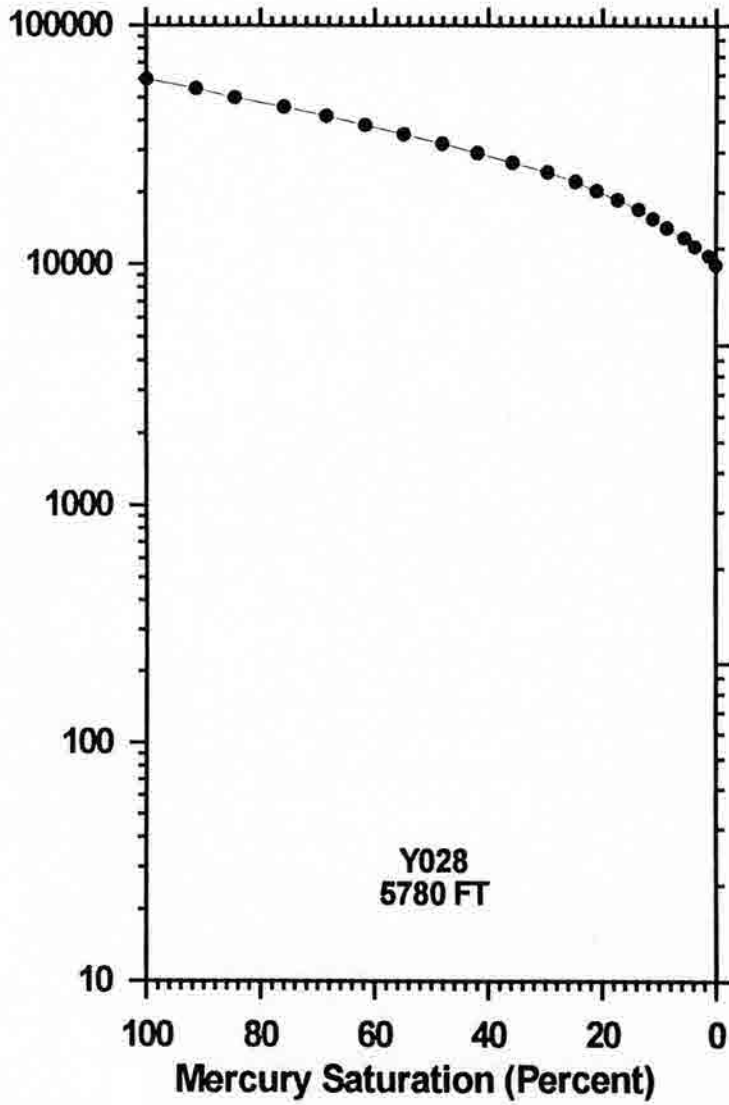


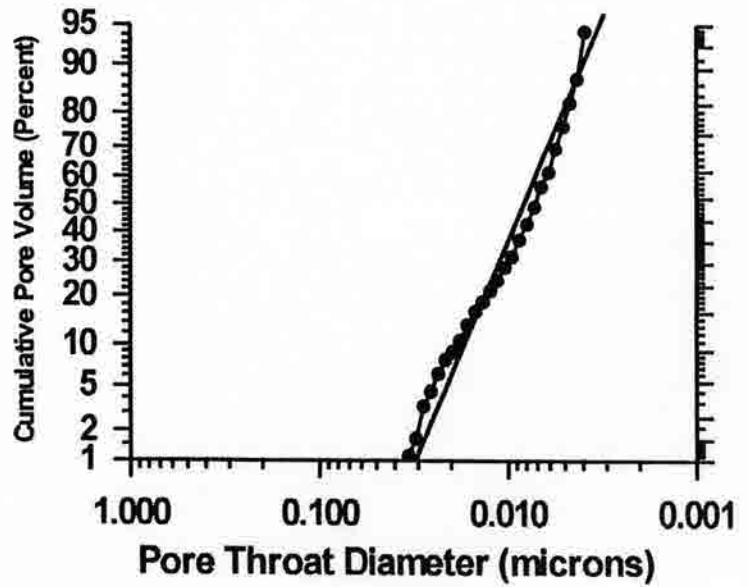
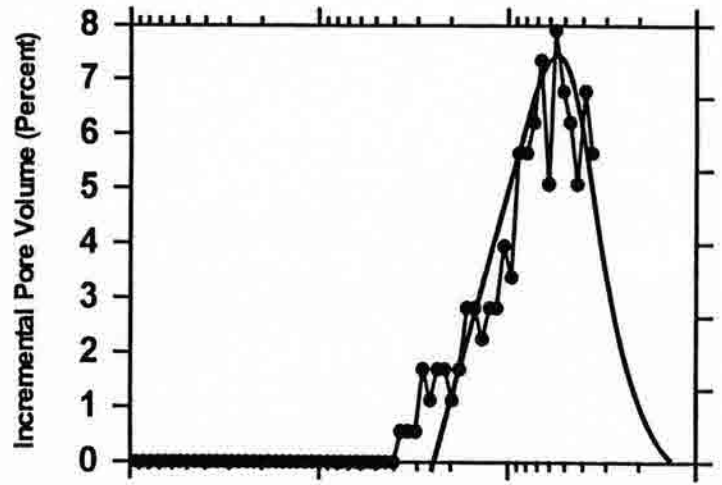
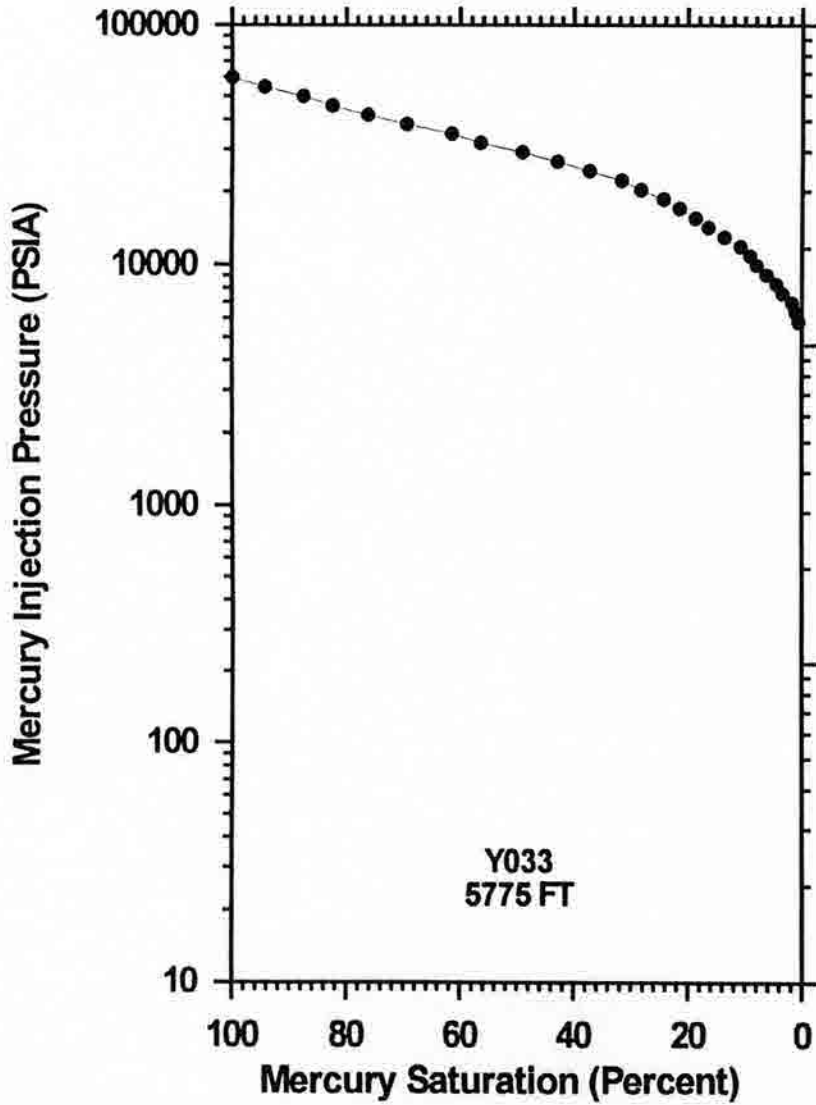


Mercury Injection Pressure (PSIA)

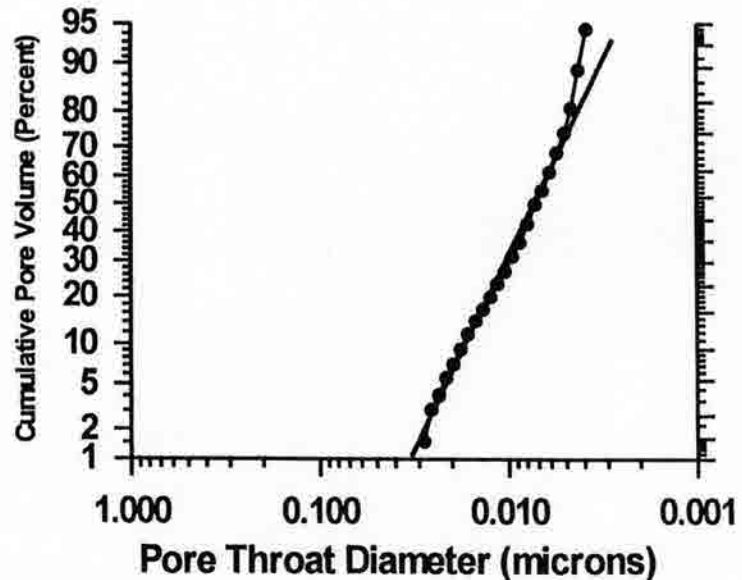
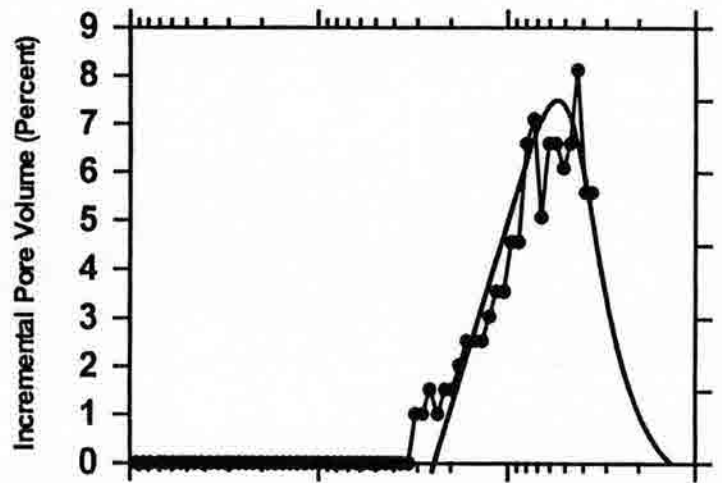
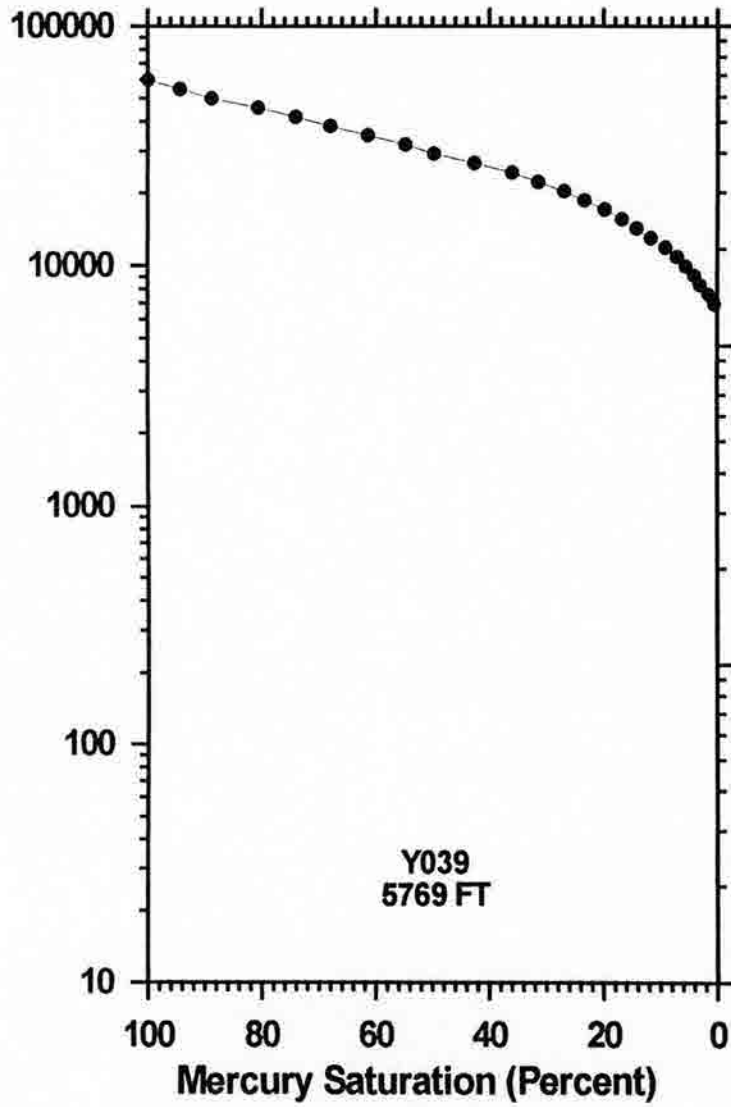


Mercury Injection Pressure (PSIA)

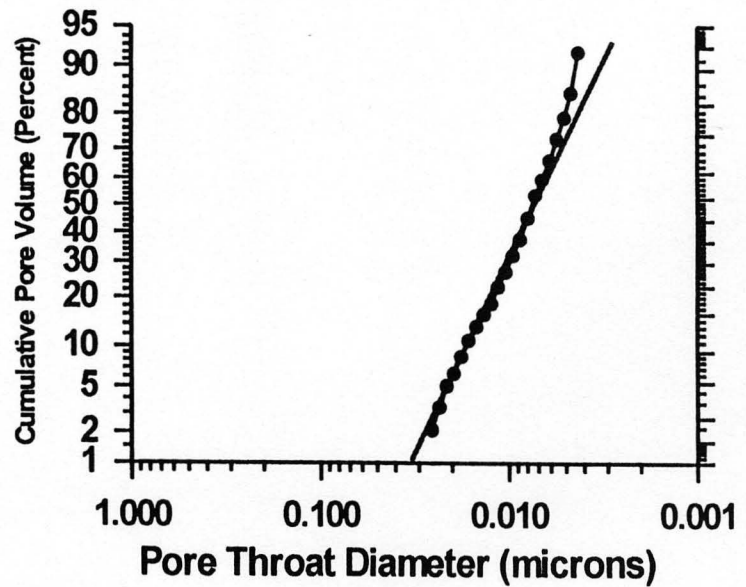
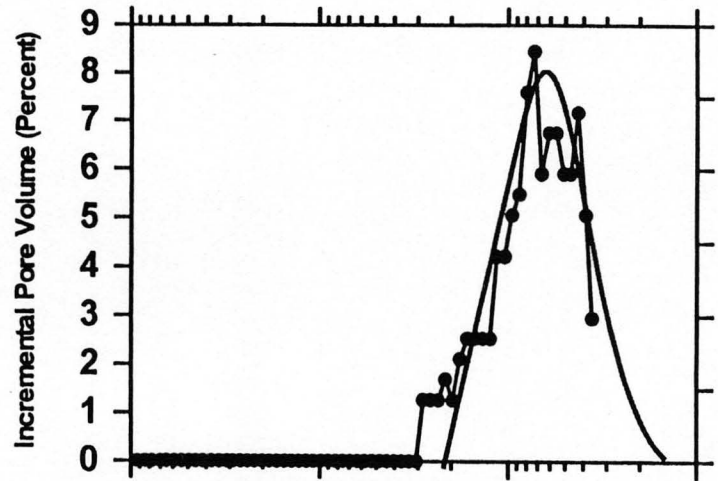
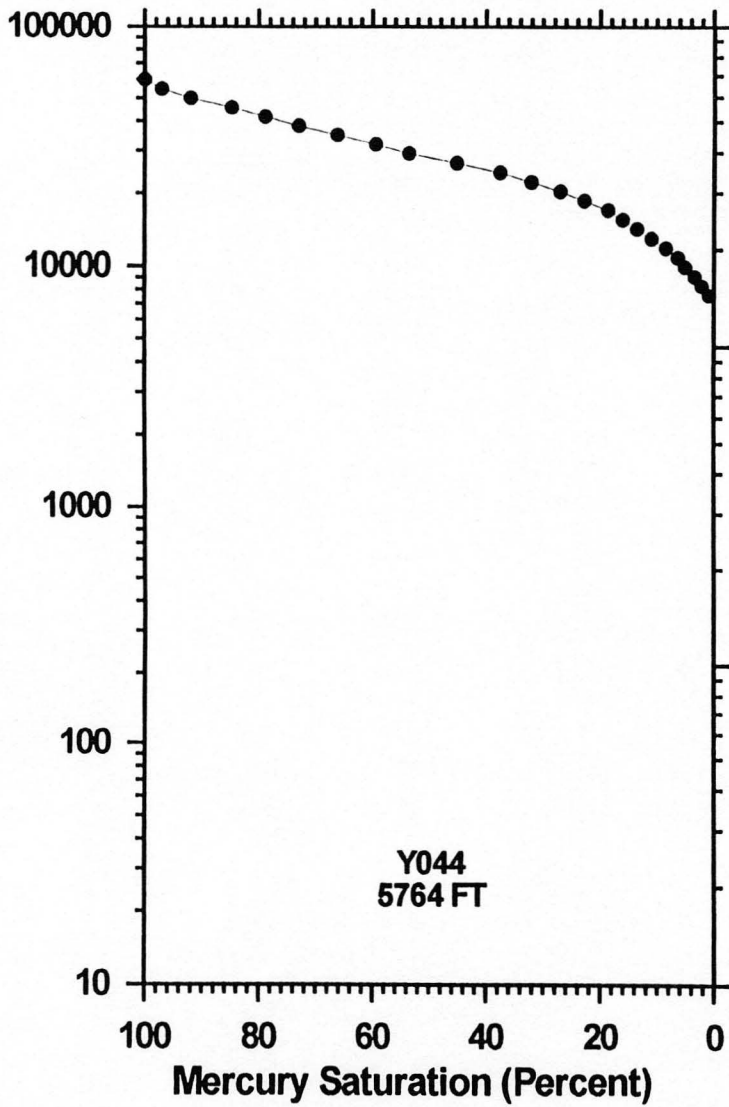




Mercury Injection Pressure (PSIA)



Mercury Injection Pressure (PSIA)



APPENDIX P

SKULL CREEK AND

GRANEROS SHALE

ORGANIC GEOCHEMISTRY

SOLDIER CANYON DAM OUTCROP, COLORADO

Total Organic Carbon and Rock Eval Pyrolysis

SOURCE QUALITY										THERMAL MATURITY	
Facies	Sample Number	Height (ft)	Total Organic Carbon	Generated (Free) Hydrocarbons	Generated Hydrocarbons	Total Hydrocarbon Generation Potential	Hydrogen Enrichment Index	Generatable Carbon Dioxide	Oxygen Enrichment Index	Transformation Ratio	Temp. of peak S2
			TOC (%)	S1 (mg HC/g rk)	S2 (mg HC/g rk)	S1 + S2 (mg HC/g rk)	HI (mg HC/g TOC)	S3 (mg CO2/g rk)	OI (mg CO2/g TOC)	"PI" (S1 / S1+S2)	Tmax (°C)
	BSC-000	0	1.09	0.07	0.14	0.21	13	0.72	66	0.33	435
	BSC-001	14	0.50	0.07	0.03	0.1	6	0.54	108	0.70	447
	BSC-002	16	0.55	0.05	0.02	0.07	4	0.41	75	0.71	324
	BSC-003	18	0.60	0.07	0.03	0.1	5	0.45	75	0.70	364
	BSC-004	20	0.49	0.04	0.02	0.06	4	0.36	73	0.67	324
	BSC-005	22	0.44	0.05	0.01	0.06	2	0.26	59	0.83	303
	BSC-006	24	0.37	0.02	0	0.02	0	0.31	84	1.00	426
	BSC-007	26	0.29	0.01	0.01	0.02	3	0.33	114	0.50	402
	BSC-008	28	0.85	0.04	0.03	0.07	4	0.49	58	0.57	321
	BSC-009	30	0.71	0.05	0.03	0.08	4	0.51	72	0.63	340
K	BSC-010	32	0.50	0.05	0	0.05	0	0.21	42	1.00	279
	BSC-011	34	0.52	0.02	0.02	0.04	4	0.26	50	0.50	364
	BSC-012	36	0.50	0.02	0	0.02	0	0.26	52	1.00	277
	BSC-013	38	0.38	0.02	0.03	0.05	8	0.32	84	0.40	347
	BSC-014	40	0.42	0.02	0.01	0.03	2	0.17	40	0.67	316
	BSC-015	42	0.46	0.04	0.02	0.06	4	0.22	48	0.67	279
	BSC-016	44	0.29	0.03	0.02	0.05	7	0.3	103	0.60	279
	BSC-017	46	0.59	0.07	0.01	0.08	2	0.41	69	0.88	319
	BSC-018	48	0.56	0.05	0.01	0.06	2	0.41	73	0.83	304
	SC-001	51	0.97	0.03	0.53	0.56	55	0.4	41	0.05	436
	SC-002	52	1.19	0.1	0.45	0.55	38	0.33	28	0.18	438

SOURCE QUALITY										THERMAL MATURITY	
Facies	Sample Number	Height (ft)	Total Organic Carbon	Generated (Free) Hydrocarbons	Generated Hydrocarbons	Total Hydrocarbon Generation Potential	Hydrogen Enrichment Index	Generatable Carbon Dioxide	Oxygen Enrichment Index	Transformation Ratio	Temp. of peak S2
			TOC (%)	S1 (mg HC/g rk)	S2 (mg HC/g rk)	S1 + S2 (mg HC/g rk)	HI (mg HC/g TOC)	S3 (mg CO2/g rk)	OI (mg CO2/g TOC)	"PI" (S1 / S1+S2)	Tmax (°C)
K	SC-003	53	1.64	0.09	0.94	1.03	57	0.4	24	0.09	435
	SC-004	54	1.79	0.18	1.88	2.06	105	0.56	31	0.09	437
	SC-005	55	1.17	0.04	0.64	0.68	55	0.46	39	0.06	437
	SC-006	56	1.06	0.03	0.54	0.57	51	0.45	42	0.05	436
	SC-007	57	1.04	0.04	0.63	0.67	61	0.43	41	0.06	435
	SC-008	58	0.56	0.01	0.14	0.15	25	0.22	39	0.07	443
A	SC-009	59	0.60	0.03	0.06	0.09	10	0.11	18	0.33	404
	SC-010	60	0.00	0	0	0		0			0
	SC-011	61	2.05	0.26	2.19	2.45	107	0	0	0.11	440
	SC-012	62	1.26	0.11	0.71	0.82	56	0.46	37	0.13	444
	SC-013	63	1.27	0.11	0.88	0.99	69	0	0	0.11	439
	SC-014	64	1.59	0.1	0.92	1.02	58	0	0	0.10	438
B	SC-015	65	0.43	0.15	1.4	1.55	326	0	0	0.10	437
	SC-016	66	1.80	0.03	0.18	0.21	10	0	0	0.14	442
	SC-017	67	2.00	0.12	1.77	1.89	89	0	0	0.06	439
	SC-018	68	0.69	0.03	0.26	0.29	38	0.29	42	0.10	441
	SC-019	69	1.19	0.07	0.8	0.87	67	0	0	0.08	439
	SC-020	70	0.64	0.1	0.32	0.42	50	0.6	94	0.24	437
	SC-021	71	0.87	0.07	0.54	0.61	62	0.53	61	0.11	436
	SC-022	72	1.11	0.1	0.8	0.9	72	1.03	93	0.11	436
	SC-023	73	1.68	0.17	1.3	1.47	77	0.88	52	0.12	434
	SC-024	74	0.47	0.06	0.1	0.16	21	0.5	106	0.38	444
	SC-025	75	0.29	0.04	0.05	0.09	17	0.26	90	0.44	407
	SC-026	76	0.40	0.03	0.04	0.07	10	0.62	155	0.43	385
	SC-027	77	0.42	0.11	0.12	0.23	29	0.57	136	0.48	435

SOURCE QUALITY										THERMAL MATURITY	
Facies	Sample Number	Height (ft)	Total Organic Carbon	Generated (Free) Hydrocarbons	Generated Hydrocarbons	Total Hydrocarbon Generation Potential	Hydrogen Enrichment Index	Generatable Carbon Dioxide	Oxygen Enrichment Index	Transformation Ratio	Temp. of peak S2
			TOC (%)	S1 (mg HC/g rk)	S2 (mg HC/g rk)	S1 + S2 (mg HC/g rk)	HI (mg HC/g TOC)	S3 (mg CO2/g rk)	OI (mg CO2/g TOC)	"PI" (S1 / S1+S2)	Tmax (°C)
B	SC-028	78	0.40	0.05	0.12	0.17	30	0.36	90	0.29	441
	SC-029	79	0.37	0.11	0.09	0.2	24	0.37	100	0.55	442
	SC-030	80	0.21	0.02	0	0.02	0	0.24	114	1.00	428
C	SC-031	82	0.34	0	0.03	0.03	9	0.07	21	0.00	425
	SC-032	84	0.22	0.01	0.06	0.07	27	0.13	59	0.14	395
	SC-033	86	0.25	0	0.01	0.01	4	0.13	52	0.00	277
	SC-034	88	0.27	0.01	0.04	0.05	15	0.1	37	0.20	374
	SC-035	90	0.42	0.01	0.02	0.03	5	0.15	36	0.33	431
	SC-036	92	0.37	0.02	0.12	0.14	32	0.09	24	0.14	449
	SC-037	94	0.42	0	0.06	0.06	14	0.04	10	0.00	385
	SC-038	96	0.29	0.01	0.07	0.08	24	0.18	62	0.13	401
	SC-039	98	0.00	0	0.04	0.04	1140	0.01	285	0.00	350
	SC-040	100	0.27	0.01	0.07	0.08	26	0.18	68	0.13	401
	SC-041	102	0.26	0.01	0	0.01	0	0.14	54	1.00	274
	SC-042	104	0.26	0.01	0.02	0.03	8	0.16	62	0.33	321
	SC-043	124	0.36	0	0.04	0.04	11	0.11	31	0.00	353
	SC-044	126	0.38	0	0.04	0.04	11	0.13	34	0.00	369
	SC-045	128	0.48	0.01	0.11	0.12	23	0.2	42	0.08	451
	SC-046	130	0.38	0	0.08	0.08	21	0.16	42	0.00	410
	SC-047	132	0.49	0.02	0.18	0.2	37	0.24	49	0.10	474
	SC-048	134	0.36	0.01	0.05	0.06	14	0.15	42	0.17	380
	SC-049	136	0.34	0	0.02	0.02	6	0.25	74	0.00	449
	SC-050	138	0.35	0	0.06	0.06	17	0.14	40	0.00	449
SC-051	140	0.39	0.01	0.04	0.05	10	0.17	44	0.20	333	
SC-052	142	0.74	0.06	0.36	0.42	49	0.3	41	0.14	440	

SOURCE QUALITY										THERMAL MATURITY	
Facies	Sample Number	Height (ft)	Total Organic Carbon	Generated (Free) Hydrocarbons	Generated Hydrocarbons	Total Hydrocarbon Generation Potential	Hydrogen Enrichment Index	Generatable Carbon Dioxide	Oxygen Enrichment Index	Transformation Ratio	Temp. of peak S2
			TOC (%)	S1 (mg HC/g rk)	S2 (mg HC/g rk)	S1 + S2 (mg HC/g rk)	HI (mg HC/g TOC)	S3 (mg CO2/g rk)	OI (mg CO2/g TOC)	"PI" (S1 / S1+S2)	Tmax (°C)
C	SC-053	144	0.38	0.02	0.03	0.05	8	0.15	39	0.40	450
	SC-054	146	0.37	0	0.49	0.49	132	0.22	59	0.00	491
	SC-055	148	0.36	0.01	0.06	0.07	17	0.19	53	0.14	372
	SC-056	150	0.31	0	0.09	0.09	29	0.14	45	0.00	387
	SC-057	152	0.29	0.03	0.06	0.09	21	0.2	69	0.33	472
	SC-058	154	0.28	0.01	0	0.01	0	0.25	89	1.00	420
Horizontal Samples of A (CS)	SCCS-1	West 40'	2.32	0.35	2.50	2.85	108	0.66	28	0.12	433
	SCCS-2	West 30'	2.83	0.43	3.36	3.79	119	0.80	28	0.11	433
	SCCS-3	West 20'	2.45	0.55	5.10	5.65	208	0.83	34	0.10	433
	SCCS-4	West 10'	2.02								
	SCCS-5	East 10'	2.47	0.31	2.35	2.66	95	0.66	27	0.12	434
	SCCS-6	East 20'	2.23	0.42	3.58	4.00	161	0.69	31	0.11	433

- F "Fair" Hydrocarbon Generation Potential ($6 > S1+S2 > 5$ mg HC/g rock)
G "Good" Hydrocarbon Generation Potential ($10 > S1+S2 > 6$ mg HC/g rock)
VG "Very Good" Hydrocarbon Generation Potential ($20 > S1+S2 > 10$ mg HC/g rock)
Ex "Excellent" Hydrocarbon Generation Potential ($S1+S2 > 20$ mg HC/g rock)

BELLEVUE OUTCROP, COLORADO
Total Organic Carbon and Rock Eval Pyrolysis

			SOURCE QUALITY						THERMAL MATURITY		
Facies	Sample Number	Height (ft)	Total Organic Carbon	Generated (Free) Hydrocarbons	Generated HC	Total Hydrocarbon Generation Potential	Hydrogen Enrichment Index	Generatable Carbon Dioxide	Oxygen Enrichment Index	Transformation Ratio	Temp. of peak S2
			TOC (%)	S1 (mg HC/g rk)	S2 (mg HC/g rk)	S1 + S2 (mg HC/g rk)	HI (mg HC/g TOC)	S3 (mg CO2/g rk)	OI (mg CO2/g TOC)	"PI" (S1/S1+S2)	Tmax (°C)
	JY-000	0	0.88	0.02	0.04	0.02	5	0.56	64	0.33	451
	JY-001	1	0.91	0.06	0.12	0.1	13	0.72	79	0.33	444
	JY-002	2	0.86	0.04	0.05	0.09	6	0.56	65	0.44	438
	JY-003	3	0.85	0.05	0.05	0.09	6	0.72	85	0.50	405
	JY-004	4	0.86	0.04	0.04	0.08	5	0.59	69	0.50	400
	JY-005	5	0.65	0.04	0.03	0.1	5	0.81	125	0.57	368
	JY-006	6	0.84	0.06	0.14	0.12	17	0.77	92	0.30	437
	JY-007	7	1.00	0.06	0.24	0.11	24	1.08	108	0.20	434
	JY-008	8	1.11	0.05	0.22	0.12	20	0.94	85	0.19	435
	JY-009	9	1.16	0.07	0.34	0.11	29	1.15	99	0.17	436
	JY-010	10	0.55	0.04	0.03	0.08	5	0.93	169	0.57	452
K	JY-011	11	0.58	0.04	0.04	0.08	7	0.66	114	0.50	393
	JY-012	12	0.65	0.04	0.03	0.07	5	0.72	111	0.57	368
	JY-013	13	0.60	0.03	0.05	0.07	8	0.69	115	0.38	423
	JY-014	14	0.75	0.04	0.06	0.09	8	0.82	109	0.40	414
	JY-015	15	0.63	0.05	0.04	0.09	6	0.92	146	0.56	388
	JY-016	16	0.59	0.04	0.03	0.07	5	0.49	83	0.57	347
	JY-017	17	0.70	0.03	0.05	0.03	7	0.49	70	0.38	412
	JY-018	18	0.54	0	0.02	0.05	4	0.48	90	0.00	303
	JY-019	19	0.46	0.05	0.02	0.09	4	0.51	111	0.71	331
	JY-020	20	0.65	0.04	0.03	0.05	5	0.64	98	0.57	342

			SOURCE QUALITY						THERMAL MATURITY		
Facies	Sample Number	Height (ft)	Total Organic Carbon	Generated (Free) Hydrocarbons	Generated HC	Total Hydrocarbon Generation Potential	Hydrogen Enrichment Index	Generatable Carbon Dioxide	Oxygen Enrichment Index	Transformation Ratio	Temp. of peak S2
			TOC (%)	S1 (mg HC/g rk)	S2 (mg HC/g rk)	S1 + S2 (mg HC/g rk)	HI (mg HC/g TOC)	S3 (mg CO2/g rk)	OI (mg CO2/g TOC)	"PI" (S1/S1+S2)	Tmax (°C)
	JY-021	21	0.57	0.01	0.02	0.03	4	0.73	128	0.33	426
	JY-022	22	0.54	0.02	0.06	0.04	11	0.66	122	0.25	330
	JY-023	23	0.50	0.02	0.11	0.04	22	0.78	156	0.15	384
	JY-024	24	0.61	0.02	0.16	0.03	26	0.8	131	0.11	428
	JY-025	25	0.94	0.01	0.12	0.03	13	0.78	83	0.08	435
	JY-026	26	0.64	0.02	0.1	0.05	16	1.04	163	0.17	437
	JY-027	27	0.73	0.03	0.12	0.06	16	0.86	118	0.20	431
	JY-028	28	0.85	0.03	0.26	0.05	31	0.88	104	0.10	437
	JY-029	29	0.90	0.02	0.14	0.03	16	0.72	80	0.13	435
	JY-030	30	0.77	0.01	0.09	0.04	12	0.45	58	0.10	432
	JY-031	31	0.67	0.03	0.06	0.04	9	0.53	79	0.33	438
	JY-032	32	0.73	0.01	0.06	0.03	8	0.32	44	0.14	438
	JY-033	33	0.52	0.02	0.03	0.06	6	0.57	110	0.40	347
K	JY-034	34	0.74	0.04	0.42	0.06	57	0	0	0.09	438
	JY-035	35	0.64	0.02	0.05	0.05	8	0.48	75	0.29	444
	JY-036	36	0.76	0.03	0.13	0.06	17	0.48	63	0.19	439
	JY-037	37	1.10	0.03	0.14	0.1	13	0.83	75	0.18	434
	JY-038	38	1.69	0.07	1.22	0.08	72	0.77	46	0.05	431
	JY-039	39	0.64	0.01	0.04	0.04	6	0.54	84	0.20	437
	JY-040	40	1.30	0.03	0.37	0.13	28	0.64	49	0.08	434
	JY-041	41	1.23	0.1	0.26	0.13	21	0.71	58	0.28	434
	JY-042	42	0.11	0.03	0	0.03	0	0.21	191	1.00	418
	JY-043	43	0.00	0	0	0.13		0			0
	JY-044	44	1.97	0.13	1.93	0.32	98	1.05	53	0.06	435
	JYC-000	44	0.17	0.05	0	0.15	0	0.17	103	1.00	278

			SOURCE QUALITY						THERMAL MATURITY		
Facies	Sample Number	Height (ft)	Total Organic Carbon	Generated (Free) Hydrocarbons	Generated HC	Total Hydrocarbon Generation Potential	Hydrogen Enrichment Index	Generatable Carbon Dioxide	Oxygen Enrichment Index	Transformation Ratio	Temp. of peak S2
			TOC (%)	S1 (mg HC/g rk)	S2 (mg HC/g rk)	S1 + S2 (mg HC/g rk)	HI (mg HC/g TOC)	S3 (mg CO2/g rk)	OI (mg CO2/g TOC)	"PI" (S1/S1+S2)	Tmax (°C)
K	JYC-001	45	1.50	0.1	0.7	0.18	47	1.59	106	0.13	433
	JYC-002	46	1.61	0.08	0.7	0.15	43	1.39	86	0.10	439
	JYC-003	47	1.31	0.07	0.6	0.14	46	0.75	57	0.10	437
	JYC-004	48	1.35	0.07	0.85	0.11	63	0.58	43	0.08	437
	JYC-005	49	1.19	0.04	0.84	0.27	71	0.5	42	0.05	441
A	JYC-006	50	2.65	0.23	4.5	0.57	170	1	38	0.05	437
	JYC-007	51	2.40	0.34	3.82	0.82	159	0.81	34	0.08	433
	JYC-008	52	3.24	0.48	4.95	0.79	153	1.05	32	0.09	434
	JYC-009	53	3.39	0.31	4.64	0.69	137	1.52	45	0.06	436
	JYC-010	54	2.81	0.38	3.75	0.51	133	0.87	31	0.09	434
B	JYC-011	55	1.75	0.13	0.98	0.19	56	0.76	43	0.12	436
	JYC-012	56	1.58	0.06	0.76	0.12	48	0.74	47	0.07	438
	JYC-013	57	1.53	0.06	0.86	0.12	56	0.75	49	0.07	437
	JYC-014	58	1.50	0.06	0.85	0.28	57	0.52	35	0.07	437
	JYC-015	59	1.39	0.22	0.75	0.26	54	0.77	55	0.23	439
	JYC-016	60	1.26	0.04	0.65	0.11	52	0.54	43	0.06	438
	JYC-017	61	1.30	0.07	0.88	0.1	68	1.07	82	0.07	439
	JYC-018	62	0.63	0.03	0.28	0.09	44	0.37	59	0.10	440
	JYC-019	63	1.21	0.06	1.02	0.13	84	0.63	52	0.06	438
	JYC-020	64	1.67	0.07	1.27	0.08	76	0.99	59	0.05	436
	JYC-021	65	0.30	0.01	0.11	0.03	37	0.23	76	0.08	447
	JYC-022	66	0.87	0.02	0.43	0.04	49	0.61	70	0.04	440
	JYC-023	67	0.97	0.02	0.55	0.03	57	0.61	63	0.04	441
	JYC-024	68	0.66	0.01	0.3	0.03	45	0.39	59	0.03	442
	JY-045	69	2.73	0.19	3.83	0.22	140	1.34	49	0.05	437

Facies	Sample Number	Height (ft)	SOURCE QUALITY						THERMAL MATURITY		
			Total Organic Carbon	Generated (Free) Hydrocarbons	Generated HC	Total Hydrocarbon Generation Potential	Hydrogen Enrichment Index	Generatable Carbon Dioxide	Oxygen Enrichment Index	Transform-ation Ratio	Temp. of peak S2
			TOC (%)	S1 (mg HC/g rk)	S2 (mg HC/g rk)	S1 + S2 (mg HC/g rk)	HI (mg HC/g TOC)	S3 (mg CO2/g rk)	OI (mg CO2/g TOC)	"PI" (S1/S1+S2)	Tmax (°C)
	JY-046	70	0.83	0.03	0.55	0.09	67	0.49	59	0.05	439
	JY-047	71	1.25	0.06	0.74	0.1	59	0.7	56	0.08	439
	JY-048	72	1.21	0.04	0.71	0.15	59	0.57	47	0.05	436
	JY-049	73	1.39	0.11	1.11	0.22	80	0.53	38	0.09	436
	JY-050	74	1.39	0.11	0.99	0.19	71	0.49	35	0.10	437
	JY-051	75	1.31	0.08	1.02	0.17	78	0.62	47	0.07	438
	JY-052	76	1.34	0.09	0.94	0.15	70	0.7	52	0.09	440
	JY-053	77	1.24	0.06	0.86	0.1	69	0.69	56	0.07	441
	JY-054	78	0.93	0.04	0.36	0.19	39	0.51	55	0.10	443
	JY-055	79	1.82	0.15	1.86	0.61	102	0.77	42	0.07	437
	JY-056	80	3.75	0.46	8.1	0.52	216	1.37	37	0.05	434
B	JY-057	81	1.15	0.06	0.47	0.17	41	0.62	54	0.11	440
	JY-058	82	1.42	0.11	1.05	0.19	74	0.79	56	0.09	438
	JY-059	83	0.59	0.08	0.21	0.19	36	0.54	92	0.28	439
	JY-060	84	1.08	0.11	0.74	0.2	69	0.7	65	0.13	437
	JY-061	85	0.47	0.09	0.17	0.16	36	0.28	60	0.35	442
	JY-062	86	0.66	0.07	0.34	0.14	52	0.45	69	0.17	435
	JY-063	87	0.29	0.07	0.09	0.17	31	0.45	156	0.44	441
	JY-064	88	1.03	0.1	0.87	0.22	85	0.8	78	0.10	433
	JY-065	89	1.18	0.12	0.92	0.48	78	0.84	71	0.12	435
	JY-066	90	2.49	0.36	3.63	0.55	146	1.91	77	0.09	436
	JY-067	91	1.81	0.19	1.98	0.3	109	1.42	78	0.09	433
	JY-068	92	1.24	0.11	1.14	0.31	92	1.03	83	0.09	433
	JY-069	93	1.81	0.2	2.17	0.3	120	1.48	82	0.08	435
	JY-070	94	1.34	0.1	1.19	0.14	89	1.26	94	0.08	436

Facies	Sample Number	Height (ft)	SOURCE QUALITY						THERMAL MATURITY		
			Total Organic Carbon	Generated (Free) Hydrocarbons	Generated HC	Total Hydrocarbon Generation Potential	Hydrogen Enrichment Index	Generatable Carbon Dioxide	Oxygen Enrichment Index	Transformation Ratio	Temp. of peak S2
			TOC (%)	S1 (mg HC/g rk)	S2 (mg HC/g rk)	S1 + S2 (mg HC/g rk)	HI (mg HC/g TOC)	S3 (mg CO2/g rk)	OI (mg CO2/g TOC)	"PI" (S1/S1+S2)	Tmax (°C)
	JY-071	96	0.24	0.04	0.01	0.11	4	0.15	63	0.80	420
C	JY-072	98	0.69	0.07	0.55	0.26	80	0.45	65	0.11	433
	JY-073	100	0.90	0.19	0.78	0.37	87	1.13	126	0.20	436
	JY-074	102	1.88	0.18	2.5	0.28	133	1.56	83	0.07	434
	JY-075	104	1.13	0.1	1.04	0.14	92	1	88	0.09	427
	JY-076	106	0.44	0.04	0.25	0.08	57	0.6	137	0.14	438
	JY-077	108	0.37	0.04	0.05	0.05	14	0.44	120	0.44	445
	JY-078	110	0.15	0.01	0	0.03	0	0.18	118	1.00	308
C	JY-079	112	0.19	0.02	0	0.03	0	0.29	154	1.00	422
	JY-080	114	0.14	0.01	0	0.02	0	0.16	115	1.00	258
	JY-081	116	0.28	0.01	0.02	0.06	7	0.2	72	0.33	279
	JY-082	118	1.71	0.05	0.1	0.07	6	0.45	26	0.33	443
	JY-083	120	0.21	0.02	0	0.03	0	0.19	90	1.00	240
	JY-084	122	0.25	0.01	0	0.02	0	0.25	100	1.00	305
	JY-085	124	0.23	0.01	0.02	0.02	9	0.31	135	0.33	279
	JY-086	126	0.23	0.01	0.01	0.02	4	0.18	78	0.50	279
	JY-087	128	0.17	0.01	0	0.02	0	0.21	125	1.00	269
	JY-088	130	0.16	0.01	0	0.06	0	0.16	100	1.00	227

- F "Fair" Hydrocarbon Generation Potential ($6 > S1+S2 > 5$ mg HC/g rock)
G "Good" Hydrocarbon Generation Potential ($10 > S1+S2 > 6$ mg HC/g rock)
VG "Very Good" Hydrocarbon Generation Potential ($20 > S1+S2 > 10$ mg HC/g rock)
Ex "Excellent" Hydrocarbon Generation Potential ($S1+S2 > 20$ mg HC/g rock)

TURKEY CREEK OUTCROP, COLORADO

Total Organic Carbon and Rock Eval Pyrolysis

Facies	Sample Number	Height (ft)	SOURCE QUALITY							THERMAL MATURITY	
			Total Organic Carbon	Generated (Free) Hydrocarbons	Generated Hydrocarbons	Total Hydrocarbon Generation Potential	Hydrogen Enrichment Index	Generatable Carbon Dioxide	Oxygen Enrichment Index	Transformation Ratio	Temp. of peak S2
			TOC (%)	S1 (mg HC/g rk)	S2 (mg HC/g rk)	S1 + S2 (mg HC/g rk)	HI (mg HC/g TOC)	S3 (mg CO ₂ /g rk)	OI (mg CO ₂ /g TOC)	"PI" (S1 / S1+S2)	Tmax (°C)
C	TC-000	0	1.59	0.06	1.24	1.3	78	0.08	5	0.05	418
	TC-005	5	0.65	0.01	0.2	0.21	31	0.07	11	0.05	413
	TC-010	10	0.61	0.07	0.06	0.13	10	0.08	13	0.54	419
	TC-015	15	0.62	0.01	0.18	0.19	29	0.21	34	0.05	427
	TC-020	20	0.92	0.01	0.31	0.32	34	0.19	21	0.03	424
	TC-025	25	0.6	0.01	0.12	0.13	20	0.84	140	0.08	427
	TC-026	26	0.29	0.02	0.06	0.08	21	0.00	0	0.25	413
B	TC-030	30	1.62	0.02	1.36	1.38	84	0.18	11	0.01	416
	TC-035	35	0.73	0.02	0.19	0.21	26	0.17	23	0.10	417
	TC-036	36	1.57	0.04	2.02	2.06	129	0.19	12	0.02	415
A	TC-037	37	2.66	0.17	5.41	5.58	203	0.37	14	0.03	414
	TC-038	38	0.32	0.01	0.07	0.08	22	0.03	9	0.13	420
	TC-039	39	1.97	0.12	5.79	5.91	294	0.09	5	0.02	408
	TC-040	40	4.24	0.46	17.55	18.01	414	0.29	7	0.03	407
	TC-041	41	4.12	0.45	16.83	17.28	408	0.26	6	0.03	410
	TC-042	42	2.97	0.22	9.63	9.85	324	0.09	3	0.02	409
	TC-043	43	3.7	0.39	14.03	14.42	379	0.12	3	0.03	410
	TC-044	44	3.5	0.23	11.41	11.64	326	0.21	6	0.02	400
	TC-045	45	3.48	0.22	9.46	9.68	272	0.18	5	0.02	409
B	TC-050	50	1.79	0.07	2.95	3.02	165	0.10	6	0.02	415
	TC-055	55	1.69	0.08	3.18	3.26	188	0.12	7	0.02	413
	TC-063	63	0.65	0.03	0.64	0.67	98	0.01	2	0.04	418
	TC-070	70	0.58	0.02	0.17	0.19	29	0.03	5	0.11	423
	TC-075	75	0.82	0.05	0.4	0.45	49	0.01	1	0.11	421
C	TC-078	80	0.63	0.03	0.1	0.13	16	0.01	2	0.23	419
	TC-081	86	0.85	0.02	0.13	0.15	15	0.00	0	0.13	415
	TC-083	90	1.01	0.02	0.15	0.17	15	0.20	20	0.12	412
	TC-085	94	0.74	0.01	0.26	0.27	35	0.00	0	0.04	411

Overall Quality:

- F "Fair" Hydrocarbon Generation Potential ($6 > S1+S2 > 5$ mg HC/g rock)
- G "Good" Hydrocarbon Generation Potential ($10 > S1+S2 > 6$ mg HC/g rock)
- VG "Very Good" Hydrocarbon Generation Potential ($20 > S1+S2 > 10$ mg HC/g rock)
- Ex "Excellent" Hydrocarbon Generation Potential ($S1+S2 > 20$ mg HC/g rock)

MEADOW SPRINGS, COLORADO
Total Organic Carbon and Rock Eval Pyrolysis

Sample Quality	Number	Depth (ft)	Facies	SOURCE QUALITY							THERMAL MATURITY	
				Total Organic Carbon	Free (Generated) Hydrocarbons	Generatable Hydrocarbons	Total Hydrocarbon Generation Potential	Hydrogen Enrichment Index	Generatable Carbon Dioxide	Oxygen Enrichment Index	Transformation Ratio	Temp. of Peak S ₂
				TOC (%)	S ₁ (mg HC /g rk)	S ₂ (mg HC /g rk)	S ₁ +S ₂ (mg HC /g rk)	HI (mg HC /g TOC)	S ₃ (mg CO ₂ /g rk)	OI (mg CO ₂ /g TOC)	"PI" (S ₁ / S ₁ +S ₂)	T _{max} (°C)
<i>G</i>	MS000	7944	A	0.19	0.39	1.54	1.93	811	0.14	74	0.20	435
	MS001	7943		0.40	0.67	5.78	6.45	1445	0.10	25	0.10	432
	MS002	7942		0.11	0.16	0.49	0.65	445	0.05	45	0.25	426
<i>G</i>	MS003	7941		0.47	0.81	7.38	8.19	1570	0.14	30	0.10	432
	MS004	7940		0.45	0.45	4.23	4.68	940	0.75	167	0.10	438
<i>G</i>	MS005	7931		0.47	1.01	7.17	8.18	1526	0.14	30	0.12	432
<i>G</i>	MS006	7938		0.46	0.78	6.46	7.24	1404	0.19	41	0.11	434
<i>VG</i>	MS009	7935	B	0.63	1.07	12.76	13.83	2025	0.17	27	0.08	431
	MS014	7930		1.90	0.55	2.13	2.68	112	0.35	18	0.21	436
	MS019	7925		1.31	0.36	1.81	2.17	138	0.15	11	0.17	436
	MS024	7920		1.07	0.29	1.49	1.78	139	0.13	12	0.16	435
	MS029	7915	C	0.71	0.22	0.64	0.86	90	0.01	1	0.26	433
	MS034	7910		0.44	0.09	0.19	0.28	43	0.00	0	0.32	429
	MS039	7905		0.63	0.11	0.43	0.54	68	0.00	0	0.20	435
	MS044	7900	D	0.70	0.44	0.60	1.04	86	0.00	0	0.42	442
	MS049	7895		0.15	0.23	0.06	0.29	40	0.00	0	0.79	415
	MS052	7890		0.23	0.45	0.12	0.57	52	0.12	52	0.79	412
	MS055	7884		Paleosol	0.11	0.05	0.04	0.09	36	0.00	0	0.56
	MS058	7880	E	2.55	0.26	3.16	3.42	124	0.36	14	0.08	441
	MS062	7872		1.36	0.18	1.00	1.18	74	0.11	8	0.15	451
	MS066	7864	Mowry	1.78	0.32	3.13	3.45	176	0.08	4	0.09	450

Overall Quality:

- F* "Fair" Hydrocarbon Generation Potential (S₁+S₂ > 5 < 6 mg HC/g rock)
- G* "Good" Hydrocarbon Generation Potential (S₁+S₂ >6 <10 mg HC/g rock)
- VG* "Very Good" Hydrocarbon Generation Potential (>10 < 20 mg HC/g rock)
- Ex* "Excellent" Hydrocarbon Generation Potential (>20 mg HC/g rock)

**Total Organic Carbon and RockEval Pyrolysis
Rooney Ranch**

Sample			Source Quality							Thermal Maturity		
Facies	Sample Number	Height (ft)	Total Org. Carbon TOC (%)	Free (Generated) HC S ₁ (mg HC/g rk)	Generatable HC S ₂ (mg HC/g rk)	Generatable Carbon Dioxide S ₃ (mg CO ₂ /g rk)	total Hydrocarbon generation Potenti S ₁ +S ₂ (mg HC/g rk)	Hydrogen Enrichment Index HI (mg HC/g rk)	Oxygen Enrichment Index OI (mg CO ₂ /g rk)	Overall Source Quality Rating	Transformation Ratio PI S ₁ /(S ₁ +S ₂)	Temp. of Peak S ₂ T _{MAX} °C
	GR-000	124	1.65	0.05	0.37	0.80	0.42	22	48	Poor	0.12	426
	GR-001	123	0.12	0.13	0.03	0.14	0.16	25	117	Poor	0.81	433
	GR-002	122	1.37	0.07	0.21	0.67	0.28	15	49	Poor	0.25	433
	GR-003	121	0.96	0.05	0.33	0.55	0.38	34	57	Poor	0.13	436
	GR-004	120	3.28	0.09	0.87	0.67	0.96	27	20	Poor	0.09	434
	GR-005	119	1.66	0.11	0.35	0.59	0.46	21	36	Poor	0.24	428
	GR-006	118	3.70	0.23	4.80	1.44	5.03	130	39	Fair	0.05	425
	GR-007	117	3.40	0.18	3.72	1.18	3.90	109	35	Poor	0.05	425
	GR-008	116	2.78	0.13	1.58	1.20	1.71	57	43	Poor	0.08	426
	GR-009	115	3.36	0.19	3.67	1.10	3.86	109	33	Poor	0.05	422
	GR-010	114	3.12	0.11	2.56	1.20	2.67	82	38	Poor	0.04	427
	GR-011	113	3.11	0.18	2.38	1.10	2.56	77	35	Poor	0.07	428
	GR-012	112	3.36	0.16	3.16	1.20	3.32	94	36	Poor	0.05	427
Upper	GR-013	111	3.42	0.13	2.63	1.19	2.76	77	35	Poor	0.05	427
Y	GR-014	110	2.71	0.10	1.41	0.97	1.51	52	36	Poor	0.07	430
	GR-015	109	2.32	0.16	1.43	2.27	1.59	62	98	Poor	0.10	434
	GR-016	108	2.88	0.13	2.32	0.95	2.45	81	33	Poor	0.05	430
	GR-017	107	2.85	0.23	2.17	1.10	2.40	76	39	Poor	0.10	427
	GR-018	106	3.55	0.18	2.49	1.32	2.67	70	37	Poor	0.07	427
	GR-019	105	3.12	0.22	2.99	1.15	3.21	96	37	Poor	0.07	424
	GR-020	104	3.11	0.15	3.20	1.84	3.35	103	59	Poor	0.04	427
	GR-021	97	1.91	0.06	0.81	1.67	0.87	42	87	Poor	0.07	427
	GR-022	96	3.71	0.12	4.46	1.63	4.58	120	44	Poor	0.03	429
	GR-023	95	2.37	0.10	2.10	1.61	2.20	89	68	Poor	0.05	428

Sample			Source Quality							Thermal Maturity		
Facies	Sample Number	Height (ft)	Total Org. Carbon TOC (%)	Free (Generated) HC S ₁ (mg HC/g rk)	Generatable HC S ₂ (mg HC/g rk)	Generatable Carbon Dioxide S ₁ (mg CO ₂ /g rk)	Generatable Total Hydrocarbon S ₁ +S ₂ (mg HC/g rk)	Hydrogen Enrichment Index HI (mg HC/g rk)	Oxygen Enrichment Index OI (mg CO ₂ /g rk)	Overall Source Quality Rating	Transformation Ratio S ₁ /(S ₁ +S ₂)	Temp. of Peak S ₂ T _{MAX} °C
Upper Y	GR-024	94	1.46	0.06	0.58	1.68	0.64	40	115	Poor	0.09	430
	GR-025	93	3.73	0.19	10.96	0.39	11.15	294	10	Very Good	0.02	420
	GR-026	92	3.56	0.17	8.85	1.05	9.02	249	29	Good	0.02	423
	GR-027	91	3.91	0.18	12.36	0.48	12.54	316	12	Very Good	0.01	421
Z	GR-028	90	1.89	0.08	1.84	0.77	1.92	97	41	Poor	0.04	428
	GR-029	89	3.09	0.15	8.85	0.65	9.00	286	21	Good	0.02	422
	GR-030	88	3.60	0.14	7.75	0.84	7.89	215	23	Good	0.02	420
	GR-031	87	3.96	0.15	8.89	1.07	9.04	224	27	Good	0.02	418
	GR-032	86	3.14	0.11	6.39	0.41	6.50	204	13	Good	0.02	420
	GR-033	85	2.93	0.11	3.72	0.97	3.83	127	33	Poor	0.03	418
	GR-034	84	3.91	0.15	7.69	0.78	7.84	197	20	Good	0.02	422
	GR-035	83	3.66	0.12	6.69	0.79	6.81	183	22	Good	0.02	419
	GR-036	82	2.97	0.16	9.18	1.72	9.34	309	58	Good	0.02	420
	GR-037	81	4.61	0.17	11.79	1.90	11.96	256	41	Very Good	0.01	416
	GR-038	80	1.19	0.07	2.55	0.33	2.62	214	28	Poor	0.03	427
	GR-039	79	5.46	0.29	18.83	0.88	19.12	345	16	Very Good	0.02	418
	GR-040	78	5.15	0.17	13.61	1.11	13.78	264	22	Very Good	0.01	416
	GR-041	77	4.50	0.41	20.94	1.69	21.35	465	38	Excellent	0.02	420
	GR-042	76	3.99	0.17	9.76	1.87	9.93	245	47	Good	0.02	419
	GR-043	75	4.65	0.31	16.79	0.52	17.10	361	11	Very Good	0.02	419
	GR-044	74	4.39	0.20	14.08	0.60	14.28	321	14	Very Good	0.01	420
	GR-045	73	4.91	0.20	17.46	1.62	17.66	356	33	Very Good	0.01	422
	GR-046	72	5.55	0.29	21.08	0.39	21.37	380	7	Excellent	0.01	420
	GR-047	71	5.88	0.32	23.04	2.35	23.36	392	40	Excellent	0.01	419
GR-048	70	4.99	0.33	20.35	2.70	20.68	408	54	Excellent	0.02	419	
GR-049	69	4.12	0.34	19.00	3.15	19.34	461	76	Very Good	0.02	417	
GR-050	68	5.04	0.36	21.80	2.94	22.16	433	58	Excellent	0.02	423	

Sample			Source Quality							Thermal Maturity		
Facies	Sample Number	Height (ft)	Total Org. Carbon TOC (%)	Free (Generated) HC S ₁ (mg HC/g rk)	Generatable HC S ₂ (mg HC/g rk)	Generatable Carbon Dioxide S ₃ (mg CO ₂ /g rk)	total Hydrocarbon generation Potenti S ₁ +S ₂ (mg HC/g rk)	Hydrogen Enrichment Index HI (mg HC/g rk)	Oxygen Enrichment Index OI (mg CO ₂ /g rk)	Overall Source Quality Rating	Transformation Ratio S ₁ /(S ₁ +S ₂)	Temp. of Peak S ₂ T _{MAX} °C
Z	GR-051	67	4.89	0.27	19.84	2.36	20.11	406	48	Excellent	0.01	419
	GR-057	61	4.80	0.26	17.79	2.11	18.05	371	44	Very Goo	0.01	420
	GR-058	60	0.97	0.21	12.64	0.82	12.85	1303	85	Very Goo	0.02	420
	GR-059	59	4.86	0.38	9.01	0.57	9.39	185	12	Good	0.04	419
	GR-060	58	4.71	0.09	1.96	0.11	2.05	42	2	Poor	0.04	418
	GR-061	57	5.04	0.28	15.00	0.81	15.28	298	16	Very Goo	0.02	417
	GR-062	56	5.15	0.24	13.75	1.08	13.99	267	21	Very Goo	0.02	416
	GR-063	55	4.55	0.28	16.02	0.91	16.30	352	20	Very Goo	0.02	416
	GR-064	54	4.56	0.36	20.98	0.47	21.34	460	10	Excellent	0.02	420
	GR-065	53	4.72	0.30	13.72	0.85	14.02	291	18	Very Goo	0.02	417
	GR-066	52	5.15	0.20	17.45	0.54	17.65	339	10	Very Goo	0.01	421
GR-067	51	4.37	0.20	14.54	0.76	14.74	333	17	Very Goo	0.01	4236	
Lower Y	GR-068	50	5.03	0.20	18.57	0.66	18.77	369	13	Very Goo	0.01	424
	GR-069	49	4.43	0.11	12.93	0.89	13.04	292	20	Very Goo	0.01	423
	GR-070	48	4.14	0.16	12.37	0.61	12.53	299	15	Very Goo	0.01	422
	GR-071	47	4.02	0.10	12.82	0.40	12.92	319	10	Very Goo	0.01	422
	GR-072	46	3.41	0.14	10.33	0.65	10.47	303	19	Very Goo	0.01	423
	GR-073	44	2.41	0.09	2.70	1.54	2.79	112	64	Poor	0.03	429
	GR-074	42	3.69	0.16	10.94	1.15	11.10	296	31	Very Goo	0.01	422
	GR-075	40	2.85	0.12	3.68	1.51	3.80	129	53	Poor	0.03	426
	GR-076	38	1.04	0.03	0.12	2.02	0.15	12	194	Poor	0.20	439
	GR-077	36	2.84	0.11	5.45	1.04	5.56	192	37	Fair	0.02	424
	GR-078	34	2.00	0.05	1.97	1.09	2.02	99	55	Poor	0.02	428
	GR-079	32	2.17	0.07	2.47	1.45	2.54	114	67	Poor	0.03	430
GR-080	30	2.04	0.07	2.93	1.03	3.00	144	50	Poor	0.02	430	
GR-081	28	2.24	0.10	3.58	1.16	3.68	160	52	Poor	0.03	430	
GR-082	26	2.09	0.07	3.34	1.03	3.41	160	49	Poor	0.02	430	

Sample			Source Quality							Thermal Maturity		
Facies	Sample Number	Height (ft)	Total Org. Carbon TOC (%)	Free (Generated) HC S ₁ (mg HC/g rk)	Generatable HC S ₂ (mg HC/g rk)	Generatable Carbon Dioxide S ₁ (mg CO ₂ /g rk)	total Hydrocarbon Generation Potential S ₁ +S ₂ (mg HC/g rk)	Hydrogen Enrichment Index HI (mg HC/g rk)	Oxygen Enrichment Index OI (mg CO ₂ /g rk)	Overall Source Quality Rating	Transformation Ratio S ₁ /(S ₁ +S ₂)	Temp. of Peak S ₂ T _{MAX} °C
X	GR-083	24	1.56	0.05	1.50	0.79	1.55	96	51	Poor	0.03	431
	GR-085	20	1.03	0.02	0.41	0.67	0.43	40	65	Poor	0.05	439
	GR-088	14	1.31	0.07	0.24	0.30	0.31	18	23	Poor	0.23	427
	GR-091	8	1.18	0.10	0.14	0.46	0.24	12	39	Poor	0.42	431
	GR-093	4	0.61	0.05	0.36	1.34	0.41	59	220	Poor	0.12	431

F "Fair" Hydrocarbon Generation Potential ($6 > S_1+S_2 > 5$ mg HC/g rock)

G "Good" Hydrocarbon Generation Potential ($10 > S_1+S_2 > 6$ mg HC/g r

VG "Very Good" Hydrocarbon Generation Potential ($20 > S_1+S_2 > 10$ mg

Ex "Excellent" Hydrocarbon Generation Potential ($S_1+S_2 > 20$ mg HC/g r

YOUNGS CORE
Total Organic Carbon and RockEval Pyrolysis

			Source Quality								Thermal Maturity	
Facies	Sample Number	Depth (ft)	Total Organic Carbon TOC (%)	Free (Generated) HC S ₁ (mg HC/g rk)	Generatable HC S ₂ (mg HC/g rk)	Generatable Carbon Dioxide S ₁ (mg CO ₂ /g rk)	Total HC Generation Potential S ₁ +S ₂ (mg HC/g rk)	Hydrogen Enrich. Index HI (mg HC/g TOC)	Oxygen Enrich. Index OI (mg CO ₂ /g TOC)	Overall Source Quality Rating	Transformation Ratio PI S ₁ /(S ₁ +S ₂)	Temp. of Peak S ₂ T _{MAX} °C
D-Sand	YO-000	5808	1.48	0.81	0.42	0.02	1.23	28	1	Poor	0.66	402
Z	YO-004	5804	3.76	0.29	1.78	0.00	2.07	47	0	Poor	0.14	435
	YO-008	5800	1.56	1.92	14.43	0.02	16.35	925	1	Very Good	0.12	433
	YO-013	5795	3.12	1.16	11.42	0.00	12.58	366	0	Very Good	0.09	434
	YO-018	5790	5.36	2.88	23.09	0.03	25.97	431	1	Excellent	0.11	432
	YO-023	5785	5.35	2.83	22.66	0.07	25.49	424	1	Excellent	0.11	433
	YO-028	5780	4.81	3.02	18.93	0.03	21.95	394	1	Excellent	0.14	433
	YO-033	5775	5.12	2.91	20.92	0.03	23.83	409	1	Excellent	0.12	434
	YO-039	5769	4.31	2.20	15.34	0.03	17.54	356	1	Very Good	0.13	434
	YO-044	5764	3.92	1.56	13.63	0.07	15.19	348	2	Very Good	0.10	435

- F "Fair" Hydrocarbon Generation Potential (6 > S₁+S₂ > 5 mg HC/g rock)
- G "Good" Hydrocarbon Generation Potential (10 > S₁+S₂ > 6 mg HC/g rock)
- VG "Very Good" Hydrocarbon Generation Potential (20 > S₁+S₂ > 10 mg HC/g rock)
- Ex "Excellent" Hydrocarbon Generation Potential (S₁+S₂ > 20 mg HC/g rock)